379

AMC PAMPHLET AD ^ 0 AMCP 706-180

PAUL M. SCHUMACHER
062-40-5056

ENGINEERING DESIGN HANDBOOK

PRINCIPLES OF EXPLOSIVE BEHAVIOR

HEADQUARTERS, U S ARMY MATERIEL COMMAND APRIL 1972

PAUL M. SCHUMACHER
062-40-5056

HEADQUARTERS
UNITED STATES ARMY MATERIEL COMMAND
WASHINGTON, DC 20315

AMC PAMPHLET
No. 706-180

10 April 1972

ENGINEERING DESIGN HANDBOOK

PRINCIPLES OF EXPLOSIVE BEHAVIOR

TABLE OF CONTENTS

Paragraph		Page
	LIST OF ILLUSTRATIONS	viii
	LIST OF TABLES	xv
	PREFACE	xvii
	CHAPTER 1. INTRODUCTION	
1-1	Introductory Remarks	1-1
1-2	Description of Explosive Processes	1-2
1-3	Types of Explosives	1-2
1-4	Some Definitions	1-4
	CHAPTER 2. THEORETICAL BACKGROUND	
2-1	Introduction	2-1
2-2	Description of the Composition	2-1
2-3	The Laws of Thermodynamics	2-4
2-4	General Thermodynamic Identities	2-10
2-5	Approximations for the Thermodynamic Properties on an Isentrope	2-16
2-6	Hydrodynamics of Reacting Continua	2-16
2-7	Uniformly Isentropic Flow in One Dimension	2-21
2-8	Conservation Conditions at a Discontinuity. The Hugoniot Equation	2-27
	References	2-31

TABLE OF CONTENTS (Cont'd)

Paragraph		*Page*
	CHAPTER 3. ENERGY OF EXPLOSIVES	
3-1	Introduction	3-1
3-2	Heat of Detonation	3-1
3-3	Thermochemistry of High Explosives	3-1
3-4	Computation of Q	3-3
3-5	Fragment Velocities	3-4
3-6	Air-blast	3-5
3-7	Underwater Performance	3-5
3-8	C-J Parameters	3-6
3-9	Maximum Work	3-6
	References	3-8
	CHAPTER 4. THERMAL DECOMPOSITION OF EXPLOSIVES	
4-1	Introduction	4-1
4-2	Decomposition Energies	4-1
4-3	Decomposition Mechanisms	4-3
4-3.1	Covalent Liquids and Solids	4-4
4-3.2	Ionic Solids (Azides)	4-6
4-3.3	Ammonium Salts	4-16
4-4	Radiation Damage in Explosive Solids	4-18
	References	4-20
	CHAPTER 5. MEASUREMENT OF DETONATION PROPERTIES	
5-1	Introduction	5-1
5-2	Detonation Velocity	5-1
5-2.1	High-speed Photography	5-1
5-2.2	Photo-optical Systems	5-4
5-2.3	Electrical Systems	5-4
5-2.4	D'Autriche Method	5-5
5-3	Detonation Pressure	5-5
5-3.1	Pressure in Adjacent Plates	5-8
5-3.1.1	Plane Wave Explosive Systems	5-9
5-3.1.2	Pressure Transducers	5-10
5-3.1.3	Particle Velocity Measurement	5-15
5-3.2	X-ray Flash Photography	5-18
5-4	Blast Wave Pressure	5-19
5-5	Detonation Temperature	5-21
5-6	Electrical Conductivity in the Detonation Zone	5-22

PAUL M. SCHUMACHER
062-40-5056

HEADQUARTERS
UNITED STATES ARMY MATERIEL COMMAND
WASHINGTON, DC 20315

AMC PAMPHLET
No. 706-180

10 April 1972

ENGINEERING DESIGN HANDBOOK

PRINCIPLES OF EXPLOSIVE BEHAVIOR

TABLE OF CONTENTS

Paragraph		*Page*
	LIST OF ILLUSTRATIONS	viii
	LIST OF TABLES	xv
	PREFACE	xvii
	CHAPTER 1. INTRODUCTION	
1-1	Introductory Remarks	1-1
1-2	Description of Explosive Processes	1-2
1-3	Types of Explosives	1-2
1-4	Some Definitions	1-4
	CHAPTER 2. THEORETICAL BACKGROUND	
2-1	Introduction	2-1
2-2	Description of the Composition	2-1
2-3	The Laws of Thermodynamics	2-4
2-4	General Thermodynamic Identities	2-10
2-5	Approximations for the Thermodynamic Properties on an Isentrope	2-16
2-6	Hydrodynamics of Reacting Continua	2-16
2-7	Uniformly Isentropic Flow in One Dimension	2-21
2-8	Conservation Conditions at a Discontinuity. The Hugoniot Equation	2-27
	References	2-31

TABLE OF CONTENTS (Cont'd)

Paragraph		*Page*
	CHAPTER 3. ENERGY OF EXPLOSIVES	
3-1	Introduction	3-1
3-2	Heat of Detonation	3-1
3-3	Thermochemistry of High Explosives	3-1
3-4	Computation of Q	3-3
3-5	Fragment Velocities	3-4
3-6	Air-blast	3-5
3-7	Underwater Performance	3-5
3-8	C-J Parameters	3-6
3-9	Maximum Work	3-6
	References	3-8
	CHAPTER 4. THERMAL DECOMPOSITION OF EXPLOSIVES	
4-1	Introduction	4-1
4-2	Decomposition Energies	4-1
4-3	Decomposition Mechanisms	4-3
4-3.1	Covalent Liquids and Solids	4-4
4-3.2	Ionic Solids (Azides)	4-6
4-3.3	Ammonium Salts	4-16
4-4	Radiation Damage in Explosive Solids	4-18
	References	4-20
	CHAPTER 5. MEASUREMENT OF DETONATION PROPERTIES	
5-1	Introduction	5-1
5-2	Detonation Velocity	5-1
5-2.1	High-speed Photography	5-1
5-2.2	Photo-optical Systems	5-4
5-2.3	Electrical Systems	5-4
5-2.4	D'Autriche Method	5-5
5-3	Detonation Pressure	5-5
5-3.1	Pressure in Adjacent Plates	5-8
5-3.1.1	Plane Wave Explosive Systems	5-9
5-3.1.2	Pressure Transducers	5-10
5-3.1.3	Particle Velocity Measurement	5-15
5-3.2	X-ray Flash Photography	5-18
5-4	Blast Wave Pressure	5-19
5-5	Detonation Temperature	5-21
5-6	Electrical Conductivity in the Detonation Zone	5-22

TABLE OF CONTENTS (Cont'd)

Paragraph		*Page*
5-7	Empirical Tests	5-24
	References	5-27

CHAPTER 6. ELEMENTARY THEORY OF THE PLANE DETONATION WAVE

6-1	Introduction	6-1
6-2	The Rankine-Hugoniot Equation	6-1
6-3	Properties of the Hugoniot Curve	6-8
6-4	Existence and Uniqueness of Flows Involving Reaction Waves	6-14
6-5	The Chapman-Jouguet Hypothesis	6-19
6-6	Theory of the Detonation Velocity and of the Thermodynamic State of the Explosion Gas	6-24
	References	6-26

CHAPTER 7. APPLICATION OF THEORY TO CONDENSED EXPLOSIVES

7-1	Introduction	7-1
7-2	The Abel Equation of State	7-2
7-3	Determination of the Detonation State from Velocity Data	7-5
7-4	Modifications of the Abel Equation	7-8
7-5	Application of the Chapman-Jouguet Condition to Mixtures With Varying Composition	7-13
7-6	Explosives Whose Products Contain a Solid Phase	7-15
7-7	The Virial Equation of State	7-16
7-8	The Halford-Kistiakowsky-Wilson Equation of State	7-18
	References	7-21

CHAPTER 8. STRUCTURE OF THE PLANE DETONATION WAVE: FINITE REACTION ZONE

8-1	Introduction	8-1
8-2	Conservation Conditions for Steady Reaction Waves in One Dimension	8-1
8-3	The Steady Deflagration Wave	8-3
8-4	The Steady Detonation Wave	8-4
8-5	Flow Behind a Chapman-Jouguet Wave	8-6
8-6	The Detonation Wave With Equilibrium Product Composition Composition	8-9
8-7	Fine Structure of Detonation in Gases and Liquids	8-14
	References	8-17

TABLE OF CONTENTS (Cont'd)

Paragraph		*Page*
	CHAPTER 9. DETONATION WAVES OF CYLINDRICAL AND SPHERICAL SYMMETRY	
9-1	Introduction	9-1
9-2	The Effect of Charge Diameter on the Detonation Velocity	9-1
9-3	Diverging Flow Within a Cylindrical Symmetric Steady Reaction Zone	9-4
9-4	Theories of the Charge Diameter Effect	9-9
9-5	The Release Wave Model	9-12
9-6	The Spherical Detonation Wave Initiated at a Point	9-13
	References	9-18
	CHAPTER 10. THERMAL EXPLOSION	
10-1	Introduction	10-1
10-2	Description of the Thermal Explosion Process	10-1
10-3	Mathematical Treatments of Thermal Explosion	10-7
10-3.1	The Heat Conduction Equation	10-7
10-3.2	Steady-state Condition $\partial T/\partial t = 0$, and the Concept of Critical Temperature and Size	10-8
10-3.3	Adiabatic Heating ($\nabla^2 T = 0$) and the Concept of Explosion Time	10-9
10-3.4	Approximate Solutions for t_e With Nonadiabatic Heating	10-10
10-3.5	Numerical Methods	10-17
10-4	Thermal Explosion of Hot Spots	10-14
10-5	Thermal Explosion and Safety in Handling High Explosives	10-18
	References	10-21
	CHAPTER 11. INITIATION OF DETONATION BY SHOCK WAVES	
11-1	Underdriven and Overdriven Detonation	11-1
11-2	The Gap Test	11-1
11-3	Shock-pressure Measurements in the Gap Test	11-2
11-4	Effects of Shock Waves in Condensed Explosives	11-3
11-5	Shock Initiation in Homogeneous and Nonhomogeneous Explosives	11-5
11-6	Thermal Explosion Theory Applied to Shock Initiation	11-10
11-6.1	Homogeneous Explosives	11-10
11-6.2	Behavior of Hot Spots	11-13
11-7	Hot Spot Creation by Shock Waves	11-17
11-8	Sensitivity to Shock Initiation	11-19

TABLE OF CONTENTS (Cont'd)

Paragraph		*Page*
11-9	Theory of Shock Wave Initiation in Solid Explosives	11-23
11-10	Low-velocity Detonation (LVD)	11-26
	References	11-31

CHAPTER 12. INITIATION AND GROWTH OF DETONATION FROM IMPACT, FRICTION, AND THERMAL SOURCES

12-1	Sensitivity to Impact and Friction	12-1
12-2	Design and Analysis of Sensitivity Experiments	12-4
12-3	Theory of Impact Sensitivity	12-6
12-4	Transition of Deflagration to Detonation	12-13
	References	12-21

CHAPTER 13. SHOCK WAVES FROM EXPLOSIVE CHARGES

13-1	Introduction	13-1
13-2	Expansion of the Explosion Products	13-3
13-3	Energy Transport by Shock Wave Propagation	13-5
13-4	Blast Waves in Air from Explosive Charges	13-7
13-5	Results of Numerical Integration of the Hydrodynamic Equations for Blast Waves in Air	13-10
13-6	Underwater and Underground Explosions	13-19
13-7	The Initial Shock Wave Pressures	13-25
13-8	An Approximate Theory of Shock Wave Propagation	13-26
13-9	Shock Wave Scaling	13-33
13-10	Explosively-produced Shock Waves in Solids	13-38
	References	13-40

CHAPTER 14. COMPUTER PROGRAMS FOR EXPLOSIVE CALCULATIONS

14-1	Introduction	14-1
14-2	Methods of Hydrodynamic Calculations	14-1
14-2.1	Introduction	14-1
14-2.2	Method of Characteristics	14-1
14-2.3	Method of Artificial Viscosity	14-5
14-2.4	Particle-in-cell Method	14-11
14-3	Equation-of-state Computations	14-11
14-4	Reaction Mechanisms for Computations	14-13
14-5	Summary of Calculations of Wave Propagation With Reactive Mechanisms	14-13
	References	14-15

TABLE OF CONTENTS (Cont'd)

Paragraph		*Page*
	APPENDIX A. EVALUATION OF THE THERMODYNAMIC PROPERTIES	
A-1	Introduction	A-1
A-2	Thermodynamic Properties of Pure Condensed Phases	A-1
A-3	Thermodynamic Properties of a Gas Mixture	A-3
A-4	Thermodynamic Properties of Heterogeneous Systems	A-6
	References	A-7
	APPENDIX B. GENERAL PROCEDURE FOR THE CALCULATION OF EQUILIBRIUM COMPOSITION	
B-1	Introduction	B-1
B-2	Linearization of the Equilibrium Conditions	B-1
B-3	Relations for an Equation of State Explicit in Pressure and Temperature	B-2
B-4	Relations for an Equation of State Explicit in Volume and Temperature	B-4
B-5	The Initial Approximation	B-5
B-6	Calculation of the Equilibrium Partial Derivatives	B-6
	References	B-7
	APPENDIX C. METHOD FOR THE DESK CALCULATION OF EQUILIBRIUM COMPOSITION OF SYSTEMS CONTAINING COMPOUNDS OF CARBON, HYDROGEN, OXYGEN, AND NITROGEN	
C-1	Introduction	C-1
C-2	Systems With Solid Carbon	C-2
C-3	Rich System Without Solid Carbon, $q_O < 2\,q_C + q_H/2$	C-2
C-4	Lean Systems Without Solid Carbon $q_O \geq 2\,q_C + q_H/2$	C-3
	APPENDIX D. IMPERFECT GAS CONTRIBUTIONS TO THE THERMODYNAMIC PROPERTIES FOR SEVERAL EQUATIONS OF STATE	
D-1	Introduction	D-1
D-2	The Abel Equation of State	D-1
D-3	The Abel Equation of State as Modified by Jones	D-1
D-4	The Abel Equation of State as Modified by Cook	D-2
D-5	The Virial Equation of State of Hirschfelder and Roseveare	D-2
D-6	The Halford-Kistiakowsky-Wilson Equation of State	D-3

TABLE OF CONTENTS (Cont'd)

Paragraph *Page*

APPENDIX E. CALCULATION OF THE DETONATION VELOCITY OF THE THERMODYNAMIC STATE OF THE EXPLOSION GAS E-1

APPENDIX F. CALCULATION OF THE DETONATION VELOCITY FOR IDEAL GASES F-1

INDEX I-1

LIST OF ILLUSTRATIONS

Fig. No.	Title	Page
1-1	Model of Explosive Charge	1-5
2-1	The Coefficients of α_{ik} and β_{ij} for the Explosion Products of TNT	2-5
2-2	Region of Influence of a Point P	2-23
2-3	Domain of Dependence of Arc AB of a Spacelike Initial Value Curve	2-24
2-4	Domain of Dependence of Arc AB of a Timelike Initial Value Curve and Arc BC of a Timelike or Characteristic Initial Valuc Curve	2-25
2-5	Straight Characteristics C_+, Piston Path, and Particle Path in a Simple Rarefaction Wave	2-26
2-6	Intersecting Straight Characteristics C_+ During Compression Wave	2-27
2-7	One-dimensional Shock Wave	2-28
2-8	Flow in a Steady One-dimensional Shock Supported by a Piston, Showing a Particle Path and C_+ Characteristics Through Points on the Particle Path	2-30
4-1	Thermal Decomposition Sigmoid Curve	4-2
4-2	Plot of Logarithm of Rate constant k vs Reciprocal of Absolute Temperature to Determine Activation Energy from Slope of the Line	4-3
4-3	Representation of the Orbital System of the Azide Ion	4-7
4-4	Schematic Showing Energy E to Excite an Electron from Valence Band to Conduction Band in Silver Azide	4-8
4-5	Showing Technique for Studying Silver Nuclei from Decomposed Silver Azide	4-10
4-6	Schematic for Determining Optical Absorption Spectra	4-11
4-7	Absorption Coefficients α as Function of Wavelength λ. At High Absorption, Photon Energy $h\nu$ Assumed to Correspond to Band Gap Energy E	4-12
4-8	Showing Exciton Levels	4-12
4-9	Energy Gaps E_1 and E_2 in Silver Azide	4-13
4-10	Schematic for Studying Photoconductivity of Crystal	4-15
4-11	Orbital System of Covalent Azide, HN_3	4-17
5-1	Elements of the Rotating Drum Camera System	5-2
5-2	Optical System in AEC-Bowen Framing Camera	5-3
5-3	Arrangement of a Kerr-effect Shutter	5-4
5-4	Block Diagram of Equipment for Measuring Detonation Velocity With Ionization Probes	5-6
5-5	Zig-zag Oscilloscope Trace Obtained With Raster Generator	5-7
5-6	D'Autriche Test System	5-8

LIST OF ILLUSTRATIONS (Cont'd)

Fig. No.	Title	Page
5-7	Plane-wave Generator (A), and Shock Wave Before (B) and After (C) It Impinges on the Metal Plate	5-11
5-8	Compressibility of Various Materials Under Shock Wave Conditions	5-12
5-9	Configuration for the Measurement of Interface Stress Using a Quartz Pressure Transducer	5-13
5-10	Configuration of Manganin-epoxy Pressure Transducer	5-14
5-11	Form of Polarization Signal from Polarization Gage	5-15
5-12	"Wedge" Technique for Measuring Free-surface Velocity and Shock Velocity	5-16
5-13	Laser Interferometer System	5-17
5-14	The Stretched-diaphragm BRL Piezoelectric Gage for Measuring Face-on Air-blast Pressures	5-20
5-15	Electrical Conductivity as a Function of Time in the Detonation Reaction Zone of Various Explosives	5-24
6-1	One-dimensional Reaction Wave	6-2
6-2	Hugoniot Curve for Detonations and Deflagrations	6-4
6-3	Nomenclature on the Hugoniot Curve for Detonations and Deflagrations	6-5
6-4	Hugoniot Curve (H), Rayleigh line (R), and Isentropes (dashed curves) for (A) Strong Detonations and Weak Deflagrations, (B) Chapman-Jouguet Detonation and Deflagration, and (C) Weak Detonations and Strong Deflagrations	6-6
6-5	Wave Path (W) and Particle Path (P) for (A) a Detonation and (B) a Deflagration With $u_o = 0$	6-7
6-6	Physically Realizable Detonation and Deflagration States	6-8
6-7	Flow in a Strong Detonation	6-16
6-8	Flow in Chapman-Jouguet Detonation	6-17
6-9	Particle Velocity Behind Detonation Waves: Strong Detonations, (A) and (B); Chapman-Jouguet Detonations (B), (C), and (D)	6-17
6-10	Flow in Weak Deflagration With Closed End	6-18
6-11	A Detonation as a Deflagration With a Precompression Shock	6-20
6-12	Attenuation of a Strong Detonation Wave by a Rarefaction Wave	6-21
7-1	Covolume Function for Detonation Products of Condensed Explosives	7-11
7-2	Covolume Function for Detonation Products of PETN	7-12
8-1	Family of Hugoniot Curves for Steady Deflagration Wave	8-4

LIST OF ILLUSTRATIONS (Cont'd)

Fig. No.	*Title*	*Page*
8-2	Family of Hugoniot Curves for Steady Detonation Wave	8-6
8-3	The von Neumann Pathological Weak Detonation	8-7
8-4	Pressure and Particle Velocity Behind an Unsupported Chapman-Jouguet Detonation	8-10
8-5	Constant Composition and Equilibrium Hugoniot Curves	8-13
9-1	Effect of Charge Diameter on the Detonation Velocity of RDX, $\rho_o = 0.9$	9-2
9-2	Cylindrical Symmetric Flow Through a Detonation Wave	9-5
9-3	Models of the Reaction Zone Employed by Wood and Kirkwood	9-8
9-4	Models of the Reaction Zone Employed by (A) Jones, (B) Eyring and Coworkers, and (C) Cook	9-11
9-5	Typical Histogram Representation of the Pressure Pulse for Use in "Release Wave" Calculations Together With the Simplified Square Pulse Approximation	9-13
9-6	Illustration of Progress of Characteristic Surfaces in a Three-dimensional Explosive Charge, as Described in the "Release Wave" Theory	9-14
9-7	Particle Velocity Behind a Spherical Detonation Wave in Pentolite, $\rho_o = 1.65$	9-16
9-8	Pressure Behind a Spherical Wave in Pentolite, $\rho_o = 1.65$	9-17
10-1	An Experiment To Illustrate the Critical Nature of a Thermal Explosion	10-4
10-2	Heat Production and Heat Loss Rates in an Experiment of the Type Depicted in Fig. 10-1	10-5
10-3	Heating Curves (Temperature vs Time) in an Experiment of the Type Depicted in Fig. 10-1 and Consistent With the Data in Fig. 10-2	10-6
10-4	Temperature Profiles for Times Near the End of the Induction Period, as Calculated for 1-in. Spheres of RDX Initially at 25°C	10-13
10-5	Explosion Times vs $1/T_s$ for RDX in Various Geometries Initially at 25°C	10-14
10-6	Graphs of $\lambda t_e/\rho c a^2$ vs $E/T_{cr} - E/T_s$ for Spheres, Cylinders, and Slabs, All Initially at 25°C	10-15
10-7	Temperature Distribution During Cooling of a Spherical Element of Inert Material That Has Been Raised Initially to a Uniform Temperature Greater Than That of the Surroundings	10-17

LIST OF ILLUSTRATIONS (Cont'd)

Fig. No.	Title	Page
11-1	Transmission of Detonation from a Donor to an Acceptor Charge	11-2
11-2	The Gap Test	11-2
11-3	Charge Assembly and Dimensions for NOL Gap Test	11-3
11-4	Shock Wave Pressure at the End of the Lucite Gap in the NOL Gap Test	11-4
11-5	Comparison of Shock Loading at 50 Percent Point With Initial Pressure in Charge	11-5
11-6(A)	Arrangement to Measure Shock and Detonation Travel in a Nonhomogeneous Solid Explosive Using the Wedge Technique	11-7
11-6(B)	Arrangement to Measure Shock and Detonation Travel in a Homogeneous Liquid Explosive (Nitromethane)	11-7
11-7	Distance vs Time Behavior in Shock Wave Initiation of Nonhomogeneous and Homogeneous Explosives	11-8
11-8	Smear Camera Record of Effect of Rough Shock Wave on Induction Time	11-9
11-9	Shock Initiation Induction Times in Nitromethane at Different Shock Pressures and at Different Initial Temperatures	11-11
11-10	Smear Camera Record Showing Effect of Bubbles in Initiation of Nitromethane	11-12
11-11	Pressure-distance Profiles at Various Times for the Shock Initiation of Nitromethane by a 92-kbar Shock	11-14
11-12	Pressure-radius Profiles at Various Times for the Development of a Detonation in Shocked Nitromethane (94.7 kbar, 1230°K) from a Spheri l Temperature Hot Spot (1404°K) of 0.292 - cm Radius	11-14
11-13	Pressure-radius Profiles at Various Times for the Development of a Detonation in Shocked Nitromethane (94.7 kbar, 1230°K) from a Spherical Temperature Hot Spot (1404°K) of 0.06 - cm Radius	11-15
11-14	Pressure-radius Profiles at Various Times for the Failure of r 0.0292-cm-radius Temperature Hot Spot (1404°K) to Initiate Propagating Detonation in Shocked Nitromethane (94.7 kbar, 1230°K)	11-16
11-15	Successive Configurations of Shock and Bubble	11-18
11-16	Isotherm Plots for the Shock in Helium Hitting a Neon Bubble	11-19
11-17	Normalized Initiation Criteria	11-21
11-18	Effect of Pulse Width on Minimum Initiating Shock Pressure	11-22

LIST OF ILLUSTRATIONS (Cont'd)

Fig. No.	Title	Page
11-19	Build-up of Shock Wave in Solid Explosive to Detonation for a Surface Erosion (Grain Burning) Law of Heat Release	11-25
11-20	Peak Pressure and Position of the Wave as a Function of Time for the Case in Fig. 11-19	11-25
11-21	Propagation Failure in Blasting Gelatin	11-27
12-1	Impace Apparatus Showing Anvil-striking Pin Assembly	12-2
12-2	Illustration of Apparatus for Determining the Friction Sensitivity of Solid Explosives	12-3
12-3	Example of a Sensitivity Test Result Comprising 100 Trials Following the Up-and-down Method	12-5
12-4	Curves for Calculating s from M When $M < 0.40$ in the Statistical Reduction of Impact Sensitivity Data	12-7
12-5	Cavity Striker, Showing Small Air Bubble Inside Cavity	12-9
12-6	Explosive Decomposition Data from the Adiabatic Furnace	12-11
12-7	Correlation Plot of 50 Percent Explosion Drop Height in the Sensitivity Test vs Critical Explosion Temperature for Hot Spot of Radius 10 μ	12-14
12-8	Charge Arrangement Used by Macek to Study Deflagration to Detonation Transition	12-16
12-9	Characteristics Diagram (C_+) for the Development of a Compression Wave from Deflagration in a Rigidly Confined High Explosive	12-18
12-10	Development of Compression Wave from Deflagration as Transposed from the Characteristics Diagram in Fig. 12-9	12-19
13-1	Development of Shock Wave About Cylindrical Explosive Charge Initiated at One End	13-2
13-2	Schematic Illustration of the Energy Retention Resulting from the Entropy Increase at the Shock Front	13-6
13-3	Pressure-distance Curves for Blast Waves in Air at Successive Times	13-8
13-4	Particle Velocity-distance Curves for Blast Waves in Air at Successive Times	13-9
13-5	Pressure-time Curves for Blast Waves in Air	13-9
13-6	Hugoniot Properties of the Shock Wave for Ideal Polytropic Air	13-11
13-7	Peak Pressure-distance Curves for Shock Waves in Air Calculated With the Point Source Model (Brode)	13-14
13-8	Pressure in Atmospheres as a Function of the Lagrange or Mass Position for the Point Source Solution at Times Indicated	13-15

LIST OF ILLUSTRATIONS (Cont'd)

Fig. No.	*Title*	*Page*
13-9	Space-time Diagram for Shocks and Contact Surface for TNT Blast in Air (Brode)	13-16
13-10	Pressure-distance Curves at Successive Times for TNT Blast Waves in Air (Brode)	13-17
13-11	Peak Pressure-distance Curve for TNT Blast Waves in Air (Brode)	13-18
13-12	Pressure-distance Curves for the Underwater Shock Wave Produced by a 300-lb TNT Charge	13-20
13-13	Pressure-time Curve for the Underwater Shock Wave Produced by a 300-lb TNT Charge	13-21
13-14	Bubble Oscillations from an Underwater Explosion	13-22
13-15	Pressure-time Curve for Underwater Pressure Waves 50 ft from a 300-lb TNT Charge	13-22
13-16	Hugoniot Properties for Shock Waves in Sea Water	13-24
13-17	Peak Pressure-distance Curve for the Underwater Explosion of TNT as Calculated by Penney and Dasgupta	13-27
13-18	Pressure-time Curves of Shock Wave in Water, Showing Dissipation at Front as Described by Kirkwood and Bethe	13-27
13-19	Peak Pressure-distance Curve for the Underwater Explosion of TNT as Calculated by Kirkwood and Brinkley	13-33
13-20	Peak Excess Pressure Ratio vs Distance in Charge Radii for TNT at a Loading Density of 1.5 g/cm^3	13-34
13-21	Peak Excess Pressure Ratio vs Distance in Charge Radii for Pentolite at a Loading Density of 1.65 g/cm^3 (Shear and Wright)	13-35
13-22	Positive Impulse-distance Curve for Pentolite	14-3
14-1	Typical Characteristic Grids in the Distance-time Plane	14-3
14-2	Characteristic Grid for Hartree Computation Scheme	14-4
14-3	Paths Traversed by Thermodynamic and Mechanical Stress Through a Shock Front; Definition of Artificial Viscous Stress	14-6
14-4(A)	Stress Histories Generated in Tungsten by an Impact With C-7 Epoxy: Quadratic Artificial Viscosity Only With a Coefficient of 4.0	14-7
14-4(B)	Stress Histories Generated in Tungsten by an Impact With C-7 Epoxy: Linear Artificial Viscosity Only With a Coefficient of 0.5	14-8
14-5	Grid for Depicting Coordinates and Time Increments	14-9

LIST OF ILLUSTRATIONS (Cont'd)

Fig. No.	*Title*	*Page*
14-6	Stress Profiles Following Impact in a Material Represented by Simple Anelastic Model	14-10
14-7	Hugoniots and Paths for Steady-state Shock and Reaction in a Homogeneous Explosive	14-12

LIST OF TABLES

Table No.	Title	Page
1-1	Typical Explosive Substances	1-6
1-2	Compositions of Some Explosive Mixtures	1-8
3-1	Some Basic Thermochemical Data	3-9
3-2	Calorimetric Determination of the Heat and Products of Detonation	3-10
3-3	Ideal Gas Free Energy Function $(G^\circ/(RT))$ for Detonation Products	3-11
3-4	Water Gas Equilibrium for Ideal Gas Products at 1 atm and 1600°K	3-12
3-5	Calculated and Observed C-J Parameters	3-13
3-6	Correlation Between Q and Oxygen Balance	3-14
3-7	Comparison of Q_{CJ} and Q_A Based on an Arbitrary Decomposition Mechanism	3-15
3-8	Comparison of Q and Gurney Constants for Plane-wave Shots	3-16
3-9	Correlation of Q and Equivalent Weights for Free Air Blast	3-17
3-10	Underwater Performance of Explosives	3-18
3-11	Correlation of Detonation Energy and Maximum Work (Ballistic Mortar)	3-19
4-1	Activation Energies and Pre-exponential Factors for Some Explosive Liquids and Solids	4-4
4-2	Thermal and Photochemical Decomposition of Some Ionic Azides	4-15
5-1	Chapman-Jouguet Pressures in Various Explosives	5-9
5-2	Experimental Detonation Temperatures	5-22
7-1	Estimates of the Detonation Properties of Composition B	7-5
7-2	The Derivatives β, κ, and λ Along the Chapman-Jouguet Locus for Composition B	7-8
7-3	Detonation Properties of Some Pure Explosives	7-10
7-4	Detonation Properties of PETN	7-13
7-5	The Adiabatic Exponent for Composition B Along the Chapman-Jouguet Locus	7-13
7-6	High Temperature Second Virial Coefficients of Gaseous Detonation Products	7-17
7-7	Detonation Properties of Some Condensed Explosives	7-18
7-8	Values of the Constants k_i	7-19
7-9	Comparison of Calculated Detonation Properties	7-20
10-1	Specific Rate Constants for First-order Isothermal Decomposition of Explosives	10-2

LIST OF TABLES (Cont'd)

Table No.	Title	Page
10-2	Typical Behavior of a Solid High Explosive Compound Following an Arrhenius Reaction Law	10-3
10-3	Critical Values for Thermal Explosion Parameters δ and θ	10-9
10-4	Approximate Solutions for Explosion Induction Times for a Semi-infinite Planar Explosive	10-12
10-5	Various Calculated Quantities for Hot Spots in RDX	10-18
10-6	Critical Diameter and Adiabatic Explosion Time for RDX	10-19
11-1	Shock Sensitivity of Solid Rocket Propellants in the NOL Gap Test	11-6
11-2	Calculated Shock Initiation Induction Times in Homogeneous Explosives	11-13
11-3	Effect of Donor Charge Diameter on Shock Sensitivity	11-23
11-4	Experimental Card-gap Test Results	11-28
11-5	Results of Low-velocity Detonation Stability Studies With NG-EGDN	11-29
11-6	LVD Gap Test for 1,2-DP: Effect of Confinement Geometry and Sonic Velocity	11-30
11-7	Correlation of Sensitivity Tests With Reaction Rates	11-30
12-1	Initiation of Explosion of PETN in the Presence of Grit	12-9
12-2	Kinetic Properties of Explosive Materials from Adiabatic Self-heating Experiments	12-12
12-3	Hot-spot Explosion Temperatures Calculated on Basis of Data in Table 12-2	12-13

PREFACE

The Engineering Design Handbooks of the U S Army Materiel Command are a coordinated series of handbooks containing basic information and fundamental data useful in the design and development of Army materiel and systems.

In the last several decades—certainly since World War II—a great deal of work, both experimental and theoretical, has been performed on explosives and their effects. There did not exist in any language a satisfactory, comprehensive compilation presenting a unified, self-consistent, theoretically competent treatment of this material. Also, a large number of interesting contributions from Government-supported and Government laboratories, which have now been declassified and should provide valuable information, was comparatively inaccessible to the average scientist and engineer.

This Handbook attempts to correct the situation. Presented is a unified treatment of the important open literature in which is included not only articles in professional journals but also the available military reports of importance. Original contributions also have been made to the theoretical portions. Much current research on explosion phenomena involves numerical solutions to complex mathematical equations of fluid dynamics, chemical kinetics, thermodynamics, and heat transport. For this reason a description of some of the novel computational techniques (computer codes) that have been developed for these purposes is included. While the Handbook is not a comprehensive treatise on explosives, it does discuss at length topic areas that are considered to be of greatest value in an exposition of the principles of explosive behavior of liquid and solid explosives, and thus provides a readily accessible collection of important theoretical and experimental results on explosives and explosive effects.

The Handbook does not cover the synthesis of explosive substances, compilation of properties of explosives, or the manufacture of explosives—these topics are the subjects of existing handbooks.

The Engineering Design Handbooks fall into two basic categories, those approved for release and sale, and those classified for security reasons. The Army Materiel Command policy is to release these Engineering Design Handbooks to other DOD activities and their contractors and other Government agencies in accordance with current Army Regulation 70-31, dated 9 September 1966. It will be noted that the majority of these Handbooks can be obtained from the National Technical Information Service (NTIS). Procedures for acquiring these Handbooks follow:

PREFACE (Cont'd)

a. Activities within AMC, DOD agencies, and Government agencies other than DOD having need for the Handbooks should direct their request on an official form to:

Commanding Officer
Letterkenny Army Depot
ATTN: AMXLE-ATD
Chambersburg, Pennsylvania 17201

b. Contractors and universities must forward their requests to:

National Technical Information Service
Department of Commerce
Springfield, Virginia 22151

(Requests for classified documents must be sent, with appropriate "Need to Know" justification, to Letterkenny Army Depot.)

Comments and suggestions on this Handbook are welcome and should be addressed to:

U S Army Materiel Command
ATTN: AMCRD-TV
Washington, D C 20315

(DA Forms 2028 (Recommended Changes to Publications), which are available through normal publications supply channels, may be used for comments/suggestions.)

CHAPTER 1 INTRODUCTION

1-1 INTRODUCTORY REMARKS

Explosives have been known and used for a very long time. Black powder—a mixture of potassium or sodium nitrate, sulfur, and carbon black—has been employed as an explosive since ancient times. Nitroglycerin, discovered in 1846 by Sombrero, and the invention of nitroglycerin-based dynamite by Nobel in 1867 can be considered as the start of the era of high explosive technology. This era which extends to current times has been the development of a vast number of military and commercial explosives and explosive applications.

The development of a fundamental theory of detonation also had its beginnings in the latter part of the 19th century, starting with the investigations by Mallard and Le Chatelier (1881) and of Berthelot and Vieille (1882) on gaseous explosions. They found that the explosion process consisted of a progressing wave of chemical reaction and distinguished two types of reaction waves. The first type is a relatively slow moving flame having linear velocities on the order of 1 to 10 cm/sec, and the second, a very much faster wave (i.e., a detonation wave) moving on the order of the speed of sound (10^4 to 10^5 cm/sec). In 1893 Shuster suggested that there is an analogy between a detonation wave, which is supported by energy release from chemical reaction, and a nonreactive shock wave, which has to be supported by a piston or similar mechanical source of energy. Shock waves had been theoretically described in detail by Riemann (1860), Lord Rayleigh, and others, and a physical model consisting of a moving discontinuity in pressure had been shown satisfactorily to account for the observed properties of shock waves. The laws of mass, momentum, and energy conservation across a discontinuous shock front had already been deduced by Rankine in 1870 and by Hugoniot in 1889. The suggestion of Shuster that a detonation wave is a reactive shock formed the basis for the development by Chapman (1899) and by Jouguet (1905) of the classical hydrodynamic-thermodynamic theory of steady-state detonation. This theory employs an idealized one-dimensional model in which it is assumed that the explosion energy is instantaneously released in a discontinuous shock front across which the conservation conditions of Rankine-Hugoniot apply. The velocity of the detonation wave was assumed to be the minimum velocity compatible with the hydrodynamic conservation equations. The Chapman-Jouguet (C-J) theory thus defined a unique steady-state detonation velocity which could be compared with experimentally observed velocities, and detailed calculations for gaseous detonations were shown to be in excellent agreement with experiment.

In the period 1940-1943, Zeldovich (USSR), von Neumann (USA), and Döering (Germany), each working independently, refined the C-J theory and extended it to the case where chemical reaction occurs in a finite zone behind the front of the detonation wave. This work was stimulated by the events of World War II, which also gave great impetus to the development of many of the modern high-speed electronic and photographic techniques for studying details of explosion phenomena.

At the present time there exists a substantial corpus of theory and experimental data that can be said to provide a good description of many aspects of explosion processes. The theory is, however, incomplete in many respects in that it deals, in the main, with idealized configurations not met with in practice and does not treat at all some of the events upon which the performance of an explosive depends. If we use the existing theory as a point of departure, there are many areas which can be fruitfully explored in the theoretical and experimental investigations.

In this handbook an attempt has been made to describe the principles of explosive behavior as they apply to condensed explosives. It has been the principal aim to present a comprehensive treatment of those topics that are necessary for an appreciation of the literature reporting the results of current research. The authors have developed most of the important relations of thermodynamics and hydrodynamics upon which the theoretical treatment of explosion

phenomena is based. The classical theory is developed rigorously and in detail, since this theory is the basis both for an understanding of actual explosion phenomena and for the theoretical investigations that are currently in progress. The treatment of topics for which theory is incomplete is necessarily more qualitative and relies heavily on discussions of experimental data and simple physical models. The techniques employed in obtaining the experimental data are therefore discussed in some detail. Much current research on explosion phenomena involves numerical solutions to complex mathematical equations of fluid dynamics, chemical kinetics, thermodynamics, hydrodynamics, and heat transport. For this reason some of the novel computational techniques (computer codes) which have been developed for these purposes have been described.

It has not been the aim of the authors to provide a comprehensive treatise on explosives, but rather to discuss at length topic areas which are thought to be of greatest value in an exposition of the principles of behavior of liquid and solid explosives.

1-2 DESCRIPTION OF EXPLOSIVE PROCESSES

Explosives are substances or mixtures of substances which are capable of undergoing exothermic chemical reaction at extremely fast rates to produce gaseous and/or solid reaction products at high pressure and temperature. In the case of a typical "CHNO" explosive such as TNT, the molecule—which contains carbon, hydrogen, nitrogen, and oxygen (see Table 1-1) undergoes a decomposition reaction followed by reduction-oxidation reactions which eventually lead to low molecular weight detonation products such as CO_2, CO, H_2O, N_2, and solid carbon (cf. Chapter 3). The chemical reactions occur in microseconds with an energy release of $\approx 10^3$ cal/g. For cast TNT this can result in a detonation wave with pressure, temperature, and velocity of $\approx$ 200,000 atm, $\approx$ 3000°K and $\approx$ 7000 m/sec, respectively. The large energy release and fast velocity of the detonation wave represent a tremendous power level of energy conversion, $\approx 5 \times 10^9$ W per sq cm of detonation front. This value can be compared with the total United States electric generating capacity of $\approx 3 \times 10^{11}$ W. It is the high power level and high reaction pressure generated which give rise to the primary application of explosives, namely, as compact sources of energy for blasting. Other applications (e.g., welding) relate to the strong shock wave that is associated with the detonation front.

Since the performance of an explosive depends strongly on its energy release in detonation, considerable theoretical and experimental effort has been carried out to predict and to measure the energy of detonation. The thermodynamic theory developed in Chapter 2 and the discussions in Chapter 3 relate directly to this subject.

Observation of a detonation wave progressing along a long cylindrical charge of explosive will show that the wave moves at constant velocity. In the more energetic military explosives this velocity may be as high as 8000 m/sec. The detonation velocity is relatively easy to measure and for many years was virtually the only experimental data available. However, with the advent of high speed electronic recording equipment, streak camera photography, flash X-ray, and manganin pressure gages, having time resolutions of $\approx 10^{-8}$ sec, it has been possible to measure detonation pressures as high as 460,000 atm, and particle velocities at the detonation front (cf. Chapter 5). Unfortunately, experimental techniques for reliable measurement of detonation temperature have not as yet been developed.

The constancy of the speed of detonation can be readily explained in terms of Chapman-Jouguet (C-J) theory and the Zeldovich-von Neumann-Döering (ZND) model, which are developed in detail in Chapters 6-8. In this approach, the detonation wave may be considered as a strong shock wave supported by energy release in a small zone of chemical reaction just behind the front of the shock, i.e., the detonation front. The almost instantaneous compression and heating of the explosive as it passes through the detonation front triggers the supporting chemical reactions.

The stable detonation velocity as described by classical C-J theory represents an upper limit or ideal detonation velocity, and strictly refers to a planar detonation wave. Such waves are indeed found to be approached in cylindrical charges of

large diameter. In practice, however, it is found that in small diameter cylindrical charges the detonation front is curved, and its velocity depends upon the degree of charge confinement and charge diameter. Also it is observed that for each explosive there is a critical value of charge diameter d_c below which a steady-state detonation will not propagate. For example, d_c is about 1 cm for cast TNT, about 10 cm for ammonium nitrate, and about 160 cm for some types of rubber-base composite propellant. The explanation of these "nonideal" detonation phenomena relates to the effects of charge expansion and lateral energy losses on the rate of chemical reaction in the detonation reaction zone. "Nonideal" detonation behavior is discussed in detail in Chapters 9 and 11.

If we take a solid explosive such as cast TNT and set a match to it, it will probably burn (deflagrate) with a linear velocity of ≈ 1 cm/sec. However, if we strongly shock the explosive it will detonate at $\approx 7 \times 10^5$ cm/sec. It can also be observed that if a burning explosive is confined or if the explosive is porous, a deflagration to detonation transition will occur some place in the material. This brings up very practical questions such as what are the conditions which cause the initiation of detonation in an explosive, and why do different explosives, or even the same explosive at different bulk densities, react differently to initiating stimuli—e.g., shock, impact, friction, spark, heat, etc.? The need to design reliable detonation initiation devices and to prevent accidental initiations lent early impetus to studies devoted to characterizing the ease of initiation or sensitivity of explosive materials.

There is now substantial evidence that all detonation initiation processes are essentially thermal in origin. By this is meant that initiating external stimuli such as shock, impact, and spark cause heating of the explosive and the creation of thermal explosion—sometimes in small localized regions of the explosive charge, i.e., hot spots. The thermal explosion, if it is of sufficient intensity, will propagate a deflagration and/or shock wave which eventually leads to the formation of a detonation wave. The factors which determine whether or not the stimulus is sufficient to cause thermal explosion and whether or not the thermal explosion is of sufficient intensity to grow to detonation are very complex, involving chemical kinetics, thermodynamics, mass and heat transport, and hydrodynamic flow. A detailed discussion of thermal explosion and its application to detonation initiation are given in Chapters 10-12.

As indicated earlier, one of the main applications of condensed explosives is as an energy source for blasting. The transmission of detonation energy to the medium surrounding an explosive relates not only to the properties of the medium but also to the properties of the explosive; e.g., detonation velocity, energy, pressure, product composition, etc. The theory of blast propagation in air and water from an spherical explosive charge is described in detail in Chapter 13. The theory is of significance in a book on explosive behavior since it sets the foundation and limitations of the concept of "TNT Equivalent" which is often used in evaluating explosive performance, as well as forming the basis of some of the experimental determinations of the energy of detonation (cf. Chapter 3).

Finally in Chapter 14 we discuss some of the equilibrium thermodynamic and time dependent hydrodynamic computer codes which are currently being used in calculating explosive properties and explosives' behavior.

1-3 TYPES OF EXPLOSIVE

It has become traditional to distinguish between various types of explosives. Most military explosives consist of pure compounds or of relatively simple mixtures of explosive compounds. In such compounds the oxygen is normally bound in nitro- or nitrate-groups, and the explosion reaction consists of the decomposition of the molecule of the explosive substance. Many commercial explosives consist of mixtures of various kinds. The mixture may consist of a substance which itself is an explosive to which are added various materials which may serve as added fuel, added oxidizer, or inerts. When inerts are present, their function is usually to serve as a thermal ballast and thus to moderate the energy available for useful work or the temperature of the gaseous products. If one or more of the ingredients of such mixtures is an explosive substance, it is useful to call the mixture a hybrid explosive. Commercial dynamites provide an example of explosives of

this type. A very large number of formulations exist, each of them tailored to meet a particular commercial need and to comply with safety requirements imposed by the particular use. Another type of explosive mixture may consist of two or more substances none of which of themselves are explosives. These may be called composite explosives. Typically they consist of mixtures of a substance serving as fuel and a substance serving as oxidizer. Mixtures of the oxidizer ammonium nitrate, which can only be exploded with great difficulty, and fuel oil are examples of this type which have recently become very prominent as cheap blasting agents.

Most explosive charges contain a main charge which is designed to accomplish the particular task for which the explosive is intended. The common explosives with a sufficiently high energy and pressure of explosion are normally somewhat difficult to initiate. These materials are called secondary explosives. Typical of this class are the military explosives TNT, RDX, and the commercial dynamites. To provide reliable initiation, the charge will contain an initiator employing a substance easily initiated by a thermal source or by mechanical shock but whose energy and pressure of explosion are too low for use as a main charge. These materials are called primary explosives. Lead azide and mercury fulminate are well-known examples. A typical explosive device (see Fig. 1-1) consists of a train composed of an initiating charge of primary explosive, a main charge of secondary explosive, and a booster charge which is initiated by the primary explosive and which accomplishes the initiation of the main charge. The booster, therefore, serves as an intermediate step in the detonation of the main charge. The more sensitive secondary explosives are employed as boosters. Tetryl and PETN are frequently used for this purpose. Blasting caps are themselves explosive trains, containing a small amount of primary explosive and a booster charge which today is often PETN.

Some typical explosive compounds are listed in Table 1-1. Table 1-2 gives the compositions of some explosive mixtures.

1-4 SOME DEFINITIONS

We wish here to define the meaning of several terms that are employed in the discussion of the properties and behavior of explosive substances. Some of these terms are in everyday use with meanings that are in varying degrees of imprecision. Some are not even capable of precise definition but are in such common use as to have a more or less established meaning through usage. The word "explosion" is in this category as is, for example, the word "fire". Some terms are susceptible to exact definition but are frequently misused; such as the word "detonation", which should only be used in the case of reaction by a detonation wave.

An *explosive* can be loosely defined as a substance capable of undergoing an explosion. More precisely we shall employ the word as we have in par. 1-2 to designate a substance or mixture of substances capable of undergoing exothermic chemical reaction with the evolution of gaseous products at an extremely high rate. Explosives may be in the gaseous, liquid, or solid state of aggregation. In this handbook we shall be mainly concerned with condensed explosives that are either liquid or solid.

An *explosion* is literally the sudden outward projection of a quantity of matter. The term is, for example, applied to the event following the rupture of a steam boiler in which steam and possibly boiler case fragments undergo a rapid excursion. The term is also applied, for example, to the event that follows the sudden admixture of liquid water to molten materials at a temperature substantially in excess of the boiling point of water. As a final example, the term applies to the event resulting from the overpressurization of any container. All of these meanings are endorsed by everyday use. However, in this handbook we shall employ the word in a more restricted sense to refer to the overall process by means of which an explosive is suddenly converted to gaseous products which, as will be shown, are at high temperature and pressure. We shall frequently refer to the chemical products of this process as explosion products.

It may be noted that explosives may undergo slow reactions to gaseous products (cf. Chapter 3). If the rate of these reactions is so slow that high temperature and high pressure are not obtained, the process is not an explosion.

The term *thermal explosion* is used in a special sense that is fully discussed in Chapter 10. It is the result of runaway exothermic chemical reaction which occurs when the rate of

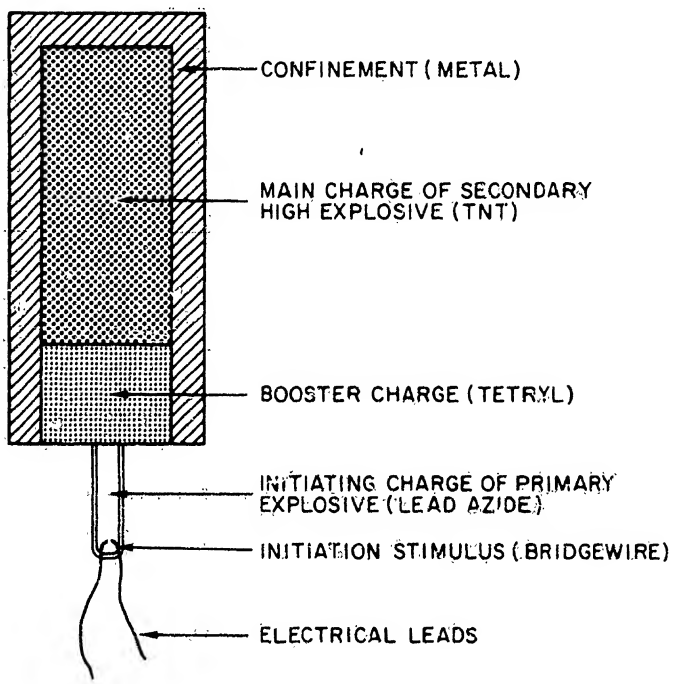

Figure 1-1. Model of Explosive Charge

evolution of heat within a reacting volume is greater than the rate at which that volume can lose heat by conduction to a heat sink which surrounds the volume. This is a precisely defined process that can be fully described by the laws of chemical reaction rates and heat conduction. For the present we wish only to note that it is a process that occurs in a static system, does not involve the flow of either reactants or products, and in consequence does not depend upon the laws of hydrodynamics.

If a substance is capable of undergoing an exothermic reaction, which we are calling an explosive, and if such a reaction is initiated in some local region of a larger mass of material, then a reaction wave may propagate from the point of initiation throughout the mass. Under these circumstances the chemical reaction takes place within the wave. Even if the mass is initially static, the propagating wave induces flow in the material and thus is governed by hydrodynamical as well as chemical considerations. If the propagation velocity is constant, the wave may be said to be *steady-state* (even though the associated flow may not be stationary everywhere in any frame of reference). In general, two flow regimes are observed. If the propagation velocity (i.e., the rate at which the wave advances into unreacted material) is less than the velocity of sound in the unreacted material, the reaction wave is said to be a *deflagration*. If a deflagration wave is held stationary by a flameholder such as a burner rim and the unreacted material flows through it, the

TABLE 1-1 TYPICAL EXPLOSIVE SUBSTANCES

(Code)	Name	Elemental Formula	Structural Formula	Principal Use
(AN)	Ammonium nitrate	$H_4N_2O_3$	$NH_4^+ NO_3^-$	solid oxidizer
(AP)	Ammonium perchlorate	H_4NO_4Cl	$NH_4^+ ClO_4^-$	solid oxidizer
(ETNEU)	Bis (N,N'-trinitroethyl) urea	$C_5H_8N_8O_{13}$	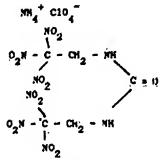	secondary high explosive
(D)	Ammonium picrate	$C_6H_6N_4O_7$	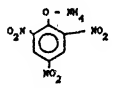	secondary high explosive
(DATNB)	Diaminotrinitrobenzene	$C_6H_5N_5O_6$	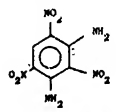	secondary high explosive
(DINA)	Diethylnitramine dinitrate	$C_4H_8N_4O_8$	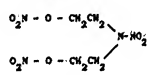	secondary high explosive
(EDNA)	Ethylenedinitramine "Haleite"	$C_2H_6N_4O_4$	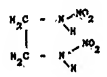	secondary high explosive
(EGDN)	Ethylene glycol dinitrate	$C_2H_4N_2O_6$	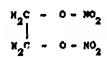	liquid explosive
(FEFO)	Bis-(2,2-dinitro-2-fluoroethyl) formal	$C_5H_6N_4O_{10}F_2$	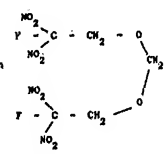	secondary high explosive
(RDX)	Cyclotetramethylene tetranitramine	$C_4H_8N_8O_8$	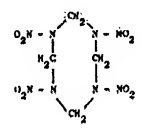	secondary high explosive
	Lead Azide	PbN_6		primary explosive

TABLE 1-1 TYPICAL EXPLOSIVE SUBSTANCES (Continued)

(Code)	Name	Elemental Formula	Structural Formula	Principal Use
	Lead styphnate	$PbC_6H_3N_3O_9$	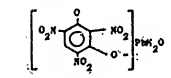	primary explosive
	Mercury fulminate	$HgC_2N_2O_2$	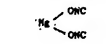	primary explosive
(NG)	Nitroglycerin	$C_3H_5N_3O_9$	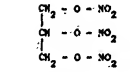	liquid secondary explosive ingredient in commercial explosives
(NM)	Nitromethane	CH_3NO_2	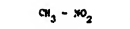	liquid secondary explosive
(PETN)	Pentaerythritol tetranitrate	$C_5H_8N_4O_{12}$	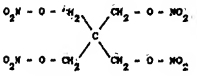	secondary high explosive used as booster
	Picric acid	$C_6H_3N_3O_7$	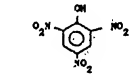	secondary high explosive
(RDX)	Cyclotrimethylene trinitramine	$C_3H_6N_6O_6$	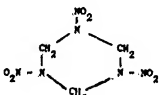	secondary high explosive used as booster
(Tetryl)	Trinitrophenyl methylnitramine	$C_7H_5O_8N_5$	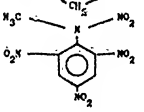	secondary explosive booster
(TNETB)	2,2,2-trinitroethyl-4,4,4-trinitrobutyrate	$C_6H_6N_6O_{14}$	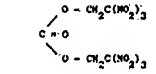	secondary high explosive
(TNM)	Tetranitromethane	CN_4O_8	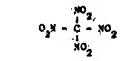	liquid explosive
(TNT)	Trinitrotoluene	$C_7H_5N_3O_6$	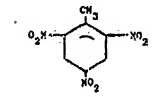	secondary high explosive

TABLE 1-2 COMPOSITIONS OF SOME EXPLOSIVE MIXTURES

Name	*Composition*
Amatol	Mixture of TNT and AN (80% AN, 20% TNT is typical)
Ammonium Nitrate Dynamite	10% NG, 80% AN, 10% carbonaceous material is typical
Baratol	67% Barium nitrate, 33% TNT
Blasting Gelatin	92% NG, 8% nitrocellulose
Composition B	60% RDX, 40% TNT (with 1% wax)
Cyclotol	Mixture of RDX and TNT (50% RDX, 50% TNT is typical)
Dynamite	Mixture of NG, sodium or potassium nitrate, and wood pulp (40% NG is typical)
PBX 9404	Plastic bonded HMX (94% HMX)
Pentolite	Mixture of TNT and PETN (50% TNT, 50% PETN is typical)

deflagration wave is the familiar flame. The propagation rate of a deflagration wave is called either the deflagration velocity or more customarily, in combustion literature, the *burning velocity*. If the propagation velocity of the reaction wave is supersonic with respect to the unreacted material, the wave is called a *detonation wave* and its velocity of propagation is called the *detonation velocity*.

It is worth noting that a process involving a detonation wave can always be called an explosion. However, not all explosions involve a detonation wave since the explosion may result from a deflagration wave or a thermal explosion.

In citing various typical explosives we have noted that they are frequently broadly classified into primary and secondary explosives, and that some secondary explosives are employed as boosters. This is a working classification based upon the use to which the substance is normally put in an explosive system or train and which is based upon a property of the material called the *sensitivity*. Primary explosives are used because they can be initiated by thermal sources such as hot wires or flames. As a class they can also be initiated by relatively mild blows. Such explosives are said to have a *high sensitivity*. In contrast, secondary explosives, as a class, are difficult to initiate from thermal sources and require a relatively severe impact to initiate explosion. These explosives are considered to have a *low sensitivity*.

The concept of sensitivity is, at least historically, a qualitative one. Sensitivity has usually been measured by a variety of different empirical tests in which samples of explosive are subjected to controlled and measurable initiation stimuli. Typical of such tests is one in which the sensitivity is measured by the distance of travel of a falling weight, onto a small mass of explosive, that is required to produce an explosion. Thus, the *impact sensitivity* of an explosive is its response to an impact test in a specific drop-weight apparatus. Similarly, the *friction sensitivity* is the response to an empirical friction test. Test results depend on the test method and also upon a variety of physical and chemical properties of the explosive in a way that is not usually well defined. In consequence, different methods of evaluating sensitivity may not place explosives in the same order of sensitivity.

CHAPTER 2 THEORETICAL BACKGROUND

2-1 INTRODUCTION

The theoretical description of explosion phenomena has relied mainly on the science of thermodynamics to provide a description of the properties of the product of the decomposition of an explosive and on the science of hydrodynamics to formulate the laws governing the motion of these products. It is the intention of this chapter to present the results of these sciences that are required in the later development of the topics covered in this handbook, and to state the assumptions that are made in order to apply the methods of these sciences to the description of explosion phenomena. The topics discussed in this chapter may be pursued in greater detail in standard treaties on thermodynamics[1,2*] and hydrodynamics[3,4].

Although this chapter and others are replete with mathematical formulas and notation, the nonmathematician will find the text material amply rewarding for the time spent in reading it—it is not essential that one be a mathematician to understand the text.

2-2 DESCRIPTION OF THE COMPOSITION

In this paragraph is defined the notation used to describe the unreacted explosive and the explosion products. As an example of the reaction equations to be considered, let us consider decomposition of the explosive TNT, $C_7H_5O_6N_3$. The predominant products are expected to be C, CO, H_2, and N_2. A conventional decomposition equation for TNT is

$$C_7H_5O_6N_3 \rightarrow C + 6CO + \frac{5}{2}H_2 + \frac{3}{2}N_2 \quad (2\text{-}1a)$$

which provides an approximation to the composition of the explosion products. A more general decomposition equation is

$$C_7H_5O_6N_3 \rightarrow M\,(q_1C + q_2CO + q_3H_2 + q_4N_2 + q_5CO_2 + q_6H_2O + q_7H) \quad (2\text{-}1b)$$

* Superscript numbers refer to references at the end of a chapter.

where q indicates the quantity (moles/gram) of a product and M is the gram-molecular weight of the explosive. It is often assumed that the composition of the mixture remains "frozen" during the flow following decomposition, i.e., that each q is constant. In the more general case considered here, each q is allowed to vary within the constraints of chemical equilibrium. In preparation for this treatment, we introduce a notation which allows development of the thermodynamics and hydrodynamics in general terms without restriction to the chemical nature of the mixtures.

We consider a mixture of s different chemical species or constituents and employ the index i-(i = 1, 2, ... s) as a *constituent index*. Thus, for example, if the list of chemical species is C, CO, etc., the index i = 1 designates the species C, the index i = 2 designates the species CO, etc. The composition of the gas phase of a mixture of many constituents can be described by the *mole numbers* n_i (i = 1, 2, ... s), where n_i (moles/gram) is the number of moles of the *i-th* constituent in unit weight (e.g., one gram) of mixture. We shall assume that any condensed phase in the mixture is a pure phase, thus excluding consideration of solid or liquid solutions, and we denote by $n_i^{(\ell)}$ and $n_i^{(s)}$ the number of moles of liquid and solid species i in unit weight of the mixture. The composition of the mixture is thus described by the numbers n_i, $n_i^{(\ell)}$, and $n_i^{(s)}$ (i = 1, 2, ... s). The phase rule imposes a restriction on the number of the quantities $n_i^{(\ell)}$ and $n_i^{(s)}$ that may be nonzero. In mixtures of practical interest, most of these quantities will be zero. If they are all zero, the system is homogeneous, consisting of a gas phase only.

We designate by c the number of different chemical elements contained in the s different species comprising the mixture and employ an index, k(k = 1, 2, ... c), as an element index. Thus, for example, if the list of elements is C, H, etc., the index k = 1 designates the element C, the index k = 2 designates the element H, etc.

The gross composition of the system can be described by the quantities a_k' (k = 1, 2, ... c), where a_k' is the number of gram-atomic weights of the k-*th* element contained in unit weight of the mixture. If the gross composition of the

system of interest is described by some other set of parameters, the quantities q'_k can always be obtained by simple consideration of stoichiometry, and we assume that this has been done. For example, the TNT formula referred to in Eq. 2-1a is associated with the set of numbers which can be represented by the vector $q' = (7/M, 5/M, 6/M, 3/M)$.

In a system containing many constituents, it is possible to select a set of constituents which are sufficient for the complete description of the gross composition. Thus if the mixture consisted of the selected constituents only, the amounts of each element present in the hypothetical system would be the same as those in the system of interest. The constituents thus sufficient to describe the system are called the *components* of the system. One possible set of components for the reaction products of TNT is given in Eq. 2-1a. The number of components is usually, but not necessarily, equal to the number of elements. For the development here in which the explosion products as well as the explosive are expressed as a sum of the components, the number of components c is set equal to the number of elements. We employ an index, j ($j = 1, 2, \ldots c$), as a *component index*. Thus, for example, if the list of components is C, CO, etc., the index $j = 1$ designates the component C, the index $j = 2$ designates the component CO, etc.

The molecular formula of the *i-th* constituent or chemical species of the mixture of explosion products can be formally represented by

$$Y^{(i)} = X_{\alpha_{i1}}^{(1)} \cdots X_{\alpha_{ik}}^{(k)} \cdots X_{\alpha_{ic}}^{(c)} \qquad (2\text{-}2)$$

where $X^{(k)}$ is the symbol of the *k-th* element and α_{ik} is the subscript (which may be zero) to this symbol in the forumla of the *i-th* species. For every species i, the array α_{ik} ($k = 1, 2, \ldots c$) defines a vector

$$y_i = (\alpha_{i1}, \ldots \alpha_{ik}, \ldots \alpha_{ic}) \qquad (2\text{-}3)$$

that can be called the *formula vector* of the *i-th* substance. As shown by Brinkley[5] it is a necessary condition for the selection of a proper set of components that the formula vectors of the selected constituents be linearly independent, which implies that the determinant $|\alpha_{ik}|$ does not vanish.

We denote by q_j (moles/gram) the number of moles of the *j-th* component in unit weight of the hypothetical system consisting of components only. The quantities q_j ($j = 1, 2, \ldots c$) are called the *stoichiometric constants* of the system for a particular choice of components. For a proper set of components we require that the stoichiometric constants q_j be greater than zero for all j. The stoichiometric constants indicate the quantity of each component without regard to phase; hence, they are sums of the mole numbers:

$$q_j = n_j + n_j^{(g)} + n_j^{(s)} \qquad (2\text{-}4)$$

Since this hypothetical system is to have the same gross composition as the system of interest, then the quantity of each element must be the same in each system. Hence

$$\sum_{j=1}^{c} \alpha_{jk} q_j = q'_k \quad \text{for } k = 1, 2, \ldots c \qquad (2\text{-}5)$$

The q_j provide a specification of the gross composition of the system that is an alternative to that provided by the q'_k.

A choice of components is generally not unique. If it is arbitrarily assumed that the chemical elements in their standard states (e.g., C, O_2, N_2 ...) are members of the system (even though the concentrations of the elementary species may be so low as to be negligible), the elements constitute a proper choice of components. The elements as atoms (i.e., in dissociated forms) always constitute a proper set of components even though they may be present in negligible concentrations. Then $q = q'$. However, use a set of components other than the elements is advantageous if the hypothetical system of components is a good approximation to the system of interest. This will be the case if it is possible to select as components the predominant species of the mixture and if the concentrations of the species that are not selected are small enough to be neglected as a reasonable approximation.

If the hypothetical system of components is an adequate representation for the mixture resulting from the decomposition of an explosive, the equation for the decomposition reaction can be written from stoichiometric

considerations alone. An example of such a simple reaction is given as Eq. 2-1a. We can generalize the decomposition of an explosive by the equation

$$X_{x_1}^{(1)} \ldots X_{x_k}^{(k)} \ldots X_{x_c}^{(c)} \rightarrow M\sum_{j=1}^{c} q_j Y^{(j)} \qquad (2\text{-}6)$$

where $(x_1 \ldots x_k \ldots x_c)$ is the formula vector of the explosive of gram-molecular weight M, and $Y^{(j)}$ represent the formulas of the constituents of a hypothetical mixture of products satisfying the critera of a proper set of components. The q_j of Eq. 2-6 satisfy Eqs. 2-5 with $q_k' = x_k/M$. A decomposition equation of the form of Eq. 2-6 is called a *conventional decomposition equation.* Conventional decomposition equations have been widely employed to obtain approximate descriptions of the composition of the products of the decomposition of explosives. The validity of the approximation cannot be judged *a priori.* In general, it is necessary to compare the results with those of a better approximation such as that resulting from the assumption that the explosion products are in thermodynamic equilibrium.

The calculation of the composition at equilibrium of a system of many constituents is carried out by a method of successive approximations. The procedure requires the specification of an initial approximation. If the calculation is to be carried out on a computer, the initial approximation must be specified in a well-defined manner. The approximation provided by the hypothetical set of components is well-suited for this purpose. It leads to a more rapid convergence of the successive approximations to the equilibrium composition than is obtained with a physically less realistic initial approximation.

We now introduce the algebra required to express the constituents in terms of the components. Then the method of calculating equilibrium composition of the product mixture can be discussed. The formula vector of the *i-th* constituent can be expressed as a linear combination of the formula vectors of the components

$$\sum_{j=1}^{c} \beta_{ij} y_j = y_i \; (i = 1, 2, \ldots s) \qquad (2\text{-}7a)$$

where y_j = formula vector of the *j-th* component. If the dissociated elements are taken to be the components, $\beta_{ij} = \alpha_{ij}$. To each of Eqs. 2-7a there corresponds a chemical reaction that can be represented formally by

$$\sum_{j=1}^{c} \beta_{ij} Y^{(j)} = Y^{(i)} \qquad (2\text{-}7b)$$

resulting in the formation of each of the constituents of the mixture from the components.

For a given choice of components, the reactions in the form of Eqs. 2-7b can always be written by inspection, using the customary rules for balancing chemical equations. The formal discussion of this paragraph is intended only to display the meaning of the coefficients β_{ij}, since it is possible to formulate a computer program that will construct a table (matrix) of the coefficients β_{ij} from the coefficients α_{ik}.

The conservation of mass by the reactions of Eqs. 2-7b can be expressed by the relations

$$M_i = \sum_{j=1}^{c} \beta_{ij} M_j \qquad (2\text{-}8)$$

where M_i and M_j (grams/mole) are the gram-molecular weights of the *i-th* constituent and *j-th* component, respectively. The conservation of mass in the system as a whole requires that

$$\sum_{i=1}^{s} (n_i + n_i^{(k)} + n_i^{(g)}) M_i = \sum_{j=1}^{c} q_j M_j \qquad (2\text{-}9)$$

On substituting Eqs. 2-7b into Eq. 2-9 and equating the coefficients of M_j, there are obtained

$$\sum_{i=1}^{s} \beta_{ij} (n_i + n_i^{(z)} + n_i^{(s)}) = q_j \qquad (2\text{-}10)$$

$(j = 1, 2, \ldots s)$. Eqs. 2-10 are the *stoichiometric conditions.*

According to the phase rule, the number of condensed phases is at most c + 1 (and this number of condensed phases can coexist in equilibrium with a gas phase only for a uniquely specified set of stoichiometric constants at a uniquely specified temperature and pressure). We simplify Eqs. 2-10 by making the assumption that any condensed phase is a pure component whose state of aggregation (solid or liquid) is known. More general threatments of heterogeneous systems present no special difficulty but result in a considerable amplification of the notation required for a

general discussion. The systems of interest in this handbook are all compatible with this restriction. With this assumption, Eqs. 2-10 can be written

$$n_j' + \sum_{i=1}^{s} \beta_{ij} n_i = q_j \qquad (2\text{-}11)$$

where n_j' is the number of moles of condensed (solid or liquid) component j in unit weight of the mixture.

If the equilibrium composition of a mixture is to be determined, the constituents to be considered must be chosen *a priori*. The selection will usually imply the neglect of certain species whose concentrations at equilibrium can be expected to be negligibly small. In general, the correctness of the choice can only by confirmed *a posteriori* by a calculation demonstrating that the concentrations of the neglected species are in fact negligible. In some applications, additional species may be arbitrarily excluded from consideration even though their equilibrium concentrations may be significant, provided kinetic consideratons imply that the rate of their formation is too small to be significant under the conditions of their application.

We may illustrate the notation of this section by considering the decomposition products of TNT. We assume *a priori* that the products consist of a mixture of solid carbon with a gas phase comprised of C, CO, H_2, N_2, CO_2, H_2O, H. In this list we have arbitrarily neglected a number of possible dissociation products; they can be included if desired. Because of the oxygen deficit in the TNT molecule, we expect the most abundant species to be C, CO, H_2, N_2, and we select these species as components. The coefficients α_{ik} of the formula vectors and β_{ij} of Eqs. 2-7 are collected in Fig. 2-1. The first four rows of the array (matrix) of the β_{ij} correspond to the identities resulting from the choice of components. The remaining rows represent the chemical reactions of Eqs. 2-7.

$$2\,CO - C = CO_2$$

$$H_2 + CO - C = H_2O$$

$$\tfrac{1}{2}H_2 = H$$

by means of which those constituents that are not components are formed from those that are. For TNT, $C_7H_5O_6N_3$,

$$q_1' = 7/M;\ q_2' = 6/M;\ q_3' = 5/M;\ q_4' = 3/M$$

where $M = 228.18$ is the molecular weight of TNT. The solution of Eqs. 2-3 is

$$q_1 = 1/M;\ q_2 = 6/M;\ q_3 = 5/2M;\ q_4 = 3/2M$$

2-3 THE LAWS OF THERMODYNAMICS

Thermodynamics is an exact mathematical science, based upon a small number of basic premises or postulates from which all the results of the science are deduced by logical processes. Application of the science to physical systems always involves additional hypotheses separate from the science itself. It is necessary to assume the relevance of the mathematical model to the physical system to the one-to-one correlation of quantities employed by the science to physically measurable properties of the system. It is also necessary, except in trivial cases, to appeal either to experiment or to other theory to evaluate the various functions required by the application of thermodynamics in their dependence upon the independent variables of the physical system.

A *thermodynamic system* (closed system) is one that interacts with the surroundings by exchanging heat and work through its boundary; an *isolated system* is one that does not interact with the surroundings. The *state* of a system is determined by the values of its various properties, the nature and necessary number of which are to be determined. A system is composed of a finite number of homogeneous parts, called phases. For some applications, it may be necessary to consider the finite number of nonhomogeneous regions forming the boundaries between pairs of homogeneous phases; for most cases, the extent of such regions is small and they can be neglected in comparison to the homogeneous regions. Some properties of the homogeneous phases are regarded as fundamental; i.e., temperature, internal energy, pressure, entropy, and volume.

Properties such as internal energy, volume and entropy are called *extensive* because their values for a given phase are proportional to the mass of the phase. The value of an extensive property of an entire system is the sum of the values of each of the constituent phases. The *molar value* of an extensive property is that for a suitably defined gram-molecular weight or mole of material. The *specific value* of an extensive property is that for

ELEMENTS

CONSTITUENTS	k =	C 1	O 2	H 3	N 4	
C	i=1	1	0	0	0	= (α_{ik})
CO	2	1	1	0	0	
H_2	3	0	0	2	0	
N_2	4	0	0	0	2	
CO_2	5	1	2	0	0	
H_2O	6	0	1	2	0	
H	7	0	0	1	0	

COMPONENTS

CONSTITUENTS	j =	C 1	CO 2	H_2 3	N_2 4	
C	i=1	1	0	0	0	= (β_{ij})
CO	2	0	1	0	0	
H_2	3	0	0	1	0	
N_2	4	0	0	0	1	
CO_2	5	-1	2	0	0	
H_2O	6	-1	1	1	0	
H	7	0	0	1/2	0	

Figure 2-1. The Coefficients α_{ik} and β_{ij} for the Explosion Products of TNT

unit weight (e.g., one gram of material. We will generally employ a capital letter to designate an extensive property for weight M of material, where M may be a suitably defined gram-molecular weight, and the lower case letter designates the value of the extensive property for unit weight. A property is called *intensive* if its value for a given phase is independent of the mass of the phase. The temperature and pressure are such intensive properties.

A *thermodynamic process* is said to have taken place if a change is observed to have taken place in any macroscopic property of the system. An *infinitesimal process* is a process in which there is only an infinitesimal change in any macroscopic property of the system. A *natural process* is an infinitesimal process that occurs spontaneously in real systems; an *unnatural process* is one that cannot occur spontaneously in real systems. *Reversible processes* are either natural or unnatural processes which can occur in either direction between two states of equilibrium.

The first law of thermodynamics for an isolated system can be stated as follows: *There exists a function of the state of a uniform phase called the energy which is conserved for any process over all the phases participating in the process.* For an infinitesimal process, the first law is

$$\sum_k dE^{(k)} = 0 \qquad (2\text{-}12)$$

where $E^{(k)}$ is the energy of the k-th phase. Note that k now refers to the phase (solid, liquid, or gas), not to the element as in the preceding paragraph. Because energy is an extensive property, the energy of the whole system is defined by

$$E = \sum_k E^{(k)} \qquad (2\text{-}13)$$

We shall here limit consideration to the case in which all of the work done on a phase is produced by the pressure exerted on the phase. We suppose that the phase is in pressure equilibrium with its surroundings in the sense that if the pressure exerted by the phase on its surroundings is p, the pressure exerted by the surroundings is $p + dp$ or $p - dp$. Under these circumstances the external work performed on the k-th phase is reversible, equals $p^{(k)}\,dv^{(k)}$, and

$$dE^{(k)} = \delta q^{(k)} - p^{(k)} dV^{(k)} \qquad (2\text{-}14)$$

where $\delta q^{(k)}$ is the heat absorbed by the k-th phase, $p^{(k)}$ is the pressure of the k-th phase, and $dV^{(k)}$ is the differential increase in volume of the phase during the process producing the change $dE^{(k)}$ in $E^{(k)}$.

The second law of thermodynamics for an isolated system can be stated as follows: *There exists a function of the state of a uniform phase called the entropy which is conserved for any reversible process and which increases for any irreversible process over all of the phases participating in the process.* For an infinitesimal process

$$\sum_k dS^{(k)} \geq 0 \qquad (2\text{-}15)$$

where $S^{(k)}$ is the entropy of the k-th phase. The equality sign refers to a reversible process and the inequality sign to an irreversible one. Because entropy is an extensive property, the entropy of the whole system is defined by

$$S = \Sigma S^{(k)} \qquad (2\text{-}16)$$

The statement of the second law is completed by the further assumption that for a particular phase participating in a reversible process

$$dS^{(k)} = \frac{\delta q^{(k)}}{T^{(k)}} \qquad (2\text{-}17)$$

where $T^{(k)}$ is the temperature of the uniform k-th phase and $\delta q^{(k)}$ is the heat absorbed by the phase from its surroundings in the reversible process producing the change $dS^{(k)}$ in $S^{(k)}$. Then Eq. 2-14 can be written

$$dE^{(k)} = T^{(k)} dS^{(k)} - p^{(k)} dV^{(k)} \qquad (2\text{-}18)$$

for a reversible process.

Note that the summation of Eqs. 2-12 and 2-15 is over all of the phases performing work or exchanging heat during the process, and the total system described by these equations is an isolated system for which the total volume is

constant and through the boundary of which no heat flows.

In textbooks on thermodynamics, it is shown that a general (reversible or irreversible) infinitesimal change in the energy $E^{(k)}$ of a phase k can be written

$$\left.\begin{aligned} dE^{(k)} &= T^{(k)}dS^{(k)} - p^{(k)}dV^{(k)} \\ &\quad + M\sum_i \mu_i^{(k)} dn_i^{(k)} \end{aligned}\right\} \quad (2\text{-}19)$$

where M is the total mass of the system (not the gram-molecular weight as in the previous paragraph) $u_i^{(k)}$ is called the chemical potential of the *k-th* phase of the *i-th* constituent. Equation 2-19 can be shown to be compatible with the first and second laws of thermodynamics.

If independent variables other than the entropy and volume are to be employed for a particular system, it is convenient to define new extensive variables: enthalpy, Helmholtz free energy, and Gibbs free energy. The new state variables are defined in terms of quantities already introduced; they do not provide additional information concerning the state. The characteristic function for the independent variables entropy, pressure, and the mole numbers is called the enthalpy, denoted by H, and defined for a phase k by

$$H^{(k)} = E^{(k)} + p^{(k)}V^{(k)} \quad (2\text{-}20)$$

For the independent variables—temperature, volume, and the mole numbers—the characteristic function is called the Helmholtz free energy, denoted by F, and defined for a phase k by

$$F^{(k)} = E^{(k)} - T^{(k)}S^{(k)} \quad (2\text{-}21)$$

For the independent variables—temperature, pressure, and the mole numbers—the characteristic function is called the Gibbs free energy, denoted by G, and defined for a phase k by

$$G^{(k)} = H^{(k)} - T^{(k)}S^{(k)} \quad (2\text{-}22)$$

For any infinitesimal process of the whole system the extensive properties satisfy the equations

$$\left.\begin{aligned} dS &= \sum_k dS^{(k)} \quad , \quad dH = \sum_k dH^{(k)} \\ dV &= \sum_k dV^{(k)} \quad , \quad dF = \sum_k dF^{(k)} \\ dE &= \sum_k dE^{(k)} \quad , \quad dG = \sum_k dG^{(k)} \end{aligned}\right\} \quad (2\text{-}23)$$

When the definitions of Eqs. 2-20, 2-21, and 2-22 are differentiated and combined with Eq. 2-19, we obtain

$$\left.\begin{aligned} dH^{(k)} &= T^{(k)}dS^{(k)} + V^{(k)}dp^{(k)} + M\sum_i \mu_i^{(k)} dn_i^{(k)} \\ dF^{(k)} &= -S^{(k)}dT^{(k)} - p^{(k)}dV^{(k)} + M\sum_i \mu_i^{(k)} dn_i^{(k)} \\ dG^{(k)} &= -S^{(k)}dT^{(k)} + V^{(k)}dp^{(k)} + M\sum_i \mu_i^{(k)} dn_i^{(k)} \end{aligned}\right\} \quad (2\text{-}24)$$

For a particular phase, the chemical potential can be defined by any one of the relations

$$\left.\begin{aligned} \mu_i^{(k)} &= \frac{1}{M}\left[\left(\frac{\partial E}{\partial n_i}\right)_{S,V}\right]^{(k)} = \frac{1}{M}\left[\left(\frac{\partial H}{\partial n_i}\right)_{S,p}\right]^{(k)} \\ &= \frac{1}{M}\left[\left(\frac{\partial F}{\partial n_i}\right)_{V,T}\right]^{(k)} = \frac{1}{M}\left[\left(\frac{\partial G}{\partial n_i}\right)_{p,T}\right]^{(k)} \end{aligned}\right\} \quad (2\text{-}25)$$

If the system consists of a single pure phase, Eqs. 2-19 and 2-24 can be written

$$\left.\begin{aligned} dE &= TdS - pdV \\ dH &= TdS + Vdp \\ dF &= -SdT - pdV \\ dG &= -SdT + Vdp \end{aligned}\right\} \quad (2\text{-}26)$$

where it is unnecessary to retain the superscript label of the phase. These expressions, for any infinitesimal process involving only a single pure phase, satisfy the first and second laws as expressed by Eq. 2-18.

The variations of Eqs. 2-23, with Eqs. 2-19 and 2-24 are arbitrary, except that the variations $dn_i^{(k)}$ must satisfy the stoichiometric conditions, Eqs. 2-10, which we write in the form,

$$\sum_k \sum_l \beta_{lj} dn_l^{(k)} = 0 \quad (2\text{-}27)$$

When the assumption is made that a process occurs at fixed composition, these connections

are automatically satisfied since

$$dn_i^{(k)} = 0 \qquad (2\text{-}28)$$

for all i and k by definition.

The equilibrium conditions are the conditions under which a process in an isolated system—as described by Eqs. 2-23 and 2-24, and subject to the stoichiometric constraints of Eq. 2-27—is a reversible process, i.e., satisfies Eqs. 2-12 and 2-15. The analysis for the case of fixed composition is given in standard thermodynamics textbooks, e.g., that of Guggenheim[2]. The analysis, when the stoichiometric conditions are expressed in the form of Eq. 2-27, has been published by Brinkley[6].

Both under constant composition constraint and under the constraint expressed by Eq. 2-27, the mechanical and thermal equilibrium conditions are obtained in the form

$$\left.\begin{aligned} p^{(k)} &= p \\ T^{(k)} &= T \end{aligned}\right\} \qquad (2\text{-}29)$$

where p and T are the uniform pressure and temperature, respectively, of the whole system. For the general stoichiometric conditions expressed by Eq. 2-27, the chemical equilibrium conditions can be obtained in the form

$$\mu_i^{(k)} = RT\sum_j \beta_{ij}\lambda_j \qquad (2\text{-}30)$$

where the λ_j are parameters that can be eliminated between Eqs. 2-27 and 2-30.

In the derivation of Eqs. 2-29 and 2-30 that has been outlined, a process occurring at constant total volume and constant total entropy in an isolated system was considered. The analysis can be extended to cases where the system of interest exchanges heat with its surroundings or performs work on its surroundings by conceiving of an isolated system consisting of the system of interest surrounded by an additional phase and separated from it by a membrane impermeable to the exchange of matter but through which heat can be transferred or upon which work can be performed, or both. If the added phase is assumed to be so large that the exchange of heat results in a negligible change in its pressure, then the process occurring in the system of interest may be at constant temperature, or constant pressure, or both. It can then be shown that Eqs. 2-29 and 2-30 are the conditions that a process be reversible when the process occurs at constant entropy and pressure, at constant temperature and volume, or at constant temperature and pressure of the system of interest. Eqs. 2-29 and 2-30 are thus the conditions for any infinitesimal process to be a reversible process and they are thus the general conditions for equilibrium.

When Eqs. 2-28 and 2-29 are satisfied, the system is in mechanical and thermal equilibrium, but is constrained to constant composition. It is a state of partial equilibrium that may provide a good approximation to the state of a transient system if relaxation times for equilibration of temperature and pressure are short and relaxation times for equilibration of composition are long compared to the time characterizing the transient nature of the system. When Eqs. 2-28 and 2-29 are satisfied, Eqs. 2-19, 2-23, and 2-24 can be written

$$\left.\begin{aligned} dE &= TdS - pdV \\ dH &= TdS + Vdp \\ dF &= -SdT - pdV \\ dG &= -SdT + Vdp \end{aligned}\right\} \qquad (2\text{-}31)$$

Eqs. 2-31 are identical with Eqs. 2-26 for a pure single phase. We conclude that *the equations for an infinitesimal process in a mixture—which maintains thermal and mechanical equilibrium during the process and also is constrained to constant composition—are identical with those for a single pure phase.*

When Eqs. 2-29 and 2-30 are satisfied, the system is in a state of complete equilibrium. It may provide a good approximation to the state of a transient system if relaxation times for equilibration of temperature, pressure, and composition are all short compared to the time characterizing the transient nature of the system. When Eqs. 2-29 and 2-30 are satisfied, Eq. 2-19 and the third of Eqs. 2-23 can be combined to give

$$dE = TdS - pdV + RTM\sum_j \lambda_j \sum_k \sum_i \beta_{ij} \alpha n_i^{(k)}$$

In view of Eq. 2-27, this expression reduces to

$$dE = TdS - pdV \qquad (2\text{-}32)$$

Similarly, Eqs. 2-23 and 2-24 result in the expression

$$\left.\begin{aligned} dH &= TdS + Vdp \\ dF &= -SdT - pdV \\ dG &= -SdT + Vdp \end{aligned}\right\} \qquad (2\text{-}33)$$

Eqs. 2-32 and 2-33 are identical with Eqs. 2-26 for a pure single phase. We conclude that *the equations for an infinitesimal process in a mixture that maintains equilibrium during the process are identical with those for a single pure phase.*

Using Eqs. 2-29 and the extensive nature of the enthalpy and free energy functions, we can also write

$$\left.\begin{aligned} H &= E + pV \\ F &= E - TS \\ G &= H - TS \end{aligned}\right\} \qquad (2\text{-}34)$$

for a mixture. These expressions have the same form as the definitions given by Eqs. 2-20, 2-21, and 2-22 for a single phase.

The energy and enthalpy are undefined to the extent of an arbitrary additive constant. The entropy is undefined to the extent of an additional arbitrary additive constant. The free energies are thus undefined to the extent of an additive constant and an additive linear function of temperature. In practice, this lack of definition occasions no difficulty since one is always concerned with the energy or entropy difference between two states and these differences are completely defined. The lack of definition can be removed by defining for each constituent of a mixture a standard state in which energy and entropy are arbitrarily assigned the value zero. It is not necessary that the standard state be physically accessible, provided a process can be defined that will produce the state of interest from the standard state and for which the change in energy and entropy can be calculated.

Now suppose that the entropy and volume are known as functions of the independent variables pressure, temperature, and the mole numbers n_i, i.e., that the functions represented by,

$$s = s(p, T; n_1, \cdots n_s)$$

$$v = v(p, T; n_1, \cdots n_s)$$

are known. The the sake of definiteness, we employ the specific entropy and specific volume. If (1) the system is a single pure phase, if (2) the system is a mixture constrained to constant composition, or if (3) the composition of the system satisfies the equilibrium and stoichiometric conditions at all values of p and T; we may regard the entropy and volume as implicitly prescribed functions of p and T only, i.e.,

$$\left.\begin{aligned} s &= s(p, T) \\ v &= v(p, T) \end{aligned}\right\} \qquad (2\text{-}35)$$

If a standard state has been defined, the third of Eqs. 2-33 and the information summarized by Eqs. 2-35 suffice to evaluate the Gibbs free energy as a function of pressure and temperature. Therefore, the function

$$g = g(p, T)$$

may be regarded as known, where g is the specific Gibbs free energy. The other thermodynamic properties are then also known. In particular, the specific energy can be regarded a known function of pressure and temperature as expressed by

$$e(p, T) = g(p, T) + Ts(p, T) - pv(p, T) \qquad (2\text{-}36)$$

Similarly, it may be supposed that the entropy and pressure are known as functions of the independent variables volume, temperature, and the mole numbers n_i,

$$s = s(v, T; n_1, \cdots n_s)$$

$$p = p(v, T; n_1, \cdots n_s)$$

Under these circumstances, we may regard the entropy and pressure as implicitly prescribed functions of v and T only, i.e.,

$$\left.\begin{aligned} s &= s(v, T) \\ p &= p(v, T) \end{aligned}\right\} \qquad (2\text{-}37)$$

If a standard state has been defined, the second of Eqs. 2-33 and the information summarized by Eqs. 2-37 suffice to determine the specific Helmholtz free energy as a function of volume and temperature

$$f = f(v, T)$$

The other thermodynamic properties are then also known. In particular, the specific energy can be regarded a known function of volume and temperature, as expressed by

$$e(v, T) = f(v, T) - Ts(v, T) \qquad (2\text{-}38)$$

Either of the expressions

$$\left.\begin{aligned} v &= v(p, T; n_1, \cdots n_s) \\ p &= p(v, T; n_1, \cdots n_s) \end{aligned}\right\} \qquad (2\text{-}39)$$

represent a relation between pressure, volume, and temperature that is called an *equation of state*. Either of the expressions

$$\left.\begin{aligned} s &= s(p, T; n_1, \cdots n_s) \\ s &= s(v, T; n_1, \cdots n_s) \end{aligned}\right\} \qquad (2\text{-}40)$$

can be evaluated if an equation of state and certain thermal data, to be specified later, are known. The information summarized by Eqs. 2-40 is sometimes called the *caloric equation of state*, although these data cannot usually be expressed in analytical form.

A similar discussion results if the pairs (s,p) and (s,v) are considered as independent variables. The energy is most naturally, from a purely thermodynamic standpoint, considered a variable of the latter pair. However, except in an approximation to be noted later, equation of state and thermal data are always presented in the forms summarized by Eqs. 2-39 and 2-40 so that the energy, regarded a function of entropy and volume, is determined parametrically by Eq. 2-38 or by Eqs. 2-36 and 2-37.

We conclude that the thermodynamic state of a system is uniquely determined by the values of two independent properties of the system (state variables) if the laws of thermodynamics, an equation of state, and the thermal data summarized by one of Eqs. 2-40 are simultaneously satisfied and if the system consists of a single pure phase, a mixture constrained to constant composition, or a mixture whose composition satisfies the stoichiometric and equilibrium conditions at all values of the independent state variables. The state of a system is uniquely specified in this way from purely thermodynamic considerations under no other circumstances.

2-4 GENERAL THERMODYNAMIC IDENTITIES

To determine the thermodynamic properties (such as energy, pressure, enthalpy, temperature, specific heat, etc.) of an actual system, it is first necessary to define or to determine its composition. It is also necessary to know the equation of state of the gaseous mixture and the equation of state of each phase present. Then the thermodynamic properties are determined by the general relations to be summarized in this paragraph. These relations are described by partial derivatives of thermodynamic quantities. To determine the properties themselves, the derivatives must be integrated along some thermodynamic path. Examples of such integrated expressions are presented in Appendix A.

The general thermodynamic relations are derived for a heterogeneous mixture. First the partial derivatives of volume with respect to temperature and pressure, are derived and then the derivatives of pressure with respect to volume and temperature are derived. Then specific heats, and derivatives of entropy, energy, enthalpy, and chemical potential are considered. Finally the adiabatic exponent and the sound speeds are derived.

The equation of state of a heterogeneous mixture is constructed from the p-v-T relations for each of the constituent phases, making use of the fact that the volume of a mixture is the sum of the volumes of its constituent phases. We will let v denote the specific volume of a mixture, V_j' the molar volume of the j-*th* condensed component, and τ the volume of the gas phase for unit weight of mixture. For a homogeneous system consisting of a gas phase only, $v = \tau$. In general, we consider

$$v = \tau + \sum_j n_j' V_j' \qquad (2\text{-}41)$$

since we have restricted our discussion to mixtures in which any condensed phase consists of a pure component.

The equation of state of a pure condensed phase is an expression giving

$$V_j' = V_j'(p, T) \qquad (2\text{-}42)$$

The dependence of the molar volume of a pure

condensed phase on pressure and temperature is usually determined for each substance by experimental measurements, and the data have been represented by a variety of empirical equations. Without such data, the molar volume of a pure condensed component may be regarded—as an approximation—a constant, and at temperatures and pressures far removed from ordinary values treated as an adjustable parameter.

The equation of state of a gas phase may be an expression giving

$$\tau = \tau(p,\ T;\ n_1, \cdots n_s) \tag{2-43}$$

Later we consider the case where pressure is a function of τ, T, and the n's. The partial molar volume of the *i-th* gaseous constituent is defined by

$$\overline{V}_i = \left(\frac{\partial \tau}{\partial n_i}\right)_{p,T} \tag{2-44}$$

In general, $\overline{V}_i$ is a function of the form $\overline{V}_i(p,\ T;\ n_1, \ldots n_s)$. In textbooks on thermodynamics, it is shown that

$$\tau = \sum_i n_i \overline{V}_i \tag{2-45}$$

Therefore, Eq. 2-41 can be written

$$v = \sum_i n_i \overline{V}_i + \sum_j n'_j V'_j \tag{2-46}$$

when the equation of state of the gas phase is explicit in temperature and pressure. The partial derivatives of the volume with respect to temperature and pressure and at constant composition are

$$\left.\begin{aligned}\left(\frac{\partial v}{\partial T}\right)_{p,n} &= \sum_i n_i \left(\frac{\partial \overline{V}_i}{\partial T}\right)_{p,n} + \sum_j n'_j \left(\frac{\partial V'_j}{\partial T}\right)_p \\ \left(\frac{\partial v}{\partial p}\right)_{T,n} &= \sum_i n_i \left(\frac{\partial \overline{V}_i}{\partial p}\right)_{T,n} + \sum_j n'_j \left(\frac{\partial V'_j}{\partial p}\right)_T\end{aligned}\right\} \tag{2-47}$$

where the subscript n means that the differentiation is to be performed at constant composition. Equilibrium partial derivatives of the volume with respect to temperature and pressure are related to the derivatives at constant composition by

$$\left.\begin{aligned}\left(\frac{\partial v}{\partial T}\right)_p &= \left(\frac{\partial v}{\partial T}\right)_{p,n} + \sum_i n_i \overline{V}_i \left(\frac{\partial\, \ln n_i}{\partial T}\right)_p + \sum_j V'_j \left(\frac{\partial n'_j}{\partial T}\right)_p \\ \left(\frac{\partial v}{\partial p}\right)_T &= \left(\frac{\partial v}{\partial p}\right)_{T,n} + \sum_i n_i \overline{V}_i \left(\frac{\partial\, \ln n_i}{\partial p}\right)_T + \sum_j V'_j \left(\frac{\partial n'_j}{\partial p}\right)_T\end{aligned}\right\} \tag{2-48}$$

where the equilibrium nature of the derivative is indicated by omitting the subscript i. The derivatives of the mole numbers with respect to temperature and pressure are to be determined from the variation of the equilibrium composition with temperature and pressure. Their explicit evaluation is described in Appendix B.

Alternatively, the equation of state of a gas phase may be an expression giving

$$p = p(\tau,\ T;\ n_1, \cdots n_s) \tag{2-49}$$

If the system consists only of a gas phase, so that $\tau = v$ the evaluation of the equilibrium partial derivatives of pressure with respect to temperature and mixture volume is straightforward. It is convenient to define

$$p_i = \left(\frac{\partial p}{\partial n_i}\right)_{\tau,T} \tag{2-50}$$

(p_i *is not* a partial molar quantity). From the ordinary rules of differentiation, we obtain the relations,

$$\left.\begin{aligned}\left(\frac{\partial p}{\partial T}\right)_\tau &= \left(\frac{\partial p}{\partial T}\right)_{\tau,n} + \sum_i n_i p_i \left(\frac{\partial\, \ln n_i}{\partial T}\right)_\tau \\ \left(\frac{\partial p}{\partial \tau}\right)_T &= \left(\frac{\partial p}{\partial \tau}\right)_{T,n} + \sum_i n_i p_i \left(\frac{\partial\, \ln n_i}{\partial \tau}\right)_T\end{aligned}\right\} \tag{2-51}$$

The derivatives of the mole numbers with respect to temperature and gas volume are to be determined from the variation of the equilibrium composition for changes in these variables. If the mixture is heterogeneous, the expressions for the partial derivatives of the pressure with respect to temperature and mixture volume are of an awkward form because of the mixed character of the equations of state. To evaluate them, we first evaluate the quantities

$$\left.\begin{aligned}\left(\frac{\partial v}{\partial \tau}\right)_{T,n} &= \left(\frac{\partial p}{\partial \tau}\right)_{T,n} \sum_j n_j' \left(\frac{\partial V_j'}{\partial p}\right)_T + 1 \\ \left(\frac{\partial v}{\partial T}\right)_{\tau,n} &= \sum_j n_j' \left(\frac{\partial V_j'}{\partial T}\right)_p + \left(\frac{\partial p}{\partial T}\right)_{\tau,n} \sum_j n_j' \left(\frac{\partial V_j'}{\partial p}\right)_T\end{aligned}\right\} \quad (2\text{-}52)$$

Eqs. 2-52 are obtained by differentiation of Eq. 2-41. Then the fixed composition partial derivatives of the pressure with respect to temperature and mixture volume can be obtained from identities.

$$\left.\begin{aligned}\left(\frac{\partial p}{\partial v}\right)_{T,n} &= \left(\frac{\partial p}{\partial \tau}\right)_{T,n} \Bigg/ \left(\frac{\partial v}{\partial \tau}\right)_{T,n} \\ \left(\frac{\partial p}{\partial T}\right)_{v,n} &= \left(\frac{\partial p}{\partial T}\right)_{\tau,n} - \left(\frac{\partial p}{\partial v}\right)_{T,n} \left(\frac{\partial v}{\partial T}\right)_{\tau,n}\end{aligned}\right\} \quad (2\text{-}53)$$

We proceed in a similar manner to evaluate the equilibrium partial derivatives. From Eq. 2-41, we obtain

$$\left.\begin{aligned}\left(\frac{\partial v}{\partial \tau}\right)_T &= \left(\frac{\partial p}{\partial \tau}\right)_T \sum_j n_j' \left(\frac{\partial V_j'}{\partial p}\right)_T + \sum_j V_j' \left(\frac{\partial n_j}{\partial \tau}\right)_T + 1 \\ \left(\frac{\partial v}{\partial T}\right)_\tau &= \sum_j n_j' \left(\frac{\partial V_j'}{\partial T}\right)_p + \left(\frac{\partial p}{\partial T}\right)_\tau \sum_j n_j' \left(\frac{\partial V_j'}{\partial p}\right)_T + \sum_j V_j' \left(\frac{\partial n_j}{\partial T}\right)_\tau\end{aligned}\right\} \quad (2\text{-}54)$$

Then the equilibrium partial derivatives of pressure with respect to temperature and mixture volume can be obtained from the identities of Eqs. 2-51, written for the equilibrium derivatives by the elimination of the subscript n.

A secondary thermodynamic property is the heat capacity. If a system is heated from temperature T to $T + dT$, the heat absorbed δq by unit weight of the system is evidently proportional to dT

$$\delta q = c\,dT$$

where c is the heat capacity per unit weight. If the changes taking place in the heating process are reversible, we may employ Eqs. 2-16, 2-17, and the second of Eqs. 2-29 to write

$$\delta q = \sum_k \delta q = T\,ds = c\,dT$$

where s is the specific entropy. If the volume is held constant during the heating process, the quantity c is called the specific heat capacity at constant volume and denoted by c_v. If the pressure is held constant during the heating process, the constant c is called the specific heat at constant pressure and denoted by c_p.

$$\left.\begin{aligned}c_v &= T\left(\frac{\partial s}{\partial T}\right)_v \\ c_p &= T\left(\frac{\partial s}{\partial T}\right)_p\end{aligned}\right\} \quad (2\text{-}55)$$

If in addition to pressure or volume the composition is assumed to remain fixed during the heating process, the heat capacities are called the heat capacities for constant composition, or more shortly, the "frozen" heat capacities. They can be denoted by $c_{v,n}$ or $c_{p,n}$, where

$$\left.\begin{aligned}c_{v,n} &= T\left(\frac{\partial s}{\partial T}\right)_{v,n} \\ c_{p,n} &= T\left(\frac{\partial s}{\partial T}\right)_{p,n}\end{aligned}\right\} \quad (2\text{-}56)$$

The expressions for specific energy e and specific enthalpy h (from Eqs. 2-26) can be written

$$de = c\,dT - p\,dv\ ,\quad dh = c\,dT + v\,dp$$

valid either for a change between equilibrium states or for a change at constant composition. It follows that alternate definitions for the heat capacities are given by the expressions

$$\left.\begin{aligned}c_v &= \left(\frac{\partial e}{\partial T}\right)_v\ ,\quad c_{v,n} = \left(\frac{\partial e}{\partial T}\right)_{v,n} \\ c_p &= \left(\frac{\partial h}{\partial T}\right)_p\ ,\quad c_{p,n} = \left(\frac{\partial h}{\partial T}\right)_{p,n}\end{aligned}\right\} \quad (2\text{-}57)$$

To evaluate the frozen heat capacity at constant volume for a heterogeneous system, we introduce the abbreviation

$$c_{\tau,n} = \left(\frac{\partial e}{\partial T}\right)_{\tau,n} \quad (2\text{-}58)$$

and employ the identity

$$c_{v,n} = c_{\tau,n} - \left(\frac{\partial e}{\partial \tau}\right)_{T,n} \left(\frac{\partial v}{\partial T}\right)_{\tau,n} \left(\frac{\partial v}{\partial \tau}\right)_{T,n} \quad (2\text{-}59)$$

Expressions for the quantities $c_{\tau,n}$ and $(\partial e/\partial \tau)_{T,n}$ are given in Appendix A, and expressions for the derivatives of the mixture volume are given by Eqs. 2-52.

To calculate the equilibrium heat capacity at constant volume for a heterogeneous system, we employ the quantity c_τ,

$$c_\tau = \left(\frac{\partial e}{\partial T}\right)_{\tau} = c_{\tau,n} + \sum_i n_i E_i \left(\frac{\partial \ln n_i}{\partial T}\right)_{\tau} + \sum_j E_j' \left(\frac{\partial n_j'}{\partial T}\right)_{\tau} \quad (2\text{-}60)$$

where we have introduced the abbreviation

$$E_i = \left(\frac{\partial e}{\partial n_i}\right)_{\tau,T} \quad (2\text{-}61)$$

and where E_j' is the molar energy of the *j-th* condensed component. The quantity E_i *is not* a partial molar quantity. An expression for E_i is given in Appendix A. Then c_v can be obtained from the identity of Eq. 2-59, written for the equilibrium derivatives by the elimination of the subscript n.

An expression connecting the frozen and equilibrium heat capacities at constant pressure can be written in the form

$$c_p = c_{p,n} + \sum_i n_i \overline{H}_i \left(\frac{\partial \ln n_i}{\partial T}\right)_p + \sum_j H_j' \left(\frac{\partial n_j'}{\partial T}\right)_p \quad (2\text{-}62)$$

where $\overline{H}_i$ is the partial molar enthalpy of the *i-th* gaseous constituent

$$\overline{H}_i = \left(\frac{\partial h}{\partial n_i}\right)_{p,T} \quad (2\text{-}63)$$

and where H_j is the molar enthalpy of the *j-th* condensed component. Expressions for the $c_{p,n}$ and H_j are given in Appendix A.

We shall have occasion to employ the fixed composition partial derivatives of several thermodynamic functions with respect to temperature and pressure or with respect to temperature and volume. They can all easily be obtained from the definitions of the functions and the thermodynamics laws by application of the rules for partial differentiation. For purposes of reference, we list certain of these relations without derivation. The derivatives of entropy with respect to pressure and volume at constant temperature are

$$\left(\frac{\partial s}{\partial v}\right)_{T,n} = \left(\frac{\partial p}{\partial T}\right)_{v,n}$$
$$\left(\frac{\partial s}{\partial p}\right)_{T,n} = -\left(\frac{\partial v}{\partial T}\right)_{p,n} \quad (2\text{-}64)$$

The derivatives of energy and enthalpy with respect to volume and pressure, respectively, at constant temperature are

$$\left(\frac{\partial e}{\partial v}\right)_{T,n} = T\left(\frac{\partial p}{\partial T}\right)_{v,n} - p$$
$$\left(\frac{\partial h}{\partial p}\right)_{T,n} = v - T\left(\frac{\partial v}{\partial T}\right)_{p,n} \quad (2\text{-}65)$$

Eqs. 2-64 and 2-65 complement Eqs. 2-56 and 2-57. The partial derivatives of the chemical potential of the *i-th* gaseous constituent can be written

$$\left(\frac{\partial \mu_i}{\partial p}\right)_{T,n} = \overline{V}_i$$
$$\left(\frac{\partial \mu_i}{\partial \tau}\right)_{T,n} = -p_i$$
$$\left[\frac{\partial(\mu_i/T)}{\partial T}\right]_{T,n} = -E_i/T^2$$
$$\left[\frac{\partial(\mu_i/T)}{\partial T}\right]_{p,n} = -\overline{H}_i/T^2 \quad (2\text{-}66)$$

Similar relations apply to the chemical potential of a pure condensed phase,

$$\left(\frac{\partial \mu_j'}{\partial p}\right)_T = V_j'$$
$$\left[\frac{\partial(\mu_j'/T)}{\partial T}\right]_p = -H_j/T^2 \quad (2\text{-}67)$$

Derivations of these relations can be found in thermodynamics textbooks.

A relation between the fixed composition heat capacity at constant pressure and that at constant volume can be obtained in either of the equivalent forms

$$\left.\begin{aligned} c_{p,n} - c_{v,n} &= -T\left(\frac{\partial p}{\partial T}\right)^2_{v,n}\left(\frac{\partial v}{\partial p}\right)_{T,n} \\ &= -T\left(\frac{\partial v}{\partial T}\right)^2_{p,n}\left(\frac{\partial p}{\partial v}\right)_{T} \end{aligned}\right\} \quad (2\text{-}68)$$

the first of which is convenient for the independent variables v and T, and the second of which is convenient for the independent variables p and T. It can be shown that an expression of the same form connects the equilibrium heat capacities

$$\left.\begin{aligned} c_p - c_v &= -T\left(\frac{\partial p}{\partial T}\right)^2_{v}\left(\frac{\partial v}{\partial p}\right)_{T} \\ &= -T\left(\frac{\partial v}{\partial T}\right)^2_{p}\left(\frac{\partial p}{\partial v}\right)_{T} \end{aligned}\right\} \quad (2\text{-}69)$$

where the equilibrium derivatives of pressure or volume are employed in evaluating the right-hand side of the equations.

The ratio of the heat capacity γ at constant pressure to that at constant volume can be defined for either the frozen heat capacities or for the equilibrium heat capacities. We define the quantities

$$\left.\begin{aligned} \gamma &= c_p/c_v \\ \gamma_n &= c_{p,n}/c_{v,n} \end{aligned}\right\} \quad (2\text{-}70)$$

Using Eqs. 2-68 and 2-69, we obtain the following useful relations:

$$\left.\begin{aligned} \gamma_n &= 1 - \frac{T}{c_{v,n}}\left(\frac{\partial p}{\partial T}\right)^2_{v,n}\left(\frac{\partial v}{\partial p}\right)_{T,n} \\ \frac{1}{\gamma_n} &= 1 + \frac{T}{c_{p,n}}\left(\frac{\partial v}{\partial T}\right)^2_{p,n}\left(\frac{\partial p}{\partial v}\right)_{T,n} \\ \gamma &= 1 - \frac{T}{c_v}\left(\frac{\partial p}{\partial T}\right)^2_{v}\left(\frac{\partial v}{\partial p}\right)_{T} \\ \frac{1}{\gamma} &= 1 + \frac{T}{c_p}\left(\frac{\partial v}{\partial T}\right)^2_{p}\left(\frac{\partial p}{\partial v}\right)_{T} \end{aligned}\right\} \quad (2\text{-}71)$$

The adiabatic exponent κ is defined by

$$\kappa = -\frac{v}{p}\left(\frac{\partial p}{\partial v}\right)_s \quad (2\text{-}72)$$

This exponent is used to describe the adiabatic expansion of gases. For detonation products κ has a value of approximately 3, and for perfect gases $\kappa = \gamma$.

By use of the thermodynamic identity

$$\left(\frac{\partial p}{\partial v}\right)_s = -\left(\frac{\partial s}{\partial v}\right)_p\left(\frac{\partial p}{\partial s}\right)_v = -\frac{c_p}{c_v}\left(\frac{\partial T}{\partial v}\right)_p\left(\frac{\partial p}{\partial T}\right)_v$$

$$= \gamma\left(\frac{\partial p}{\partial v}\right)_T$$

Eq. 2-72 can be written

$$\kappa = -\gamma\left(\frac{v}{p}\right)\left(\frac{\partial p}{\partial v}\right)_T \quad (2\text{-}73)$$

An adiabatic exponent for fixed composition κ_n can also be defined by

$$\kappa_n = -\frac{v}{p}\left(\frac{\partial p}{\partial v}\right)_{s,n} = -\gamma_n\left(\frac{v}{p}\right)\left(\frac{\partial v}{\partial p}\right)_{T,n} \quad (2\text{-}74)$$

If Eqs. 2-73 and 2-74 are combined with Eqs. 2-71, we obtain the useful expressions

$$\left.\begin{aligned} \kappa_n &= -\frac{v}{p}\left(\frac{\partial p}{\partial v}\right)_{T,n} + \frac{vT}{pc_{v,n}}\left(\frac{\partial p}{\partial T}\right)^2_{v,n} \\ \frac{1}{\kappa_n} &= -\frac{p}{v}\left(\frac{\partial v}{\partial p}\right)_{T,n} - \frac{pT}{vc_{p,n}}\left(\frac{\partial v}{\partial T}\right)^2_{p,n} \\ \kappa &= -\frac{v}{p}\left(\frac{\partial p}{\partial v}\right)_{T} + \frac{vT}{pc_v}\left(\frac{\partial p}{\partial T}\right)^2_{v} \\ \frac{1}{\kappa} &= -\frac{p}{v}\left(\frac{\partial v}{\partial p}\right)_{T} - \frac{pT}{vc_p}\left(\frac{\partial v}{\partial T}\right)^2_{p} \end{aligned}\right\} \quad (2\text{-}75)$$

The sound velocity c is defined by

$$c^2 = \left(\frac{\partial p}{\partial \rho}\right)_s = \kappa p v \quad (2\text{-}76)$$

where $\rho = 1/v$ is the density of the mixture. A fixed composition or frozen sound velocity c_n can be similarly defined by

$$c_n^2 = \left(\frac{\partial p}{\partial \rho}\right)_{s,n} = \kappa_n p v \qquad (2\text{-}77)$$

Eqs. 2-75 can be combined with the definition of the sound velocity to obtain useful expressions relating this quantity to the derivatives of the equation of state. We obtain the relations

$$\left.\begin{aligned} c_n^2 &= -v^2\left[\left(\frac{\partial p}{\partial v}\right)_{T,n} - \frac{T}{c_{v,n}}\left(\frac{\partial p}{\partial T}\right)^2_{v,n}\right] \\ &= -v^2\left[\left(\frac{\partial v}{\partial p}\right)_{T,n} + \frac{T}{c_{p,n}}\left(\frac{\partial v}{\partial T}\right)^2_{p,n}\right]^{-1} \\ c^2 &= -v^2\left[\left(\frac{\partial p}{\partial v}\right)_{T} - \frac{T}{c_v}\left(\frac{\partial p}{\partial T}\right)^2_{v}\right] \\ &= -v^2\left[\left(\frac{\partial v}{\partial p}\right)_{T} + \frac{T}{c_p}\left(\frac{\partial v}{\partial T}\right)^2_{p}\right]^{-1} \end{aligned}\right\} \qquad (2\text{-}78)$$

Physically, the frozen sound velocity corresponds to the velocity of propagation of sound waves in a limit attained at high frequency and the equilibrium sound velocity corresponds to the propagation velocity of sound waves in a limit attained at low frequency.

A differential coefficient which is complementary to the adiabatic exponent κ and which is useful in analysis where volume and entropy are taken as independent variables can be defined for an equilibrium system by

$$\beta = \frac{v}{T}\left(\frac{\partial p}{\partial s}\right)_v \qquad (2\text{-}79)$$

and for a system constrained to fixed composition by

$$\beta_n = \frac{v}{T}\left(\frac{\partial p}{\partial s}\right)_{v,n} \qquad (2\text{-}80)$$

These quantities are related to derivatives of the equation of state by

$$\left.\begin{aligned} \beta_n &= \frac{v}{c_{v,n}}\left(\frac{\partial p}{\partial T}\right)_v \\ \beta &= \frac{v}{c_v}\left(\frac{\partial p}{\partial T}\right)_v \end{aligned}\right\} \qquad (2\text{-}81)$$

It is sometimes useful to regard the energy as a function of pressure and volume, with the partial derivatives

$$\left(\frac{\partial e}{\partial v}\right)_{p,n} = \frac{p}{\lambda_n} \; ; \left(\frac{\partial e}{\partial v}\right)_p = \frac{p}{\lambda} \qquad (2\text{-}82)$$

which define the coefficient λ_n for a system constrained to fixed composition and the coefficient λ for an equilibrium system. The corresponding derivatives of the energy with respect to the pressure are

$$\left(\frac{\partial e}{\partial p}\right)_{v,n} = \frac{v}{\beta_n} \; ; \left(\frac{\partial e}{\partial p}\right)_v = \frac{v}{\beta} \qquad (2\text{-}83)$$

The coefficients λ,β, and κ are not independent, but are related by the expression

$$\kappa = \beta\left(\frac{1}{\lambda} + 1\right) \qquad (2\text{-}84)$$

An analogous relation exists between the corresponding coefficients for a system of fixed composition.

Integrated expressions for the thermodynamic properties of a gas mixture, of a condensed phase, and of a composite heterogeneous system are derived in Appendix A. These expressions give the property of interest as the sum of two terms: the first is the value for an ideal system and the second is the contribution arising from the nonideal nature of the actual system. Terms of the second type involved integrals of the equation of state. In Appendix D, we list the gas imperfection contributions to the various thermodynamic properties as evaluated for several equations of state that have been employed to describe properties of the explosion products of explosives.

It has been noted that the equilibrium mixture is often employed to represent the composition of real mixtures of explosion products. The composition of this mixture is determined by the stoichiometric conditions, Eqs. 2-10, and by

the chemical equilibrium conditions, Eqs. 2-30. Because Eqs. 2-10 are linear in the mole numbers, while Eqs. 2-30 are linear in the logarithms of the mole numbers, an iterative procedure must be employed to determine the equilibrium mixture. A general method to solve these algebraic equations is formulated in Appendix B. This method can be employed as the basis for a computer program of very broad application, but it is not well adapted for hand calculations. In Appendix C, there is presented a simplified method of computation for systems containing compounds of carbon, hydrogen, oxygen, and nitrogen in which, with the chemical nature of the system specified, it is possible to achieve a partial separation of the variables and thus to simplify markedly the computational process.

2-5 APPROXIMATIONS FOR THE THERMODYNAMIC PROPERTIES ON AN ISENTROPE

It is possible to perform an exact calculation of all of the properties of the system, provided that the equations of state exist for the various phases comprising the system. This calculation, however, involves a large number of successive numerical steps, and the dependence of a property such as the energy on the independent state variables such as entropy and volume, i.e., the function $e(v,s)$ is obtained implicitly and not analytically. For some theoretical investigations, there is a need for approximate analytical expressions of such functions.

For an ideal gas of constant composition, the adiabatic exponent defined by Eq. 2-74 is equal to the ratio of the heat capacity at constant pressure to that at constant volume, $\kappa = \gamma$. The thermodynamic properties of an ideal gas are frequently represented with sufficient accuracy by the assumption that γ is a constant. Such a gas is called an ideal polytropic gas. The thermodynamic properties of such gases can be expressed in relatively simple form and the approximation has been extensively employed in the development of the hydrodynamics of compressible fluids such as air for which at moderate temperatures and pressures the polytropic assumption is a good approximation.

For the products of condensed explosives, it has been experimentally found that the adiabatic exponent γ is, to a good approximation, independent of the density and a function of entropy only for a considerable range of pressure. It seems proper to designate as a nonideal polytropic gas any gas for which κ is constant on an isentrope.

If the adiabatic exponent is a function of entropy only, Eq. 2-72 can be integrated along a path of constant entropy with the result

$$p = Av^{-\kappa} = A\rho^{\kappa} \qquad (2\text{-}85)$$

where $\rho = 1/v$ is the density and $A = A(s)$ is a function of entropy only. Eq. 2-85 can also be expressed in the form

$$p(v,s') = p'(v'/v) = p'(\rho/\rho') \qquad (2\text{-}86)$$

where $p' = p(v',s')$ and $\kappa = \kappa(s')$. From Eq. 2-32, $(\partial e/\partial v)_s = -p$. Using Eq. 2-85 and integrating along a path of constant entropy, we obtain

$$e = \frac{A}{\kappa - 1} v^{-\kappa+1} + B = \frac{pv}{\kappa - 1} + B \qquad (2\text{-}87)$$

where $B = B(s)$ is a function of entropy only. Eq. 2-87 can also be expressed in the form

$$e = e' + \frac{1}{\kappa - 1}(pv - p'v') \qquad (2\text{-}88)$$

where $e' = e(v',s')$. The enthalpy $h = e + pv$ is given by

$$\left.\begin{aligned} h &= \left(\frac{\kappa}{\kappa - 1}\right) pv + B \\ &= h' + \frac{\kappa}{\kappa - 1}(pv - p'v') \end{aligned}\right\} \qquad (2\text{-}89)$$

where $h' = h(p's')$. By using Eq. 2-76, the sound velocity c can be introduced into Eqs. 2-87 and 2-89 with the result

$$\left.\begin{aligned} c^2 &= \kappa pv = \kappa(\kappa - 1)(e - B) \\ &= (\kappa - 1)(h - B) \end{aligned}\right\} \qquad (2\text{-}90)$$

2-6 HYDRODYNAMICS OF REACTING CONTINUA

The fundamental differential equations of motion for a reacting fluid are derived in this paragraph. For one-dimensional problems they are simplified to the usual Eulerian and Lagrangian equations. In par. 2-7 the method of

characteristics is applied to the one-dimensional problem. The treatment of shock waves as discontinuities is given in par. 2-8.

In the macroscopic description of a physical system, the information concerning the state at one instant of time may be considered adequate if one can obtain from it a reasonable description of the state at some later time. It is assumed that the process can be performed in series (making each estimate from the previous estimate) over subintervals of the desired time interval with the final result insensitive to the length of the subinterval. One expects the procedure to fail for information of a given type if the subintervals become much smaller than a critical time interval, characteristic of the system and of the type of information, which can be called the "time resolution". This paragraph is confined to the consideration of systems and of time resolutions for which adequate information consists of a knowledge of the spatial distribution of the following densities:

(1) The concentrations ρn_i expressed in moles per unit volume of each of the chemical constituents of the system, where ρ is the mass density.

(2) The momentum density $\vec{m} = \rho\vec{u}$, where $\vec{u}$ is the (vector) particle velocity

(3) The total energy density $\rho(e + u^2/2)$, where e is the specific energy as measured by an observer moving with the fluid and $u^2/2$, $u^2 = |\vec{u}|^2$, is the specific kinetic energy of mass motion as measured by a fixed observer.

We simplify the system at the outset by making several assumptions:

(1) The velocity of each individual species is that of the mixture; therefore the diffusion of gaseous species is neglected and any condensed species is completely entrained in the flow.

(2) Heat conduction is neglected.

(3) The fluid is inviscid; hence no energy is dissipated by mechanical processes except across shock discontinuities.

(4) The only force acting on the fluid is the hydrostatic pressure (gravity and other body forces are neglected).

These four assumptions produce a valid model for the flows with which we are principally concerned, where the bulk velocity of the fluid is large compared to relative velocities of heat and diffusion. The model without heat conduction or diffusion is not an accurate one for the flow associated with ordinary flame propagation. For derivations of the flow equations in which these simplifying assumptions are not made, reference is made to a review by Richardson and Brinkley[8].

The next step is the derivation of the rate of change of any property of the fluid. Consider any vector or scalar property of position and time, $G(\vec{r},t)$, where $\vec{r}$ is the position vector and V is a movile volume whose surface a moves with velocity $\vec{u}$. Now, the total rate of change is separated into a partial derivative with respect to time and a convective term (for this derivation, see Band[9], for example).

$$\frac{d}{dt}\int_V G\,dV = \int_V \frac{\partial G}{\partial t}\,dV + \int_a G\vec{u}\cdot d\vec{a} \qquad (2\text{-}91)$$

where $d\vec{a} = \vec{n}\,da$, $\vec{n}$ is an outward pointing normal to the surface, da is a differential surface area and $G\vec{u}$ is interpreted as a dyadic if G is a vector (see Gibbs[10] for an introduction to dyadics). The left hand term expresses the time rate of the quantity G averaged over the volume V. It is equal to the sum of the contributions of each stationary volume element dV and the changes associated with the movement of the surface. If the velocity vector $\vec{u}$ is defined everywhere in the volume, the surface integral may be transformed with the aid of the Gauss integral theorem and we obtain the general kinematical relation,

$$\frac{d}{dt}\int_V G\,dV = \int_V \left[\frac{\partial G}{\partial t} + \nabla\cdot(\vec{u}G)\right] dV \qquad (2\text{-}92)$$

Consider an arbitrary mobile volume V whose surface moves with the particle velocity u. In the absence of diffusion, the time rate of change of the species i in V can be written

$$\frac{d}{dt}\int_V \rho n_i\,dV = \int_V R_i\,dV \qquad (2\text{-}93)$$

where R_i is the reaction rate. Using Eq. 2-92, we have

$$\int_V \left[\frac{\partial(\rho n_i)}{\partial t} + \nabla\cdot(\vec{u}\rho n_i) - R_i\right] dV = 0 \qquad (2\text{-}94)$$

Since the surface of the volume moves with velocity $\vec{u}$, the total mass in V is conserved

$$\frac{d}{dt}\int_V \rho dV = \int_V \left[\frac{\partial \rho}{\partial t} + \nabla \cdot (\rho \vec{u})\right] dV = 0 \quad (2\text{-}95)$$

Considering again the mobile volume V previously defined, one can obtain the equation for momentum transport by a straightforward application of Newton's second law of motion. According to this law, the total force acting on the mass of fluid in V is equal to the rate of change of linear momentum of the fluid in V. For an inviscid fluid in the absence of body forces, we have

$$-\int_a p d\vec{a} = \frac{d}{dt}\int_V \rho \vec{u} dV \quad (2\text{-}96)$$

since the force normal to the area $d\vec{a}$ is $-p\vec{n}$. Using Eq. 2-92 with $G = p\vec{u}$, we have

$$\int_V \left[\frac{\partial(\rho \vec{u})}{\partial t} + \nabla \cdot (\vec{u}\rho\vec{u}) + \nabla p\right] dV = 0 \quad (2\text{-}97)$$

where the integral of the pressure over the surface is transformed to a volume integral by the use of Gauss' theorem. The time rate of change of the total energy is equal to the rate at which work is performed on the material in V if the conduction of heat is neglected. Thus,

$$\frac{d}{dt}\int_V \rho(e + u^2/u) = \int_a p\,\vec{u} \cdot d\vec{a} \quad (2\text{-}98)$$

Again using Eq. 2-92 and Gauss' theorem to transform the surface integral, we obtain

$$\int_V \left\{\frac{\partial}{\partial t}[\rho(e + u^2/2) + \nabla \cdot \vec{u}(e + u^2/2), + \nabla \cdot (\vec{u}p)]\right\} dV = 0 \quad (2\text{-}99)$$

The volume V of Eqs. 2-94, 2-97, 2-99, and 2-93, is arbitrary. Therefore, the integrands of each expression must equal zero, giving

$$\left.\begin{aligned}
&\frac{\partial \rho}{\partial t} + \nabla \cdot (\vec{u}\rho) = 0 && \text{mass conservation}\\
&\frac{\partial(\rho\vec{u})}{\partial t} + \nabla \cdot (\vec{u}\rho\vec{u}) = -\nabla p && \text{momentum conservation}\\
&\frac{\partial}{\partial t}[\rho(e + u^2/2)] + \nabla \cdot \vec{u}\rho(e + u^2/2) = -\nabla \cdot (\vec{u}p) && \text{energy conservation}\\
&\frac{\partial(\rho n_l)}{\partial t} + \nabla \cdot (\vec{u}\rho n_l) = R_l
\end{aligned}\right\} \quad (2\text{-}100)$$

The equation of mass conservation is used to simplify the other three equations, and the energy equation is further simplified by using the momentum equation. After some manipulation, Eqs. 2-100 become

$$\left.\begin{aligned}
&\frac{\partial \rho}{\partial t} + \nabla \cdot (\vec{u}\rho) = 0\\
&\frac{\partial \vec{u}}{\partial t} + \vec{u} \cdot \nabla\vec{u} = -\frac{1}{\rho}\nabla p\\
&\frac{\partial e}{\partial t} + \vec{u} \cdot \nabla e = -\frac{p}{\rho}\nabla \cdot \vec{u}\\
&\frac{\partial n_l}{\partial t} + \vec{u} \cdot \nabla n_l = R_l/\rho
\end{aligned}\right\} \quad (2\text{-}101)$$

A more familiar form of these equations of hydrodynamics is obtained by introducing a total time derivative by the definition

$$\frac{d}{dt} = \frac{\partial}{\partial t} + \vec{u} \cdot \nabla \quad (2\text{-}102)$$

by means of which the rates of change are measured by an observer moving with the fluid. Then Eqs. 2-101 become

$$\left.\begin{aligned}
&\frac{d\rho}{dt} + \rho\nabla \cdot \vec{u} = 0 && \text{mass conservation}\\
&\frac{d\vec{u}}{dt} + \frac{1}{\rho}\nabla p = 0 && \text{momentum conservation}\\
&\frac{de}{dt} - \frac{p}{\rho^2}\frac{d\rho}{dt} = 0 && \text{energy conservation}\\
&\frac{dn_l}{dt} = R_l/\rho
\end{aligned}\right\} \quad (2\text{-}103)$$

and the last equation can be taken as a definition of the quantity R_l. Rates R_l of production of the constituents of the mixture are not all independent but most obey the stoichiometric conditions of par. 2-2. Thus, only $s - c$ of the quantities R_l may be regarded as independent.

The further development of the theory of irreversible processes of nonuniform systems that are not in equilibrium is based on two assumptions: (1) temperature T and chemical potentials μ_l can be defined as functions of the fundamental densities ρn_l, $\rho\vec{u}$, and $\rho(e + u^2/2)$; (2) T and μ_l can, to a good approximation, be

regarded as point functions of the fundamental densities. To simplify the development, we shall assume initally that all infinitesimal processes, including chemical ones, in a given volume element are reversible. (Later, we shall explore the analysis without this assumption.) With this assumption of reversibility we can regard a given volume element as being in equilibrium. The assumption of local reversibility makes it possible to employ the thermodynamic relations between the various state variables in a nonuniform system.

Eq. 2-19 for a general change in the energy can be written

$$\frac{de}{dt} = T\left(\frac{ds}{dt}\right) + \frac{p}{\rho^2}\left(\frac{d\rho}{dt}\right) + \frac{1}{\rho}\sum_i \mu_i R_i \qquad (2\text{-}104)$$

(For simplicity, we assume that the system is a gas mixture. Our conclusions are unchanged if condensed phases are present, although the assumptions of this paragraph require that such phases be completely entrained in the flow.) The reaction rates must satisfy the stoichiometric conditions, Eqs. 2-27, and therefore

$$\sum_i \beta_{ij} R_i = 0 \quad (j = 1, 2, \ldots c) \qquad (2\text{-}105)$$

Now, if chemical changes in the system are reversible, the equilibrium conditions, Eqs. 2-30, are satisfied, and Eq. 2-104 can be written

$$\frac{de}{dt} = T\left(\frac{ds}{dt}\right) + \frac{p}{\rho^2}\left(\frac{d\rho}{dt}\right) + \frac{RT}{\rho}\sum_j \lambda_j \sum_i \beta_{ij} R_i \qquad (2\text{-}106)$$

Therefore, if all of the changes, including chemical ones, are reversible,

$$\frac{de}{dt} = T\left(\frac{ds}{dt}\right) + \frac{p}{\rho^2}\left(\frac{d\rho}{dt}\right) \qquad (2\text{-}107)$$

Combining this equation with the energy transport equation 2-103, it follows that

$$\frac{ds}{dt} = 0 \qquad (2\text{-}108)$$

Eq. 2-108 states that the entropy contained in an element of fluid does not change as the element moves if diffusion and heat conduction are neglected, if the dissipative effects of viscosity are neglected, and if all changes in state of the element are reversible.

If the processes represented by Eq. 2-104 are not reversible, the assumption of local equilibrium is no longer possible. In considering a single element of volume one must now employ a quasi-thermodynamics, the justification of which is beyond the scope of this paragraph. However, the results are that one can define a specific entropy s such that for a fixed volume element

$$Td(\rho s) = d(\rho e) - \sum_i \mu_i d(\rho n_i) \qquad (2\text{-}109)$$

in which T and μ_i are calculated as though the element were in thermodynamic equilibrium. This expression can be transformed to

$$Tds = de - \left(\frac{p'}{\rho^2}\right) d\rho - \sum_i \mu_i \, dn_i \qquad (2\text{-}110)$$

where $p' = \rho(Ts - e + \sum_i \mu_i \, dn_i)$

The quantity p' is evidently the thermodynamically defined pressure. In general, it differs from the dynamically defined quantity of this paragraph because of the irreversible chemical reactions. It is usually a good approximation to assume that the thermodynamic and dynamic pressures are identical. Then the equation for entropy transport becomes

$$\rho\left(\frac{ds}{dt}\right) = -\sum_i \frac{\mu_i R_i}{T} > 0 \qquad (2\text{-}111)$$

If chemical reactions are irreversible, the entropy contained in an element of fluid changes in accord with Eq. 2-111 as a consequence of the entropy increase during an irreversible process.

A steady flow is defined as one in which all of the partial derivatives with respect to time are zero. A flow is called subsonic, sonic, or supersonic at a point as $u = |\vec{u}|$ is less than, equal to, or greater than the velocity of sound c at that point in the particular coordinate system being used.

Eqs. 2-103 are to be solved subject to initial and boundary conditions and to a specification of the state of the fluid, i.e., a knowledge of the function

$$e = e(\rho, p; \ldots n_i \ldots)$$

If all of the processes occurring are reversible, so that the energy transport equation can be replaced by the entropy transport equation as expressed by Eq. 2-108, then the state of the system is sufficiently specified if the function

$$p = p(\rho, s)$$

is known. Under these circumstances, Eqs 2-103 can also be expressed in the form

$$\left.\begin{aligned} &\frac{1}{c^2}\left(\frac{dp}{dt}\right) + \rho\nabla\cdot\vec{u} = 0 \\ &\frac{d\vec{u}}{dt} + \left(\frac{1}{\rho}\right)\nabla p = 0 \\ &\frac{ds}{dt} = 0. \end{aligned}\right\} \quad (2\text{-}112)$$

which involves derivatives of only the pressure and particle velocity.

Eqs. 2-103, and their alternative forms are called the Eulerian equations of hydrodynamics. When supplemented—as previously mentioned by initial and boundary conditions and by an equation of state, they can in principle be solved to determine p, ρ, and $\vec{u}$ regarded as functions of position and time. The initial conditions consist of a knowledge of these quantities as functions of position at some time which is taken as the initial instant. Boundary conditions are of two types, kinematical (velocity and displacement conditions) and physical (pressure). A kinematical condition is the requirement that the components of velocity normal to an interface be equal on both sides of the interface. A physical condition that must be satisfied by an inviscid fluid in contact with a rigid boundary is that the pressure shall be normal to the boundary. In the case of two inviscid fluids presenting a surface of separation, the physical condition to be satisfied is that the pressure shall be continuous at the boundary in passing from one side to the other. The surface separating two fluids or the same fluid at different densities is called a contact surface.

The equations of hydrodynamics comprise a system of partial differential equations of the first order that are quasi-linear, i.e., the partial derivatives appear linearly. Formal solutions of these equations can be obtained only in special cases.

As an example, the Eulerian equations of hydrodynamics for nondissipative ($ds/dt = 0$) flow can be written for motion in one dimension in the form

$$\left.\begin{aligned} &\frac{d\rho}{dt} + \rho\left(\frac{\partial u}{\partial x}\right) = 0 \\ &\frac{du}{dt} + \frac{1}{\rho}\left(\frac{\partial p}{\partial x}\right) = 0 \end{aligned}\right\} \quad (2\text{-}113)$$

where u is the particle velocity in the x-direction. The Eulerian equations for one-dimensional radial flow with spherical symmetry can be written

$$\left.\begin{aligned} &\frac{d\rho}{dt} + \rho\left(\frac{\partial u}{\partial r}\right) + \frac{2u\rho}{r} = 0 \\ &\frac{du}{dt} + \frac{1}{\rho}\left(\frac{\partial p}{\partial x}\right) = 0 \end{aligned}\right\} \quad (2\text{-}114)$$

where u is now the particle velocity in the direction of the radial coordinate r.

There is another mode of expression of the fundamental equations called the Lagrangian form. The label coordinates of a point may consist of its position coordinates or Eulerian coordinates at the initial instant of time. Thus a partial derivative with respect to time at constant values of the label coordinates has the same meaning as the operator d/dt in Eulerian coordinates, and

$$\vec{u} = \frac{\partial \vec{r}}{\partial t}$$

where $\vec{r}$ is the position vector of a point at time t. The Lagrangian representation is especially useful for problems in which interfaces and boundaries must be preserved and in which high precision in the conservation of mass and momentum is desired. Lagrangian is generally superior to Eulerian for one-dimensional problems but not necessarily for two- or three-dimensional problems.

As an example of the Lagrange representation, we may consider the case of plane flow in one dimension and let the label coordinate of a particle x_o to be the value of its position (Eulerian) coordinate x at $t = 0$. The particle velocity is given by

$$u = (\partial x/\partial t)_{x_o} \quad (2\text{-}115)$$

The form taken by the equation of continuity in Lagrangian coordinates is most easily deduced for the particular initial circumstances of the fluid. Suppose that the fluid is initially uniform with constant density ρ_o. The conservation of mass can be expressed by

$$x_o\rho_o = \int_{x(o,\,t)}^{x(x_o,\,t)} \rho(x,\,t)\,dx \quad (2\text{-}116)$$

where $x(x_o,t)$ is the Eulerian coordinate at time t of the point whose Eulerian coordinate at $t = 0$ was x_o, and $x(o,t)$ is the Eulerian coordinate of the point that was on a plane through the origin at $t = 0$. Differentiating this expression with respect to x_o at constant t, we obtain the Lagrangian equation of continuity for plane flow of an initially uniform fluid in the form

$$\left(\frac{\partial x}{\partial x_o}\right)_t = \frac{\rho_o}{\rho} \tag{2-117}$$

The Lagrangian equation of motion for the same fluid in plane flow can be obtained from the second of Eqs. 2-113 by the use of Eqs. 2-115 and 2-117. We obtain

$$\left(\frac{\partial^2 x}{\partial t^2}\right)_{x_o} + \frac{1}{\rho_o}\left(\frac{\partial p}{\partial x_o}\right)_t = 0 \tag{2-118}$$

For nondissipative flow, the entropy transport equation has the form

$$\left(\frac{\partial s}{\partial t}\right)_{x_o} = 0 \tag{2-119}$$

The Lagrangian form envisages the possibility of obtaining a description of the properties of the flow, including the Eulerian coordinates, as functions of the time and the label coordinates.

2-7 UNIFORMLY ISENTROPIC FLOW IN ONE DIMENSION

We will consider an application of the fundamental equation to a flow for which a formal solution is possible. The flow is considered to be in one direction—e.g., the x-direction—which means that the properties of the flow are functions of the x-coordinate only and independent of the y- and z-coordinates in a rectangular coordinate system. Whenever there is a portion of the x-t plane in which all the material is on the same isentrope—i.e., when the material is uniformly isentropic or homentropic—it is possible to transform the fundamental equations of par. 2-6 to another form that is due to Riemann.

For nondissipative flow as described by the entropy transport equation in the form of Eq. 2-108, the pressure and the sound velocity vary within the flow as functions of the density only. It is then convenient to introduce the quantity

$$\left.\begin{aligned} \sigma &= \int^{\rho} (c/\rho)\,d\rho \\ (\partial\sigma/\partial\rho)_s &= c/\rho \end{aligned}\right\} \tag{2-120}$$

where the integral is along a path of constant entropy and where c is the sound velocity, defined by Eq. 2-76. The quantity σ is undefined to the extent of an additive constant which can be arbitrarily assigned for convenience of calculation by the assignment of a lower limit of integration. Then Eqs. 2-113 and 2-108 can be written

$$\left.\begin{aligned} &\frac{\partial\sigma}{\partial t} + u\left(\frac{\partial\sigma}{\partial x}\right) + c\left(\frac{\partial u}{\partial x}\right) = 0 \\ &\frac{\partial u}{\partial t} + u\left(\frac{\partial u}{\partial x}\right) + c\left(\frac{\partial\sigma}{\partial x}\right) = 0 \\ &\frac{\partial s}{\partial t} + u\left(\frac{\partial s}{\partial x}\right) = 0 \end{aligned}\right\} \tag{2-121}$$

Addition and subtraction of the first two of these equations yields the new set

$$\left.\begin{aligned} &\left[\frac{\partial}{\partial t} + (u + c)\frac{\partial}{\partial x}\right](\sigma + u) = 0 \\ &\left[\frac{\partial}{\partial t} + (u - c)\frac{\partial}{\partial x}\right](\sigma - u) = 0 \\ &\left[\frac{\partial}{\partial t} + u\frac{\partial}{\partial x}\right]s = 0 \end{aligned}\right\} \tag{2-122}$$

which is due to Riemann. The form of Eqs. 2-122 suggests the definition of three characteristic directions—labeled C_+, C_-, and C_o—by the definitions

$$\left.\begin{aligned} C_+ &: \frac{dx}{dt} = u + c \\ C_- &: \frac{dx}{dt} = u - c \\ C_o &: \frac{dx}{dt} = u \end{aligned}\right\} \tag{2-123}$$

A *characteristic curve* in the x,t plane is defined as one that is tangent at every point to a characteristic direction. Thus, Eqs. 2-123 are the equations for the characteristic curves. The characteristics C_o are evidently the particle

paths in the x-t plane. With these definitions, Eqs. 2-122 can be interpreted as stating that on characteristic curves C_+

$$\bar{r} = \sigma + u = \text{constant} \qquad (2\text{-}124)$$

on characteristic curves C_-

$$\bar{s} = \sigma - u = \text{constant} \qquad (2\text{-}125)$$

while on the particle paths C_0, the entropy is constant. The entropy transport equation states that if the entropy is initially constant, it will remain constant for flow without discontinuities in the x-t plane.

The quantities $\bar{r}$ and $\bar{s}$ are called the Riemann invariants. If they are known at a given point, then u and σ are known there, i.e.,

$$\left.\begin{aligned} \sigma &= (\bar{r} + \bar{s})/2 \\ u &= (\bar{r} - \bar{s})/2 \end{aligned}\right\} \qquad (2\text{-}126)$$

From these, the density can be obtained from Eq. 2-120 and the pressure from the equation of state. For materials with a constant adiabatic exponent, as described in par. 2-5

$$\sigma = 2c/(\kappa - 1)$$

An especially simple case occurs for $\kappa = 3$, since then $\sigma = c$, $\bar{r} = c + u$, and $\bar{s} = c - u$. The first two of Eqs. 2-123 become

$$\left.\begin{aligned} C_+ &: \frac{dx}{dt} = \bar{r} \\ & \qquad (\kappa = 3) \\ C_- &: \frac{dx}{dt} = -\bar{s} \end{aligned}\right\} \qquad (2\text{-}127)$$

Since $\bar{r}$ is constant along curves C_+ and $\bar{s}$ is constant along lines C_-, Eqs. 2-127 can be integrated to give

$$C_+ : x = \bar{r}t + \text{constant}$$

$$C_- : x = -\bar{s}t + \text{constant}$$

so that the characteristic curves of each kind are straight lines for $\kappa = 3$. This case is of practical interest because the explosion products for condensed explosives have an adiabatic exponent that is near the value 3 and, consequently, flows for which $\kappa = 3$ present the qualitative feature of the flows of such gases.

In general, the characteristic curves have the following useful properties:

(1) There is a curve of each type through every point on the x-t plane.

(2) If curves of a given type having different values of the invariant associated with that type intersect at a point, the flow cannot remain continuous because different values of the dependent variables would be obtained if one characteristic or the other were used in computation. Thus, there will be a discontinuity in u, ρ, etc. at that point.

(3) If, in a given region, $\bar{s}$ has the same value along adjacent C_- curves, the C_+ curves are straight lines in that region. For $\bar{r}$ is constant along a C_+ curve which will cross the C_- curves and if $\bar{s}$ is also constant along the C_+ curves, both u and σ, therefore u and c, and therefore the slope of the C_+ curves must be constant.

(4) Similarly, if $\bar{r}$ has the same value along adjacent C_+ curves in a given region, the C_- curves are straight lines in that region.

(5) A weak discontinuity (not a shock), i.e., a discontinuity in a derivative of a function without a change in the function itself, is propagated into the flow from a boundary along a characteristic curve.

If both the density and the particle velocity are known along a line in the x-t plane, then $\bar{r}$ and $\bar{s}$ and the two characteristic directions can be calculated for each point along the line. Such a line may be the x-axis, in which case the information on the line describes the initial state of the fluid. Information may also be given as to one or more properties of the flow along additional paths in the x-t plane. For example, the path of a piston may be prescribed along which the velocity u is known. Similarly, the path of a shock wave may be given along which, as we shall see, the density and particle velocity are known. It is necessary to consider briefly the amount of initial and boundary information that is required, from which the propagation equations—Eqs. 2-124, 2-125, and 2-126—uniquely determine the flow. If a point following a given curve in the x-t plane moves supersonically with respect to the local flow, i.e.,

$$|dx/dt - u| > c$$

then the curve is called spacelike; if such a point moves subsonically with respect to the local flow, i.e.,

$$|dx/dt - u| < c$$

then it is called timelike, and if such a point

moves sonically with respect to the local flow, i.e.,

$$|dx/dt - u| = c$$

then the curve is a characteristic. In general, the characteristic curves are not perpendicular to the direction of flow. There is, therefore, a downstream direction on the characteristic curves of each type. If an initial value curve is spacelike, it lies outside the region between the directions of the two characteristic curves; if it is timelike, it lies inside the region between the directions of the characteristic curves. If an initial value curve coincides with a characteristic, a point moving along the curve moves with respect to the local flow with the velocity of sound, i.e.,

$$|dx/dt| = c$$

The x-axis is spacelike. The path of a piston moving subsonically with respect to the local flow is timelike.

If the values of the dependent variables u and σ (or Γ and $\overline{\Gamma}$) are changed at a particular point, this change can only affect the properties of the flow in a *region of influence* of that point, which is the angular region between the characteristics through the point. The region of influence of a point P is sketched in Fig. 2-2. Now, consider the arc AB of a spacelike initial value curve, as shown in Fig. 2-3. It is evident that points in the x-t plane lying outside of the region enclosed by the C_+ characteristic through A, the C_- characteristic through B and the arc AB are unaffected by the values of the dependent variables on the arc AB. The region thus enclosed is called the *domain of dependence* of the spacelike arc AB since this region contains all of the flow determined by the given initial values on AB, including the end points, then the flow is unique and continuous in the domain of dependence, including its boundaries. If the arc AB is on a timelike curve, a second intersecting curve—which may be either another timelike curve or a characteristic curve—is required, as shown in Fig. 2-4, to obtain a downstream domain of dependence. It can be shown that only one dependent variable must be specified on each such timelike or characteristic curve (both being known at the intersection) to obtain a unique flow in the domain of independence.

In certain flows, the invariant s is constant over a certain region. The C_+ characteristic curves are then straight lines, as has already been mentioned. Flows of this type are called progressive simple waves. As an example of this type of flow, consider the case of an infinite

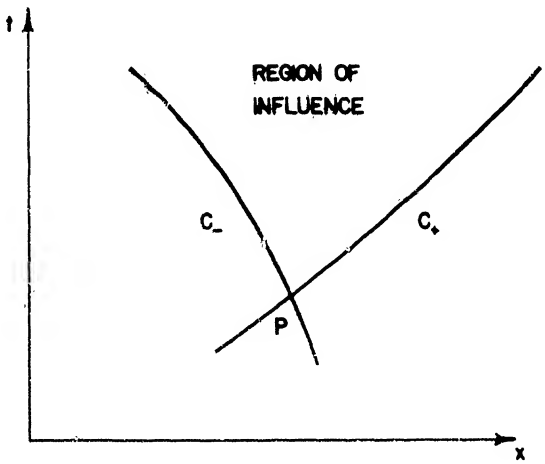

Figure 2-2. Region of Influence of a Point P

tube closed at one end by a piston initially at rest. At the initial instant of time, the material in the cylinder is at rest with $u = \sigma = 0$ (the lower limit of integration of Eq. 2-120 is here taken to be ρ_o, the density of the undisturbed material). Thus, on the spacelike x-axis, $\bar{r} = \bar{s} = 0$. Therefore, both kinds of characteristic curves originating on the x-axis are straight lines. The C_- characteristics through points on the x-axis cover the whole x-t plane since the tube is supposed to be infinitely long. Therefore, if $\bar{s} = 0$ on the x-axis; $\bar{s} = 0$, $u = \sigma$, and $\bar{r} = 2u$ everywhere, and the C_+ characteristics are straight lines everywhere. Suppose as shown in Fig. 2-5, that the piston begins to move in the negative x-direction at the initial instant of time thus initiating a rarefaction wave moving down the tube in the positive x-direction. The particle velocity on the piston path is equal to the piston velocity and r is known on this path. Since the C_+ characteristics are straight lines, their slope is constant. Since $\bar{r}$ is changing from one C_+ characteristic to another, the slopes of the C_+ characteristics increase in moving backward into the flow and the C_- characteristics are curved. If the piston path is specified, an analytic solution of the flow equations is easily constructed. Now suppose that the acceleration of the piston ceases and its (backward) velocity becomes constant. The characteristics of both types originating on this part of the piston path are then straight lines. The flow in the x-t plane thus consists of three regions:

(1) The initial undisturbed region of uniform density and zero particle velocity between the x-axis and the C_+ characteristic labeled A in Fig. 2-5.

(2) The simple wave generated by the accelerating piston in the region between the C_+ characteristics labeled A and B.

(3) The final state in the region to the left of the C_+ characteristic labeled B of uniform density and particle velocity accommodated to the piston velocity.

It will be noticed that the front of the rarefaction wave propagates with the velocity of

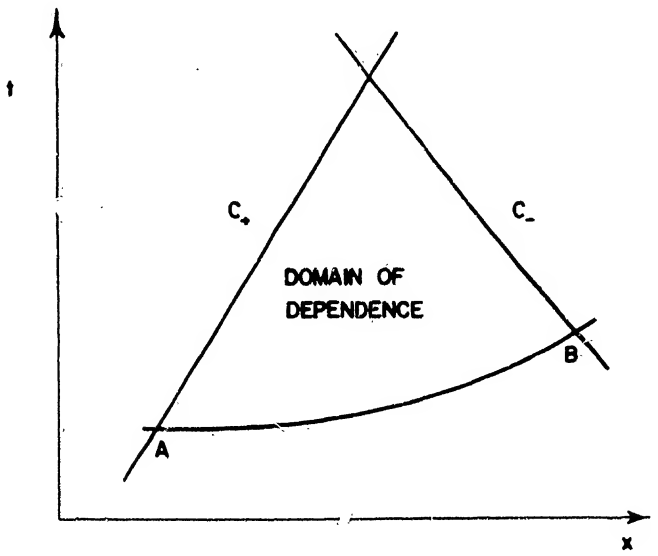

Figure 2-3. Domain of Dependence of Arc AB of a Spacelike Initial Value Curve

sound in the undisturbed medium while the rear of the wave propagates with the velocity of sound in the final medium of reduced density plus the (negative) particle velocity in the final medium. Therefore, the rarefaction wave broadens as it passes down the tube, and no strong discontinuities occur. If the piston had been instantaneously accelerated to its final velocity, all of the C_+ characteristics in the wave region would have emerged from the point at which the piston motion began. Such a wave is called a *centered* simple wave.

Now, in contrast to the flow just discussed, suppose that the direction of the piston is in the positive x-direction, as shown in Fig. 2-6, generating a progressive compression wave. The resulting flow remains a simple wave with $\bar{v} = 0$ everywhere and, consequently, with C_+ characteristics that are straight lines. In this case, however, the C_+ characteristics originating on the piston path do not diverge but converge, and they must in consequence intersect. It has been noted that the flow cannot remain continuous if two characteristics of the same type overtake each other, for different values of the flow variables obtain on each of the intersecting characteristics. The discontinuity that appears in a progressive compression wave is called a *shock wave* and, in any such compression wave, shock waves form in the body of the fluid. The boundary between a region where characteristics of the same type intersect and one where they do not is an envelope of these characteristics. Intersecting characteristics of the same type being physically impossible, the shock wave begins at the first point of that envelope. If the piston is instantaneously accelerated to some final finite velocity, the envelope begins on the piston path.

It can be concluded that compression waves of finite amplitude cannot propagate without the formation of shock waves. Each of the two

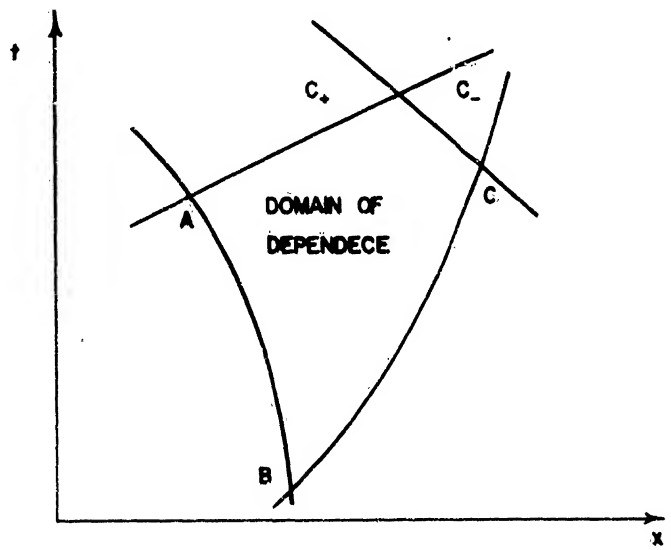

Figure 2-4. Domain of Dependence of Arc AB of a Timelike Initial Value Curve and Arc BC of a Timelike or Characteristic Initial Value Curve

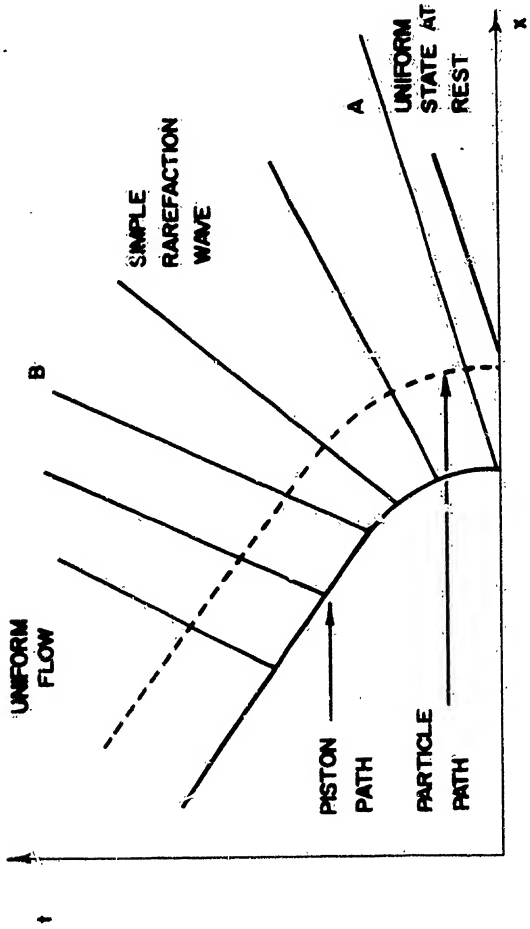

Figure 2-5. Straight Characteristics C_+, Piston Path, and Particle Path in a Simple Rarefaction Wave

characteristic curves passing through a point corresponds to a sound wave, the one to a forward-moving wave and the other to a backward-moving wave. The intersection of two C_+ characteristics corresponds physically to the overtaking of one forward-moving sound wave by a later one with higher velocity. When later sound waves overtake earlier ones, there is a steepening of wave profiles until discontinuities of the dependent quantities velocity, pressure, and density are formed. That such discontinuities should form in the case of compression waves supported by an accelerating piston is apparent in the fact that the sound velocity is greater in the compressed, adiabatically heated medium resulting from the piston motion than in the undisturbed medium.

The one-dimensional unsteady flow equations that have been discussed in this paragraph are an example of a general case involving two simultaneous first order partial differential equations for which two real characteristic directions can be defined and which, for that reason, are said to form a hyperbolic system. If the equations are linear, as in the example of this paragraph, they are said to be reducible. The equations for two-dimensional, steady, irrotational, uniformly isentropic flow form such a reducible hyperbolic system. The theory of hyperbolic systems of equations is treated in detail by Courant and Friedrichs[3].

2-8 CONSERVATION CONDITIONS AT A DISCONTINUITY. THE HUGONIOT EQUATION

A shock wave consists of a very thin region in which the properties of the undisturbed medium very rapidly become those of the shocked medium. The structure of this region is determined by the viscosity of the medium and is affected by the irreversible process of heat conduction along the very steep temperature

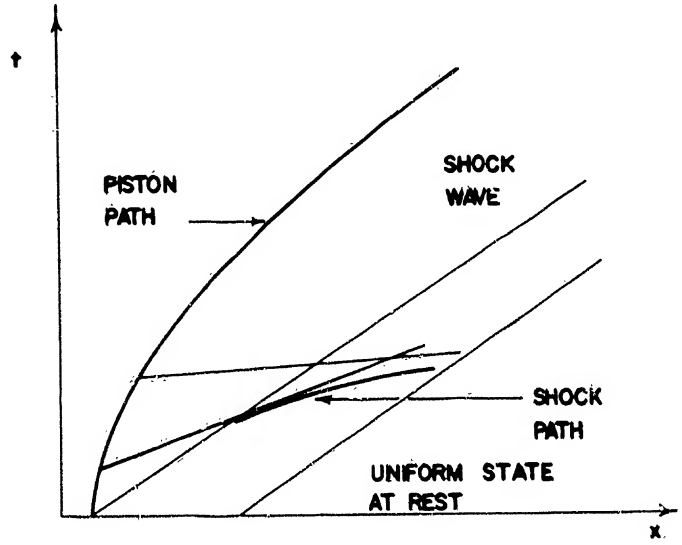

Figure 2-6. Intersecting Straight Characteristics C_+ During Compression Wave

gradient existing in the transition region. In the mathematical treatment of shock waves, it is usual to idealize them by supposing that the dependent variables change discontinuously from their initial to their final states at a mathematical surface of zero thickness. It can be assumed that (1) the flow involving such a discontinuity is determined by the laws of conservation of mass, momentum, and energy; and that (2) the irreversible nature of the discontinuous process is described by the condition that the entropy does not decrease. Apart from the discontinuity, the flow can be described by the differential equations for continuous flow described in par. 2-6. A more complete discussion of shock waves is given by Rice, McQueen, and Walsh[11].

We consider a shock wave propagating in one dimension in the direction of increasing values of the coordinate x, and we denote its velocity with respect to the undisturbed material by U. Employing the notation exemplified in Fig. 2-7, we fix the origin of the x-coordinate in the moving shock wave and denote the velocity of undisturbed material and shocked material with respect to this origin and in the direction of increasing x by w_o and w_1, respectively. If u_o and u_1 are the corresponding velocities relative to a fixed coordinate system,

$$w_o = -U, \; w_1 = u_1 - u_o - U \qquad (2\text{-}128)$$

The undisturbed medium is at pressure p_o, density ρ_o, and has specific energy e_o; and the shocked material is at pressure p_1, density ρ_1, and has specific energy e_1.

In a time dt, an amount of mass $-\rho_o w_o dt$ is brought up to a unit area of the moving discontinuity from the right and an amount of mass $-\rho_1 w_1 dt$ is removed from unit area to the left. When dt is made very small so that the layers on either side of the discontinuity are infinitesimal, the mass brought up on the right must equal that removed to the left, so that

$$\rho_o w_o = \rho_1 w_1 \qquad (2\text{-}129)$$

even if U is not a constant. Similarly, the change in momentum of a thin slice of matter of mass $\rho_o w_o$ per unit area must be equal to the resultant force acting on unit area, so that

$$\rho_o w_o^2 - \rho_1 w_1^2 = p_1 - p_o \qquad (2\text{-}130)$$

even if U is not a constant. Finally, the work done on the matter in the thin slice by the forces acting on it must be equal to the increase in energy of the matter in the slice, so that

$$e_1 + w_1^2/2 - e_o - w_o^2/2 = p_o v_o - p_1 v_1 \qquad (2\text{-}131)$$

even if U is not a constant. For the irreversible process at the shock discontinuity, the second law of thermodynamics requires that

$$s_1 > s_o \qquad (2\text{-}132)$$

By rearrangement, Eqs. 2-129 and 2-130 may be written in the form

$$\left.\begin{aligned} \rho_o w_o &= \rho_1 w_1 \\ p_1 - p_o &= \rho_o w_o (w_o - w_1) \end{aligned}\right\} \qquad (2\text{-}133)$$

Eqs. 2-133 are called the mechanical conservation conditions. When they are used to

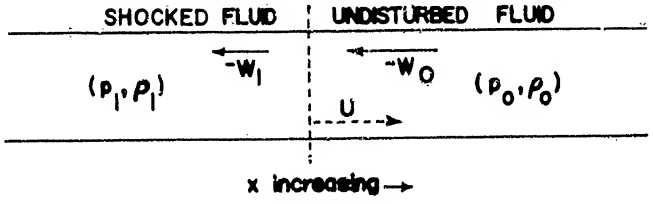

Figure 2-7. One-dimensional Shock Wave

simplify Eq. 2-131, we obtain

$$e_1 - e_o = \tfrac{1}{2}(p_1 + p_o)(v_o - v_1) \qquad (2\text{-}134)$$

Eq. 2-134 was obtained by Rankine and by Hugoniot, and it is called the Rankine-Hugoniot equation. It contains thermodynamic quantities only. With thermal data and an equation of state of the material, the quantities $e_1 = e(p_1, v_1)$ and $e_o = e(p_o, v_o)$ are determined, and therefore Eq. 2-134 describes a curve in the p-t plane for given values of p_o and v_o, which is the locus of all states (p_1, v_1) which satisfy the conservation conditions for a given initial undisturbed state. The curve is called the Hugoniot curve and it is said to be centered on the point (p_o, v_o).

Shock waves are stable, i.e. they do not break up into several shocks nor become a gradually rising wave, if the isentropes satisfy the condition

$$\left(\frac{\partial^2 p}{\partial v^2}\right)_s > 0$$

When this condition is satisfied, the Hugoniot curve represents states which can be reached by a shock process from the initial state (p_o, v_o), and shock wave of rarefaction do not exist.

If the state of the fluid is known on one side of the shock wave, the shock velocity and state on the other side of the shock wave are completely determined by Eqs. 2-133 and 2-134 if one additional quantity is given. The additional quantity may be either a state variable, the shock wave velocity or the particle velocity, except that if the particle velocity is given as the additional quantity, it is necessary to specify which is the downstream side of the shock wave.

Additional properties of the shock wave can be deduced directly from Eqs. 2-133. Since $p_1 > p_o$, it follows that $w_o > w_1$, i.e., that the flow is decelerated in passing through the shock front. It then follows that $\rho_1 > \rho_o$, from the first of the mechanical conditions. It can also be shown—as, e.g., by Courant and Friedrichs—that the flow velocity relative to a shock wave is supersonic ahead of the wave and subsonic behind it. Therefore, C_+ characteristics through a point behind a shock wave overtake the wave and the shock overtakes C_+ characteristics ahead of it. Fig. 2-8 illustrates the flow in a steady plane shock wave supported by a piston propagating into a uniform fluid at rest.

For many applications of the shock wave conservation equations, the undisturbed medium is at rest in a stationary coordinate system. For this case, the mechanical conservation conditions can be written in the form

$$\left.\begin{aligned} u_1 &= U(1 - \rho_o v_1) \\ p_1 - p_o &= \rho_o u_1 U \end{aligned}\right\} \qquad (2\text{-}135)$$

In this case, the particle velocity of the shocked material is seen to be directed toward the shock front.

The conservation equations of this paragraph provide relations between the dependent variables on the two sides of the shock discontinuity. In the regions where the flow is continuous, it is described by the differential equations of par. 2-6. The complete flow is thus determined by solutions of the differential equations that are subject to conditions specified on the shock path which is to be regarded as a kind of initial value curve.

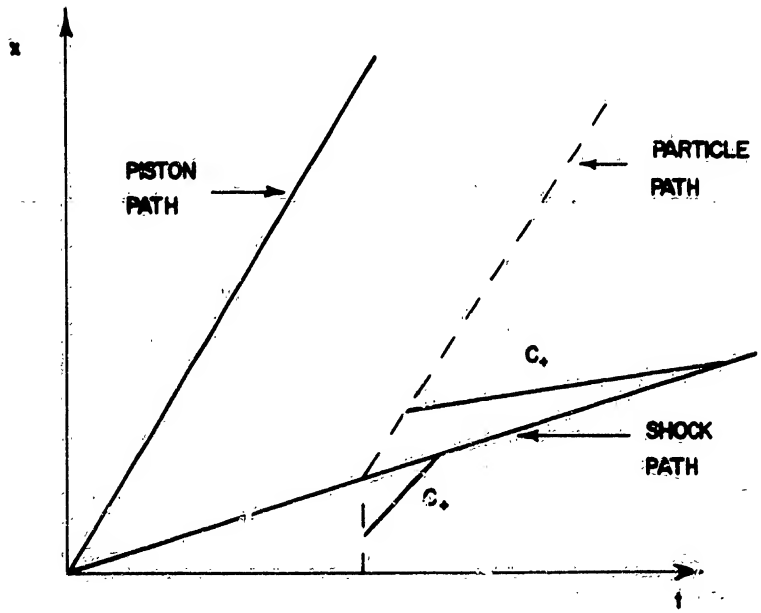

Figure 2-8. Flow in a Steady One-dimensional Shock Supported by a Piston, Showing a Particle Path and C_+ Characteristics Through Points on the Particle Path

REFERENCES

1. J. Willard Gibbs, *The Scientific Papers of J. Willard Gibbs*, Vol. 1, *Thermodynamics*, Dover Publications, Inc., New York, New York, 1961.
2. E. A. Guggenheim, *Thermodynamics, An Advanced Treatment for Chemist and Physicists*, Interscience Publishers, New York, 1957.
3. R. Courant and K. O. Friedrichs, *Supersonic Flow and Shock Waves*, Interscience Publishers, Inc., New York, 1948.
4. R. D. Richtmeyer and K. W. Morton, *Difference Methods for Initial Value Problems*, 2nd Edition, Interscience Publishers, New York, 1967.
5. S. R. Brinkley, Jr., "Note on the Conditions of Equilibrium for Systems of Many Constituents", J. Chem. Phys. 14, 563-564, 686 (1946).
6. S. R. Brinkley, Jr., "Calculations of the Equilibrium Composition of Systems of Many Constituents", J. Chem. Phys. 15, 107-110 (1947).
7. S. R. Brinkley, Jr., "Computational Methods in Combustion Calculations", *High Speed Aerodynamics and Jet Propulsion—Combustion Processes*, Princeton Univ. Press, Princeton, New Jersey, 1956, Vol. II, pp. 64-97.
8. J. M. Richardson and S. R. Brinkley, Jr., "Mechanics of Reacting Continua", *High Speed Aerodynamics and Jet Propulsion—Combustion Processes*, Princeton Univ. Press, Princeton, New Jersey, 1956, Vol. II, pp. 203-15.
9. William Band, *Introduction to Mathematical Physics*, Van Nostrand, Princeton, New Jersey, 1959.
10. J. Willard Gibbs, *Vector Analysis*, Dover Publications, Inc., New York, New York, 1960.
11. M. H. Rice, R. G. McQueen, and J. M. Walsh, "Compression of Solids by Strong Shock Waves", *Solid State Physics*, Vol. 6, F. Seitz and D. Turnbull, Ed., Academic Press, New York, 1958.

CHAPTER 3 ENERGY OF EXPLOSIVES

3-1 INTRODUCTION

Explosives are substances that rapidly liberate their chemical energy as heat to form gaseous and solid decomposition products at high pressure and temperature. The hot and very dense detonation products produce shock waves in the surrounding medium and upon expansion impart kinetic energy to the surrounding medium. The energy released in the detonation process and the energy available after some degree of expansion respectively measure the ability of the explosive to generate shocks and to impart motion to the environment. Consequently the energy of an explosive is a measure of its performance. Moreover the heat release in the detonation is an important quantity, as will be shown, in the thermo-hydrodynamic Chapman-Jouguet (C-J) theory of detonation (see Chapter 6 for a discussion of the C-J theory).

3-2 HEAT OF DETONATION

In principle, Q, the heat released in a detonation, is obtained for some standard state by Hess' law according to

$$Q = \sum^{i}_{n} n_i (\Delta H_f^\circ)_i - \sum^{m} m_j (\Delta H_f^\circ)_j \qquad (3\text{-}1)$$

where n_i is the number of moles the *i-th* species of detonation products whose standard heat of formation is $(\Delta H_f^\circ)_i$ and m_j is the number of moles of unreacted explosive of the *j-th* species whose standard heat of formation is $(\Delta H_f^\circ)_j$. If the Lewis and Randall convention is used, the right hand side of Eq. 3-1 would be negative for an exothermic reaction. However, it is customary to have Q positive for exothermic reactions. Thus $Q = -\Delta H_{reaction}$ where $\Delta H_{reaction}$ is the right hand side of Eq. 3-1. In practice it turns out that the compositions of the detonation products in the C-J state, or at different degrees of expansion, are unknown. Since chemical equilibria can be influenced by the total pressure of the system, the product composition and consequently Q can change as the products expand and the total pressure decreases. Expansion also results in cooling and consequent product composition change. Below some temperature, chemical reaction rates become so slow that further temperature and pressure decrease (expansion) produces virtually no further change in composition, i.e., the composition is "frozen". Thus any calorimetric measurement of the heat of detonation ΔH_d, may not be the Q for the C-J state, but the heat of reaction for some expanded "frozen" equilibrium composition. Measured heats of reaction will vary depending on how the calorimeter measurements are made, i.e., on how much the products are allowed to expand before the composition is frozen. This is probably the main reason why many conflicting values of ΔH_d have been reported. Further confusion arises from the fact that sometimes calorimetric heats of detonation are "corrected" for the heat of vaporization of water (one of the major detonation products in secondary explosives). In a calorimeter measurement water is in its liquid state, but under detonation conditions it is in the gaseous state. Thus to obtain Q from calorimeter measurements a heat of vaporization correction should be made, but unfortunately it is not always possible to estimate how much water was present under detonation conditions even though the amount of water formed during the reaction in the calorimeter has been determined.

3-3 THERMOCHEMISTRY OF HIGH EXPLOSIVES

Thermochemical data and empirical formulas for several explosives, explosive mixtures, and ingredients of explosive mixtures are given in Table 3-1, together with data for their major decomposition products. These are important quantities from which theoretical properties of explosives can be calculated. There is no obvious correlation between ΔH_f° or ΔH_d and the "stability" or "sensitivity" of an explosive. For example, NG and PETN which are known to be "sensitive" have large negative ΔH_f°'s, i.e., these compounds are thermally stable with respect to their constituent elements. On the other hand TNT which is quite "insensitive" is almost thermoneutral with respect to its elements.

HMX and RDX which are certainly less "sensitive" than PETN or NG are thermally unstable with respect to their elements. Similarly ΔH_d's do not correlate with sensitivity, e.g., tetryl is much more "sensitive" than nitromethane but $(\Delta H_d)_{NM} > (\Delta H_d)_{tetryl}$. Moreover it does not necessarily follow that a positive ΔH_f° results in a large ΔH_d, e.g., $(\Delta H_d)_{tetryl} < (\Delta H_d)_{PETN}$.

By far the best available determinations of ΔH_d and product composition are those of Ornellas[1]. His results are given in Table 3-2. Note the excellent thermal and material balance obtained. Certain useful generalization can be drawn from these data, namely:

1. Confinement increases ΔH_d and changes product composition in oxygen-negative explosives but not in oxygen-balanced explosives (see par. 3-4 and Table 3-6).

2. In confined oxygen-negative explosives, at large packing density, an appreciable amount of solid carbon is found in the products even though sufficient oxygen is available to form CO, e.g., in HMX.

3. The fluorine of fluorine-containing explosives appears as HF in the detonation products.

Consider the data of Ornellas (Table 3-2) for unconfined explosives. If the products for unconfined shots expand very rapidly so that the pressure becomes much less than P_{CJ} at T_{fr}, the temperature at which equilibria are frozen, then these products should approach perfect gas behavior at T_{fr}. If we know the equilibria involved and their ideal equilibrium constants as a function of temperature, we can compute T_{fr}. Table 3-3 gives the free energy function G°/RT for the important detonation products of CHNO* explosives. From these data $\Delta G^\circ/(RT)$ can be obtained for different temperatures for the reactions of interest, and ideal equilibrium constants computed according to

$$\ell nK = -\Delta G^\circ/(RT) \qquad (3\text{-}2)$$

where

G° = standard state Gibbs free energy
R = gas constant
T = absolute temperature

Let us assume that the water-gas reaction

$$CO_2 + H_2 = CO + H_2O \qquad (a)$$

is the controlling equilibrium. To illustrate the computation we will use PETN, $C_5H_8N_4O_{12}$, as an example. Let X be the number of moles of CO_2 at equilibrium, and C, H, O the original gram atoms of carbon, hydrogen and oxygen respectively. Then from mass balance and Raoult's law

$$\left.\begin{aligned} p_{CO} &= \frac{P(C-X)}{n_t} \\ p_{CO_2} &= \frac{PX}{n_t} \\ p_{H_2O} &= \frac{P}{n_t}(O-C-X) \\ p_{H_2} &= \frac{P}{n_t}(\tfrac{1}{2}H+C-O+X) \end{aligned}\right\} \qquad (3\text{-}3)$$

where

n_t = total number of moles of gas at equilibrium
p = partial pressure
P = total pressure at equilibrium

The ideal equilibrium constant for reaction (a) is

$$K_a = \frac{p_{CO}p_{H_2O}}{p_{CO_2}p_{H_2}} = \frac{(C-X)(O-C-X)}{X(\tfrac{1}{2}CH+C-O+X)} = \frac{(5-X)(7-X)}{X(X-3)}$$

For PETN with $K = 2.96$ corresponding to $T_{fr} = 1600°K$:

X = 3.50 = moles CO_2 per mole of PETN
$C-X$ = 1.50 = moles CO per mole of PETN
$O-C-X$ = 3.50 = moles H_2O per mole of PETN
$\tfrac{1}{2}H+C-O+X$ = 0.50 = moles H_2 per mole of PETN
$N/2$ = 2.00 = moles N_2 per mole of PETN

This equilibrium mixture matches almost exactly the composition found by Ornellas[1] for unconfined PETN (see Table 3-2). In Table 3-4 we show that for $T_{fr} = 1600°K$ the computed ideal gas mixtures for HMX, TNT, as well as PETN, agree closely with the results of Ornellas for unconfined charges.

Other reactions which must be considered at high pressures (confined charges) are

$$2CO = CO_2 + C(s) \qquad (b)$$

$$CO + H_2 = H_2O + C(s) \qquad (c)$$

* Since these are the explosives of military interest all the subsequent discussion in this chapter will be confined to CHNO explosives.

At low total pressures (unconfined charges) the data in Table 3-3 give $K_c \approx 9 \times 10^{-5}$ and $K_b \approx 4 \times 10^{-5}$ for the equilibria (b) and (c) at T_{fr} = 1600° K. Thus the neglect of reactions (b) and (c) at low pressure is entirely justified. According to Le Chatelier's Principle, reactions (b) and (c) will shift to the right at high pressure, and we should expect more CO_2, H_2O and C(s) for confined charges than for unconfined charges. At high pressures, the ideal gas laws are no longer applicable and simple computations of equilibrium compositions are no longer possible without the appropriate *PVT* equation of state for the products. Ornellas[1] has made computations for C-J isentrope compositions at 1500° K and at 1800° K using the Becker-Kistiakowsky-Wilson (BKW) and Lennard-Jones Devonshire (LJD) equations of state for the products. Agreement between observed and computed product compositions is quite good. This suggests that T_{fr} for confined charges is between 1500° and 1800° K in agreement with T_{fr} = 1600° K for unconfined charges.

At high pressures and temperatures of the order of 1500° to 2000° K the reactions

$$N_2 + 3H_2 = 2NH_3 \qquad (d)$$

$$C(s) + 2H_2 = CH_4 \qquad (e)$$

are no longer neglible if the equilibrium mixture (before considering reactions (d) and (e)) contains appreciable H_2. Equilibria (a) through (e) account for all the observed products (Table 3-2) with the exception of very minor amounts of HCN.

3-4 COMPUTATION OF *Q*

Examination of computations for unconfined charges (perfect gas) as well as the more elaborate calculations for confined charges BKW, LJD, etc.) clearly show that when an explosive contains sufficient oxygen to convert all its hydrogen to steam and its carbon to CO_2 (oxygen-balanced), the water gas equilibrium completely determines the composition of the products. This equilibrium is rather insensitive to the total pressure at equilibrium. Confirmation of these theoretical computations is found in Ornellas' data for confined and unconfined PETN (Table 3-2) which show essentially the same product composition at high pressure and at ambient pressure. Conversely, in oxygen deficient explosives equilibria (b) through (e) play an important role and as expected, the product compositions for an oxygen-negative explosive are very different for confined and unconfined charges (Table 3-2).

We now return to the question of *Q* the heat released in a detonation and its relationship to ΔH_d which is determined calorimetrically. *Q* cannot be measured directly. It can be computed if a *PVT* equation of state is known for the dense detonation products. Since there is no general agreement about the proper form of a *PVT* equation of state for detonation products, the best we can do is to compare *Q*'s computed with different equations of state. This is done in Table 3-5 using three rather different equations of state. Somewhat unexpectedly it turns out that *Q* is quite insensitive to the type of equation of state used. Thus *Q*'s computed, for a given explosive at a given density but using different equations of state, agree closely. What appears to be even more remarkable is that for explosives that are not too deficient in oxygen

$$Q \approx \Delta H_d \qquad (3\text{-}4)$$

and for oxygen deficient explosives

$$Q \approx 1.1\,\Delta H_d \qquad (3\text{-}5)$$

where the calorimetric measurements ΔH_d were made on confined explosives. Actually this coincidence is not totally unexpected. In a calorimeter water is in the liquid state and even for strong confinement one might expect some pressure drop before the thermal measurements are completed. In the C-J state, water is gaseous and the pressure is at its highest possible level. If there were no pressure drop, then $\Delta H_d > Q$ by the heat of vaporization of water. However there is some pressure drop and, consequently, the equilibria of such reactions as (b) and (c) lie further to the right in the C-J state than in the calorimeter. Reactions (b) and (c) (as well as (d) and (e) the less important reactions) are exothermic, and their greater degree of completion in the C-J state tends to compensate for the effect of the heat of vaporization of water.

Some further conclusions may be drawn from the data in Table 3-5. As already stated, at a

fixed density for a given explosive, Q does not change with the equation of state but the computed C-J temperatures *do change*. The computed C-J pressures (which are generally in reasonable agreement with experiment) *do not change* appreciably with these equations of state, but *do change* strongly with initial density. Now for a given equation of state, a change in initial density produces a much greater change in the computed pressure than in the computed temperature. This computed pressure change is confirmed by experiment. Note that the computed Q for a particular explosive in all cases decreases as the computed pressure decreases but that it is fairly independent of the computed temperatures. This same trend appeared in the data of Table 3-2 where the freeze-out temperatures for all the explosives were about 1600°K but the equilibrium pressures and product compositions varied depending on whether the explosive was confined or unconfined. Thus it appears that product composition (which determines Q) is more strongly influenced by the final pressure than by the final temperature of the system.

The relative nondependence of Q on C-J temperature may be rationalized as follows. For oxygen-balanced or oxygen-rich explosives, the water gas equilibrium (reaction(a)) is the primary reaction which determines the product composition. This equilibrium changes rather slowly with temperature and furthermore small changes in equilibrium composition produce very little change in Q because reaction (a) is almost thermo-neutral, i.e., $(\Delta H_f^\circ)_{CO_2} \approx (\Delta H_f^\circ)_{CO} + (\Delta H_f^\circ)_{H_2O}$. For oxygen-poor explosives the explanation is not as apparent. Reactions (b) and (c) are sensitive to temperature, and they are not thermo-neutral. It may be that equilibria (b) and (c) lie far to the right (as written) over wide ranges of detonation temperature and pressure.

Two further generalizations can be made about the results in Table 3-5. If we arrange explosives according to their oxygen balance in order of increasing unbalance, as we have done in Table 3-6, then it becomes apparent that the largest Q's are obtained with balanced explosives and that the Q's decrease fairly slowly for moderately oxygen-poor explosives, and more rapidly for oxygen-rich explosives. The reader must be warned that there are exceptions to this generalization—(e.g., Explosive D and Hydrazine nitrate in Table 3-6).

A more fruitful approach to *a priori* estimates of Q is shown in Table 3-7. It is clear that Q's based on the best available computations agree closely with Q_A's computed solely on the basis of initial explosive composition and thermochemistry with the arbitrary assumptions:

(1) All the initially available hydrogen forms steam.

(2) Any oxygen remaining forms CO_2.

(3) Any carbon remaining appears as solid graphite.

(4) All the nitrogen goes to N_2.

Thus quite accurate estimates of Q appear possible if the initial explosive composition and ΔH_f° of this composition are known.

3-5 FRAGMENT VELOCITIES

One of the most useful functions of a secondary explosive is its ability to produce and accelerate fragments formed from its immediate environment. It seems likely that the efficiency of an explosive in accelerating fragments should be related to the energy contained in the explosive. The discussion which follows will show that this expectation is fulfilled.

The so-called Gurney formulas[5] are very successful in determining terminal fragment velocities. These formulas are derived on the basis of three fundamental assumptions, namely:

(1) The chemical energy of the explosive is converted into kinetic energy of fragments and detonation products.

(2) The velocity distribution of the detonation products varies linearly from zero to the velocity of the fragment.

(3) The density of the products is uniform or at lease independent of position, i.e., $\rho = \rho(t)$ but $\rho \neq \rho(x)$.

For cased cylindrical explosive charges these assumptions lead to

$$V = \sqrt{2E}\sqrt{\frac{C/M}{1 + C/2M}} \qquad (3\text{-}6)$$

where

V = terminal fragment velocity (no air drag)
$\sqrt{2E}$ = empirical Gurney constant (having the dimensions of V)
C = weight of explosive
M = weight of casing

For the case of a plane wave detonation accelerating a flat plate, the Gurney formula is

$$V = \sqrt{2E}\sqrt{\frac{3}{1 + 5M/C + 4(M/C)^2}} \qquad (3\text{-}7)$$

Gurney constants computed from experimental data obtained from several sources are compared with Q in Table 3-8. On the average (with Q obtained from Eq. 3-4, using experimental ΔH_d) $\sqrt{2E}/\sqrt{2Q} \approx 0.95$, however, there may be a trend for this ratio to decrease as ρ_o decreases. The results for TNT are contradictory. The only available information for nitromethane (NM) makes it appear as an inefficient plate driving explosive. Nevertheless, the data in Table 3-8 clearly show that in one-dimensional detonations the chemical energy of explosives is very efficiently converted into kinetic energy (around 90% conversion) of fragments and explosion products.

3-6 AIR-BLAST

The efficiency of an explosive in producing air-blast is usually given in terms of equivalent weight, i.e., the weight of TNT (or some other standard explosive) to give the same air-blast overpressure as the test explosive where both measurements are made at a fixed distance from the charges (see Chapter 13). For measurements made far away from the explosive charge, Landau and Lifshitz[2] have shown that the overpressure is proportional to the initial energy of the explosive, i.e., to mQ where m is the mass of explosive; consequently,

$$\text{equivalent weight} = m^o/m = Q/Q^o \qquad (3\text{-}8)$$

where the superscript o refers to the standard explosive.

Experimental equivalent weights are compared to computed Q/Q_{TNT} and to experimental $\Delta H_d/(\Delta H_d)_{TNT}$ in Table 3-9. Agreement between m_{TNT}/m and Q/Q_{TNT} is seen to be quite good. $\Delta H_d/(\Delta H_d)_{TNT} > m_{TNT}/m$ except for Comp. B and Pentolite which contain large proportions of TNT. This is not surprising since it is Q and not ΔH_d which should correlate with equivalent weights. Using the approximation of Eq. 3-5 brings the ΔH_d ratios into much better agreement with the equivalent weight ratios, except in the case of aluminized explosives for which the "corrected" ΔH_d ratio is still greater than the equivalent weight ratio. This suggests that in unconfined aluminized explosive charges the aluminum does not contribute all its chemical energy presumably because the aluminum reactions are slower than the other detonation reactions.

3-7 UNDERWATER PERFORMANCE

Price[3] has suggested that a criterion of the underwater performance of an explosive is given by the sum of the shock wave energy (at a fixed distance which is large compared to the explosive dimensions) and the oscillating bubble energy. To a first approximation both shock energy and bubble vary directly with explosive weight, and the sum should be approximately equal to the chemical energy of the explosive[4]. Consequently, Eq. 3-8 is also applicable to underwater explosions if the m's are the sums of equivalent weights for shock wave and bubble energies. The data in Table 3-10 show excellent agreement between equivalent weights and Q/Q_{TNT} except for two explosives (TNETB and PETN) which have only slight oxygen deficiences. As discussed in par. 3-3 the composition and, consequently, Q for these two explosives do not change with confinement. For the other explosives in Table 3-10, and particularly for TNT, composition could be affected by confinement in the direction of smaller Q as confinement is reduced. It is conceivable that the computed Q's for the oxygen negative explosives are overestimates of the actual Q's for the conditions of the experiment, and consequently Q_{PETN}/Q_{TNT} or Q_{TNETB}/Q_{TNT} should be larger than shown in Table 3-10.

Note that aluminum greatly adds to the underwater performance of aluminized explosives. Presumably this is due to the longer confinement period of the surrounding water which allows the aluminum reactions to go to completion before too much expansion occurs.

3-8 C-J PARAMETERS

In par. 3-4 we indicated that calculated Q's for dense explosives are insensitive to the form of *PVT* equation of state used in the computation. This means that Q, if available experimentally, is a poor criterion for choosing the best equation of state. On the other hand quite good estimates of Q appear possible based on Q_A or ΔH_d. These estimates can then be used to get approximate values of T_V the equilibrium temperature of a constant volume explosion, P_{CJ} the Chapman-Jouguet pressure, and D the steady detonation velocity. Approximate values for T_V can be obtained from

$$T_V \approx \frac{Q_A}{\Sigma n_i \bar{c}_i} + T_o \qquad (3\text{-}9)$$

where

Q_A = heat released in an explosion computed on initial explosive composition and thermochemistry and arbitrary assignment of products shown in par. 3-4.

n_i = number of moles of gas at equilibrium estimated from arbitrary reactions used in obtaining Q_A

$\bar{c}_i$ = specific heats of products averaged over the temperature range $T_V - T_o$

The T_V obtained from Eq. 3-9 should represent an upper limit to T_{CJ}, since all the chemical energy is assumed to go into thermal energy of the products and no allowance is made for energy of repulsion which surely must be present in the highly compressed C-J state. If the detonation products obey the polytropic gas law, i.e., PV^{κ} = constant, then

$$D \approx 2Q_A(\kappa^2-1) \qquad (3\text{-}10)$$

and

$$P_{CJ} \approx 2Q_A \rho_o(\kappa - 1) \qquad (3\text{-}11)$$

Agreement between experimental values of D and P_{CJ}, and those computed using Eqs. 3-10 and 3-11 is only moderately good. Using Q_A (or Q) and $\kappa = 2.5$ the average deviation of computed and experimental D's (detonation velocity) is 5% (+5 to -13% maximum deviation) for 13 almost voidless explosives. For these same explosives the average deviation of computed and experimental P_{CJ} is 6%(+15 to -11% maximum deviation). For ten other explosives for which experimental data are also available the deviation is greater than that given. Seven of these ten explosives contain NM or TNM or both. For other values of κ, agreement is even poorer.

A better approach for estimating P_{CJ} is to use experimental D values which are often available where experimental P_{CJ} data are not. A convenient equation to use is

$$P_{CJ} = \frac{\rho_o D^2}{\kappa + 1} \qquad (3\text{-}12)$$

Calculations on 26 explosives (some of these are at about 1/2 of voidless density), using Eq. 3-12 and experimental D and P_{CJ}, give an average κ of 2.8 with a maximum range of 2.4 to 3.0. Four explosives which give κ's outside the above range are NM, TNM and two aluminized Comp B mixtures.

3-9 MAXIMUM WORK

In an adiabatic process, according to the first law, the maximum work W_{max} that an element of explosive can do on its surroundings is $-\Delta E$ (note that the term adiabatic refers to no heat gain or loss by the element from or to the surroundings). For a constant volume explosion, explosion products (formed in an exo-thermic reaction) assumed to be a polytropic gas, and neglecting the Pv term for the solid unreacted explosive,

$$\left.\begin{aligned} \Delta E = E_f - E_o &\approx \Sigma(\Delta H_f^o)_{products} \\ &+ \frac{P_o v_f}{\gamma - 1} - \Sigma(\Delta H_f^o)_{explosive} \\ &= Q_{c.v.} + \frac{P_o v_f}{\gamma - 1} = - W_{max} \end{aligned}\right\} \qquad (3\text{-}13)$$

For a polytropic gas v_f may be related to v_o according to

$$P_i v_o^{\kappa}/2 = P_i v_i^{\kappa} \text{ and } P_i v_i^{\gamma} = P_o v_i^{\gamma}$$

where the subscript i refers to some intermediate state above which the polytropic coefficient is κ and below which the coefficient is $\gamma = c_p/c_v$, $P_{c.v.} = P_i/2$ is the constant volume explosion pressure, and the subscript o refers

to the standard explosive. For typical values of the parameters involved and an arbitrary assignment of $(P_j/P_i)/2 = 10^3$ it can be shown that

$$\frac{P_o v_f}{(\gamma-1)\, Q_{c.v.}} \leq 0.04.$$

Consequently for a constant volume (c.v.) explosion

$$W_{max} \approx Q_{c.v.} \qquad (3\text{-}14)$$

Eq. 3-13 is also applicable to a C-J detonation except that v_f for a C-J detonation is different from v_f for a constant volume explosion. For a C-J detonation

$$P_j v_j^{\kappa} = P_j[v_o \kappa/(\kappa + 1)]^{\kappa}$$

$$= P_i v_i^{\kappa} \text{ and as before } P_i v_i^{\gamma} = P_o v_f^{\gamma}$$

With the same assumptions as before $\frac{P_o v_f}{(\gamma-1)Q} \leq 0.03$ and

$$W_{max} \approx Q \qquad (3\text{-}15)$$

Because the pressures are different and consequently the chemical equilibria could be different Q does not necessarily equal $Q_{c.v.}$. The data in Table 3-5 suggest that $Q > Q_{c.v.}$ because $P_j > P_{c.v.}$.

There are no completely unambiguous measurements of the maximum work done by an explosive; however, the Ballistic Mortar probably comes closest to being a valid test of the maximum work. In this test a standard weight of explosive is fired in a suspended mortar with a tightly fitting steel projectile and the angle of recoil of the mortar is measured. Results are generally expressed in terms of a standard explosive, e.g., TNT. In Table 3-11 we compare measured Ballistic Mortar results with Q where both quantities are taken relative to TNT. It is obvious that correlation is poor. If the comparison is made with ΔH_d rather than Q, correlation is much better and it becomes better yet if one arbitrarily assigns $(\Delta H_d)_{TNT} = 1.00$ kcal/g rather than the measured $(\Delta H_d)_{TNT} = 1.09$ kcal/g for tightly confined charges[1]. As already discussed the heat release of TNT, but not of other explosives such as PETN, is strongly influenced by confinement. The explosive loads in the Ballistic Mortar are generally at fairly low packing densities so that detonation products can expand slightly before the projectile starts to move. During the period of acceleration of the projectile there is further gas expansion and re-equilibration of products. The whole process appears to be quite similar to what is happening in a partially confined charge fired in a calorimeter. Thus one might expect that ΔH_d, and not Q is a better measure of the "maximum work" measured by the Ballistic Mortar. In Table 3-2 we show that ΔH_d for TNT varies from 0.68 to 1.09 kcal/g depending on the degree of confinement. Consequently, the arbitrary choice of $(\Delta H_d)_{TNT} = 1.00$ kcal/g is not unreasonable in this case.

In the Ballistic Mortar, as in air-blast and fragment propulsion, aluminized explosives do not perform as well as expected from their theoretical Q values.

REFERENCES

1. D. L. Ornellas, J. Phys. Chem. 72, 2390 (1968) and Ornellas et al., Rev. of Sci. Instr. 37, 907 (1966).
2. L. D. Landau and E. M. Lifshitz, Fluid Mechanics 6, 372-377, 392-396 (1959).
3. D. Price, Chem. Rev. 59, 821 (1959).
4. R. M. Cole, *Underwater Explosions*, Princeton Univ. Press, Princeton, N. J., 1948.
5. W. Gurney, BRL Report 405, 1943.

TABLE 3-1. SOME BASIC THERMOCHEMICAL DATA

a. Pure Explosives	Empirical Formula	Formula Weight	ΔH_f° [1], kcal/mol	ρ_0, g/cc	ΔH_d [2], kcal/g	Source[3] of ΔH_d
Nitroglycerin (NG)	$C_3H_5N_3O_9$	227	-90.8		-	-
PETN	$C_5H_8N_4O_{12}$	316	-126.7	1.74	1.49	LRL
RDX	$C_3H_6N_6O_6$	296	+ 17.9	1.80	1.46	LRL
TNT	$C_7H_5N_3O_6$	227	- 17.5	1.53	1.09	LRL
Nitromethane (NM)	CH_3NO_2	61	- 27.0	1.13	1.23	LRL
Tetranitromethane (TNM)	$C(NO)_4$	196	+ 13	1.64	-	-
PEPO	$C_3H_6N_4O_{10}F_2$	320	-178.8	1.60	1.28	LRL
HDX	$C_2H_6N_6O_6$	222	+ 31.7	1.63	1.36(a)	LRL
Tetryl	$C_7H_5N_5O_8$	287	+ 8	1.50	1.17	LRL
DATNO	$C_6H_5N_5O_6$	243	- 36.9	1.80	1.01	LRL
TUS	$C_6H_6N_6O_{14}$	386	-118.6	1.70	1.47	NOL
NTNEU	$C_5H_6N_8O_{13}$	386	- 72.4	1.60	1.50	NOL
Picric Acid	$C_6H_3N_3O_7$	229	- 38.3		1.03	ARDE
Ammonium Picrate (explosive D)	$C_6H_6N_4O_7$	246	- 97.0	-	-	-
b. Explosive Mixtures						
PBX9404	$C_{1.40}H_{2.75}N_{2.57}O_{2.69}$	100g	+ 4	1.85	1.40	LAL
Comp B-3	$C_{2.06}H_{2.81}N_{2.18}O_{2.67}$	100g	+ 6	1.69	1.24	LAL
50/50 Cyclotol	$C_{10}H_{11}N_8O_{12}$	449	+ 3.1		1.16	ARDE
60/40 Amatol	$C_{1.88}H_{4.11}N_{1.79}O_{3.09}$	100g	- 48.4	1.66	1.08	NOL
c. Oxidizers						
Ammonium Nitrate (AN)	NH_4NO_3	80	- 87		-	-
Potassium Nitrate (KN)	KNO_3	101.1	-118		-	-
Ammonium Perchlorate (AP)	NH_4ClO_4	117.5	- 71		-	-
Liquid Oxygen (LOX)	O_2	32	- 3		-	-
Tetranitromethane	$C(NO_2)_4$	196	+ 13		-	-
d. Fuels						
Aluminum	Al	27	0		-	-
Carbon	C	12	0		-	-
Petroleum (Pet)	(CH_2)	14	- 7		-	-
Cellulose (Cel)	$(C_6H_{10}O_5)$	162	-224		-	-
Sulfur	S	32	0		-	-
e. Reaction Products						
Carbon Monoxide	CO	28	-26.4		-	-
Carbon Dioxide	CO_2	44	-94.0		-	-
Water (Gas)	H_2O	18	-57.8		-	-
Hydrogen Chloride	HCl	36.5	-22.1		-	-
Hydrogen Fluoride	HF	20	-64.2		-	-
Sulfur Dioxide	SO_2	64	-71.0		-	-
Aluminum Oxide	Al_2O_3	102	-398.1		-	-
Potassium Oxide	K_2O_3	94.2	-86.4		-	-

[1] Standard heat of formation at 298°K and 1 atm.

[2] Calorimetrically determined heat of detonation in inert atmospheres for explosive at ρ_0; explosives were confined unless indicated; $H_2O(\ell)$

[3] LRL = Lawrence Radiation Laboratory
NOL = Naval Ordnance Laboratory
ARDE = Armament Research and Development Establishment (U.K.)

(a) Unconfined.

TABLE 3-2. CALORIMETRIC DETERMINATION OF THE HEAT AND PRODUCTS OF DETONATION[1]

EXPLOSIVE	PETN	PETN	HMX	HMX	TNT	TNT	NM	FEFO
Condition	Confined	Unconfined	Confined	Unconfined	Confined	Unconfined	Confined	Confined
ρ_o (g/cc)	1.74	1.74	1.80	1.80	1.53	1.53	1.13	1.60
ΔH_d (k cal/g)	1.49	1.50	1.48	-	1.09	-	1.23	1.28
$(\Delta H_d)_{cal_c}$ (k cal/g)*	1.50	1.51	1.51	1.33	1.16	0.68	1.25	1.35
Products Mole/mole								
CO_2	3.39	3.50	1.92	1.44	1.25	0.063	0.261	3.16
CO	1.64	1.59	1.06	2.65	1.98	5.89	0.550	1.88
CH_4	0.003	<0.0002	0.039	0.0006	0.099	0.009	0.083	0.001
C(s)	none	none	0.97	none	3.65	1.01	0.095	none
$H_2O(\ell)$	3.50	3.45	3.18	2.50	1.60	0.17	0.882	2.14
H_2	0.45	0.51	0.30	1.53	0.46	2.31	0.294	0.046
N_2	2.00	2.00	3.68	4.01	1.32	1.36	0.394	1.99
NH_3	0.037	<0.002	0.395	none	0.162	0.022	0.118	0.023
HCN	none	none	0.008	0.0006	0.020	0.024	0.008	-
HF	-	-	-	-	-	-	-	1.87
Empirical formula of explosives based on products**								
C	5.03	5.01	4.00	4.09	2.00	6.99	0.99(a)	5.04(b)
H	8.02	7.92	8.31	8.06	5.03	5.08	3.04	6.30
N	4.04	4.00	7.77	8.04	2.68	2.76	0.92	4.00
O	11.92	11.99	8.08	8.03	6.09	6.19	1.95	10.34
F	-	-	-	-	-	-	-	1.87

* From product composition and ΔH_f^o's of Table 3-1.

** Compare with empirical formula of Table 3-1.

(a) Analysis of original material gave $C_{1.00}H_{2.96}N_{.96}O_{1.92}$.

(b) Analysis of original material gave $C_{5.00}H_{5.74}N_{4.09}O_{10.06}F_{1.87}$.

TABLE 3-3. IDEAL GAS FREE ENERGY FUNCTIONS ($G^o/(RT)$) FOR DETONATION PRODUCTS

T, °K	CO_2	CO	H_2O	H_2	C(s)	NH_3	N_2	CH_4	H	O
1000	-75.69	-38.88	-53.94	-17.49	-1.522	-31.70	-24.95	-34.17		
1400	-63.66	-36.03	046.77	018.39	-2.064	-31.44	-25.97	-33.38		
1500	-61.74	-35.61	-45.66	-18.59	-2.190	-31.49	-26.20	-33.38		
1600	-60.09	-35.26	-44.70	-18.78	-2.312	-31.57	-26.43	-33.41	-0.435	-2.84
1800	-57.42	-34.72	-43.17	-19.14	-2.454	-31.79	-26.84	-33.59		
2000	-55.36	-34.34	-42.00	-19.47	-2.764	-32.06	-27.24	-33.85	-3.31	-7.06
2500	-51.89	-33.79	-40.11	-20.20	-3.256	-32.83	-28.12	-34.70		
3000	-49.83	-33.58	-39.07	-20.84	-3.686	-33.65	-28.89	-35.67		
4000	-47.70	-33.58	-38.19	-21.90	-4.406	-35.24	-30.19	-37.61	-11.41	-16.11
5000	-46.81	-33.81	-37.99	-22.77	-4.996	-36.67	-31.29	-39.41	-13.34	-18.13

TABLE 3-4 WATER GAS EQUILIBRIUM FOR IDEAL GAS PRODUCTS AT 1 ATM AND 1600° K

Product Composition, moles/mole	*Explosive* PETN	HMX	TNT	NM
CO_2	3.50	1.46	0.043	0.25
CO	1.50	2.54	5.86	0.75
H_2O	3.50	2.54	0.057	0.75
H_2	0.50	1.46	2.46	0.75
N_2	5.50	4.00	1.50	0.50
C(s)	None	None	1.09	-----
NH_3	1.5×10^{-5}	1×10^{-4}	1.5×10^{-4}	-----
CH_4	None	None	0.012	-----
Q* kcal/g	1.41	1.24	0.67	0.98

*Based on computed composition, $H_2O_{(g)}$

TABLE 3-5. CALCULATED AND OBSERVED C-J PARAMETERS

Explosive	ρ_o, g/cc	Q, kcal/g			P, kbar			T, °K		
		Meder*	Fickett**	Zuberev***	Meder	Fickett	Zuberev	Meder	Fickett	Zuberev
PETN	1.77	1.52	--	1.49	319	--	310	2830	--	4400
	1.77		ΔH_d = 1.49			340(1)			4200(1)	
	1.67	1.52	1.49(a)	1.45	260	231(a)	270	3020	4500(a)	4500
	1.67					310(2)			3400&30(2)	
	1.00	1.39	1.42	--	102	90	88	3970	4750	4650
RDX	1.80	1.48	1.49	1.47	347	325	340	2580	4040	4000
	1.80		$\Delta H_d \simeq 1.46$(b)			347(3); 370(3)			3700(1)	
	1.40	1.43	1.43	--	200	192	--	3270	4380	--
	1.40	--	--	--		213(3)				
	1.20	1.38	--	--	142	--	153(c)	3475	--	4540
	1.20					152(3)				
	1.00	1.33	1.29	1.33	108	104	104	3600	4375	4560
HMX	1.90	1.48	--	--	395	--	--	2368	--	--
	1.90	ΔH_d = 1.48				390(2)				
NM	1.13	1.30	1.37	--	130	125		3120	3800	
	1.13	ΔH_d=1.23				129(3) 144(2)			3400(4)(2) 3700(1)	
TNT	1.63	1.27	1.28	1.25	206	184	184	2940	3660	3740
	1.63					225(2)				
	1.58					202(3)				
	1.53	ΔH_d = 1.09								
	1.40 1.45		1.24	--	145	131 178(2) 167(3)	--	3110	3720	--
	1.00	1.14	1.11	1.16	76	71	73	3200	3630	3870
	1.05					113(2)				
	1.00					66(3)				
DATB	1.79	1.12	--	--	265	--	--	2565	--	--
	1.79	ΔH_d=1.01				259(2)				
Tetryl	1.70	1.42	--	1.40	282	--	250	2920	--	4000
	1.70					265(1)			2950(1)	
	1.50		ΔH_d=1.17							
TNM	1.64	0.56	0.53	--	163	132	--	1540	2440	--
	1.64					159(2)			2900(2) 3100(1)	
2/3NM/1/3TNM	1.40	1.44	1.50	--	192	153	--	3565	4455	--
						169(2)			3580(2)	
0.80NM/0.20TNM	1.31	1.59	1.62	--	181	156	--	4000	5040	--
	1.31					156(2)			3730(2)	
NG	1.60	1.48	1.46	--	347	308	--	3220	4680	--
	1.60					253(2)			4000(1)	
TNT/RDX(d)	1.70	1.45	--	--	300		--	3008	--	--
BTNEU(d)	1.66	1.49	--	--	333	--		3935	--	--

* Meder LA 2800; 1963.

** Fickett LA 2712, 1962.

*** Zuberev and Telegin, Doklady 156, 452, (1964).

(1) Apin and Voskoboinikov, RMPT 117, No. 3, (1961).

(2) Cited in LA 2800.

(3) Dremin and Pokhil, Doklady 120, 806, (1958).

(a) ρ_o = 1.60 g/cc.

(b) Assumed to be the same as for HMX.

(c) ρ_o = 1.25 g/cc.

(d) NOL computation using BKW equation.

TABLE 3-6. CORRELATION BETWEEN Q AND OXYGEN BALANCE

Explosive	ρ_o, g/cc	Q*, kcal/g	Oxygen Balance**
0.8 NM/0.2 TNM	1.31	1.61	0.00
BTNEU	1.86	1.49	0.00
NG	1.60	1.47	+3.5
TNETB	1.70	1.45	-4.0
PETN	1.77	1.50	-10.0
2/ 3NM/1/ 3TNM	1.40	1.30	+15.1
HMX	1.90	1.48	-22.0
RDX	1.80	1.48	-22.0
NM	1.13	1.33	-39.3
Comp. B	1.7	1.41	-40.3
Tetryl	1.70	1.41	-47.4
TNT	1.63	1.27	-77.0
TNM	1.64	0.55	+49.0
Explosive D	1.50	1.27	-52
DATNB	1.79	1.12	-56
Hydrazine nitrate	1.63	0.90	+8.4

*Average value shown in Table 3-5

**Oxygen balance = $-\frac{1600}{\text{formula weight}}$ [2C atoms +H/2 atoms - O atoms]

TABLE 3-7. COMPARISON OF Q_{CJ} AND Q_A BASED ON AN ARBITRARY DECOMPOSITION MECHANISM

Explosive		ρ_o, g/cc	Q,* kcal/g	Q_A,** kcal/g
PETN	$C_5H_8N_4O_{12}$	1.75	1.50	1.52
BTNEU	$C_5H_6N_8O_{13}$	1.86	1.49	1.48
RDX	$C_3H_6N_6O_6$	1.80	1.48	1.48
HMX	$C_4H_8N_8O_8$	1.90	1.48	1.48
TNETB	$C_6H_6N_6O_{14}$	1.70	1.45	1.43
TETRYL	$C_7H_5N_5O_8$	1.70	1.41	1.43
NM	CH_3NO_2	1.13	1.33	1.36
TNT	$C_7H_5N_3O_6$	1.63	1.27	1.28
PICRIC ACID	$C_6H_3N_3O_4$	1.7	1.23	1.25
DATNB	$C_6H_5N_5O_6$	1.79	1.12	1.12
Explosive D	$C_6H_6N_4O_7$	1.70	1.07	1.08
PBX 9404	$C_{1.40}H_{2.75}N_{2.57}O_{2.69}$	1.84	1.46	1.47
COMP.B-3	$C_{2.05}H_{2.51}N_{2.15}O_{2.67}$	1.7	1.40	1.39
OCTOL	$C_{6.84}H_{10.03}N_{9.22}O_{10.43}$	1.81	1.43	1.43

* From Table 3-5, and NOL and LASL compilations.

** From arbitrary decomposition mechanism assigning all available oxygen to H_2O and CO_2 with excess carbon appearing as C(s).

TABLE 3-8. COMPARISON OF Q AND GURNEY CONSTANTS FOR PLANE-WAVE SHOTS

HE	ρ_o, g/cc	$\sqrt{3Q}$*, mm/μsec	$\sqrt{2E}$**, mm/μsec	$\sqrt{2E/2Q}$	Source
Baratol	2.61	~2.0	1.94 1.72 min	~0.97 ~0.86 min	SRI
83/17 HMX/Teflon	1.911	3.24[a]	3.22	0.995	LRL
86/14 HMX/Fluorcarbon	1.894	3.26[a]	3.32	1.02	LRL
HMX	1.891	3.52	3.55	1.01	LRL
HMX	1.89	3.52	≥3.45	≥0.980	SRI
84/16 HMX/Kel-F	1.882	3.27[a]	3.28	1.00	LRL
80/20 HMX/Viton	1.876	3.15[a]	3.14	0.995	LRL
90/10 HMX/Viton	1.865	3.38[a]	3.32	0.980	LRL
85/15 HMX/Viton	1.865	3.24[a]	3.19	0.984	LRL
PBX 9404	1.841	3.42	3.38	0.988	LRL
PBX 9404	1.84	3.42	3.21	0.938 (0.99 max)	SRI
78/22 HMX/TNT	1.821	3.41[b]	3.29	0.965	LRL
88/12 HMX/Fluorcarbon	1.798	3.30[a]	3.17	0.960	LRL
90/10 RDX/Kel F	1.787	3.22[a]	3.13	0.972	LRL
90/10 HMX/Urethane Polymer	1.777	3.38[a]	3.14	0.929	LRL
PETN	1.765	3.57	3.36	0.940	LRL
77/23 Cyclotol	1.754	3.35[b]	3.14	0.938	LRL
92/8 HMX/PE	1.719	3.42[a]	3.10	0.905	LRL
Comp. B grd.A	1.717	3.26	2.990	0.915	LRL
Comp. B-3	1.68	3.22	2.99	0.930	SRI
Comp. B-3	1.68	3.22	3.00	0.933	NOL
90/8/2 RDX/P.S./D.O.P	1.675	3.27[a]	2.97	0.908	LRL
TNT	1.630	3.02	2.54	0.84 min	LRL
TNT	1.630	2.37[d]	2.54	1.07 max	"
TNT	pressed	3.02	<3.00	<0.99[c]	SRI
TNT	pressed	3.02	≤2.95	≤0.98[c]	LASL
NM	1.143	3.21	2.18	0.68	LRL
NM	1.143	2.86[d]	2.18	0.76 min	"

* $Q \equiv \Delta H_d$ for confined charges.

** Determined by Eq. 3-6 using experimental data.

(a) $Q = (\%HMX)(Q_{HMX})$, i.e., all other materials assumed inert.

(b) $Q = \Sigma n_i Q_i$

(c) Plane wave lens contributes to driving the metal.

(d) Based on ΔH_d for unconfined charges (see Table 3-4).

TABLE 3-9. CORRELATION OF Q AND EQUIVALENT WEIGHTS FOR FREE AIR BLAST

Explosive	ρ_o, g/cc	Q,* kcal/g	Experimental ΔH_d, kcal/g	Equivalent Weight**	Q/Q_{TNT}	$\Delta H_d/(\Delta H_d)_{TNT}$
TNT	1.6	1.27	1.09	1.00	1.00	1.00
TNETB	1.7	1.45	1.47	1.13	1.14	1.35
Comp B-3	1.7	1.40 (a)	1.24	1.13	1.10	1.14
98/2 RDX/Wax	1.6	1.45 (b)	1.45 (b)	1.19	1.14	1.33
95/5 RDX/Wax	1.6	1.41 (b)	1.41 (b)	1.19	1.11	1.29
91/9 RDX (Comp. A-3)	1.6	1.35 (b)	1.35 (b)	1.09	1.06	1.24
PETN	1.55	1.48	1.49	≈1.2 (c)	1.17	1.36
50/50 Pentolite	1.6	-	1.29 (b)	1.16	-	1.18
Explosive D		≈1.07 (d)	-	≈0.85	0.84	-
Aluminized explosives						
80/20 Tritonal	1.7	≈1.8 (e)	1.63	1.07	≈1.4	1.52
HBX-3	1.8	-	1.995	1.16	-	1.83
Minol II	1.7	-	1.51	1.24	-	1.39
Torpex II	1.7	-	1.60	1.23	-	1.47

* Average of values shown in Table 3-5.

** Taken from J. Petes, Annals N.Y. Academy of Sciences 152, 315 (1968).

(a) Assumed slightly smaller than the 1.42 to 1.45 kcal/g computed by LJD or BKW methods for 64/36 RDX/TNT.

(b) $Q = \Sigma\, n_i Q_i$

$\Delta H_d = \Sigma\, n_i (\Delta H_d)_i$

(c) Unpublished data, Stanford Research Institute

(d) NOL calculation using the BKW equation

(e) Based on $1/3\ C_7H_5N_3O_6 + 0.7Al_2O_3 = 0.83H_2O + 7/3\ C(s) + 1/2N_2$

TABLE 3-10. UNDERWATER PERFORMANCE OF EXPLOSIVES

Explosive	Equivalent Weight*	Q/Q_{TNT}
TNETB	1.28	1.14
PETN	1.25	1.18
HMX	1.19	1.17
RDX	1.16	1.17
95/5 RDX/Wax	1.13	1.11 (a)
75/25 Cyclotol	1.12	1.12 (a)
Comp. B	1.11	1.11
50/50 Pentolite	1.09	1.09 (a)
Tetryl	1.08	1.11
Explosive D	0.91	0.84 (b)
Aluminized		
70/30 TNETB/Al	1.80	≈1.90 (c)
HBX-3	1.59	≈1.57 (d)
70/5/25 RDX/Wax/Al	≈1.60	≈1.7 (e)

* Relative to TNT, this is the equivalent weight for shock energy + bubble energy. Data taken from Ref. 3.

(a) $Q \equiv \Sigma\, n_i Q_i$; wax, if present, assumed inert

(b) NOL computation of Q

(c) $Q_A = 2.42$ kcal/g for $C_6H_6N_6O_{14} + 6Al = 3Al_2O_3 + 3H_2O + CO_2 + 5C + 3N_2$

(d) Assuming $Q = \Delta H_d$

(e) $Q_A \approx 2.2$ kcal/g for $1/3\ C_3H_6N_6O_6 + 0.98\ Al =$
$0.49Al_2O_3 + 0.53H_2O + 0.47H_2 + C(s) + N_2$

TABLE 3-11. CORRELATION OF DETONATION ENERGY AND MAXIMUM WORK (BALLISTIC MORTAR)

Explosive	Ballistic Mortar Relative to TNT	Q/Q_{TNT}	$\Delta H_d/(\Delta H_d)_{TNT}$	
			$(\Delta H_d)_{TNT} = 1.09$	$(\Delta H_d)_{TNT} = 1.00$ kcal/g
HMX	1.50	1.17	1.36	1.48
RDX	1.50	1.17	1.36	1.48
PETN	1.45	1.18	1.37	1.50
NG	1.40	1.16	1.35	1.46
TNETB	1.36	1.14	1.35	1.48
Comp. A-3	1.35	1.06[a] [b]	1.24[a] [b]	1.35[a] [b]
Comp. B	1.33	1.10	1.14	1.24
Tetryl	1.2 to 1.3	1.11	1.07	1.17
Pentolite	1.26	1.02[a]	1.18[a]	1.29[a]
Picric Acid	1.12	0.97	0.95	1.03
DATNB	1.00	0.88	0.93	1.01
Explosive D	0.99	0.84	0.98	1.07
Minol 2	1.43	-	1.39	1.51
Torpex 2	1.38	-	1.47	1.60
Tritonal 80/20	1.24	-	1.50	1.65
HBX-3	1.11	-	1.83	2.00

(a) $Q = \Sigma n_i Q_i$; $\Delta H_d = \Sigma n_i (\Delta H_d)_i$

(b) Assumed wax is completely inert

CHAPTER 4 THERMAL DECOMPOSITION OF EXPLOSIVES

4-1 INTRODUCTION

Explosive liquids and solids can be decomposed by heat and light at relatively moderate temperatures. During decomposition, considerable heat is liberated since these reactions are exothermic. When the rate of decomposition in the condensed phase is sufficiently high, then an explosion may result due to self-heating, i.e., the heat generated during decomposition exceeds heat loss to the ambient by conduction and other means. This phase of decomposition (self-heating) is analyzed in Chapter 10. It is clear that detailed information on the stability of liquids and solids is needed for two reasons. First, to determine the conditions under which the unstable materials may be handled with some degree of safety. Second, to determine the conditions under which explosion will result since many explosions are preceded by a phase of rapid decomposition.

The first step in assessing the stability of a liquid or solid is to consider the thermochemical properties. Detailed information is needed on rates of decomposition, activation energies, and heats of decomposition. Some information on these properties is becoming available but there is considerable discrepancy in the values quoted by different workers. There is also a lack of reliable values for many of the thermal properties such as specific heat, thermal expansion, thermal conductivity, and other similar properties.

If the conditions under which explosion develops are to be controlled, then it is vital to understand the mechanism of the decomposition. This has been recognized in the last ten to fifteen years, and there are active centers of research throughout the world concentrating on this problem. Liquid explosives are usually characterized by covalent bonds, and there is considerable background of research for related materials to make it possible to propose reasonable decomposition mechanisms. At the same time, the development of modern equipment makes possible the analysis and identification of intermediates in small concentrations and of short life. Mass spectrometers, electron spin resonance and nuclear magnetic resonance equipment, chromatography, and spectroscopy are all being employed in this connection.

The majority of explosive materials, however, are solids and here the situation is more complex. The decomposition may be mainly a surface reaction or it may develop in the bulk material. Defects and impurities can influence the course of the reactions. It is perhaps essential to have a phase change or to melt the solid before an appreciable decomposition rate can be measured. The methods used to study explosive solids follow closely those developed for the study of semiconductors. It is necessary to show the nature of the bonds in the solid and to decide whether the solid is ionic or covalent. Covalent solids can be of the valence type or of the molecular type. For this purpose, studies are being made of the optical properties of the solid (ultraviolet, visible, and infrared spectra; refractive index; birefringence), as well as electrical properties (conductivity at low and high temperature), photoconductivity, crystallographic studies, and electron microscope and electron diffraction studies. In this way much has been learned about simple azides although it cannot be said that one can yet speak with confidence about solids such as lead azide.

4-2 DECOMPOSITION ENERGIES

The decomposition of most liquid and solid explosives results in the formation of gas. The simplest way to follow the reaction is to make pressure, time measurements in a closed system at constant volume. These curves are sigmoid in shape (Fig. 4-1), and from such curves the rate constant k can be obtained. Numerous relations have been obtained experimentally for solids, for example

$$\ln p = kt + \text{constant} \tag{4-1}$$

$$\ln \left(\frac{p_f}{p_f - p} \right) \tag{4-2}$$

where p is the gas pressure at time t and p_f the final gas pressure. For many solids nuclei are formed in localized regions, and these play a role

in the decomposition. These nuclei grow and eventually overlap and interfere. Many investigators have derived expressions to fit the experimental curves in terms of the production of nuclei. Thus, Prout and Tompkins give the relation

$$\ell n \left(\frac{\alpha}{1 - \alpha} \right) = kt + c \qquad (4\text{-}3)$$

where c is a constant and α the fraction of explosive decomposed; this holds for the decomposition of many solids such as permanganates and oxalates, and some of the azides. Another relation by Avrami and Erofeev is gaining in popularity. Their analysis involving three-dimensional growth of nuclei is of the form

$$- \ell n \, (1 - \alpha) = (kt)^n \qquad (4\text{-}4)$$

For some reactions $n = 4$ at the beginning of the reaction and $n = 3$ in the decay period.

When melting takes place, the nature of the rate equation is modified. The decomposition of liquid explosives has been successfully followed by determining the concentration of one of the products of decomposition with time, e.g., the formation of nitrogen dioxide during the decomposition of the nitrate esters or the nitro compounds. Here, of course, the assumption is made that the nitrogen dioxide is one of the primary products of decomposition. It is not intended to list here all the various methods in use to follow decomposition since these are too numerous. Accounts can be found in *Chemistry of the Solid State*[4], *Reactivity of Solids*[2], and in many other Symposia and papers published in recent years.

Once the rate constant has been determined, then a study of the variation of the rate constant k with absolute temperature T gives a measure

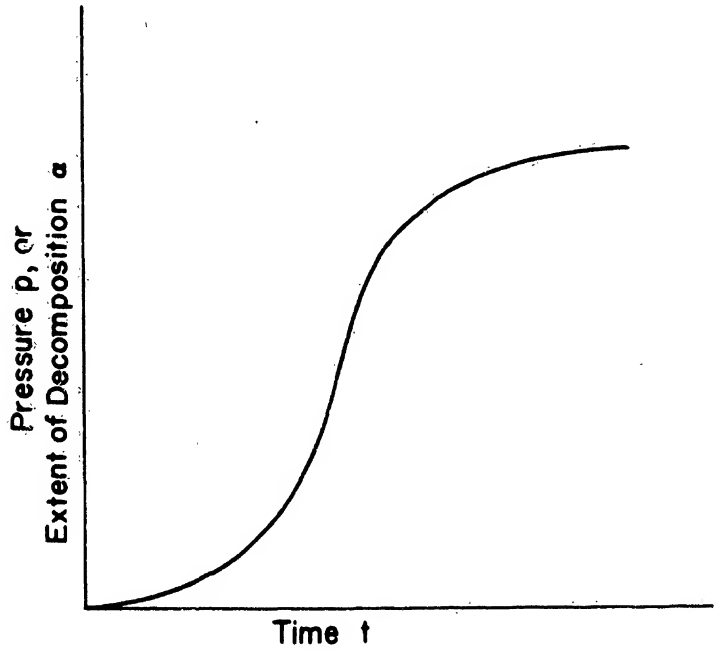

Figure 4-1. Thermal Decomposition Sigmoid Curve

the activation energy E (refer to Fig. 4-2) from the general relation

$$k = Z \exp\left[-E/(RT)\right] \qquad (4\text{-}5)$$

where Z is the pre-exponential factor and R the gas constant. Unless it is stated specifically, the values for E are usually the overall activation energies. Of greater interest is the value for the activation energy for each individual step in the decomposition complex of reactions; these are gradually becoming available. More refined equations are available for analysis of rate measurements but the experimental results obtained so far do not lend themselves to the use of advanced theory.

Values which have been given for activation energies of various explosives are listed in Table 4-1. These have been selected as possible values but the agreement between different investigators is not good. Both E and Z may vary with temperature, particularly at high temperatures. Autocatalysis may also take place and the products of decomposition can exert a profound influence on the rate. The table is included to give an idea of the magnitude of the energies, however, too much reliance should not be placed on the absolute values given. The values usually range between 30 and 50 kcal/mole, and are not very different from those normally found for many other nonexplosive materials. This is not surprising as the processes involved in the decomposition of explosive and nonexplosive systems can be very similar. It is the exothermic nature of many of the decompositions that makes the reaction run away to explosion. Chain mechanisms may also play a part in the decomposition.

4-3 DECOMPOSITION MECHANISMS

It will be convenient to consider explosives in three groups:

(1) *Covalent liquids and solids* (the organic nitrates and nitrocompounds). Here the initial

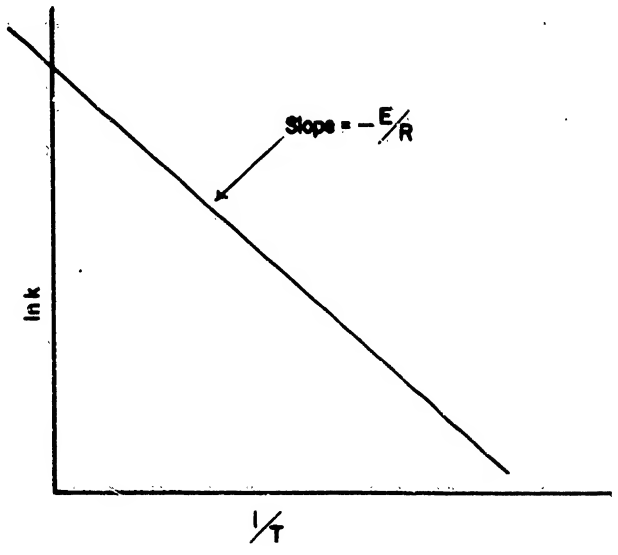

Figure 4-2. Plot of Logarithm of Rate Constant k vs Reciprocal of Absolute Temperature to Determine Activation Energy from Slope of the Line

TABLE 4-1 ACTIVATION ENERGIES AND PRE-EXPONENTIAL FACTORS FOR SOME EXPLOSIVE LIQUIDS AND SOLIDS

Compound	*Temperature Range*, °C	E_a, kcal/mole	$\log Z$ sec^{-1}
Nitroglycerin	160-190	50	23.5
Tetryl	211-260	38.4	15.4
Ethylene dinitramine	174-178	30.5	12.8
PETN	160-230	47	19.8
TNT	—	37	—
DINA	—	35.5	—
Picric acid	153	58	—
Lead azide	—	36-38	
Silver azide	below 190	44	
	above 190	31	
Mercury fulminate	100-115	32.2	
Lead styphnate	225-255	40 ?	

step in the decomposition is usually bond fission and a free radical mechanism applies. Intramolecular elimination reactions have also been considered.

(2) *Ionic solids.* Many of the primary explosives such as the azides, metal picrates, and acetylides belong to this group; electronic processes will dominate the reaction mechanism.

(3) *Ammonium salts.* Ammonium salts in principle belong to group (2) since they are generally ionic solids. There are, however, two possible paths for the decomposition, and for this reason they are considered separately.

4-3.1 COVALENT LIQUIDS AND SOLIDS

There is no doubt that the *organic nitrates* form the only class of materials which have been studied in a systematic way. It is generally agreed that the first step in the decomposition is the fission of the oxygen-nitrogen bond in which an alkoxyl radical is produced. This is also the rate determining step. Thus, for a simple compound such as methyl nitrate

$$CH_3ONO_2 \rightarrow CH_3O + NO_2$$

The activation energies favored by Gray[7,8] for the decomposition are methyl nitrate, 38.4 kcal/mole; ethyl nitrate, 36.4 kcal/mole; n-propyl nitrate, 37.6 kcal/mole; and this is equated to the energy required in the bond fission process given in the given decomposition reaction. The reactions in the gas phase in particular are homogeneous with pre-exponential factors approximately equal to 10^{13}. The decompositions are also inhibited by the addition of nitrogen dioxide and nitric oxide by the possible reactions of the alkoxyl radicals RO in the manner

$$RO\cdot + NO_2 \rightarrow RONO_2$$

$$RO\cdot + NO \rightarrow RONO$$

thus indicating the way in which nitrates may be reformed and also how nitrites can be produced during decomposition of the nitrate esters.

The alkoxyl radicals can undergo a variety of reactions and rearrangements, and in the case of the simpler alkoxyl radicals these have been described in detail in a review by Gray and Williams[8]. There may be association with radicals, hydrogen abstraction, rearrangements (isomerization), decomposition of the radical to simpler radicals and aldehydes or ketones, disproportionation, and decomposition by

radical attack. It is evident that all these reactions can lead to complex products and these are found in the decomposition products.

For the decomposition of a nitrate ester such as n-propyl nitrate the following set of equations may be written as a sequence of reactions during decomposition:

$$n\text{-}C_3H_7ONO_2 \rightarrow n\text{-}C_3H_7O + NO_2$$

$$n\text{-}C_3H_7O \rightarrow$$

$$C_2H_5\cdot + NO_2 \rightarrow C_2H_5O\cdot + NO$$

and some $C_2H_5NO_2$

$$C_2H_5O\cdot \rightarrow CH_3\cdot + CH_2O$$

$$CH_3\cdot + NO_2 \rightarrow \text{etc.}$$

$$n\text{-}C_3H_7O + NO \rightarrow n\text{-}C_3H_7ONO$$

etc.

Schemes such as this have been proposed for many nitrates and related esters. What is needed is the activation energy for each step; some of these are now known fairly accurately.

Systems such as glycol dinitrate, nitroglycerin, and PETN will behave in the same way but, since there are more nitrate groups in each molecule, there is difficulty in working out the precise order of the steps to the final products. Thus, glycol dinitrate would be assumed to decompose ideally in the manner

$$NO_2OCH_2CH_2ONO_2 \rightarrow 2NO_2 + \cdot OCH_2CH_2O$$

$$\downarrow$$

$$2\,CH_2O$$

or for more complex dinitrates ·

$$\begin{array}{l} (CH_3)_2CO \,\rfloor\, NO_2 \\ \quad\ \ \lceil \\ \quad\ \ CH_2 \rightarrow 2\,(CH_3)_2CO + 2\,NO_2 + C_2H_4 \\ \quad\ \ \lfloor \\ \quad\ \ CH_2 \\ \quad\ \ \lfloor \\ (CH_3)_2CO \,\rceil\, NO_2 \end{array}$$

For PETN, nitroglycerin, and related systems, carbonyl compounds—such as formaldehyde, more complex aldehydes and ketones—are formed simultaneously, and these together with the alkyl radicals are oxidized by the nitrogen dioxide. The decomposition of nitroglycerin accelerates if the products are allowed to accumulate or if water or acids are introduced. Apart from gaseous products—such as NO, N_2O, H_2O, CO, CH_4, N_2, and HCN—liquid and solid residues of complicated structure are also found.

The nitrate esters are also decomposed by ultraviolet light, and again it is assumed that the initial step is bond fission. First there is the formation of an excited state

$$RONO_2 \xrightarrow{h\nu} \underset{\text{excited state}}{RONO_2^*} \rightarrow RO + NO_2$$

which may revert to the ground state or dissociate to give free radicals.

Andreev has made an extensive study of the decomposition of nitrate esters, and of the effect of products and additives on the reaction rate. He followed the decomposition of PETN in a variety of physical states: the solid, molten, dissolved, and gaseous states. The rate of decomposition is greatest in the gaseous state and least in the solid state.

The nitro compounds have also been studied in some detail. A review of the decomposition of nitromethane by Makovsky and Lenji[10] records the information available up to 1958. The vapor phase decomposition at different temperatures and pressures has been followed by static and flow methods. The reaction has been shown to be first order and a large number of the products of decomposition identified. These include NO, N_2O, H_2O, CO, CH_4, CO_2, and traces of C_2H_2, C_2H_6, and NO_2. More complicated products are formed at high pressures, e.g., HCN, CH_3CN, HCHO, etc. The overall activation energy for decomposition is in the region of 50-53 kcal/mole. Most investigators favor bond fission as the initial step in the decomposition

$$CH_3NO_2 \rightarrow CH_3\cdot + NO_2$$

Numerous other steps have been proposed to account for the products of decomposition, and some of these are given to indicate the type of reactions envisaged.

$$CH_3\cdot + CH_3NO_2 \rightarrow CH_4 + \cdot CH_2NO_2$$

$$\cdot CH_2NO_2 + NO_2 \rightarrow CH_2O + NO + NO_2$$

$$CH_2O + NO_2 \rightarrow CO + NO + H_2O$$

$$2\ CH_3\cdot \rightarrow C_2H_6$$

Reactions of the type

$$CH_3\cdot + NO \rightarrow CH_3NO \rightarrow CH_2{=}NOH \rightarrow HCN + H_2O$$

are also probable reactions.

On the other hand at high pressures, in the region 12-40 atm, Makovsky[10] and Guenwald consider the reactions

$$CH_2NO_2 \rightarrow CH_2NO + O$$

$$O + CH_3NO_2 \rightarrow CH_2O + HNO_2, \text{ etc.}$$

may also take place. The photolysis of nitromethane has been studied recently by Nicholson[12] who postulates bond fission as the initial step in the decomposition.

The decomposition of the higher nitro alkanes—e.g., nitroethane, 1 and 2 nitropropane—has also been studied though in less detail. For nitroethane, values of the activation energy ranging between 41 and 46 kcal/mole seem to be the most reliable. There is considerable debate concerning the first step in the decomposition. The C-N bond strength is estimated at 58 kcal and the activation energy measured is some 10 kcal smaller than this for nitroethane. Possible schemes starting with

$$C_2H_5NO_2 \rightarrow C_2H_5 + NO_2$$

as the first step have been evolved but the alternative reaction

$$C_2H_5NO_2 \rightarrow C_2H_4 + HNO_2$$

is a strong candidate. For this reason the detailed schemes for the two rival mechanisms will not be given; the details may be found in the literature.

For 2-nitropropane, a careful study by Smith and Calvert[11] gives the following expression for the decomposition rate constant:

$$k = 1.11 \times 10^{11} \exp\ [-39.3/(RT)],\ \text{sec}^{-1} \quad (4\text{-}6)$$

This is based on propylene formation in a static system. Many of the arguments put forward for nitroethane also apply to the nitropropane system. Again, there is disagreement as to the first step of the decomposition but the weight is perhaps in favor of a step of the kind

$$CH_3CHNO_2CH_3 \rightarrow CH_2{=}CHCH_3 + HNO_2$$

Here, intramolecular elimination of propylene and nitrous acid takes place via a cyclic activated complex. This is followed by a series of radical reactions. Some of those proposed are

$$HNO_2 \rightarrow OH + NO$$

$$OH + CH_3CHNO_2CH_3 \rightarrow H_2O + CH_3\dot{C}NO_2CH_3$$

$$\rightarrow H_2O + CH_3CHNO_2CH_2\cdot$$

$$CH_3\dot{C}NO_2CH_3 \rightarrow CH_3COCH_3 + NO$$

$$CH_3CHNO_2CH_2\cdot \rightarrow CH_2CHNO + CH_2O$$

$$\rightarrow CH_3CH{=}CH_2 + NO_2$$

$$CH_3CHNO \rightarrow CH_3CNOH$$

$$CH_3CNOH + NO \rightarrow CH_3CN + HNO_2$$

The higher aliphatic nitrocompounds have not been studied in sufficient detail for likely mechanisms to be proposed. This is also true for some of the aromatic compounds such as picric acid.

4-3.2 IONIC SOLIDS (AZIDES)

From the practical point of view, lead azide is the most interesting of the azides. On the qualitative side considerable information exists on rates of decomposition, explosion temperatures and the like. It has only been realized in recent years, however, that one needs to go further into this problem of the decomposition of the azides. Figures were available but no real understanding of the mechanism of decomposition; this is still true to some extent.

A start has been made on the simpler azides in the solid state which are represented as $M N_3$,

and on the related compounds—the fulminates CH O and cyanamides CN_2^{2-} —since these form an isoelectronic series. Consider a solid like KN_3. It is known that it is composed of ions K_+ and N_3^-, and that it is a relatively stable compound. The azide ion is a linear symmetrical group $N^{1.13\text{Å}}N^{1.16\text{Å}}N^-$ with sixteen valence electrons, and the orbital system can be represented simply as in Fig. 4-3 where the σ-bonds, lone pairs, and the π-bonds are indicated. The orbitals which are of interest from the point of view of electronic transitions are the delocalized π_{x_2} and π_{y_2} nonbonding orbitals since electrons will be excited from these orbitals to higher orbitals.

The azide ion is also isoelectronic with the CO_2 molecule and all the values for the vibration frequencies—symmetrical stretching, asymmetrical stretching, and bending—are known from infrared and Raman spectra. From these, force constants may be calculated.

If one considers a simple series of the monovalent azides—KN_3, TlN_3, AgN_3, CuN_3, $Hg_2(N_3)_2$—and organic azides (solid), it is found that the stability varies in the order $KN_3 > TlN_3 > AgN_3 > CuN_3 < Hg_2(N_3)_2 <$ solid azides. The stability decreases along the series K to Cu as the ionization potential I increases, or more accurately as $(I - E)$ increases. Here E is the electron affinity of the azide (N_3) radical and is in the order of 2.8 ev, although higher values than this have been quoted. The problem is to explain why the stability varies in this way; a reasonable explanation can be given if we use the band theory of solids.

In the case of KN_3, I=4.32 ev, $E \approx 2.8$ ev; therefore $(I - E)$ is small. For greatest stability, the solid should be composed of ions K^+ and N_3^-. The structure is tetragonal and all metal-nitrogen distances are the same. It has properties typical of ionic solids such as KBr, the refractive index is low (of the order 1.5), and the optical absorption edge occurs in the vacuum ultraviolet part of the spectrum. The silver salts AgN_3 and AgBr, however, are unstable solids and readily decompose on heating, or during irradiation with light of suitable wave length or ionizing radiation.

$$2AgN_3 \xrightarrow{kT} 2Ag + 3N_2 + Q$$

similar to

$$2AgBr \rightarrow 2Ag + Br_2$$

where Q represents the heat of decomposition.

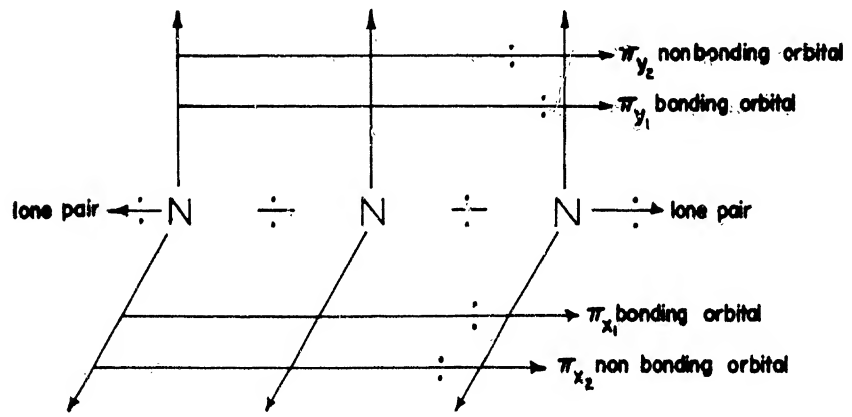

Figure 4-3. Representation of the Orbital System of the Azide Ion

The bromides are mentioned since there is in fact a close resemblance between the behavior of the azides and the corresponding bromides. The ionic radii of Ag^+ and of K^+ are 1.26Å and 1.33Å, respectively, which are not too different. On the other hand, the structure of AgN_3 is orthorhombic, and there are directed bonds. In the solid, there are four long silver-nitrogen bonds of 2.79Å and four short bonds of 2.56Å. The solid has a partial layer-type structure. The physical properties depend markedly on crystal direction. The refractive index is high and is approximately 2.0 for light of long wave length, and the optical absorption edge is now much further into the visible part of the spectrum. All these properties indicate a departure from an ionic type of lattice in the silver salt.

The decomposition of silver azide by heat is exothermic to the extent Q=148 kcal/mole. From the given chemical equation it is clear that while the lattice is composed mainly of ions, the products are neutral, so that an electron transfer mechanism must operate at some stage of the decomposition. Before the mechanism of the decomposition can be established, it is necessary to determine the electron energy levels in the solid—in other words the energy E required to excite an electron from the valence band to the conduction band where, as in Fig. 4-4, we assume the valence band is formed by the overlap of orbitals of the azide N_3^- ions while the conduction band is formed by the overlap of orbitals of the metal M^+ ions.

On the experimental side the overall activation energy for the decomposition of silver azide has been determined from pressure-time curves, and below 190°C the value is 44 kcal/mole or 1.9 ev molecule. Some information is also available on the collapse of the lattice in passing from silver azide to metallic silver. This is obtained from electron diffraction studies of a crystal as it decomposes under the action of an electron beam in the diffraction camera. Oriented silver is formed with lattice parameters slightly greater

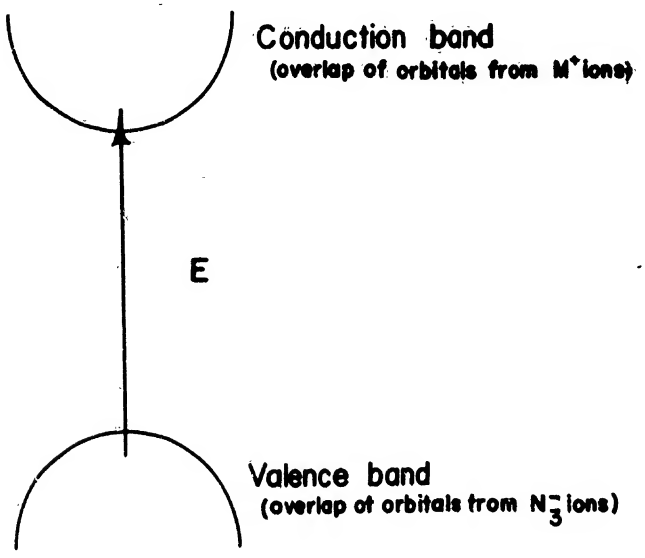

Figure 4-4. Schematic Showing Energy E to Excite an Electron from Valence Band to Conduction Band in Silver Azide

than for normal silver, and it is concluded that a diffusion of silver takes place to lattice sites made vacant by the removal of azide ions N_3^- during decomposition. This will give oriented silver nuclei with large silver-silver spacings. Finally, there is a collapse to normal silver. The silver that is formed during decomposition is very mobile and appears on the surface mainly as discrete nuclei which grow in size until they cover the whole of the surface. The nuclei may be less than 10Å in diameter (the limit of resolution of the electron microscope used to determine their size) to greater than 2000Å. These nuclei play an important part in the decomposition, and for this reason a knowledge of their size and distribution is needed. The technique used is simple. Crystals of silver azide are heated or irradiated with light giving a surface film of silver, which consists of the large and small nuclei as illustrated In Fig. 4-5(A). A carbon film is evaporated on to the nuclei (Fig. 4-5(B), and undecomposed silver azide dissolved away in dilute ammonia solution. The carbon film floats on the liquid surface and is picked up on an electron microscope grid which is then studied in the normal way. It is possible that silver forms internally along dislocations in the crystal in the manner found by Mitchell and illustrated in Fig. 4-5(C). No evidence for this type of behavior has as yet been found for the azides. Even with crystals of silver cyanamide which resembles silver azide but which are more stable, the silver is mainly at the surface. This has been verified frequently in electron microscope studies. The situation, as far as dislocations and their influence on the decomposition of the azides is concerned, is that a possibility exists that they do play a part in the decomposition but direct proof is not at present available. An etching technique might perhaps give better results. The main decomposition seem to take place at the surface.

Reference was made earlier to use of the band theory of solids in connection with the explanation of the stability of azides, and it was stated that it is necessary to determine electron energy levels in the solid. The simplest way to determine energy gaps is from the optical and electrical properties of the solid. The optical absorption spectra are determined in the normal way, and one can represent the light path as in Fig. 4-6. If I_o is the incident intensity of light and I the transmitted intensity, then in the ideal case the absorption coefficient α in cm^{-1} is given by the expression $I=I_o e^{-\alpha t}$, where t is the thickness of the crystal in cm. Absorption coefficients α are determined as functions of the wavelength of light γ and for values of α in the region of high absorption corresponding to 10^5 to 10^6 cm^{-1}, it is assumed that photon energies $h\nu$ correspond to the band gap E as shown in Fig. 4-7. Here one is concerned with direct transitions from the valence band to the conduction band for values of the wave vector $k = 0$. On a simple ideal this would correspond to the energy required for the following process but this concept should not be pushed too far:

$$N_3^- \rightarrow N_3 + e$$

azide ion in lattice	azide radical (positive hole)	electron in conduction band

Measurements of the absorption spectra at low temperatures, particularly at liquid helium temperatures, reveal the presence of excited states. These are exciton levels and lie below the conduction band (Fig. 4-8). They form a hydrogen-like series and their frequency is given by an expression of the form

$$\nu_n = \nu_\infty - R/n^2 \qquad (4\text{-}7)$$

where ν_n is the frequency corresponding to the exciton of quantum number n, ν_∞ is the frequency of the series limit, and R is an exciton Rydberg constant. In the case of the alkali metal azides, Deb has resolved the $n = 1, 2$ and 3 lines and has found that at liquid helium temperatures the band gap for KN_3 is 8.6 ev corresponding to light of wavelength 1450Å in the vacuum ultraviolet, and the $n = 1$ exciton line occurs at 1895Å or 6.6 ev. These gaps are quite large.

Exciton levels have also been identified in TlN_3 and AgN_3. However, one now finds that the absorption edge is in the vicinity of 3500 Å or 3.5 ev for silver azide. The values for the gaps are: E_1 = 3.5 ev optical; E_2 = 0.6 ev optical (see Fig. 4-9). These are much smaller than for potassium azide.

E_1 can also be estimated from electrical conductivity measurements at high temperatures but the interpretation of the results is not always easy since both ionic and electronic conductivity have to be considered. E_2 can also

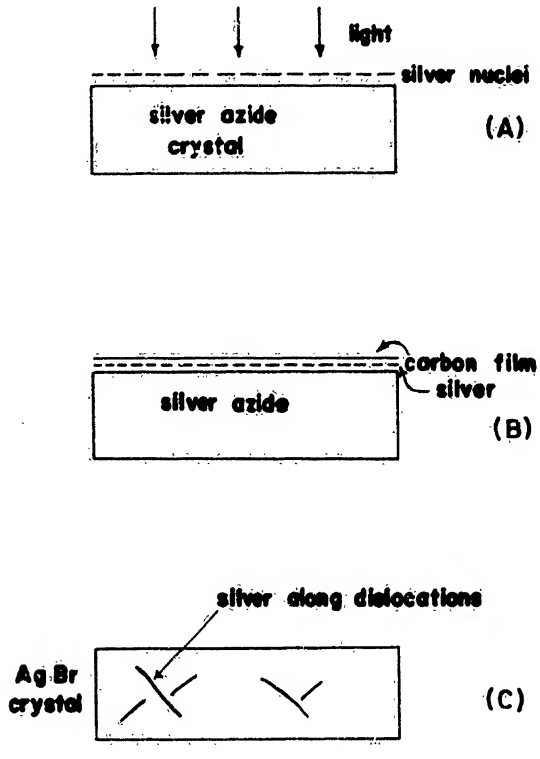

Figure 4-5. Showing Technique for Studying Silver Nuclei from Decomposed Silver Azide

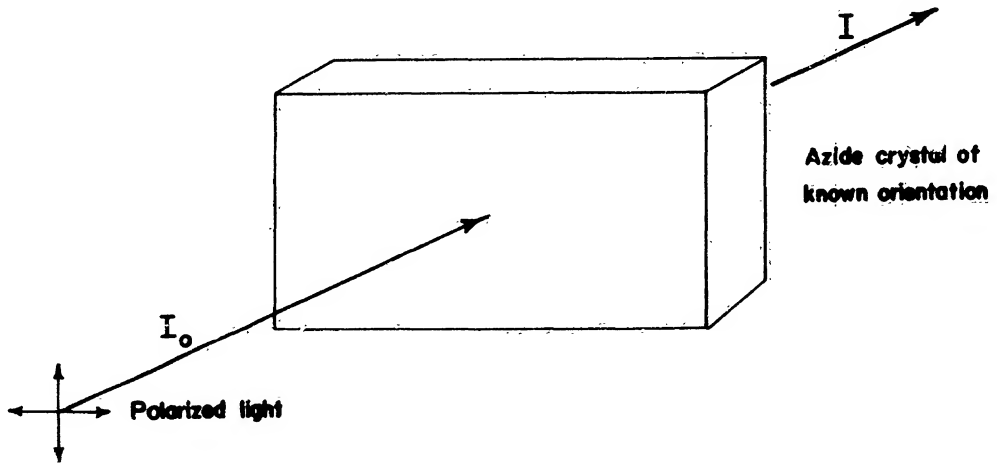

Figure 4-6. Schematic for Determining Optical Absorption Spectra

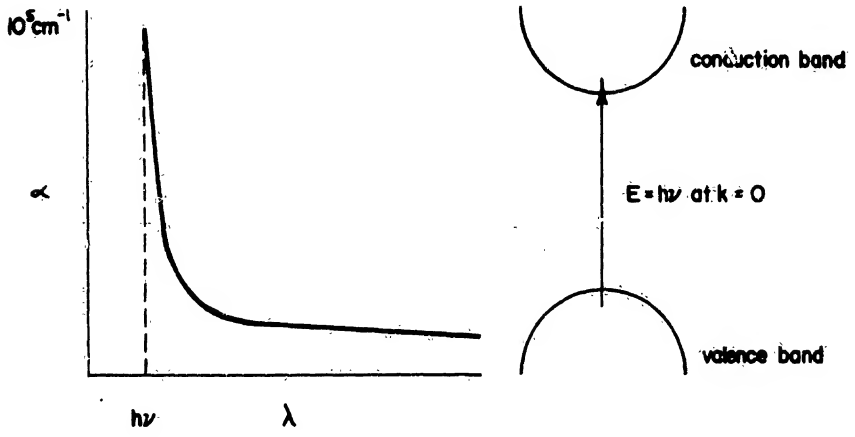

Figure 4-7. Absorption Coefficients α as Function of Wavelength λ. At High Absorption, Photon Energy hν Assumed to Correspond to Band Gap Energy E

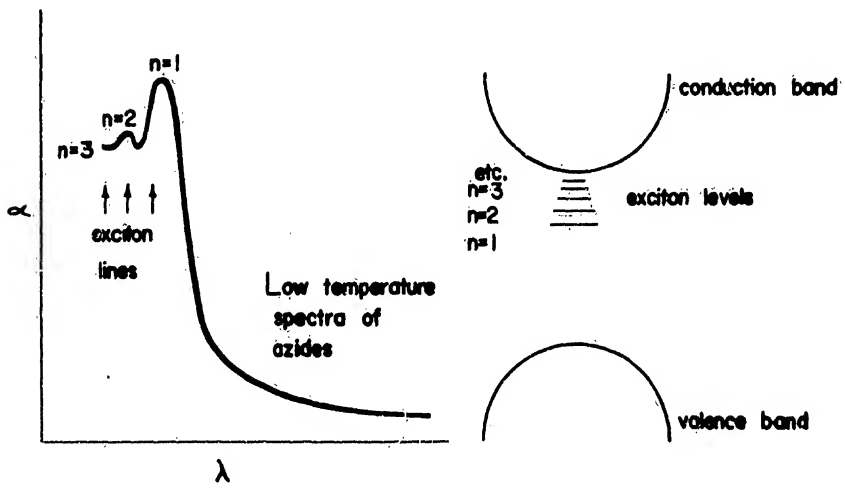

Figure 4-8. Showing Exciton Levels

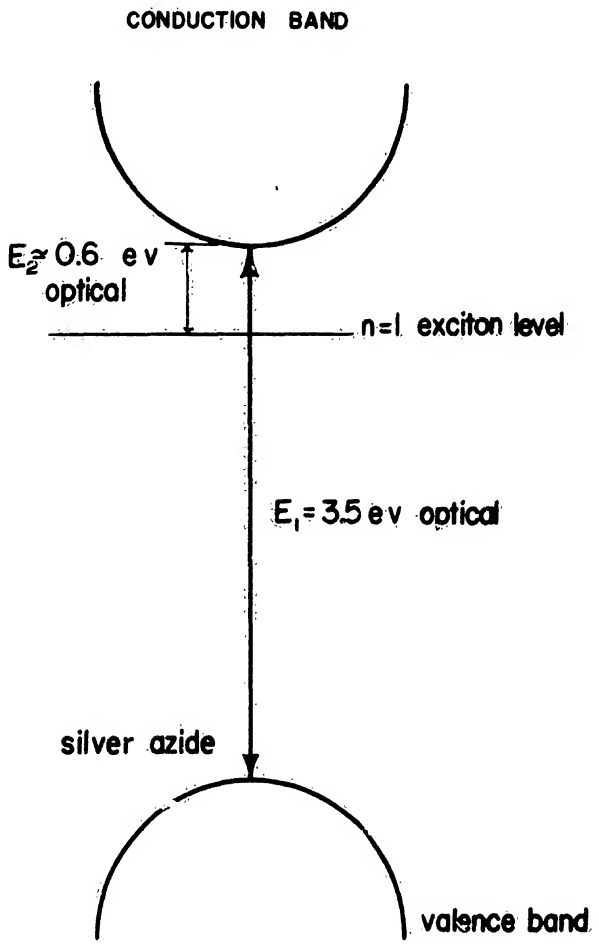

Figure 4-9. Energy Gaps E_1 and E_2 in Silver Azide

be estimated from photoconductivity experiments. Here it is assumed that one measures the thermal energy required to dissociate optically formed excitons in the manner

$$N_3^- + h\nu \rightleftharpoons N_3^{-*} \xrightarrow{\text{heat}} N_3 + (e)$$

exciton

Both TlN_3 and AgN_3 are good photoconductors when they are irradiated with light near to the optical absorption edge. The experiment is quite a simple one, and a schematic diagram is shown in Fig. 4-10. Light of known wavelength is allowed to fall on to a crystal held at a DC potential of a few volts. A photocurrent will result and the magnitude of this photocurrent depends on the wavelength of the light and the temperature of the crystal. Since the resistance of the crystal is usually high, of the order of 10^{10} Ω cm., the photocurrents are very small and can be in the region of 10^{-12} A. For this reason electrometers are in general used to record the currents. From the variation in photocurrent with temperature it is possible to determine an activation energy for the photoconduction process; for silver azide this is in the region 0.38 ev. This is a thermal energy which can be shown to be in good agreement with the value E_2 obtained optically.

Energy gaps obtained from spectroscopic measurements give optical energies. One also needs to know thermal energy gaps. These are not the same, and arguments based on the Franck-Condon principle led Mott and Gurney to give the approximate relation

$$E_t = E_o \left(\frac{K_o}{K}\right) \qquad (4\text{-}7)$$

where E_t is a thermal energy, E_o the corresponding optical energy, K_o the high frequency dielectric constant, and K the static or low frequency dielectric constant. K_o is estimated from values for the refractive index n and for values of n corresponding to wavelengths well away from the absorption edge $K_o = n^2$. Substituting the appropriate values for silver azide, one obtains for E_t a value of 1.88 ev. This is the thermal energy required to excite an electron from the valence band to the conduction band. This agrees remarkably well with the activation energy for thermal decomposition of 1.9 ev (below 190°C) determined from pressure-time curves. It is suggested in fact that E_1 in Fig. 4-9 for silver azide is connected with thermal decomposition and E_2 with the activation energy for photochemical decomposition. It is, therefore, possible to propose a generalized scheme for the thermal and photochemical decomposition of the heavy metal azides. This is shown in Table 4-2.

It must be emphasized that this scheme is very general. The detailed mechanism is much more complex since the presence of point defects, dislocations, impurities, metal particles and the like have been ignored. In a general sense, however, it is probably correct and resembles in outline the mechanism of decomposition of silver bromide in the photographic process.

An attempt can also be made to explain how the stability decreases along the azide series K, Tl, Ag, Cu. Along this series E_1 is found to decrease quite appreciably; this can mean that the rate of decomposition at a given temperature can be higher. The situation with KN_3 is a little more complicated. The band gaps are very large and the exciton level $n = 1$ is well below the conduction band. With KN_3 Jacobs and Tompkins assume that during decomposition, for example by light, excitons are formed. These may be trapped at vacant lattice sites, for example where K^+ ions are missing. The electron from the exciton is then lost to form an F center. The positive holes (N_3) finally can give nitrogen gas. Such a mechanism is plausible because just as in the case of the alkali halides, color centers of the F center type readily form in the alkali azides and could play a part in the decomposition.

As soon as the ionization potential becomes too large—e.g., $I > 8.0$ ev—the solid is no longer composed of ions but a covalent type of solid is formed. Examples are mercurous azide $Hg_2(N_3)_2$, hydrazoic acid HN_3, and the organic azides. There are now directed bonds to one end of the azide group

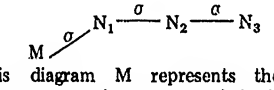

In this diagram M represents the metal, hydrogen or organic groups, and the bonds are shown. The distance N_1N_2 is now much larger than N_2N_3. For example in methyl azide, CH_3N_3, the bond lengths and bond angles are:

TABLE 4-2 THERMAL AND PHOTOCHEMICAL DECOMPOSITION OF SOME IONIC AZIDES

Thermal Decomposition	*Photochemical Decomposition*	
	Exciton formation	*Direct transition*
(1) $N_3^- = N_3 + e$ formation of positive hole and electron in the conduction band.	(1) $N_3^- + h\nu = N_3^*$ formation of an exciton	(1) $N_3^{-*} + h\nu = N_3 + e$
(2) $2N_3 \rightarrow 3N_2$ reaction of two positive-holes at the surface to give nitrogen.	(2) $N_3^{-*} \overset{kT}{\rightarrow} N_3 + e$ thermal dissociation of optically formed exciton: (rate determining step) followed by steps 2,3 column 1.	
(3) $Ag_n + Ag^+ + e \rightarrow Ag_{n+1}$ absorption of silver ion at a metal nucleus and electron capture.		

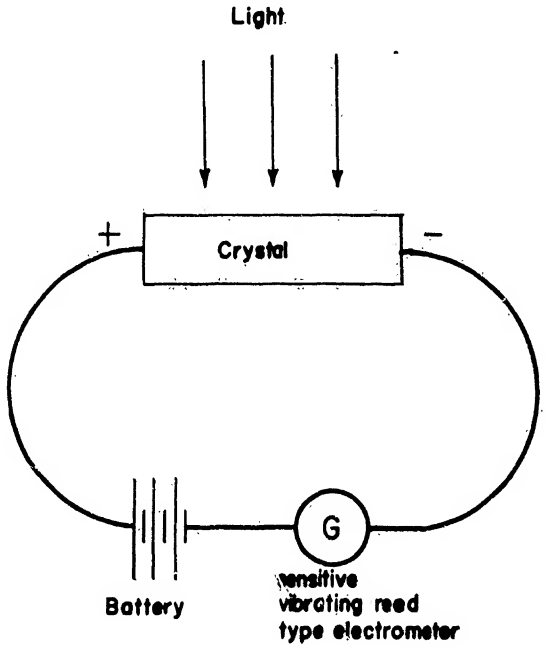

Figure 4-10. Schematic for Studying Photoconductivity of Crystal

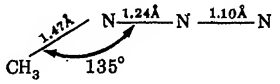

If we consider hydrazoic acid as the simplest of these covalent azides, the orbital system may be written as shown in Fig. 4-11.

There now exist differences in physical properties to the ionic azides in vibration frequencies, since all are now infrared active, and in the decomposition behavior to heat and light. The initial step in the decomposition is probably bond fission, e.g., of the longest N-N bond,

$$MN_3 \xrightarrow[\text{light}]{\text{heat}} MN + N_2$$

$$HN_3 \rightarrow HN + N_2$$

The subsequent steps in the decomposition depend on the stability of MN if M is a metal atom, or on the reactivity of the free radical if it is of the type HN. For example, ammonium azide can be formed from hydrazoic acid. The detailed mechanism is, however, the subject of rather violent argument and controversy at the present time, so that all the steps will not be given here. In the case of the organic azides the radical RN· can undergo rearrangement particularly if it is of the complex variety and is derived, for example, from triphenyl methyl and similar groups R. Usually the covalent azides are more stable than the ionic azides, although the statement must be qualified to some extent since some of the covalent azides are exceedingly unstable, e.g., BrN_3, IN_3, NON_3 and the like. Solid HN_3 is also said to be very unstable but there is no reliable information on this point.

A number of other systems are being studied in the same way as the azides. The list would include the acetylides, fulminates, styphnates, and picrates. At the present time it is impossible to predict accurately the properties of these solids. Potassium fulminate, for example, is one of the most unstable materials in this list and the reason for this is not clear. It should in fact be a reasonably stable solid from what one knows of the structure and other properties.

The solids previously discussed are all of the simple type. In the case of azides and acetylides formed from transition metals such as nickel and cobalt, the situation is a little more complicated. Here one deals with coordination complexes; ligand-field theory, the study of the effects of environment of anions on the energies of the d-orbitals of the cation, has proved valuable in discussing the optical and magnetic properties and the stability of these solids.

4-3.3 AMMONIUM SALTS

The decomposition of both ammonium nitrate and ammonium perchlorate has been studied extensively. These are widely used as explosive materials. The decomposition can, however, be quite complex since the physical state of the solid may change and it is possible to have sublimation and melting. Ammonium nitrate in the solid state can undergo a large number of phase changes over a relatively small temperature range. This has led to useful information on rotation of the nitrate ion and diffusion of the ammonium ions in the solid.

Between 210°-260°C ammonium nitrate gives off nitrous oxide and water, but above 300°C explosion can take place. Some nitrogen is produced and impurities, for example Cl^-, can have a profound effect on the decomposition. The overall decomposition can be represented by

$$NH_4NO_3 \rightarrow N_2O + 2\ H_2O$$

Bircumshaw has discussed the decomposition of ammonium perchlorate. The solid exists in two modifications, orthorhombic below 240°C and cubic above 240°C. The products of decomposition are oxygen, nitrogen, chlorine, chlorine dioxide, nitrous oxide, nitrogen tetroxide, hydrochloric and perchloric acids, and water. An unusual phenomenon is observed during thermal decomposition of single crystals below 300°C. An amorphous solid is left as a residue and, strangely enough, this is also ammonium perchlorate. A similar observation has also been made for sodium azide by Secco.

The decomposition of ammonium perchlorate, like ammonium nitrate, depends very markedly on the surface area of the solid. In the case of ammonium nitrate, considerable effort has gone into the preparation of a solid of low density (ca. 0.5) and high surface area. This material is said to be very sensitive to shock but there is

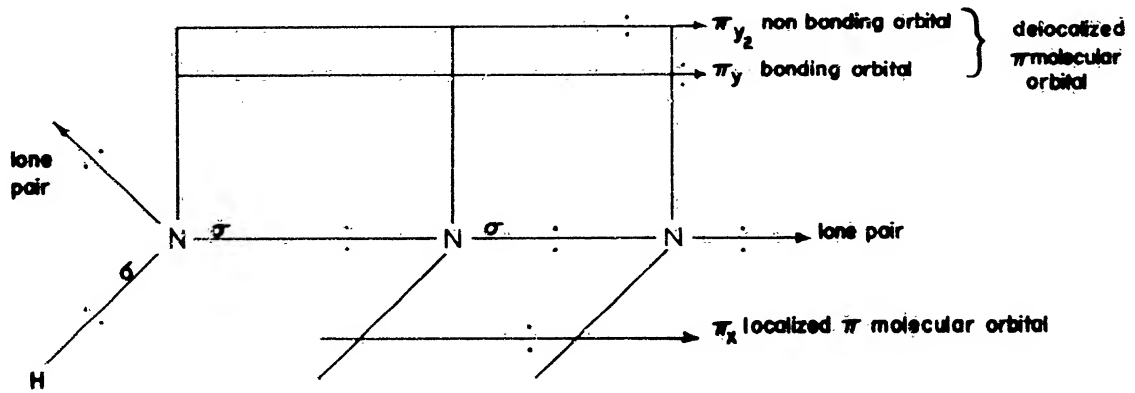

Figure 4-11. Orbital System of Covalent Azide, HN_3

some disagreement on this. The effect of metal oxide catalysts on the decomposition of ammonium perchlorate can be quite marked. Manganese dioxide, nickel oxide, chromic oxide, cupric oxide, and zinc oxide have all been tried; for example, the addition of zinc oxide can have a profound effect. In this case, the rate and extent of decomposition can be increased, and the explosion temperature can be lowered by some 200°C. Many of these effects have been interpreted in terms of electronic processes which occur during decomposition; accordingly, detailed knowledge of the catalyst, particularly by its semiconductor properties, is needed. Carbon has also been added to ammonium perchlorate and can influence the kinetics of the decomposition.

The ammonium salts are ionic solids and just as for the azides, electron transfer can occur during decomposition. On a molecular scale one may visualize the NH_4^+ and ClO_4^- ions in the solid, and the formation of NH_4 and ClO_4 radicals (under the action of suitable stimuli) and their subsequent reactions. Another possibility, however, is the dissociation of NH_4ClO_4 according to the equation

$$NH_4ClO_4 \rightarrow NH_3 + HClO_4$$

This is referred to as *proton transfer* and the reaction will be dominated by the subsequent decomposition and reactions of $HClO_4$. Which of these two mechanisms will operate will depend on temperature, and Galwey and Jacobs[13] have suggested that below 280°C the electron transfer mechansim is the important one. Here only 30 percent of the solid decomposes and, as mentioned, the residue is still NH_4ClO_4 in an amorphous form. The activation energy for decomposition is 32 kcal/mole. At higher temperatures, 350° - 400°C, the proton transfer mechanism will be the more important and the activation energy for decomposition is 39.5 kcal/mole. The proton transfer takes place on the surface of the solid followed by the oxidation of the ammonia gas.

Some of the steps in the decomposition of perchloric acid which have been proposed are

$$2HClO_4 \rightarrow H_2O + Cl_2O_7$$

$$2Cl_2O_7 \rightarrow 2Cl_2 + 7O_2 \quad \text{(probably a chain reaction)}$$

$$4NH_3 + 5O_2 \rightarrow 6H_2O + 4NO$$

The overall decomposition may be represented as $2NH_4ClO_4 \rightarrow 4H_2O + 2NO + O_2 + Cl_2$

Similar schemes have also been proposed for ammonium nitrate. One favored by Russian workers is

$$NH_4NO_3 \rightleftharpoons NH_3 + HNO_3$$

$$\downarrow$$

$$NO_2 + H_2O + O_2$$

$$NH_3 + NO_2 \rightarrow NH_2\cdot + HNO_2$$

$$NH_2\cdot + NO_2 \rightarrow NH_2NO_2$$

$$\downarrow$$

$$N_2O + H_2O$$

$$NO + NH_2\cdot \rightarrow NH_2NO \rightarrow H_2O$$

etc.

As in many schemes of this kind, there is no problem in writing down possible free radical reactions. The main difficulty is to determine whether these in fact do take place and the energies involved in the processes.

4-4 RADIATION DAMAGE IN EXPLOSION SOLIDS

Explosive solids have been subjected to a variety of ionizing radiations and nuclear particles. There are electron beams, x-and γ-rays, α particles, H^3 nuclei, neutrons, proton fission fragments and doubtless others not listed here. These would include mesons and those particles discovered in recent years. Decomposition can be induced in solids by these particles and, by taking nonexplosive solids as models, some insight into the radiation damage that is produced can be obtained. For the lighter particles the damage caused is studied by a variety of techniques. Optical and electrical properties, spin resonance techniques, chemical methods to identify new species, radioactive techniques — all are studied to determine changes within the crystal such as interstitials, vacancies, free radicals, color centers, and impurity formation. When the damage is extensive as with fission fragments, high resolution electron microscopy coupled with Moire' fringe techniques can show tracks and dislocation loops in the crystal

For ionic solids the main damage is caused by ionization, and electron processes, similar to those discussed earlier, operate. In addition, thermal effects, recoil, and decomposition of the anion may occur depending on the nature of the radiation. Covalent solids are in general more stable. Point defects can be created, and strain and dislocations introduced into the lattice. Localized decomposition has also been found. Fission fragments can cause an appreciable increase in surface area of the solid. All of these factors can influence the rate of the subsequent decomposition. Although the rates of decomposition may be enhanced, the effects observed up to the present have not been very spectacular. In no case has an explosion resulted with the possible exception of electron bombardment and here heating has been shown to be responsible for the explosion. This is perhaps a fortunate result since explosive solids are already sufficiently dangerous to handle, without the added concern of excessive sensitization by ionizing radiation.

REFERENCES

Books:

1. F. P. Bowden and A. D. Yoffe, *Fast Reactions in Solids*, Butterworths, 1958.
2. J. H. De Boer, Ed., *Reactivity of Solids*, Elsevier, 1961.
3. C. B. Colburn, Ed., *Developments in Inorganic Nitrogen Chemistry*, Elsevier, 1965. Chapter on Inorganic Azides by A. D. Yoffe.
4. W. E. Garner, Ed. *Chemistry of the Solid State*, Butterworths, 1955. Contains a number of excellent chapters on decomposition of explosives.
5. "Radiation Damage in Solids", Course 18, 1962, Proceedings of the International School of Physics, "Enrico Fermi", Academic Press.

Reviews:

6. F. P. Bowden and A. D. Yoffe, Endeavour 21, 125 (1962). See also A. D. Yoffe, *Proc. Royal Inst. Chem.*, 1961, p. 174 on properties of sensitive compounds.
7. B. L. Evans, P. Gray and A. D. Yoffe Chem. Rev. 59, 515 (1959) for review on azides. Also P. Gray, Quart. Rev. Chem. Soc., London, 17, 441 (1963).
8. P. Gray and A. Williams, Chem. Rev. 59, 239 (1959) on the thermochemistry and reactivity of alkoxyl radicals.
9. A. Mace., Chem. Rev. 62, 41 (1962), sensitivity of explosives.
10. A. Makovsky and L. Lenji, Chem. Rev. 58, 627 (1958), on nitromethane.

The following references are given to act more as a source of reference than to show priority over other investigations.

11. Trudy E. Smith and J. C. Calvert, J. Phys. Chem. 63, 1305 (1959), thermal decomposition of 2-nitropropane.
12. A. J. C. Nicholson, Nature 190, 143 (1961), Photolysis of nitromethane.
13. A. K. Galwey and P. W. M. Jacobs, *J. Chem. Soc.*, p. 837, (1959); p. 5031, (1960). High temperature thermal decomposition of ammonium perchlorate.
14. F. Solymosi and L. Revesz, Zeit. fur Anorg. Chem. 322, 86 (1963). Thermal decomposition of ammonium perchlorate in the presence of zinc oxide.
15. R. D. Smith, Trans. Faraday Soc. 53, 1340 (1957). Thermal decomposition of ammonium nitrate.
16. R. N. Brown and A. C. McLaren, Proc. Roy. Soc. (London) 266A, 329 (1962). Mechanism of thermal transformations in solid ammonium nitrate.
17. Abstracts of Russian work on nitrate esters — the work of K. K. Andreev and coworkers; see Chem. Abstr. 60, 2713 (1964).
18. Some recent work on radiation damage of explosives. See T. B. Flanagan, J. Phys. Chem. 66, 416 (1962). Lead styphnate.
19. J. Jack, Trans. Faraday Soc. 59, 947 (1963). Thermal decomposition of irradiated lead azide.

CHAPTER 5 MEASUREMENT OF DETONATION PROPERTIES

5-1 INTRODUCTION

In Chapters 2 and 6, relationships among the detonation parameters are derived and discussed. Some of these parameters—namely, velocity and conductivity—are readily measurable quantities. Others, such as pressure and temperature are difficult if not impossible to measure at the present time. In this chapter the current and most commonly used techniques for the measurement of detonation parameters are presented. The techniques are grouped according to the parameter being measured. Where a technique is applicable to the measurement of several parameters, it is discussed in detail only when first encountered. Date representative of some of the techniques are included. More extensive data may be found in the references.

5-2 DETONATION VELOCITY

Detonation velocity D is the most readily measured property of the detonation wave. Consequently, much of detonation theory centers on this quantity. A large body of theory concerns the state of the explosive products, a state which was perhaps the most unusual condition of matter prior to the advent of nuclear explosions. The explosive products in the detonation wave consist mainly of gases, sometimes mixed with solid particles of carbon or metal oxides, at a very high temperature at a density greater than that of the original solid or liquid explosive. The pressure is enormous; and the behavior, therefore, is far from the near ideal-gas behavior evidenced under more normal conditions. The nonideality of the product gases makes the detonation velocity in condensed explosives depend strongly on the initial bulk density of the explosive ρ_o. The detonation velocity in gas mixture does not change very much with initial density. Empirically, the dependence of D on ρ_o can be expressed quite accurately by a linear formula: $D = D_1 + M/\rho_o$, where D_1 is the detonation velocity at unit density. Data on the dependence of detonation velocity on initial density have been the major source of information about the equation of state of the product gases; and, although the exact equation of state cannot be determined on the basis of these data alone, a considerable body of knowledge on this subject has been obtained. This topic is taken up in Chapter 7.

5-2.1 HIGH-SPEED PHOTOGRAPHY

The extremely high and remarkably constant wave velocity was the phenomenon that first attracted scientific attention to the study of detonation. The major experimental tool for observing this pheonomenon has been and still remains high-speed photography[1]; to describe all the ingenious cameras that have been developed for this specific purpose would demand a book in itself. The discussion which follows is, therefore, limited to the most commonly used cameras.

The classical work was done with a rotating-drum or a rotating-mirror camera. This type of device, sometimes called a "streak" camera, is useful primarily for measuring the velocity of a wave front or the motion of a surface. (The drum camera principle is illustrated in Fig. 5-1.) The field of view of the camera lens is masked except for a narrow slit parallel to the rotational axis of the camera. The camera is aligned so the slit is parallel to the direction in which velocity is to be recorded; for example, to measure detonation velocity, the camera is set up so that the slit is parallel to the axis of the explosive stick. The rotating-drum camera has the film mounted on a rotating cylinder, preferably on the inside so that it does not fly off. The image of the luminous wave front leaves a diagonal trace on the film, the slope of which is a measure of the velocity. A rotating-mirror camera is similar, except that the film is stationary and the image is swept over it by means of a rotating plane mirror. This makes possible much higher effective speeds.

The precision of a velocity measurement with a streak camera depends among other things on the "writing speed", i.e., the velocity of the image on the film. Present-day cameras of this type have a speed of up to 10 mm per μsec. With such devices, velocity can be measured with an accuracy of about 0.1 percent.

Although streak cameras have provided many of the important data concerning detonation, they do not furnish an image that allows one to

PAUL M. SCHUMACHER
062-40-5056

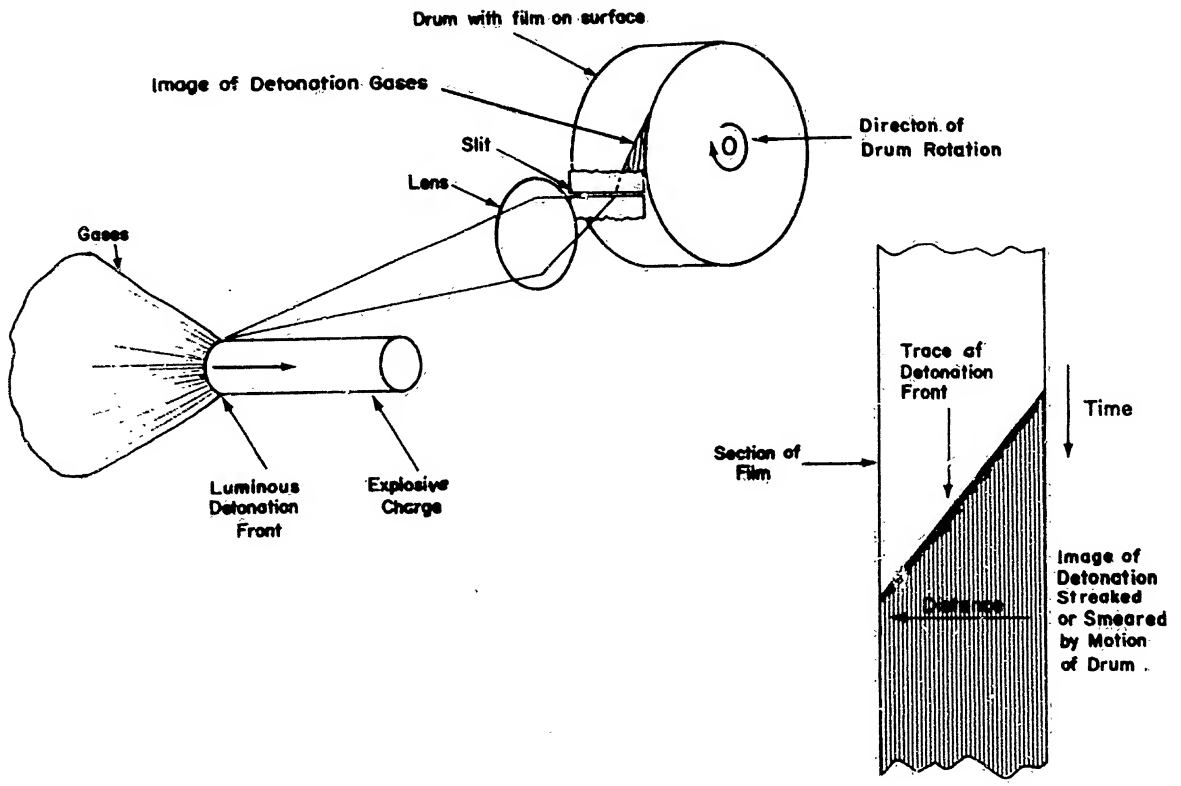

Figure 5-1. Elements of the Rotating Drum Camera System

directly "see" a phenomenon. Great advances came about during World War II, therefore, when very high-speed motion picture cameras (or "framing" cameras as they are usually called) were developed. (The principal elements in the scheme are depicted in Fig. 5-2.) With these devices, rates up to 15×10^6 frames per second have been obtained. Such cameras are now available commercially. A rotating mirror is used to sweep the image over a bank of individual "relay" lenses that serve to "stop" the motion in discrete intervals and project on the film a sequence of stationary images, one for each lens. Thus, the number of frames is limited by the number of lenses. A common camera of this type has some 24 lenses and supplies a corresponding number of sequential photographs.

So-called "image dissection" has been applied to obtain much higher effective framing rates, up to 10^8 or even 10^9 frames per second. This technique involves dividing the image into elements that are "scrambled" on the film, thereby reducing the length of film that has to be scanned in each frame by the rotating mirror. To reassemble the image, the separate parts are "unscrambled" by reversing the process. Image dissection results in a loss of detail in those techniques where portions between elements are actually not recorded on the film, or loss of resolution when optical distortion of the separate parts is involved in displacing or compressing the images on the film.

In photographing many high-explosive phenomena the self-light produced by the detonation is all that is needed to form the desired image on the photographic plate. But in some cases external illumination is needed. A common light source for this purpose is the argon flash charge. Essentially this is just an explosive charge such as Composition B in an atmosphere of argon. Because argon is monatomic and has a high electronic excitation energy, the shock wave near the surface of an explosive charge produces a very high temperature and thus an intense source of light. By tailoring the geometry of the charge and the size and shape of the argon envelope, the intensity and duration of the light can be modified to suit the experiment. Timing of the light flash can be synchronized by use of a suitable circuit to fire the charge. The peak luminosity of the argon flash charge is said to be 5 to 7 million candlepower per square centimeter. Duration may be varied from as little as 10^{-8} sec to several hundred microseconds.

Another light source for high-speed photography is the exploding wire. Electrical energy stored at high voltage in a condenser is discharged into a fine wire of silver or copper. A bright flash is obtained, lasting for 50 to 60 μsec. Alternatively, a spark discharge is often used to obtain a very brief exposure.

Single-exposure photographs of exploding charges can be made in a variety of ways. If the self-luminosity is not too great, an argon flash charge or a spark of brief duration can be used. Or, if the luminosity of the charge itself is too high, the motion can be stopped by means of a high-speed shutter[2]. One type of shutter exploits the Kerr effect (see Fig. 5-3), which is the polarization of light passing through certain liquids when they are subjected to a high electric field. The Kerr shutter uses nitrobenzene in a glass cell containing two electrodes. The cell is

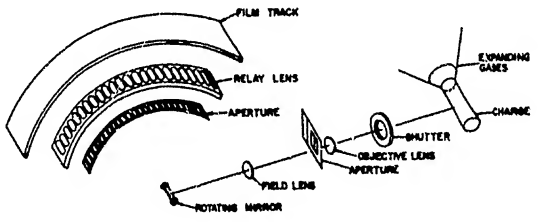

Figure 5-2. Optical System in AEC-Bowen Framing Camera

situated between crossed Nicol prisms, and the assembly is placed in front of the camera lens. When an electrical pulse of short duration is applied to the electrodes, light is allowed to pass. The open time of the Kerr cell can be as small as a few nanoseconds (10^{-9} sec). Another type of shutter which is more convenient but not as fast exploits the Faraday, or magneto-optic, effect. Here polarization is produced in a dense flint glass plate by inducing a strong magnetic field.

5-2.2 PHOTO-OPTICAL SYSTEMS

While mechanical and optical techniques have been highly developed in the photography of detonation phenomena, the possibilities that exist in the field of electronics involving, for example, the photoelectric effect and the cathode ray tube have only recently been exploited. Ingenious work in this area is the work of J. S. Courtney-Pratt[3] which has been directed especially toward the study of fast events on a micro scale, such as the initiation of detonation in a single crystal of lead azide. One application is the image-converter tube in which a photosensitive screen acts as the source of electrons (cathode) in a cathode ray tube. With this device the intensity of the image can be amplified many fold. Also, by means of electrostatic or magnetic deflection of the electrons, the image can be scanned at very high speed. A combination of these techniques makes it possible to achieve effective writing speeds some 100 times greater than those in a rotating mirror camera. Also, a very effective shutter for single-frame or multiframe photographs can be obtained by "gating" the passage of electrons in the image converter tube. Several image converter cameras are presently available commercially.

5-2.3 ELECTRICAL SYSTEMS

Although the streak camera is an important and in some cases indispensable tool for measuring detonation velocity, a more convenient technique[4] commonly employed in routine work is the use of "ionization probes". These detect the passage of the detonation wave as a result of the electrical conductivity in the reaction zone. A series of two or more such probes are imbedded in the charge, spaced at intervals along the surface. By means of suitable electrical circuits, the passage of the detonation wave front is signaled to a cathode ray tube and displayed on a time base. The average detonation velocity between two probes may

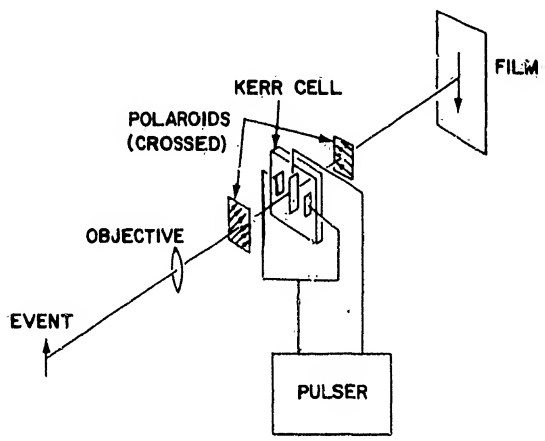

Figure 5-3. Arrangement of a Kerr-effect Shutter

then be calculated from the separation distance and the time interval between signals.

The ionization probe itself may consist of two wires held a small distance apart with a voltage source—such as a charged condenser—applied across the gap and a series resistance to indicate the passage of current. A convenient type of probe for many purposes consists of a pair of enamel-covered wires that are twisted together. The enamel is quickly burned off in the heat of the detonation front.

For the time base, a combination of a triangle-wave generator applied to the horizontal deflection plates of an oscilloscope and a single linear sweep applied to the vertical plates gives a zig-zag raster of long duration and high resolution. Time markings may be applied by means of either beam intensity modulation or beam deflection. The circuit elements are shown schematically in Fig. 5-4, and the type of record obtained is shown in Fig. 5-5.

The common ionization probe method is useful only for obtaining average velocities in a series of intervals. When one wants to measure accurately a rapidly changing velocity (for example, in ionization experiments), a variation of this technique can be used which yields a continuous distance-time trace like that given by a streak camera. In this arrangement two long parallel lengths of resistance wire are inserted on the axis of the explosive charge and attached to a voltage source. As the detonation wave advances it effectively shorts out the two wires at the wave front and thus reduces the series resistance in the electrical circuit by the fractional extent to which the wave has progressed along the length of the wires from the open end. By suitable circuitry a resistance vs time trace can be displayed on an oscilloscope screen, which is essentially equivalent to distance vs time for the detonation wave.

Still another method of measuring detonation velocity has been studied by Cook[1]; this involves using the explosive charge as a wave guide for microwaves.

5-2.4 D'AUTRICHE METHOD

Besides these relatively sophisticated techniques, there is a simple velocity test known as the D'Autriche method. This is still used to some extent in routine testing of dynamites. It employs a detonating cord as a standard and gives a measure of the velocity in the test stick compared to that in the cord. The test arrangement is shown in Fig. 5-6. The ends of a loop of detonating cord are inserted in the test stick and the middle is taped to a metal "teller" rod (lead or steel are often used). The exact mid-point of the detonating cord is marked on the teller rod. When the stick detonates it induces detonation in the two ends of the detonating cord, not simultaneously, but at an interval between equal to the test base line ℓ_t divided by the detonation velocity D_t in the test stick. The two detonation fronts traveling from opposite ends of the cord with a speed D_s converge at some point a distance ℓ_s beyond the mid-point toward the rear end of the loop. At the point of meeting head-on, the detonation waves produce a sharp dent in the teller rod which is readily identified. The ratio D_t/D_s of the velocities is equal to one-half the ratio ℓ_t/ℓ_s of the lengths and if D_s is known, D_t can be determined. The accuracy, of course, depends on the reliability of the value for D_s and on the care with which the test is carried out.

5-3 DETONATION PRESSURE

The problem of measuring the extremely high and short-lived pressure in the detonation wave initially seems insurmountable. Theory predicts the magnitude to be some hundreds of kilobars, a level that may be compared, for example, to a head of water thousands of miles deep. These pressures equal or exceed the highest levels that can be produced in any other way at the present time. Indeed, the generation of shock waves in materials placed in contact with high explosives or impacted by explosively accelerated plates affords an important unique means for studying certain phenomena at the limit of man-made pressures.

No direct standards or scales are available against which pressures of this magnitude can be compared. However, a sound basis for the determination of pressure is provided in the laws of motion. In fact, we now posess very accurate measurements of pressure in the detonation of various explosives, plus a wealth of precise data on the behavior of many inert materials at these high pressures[5].

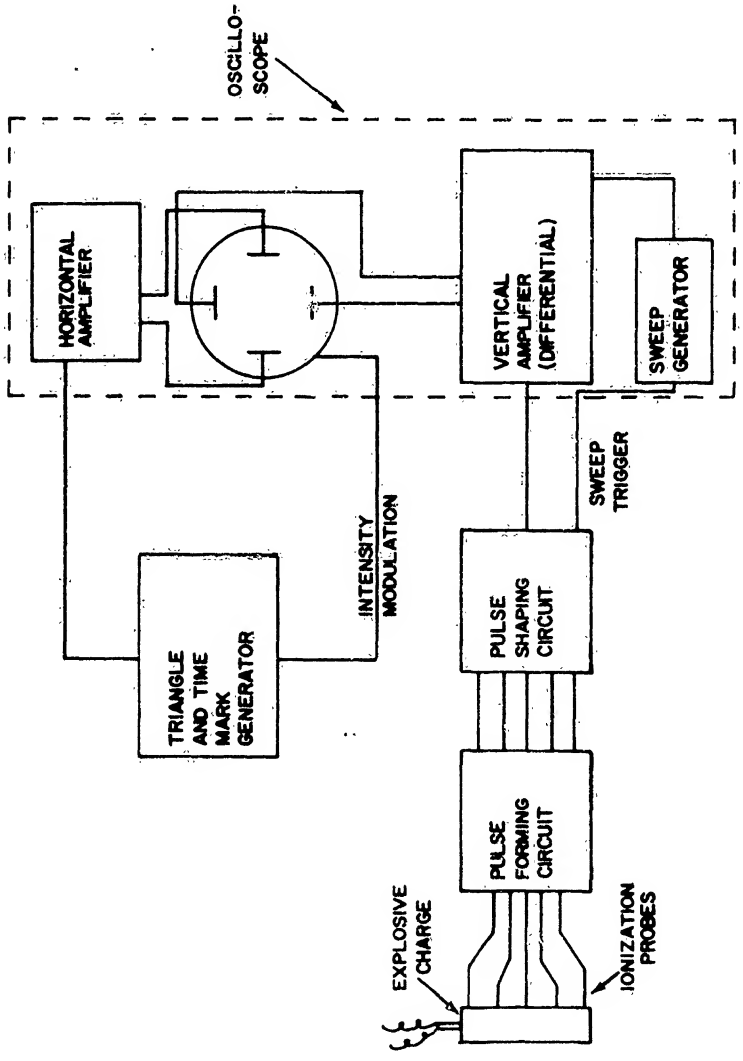

Figure 5-4. Block Diagram of Equipment for Measuring Detonation Velocity With Ionization Probes

The mechanical conservation equation expressing conservation of momentum across a shock front (Eq. 2-133 of Chapter 2) relates pressure across the front $p_1 - p_o$ to three measurable quantities—initial density ρ_o of the unshocked material, shock velocity U, and particle velocity u_1 of the shocked material—according to

$$p_1 - p_o = \rho_o u_1 U \tag{5-1}$$

In a steady state wave, U is readily measured. Determination of p_1 hinges, then, on finding u_1. In general, two ways are possible to determine u_1, the most common being to measure the velocity u_{fs} at a free surface. For a shock wave in a condensed nonporous medium, u_{fs} may be equated without much error to exactly twice u_1, i.e.,

$$u_{fs} = 2u_1 \tag{5-2}$$

Eq. 5-2 is rigorous only in the infinitesimal acoustic approximation. It amounts to neglecting the entropy increase at the shock front and the energy dissipated in plastic deformation. For many condensed, nonporous materials, Eq. 5-2 is a reasonable approximation at high pressure.

Another method of obtaining u_1 is to measure the density ρ_1 behind the shock front by flash X-ray densitometry. This value may then be used to determine u_1 through the equation for conservation of mass (Eq. 2-129)

$$\rho_o U = \rho_1 (U - u_1) \tag{5-3}$$

A close estimate of the particle velocity associated with the C-J pressure (equilibrium

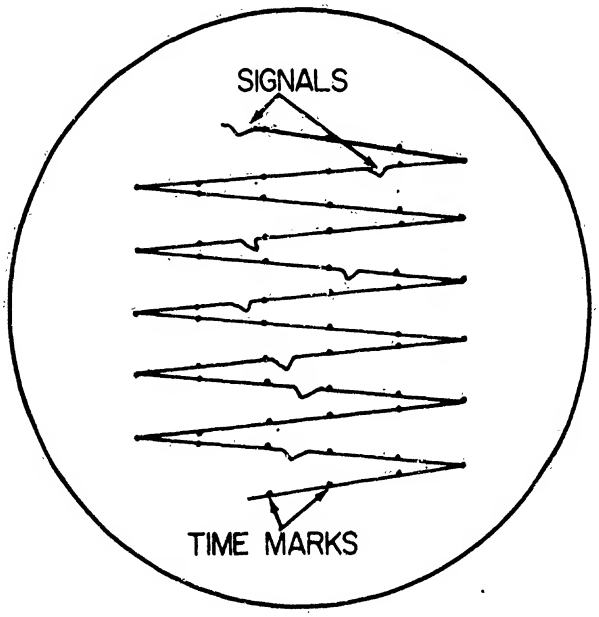

Figure 5-5. Zig-zag Oscilloscope Trace Obtained With Raster Generator

pressure at the end of the reaction zone) in a detonating explosive can be obtained from a theoretical equation due to H. Jones[6], which is discussed in par. 7-3. This equation (Eq. 7-30) relates u_1 to detonation velocity and other properties of the explosive.

$$u_1 = D/[g_o(2 + \alpha)] \qquad (5\text{-}4)$$

where $g_o = 1 + d\ell nD/d\ell n\ \rho_o$, and α is a dimensionless number that depends on certain thermodynamic properties. The value of α is close to 0.25. For many explosives g_o is approximately equal to 1.7; hence, one may estimate u_1 from D by the approximate relation

$$u_1 = 0.26\ D \qquad (5\text{-}5)$$

Combining Eq. 5-5 and Eq. 5-1, one obtains (neglecting p_o)

$$p_1 = 0.26\rho_o D^2 \qquad (5\text{-}6)$$

Eq. 5-6 gives values usually within a few percent of those determined experimentally.

Pressure measurements obtained at the Los Alamos Laboratory[7,8] are given in Table 5-1. The number of significant figures reported is indicative of the accuracy of this work. The last line of the table gives the pressure calculated by substitution of the values for ρ_o and D in the approximate relation Eq. 5-6. The agreement shows that this is indeed quite a useful formula.

5-3.1 PRESSURE IN ADJACENT PLATES

Pressures in the detonation wave have been very accurately determined by the measurement of pressure in a metal plate in contact with an explosive. The method was proposed by Goranson[9] at Los Alamos in 1945, but such were the rigors of the technique that results were not forthcoming until some ten years later [5-9]. Both the theory and the methods in this type of experiment are somewhat involved and cannot be discussed fully here. The reader is

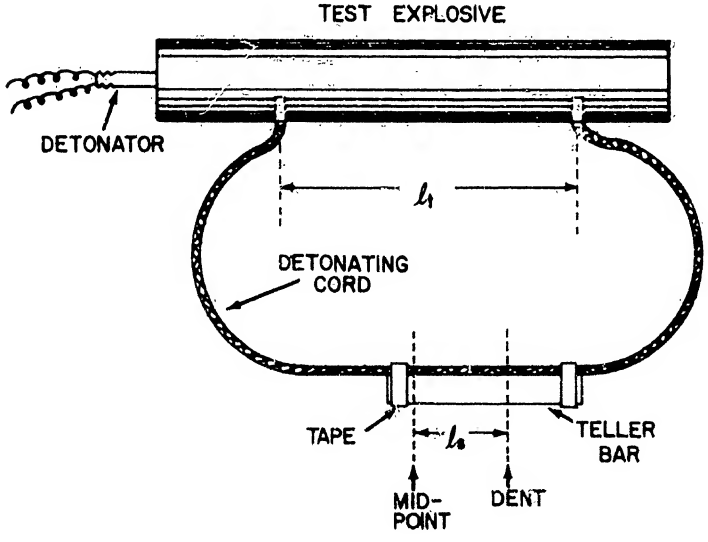

Figure 5-6. D'Autriche Test System

TABLE 5-1 CHAPMAN-JOUGUET PRESSURES IN VARIOUS EXPLOSIVES

Parameter	RDX[5]	TNT[5]	63/37 Comp. B[7]	64/36 Comp. B[5]	77/23 Cyclotol[5]
Density ρ_o, g/cm^3	1.767	1.637	1.67	1.713	1.743
Detonation Velocity D, m/sec	8639	6942	7868	8018	8252
C-J Pressure, kbar: meas.	337.9	189.1	272	292.2	312.5
Eq. 5-6	345	207	272	290	312

referred for details to the given references. However, the basic ideas are simple. The pressure p_m behind the shock wave in the metal plate is determined through Eqs. 5-1 and 5-2 by a simultaneous measurement of shock wave velocity U and free-surface velocity u_{fs}. This determination is made for several thicknesses of metal and extrapolated to zero or near-zero thickness, depending on whether the initial pressure in the precursor shock (the so-called "von Neumann spike") or the Chapman-Jouguet pressure is desired (see Fig. 5-7). The reason an extrapolation must be made is that the shock front in the metal is continually attenuated as it passes through the metal because of the "overtaking" effect of the rarefaction traveling behind it. Thus, if one wishes to determine the pressure at the interface between metal and explosive at the instant the detonation front first reaches that point, it is necessary to know the shock and free-surface velocity that would be produced in an infinitely thin plate. When the initial pressure p_m in the metal at the interface is known, pressure p_x in the incident detonation wave can be calculated from the "impedance-match" formula that governs the interaction which the wave experiences at the interface. An approximate but quite accurate version of this formula was deduced by Duff and Houston[7]; it is

$$p_m/p_x = 2\rho_m U_m/(\rho_x U_x + \rho_m U_m) \qquad (5\text{-}7)$$

where ρ is the initial density, U the shock wave velocity, and the subscripts m and x refer to metal and explosive, respectively.

The pressure in the adjacent plate is usually determined by measuring particle velocity, free surface velocity, or stress transmitted to a second material. Techniques for generation of pressure pulses and measurement of pressure in the second material are discussed in the next three subparagraphs.

5-3.1.1 Plane Wave Explosive Systems

A prerequisite for measurements of pressure in plates is a means to obtain a very flat (planar) detonation wave front. Since the wave is initiated in a small area by a detonator cap, it starts out as a spreading spherical front. The problem is, therefore, to make an explosive "lens" that will convert the diverging wave front to a plane. This development came about at the Los Alamos Scientific Laboratory shortly after World War II. The "plane wave lens" has become indispensible for studying strong shock waves. The Los Alamos experiments customarily employ an 8-in.-diameter lens to initiate detonation in a precisely machined block of explosive. Experimental observations are confined to the central portion of the charge to avoid edge effects (rarefactions due to lateral expansion). Fig. 5-7(A) shows the charge geometry.

Fig. 5-7(B) shows the contour (pressure vs distance) of the detonation wave in the explosive charge before it reaches the explosive-metal interface. The wave front is a shock, and this is followed by a very rapid pressure decay in the narrow region where chemical reaction takes place. This portion is called the "von Neumann spike". Following the steep decay, a much more gradual pressure drop occurs in the rarefaction that proceeds from the detonating end of the charge. This portion is called the "Taylor wave". The Chapman-Jouguet point (C-J point) is at the juncture of these two portions, i.e., at the termination of the "von Neumann spike". At this point chemical

reaction is virtually complete. The C-J conditions determine the detonation velocity as well as other important parameters of the explosive. This subject is discussed in Chapter 6. The von Neumann region and the Taylor wave are described in Chapter 8 which deals with the structure in the detonation.

Fig. 5-7(C) shows the shape of the shock wave at a later time, after it has crossed the explosive/metal interface. Since most metals have a higher acoustic impedance than explosives (i.e., ρU higher for the metal than for the explosive), a shock wave rather than a rarefaction is reflected back from the metal surface into the detonation product gases in the explosive. This reflection occurs at the instant the shock wave meets the interface and, since pressure must always be equal on both sides of the interface, the transmitted shock advancing into the metal has at that moment the same pressure as the reflected shock in the explosive. However, as the two shock fronts advance, traveling in opposite directions away from the interface, the pressures change. The reflected shock changes because the wave is traveling back into a more rarefied region behind the detonation front. The transmitted shock changes because the front is constantly attenuated by the rarefaction behind it. The steep von Neumann spike region rapidly disappears in the metal since there is now no reaction process to feed energy to the shock front. Duff and Houston found that the spike vanished at a point about 1 mm from the interface of an aluminum plate in contact with Composition B. Fig. 5-7(C) shows the configuration after the spike has disappeared in the transmitter wave.

The wealth of information harvested from experiments involving measurements in adjacent plates is illustrated by data for water, Plexiglas, and aluminum shown in Fig. 5-8. These data were taken from Ref. 10. Such curves are known as Hugoniot curves (see par. 2-8) and reflect the compressibility of the material under dynamic conditions in a shock wave. The data of Professor Bridgman for Plexiglas[11] are also plotted in Fig. 5-8; these are isothermal points obtained in static experiments. They lie somewhat below the Hugoniot curve, as would be expected, but their position is consistent with the dynamic measurements. Comparison of the pressure range covered by dynamic measurements with that explored by Bridgman demonstrates the power of these new techniques.

At the present time the equation of state in the hundreds of kilobar range is known for about thirty metals as well as for many other materials. Recent measurements have yielded data in the megabar region for a number of materials[39]. With this information now available, and with certain simplifying assumptions, only the free-surface velocity is needed to determine pressure in a given experiment since the shock wave velocity can be calculated from the particle velocity by use of the equation of state.

5-3.1.2 Pressure Transducers

Recent work at several laboratories has resulted in the development of several devices for the measurement of pressure. These are the piezoelectric "quartz gage"[1,2,15] and a piezoresistive "manganin gage"[16-18] both of which are now being extensively applied to study the response of solids to shock waves. The manganin gage has also been employed in underground nuclear test programs as an "in-material" gage, measuring the stress history of earth media close to a nuclear event.

The quartz gage is well suited to the measurement of interface stress pulses up to several tens of kbars and with durations less than the transit time through the gage. The high time resolution of the gage is a consequence of the fact that the output signal from the gage is proportional to the instantaneous pressure difference across its faces. Hence, the gage need not come into mechanical equilibrium with its surroundings before a valid measurement of interface stress can be made. Fig. 5-9 shows a quartz gage in place on a block of metal, the rear face of which has been subjected to an impulse from an explosive plane wave generator. This impulse creates a shock wave propagating from left to right in the specimen. As the stress wave enters the x-cut quartz disk comprising the gage, a polarization vector P is produced by the relative displacement of the Si^{4+} ions and the O^{2-} ions in the quartz structure. Hence, the electric displacement vector $\vec{D} = \vec{P} + \epsilon_0 \vec{E}$ in the crystal changes with time, and for external short

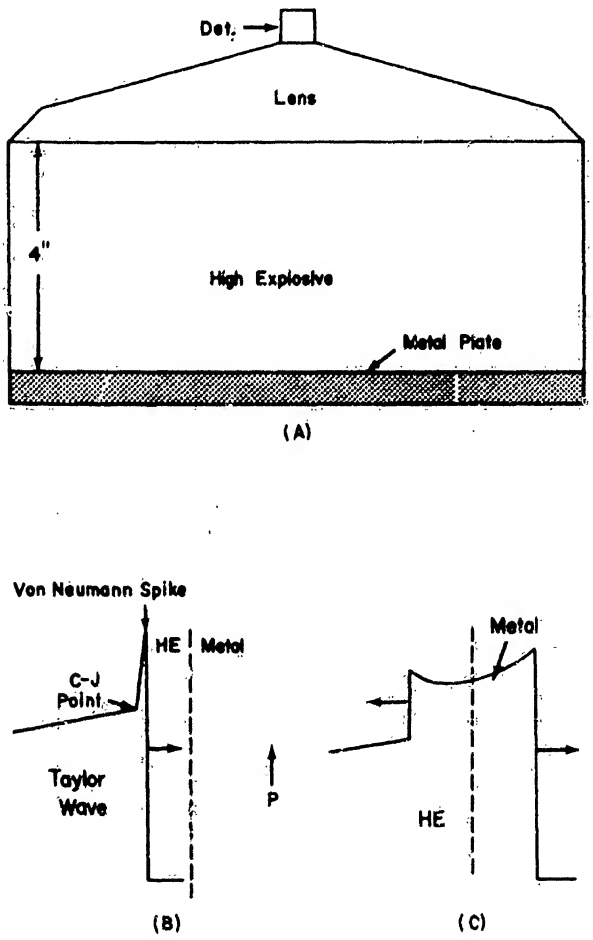

Figure 5-7. Plane-wave Generator (A), and Shock Wave Before (B) and After (C) It Impinges on the Metal Plate

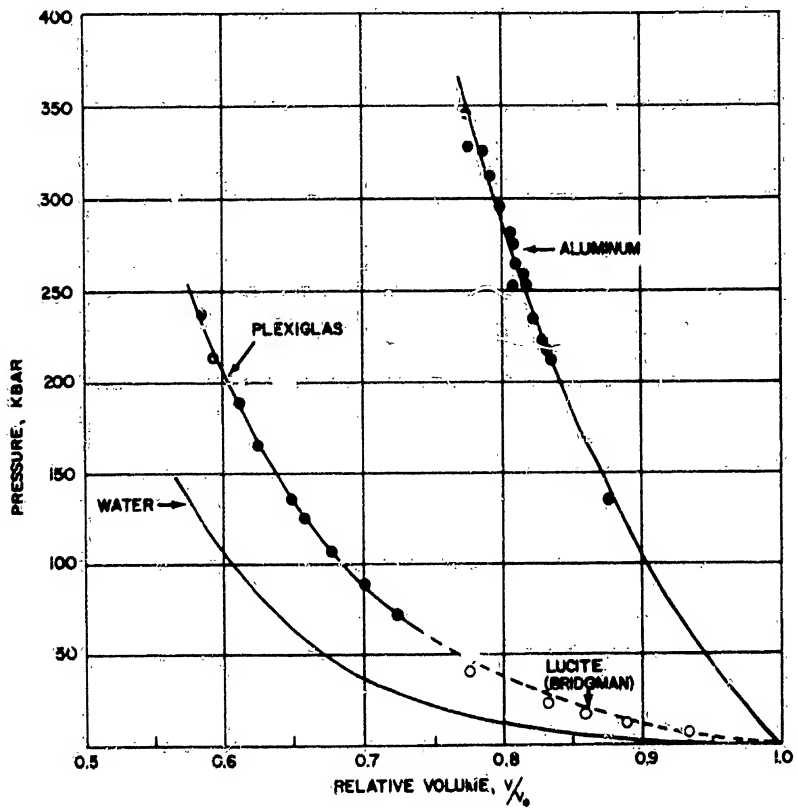

Figure 5-8. Compressibility of Various Materials Under Shock Wave Conditions

circuit conditions it is shown in Ref. 14 that one has

$$i(t) = A\left(\frac{dP}{dt}\right) = \frac{fAU}{\ell}\ [\sigma_o - \sigma_\ell] \qquad (5\text{-}8)$$

where $i(t)$ denotes the short circuit current, A the area of the crystal, f a piezoelectric constant, U the shock velocity in the quartz, ℓ the length of the crystal, and σ_o and σ_ℓ represent the x-components of stress at the stressed electrode and the rear face of the quartz crystal, respectively. Eq. 5-8 is derived with the aid of several assumptions, the details of which are given in Ref. 14. This equation provides a means of measuring the time dependence of $\sigma_o(t)$ by monitoring $i(t)$. Experimentally, it is found that Eq. 5-8 can be used for peak stress amplitudes of a few tens of kbars. The short-circuit current $i(t)$ is monitored by photographing, with the aid of an oscilloscope, the incremental time-dependent voltage $V(t) = Ri(t)$ developed across a small resistance R. We shall not describe here the procedures necessary to ensure that the observed voltage transient $V(t)$ is accurately proportional to the stress difference across the crystal, referring the reader instead to Refs. 13 through 15 for details of experimental technique and gage construction.

The piezoresistive manganin gage utilizes the change in resistance resulting from a change in resistivity and volume under compression as a measure of the applied stress. A common form of the gage consists of a fine wire embedded a small distance into a block of nonconducting material, usually a plastic. The block is placed in contact with the specimen such that the wire is near the interface. The response of the wire is a measure of the x-component of interface stress. The manganin gage has been used to much higher pressure than the quartz gage (several hundred rather than a few tens of kilobars). Also, recording times available with the manganin gage can be quite long: of the order of 10 μsec. In addition, the manganin gage can be embedded in a thin wafer within solids that are to be shock loaded, providing an in-material measurement of the x-component rather than a rear-surface measurement as does the quartz gage. Measurement uncertainties arising from impedance mismatch are thereby minimized.

The principle of operation of the piezoresistive transducer is simple. The application of pressure changes the resistivity and volume of a gage wire, the resistance of which is monitored by measuring the voltage developed across the gage when a steady current flows in it. In practice, use is made of a pulsed gage current to obtain substantial output voltage. Pulsed currents minimize heating of the gage wire unduly. Fig. 5-10 shows the configuration of a particular gage used in laboratory pressure measurements[15]. The current leads of the four-terminal resistor are marked I while the voltage leads are marked V. A flat-topped constant current pulse of about 3A peak amplitude is turned on approximately 2

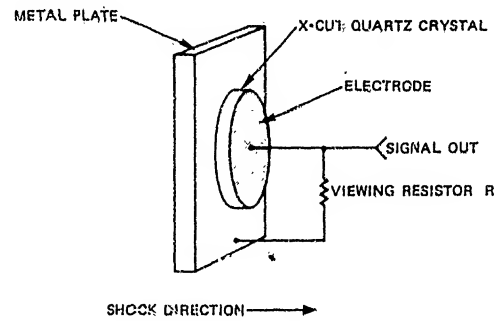

Figure 5-9. Configuration for the Measurement of Interface Stress Using a Quartz Pressure Transducer

μsec before the shock wave arrives at the gage wire. By Ohm's law, the change in gage wire resistance is directly proportional to the amplitude of the incremental voltage developed across it, and since the resistance change is in turn proportional to the pressure, the manganin gage provides a simple way of measuring dynamic pressures. The gage factor, i.e., the constant k in the equation $R(P) = kP$ where R denotes resistance and P stands for pressure, is determined by calculating pressure from a measurement of free-surface velocity U_{fs} and the shock velocity U of a shocked material in which the gage is embedded and then by applying the Hugoniot jump conditions discussed in par. 5-3 to determine the pressure associated with the shock wave. Simultaneously, the voltage transient $V(t)$ is measured across the gage. By repeating this experiment several times, one can obtain a set of point for a calibration curve relating P and $R(P)$. The relation appears to be accurately linear to about kbar. The value of k is on the order of 0.0029 ohm/ohm/kbar and varies with the alloy composition[16].

A pressure transducer utilizing a rotational polarization effect caused by the passage of a shock wave through dielectric materials consisting of polar molecules has also been developed[19-21], although it appears to have been less frequently applied in shock physics experiments than either the manganin gage or the quartz gage. The principle of operation of this polarization gage is qualitatively similar to that of the quartz gage. The advancing shock wave aligns permanent dipoles present in polar dielectrics so as to cause a polarization vector to appear in these materials. This effect causes the plane parallel capacitor consisting of the dielectric and two metallic electrodes to become charged. The current from this capacitor is monitored by measuring the voltage drop across a small resistor in an external circuit. Such a transducer has a fast response and is, therefore, well suited to the study of details of shock wave structure. The available recording time is typically 2 to 3 μsec. Fig. 5-11 illustrates the kind of record obtained. The polarization transducer appears to be less convenient to use than either the manganin gage or the quartz gage

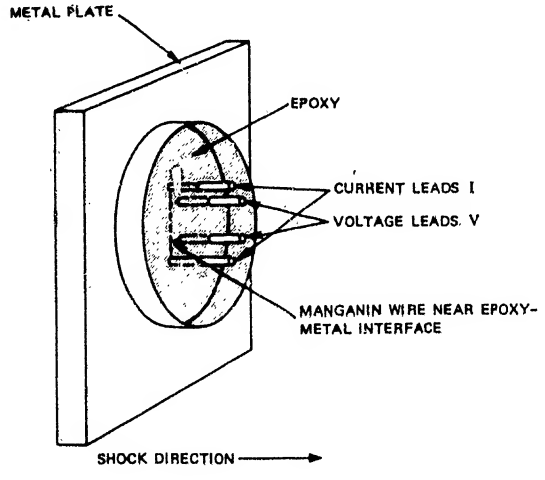

Figure 5-10. Configuration of Manganin-epoxy Pressure Transducer

since a threshold pressure of about 30 kbars exists, below which no output signal is obtained, and since the pressure versus output current relations are nonlinear in ways specific to the particular dielectric materials used.

One other pressure transducer will be mentioned here, i.e., the "sulfur gage" described in Ref. 21. Sulfur exhibits a large decrease of electrical resistance when it is subjected to pressures in the detonation range, changing from an excellent insulator a 1 bar to a good conductor at 200 kbar. This property has been exploited in a transducer to measure pressures in shock waves [21-22]. The response of the sulfur gage is nonlinear; also unlike manganin, the plot of resistivity versus pressure for sulfur exhibits marked curvature. In addition, above 200 kbar the resistivity of sulfur is so low that its measurement is inconvenient. For these reasons, comparatively little work has been published in which the sulfur gage has been used to monitor pressure wave profiles.

5-3.1.3 Particle Velocity Measurement

Various means have been employed to measure shock and free-surface velocities in the metal plate[23]. The earliest work employed a pin technique. Pointed metal pins were spaced at graded distances from the free surface. When the surface was impelled forward by the impacting shock front, it made contact with each of the pins in turn. The pins were wired to separate pulse-forming circuits, and the pulses produced on contact were displayed on a high-speed oscilliscope sweep. In this way the free surface velocity was measured. To determine shock velocity, small wells were drilled at various depths in the surface of the plate and in each well a pin was placed almost in contact with the bottom surface. Thus, as the shock wave arrived at each of these points (before reaching the main free surface) it caused a contact to be made almost instantly. In this way the shock wave velocity was measured inside the metal plate within a short distance of the free surface. What is desired is an instantaneous reading of shock velocity at the surface. Since the shock is constantly attenuating (a typical rate of attenuation 0.5 in. from the explosive/metal interface is 10 percent per in.), it is necessary to have velocity measurements within a few tenths of a millimeter of the surface. The technique, therefore, requires the utmost precision in machining the test specimens. Nonplanarity in the detonation front can also lead to serious errors. Work in this field, therefore, represents the culmination of patient effort in a most demanding endeavor.

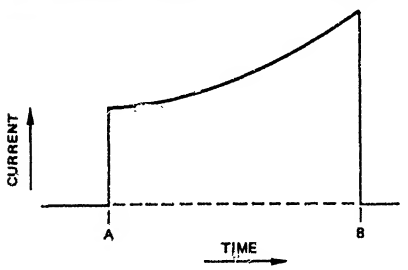

A Shock front enters dielectric
B Shock front arrives at second electrode

Figure 5-11. Form of Polarization Signal from Polarization Gage

Another means to measure shock and free-surface velocities is the "Lucite wedge" technique[5] illustrated in Fig. 5-12(A). A flat-bottom groove is milled in the form of a ramp, making an angle of 10° with the metal surface. One end of a Lucite rod of rectangular cross section is placed in the ramp and the other end extending about an equal distance beyond, forming a wedge-shaped space between the rod and the metal surface. The Lucite rod does not rest directly on the metal surface in the ramp but is shimmed up so that there is a narrow gap between. Likewise, a thin metal sheet is placed over the under surface of the overhanging portion of Lucite and separated by shims so as to form a narrow gap at the surface of this portion of the rod. The gap under the Lucite rod is filled with argon. When the argon is suddenly compressed because of the movement of metal beneath, it flashes brightly. A streak camera is set up with the slit parallel to the long axis of the Lucite rod; a photograph like that shown in Fig. 5-12(B) is obtained. This yields the shock velocity and the free surface velocity on the same photograph. In later work it was found that a coating of paint filled with "microballoons" (very tiny, hollow plastic

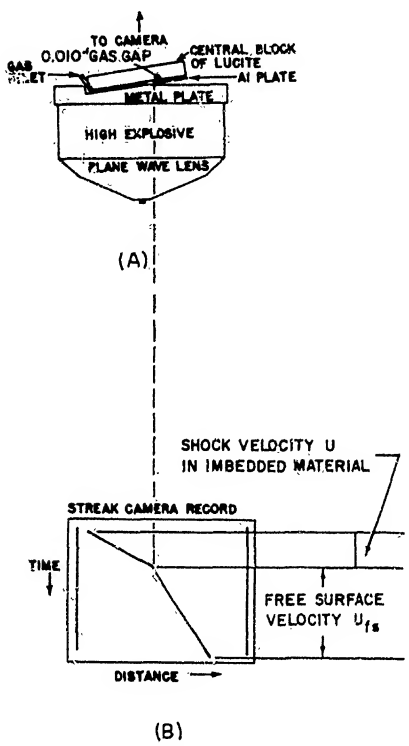

Figure 5-12. "Wedge" Technique for Measuring Free-surface Velocity and Shock Velocity

spheres) could be substituted for the argon-filled gap with equal effect.

A third method for measuring velocities employs Lucite and argon gaps in a similar way but does not use the wedge. Instead, the free-surface velocity is measured across a fixed gap between a Lucite block and the metal surface. Shock velocities are measured by attaching small metal blocks of various thicknesses to the surface of the main plate and recording the transit time of the shock wave in each by the argon-gap method.

The most recent advances in the measurement of particle velocity are the Faraday foil[24] and the laser interferometer, techniques[25]. With the interferometer, the movement of a reflecting surface can be monitored as a function of time. The surface can be a free surface or in transparent materials a reflecting plane within or between two specimens. The Faraday foil technique provides a measurement of particle velocity in nonconductors. These two techniques are described here briefly. More detailed information can be found in the references.

The laser interferometer is shown schematically in Fig. 5-13. The parameter measured is the free surface velocity of the specimen material. The principle of operation is as follows. Light from the single frequency gas laser is focused on the surface of the target by means of a lens L1. The reflected light is recollimated by L2, and then split by a beam splitter B1. Half the light traverses the delay leg and is recombined with the undelayed half at beam splitter B2. The photomultiplier then records a signal whose brightness depends on the relative phases of the two beams. Since the delay leg is fixed and the wavelength of the input light is a function of free surface velocity (Doppler shift), the number of fringes recorded at the photomultiplier is related to the free surface velocity. The relationship can be derived as follows[25]. The Doppler shift is given by

$$\Delta\lambda(t) = -\left(\frac{2\lambda}{c}\right) u(t) \qquad (5\text{-}9)$$

where λ is the wavelength, c the speed of light, and $u(t)$ is the speed of the reflecting surface at time t. The delay leg length $N\lambda$ is

$$N\lambda = c\tau \qquad (5\text{-}10)$$

where τ is the time for light to traverse the delay leg. Differentiating Eq. 5-10 gives

$$\Delta N(t) = -\left(\frac{c\tau}{\lambda^2}\right) \Delta\lambda(t) \qquad (5\text{-}11)$$

and substituting for $\Delta\lambda$ in Eq. 5-9 from Eq. 5-11 gives

$$u(t) = \left(\frac{\lambda}{2\tau}\right) \Delta N(t) \qquad (5\text{-}12)$$

The number of fringes ΔN as a function of time are thus related to the reflecting surfaces velocity by a constant $\lambda/(2\tau)$.

The major advantages of the laser interferometer over previous free surface systems are the high time resolution and the high surface velocity capability. The limitations in rise time are limited by the capability of the photomultiplier or oscilloscope recording system. The bandwidth of each system is typically 600 MHz or a response time of ≈ 1 nsec.

The Faraday foil technique utilizes the voltage generated between ends of a conductor moving in a stationary magnetic field as a measure of foil velocity. Experimentally, a metal foil, small in the direction of shock propagation is placed in or between sections of a sample. The sample is placed in a uniform magnetic field and, as the sample is accelerated by the passage of a stress wave, the foil moves with the sample. The voltage induced across the foil is monitored as a function of time on an oscilloscope.

The relation between the voltage induced and particle velocity is

$$V = \vec{\ell} \cdot \left(\vec{u} \times \vec{H}/10^4 \right) \qquad (5\text{-}13)$$

where $\vec{\ell}$ is the length of conductor in millimeters, $\vec{u}$ is particle velocity in millimeters per microsecond, $\vec{H}$ is the field strength in gauss,

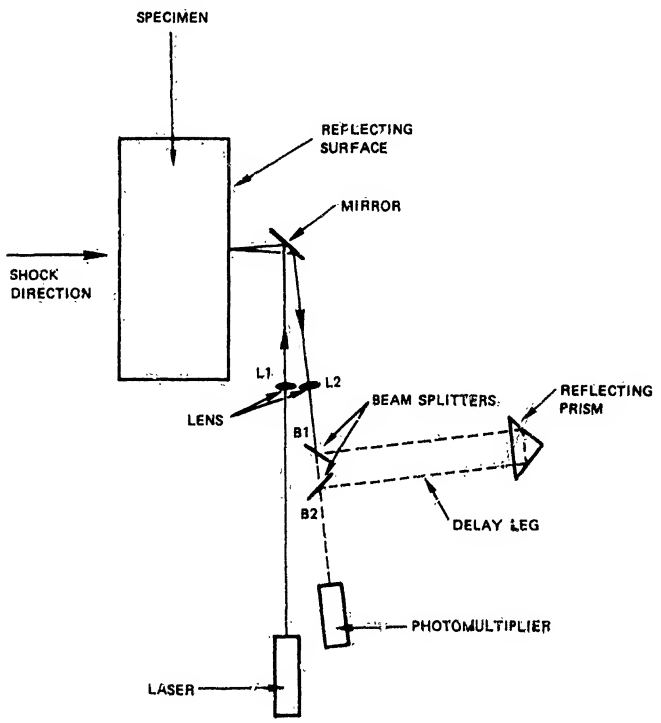

Figure 5-13. Laser Interferometer System (The velocity of the reflecting surface is related to the number of fringes observed by the photomultiplier.)

and V is the voltage in volts. The accuracy of measurement is limited by the ability to measure $\vec{H}$ and the effective length $\vec{\ell}$ of the conductor, and by a knowledge of the magnetic susceptibility change of the sample during shock loading.

Advantages of the Faraday foil technique are (1) high time resolution, (2) simplicity, and (3) most important, the capability of measurement within a test specimen. Disadvantages are the difficulty in calibration of the system and the restriction to measurement in a nonconductor.

5-3.2 X-RAY FLASH PHOTOGRAPHY

The use of X-ray holds great promise for the study of explosives but until quite recently X-ray sources have been inadequate to exploit the technique fully.

X-ray absorption furnishes an absolute measure of the density of matter. However, in many applications the important observations to be made with X-rays concern the geometrical relationships of shock fronts and contact surfaces; it is in this area where X-rays, because they make it possible to "see inside" the detonating explosive, provide a uniquely appropriate tool. Until now the difficulty has been the inability of available sources to penetrate charges more than a few inches in diameter. This has been a serious limitation. The advent of PHERMEX[28] will greatly reduce this problem.

The major published work with flash X-rays has been done by Schall[27] at Weil am Rhine (Institute de Saint Louis in France). In Ref. 27 Schall lists three determinations of detonation pressure based on flash X-ray photographs. One method involves the acceleration of a brass plate in contact with explosive. By measuring the curvature of the plate in the vicinity of the wave front, Schall estimated the pressure in Composition B to be 1.6×10^5 atm. This figure must underestimate the pressure at the front because it is obtained from an average value of the acceleration during the expansion of the explosive gas against the plate. Accordingly, the figure is not the instataneous initial value that relates to p_1.

Another pressure estimate reported by Schall was derived from an X-ray photograph showing the boundary of the expanding gas from an unconfined charge. Schall used the following approximate theoretical expression, ascribed to W. Döering and G. Burkhardt[28], which relates the angle α that this boundary makes with the charge axis and the effective adiabatic exponent of the product gases κ:

$$\alpha = \frac{\pi}{2}\left(\frac{\kappa + 1}{\kappa - 1}\right) - 1 \qquad (5\text{-}14)$$

From the observed angle of 40°, κ was calculated using Eq. 5-14. The value found was 2.8. The theory of detonation (Chapter 6) shows that the particle velocity u_1 is equal to $D/(\kappa + 1)$; hence, from Eq. 5-1

$$p_1 = \rho_o D^2/(\kappa + 1) \qquad (5\text{-}15)$$

Substituting the value for κ in Eq. 5-11, Schall obtained a value of 2.5×10^6 atm for the detonation pressure in Composition B.

It may be noted that the value of κ obtained by Schall from this simple measurement agrees very well with the value of 2.77 obtained from the isentrope as determined by Deal. Also, the factor $1/(\kappa + 1)$, which on the basis of Schall's work has a value of 0.26, agrees with the number obtained independently from the theoretical expression of Jones in Eq. 5-5. We have previously pointed to the agreement between pressures obtained from Jones' expression and the measured data (Table 5-1). Taken all together, these observations form a highly consistent picture.

By comparing the optical density in the X-ray photograph immediately behind the wave with that in front, Schall was able to estimate the ratio ρ_1/ρ_o, and hence to calculate the pressure, using Eq. 5-4 to find u_1 in terms of D. In this way he obtained a value of 1.9×10^5 atm for the detonation pressure in Composition B. This value is about 30 percent too low. The error is probably indicative of the limitations of the equipment in precise quantitative measurements of this kind.

An additional method of measuring detonation pressures involves flash X-rays to measure wave velocities in adjacent plates. Perpendicular incidence of a detonation at an interface can have one of several effects, depending on the impedance match between the explosive and the particular inert medium in contact. For dense metals, such as steel or lead, perpendicular incidence always results in a reflected shock. However, if the direction of

wave propagation is parallel to the surface of the metal or at a small angle, a rarefaction is produced in the explosive by the interaction. As the angle of incidence is increased, a point is reached where neither a rarefaction nor a shock is reflected, i.e., a "match" is obtained. This condition can be detected in flash X-ray photographs. Dr. Jane Dewey[30] of Ballistic Research Laboratories showed that when this condition of no reflection occurs, the detonation pressure can be calculated from a relationship involving the angle of incidence α and the angle δ by which the surface of the metal is depressed at the edge of the advancing detonation front. The relation is

$$p_1 = \frac{\rho_o D^2 \sin \delta}{\cos \alpha \sin (\alpha + \delta)} \qquad (5\text{-}16)$$

Observation of the precise angle for zero reflection proved to be difficult but the pressure values obtained independently in this manner confirm the validity of figures derived by other methods.

Work done with X-rays up to the present time thus corroborates very well the data obtained from other more precise but less direct types of measurements of the properties in the detonation wave. With the new commercially available high energy machines, much greater precision in data of this sort should be possible. More importantly, we should be able to learn a great deal more about three-dimensional effects in the detonation wave (e.g., the effect of the charge boundary) than is known at present.

5-4 BLAST WAVE PRESSURE

Precise measurements of shock wave pressures in air or under water are usually made by means of piezoelectric transducers. The favorite piezoelectric material is tourmaline but quartz has also been used. A good description of piezoelectric blast gages and how they are used is given in Ref. 31.

Measurement of pressure in air blast waves poses a special problem because of the large particle velocity or "wind" associated with the shock. The presence of the gage itself disturbs the flow in the medium and this can lead to serious errors unless special precautions are taken in the construction and mounting of the transducer. There are two well-defined ways to measure the pressure in the blast wave, usually referred to as "side-on" and "face-on." The first term applies to a measurement of the pressure sensed on the face of a transducer when it is oriented along the direction of travel of the shock wave, i.e., in a direction perpendicular to the shock front. Ideally, the gage should be mounted in an infinite baffle, or wall, which is aligned along a radius from the explosive charge. If the charge were fired on the ground, a side-on measurement could be made by mounting the gage flush with the ground surface. For side-on measurements in free air, the piezoelectric element must be mounted in a baffle of sufficient size and suitably shaped at the leading edge to minimize the distortion of the pressure field produced by the blast wave around the gage. Construction of a gage designed for this purpose at the Ballistic Research Laboratories is shown in Fig. 5-14.

Face-on measurement refers to the recording of pressure behind the reflected shock produced when the air blast wave strikes a massive wall at normal incidence. Since the air is brought to rest by the reflection, no problem of aerodynamic distortion arises here. A serious source of spurious signals in this case, however, is mechanical vibration of the wall or components of the mounting fixture. Special precautions must be taken to eliminate these undesirable effects. The peak overpressure of a face-on measurement is twice that of a side-on measurement at very low pressure levels (acoustic approximation) and increases to several times the side-on pressure, at higher pressures.

For the shock waves produced in air by high explosives, the most important parameters are the peak pressure and positive impulse $\int p dt$. Under water, the energy quantity obtained by evaluating the integral $\int p^2 dt$ under the pressure-time curve is also important for some considerations. A pressure and flow phenomenon known as the "bubble pulse", which follows at some distance behind the shock front, is also important in underwater effects. Some characteristics of shock waves in air and water are discussed in Chapter 13.

Various mechanical devices have been used to record shock wave effects both in air and underwater. The best known of these is the diaphragm or "Bikini" gage, the latter name deriving from the use of this device at the first

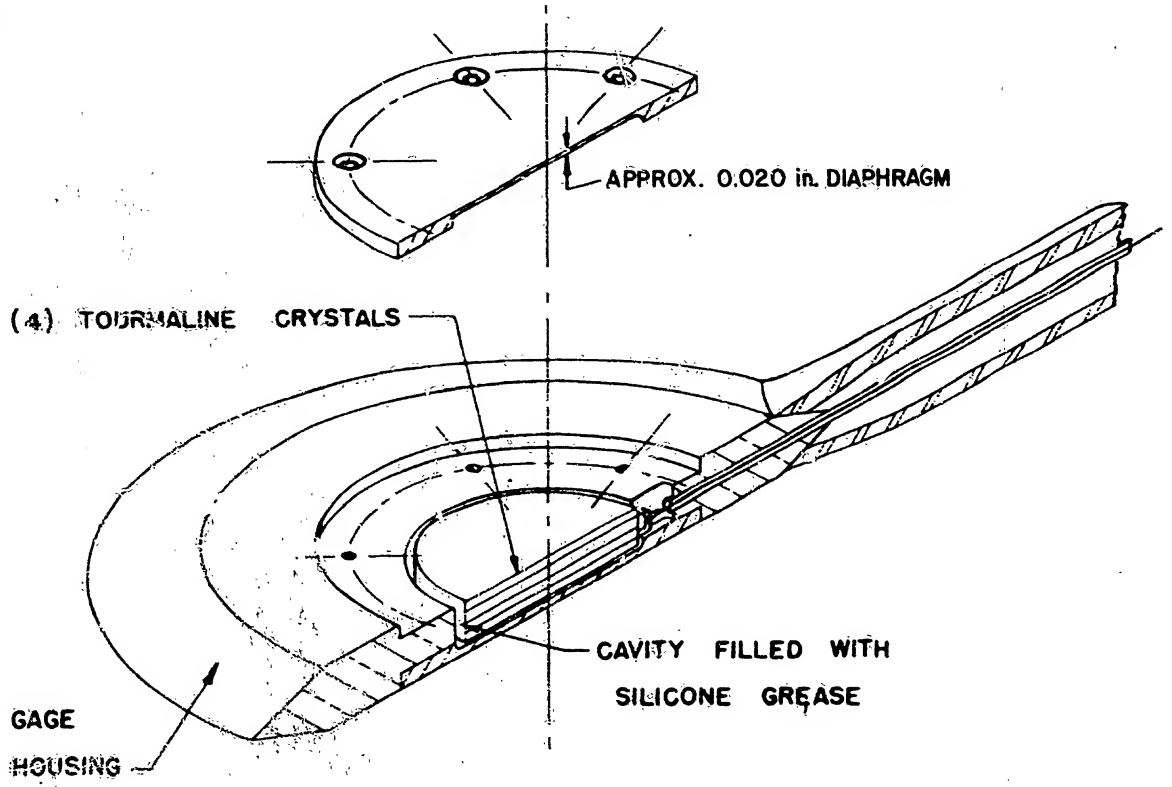

Figure 5-14. The Stretched Diaphragm BRL Piezoelectric Gage for Measuring Face-on Air-blast Pressures

nuclear bomb tests at Bikini Island after World War II. This gage consists of a sheet of aluminum foil clamped between two steel plates which have circular openings of various diameters. Several of these gages are placed face-on to the blast at various distances from the charge. After the charge is fired, the gages are inspected to determine the smallest-diameter hole in which the aluminum foil is broken in each case. This is a measure of the peak blast overpressure. These gages can be calibrated with known charges by means of the peak-pressure vs distance curves that have been compiled from piezoelectric data. If a sufficient number of diaphragm gages is used on a test so that significant statistical averages can be taken, these devices produce quite reliable information.

A mechanical gage for measuring blast impulse close to explosive charges is described in Ref. 32. This gage consists simply of a projectile in a cylindrical barrel which is mounted in the wall of a heavy concrete enclosure strong enough to withstand the blast. The projectile is placed on the mouth of the tube where it is exposed to the incident blast wave. It acquires a velocity proportional to the positive impulse in the wave. This gage appears to give quite accurate absolute measurements in a region where delicate piezoelectric instrumentation is not entirely practical.

Dewey[33], at the Shuffield Experimental Station in Alberta, Canada, has developed a technique to measure the air velocity associated with the blast wave. The method involves measuring the displacement of smoke trails in motion picture photographs. It is applicable especially to large charges of chemical explosives and to nuclear explosions. Good agreement with theoretical predictions has been obtained, except for oxygen-poor explosives like TNT. In the case of the latter, the detonation products continue to burn in the oxygen of the air. The relatively slow release of energy from this source causes an outward flow of air which contributes to the pressure and particle velocity in the "tail" of the blast wave. However, even for TNT, the particle velocity data at short distances behind the shock front are in good agreement with theory.

5-5 DETONATION TEMPERATURE

The agreement of various values of detonation pressure reviewed in this chapter may convey the impression that our knowledge of the detonation state is quite secure. Actually this is far from true. Except for Eq. 5-5, which is based on a theoretical deduction of Jones, the consistency of various estimates of pressure is merely testimony to the accuracy of experimental observations. The concepts from which these various means to measure pressure are derived are the continuity equation (conservation of matter) and the equation of motion (Newton's second law). The energy relation is not involved. Hence, experimental observations of pressure tell nothing about the thermal properties of the explosion products. This is obviously a matter of considerable interest, yet, strange to say, it has received relatively little attention from workers in this field. The reasons are not apparent because measurement of temperature would not seem to be fraught with unusual difficulties compared with other experimental determinations on explosives.

A method to measure detonation temperature and some experimental results are described by Gibson and his coworkers in Ref. 34. The temperature determination depends on measurement of the relative intensity of light at two different wavelengths and is based on the Wien displacement law (or Planck's distribution law). There are several assumptions implicit in this method: (1) that the emissivity of the medium at the two wavelengths is the same; this assumption is not likely to lead to serious errors, and (2) that the contribution to the measured light levels by the cooled expansion products is small. The apparatus was calibrated by standard methods, using a source of known temperature. Narrow bands of radiation at various wavelengths were obtained with a grating spectrograph. Several cross-checks were made in the determinations.

A summary of the temperature results for various explosives is given in Table 5-2. The authors varied the density of the explosives through a considerable range with the hope of answering the rather crucial question: whether the temperature increases or decreases when density is raised. They interpreted their results to show one trend in some cases and the other in other cases. However, the scatter is rather large and, if the few data for explosives with initial density below about 1.20 g/cm^3 are left out one is forced to conclude that these

measurements demonstrate no statistically significant trend one way or another. Therefore, in Table 5-2 the values in the density range 1.20 to 1.60 g/cm^3 for each explosive have been averaged. The figures in the table have probably have an experimental standard error of about 100° to 200° K.

The results in Table 5-2 are not consistent with theoretical values corresponding to any one of the several equations of state that have been suggested to describe the behavior of detonation products. The equation of state is an important part of the theoretical treatment of high explosives; and Chapter 7 is largely devoted to this subject. If one divides the equations of state that have been proposed into those which (1) postulate that little or none of the internal energy in the detonation products is due to intermolecular repulsive forces and (2) those which postulate that a relatively large fraction of the energy is in this form, these results generally favor the former. Indeed the measured temperatures in Table 5-2 for PETN, RDX, and EDNA are comparable with the highest values to result from any of the state equations that has been proposed.

A serious problem in experimental measurement of detonation temperature is due to the very high temperature produced in gases either on the inside or on the outside and in the vicinity of the explosive charge. Unless great precautions are taken, it is quite possible that radiation from shock-heated gases will be mistaken for radiation from the detonation products themselves. Since the luminosity depends on the fourth power of temperature, a relatively small quantity of gas at a very high temperature can contribute a very large amount of radiation. This effect was discovered by Gibson[34] who found that replacing the air occluded in the explosive charge with propane—propane having a much lower ratio of specific heats—led to much lower apparent temperatures, especially in charges of low bulk density. The authors reported, however, that these gas effects were essentially eliminated when the charges were "impregnated" with propane.

It may be significant that the temperature reported for nitroglycerin in Table 5-2 is considerably lower than would be expected in comparison with that for the other highly energetic explosives PETN and RDX. No matter which equation of state is chosen, the calculated detonation temperature of nitroglycerin is among the highest for any explosive, and yet it is far down on the scale in Table 5-2. This may be indicative that occluded gas effects, which are certainly not serious in liquid explosives like nitroglycerin, were not entirely eliminated in spite of the pains taken by the authors of Ref. 34 in this regard.

In concluding this review of detonation temperature, one is compelled to say that no completely satisfactory solution has been forthcoming up to this time. Workers in the field of detonation physics have in this area a challenging problem for the future.

5-6 ELECTRICAL CONDUCTIVITY IN THE DETONATION ZONE

Considerable interest in recent years has centered on the study of electrical conductivity in the detonation zone of high explosives. In some explosives the conductivity is relatively large, and there has been considerable speculation about the source of this

TABLE 5-2 EXPERIMENTAL DETONATION TEMPERATURES [34]

Explosive	*T*,° K	*Explosive*	*T*,° K
PETN	5720	Nitroglycerin	4020 (high order) 3200 (low order)
RDX	5550	Nitromethane	3800
EDNA	5430	Dynamite	
Tetryl	5180	(ρ_o = 1.05 g/cm^3)	2670

phenomenon. Here we shall only attempt to describe briefly the experimental methods and indicate the nature of some of the results. The reader may refer to the original works listed in the references cited in this paragraph for detailed interpretations.

In principle, various methods that have been used to measure conductivity are similar, although they differ in experimental detail and rigor of treatment. By measurement of the current i conducted between two electrodes in contact with a detonating charge when a voltage V is impressed, the resistance R is determined according to Ohm's law, i.e., $R = V/i$. At any given instant the electrodes make contact with a conducting zone of some given shape which may either be conjectured or experimentally mapped out in some way. If the conducting zone is considered to have uniform conductivity σ throughout, the value of this quantity may be obtained from R through the use of a factor K, which may be called the effective "cell constant"; thus, $\sigma = K/R$. The term "cell constant" derives from the more familiar problem of measuring the conductivity of an electrolyte solution in a "cell" or container into which the electrodes dip. The cell constant in this case is determined by the size, shape, and separation of the electrodes; the size and shape of the cell; and the placement of the electrodes in the cell or, in a word, by the "geometry" of the measuring device.

In Ref. 35 Jameson describes a method of placing electrical probes within the charge and by this means determining the shape of the zone having a high electrical conductivity. He finds that this is of a conical shape, the base of the cone being coincident with the detonation shock front and comprising the full cross section of the charge at this point. The conical surface presumably represents the front of the advancing rarefaction or "release" wave that spreads into the detonation zone from the free surface. Jameson made a "mock-up" of the conical conducting zone from graphite sheets of known electrical conductivity and in this way determined the cell constant K for the particular electrode arrangement used in the explosive experiment. The implicit assumption here is that σ is constant throughout the highly conducting zone mapped out by the probes. The value determined in this way for the resistivity of Composition B was 0.29 ohm-cm. Within an order of magnitude this agrees with values reported by other workers[36].

The method reported by Hayes[37] is considerably more elaborate. In the first place, Hayes extended the time resolution of his measurements about 1000-fold over other workers, employing nanosecond circuitry where others had used microsecond circuitry. And, instead of assuming that the conductivity throughout the detonation zone is constant, he has assumed that it varies as a function of time (or distance) behind the shock front, and has determined this function by an elaborate scheme using a high-speed digital computer to analyze the observed electrical wave form from the conductivity probe. Hayes discovered that the onset of conductivity begins immediately at the precursor shock front (see Chapter 8) and in some cases passes a peak within a few nanoseconds (which means, in terms of distance, only some several microns) behind the front. As between various explosives, the peak conductivity varies by orders of magnitude; also the variation of conductivity with time is decidedly different in various cases. Undoubtedly, this reflects wide differences in the reaction kinetics and in the physical and chemical nature of the reaction products.

Fig. 5-15, reproduced from Ref. 37, shows the conductivity profile in the detonation zone for three explosives: nitromethane, Composition B, and liquid TNT. Here, conductivity is shown as a function of time. For purposes of orientation, time may be derived from distance at the rate of about 6 microns/nsec. Thus, the full scale on the abscissa of Fig. 5-15 corresponds to little more than 1 mm. The units on the ordinate scale in Fig. 5-15 may be divided into 100 to obtain the resistivity in ohm-cm. Thus the lowest resistivity recorded for nitromethane is about 1 ohm-cm, for Comp. B about 0.1 ohm-cm, and for liquid TNT about 0.01 ohm-cm. The close agreement in the case of Comp. B with the value given by Jameson may be noted.

The highest value of conductivity in detonating explosives that has been recorded thus far (liquid TNT, Ref. 37) compares with that for an intrinsic semiconductor like germanium. It is less by a factor of 10 than the conductivity of graphite. If considered as a gaseous plasma, the detonation zone in liquid

TNT has a rather high conductivity; but, if it is considered as a condensed phase comparable with carbon black, for example, its conductivity is not surprising. Hayes' finding in Ref. 37 that the peak conductivity of various explosives shows a close correlation with the amount of solid carbon in the detonation products may, therefore, have a significant bearing on the nature of this phenomenon.

5-7 EMPIRICAL TESTS

In the early development of explosives, a number of empirical tests evolved to measure various "qualities" and "quantities" associated with the explosives. Among the qualities that different explosives possessed in varying degree was what came to be known by the French term "brisance" which was meant to reflect the shattering ability of an explosive, as distinguished from the "power" or ability to do work in moving rock, etc. Thus, it was recognized that the work capability was an extensive property that depended on the quantity of explosive; and the term "power", which in this connection is quite confusing to physicists, meant a "specific" property related

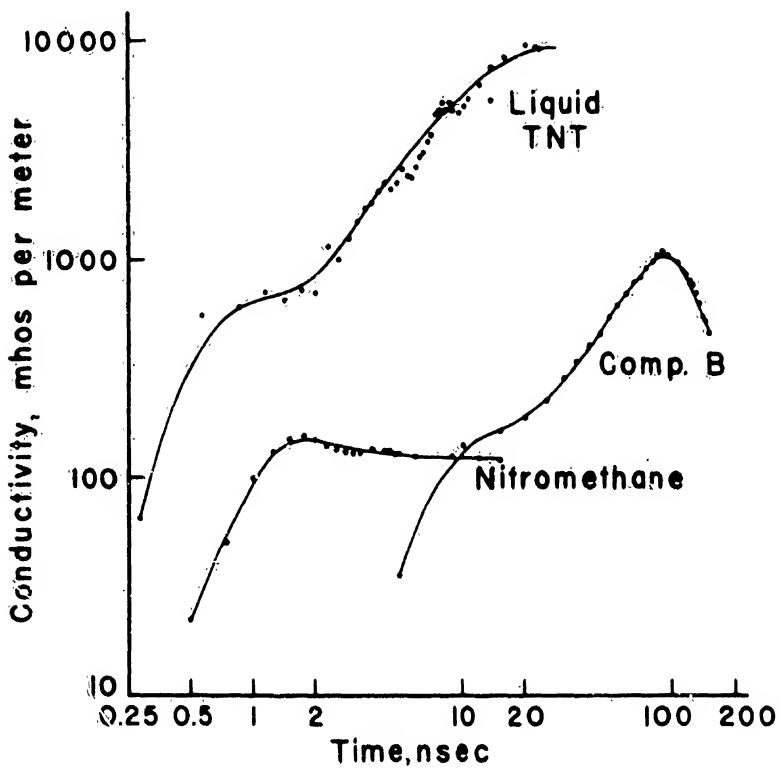

Figure 5-15. Electrical Conductivity as a Function of Time in the Detonation Reaction Zone of Various Explosives

phenomenon. Here we shall only attempt to describe briefly the experimental methods and indicate the nature of some of the results. The reader may refer to the original works listed in the references cited in this paragraph for detailed interpretations.

In principle, various methods that have been used to measure conductivity are similar, although they differ in experimental detail and rigor of treatment. By measurement of the current i conducted between two electrodes in contact with a detonating charge when a voltage V is impressed, the resistance R is determined according to Ohm's law, i.e., $R = V/i$. At any given instant the electrodes make contact with a conducting zone of some given shape which may either be conjectured or experimentally mapped out in some way. If the conducting zone is considered to have uniform conductivity σ throughout, the value of this quantity may be obtained from R through the use of a factor K, which may be called the effective "cell constant"; thus, $\sigma = K/R$. The term "cell constant" derives from the more familiar problem of measuring the conductivity of an electrolyte solution in a "cell" or container into which the electrodes dip. The cell constant in this case is determined by the size, shape, and separation of the electrodes; the size and shape of the cell; and the placement of the electrodes in the cell or, in a word, by the "geometry" of the measuring device.

In Ref. 35 Jameson describes a method of placing electrical probes within the charge and by this means determining the shape of the zone having a high electrical conductivity. He finds that this is of a conical shape, the base of the cone being coincident with the detonation shock front and comprising the full cross section of the charge at this point. The conical surface presumably represents the front of the advancing rarefaction or "release" wave that spreads into the detonation zone from the free surface. Jameson made a "mock-up" of the conical conducting zone from graphite sheets of known electrical conductivity and in this way determined the cell constant K for the particular electrode arrangement used in the explosive experiment. The implicit assumption here is that σ is constant throughout the highly conducting zone mapped out by the probes. The value determined in this way for the resistivity of Composition B was 0.29 ohm-cm. Within an order of magnitude this agrees with values reported by other workers[36].

The method reported by Hayes[37] is considerably more elaborate. In the first place, Hayes extended the time resolution of his measurements about 1000-fold over other workers, employing nanosecond circuitry where others had used microsecond circuitry. And, instead of assuming that the conductivity throughout the detonation zone is constant, he has assumed that it varies as a function of time (or distance) behind the shock front, and has determined this function by an elaborate scheme using a high-speed digital computer to analyze the observed electrical wave form from the conductivity probe. Hayes discovered that the onset of conductivity begins immediately at the precursor shock front (see Chapter 8) and in some cases passes a peak within a few nanoseconds (which means, in terms of distance, only some several microns) behind the front. As between various explosives, the peak conductivity varies by orders of magnitude; also the variation of conductivity with time is decidedly different in various cases. Undoubtedly, this reflects wide differences in the reaction kinetics and in the physical and chemical nature of the reaction products.

Fig. 5-15, reproduced from Ref. 37, shows the conductivity profile in the detonation zone for three explosives: nitromethane, Composition B, and liquid TNT. Here, conductivity is shown as a function of time. For purposes of orientation, time may be derived from distance at the rate of about 6 microns/nsec. Thus, the full scale on the abscissa of Fig. 5-15 corresponds to little more than 1 mm. The units on the ordinate scale in Fig. 5-15 may be divided into 100 to obtain the resistivity in ohm-cm. Thus the lowest resistivity recorded for nitromethane is about 1 ohm-cm, for Comp. B about 0.1 ohm-cm, and for liquid TNT about 0.01 ohm-cm. The close agreement in the case of Comp. B with the value given by Jameson may be noted.

The highest value of conductivity in detonating explosives that has been recorded thus far (liquid TNT, Ref. 37) compares with that for an intrinsic semiconductor like germanium. It is less by a factor of 10 than the conductivity of graphite. If considered as a gaseous plasma, the detonation zone in liquid

TNT has a rather high conductivity; but, if it is considered as a condensed phase comparable with carbon black, for example, its conductivity is not surprising. Hayes' finding in Ref. 37 that the peak conductivity of various explosives shows a close correlation with the amount of solid carbon in the detonation products may, therefore, have a significant bearing on the nature of this phenomenon.

5-7 EMPIRICAL TESTS

In the early development of explosives, a number of empirical tests evolved to measure various "qualities" and "quantities" associated with the explosives. Among the qualities that different explosives possessed in varying degree was what came to be known by the French term "brisance" which was meant to reflect the shattering ability of an explosive, as distinguished from the "power" or ability to do work in moving rock, etc. Thus, it was recognized that the work capability was an extensive property that depended on the quantity of explosive; and the term "power", which in this connection is quite confusing to physicists, meant a "specific" property related

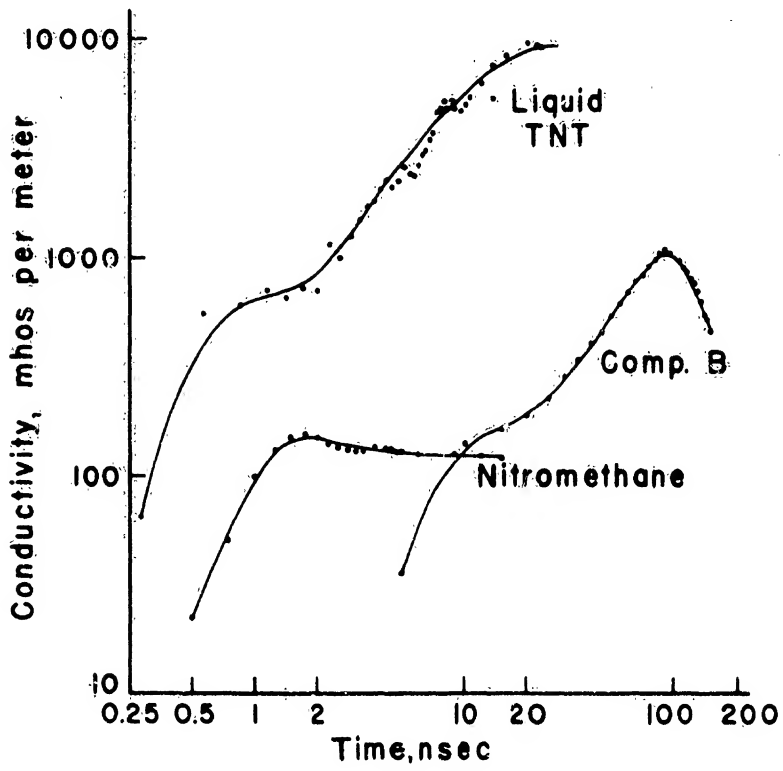

Figure 5-15. Electrical Conductivity as a Function of Time in the Detonation Reaction Zone of Various Explosives

to the available work per unit weight. Brisance, on the other hand, is what one would call an intensive property, which does not depend on the quantity of explosive involved, provided, of course, it is properly detonated.

Various tests were used that were supposed to measure either one or the other of the properties, brisance and power. A typical brisance test, for example, was the plate-dent test. An explosive cartridge of a certain diameter was placed on end in contact with a steel plate of given dimensions and then detonated from the opposite end. The depth of the dent was taken to be a measure of brisance. It was noted that the depth was sensibly independent of the length of the cartridge, provided it was not so short that initiation effects interfered. One recognizes that the test indication in this case, i.e., the depth of the dent, is probably closely related to the detonation pressure which is independent of charge length when the detonation wave is fully developed. Other intrinsic properties like density may also be related to this phenomenon.

Among the tests for power were the lead block test and the Ballistic Mortar test. These are described in Chapter 3. In this case the test indication—e.g., the volume of the cavity in the block, or the swing of the mortar pendulum—were found to be approximately proportional to the quantity of explosive used in the test.

Although empirical tests such as these have been largely superseded, except, in some cases, for the routine testing of commercial explosives, they raise an interesting question: In arriving at a relative figure of merit for the explosive, how is the test indication to be used? It was common practice to use the test indication itself—for example, the volume of the cavity in cubic centimeters for the lead block test, or the pendulum arc in degrees for the ballistic mortar test. Obviously, the procedure is arbitrary in any case. Nevertheless, one is inclined to say, on the basis of a given test, that a certain explosive is so many percentage points better than another; however, such a statement may be quite misleading, especially if the test indication is a highly nonlinear function of the weight of the test charge. Under these circumstances, it is preferable to compare the explosive on the basis of "equivalent weights", i.e., on the basis that it requires a certain percentage more of one explosive to give the *same* test indication as that given by another explosive. Indeed, if two different empirical tests (such as the lead block and the ballistic mortar) relate to the same basic extensive property in the explosive, then the relative equivalent weights for various explosives as registered in the two tests will be the same. If such is the case, there is obviously some justification for using these test numbers to compare explosives.

The following analysis of this problem is quoted from Ref. 38.

"Consider a test that yields some measurable indication I, such as a length, a volume, etc. The quantity I may be a function of several properties of the explosive charge—such as heat of explosion, available work, detonation velocity, or detonation pressure. (In addition, of course, I is functionally dependent on various parameters of the test device; but, because the test is standardized, these parameters appear as constant factors in the functional expression.) Heat and work are examples of what have been termed extensive properties; the quantity G representing such a property is proportional to the mass m of the explosive (i.e., $G = gm$. Detonation velocity and pressure, on the other hand, are examples of intensive properties, which are independent of the amount of explosive (aside from certain nonideal effects that are important for small amounts). Representing the intensive properties by the symbol g', we may write, in general,

$$I = F(gm, g') \tag{5-17}$$

"In the case where I is a function of only a single extensive property or linear combination of such properties, we can write for two different explosives 1 and 2

$$\left.\begin{aligned} I_1 &= f(g_1 m_1) \\ I_2 &= f(g_2 m_2) \end{aligned}\right\} \tag{5-18}$$

If I_1 is made equal to I_2, then

$$g_1 m_1 = g_2 m_2 \tag{5-19}$$

and

$$\frac{m_1}{m_2} = \frac{g_2}{g_1} \tag{5-20}$$

REFERENCES

1. M. A. Cook, *The Science of High Explosives*, Chap. 2, "Modern Instrumentation and Methods", Reinhold, New York, 1958.
2. W. G. Sykes, "Study of Fast Events", Science 130, 1051 (1959).
3. J. S. Courtney-Pratt, "Some New Methods of Fast Photography and Their Application to Combustion Processes", *Fourth Symposium (International) on Combustion*, The Williams and Wilkins Company, Baltimore, 1953.
4. A. W. Campbell, M. E. Malin, T. J. Boyd, Jr., and J. A. Hull, "Precision Measurement of Detonation Velocities in Liquid and Solid Explosives", Rev. Sci. Instr. 27, 567 (1956).
5. M. H. Rice, R. G. McQueen, and J. M. Walsh, "Compression of Solids by Strong Shock Waves", *Solid State Physics*, Vol. 6, Frederick Seitz, Ed., Academic Press, New York, 1958.
6. H. Jones, European Scientific Notes 3, 388 (1949); *Third Symposium on Combustion, Flames, and Explosion Phenomena*, The Williams and Wilkins Company, Baltimore, 1949, p. 590.
7. R. E. Duff and E. Houston, "Measurement of the Chapman-Jouguet Pressure and Reaction Zone Length in a Detonating High Explosive", J. Chem. Phys. 23, 1268 (1955).
8. W. E. Deal, "Measurement of Chapman-Jouguet Pressure for Explosives", J. Chem. Phys. 27, 796 (1957).
9. R. W. Goranson, D. Bancroft, B. L. Burton, T. Blechar, E. E. Houston, E. F. Gittings and S. A. Landeen, "Dynamic Determination of the Compressibility of Metals", J. Appl. Phys. 26, 1472 (1955).
10. N. L. Coleburn, *The Dynamic Compressibility of Solids from Single Experiments Using Light Reflection Techniques*, NAVWEPS Rep. No. 8026, U. S. Naval Ord. Lab., Silver Spring, Md., 1960.
11. P. W. Bridgman, "Rough Compression of 177 Substances to 40,000 kg/cm^2", Proc. Am. Acad. Arts Sci. 76, 71-87 (1948).
12. R. G. McQueen, "Laboratory Techniques for Very High Pressures and the Behavior of Metals Under Dynamic Loading", *Metallurgy at High Pressures and High Temperatures*, K. A. Gschneider, Jr. et al., Ed., Gordon and Breach Science Publishers, Inc., New York, 1964.
13. R. A. Graham, "Technique for Studying Piezoelectricity under Transient High Stress Condition", R.S.I. 32, 1308, 1961.
14. R. A. Graham, et al., "Piezoelectric Current From Shock Loaded Quartz—A Submicrosecond Stress Gage", J. Appl. Phys. 36, 1775 (1965).
15. W. J. Halpin, et al., "A Submicroscopic Technique for Simultaneous Observation of Input and Propagated Impact Stresses", ASTM Special Technical Publication No. 336, *Symposium on Dynamic Behavior of Materials*, Philadephia, 1963.
16. D. Bernstein and D. Keough, "Piezoresistivity of Manganin", J. Appl. Phys. 35, No. 5, 1471-1474 (1964).
17. D. D. Keough, *Pressure Transducer for Measuring Shock Wave Profiles, Phase IX: Additional Gage Development*, Final Report DASA No. 49-146-XZ-096, SRI Project GSU-3713, Stanford Research Institute, November 30, 1964.
18. D. D. Keough, *Procedure for Fabrication and Operation of Manganin Shock Pressure Gages*, Technical Report No. AFWL-TR-68-57, SRI Project PGU-6979, Standford Research Institute, August 1968.
19. F. E. Allison, "Shock Induced Polarization in Plastics, I. Theory", J. Appl. Phys. 36, 2111 (1965).
20. G. E. Hauver, "Shock-Induced Polarization in Plastics, II. Experimental Study of Plexiglass and Polystyrene", J. Appl. Phys. 36, 2113 (1965).
21. R. J. Eichelberger and G. E. Hauver, "Solid State Transducers for Recording of Intense Pressure Pulses", *Les Ondes de Detonation*, Colloques Internationaux du Centre National de la Recherche Scientifique, Gil-sur-Yvette, 1961.
22. G. E. Hauver and P. H. Netherwood, *Pressure Profiles of Detonating Baratol*

REFERENCES (Cont'd)

Measured with Sulfur Gages, BRL Technical Note No. 1452, Aberdeen Proving Ground, Md., 1962.

23. D. G. Doran, *High Pressure Measurement*, Giardini and Lloyd, Eds., Butterworth, Washington, D.C., 1963.
24. W. Murri, C. Petersen, and M. Cowperthwaite, "Hugoniot and Release Adiabat Measurements for Selected Geologic Materials", J. Geophys. Res. 75, No. 11 (1970).
25. L. M. Barker, "Fine Structure of Compressive and Release Wave Shapes in Aluminum Measured by the Velocity Interferometer Technique", *Symposium High Dynamic Pressure*, Paris, France, 11-15 September 1967.
26. D. Venable, "PHERMEX", *Physics Today* 17, 19 December 1964.
27. R. Schall, "Methoden and Ergebnisse der Detonations Druckbestimmung bei festen Sprengstoffen", Zeit. f. Elektrochemie, 61, 629 (1957).
28. W. Döering and G. I. Burkhardt, Tech. Rpt. No. F.T.S.-1227-118 (GDAM 9-T-46).
29. W. E. Deal, "Measurement of the Reflected Shock Hugoniot and Isentrope for Explosive Reaction Products", Phys. Fluids 1, 523 (1958).
30. J. W. Gehring, Jr. and J. Dewey, *An Experimental Determination of Detonation Pressure in Two Solid High Explosives*, BRL Report No. 935, Ballistic Research Laboratories, Aberdeen Proving Ground, Md., 1955.
31. R. H. Cole, *Underwater Explosions*, Princeton University Press, Princeton, N. J., 1948, p. 159 ff.
32. O. T. Johnson, J. C. Patterson, II, and W. C. Olson, *A Simple Mechanical Method for Measuring the Reflected Impulse of Air Blast Waves*, BRL Memorandum Report No. 1088, Aberdeen Proving Ground, Md., 1957.
33. J. M. Dewey, "The Air Velocity in Blast Waves from TNT Explosions", Proc. Roy. Soc. A 279, 366 (1964).
34. F. C. Gibson, M. L. Bowser, C. R. Summers, F. H. Scott, and C. M. Mason, "Use of an Electro-Optical Method to Determine Detonation Temperatures in High Explosives", J. Appl. Phys. 29, 628 (1958).
35. R. L. Jameson, *Electrical Measurements in Detonating Pentolite and Composition B*, BRL Memorandum Report No. 1371, Aberdeen Proving Ground, Md., 1961.
36. M. A. Cook, *The Science of High Explosives*, Chap. 7, "Ionization, Electrical, Magnetic and Electromagnetic Phenomena Accompanying Detonation", Reinhold Publishing Corp., New York, 1958.
37. B. Hayes, "Electrical Measurements in Reaction Zones of High Explosives", *Tenth Symposium (International) on Combustion*, The Combustion Institute, 1965.
38. W. E. Gordon, F. E. Reed, and B. A. Lepper, "Lead Block Test for Explosives", Ind. Eng. Chem. 47, 1794 (1955).
39. L. V. Altshuler, S. B. Kormer, M. I. Brazhnik, L. A. Vladimirov, M. P. Speranskaya, and A. I. Funtikov, "The Isentropic Compressibility of Aluminum, Copper, Lead, and Iron at High Pressures", Soviet Physics JETP (translation) II (4), 766 (1960).

CHAPTER 6 ELEMENTARY THEORY OF THE PLANE DETONATION WAVE

6-1 INTRODUCTION

The first theoretical description of detonation waves was given by Chapman in 1899 and independently by Jouguet more than a decade later. When considered in detail, reaction waves in substances capable of exothermic reaction are of very considerable complexity. The elementary theory, as formulated by Chapman and Jouguet, is based on a highly idealized model. In spite of this fact, this simple theory reproduces the main features of the phenomenon with remarkable fidelity. The success of the simple theory has two important consequences: (1) it remains the principal computational tool for the evaluation of detonation wave properties, and (2) it provides the basis from which more detailed theoretical descriptions of particular phenomena are obtained by elaboration of the model.

The classical theory of Chapman and Jouguet is concerned with the propagation of a detonation wave at a constant velocity in one dimension as, for example, in the direction of the axis of a cylindrical stick of explosive. The initiation process requires a separate discussion. Because of the continuing relevance of this theory to the description of detonation phenomena, this chapter is devoted to a detailed development of its consequences.

6-2 THE RANKINE-HUGONIOT EQUATION

In formulating a simple model to serve as the basis of the elementary thermodynamic-hydrodynamic theory of the detonation wave, it is assumed that the chemical reaction by means of which the explosive is transformed into its products takes place instantaneously so that there is a sharply defined reaction front—treated as a mathematical discontinuity—advancing into the unreacted explosive. The transition across such a front is then similar in many respects to the transition across a shock front. In particular, it must be subject to the general conservation laws that apply across any discontinuity.

We consider a wave of chemical reaction propagating in one dimension in the direction of increasing values of the coordinate x, and we denote its velocity with respect to the unreacted material by D. Employing the notation exemplified by Fig. 6-1, we fix the origin of the x-coordinate in the moving reaction wave and denote the velocity of unreacted material and reaction products with respect to this origin and in the direction of increasing x by w_o and w, respectively. If u_o and u_1 are the corresponding velocities relative to a fixed coordinate system,

$$w_o = -D;\ w_1 = u_1 - u_o - D \tag{6-1}$$

The explosive is at pressure p_o and density ρ_o, and the reaction products are at pressure p_1 and density ρ_1. The variables characterizing the flow and those descriptive of the thermodynamic state are supposed to be uniform over any plane perpendicular to the x-axis.

The conservation of mass and momentum across the discontinuity, comprising the reaction front, are expressed by the mechanical conservation conditions which in the present nomenclature can be written

$$\begin{aligned} \rho_o w_o &= \rho_1 w_1 = -\rho_o D = m \\ p_1 - p_o &= \rho_o w_o^2 - \rho_1 w_1^2 = m(w_o - w_1) \end{aligned} \tag{6-2}$$

where m is the mass flux through the reaction wave. When the condition for the conservation of energy is combined with these mechanical conditions, we obtain, as in the treatment of a simple shock wave (par. 2-8), the Rankine-Hugoniot equation

$$e_1 - e_o = \tfrac{1}{2}(p_1 + p_o)(v_o - v_1) \tag{6-3}$$

which, for brevity, we shall refer to as the Hugoniot equation. Here, $v = 1/\rho$ is the specific volume; e_o and e_1 are the specific energy functions for unreacted material and reaction products, respectively. If the products are assumed to be in thermodynamic equilibrium or if their concentrations are arbitrarily specified, then their thermodynamic state is specified and

$$e_1 = e(p_1, v_1) \tag{6-4}$$

where $e(p,v)$ is a known function of the state variables. The Hugoniot equation is thus a relation between thermodynamic quantities that determines the pressure p_1 as a function of the specific volume v_1 for specified initial pressure p_o, initial volume v_o, and for specified explosive for which c_o at these initial conditions is fixed. It describes all of the states (p_1,v_1) for given initial state (p_o, v_o) and given explosive that are compatible with the conservation conditions. These states will be said to be centered on (p_o, v_o). In terms of the specific enthalpy function

$$h = e + pv \tag{6-5}$$

the Hugoniot equation can be written in the alternative form

$$h_1 - h_o = \tfrac{1}{2}(p_1 - p_o)(v_1 + v_o) \tag{6-6}$$

The conservation conditions, Eqs. 6-2 and either Eq. 6-3 or Eq. 6-6 have the same form as for shock waves. However, an essential difference arises from the fact that the specific energy and specific enthalpy functions of the reaction products are different from the specific energy or specific enthalpy of the unreacted material, respectively. In fact, the exothermal nature of the reaction process is expressed by the assumption that the energy and enthalpy of the products are less than the energy and enthalpy, respectively, of the unreacted material when the two quantities are compared at the same pressure and specific volume. This assumption is sufficient to assure the existence of reaction waves of finite propagation velocity in the one-dimensional, instantaneous reaction approximation that is employed in this chapter as a model. In particular, it requires that

$$e(p_o, v_o) < e_o \text{ and } h(p_o, v_o) < h_o$$

which are equivalent.

The heat evolved during the decomposition of unit weight of explosive at constant temperature and pressure can be evaluated from standard thermochemical data. Denote this quantity by q and the initial temperature by T_o, then

$$q = h_o - h(p_o, T_o) \tag{6-8}$$

It is conventional to define an exothermal reaction as one for which q, the thermochemical heat of reaction, is positive; explosives of practical importance are indeed characterized by $q > 0$. However, Eq. 6-7 implies the requirement that

$$q > h(p_o, v_o) - h(p_o, T_o) \tag{6-9}$$

the right-hand side of which is negative for real materials. Consequently, Eq. 6-7 can be satisfied and, in the present approximation, reaction waves can exist for materials whose heat of decomposition q is negative so long as Eq. 6-9 is satisfied. Eq. 6-7 is evidently satisfied by all explosives characterized by the stronger condition, $q > 0$.

Now, consider the point on the Hugoniot curve for which $v_1 = v_o$. This point corresponds to an hypothetical conversion of the explosive to its products at constant volume. Eq. 6-3 reduces to

$$e(p_1, v_o) = e_o \tag{6-10}$$

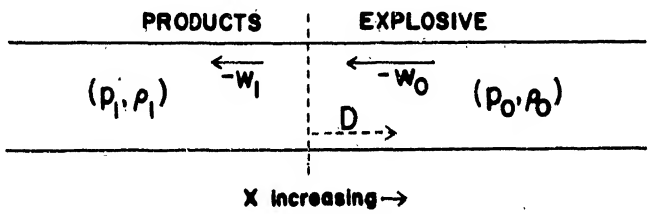

Figure 6-1. One-dimensional Reaction Wave

an implicit relation that can be solved for the pressure if the specific energy function is known. This pressure, which we denote by p_e and call the pressure for constant volume explosion, is determined by the specific energy of the explosive and its initial density, a fact made explicit by the notation

$$p_e = p(e_o, v_o) \tag{6-11}$$

since we can regard the pressure as a function $p(e,v)$ of the specific energy and specific volume. Eq. 6-7, together with the basic assumption that

$$(\partial e/\partial p)_v > 0$$

for real systems, shows that $p_e > p_o$. Similarly, consider the point for which $p_1 = p_o$. This point corresponds to a hypothetical reaction at constant pressure. Eq. 6-6 reduces to

$$h(p_o, v_1) = h_o \tag{6-12}$$

an implicit relation that can be solved for the specific volume if the specific enthalpy function is known. This quantity, which we denote by v_c and call the specific volume for constant pressure combustion, is determined by the specific enthalpy of the intact material and by the initial pressure, a fact made explicit by the notation

$$v_c = v(h_o, p_o) \tag{6-13}$$

since we can regard the specific volume as a function $v(h,p)$ of the specific enthalpy and pressure. Eq. 6-7 together with the basic assumption that

$$(\partial h/\partial v)_p > 0$$

for real systems, leads to the conclusion that $v_c > v_o$. Thus, we have shown that the Hugoniot curve passes through the points (p_e, v_o) with $p_e > p_o$ and (p_o, v_c) with $v_c > v_o$, instead of through the point (p_o, v_o) as in the case of the nonreactive shock wave. This characteristic of the Hugoniot curve for a reaction wave is a consequence of the exothermal nature of the reaction. In par. 6-3, it is shown that the pressure p_1 satisfying the Hugoniot equation centered on given initial conditions increases with decreasing specific volume v_1 and that the Hugoniot curve is concave upward in the (p,v)-plane.

The mechanical conservation conditions can be combined to yield the relation

$$-\rho_o^2 D^2 = (p_1 - p_o)/(v_1 - v_o) \tag{6-14}$$

Eq. 6-14 describes a straight line in the (p_1, v_1)-plane that is called the Rayleigh line. It is the chord connecting the point (p_1, v_1) to the point (p_o, v_o). The propagation velocity D is evidently proportional to the square root of the negative slope of the Rayleigh line. Since the left-hand member of this expression cannot be positive, the pressure and specific volume must increase or decrease in an opposite sense in passing through the reaction wave. More explicitly, it is evident that $v_1 \leq v_c$ if $p_1 \geq p_e > p_o$ and $p_1 \leq p_o$ if $v_1 \geq v_c > v_o$. Furthermore, points for which $p_e > p_1 > p_o$ and $v_o < v_1 < v_c$ do not represent states with a real propagation velocity and are excluded because they have no physical meaning. Thus, the Hugoniot curve consists of two branches, as shown in Fig. 6-2. The branch for which $v_1 \leq v_o$ is called the detonation branch; that for which $p_1 \leq p_o$ is called the deflagration branch. From Eq. 6-14, it is seen that the propagation velocity is infinite for constant volume explosion, $v_1 = v_o$ and $p_1 = p_e$, implying instantaneous conversion of the explosive to its products. This state is to be regarded a limiting one for reaction waves propagating at very high velocity. When $p_1 = p_o$ and $v_1 = v_c$, the propagation velocity is zero. The constant pressure combustion state is thus a limiting one for reaction waves propagating with a small velocity.

Transitions on the deflagration branch of the Hugoniot curve are seen to possess the qualitative properties ascribed to ordinary combustion waves. In fact the flame temperature is usually calculated on the assumption that it differs negligibly from the temperature of the constant pressure combustion state and it is customary, in the theory of flame propagation, to assume that the pressure drop through the combustion wave is negligible. The deflagration branch of the Hugoniot curve does not, however, provide a useful description of combustion waves propagating with small velocity because the idealization of the wave as a discontinuous

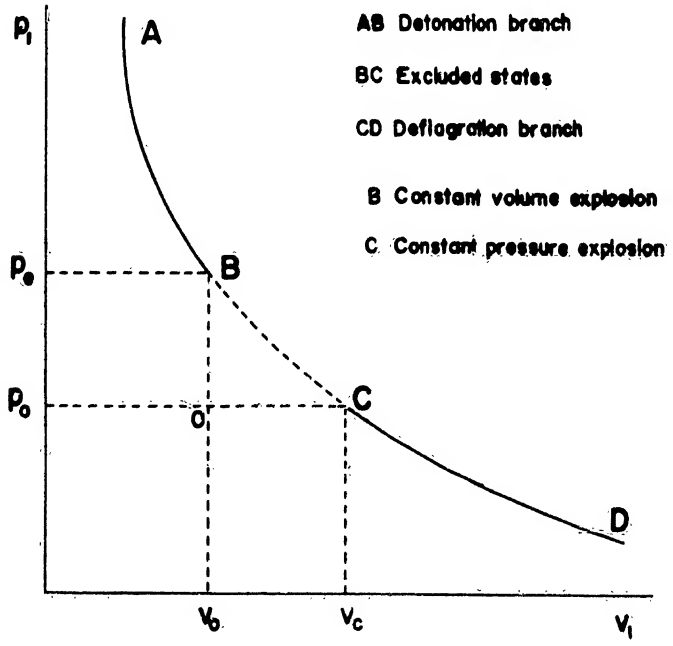

Figure 6-2. Hugoniot Curve for Detonations and Deflagrations

transition is too extreme to provide a useful model. The waves described by the detonation branch of the Hugoniot curve are compressive. Therefore, we expect that the detonation wave observed in an actual explosive will be described, in terms of the simple model employed here, by some point on the detonation branch of the Hugoniot curve. After an examination of the properties of the flows associated with each of these branches, it is possible to understand why the model affords a good description of detonation waves but not of combustion waves.

The properties of the Hugoniot curve and of the flows associated with the final states determined by it are deduced in detail in par. 6-3. Here, we summarize the results of that analysis. For one final state represented by a point on the detonation branch and for one final state represented by a point on the deflagration branch, the Rayleigh line is tangent to the Hugoniot curve. These two states are called Chapman-Jouguet states. Points on the detonation branch of the Hugoniot curve for which the pressure is greater than that at the Chapman-Jouguet point are called strong detonations, and those for which the pressure is less than the Chapman-Jouguet pressure are called weak detonations. Points on the deflagration branch are called weak or strong deflagrations, according to whether the pressure is greater than or less than, respectively, the pressure of the Chapman-Jouguet deflagration. A Rayleigh line with a slope somewhat less than that through the Chapman-Jouguet detonation—i.e., corresponding to a greater value of D—intersects the detonation branch at two points, one a weak detonation and the other a strong detonation. Similarly, a Rayleigh line with a slope somewhat greater than that through the Chapman-Jouguet deflagration—i.e.,

corresponding to a smaller value of D—intersects the deflagration branch at two points, one a weak deflagration and the other a strong deflagration. These definitions are shown on Fig. 6-3. We note that, except for the Chapman-Jouguet state, there are two detonations, one weak and one strong, satisfying the conservation conditions and having the same propagation velocity. A similar statement applies to the deflagration branch of the Hugoniot curve. There are no more than the two intersections of a given Rayleigh line with either branch of the curve.

The Chapman-Jouguet states on the Hugoniot curve have certain unique properties which are stated here and which are deduced the next paragraph. Among the various processes starting from the specified initial state, a Chapman-Jouguet detonation leads to a minimum value for the propagation velocity D, relative to the unreacted material, and a Chapman-Jouguet deflagration leads to a maximum value of this quantity. The entropy of the reaction products varies along the Hugoniot curve. The entropy also attains a stationary value at a Chapman-Jouguet point, a minimum for a detonation and a maximum for a deflagration. The Hugoniot curve is tangent at a Chapman-Jouguet point to the isentrope passing through that point. Since the Rayleigh line through a Chapman-Jouguet point is tangent to the Hugoniot curve, it is also tangent to the isentrope through the Chapman-Jouguet point at that point. Chapman in 1899 recognized that

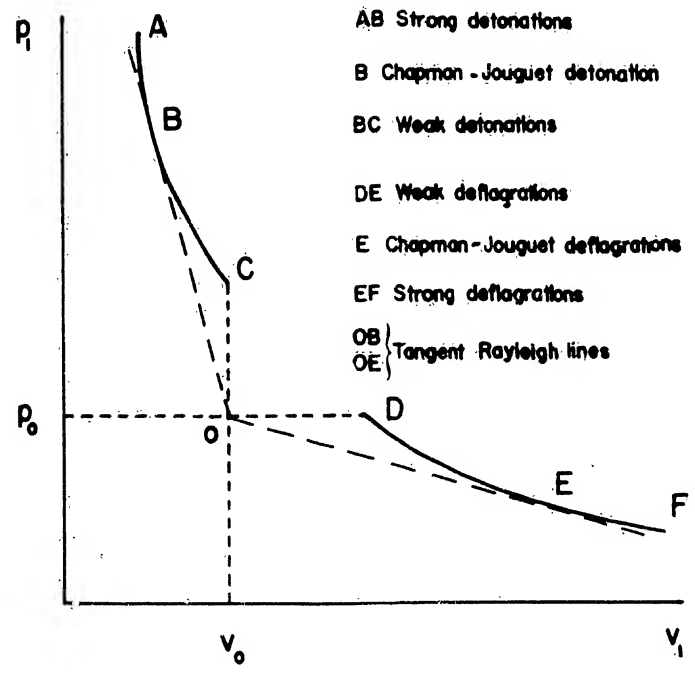

Figure 6-3. Nomenclature on the Hugoniot Curve for Detonations and Deflagrations

the detonation velocity corresponding to a tangent Rayleigh line is a minimum.

In the regions of strong detonations and weak deflagrations, the isentropes rise with increasing pressure more steeply than the Rayleigh line and less steeply than the Hugonoit curve. Conversely, in regions of weak detonations and strong deflagrations, the isentropes rise with increasing pressure less steeply than the Rayleigh line and more steeply than the Hugoniot curve. These relationships are indicated in Fig. 6-4. It is seen that the isentrope through the intersection of a Rayleigh line with the Hugoniot curve always lies between the Rayleigh line and the Hugoniot curve.

As a direct consequence of the nature of the variation of entropy along the Hugoniot curve, certain qualitative statements can be made as to the nature of the flows associated with states represented by points on the various sections of the curve. These conclusions result from the mechanical conservation conditions and are derived in the next paragraph. As summarized, they have been called Jouguet's rule. It is shown that the flow of the reaction products relative to the reaction front is subsonic behind a strong detonation or weak deflagration, sonic behind a Chapman-Jouguet detonation or deflagration, and supersonic behind a weak detonation or strong deflagration. If we refer to Fig. 6-3, these statements are expressed by the relations

$$\left.\begin{aligned} |w_1| &< c_1 \text{ on AB and DE} \\ |w_1| &= c_1 \text{ at B and E} \\ |w_1| &> c_1 \text{ on BC and EF} \end{aligned}\right\} \quad (6\text{-}15)$$

where c_1 is the velocity of sound at the point (p_1, v_1). It is also shown that the flow of the intact material relative to the reaction front is supersonic ahead of a detonation wave and subsonic ahead of a deflagration wave. Again referring to Fig. 6-3, these statements are expressed by the relations,

$$\left.\begin{aligned} D &> c_o \text{ on ABC} \\ D &< c_o \text{ on DEF} \end{aligned}\right\} \quad (6\text{-}16)$$

where c_o is the speed of sound in the unreacted material at pressure p_o and specific volume v_o.

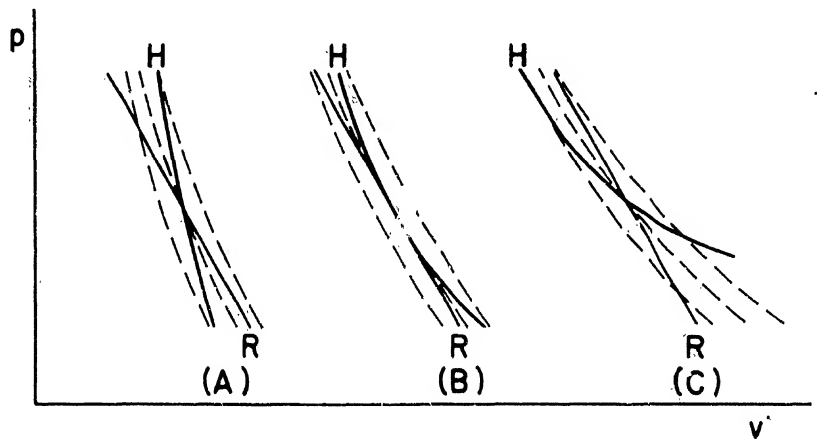

Figure 6-4. Hugoniot Curve (H), Rayleigh Line (R), and Isentropes (dashed curves) for (A) Strong Detonations and Weak Deflagrations, (B) Chapman-Jouguet Detonation and Deflagration, and (C) Weak Detonations and Strong Deflagrations

Consideration of the mechanical conservation conditions reveals a further distinction between detonations and deflagrations. Eqs. 6-1 and 6-2 can be combined to yield

$$\frac{u_1 - u_o}{v_1 - v_o} = \rho_o^2 D^2 \qquad (6\text{-}17)$$

the right-hand member of which is negative. This relation shows that the material velocity decreases in passing through a stationary detonation front, for which $v_1 < v_o$, and increases in passing through a stationary deflagration front, for which $v_1 > v_o$. If the unreacted material is at rest relative to fixed coordinates (1) $u_o = 0$ and $u_1 < 0$ if the reaction wave is a deflagration, and (2) $u_1 > 0$ if the reaction wave is a detonation. The change of material velocity in passing through the reaction front is compared in Fig. 6-5 for a detonation and a deflagration with the unreacted material at rest. For a detonation wave, the motion of the reaction products is directed toward the reaction front, and for a deflagration wave the motion of the reaction products is away from the reaction front. For the Chapman-Jouguet detonation in an explosive at rest, the expression of Eq. 6-15 can be written

$$D = u_1 + c_1 \qquad (6\text{-}18)$$

Jouguet in 1905[5] recognized that the propagation of the detonation wave for which the Rayleigh line is tangent to the Hugoniot curve is sonic with respect to the reaction products.

The conservation laws, when applied across the reaction front, simply enumerate all of the states and describe the associated flows on either side of the front that are accessible for a given material at specified initial conditions. Physical reality does not present all of the states that are possible for the simplified model that has been employed. When the model is refined by removing the assumption of an infinitely fast reaction and by considering a reaction zone of finite thickness it will be concluded that weak detonations do not usually exist and strong deflagrations can never exist. Anticipating the result of that analysis, we shall give no further consideration to these sections of the Hugoniot curve, restricting the discussion to those sections representing physically realizable states that are shown on Fig. 6-6.

Jouguet's rule indicates the reason why a theoretical description of a reaction wave based on the laws of conservation across the reaction front can be useful for a detonation wave and at the same time not useful for a combustion wave. Since the flow ahead of a deflagration wave is subsonic with respect to the wave, the flow ahead of the wave is influenced by the deflagration wave itself. This is not the case for a detonation wave where the flow of the unreacted explosive is supersonic with respect to

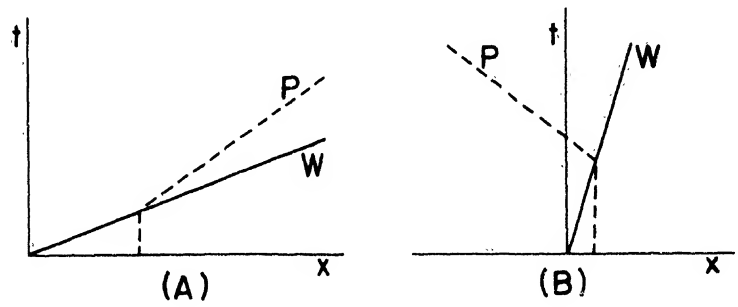

Figure 6-5. Wave Path W and Particle path P for (A) a Detonation and (B) a Deflagration With $u_o = 0$

the detonation front. It is, in fact, a consequence of this distinction that flows associated with deflagration waves have one more degree of indeterminacy than flows associated with detonation waves, and this additional degree of indeterminacy requires consideration of the conduction of heat and diffusion of molecular species on each side of the wave. We shall continue the analysis of weak deflagration waves in the next paragraph because the results obtained will find an application subsequently.

6-3 PROPERTIES OF THE HUGONIOT CURVE

In this paragraph, the properties of the Hugoniot curve and of the flows associated with it will be deduced. We assume the existence of an equation of state, both for the unreacted material and for the reaction products. The equation of state for either medium is of the form $p = p(v,s)$ if the entropy and specific volume are taken as independent state variables. We assume again that

$$\frac{\partial p}{\partial v} = -\rho^2 c^2 < 0$$
$$\frac{\partial^2 p}{\partial v^2} > 0, \quad \frac{\partial p}{\partial s} > 0 \tag{6-19}$$

These assumptions have the effect of specifying curves of constant entropy, $s(p,v)$ = constant, which form a nonintersecting family in the (p,v)-plane, decreasing and concave toward positive v and with the entropy increasing on

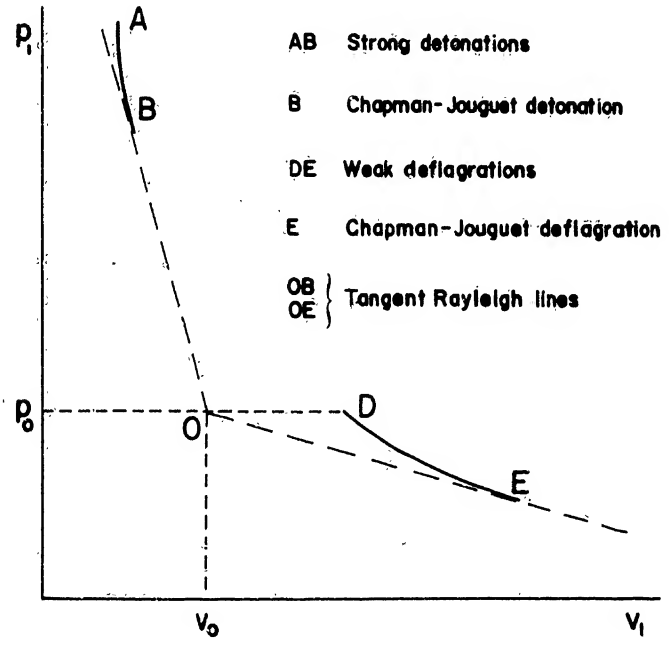

Figure 6-6. Physically Realizable Detonation and Deflagration States

any radius from the origin. We assume that the composition of the unreacted material is fixed and given by the initial specifications of the system, and that the reaction products are in thermodynamic equilibrium. Then for either medium, the second law of thermodynamics is expressed by

$$de = Tds - pdv \qquad (6\text{-}20^*)$$

and the derivatives of Eqs. 6-19, in the case of the reaction products, are taken at equilibrium composition*. The exothermic character of the reaction is expressed by the requirement that for the same pressure and specific volume the specific energy of the unreacted material is greater than the specific energy of the reaction products.

The discussion of the properties of the Hugoniot curve is facilitated by the definition of the Hugoniot function

$$H(p,v) = e(p,v) - e(p_o,v_o) + \tfrac{1}{2}(p + p_o)(v - v_o) \qquad (6\text{-}21)$$

In terms or this function, the Hugoniot equation Eq. 6-3, can be written

$$H(p_1,v_1) = e_o - e(p_o,v_o) = J(p_o,v_o) \qquad (6\text{-}22)$$

The exothermal character of the reaction is expressed by the requirement that $J(p_o,v_o) > 0$.

First, we want to prove that the entropy has at most a single extremum on a straight line in the (p,v)-plane and that such an extremum is a maximum. A ray R through the point (p_o,v_o) can be represented in terms of the parameter r and two constants a and b by

$$p = p_o + ar \quad , \quad v = v_o + br \qquad a = p_1 - p_o \quad , \quad b = v_1 - v_o \qquad (6\text{-}23)$$

Then, on R, $dp = adr$, $dv = bdr$, and

$$\frac{ds}{dr} = a\left(\frac{\partial s}{\partial p}\right) + b\left(\frac{\partial s}{\partial v}\right) = \frac{\partial s}{\partial p}\left[a - b\left(\frac{\partial p}{\partial v}\right)\right] \qquad (6\text{-}24)$$

*Since Eq. 6-20 applies either to changes at equilibrium or to changes at an arbitrarily specified composition, the analysis of this paragraph is also applicable if it is assumed that the explosion products are constrained to such an arbitrarily specified constant composition.

At an extremum, $ds/dr = 0$, so that an extremum

$$\frac{\partial p}{\partial s}\left(\frac{d^2s}{dr^2}\right) = -\,b^2\left(\frac{\partial^2 p}{\partial v^2}\right) \qquad (6\text{-}25)$$

By Eqs. 6-19, $\partial p/\partial s > 0$ and $\partial^2 p/\partial v^2 > 0$. Therefore, at an extremum $d^2s/dr^2 < 0$. We have proved that the extremum, if it exists, must be a maximum. Therefore, the entropy can attain at most one such stationary value on a straight line or ray through (p_o,v_o) in the (p,v)-plane.

Now, consider the value of the Hugoniot function $H(p,v)$ along the ray R represented by Eqs. 6-23. Differentiating Eq. 6-21 at constant p_o and v_o, we obtain

$$dH = de + \tfrac{1}{2}(p + p_o)dv + \tfrac{1}{2}(v - v_o)dp \qquad (6\text{-}26)$$

and with Eq. 6-20, this becomes

$$dH = Tds - \tfrac{1}{2}(p - p_o)dv + \tfrac{1}{2}(v - v_o)dp \qquad (6\text{-}27)$$

Therefore, on the ray R

$$dH = Tds \qquad (6\text{-}28)$$

If both the entropy and the Hugoniot function are considered functions of the parameter r on the ray R, we have proved that they are simultaneously stationary if either one is stationary. Furthermore, since a stationary value of the entropy is a maximum, a stationary value of the Hugoniot function is a maximum on R. Since the entropy can attain at most one maximum on a ray R, it follows that the Hugoniot function can attain at most one maximum on R.

Having shown that the entropy and the Hugoniot function simultaneously attain maxima at not more than one point on any ray in the (p,v)-plane, we want to prove that there is one such point on any Rayleigh line corresponding to finite propagation velocity. In view of Eq. 6-24, the entropy is a maximum on R if

$$\frac{\partial p}{\partial v} = -\,\rho^2 c^2 = a/b \qquad (6\text{-}29)$$

Along any Rayleigh line, defined by Eq. 6-14

$$a/b = -\,\rho_o^2 D^2 < 0 \qquad (6\text{-}30)$$

Therefore, the entropy—and simultaneously, the Hugoniot function—attains a maximum at a point (p,v) determined by

$$\left.\begin{aligned} \rho c &= \rho_o D \\ p &= p(v,s), \quad c = c(v,s) \end{aligned}\right\} \tag{6-31}$$

together with Eqs. 6-22, where the sound speed c is a positive quantity and a function of the state of the gas. Eq. 6-31 is the condition that a line of slope a/b be tangent to an isentrope. By Eqs. 6-19, the slope of any isentrope is always negative, increasing monotonically with increasing v. For a gas, the slope tends asymptotically to zero as v increases indefinitely. Therefore, any isentrope has a point of tangency with a line of specified slope a/b if $a/b < 0$, and such a line is parallel to the Rayleigh line of the same slope through a fixed initial point. Since, by Eqs. 6-19, the entropy increases monotonically along any radius through the origin in the (p,v)-plane, there exists an isentrope whose tangent of specified slope a/b passes through the fixed initial point and is thus identical with the Rayleigh line. Therefore, Eqs. 6-22 and 6-31 always possess a solution. We have proved that the entropy and the Hugoniot function simultaneously attain maxima at one and only one point on every Rayleigh line corresponding to finite propagation velocity.

Each point (p_1,v_1) on the Hugoniot curve described by Eq. 6-22 is on a Rayleigh line defined by Eq. 6-14, when the propagation velocity D is fixed by the point (p_1,v_1). Since the Hugoniot function is constant on the Hugoniot curve and since it attains a maximum on a Rayleigh line, the Rayleigh line through (p_1,v_1) must have a second intersection with the Hugoniot curve—i.e., (p_1',v_1')—unless (p_1,v_1) is a point on the Rayleigh line at which the Hugoniot function is a maximum. Since the Hugoniot function attains only a single maximum on a Rayleigh line, a Rayleigh line cannot intersect the Hugoniot curve at more than two points. We now consider the case of two intersections and, for definiteness, we let $v_1' < v_1$. Then the requirement that the slope of the Rayleigh line be negative implies that $p_1' > p_1$. We call the point (p_1',v_1') an upper point and the point (p_1,v_1) a lower point. An upper point on the detonation branch of the Hugoniot curve is a strong detonation; on the deflagration branch, an upper point is a weak deflagration. A lower point on the detonation branch is a weak detonation, and a lower point on the deflagration branch is a strong deflagration.

Since the Hugoniot function has the same value at the two points (p_1,v_1) and (p_1',v_1') of the intersection of a Rayleigh line with the Hugoniot curve, it attains a maximum at some intermediate point. The entropy attains a maximum at the same intermediate point. Therefore

$$\left.\begin{aligned} \frac{ds}{dr} &> 0 \text{ at } (p_1,v_1) \\ \frac{ds}{dr} &< 0 \text{ at } (p_1',v_1') \end{aligned}\right\} \tag{6-32}$$

on the detonation branch (where $v_1 < v_o$) and

$$\left.\begin{aligned} \frac{ds}{dr} &< 0 \text{ at } (p_1,v_1) \\ \frac{ds}{dr} &> 0 \text{ at } (p_1',v_1') \end{aligned}\right\} \tag{6-33}$$

on the deflagration branch (where $v_1 > v_o$). Since $\partial p/\partial s > 0$ by Eq. 6-19, we can write, for either branch

$$\begin{aligned} \frac{1}{v_1 - v_o}\left(\frac{\partial p}{\partial s}\right)\left(\frac{ds}{dr}\right) &< 0 \text{ at } (p_1,v_1) \\ \frac{1}{v_1 - v_o}\left(\frac{\partial p}{\partial s}\right)\left(\frac{ds}{dr}\right) &> 0 \text{ at } (p_1',v_1') \end{aligned} \tag{6-34}$$

By use of Eqs. 6-23, 6-24, and 6-30, these inequalities become

$$\left.\begin{aligned} \rho_1^2 c_1^2 - \rho_o^2 D^2 &< 0 \text{ at } (p_1,v_1) \\ \rho_1^2 c_1^2 - \rho_o^2 D^2 &> 0 \text{ at } (p_1',v_1') \end{aligned}\right\} \tag{6-35}$$

Because of the conservation of mass across the discontinuity, Eq. 6-2, these statements can be transformed to

$$\left.\begin{aligned} |U_1| &> c_1 \text{ at } (p_1,v_1) \\ |U_1| &< c_1 \text{ at } (p_1',v_1') \end{aligned}\right\} \tag{6-36}$$

We have proved that the gas flow relative to the reaction front is subsonic behind an upper point, i.e., a strong detonation or weak deflagration;

and supersonic behind a lower point, i.e., a weak detonation or strong deflagration. These conclusions form a part of Jouguet's rule.

If a Rayleigh line intersects the Hugoniot curve at a single point, then the Hugoniot function attains a maximum on the Rayleigh line at the point of intersection. Consequently, the entropy is a maximum on the Rayleigh line at the point of intersection and

$$\frac{ds}{dr} = 0 \tag{6-37}$$

Using Eqs. 6-23, 6-24 and 6-30, we have, at such an intersection,

$$\rho_1^2 c_1^2 = \rho_o^2 D^2 \tag{6-38}$$

and this relation implies that

$$|U_1| = c_1 \tag{6-39}$$

If the Rayleigh line intersects the Hugoniot curve at a single point, the state described by such an intersection is a Chapman-Jouguet state. We have proved that the gas flow relative to the reaction front is sonic behind a Chapman-Jouguet state. This is the property formulated by Jouguet in 1905, and this conclusion forms another part of Jouguet's rule.

We have noted that the Hugoniot function attains a stationary (maximum) value on the Rayleigh line through a Chapman-Jouguet point at the Chapman-Jouguet point. Along the Hugoniot curve, $dH(p_1, v_1) = 0$. Therefore, the Rayleigh line through the Chapman-Jouguet point is tangent at that point to the Hugoniot curve, i.e.,

$$\frac{dp_1}{dv_1} = \frac{p_1 - p_o}{v_1 - v_o} = -\rho_o^2 D^2 \tag{6-40}$$

at a Chapman-Jouguet point. Since this Rayleigh line is also tangent to the isentrope passing through the Chapman-Jouguet point, the Hugoniot curve is tangent at a Chapman-Jouguet point to the isentrope through the point. It follows that the entropy attains a stationary value on the Hugoniot curve at a Chapman-Jouguet point. Thus, we have shown that

$$\frac{dp_1}{dv_1} = -\rho_1^2 c_1^2 \tag{6-41}$$

at a Chapman-Jouguet point, an expression that can be obtained by combining Eqs. 6-38 and 6-40, and we have also shown that

$$ds_1 = 0 \tag{6-42}$$

on the Hugoniot curve, an expression that can be obtained from Eq. 6-27 with $dH(p_1, v_1) = 0$ and Eq. 6-40. If the equation of the Rayleigh line, Eq. 6-14 is differentiated,

$$DdD = \left(\frac{v_o}{v_1 - v_o}\right)^2 \left[\tfrac{1}{2}(p_1 - p_o)dv_1 - \tfrac{1}{2}(v_1 - v_o)dp_1\right] \tag{6-43}$$

Using Eq. 6-40, we see that

$$dD = 0 \tag{6-44}$$

at a Chapman-Jouguet point. We have proved that among the various reactive flows described by the Hugoniot curve, the flow for a Chapman-Jouguet point leads to a stationary value for the velocity of the reaction front relative to the unreacted material. This is the property identified by Chapman in 1899.

Along the Hugoniot curve, where $dH(p_1 v_1) = 0$, Eq. 6-27 is

$$T_1 ds_1 = \tfrac{1}{2}(p_1 - p_o)dv_1 - \tfrac{1}{2}(v_1 - v_o)dp_1 \tag{6-45}$$

The pressure is given by the equation of state as a function of specific volume and entropy. Using Eqs. 6-19, we can write

$$dp_1 = -\rho_1^2 c_1^2 dv_1 + (\partial p/\partial s)_1 ds_1 \tag{6-46}$$

and transform Eq. 6-45 to

$$\left.\begin{aligned} AT_1\left(\frac{ds_1}{dv_1}\right) &= \tfrac{1}{2}(v_1 - v_o)(\rho_1^2 c_1^2 - \rho_o^2 D^2) \\ A &= 1 + \tfrac{1}{2}(v_1 - v_o)\left(\frac{1}{T_1}\right)\left(\frac{\partial p}{\partial s}\right)_1 \end{aligned}\right\} \tag{6-47}$$

where we have employed Eq. 6-14 to eliminate the pressure difference $p_1 - p_o$.

Before discussing the implication of Eq. 6-47, it is necessary to consider the behavior of the function A. Since $\partial p/\partial s > 0$ by Eqs. 6-19, this quantity is clearly positive everywhere on the

deflagration branch of the Hugoniot curve, where $v_1 > v_o$, and at the point on the detonation branch for constant volume explosion, $v_1 = v_o$. Consequently, on the deflagration branch, in view of Eqs. 6-35,

$$\frac{ds_1}{dv_1} > 0 \text{ if } \rho_1^2 c_1^2 > \rho^2 D^2 \qquad (6\text{-}48)$$

i.e., for a weak deflagration; and

$$\frac{ds_1}{dv_1} < 0 \text{ if } \rho_1^2 c_1^2 < \rho_o^2 D^2 \qquad (6\text{-}49)$$

i.e., for a strong deflagration. From Eqs. 6-42 and 6-45 we obtain the relation

$$DdD = \left(\frac{v_o}{v_1 - v_o}\right)^2 T_1 ds_1 \qquad (6\text{-}50)$$

from which we infer that

$$\frac{dv_1}{dD} > 0 \text{ or } \frac{dv_1}{dD} < 0 \qquad (6\text{-}51)$$

for a weak or for a strong deflagration, respectively. If the slope of the Rayleigh line is increased, so that the velocity D is decreased, we see that the specific volume of the upper (weak deflagration) intersection with the Hugoniot curve decreases and the specific volume of the lower (strong deflagration) intersection increases. In the limit of zero slope and zero velocity, the upper intersection must coincide with the specific volume for constant pressure combustion since $p_o = p_1' > p_1$. The specific volume of the lower intersection tends toward infinity as the slope of the Rayleigh line tends toward zero because of Eq. 6-14. Conversely, if the slope of the Rayleigh line is decreased, so that the velocity D is increased, the specific volume of the upper intersection increases and the specific volume of the lower intersection decreases. Since $v_1' < v_1$, these intersections eventually coalesce as the slope of the Rayleigh line continues to decrease. It has been shown that such a single point of intersection is a Chapman-Jouguet point.

Before applying Eq. 6-47 to the detonation branch of the Hugoniot curve, we want to show that the coefficient A is positive everywhere on this branch. To do this, we can adapt an analysis due to Becker. Consider any Rayleigh line intersecting the Hugoniot curve at two points—i.e., (p_1', v_1') and (p_1, v_1)—where $v_1' < v_1$ so that $p_1' > p_1$. Each of these points satisfies the Hugoniot equation, Eq. 6-22. If e_o is eliminated between the two relations obtained when Eq. 6-22 is specialized in turn to the two points and if account is taken of the fact that both points are on the same Rayleigh line, it is easy to show that

$$e(p_1', v_1') - e(p_1, v_1) = \tfrac{1}{2}(p_1' + p_1)(v_1 - v_1') \qquad (6\text{-}52)$$

This relation will be recognized to be the Hugoniot equation centered on (p_1, v_1) for a shock wave in the reaction products, and it is a condition that a shocked state (p', v') must satisfy for given initial state (p_1, v_1). (Eq. 6-52 coincides with Eq. 6-20 only at the two points of intersection of the Rayleigh line with the reaction Hugoniot curve.) Now, we consider p_1' and v_1' to be variables satisfying Eq. 6-52 and obtain, by differentiation at constant p_1 and v_1 and the use of Eq. 6-19, the relation

$$T_1' \, ds_1' = \tfrac{1}{2}(p_1' - p_1)dv_1' - \tfrac{1}{2}(v_1' - v_1)dp_1' \qquad (6\text{-}53)$$

where the prime indicates that the quantity so designated is evaluated at (p_1', v_1'). We again regard the pressure a function of entropy and specific volume so the relation equivalent to Eq. 6-46 applies, and Eq. 6-53 becomes

$$\left[1 + \tfrac{1}{2}(v_1' - v_o)\left(\frac{1}{T_1'}\right)\left(\frac{\partial p}{\partial s}\right)_1'\right](T_1')\frac{ds_1'}{dv_1'} = (v_1' - v_1)\left[(\rho_1' c_1')^2 - \rho_o^2 D^2\right] \qquad (6\text{-}54)$$

where we have again employed the fact that the two points are on the same Rayleigh line. By Eq. 6-35, the right hand member of Eq. 6-52 is negative. It has been shown, as for example by Courant and Friedrichs, that $ds_1'/dv_1' < 0$ for a shock wave described by Eq. 6-52 in a medium whose equation of state conforms to Eqs. 6-19. Therefore

$$1 + \tfrac{1}{2}(v_1' - v_1)\left(\frac{1}{T_1'}\right)\left(\frac{\partial p}{\partial s}\right)_1' > 0 \qquad (6\text{-}55)$$

The specific volume v_1 of the lower intersection can be allowed to approach as closely as is desired the initial volume v_1 so that $p_1 \to p_e$ as $v_1 \to v_o$. Then, it is necessary that $p_1 \to \infty$ as $v_1 \to v_o$. From Eq. 6-55, we conclude that $A > 0$ as

the pressure increases indefinitely. We have noted that $A > 0$ when $v_1 = v_o$. Since the pressure and temperature, and their derivatives are continuous functions of the entropy and specific volume; the coefficient A, the derivative ds_1/dv_1, and the right-hand member of the first of Eq. 6-47 must be continuous on the Hugoniot curve. Therefore, the coefficient A which has been shown to be positive for the maximum and minimum values of v_1 on the detonation branch of the Hugoniot curve, is positive everywhere on the detonation branch of the Hugoniot curve.

From Eq. 6-47, we now conclude that on the detonation branch of the Hugoniot curve

$$\frac{ds_1}{dv_1} < 0 \text{ if } \rho_1^2 c_1^2 > \rho_o^2 D^2 \qquad (6\text{-}56)$$

i.e., for a strong detonation; and

$$\frac{ds_1}{dv_1} > 0 \text{ if } \rho_1^2 c_1^2 < \rho_o^2 D^2 \qquad (6\text{-}57)$$

i.e., for a weak detonation. Using Eq. 6-50, we infer that

$$\frac{dv_1}{dD} < 0 \text{ or } \frac{dv_1}{dD} > 0 \qquad (6\text{-}58)$$

for a strong or for a weak detonation, respectively. If the slope of the Rayleigh line is decreased, so that the velocity D is increased, we see that the specific volume of the upper (strong detonation) intersection with the Hugoniot curve decreases and the specific volume of the lower (weak detonation) intersection increases. In the limit of negatively infinite slope and infinite velocity, the lower intersection must coincide with that for constant volume explosion since $v_1' < v_1 = v_o$. The pressure of the upper intersection tends toward infinity as the slope of the Rayleigh line becomes negatively infinite, because of Eq. 6-14. Conversely, if the slope of the Rayleigh line is increased so that the velocity D is decreased, the specific volume of the upper intersection increases and the specific volume of the lower intersection decreases. Since $v_1' < v_1$, these intersections eventually coalesce as the slope of the Rayleigh line continues to increase. Such a single point of intersection has been shown to be a Chapman-Jouguet point.

The character of the stationary values of entropy and propagation velocity at Chapman-Jouguet points can be described specifically. Differentiating Eq. 6-47 and using Eqs. 6-38 and 6-42, we obtain

$$AT_1\left(\frac{d^2 s_1}{dv_1^2}\right) = -\tfrac{1}{2}(v_1 - v_o)\left(\frac{\partial^2 p}{\partial v^2}\right)_1 \qquad (6\text{-}59)$$

at a Chapman-Jouguet point. Since $\partial^2 p/\partial v^2 > 0$ by Eqs. 6-19 and since $A > 0$, we conclude that

$$\frac{d^2 s_1}{dv_1^2} < 0 \text{ or } \frac{d^2 s_1}{dv_1^2} > 0 \qquad (6\text{-}60)$$

for a Chapman-Jouguet deflagration or detonation, respectively. From Eq. 6-60 we have

$$\frac{d^2 D^2}{dv_1^2} = 2\left(\frac{v_o}{v_1 - v_o}\right)^2 (T_1)\frac{d^2 s_1}{dv_1^2} \qquad (6\text{-}61)$$

at a Chapman-Jouguet point. Therefore,

$$\frac{d^2 D^2}{dv_1^2} < 0 \text{ or } \frac{d^2 D^2}{dv_1^2} > 0 \qquad (6\text{-}62)$$

for a Chapman-Jouguet deflagration or detonation, respectively. It follows that the entropy and propagation velocity are relative maxima at a Chapman-Jouguet deflagration and relative minima at a Chapman-Jouguet detonation. Since the entropy is a maximum at a Chapman-Jouguet deflagration, there is at most one Chapman-Jouguet point on the deflagration branch of the Hugoniot curve. We have demonstrated the existence of one such point separating a region of strong deflagrations from one of weak deflagrations. Therefore, the deflagraion branch consists of two sections, the one consisting of a strong deflagration and the other of weak deflagrations, separated by a Chapman-Jouguet point. Similarly, we conclude that the detonation branch of the Hugoniot curve is divided by a Chapman-Jouguet point into an upper section consisting of strong detonations and a lower section consisting of weak detonations. The properties now attributed to the Hugoniot curve require that

$$\frac{dp_1}{dv_1} < 0\,, \quad \frac{d^2 p_1}{dv_1^2} > 0 \qquad (6\text{-}63)$$

and these properties are a direct consequence of

the assumptions regarding the equation of state that are expressed by Eqs. 6-19.

In order to establish Jouguet's rule for the state ahead of the reaction front, we define a Hugoniot function H_o for the unreacted material by

$$H_o(p,v) = e_o(p,v) - e_o(p_1,v_1) + \tfrac{1}{2}(p + p_1)(v - v_1) \qquad (6\text{-}64)$$

where we regard the final state (p_1, v_1) as fixed and where $e_o(p,v)$ is the specific energy function for the unreacted material. The Hugoniot equation, Eq. 6-24, can now be written

$$H_o(p_o,v_o) = e(p_1,v_1) - e_o(p_1,v_1) = -J(p_1,v_1) \qquad (6\text{-}65)$$

where the exothermal nature of the reaction is expressed by the requirement that $J(p_1,v_1) > 0$. The curve defined by Eq. 6-65 is sketched in Fig. 6-3. It consist of two branches, one of which is the locus of initial states from which the specified final state can be reached when the final state is a detonation, the other being the locus of initial states when the same final state is a deflagration. An analysis identical to that previously employed demonstrates that the Hugoniot junction and entropy of the unreacted material attain one and only one stationary value along the Rayleigh line and that this stationary value is, for each function, a maximum. In the present case, a Rayleigh line can have only a single intersection with either branch of the Hugoniot curve defined by Eq. 6-65. If a second intersection with one of the branches were to exist, the function H_o, which vanishes at (p_1,v_1), would have the same negative value at each intersection and hence a minimum on the Rayleigh line between the two intersections; this is impossible. Therefore, a second intersection with the same branch of this curve is impossible. For the present choice of variables, the Rayleigh line can be represented in terms of a parameter r_o by

$$\left.\begin{aligned} p &= p_1 + ar_o \quad , \quad v = v_1 + br_o \\ a &= p_o - p_1 \quad , \quad b = v_o - v_1 \end{aligned}\right\} \qquad (6\text{-}66)$$

where $a/b = -\rho_o^2 D^2$ by Eq. 6-14. The expression analogous to Eq. 6-24 for the unreacted material is

$$\frac{ds_o}{dr_o} = \left(\frac{\partial s_o}{\partial p}\right)_o \left(a + b\,\rho_o^2 c_o^2\right) \qquad (6\text{-}67)$$

Since the entropy attains a maximum on the Rayleigh line at a point between (p_1,v_1) and (p_o,v_o), it follows that $ds_o/dr_o < 0$ at (p_o,v_o) for an intersection with either branch. If we recall that $\partial s/\partial p > 0$ by Eqs. 6-19, Eqs. 6-66 and 6-67 lead to the result

$$(v_o - v_1)(c_o^2 - D^2) < 0 \qquad (6\text{-}68)$$

Therefore $D > c_o$ if $v_1 > v_o$ and the final state is a deflagration, and $D < c_o$ if $v_1 < v_o$ and the final state is a detonation. We have shown that the flow relative to the reaction front is subsonic ahead of a deflagration wave and supersonic ahead of a detonation wave. These statements form part of Jouguet's rule.

6-4 EXISTENCE AND UNIQUENESS OF FLOWS INVOLVING REACTION WAVES

The Hugoniot equation does not suffice to determine uniquely a reaction state and propagation velocity that can be identified with the unique detonation wave that is usually observed experimentally. Therefore, it is necessary to supplement the conservation conditions with additional information. The source of this information is the nature of the entire flow field on each side of the reaction discontinuity. These flow fields are determined by the partial differential equations of hydrodynamics. The equations must be satisfied in any region that is free of discontinuities and they are to be solved, in the present case of flow in one dimension, subject to initial conditions specified on the x-axis and to boundary conditions specified on the rear boundary. If the problem is formulated in this manner, the mechanical conditions across the reaction front and the Hugoniot equation are supplementary conditions that must be satisfied on each side of the discontinuity by the solutions of the hydrodynamic equations in the continuous regions. They can be thought of as connecting the solution in one region, that of the unreacted material, to the solution in the adjacent region, that of the reaction products. In serving this purpose, they implicitly prescribe the path, e.g.,

$x(t)$, of the reaction wave in the (x,t)-plane. The existence and uniqueness of solutions of the hydrodynamic equations in flows involving a reaction front has been discussed in an elegant manner by Courant and Friedrichs, whose treatment is followed in this paragraph.

In par. 2-7, it is remarked that a curve in the (x,t)-plane on which are specified data to which the hydrodynamic equations are subject is timelike if the flow relative to the curve is subsonic, and that such a curve is spacelike if the flow relative to the curve is supersonic. It is shown that the solution of a flow problem in a region between two curves is unique in two cases: if both curves are timelike, one quantity is specified on each curve and two quantities are specified at their intersection; or if one curve is spacelike with two quantities specified on it, the other curve is timelike with one quantity specified on it. With the aid of Jouguet's rule, these principles can be employed to consider the determinacy of flows involving a detonation wave.

For definiteness, we consider a semi-infinite mass of explosive, initially at rest with $u_o = 0$, extending from $x = 0$ to $x = \infty$; and we assume that a reaction propagating in the direction of positive x begins on the plane $x = 0$ at the time $t = 0$. Although one is usually concerned with the case where the end $x = 0$ is completely open or consists of a rigid wall, it is illuminating to consider the more general problem in which the end is conceived to be a piston which starts to move from the end $x = 0$ at the time $t = 0$ with specified constant velocity u_p.

The path P of the piston in the (x,t)-plane is timelike since it is identical with that of the particles adjacent to it. The particle velocity of the adjacent particles is equal to the piston velocity u_p so that u is specified on the path P. The initial values $u = u_o = 0$ and $p = p_o$ are specified on the x-axis which is to be regarded as spacelike. However, these regions are separated by the unknown path W of the reaction wave, and it is necessary to consider separately the flow in the two regions into which the (x,t)-plane is divided by W. We may suppose that the propagation velocity of the wave, i.e., the slope of W, is arbitrarily fixed and constant.

If the wave is a detonation, W is, by Jouguet's rule, supersonic when observed from the unreacted material. Then, between W and the x-axis, the flow is uniquely determined by the quantities prescribed on the x-axis at $t = 0$ so that u and p are constant everywhere in that region and equal to u_o and p_o, respectively. The conservation conditions across the wave front, Eqs. 6-2 and 6-3, then prescribe u_1 and p_1 for the specified value D of the slope of W. We may now regard W as an initial curve for the region between P and W on which the quantities $u = u_1$ and $p = p_1$ are prescribed.

Now suppose that W represents a strong detonation. By Jouguet's rule, W is timelike when observed from the reaction products. Since P and W are both timelike, their slopes u_p and D cannot both be arbitrarily specified. This is because the value of u on W, which is fixed by the initial conditions and the velocity D, is also fixed in accordance with the existence rule by the specification of u on P, of p on W, and of u and p at the intersection of P and W. Therefore, for a strong detonation wave of specified propagation velocity, it is necessary to adjust the piston path P so that $u_p = u_1$. It follows that the flow between the piston and the strong detonation wave is uniform with

$$\left.\begin{aligned} p &= p_1 \\ u &= u_1 = u_p \end{aligned}\right\} \qquad (6\text{-}69)$$

and that the flow for a strong detonation is completely determined by the piston velocity and initial conditions. If the first of Eqs. 6-2 is combined with Eq. 6-1, then when $u_o = 0$ we have

$$u_1 = D(1 - v_1\rho_o) \qquad (6\text{-}70)$$

Differentiating with respect to v_1 at constant ρ_o, we obtain

$$\frac{du_1}{dv_1} = \left(\frac{u_1}{D}\right)\frac{dD}{dv_1} - \rho_o D \qquad (6\text{-}71)$$

for a strong detonation, $dD/dv_1 < 0$. Therefore $du_1/dv_1 < 0$. If we denote by u_1^* the particle velocity of the reaction products for a Chapman-Jouguet detonation, we conclude that the velocity of the piston, supporting a strong detonation, is subject to the restriction

$$u_p \geq u_1^* \qquad (6\text{-}72)$$

We have shown that just one flow involving a strong detonation is possible and that the piston velocity must satisfy Eq. 6-72. In the limit given by the equality sign, the detonation is a Chapman-Jouguet detonation. The flow in a strong detonation is illustrated by Fig. 6-7 in which are shown the piston path P, the wave path W, and a typical particle path.

We must now consider flows involving a detonation wave for which $u_p < u_1^*$. It is to be noted that flows involving weak detonation cannot be excluded on dynamical grounds when the reaction zone is represented by a mathematical discontinuity. By Jouguet's rule, the wave path of a weak detonation is supersonic or spacelike when viewed from the reaction products, and a flow associated with a weak detonation consequently possesses a higher degree of indeterminacy than is the case for strong detonations. For this reason, it is possible to construct flows involving a weak detonation and compatible with a prescribed piston velocity in a number of ways. Thus, the uniqueness of a particular flow cannot be demonstrated, as was possible for a strong detonation. In fact, if shock waves in the reaction products are admitted as part of the solution, the flow behind a weak detonation can be accommodated to a piston velocity satisfying Eq. 6-72. These solutions are not discussed further since it has been noted that weak detonations are eliminated by consideration of the structure of the reaction zone.

For the case $u_p < u_1^*$, a flow involving a Chapman-Jouguet detonation can be constructed and is therefore possible. In this case, the particle velocity, equal to u_1^* behind the detonation wave, is adjusted to the piston velocity u_p by a centered rarefaction wave. Since a Chapman-Jouguet detonation wave front, (Eq. 6-18), and the head of the rarefaction wave moves with the same velocity, the rarefaction wave follows the detonation front immediately. The wave path W and the characteristic C_+ issuing from the point $x = 0$, $t = 0$ coincide. This flow is illustrated by Fig. 6-8 which shows the piston path P, the wave path W, a typical particle path and characteristics C_+ through the centered rarefaction wave. In particular, if the end $x = 0$ is fixed—so that $u_p = 0$ or open, corresponding to $u_p < 0$—a Chapman-Jouguet detonation is possible. The Chapman-Jouguet hypothesis consists of the assumption that it is this flow that actually exists in the case of an unsupported detonation wave in the absence of a piston. Weak detonation waves having been eliminated from consideration, it is likely that no other solution exists.

In Fig. 6-9, the particle velocities at a given instant of time between the wave front and the piston are compared for four different values of the piston velocity. For two of these values, strong detonations result and for the other two, one of them representing zero piston velocity, the detonation is a Chapman-Jouguet

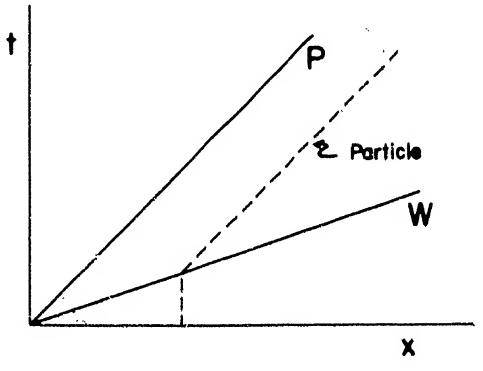

Figure 6-7. Flow in a Strong Detonation

detonation. A graph of the pressure would be qualitatively similar to this figure.

In a deflagration process, the wave path W is timelike with respect to the unreacted material in accordance with Jouguet's rule. Consequently, the flow in the unreacted material is not determined by the prescribed values of pressure and particle velocity, p_o and u_o, on the x-axis, and one quantity can be arbitrarily prescribed on W. By Jouguet's rule, the wave path W is also timelike with respect to the reaction products if the wave is a weak deflagration. It follows that the flow is uniquely determined when one quantity, the path W or a quantity ahead of W, is prescribed. For a deflagration process with $v_1 > v_o$, we have $\bar{u}_1 < 0$ by Eq. 6-17. It is possible for the wave to move into the unreacted material at rest only if the

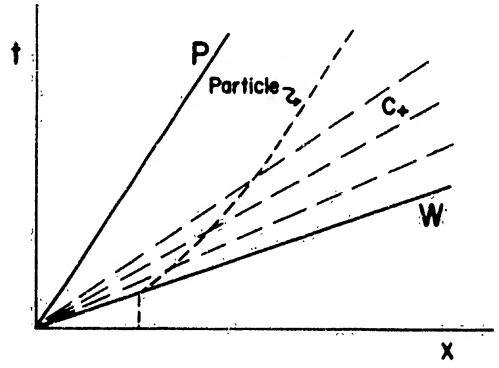

Figure 6-8. Flow in Chapman-Jouguet Detonation

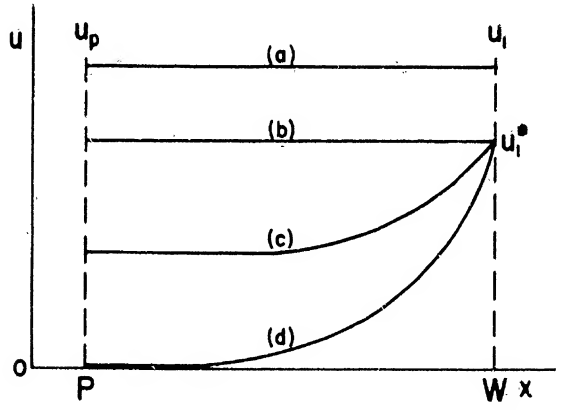

Figure 6-9. Particle Velocity Behind Detonation Waves: Strong Detonation (a) and (b); Chapman-Jouguet Detonations (b), (c), and (d)

the piston is withdrawn with a speed at least equal to that of the reaction products behind the front, $u_p < u_1$. If $u_p > u_1$, and in particular if $u_p = 0$, the pattern of the flow must involve a new feature. In this case, the adjustment of the particle velocity to that at the rear boundary is possible only if a precompression shock wave is generated by the deflagration wave in the unreacted material of a suitable strength so that after the particles are accelerated in the forward direction by the shock wave they are retarded by the deflagration wave and so attain the velocity obtaining at the rear boundary. This flow is illustrated in Fig. 6-10 for a closed end, $u_p = 0$, where the shock path S, the wave path W, and a particle path are shown. The occurrence of a precompression shock wave is in conformity with Jouguet's rule. Since the flow ahead of the deflagration wave is subsonic relative to the wave front, the wave influences the state of the material ahead of it. For any arbitrarily prescribed wave path W and piston path with $u_p > u_1$, there is a uniquely determined precompression shock S and flow between S and P. It is to be noted that flows exist for a specified shock wave involving arbitrarily chosen strong deflagration waves followed by rarefaction or shock waves. Strong deflagration waves having been eliminated from consideration, it is likely that the solution described involving a weak deflagration is the only solution that exists. One degree of indeterminacy remains: either shock path S or the wave path W can be chosen arbitrarily with a prescribed piston velocity. Additional information, to be found by an examination of reaction and transport processes in the interior of the wave, must be employed uniquely to determine the flow.

We conclude this discussion of the flows associated with reaction waves by showing that a deflagration wave with its precompression shock wave is formally equivalent to a detonation wave. Through a shock wave of velocity U, the pressure of the unreacted material is raised from p_o to p' and the specific volume decreased from v_o to v'. The mass flux m through the shock wave is, by the continuity equation,

$$m = \rho_o w_o = \rho' w' \tag{6-73}$$

where $p' = 1/v'$ and w' is the flow velocity of the shocked unreacted material relative to the shock front. Through the deflagration wave of velocity D, the pressure is reduced from p' to p_1 and the specific volume increased from v' to v_1. If the mass flux is the same through both waves,

$$m = \rho' w' = \rho_1 w_1 \tag{6-74}$$

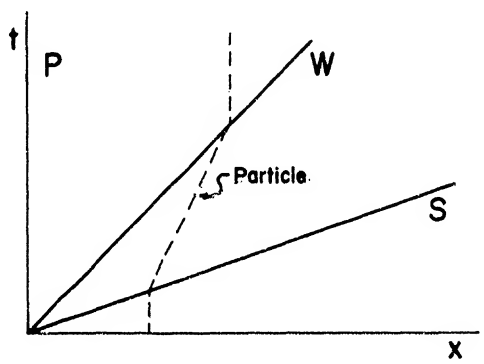

Figure 6-10. Flow in Weak Deflagration With Closed End

and therefore

$$\rho_o w_o = \rho_1 w_1 \qquad (6\text{-}75)$$

The conservation of momentum through the shock and deflagration waves requires that

$$\left.\begin{aligned} p' - p_o &= \rho_o w_o^2 - \rho'(w')^2 \\ p_1 - p' &= \rho'(w')^2 - \rho_o w_1^2 \end{aligned}\right\} \qquad (6\text{-}76)$$

so that, by the elimination of p',

$$p_1 - p_o = \rho_o w_o^2 - \rho_1 w_1^2 \qquad (6\text{-}77)$$

These conservation conditions can be combined to yield

$$\frac{p' - p_o}{v' - v_o} = \frac{p_1 - p'}{v_1 - v'} = \frac{p_1 - p_o}{v_1 - v_o} = m^2 \qquad (6\text{-}78)$$

The Hugoniot equations for the shock and deflagration waves are

$$\left.\begin{aligned} e_o(p',v') - e_o(p_o,v_o) &= \tfrac{1}{2}(p' + p_o)(v_o - v') \\ e(p_1,v_1) - e_o(p',v') &= \tfrac{1}{2}(p_1 + p')(v' - v_1) \end{aligned}\right\} \qquad (6\text{-}79)$$

respectively, where $e_o(p,v)$ is the specific energy function of the unreacted material. Eliminating $e_o(p',v')$ from these expressions and using Eq. 6-78, we obtain

$$\left.\begin{aligned} &e(p_1,v_1) - e_o(p_o,v_o) \\ &= \tfrac{1}{2}(p_1 + p_o)(v_o - v_1) \end{aligned}\right\} \qquad (6\text{-}80)$$

Eqs. 6-75, 6-77 and 6-80, are identical with Eqs. 6-2 and 6-3 for a single reaction process from the state (p_o, v_o) to the state (p_1, v_1). The shock and deflagration waves have the same propagation velocity $D = U$ when the mass flux is the same through each wave and, by Eq. 6-78, the points (p',v') and (p_1,v_1) lie on the same Rayleigh line. Fig. 6-11, illustrating the Hugoniot curve for the (weak) deflagration and the shock wave, shows that the equivalent single process is a detonation. The curve $A'AO$ is the Hugoniot curve of the shock wave, centered on (p_o,v_o), in the unreacted material, given by the first of Eqs. 6-79. The curve $B'B$ is the deflagration branch of the reaction Hugoniot curve centered on (p',v'), given by the second of Eqs. 6-79, and also the detonation branch of the reaction Hugoniot curve centered on (p_o,v_o), given by Eq. 6-80. The Rayleigh line ABO is drawn tangent to the reaction Hugoniot curve and thus corresponds to a Chapman-Jouguet detonation centered on (p_o,v_o) or to a Chapman-Jouguet deflagration centered on (p', v'). The Rayleigh line $A'B'O$ corresponds to a strong detonation or a weak deflagration. It is evident that a strong detonation is formally equivalent to a weak deflagration preceded by a shock and a Chapman-Jouguet detonation to a Chapman-Jouguet deflagration preceded by a shock, the mass flux through shock and deflagration waves being identical.

6-5 THE CHAPMAN-JOUGUET HYPOTHESIS

The Chapman-Jouguet hypothesis states that the detonation wave for which

$$w_1 = C_1 \qquad (6\text{-}81)$$

is the one that actually occurs when the reaction wave is unsupported. The assumption that the flow satisfying Eq. 6-81 is to be identified with the experimentally observed unsupported detonation wave was advanced independently by Chapman and by Jouguet. This hypothesis selects one state from the continuum of states described by the Hugoniot equation and compatible with the conservation conditions. Consequently, Eq. 6-81 together with the conservation conditions, Eqs. 6-2 and 6-3, and an equation of state for the reaction products suffices to determine the detonation velocity, the state of the reaction products, and their velocity with respect to the detonation front. These relations thus constitute a theory of the detonation wave. It can be used to calculate the detonation properties for particular explosives, and the calculated values can be tested by comparison with experiment.

Support was given to the Chapman-Jouguet hypothesis by the agreement obtained between calculated and observed properties of the detonation wave for explosives expected to conform to the model of one-dimensional flow and for which an equation of state is known. The detonation wave propagating along a pipe filled with an explosive gas mixture appears to

fulfill this conditions. For such a system, the ideal gas equation of state is sufficiently accurate. Of particular interest, because of the frequency of citation in the literature, is the work of Lewis and Friauf[6], who carried out the first critical experimental test of theory. They treated mixtures of hydrogen and oxygen, diluted by various gases, and in their calculations they considered the effect of dissociation equilibria on the final composition of the gases. Good agreement was obtained between calculated and observed values of detonation velocity. The mixtures presented a considerable variation in the energy released and in the initial density. For this mixture, elementary theory adequately predicts the principal properties of the detonation wave.

In theoretical justification of the Chapman-Jouguet hypothesis, strong detonations can at once be eliminated as states to be identified with an unsupported wave. It was shown in the last paragraph that strong detonations exist only for a supported wave where the piston velocity is greater than the particle velocity behind a Chapman-Jouguet wave. If the piston velocity is less than this limiting value, and in particular if the rear boundary is either fixed or free, rarefaction waves from the rear boundary can eventually overtake and attenuate a strong detonation because of the subsonic nature of the flow behind it. The process of attenuation will cease when the wave has decayed to a Chapman-Jouguet wave because the flow behind the wave then becomes sonic. Therefore, we conclude that a strong detonation is hydrodynamically unstable if the wave is unsupported.

To illustrate this point further, consider the hypothetical situation represented by Fig. 6-12, in which the piston P, initially supporting a strong detonation wave, is suddenly stopped, creating at that instant a rarefaction wave that overtakes and weakens the detonation wave. The

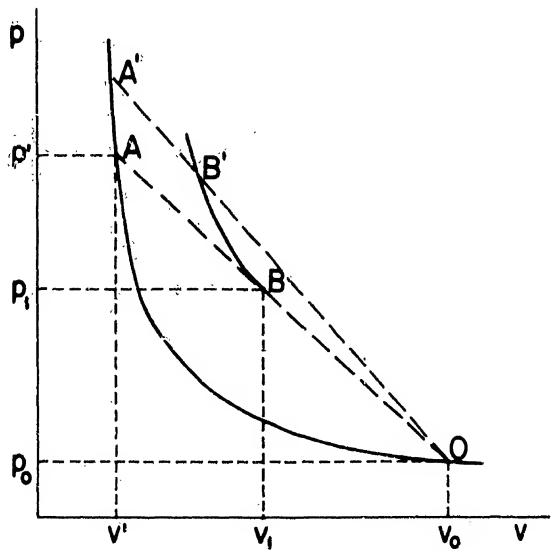

Figure 6-11. A Detonation as a Deflagration With a Precompression Shock

initial straight portion of *W* represents the strong detonation wave, the later straight portion the Chapman-Jouguet wave, and the curved portion a transition region. Two particle paths are shown, one through the strong detonation and the other through the Chapman-Jouguet detonation.

Prior to about 1940, when the analysis was refined by consideration of the finite extent of the reaction zone, weak detonations were eliminated by unconvincing plausibility arguments. Becker[7] showed that the entropy of a strong detonation state is greater than that of the weak detonation state with the same propegation velocity and inferred that the former state is therefore the more probable. Weak detonations being thermodynamically unstable relative to the corresponding strong detonations and strong detonations being dynamically unstable, he concluded that the Chapman-Jouguet detonation wave is the stable one. Scorah[8] showed the Helmholtz free energy to be a minimum for the Chapman-Jouguet state. He interpreted this result to mean that the Chapman-Jouguet state corresponds to a maximum degradation of energy and is therefore the most probable one. Commenting on the generally unsatisfactory nature of thermodynamic arguments of this sort, Zeldovich[9] remarked that an increase in entropy does not guarantee the existence of a shock; a piston to compress the gas is also necessary.

Brinkley and Kirkwood[10] have treated the dynamic stability of the detonation wave by considering the energy available in the explosive products to support the propagation of the detonation front and the hydrodynamic conditions operating in the flow behind the front. Their analysis is developed in the paragraphs which follow.

The propagation of a detonation front, like the propagation of an unreactive shock wave, requires a continuous supply of energy from the rear. The work done by the medium to the rear of the front on the intact medium ahead of the front in the time element dt is $p_1 u_1 dt$, the subscript 1 being used to designate conditions immediately to the rear of the front at an instant of time t_1. If we now fix attention on the total mass of explosion products initially

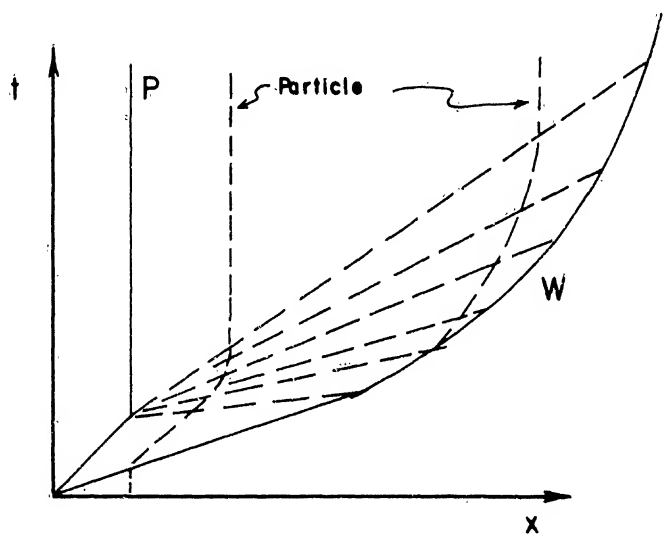

Figure 6-12. Attenuation of a Strong Detonation Wave by a Rarefaction Wave

contained in the region from the rear boundary $x_o = 0$ to the plane $x_o = x_1$ for times subsequent to the instant t_1 when the wave front reaches x_1, we note that the total work done by this portion of the medium on the medium ahead of it, designated $W(x_1)$, is

$$W(x_1) = \int_{t_1}^{\infty} pu\,dt \qquad (6\text{-}82)$$

where the integral is along the particle path of the particles initially at the point x_1.

The secular behavior of the integrand pu (for a given element of the medium) has an important bearing on the behavior of the detonation wave when it is in an unsteady state. The proof which follows shows that the sign of $[\partial(pu)/\partial t]_{x_1}$, determines the sign of the acceleration of the wave front.

Defining for the Lagrangian rate of change of the quantity pu a time constant μ to be evaluated at the shock front, i.e.,

$$\frac{1}{\mu} = -\frac{1}{p_1 u_1}\left[\frac{\partial(pu)}{\partial t}\right]_{x_1} \qquad (6\text{-}83)$$

we make the arbitrary assumption that $\mu > 0$ after external or self-generated initiation effects have died out and the wave has become self-sustaining.

Although this assumption is made *a priori*, there is strong reason to accept its validity. It can readily be shown, for example, that this condition follows if there is a rarefaction immediately behind the detonation front, a rarefaction being defined for this purpose by the two conditions

$$\frac{d\rho}{dt} < 0, \left(\frac{\partial p}{\partial x}\right)_t > 0 \qquad (6\text{-}84)$$

Since—in the absence of shocks in the flow—a given element of matter remains in an isentropic condition, the pressure will decrease when the density decreases. Also, the flow velocity will decrease when the pressure gradient is positive according to the equation of motion. Therefore the presence of a rarefaction as so defined is a sufficient condition for μ to be positive.

We now proceed to establish a connection between this condition on μ and the secular behavior of an unsteady detonation.

For inviscid flow without heat conduction, the hydrodynamic equations of continuity and momentum can be written in terms of a Lagrangian space coordinate (see par. 2-6) for flow in one dimension in the form

$$\left.\begin{aligned} \frac{\rho}{\rho_o}\left(\frac{\partial u}{\partial x_o}\right) + \frac{1}{\rho c^2}\left(\frac{\partial p}{\partial t}\right) &= 0 \\ \frac{\partial u}{\partial t} + \frac{1}{\rho_o}\left(\frac{\partial p}{\partial x_o}\right) &= 0 \end{aligned}\right\} \qquad (6\text{-}85)$$

The Lagrangian coordinate x_o is the position of the element of fluid at $t = 0$ whose position at time t is x. The time and Lagrangian coordinate are taken to be independent variables and the Eulerian coordinate x is regarded a function $x(x_o, t)$ with

$$u = \frac{\partial x}{\partial t} \text{ and } \rho_o = \rho\left(\frac{\partial x}{\partial x_o}\right) \qquad (6\text{-}86)$$

Eqs. 6-85 are supplemented by the entropy transport equation, which is not explicitly employed; by initial and boundary conditions; and by the conservation conditions across the reaction discontinuity which implicitly prescribe the path of the discontinuity in the (x_o, t)-plane. As has previously been pointed out, the discontinuity conditions prescribe a one-parameter continuum of possible detonation states and can be used, when supplemented by an equation of state, to express all of the detonation properties as functions of any one of the properties selected as argument. For convenience, the unreacted explosive is assumed to be at rest. The second of Eqs. 6-2 can then be written

$$p_1 - p_o = \rho_o u_1 D \qquad (6\text{-}87)$$

An operator in which the detonation wave is stationary is defined by

$$\frac{d}{dt} = \frac{\partial}{\partial t} + D\frac{\partial}{\partial x_o} \qquad (6\text{-}88)$$

If Eqs. 6-85 are specialized to the high pressure side of the detonation wave and the partial time derivatives eliminated with the aid of Eq. 6-88, we obtain

$$\frac{dp_1}{dt} = D\left(\frac{\partial p}{\partial x_o}\right)_1 - \frac{(\rho_1 c_1)^2}{\rho_o}\left(\frac{\partial u}{\partial x_o}\right)_1$$
$$\frac{du_1}{dt} = D\left(\frac{\partial u}{\partial x_o}\right)_1 - \frac{1}{\rho_o}\left(\frac{\partial p}{\partial x_o}\right)_1 \qquad (6\text{-}89)$$

where the subscript unity indicates that the quantity so designated is to be evaluated immediately behind the detonation wave. Since the detonation front is assumed to be a mathematical discontinuity, the conservation conditions across the discontinuity must be satisfied whether or not the state behind the wave is steady. Eq. 6-87 can therefore be differentiated, with the result

$$\frac{dp_1}{dt} = \frac{\rho_o D}{g}\left(\frac{du_1}{dt}\right)$$
$$g = 1 - \rho_o u_1\left(\frac{dD}{dp_1}\right) \qquad (6\text{-}90)$$

Also from Eq. 6-88 and the definition of μ, we can write

$$\frac{1}{p_1}\left(\frac{dp_1}{dt}\right) + \frac{1}{u_1}\left(\frac{du_1}{dt}\right) = \frac{D}{p_1}\left(\frac{\partial p}{\partial x_o}\right)_1 + \frac{D}{u_1}\left(\frac{\partial u_1}{\partial x_o}\right)_1 - \frac{1}{\mu} \qquad (6\text{-}91)$$

Eqs. 6-89, 6-90, and 6-91 can be solved for dp_1/dt in terms of μ and the properties of the reaction products behind the detonation front. The result can be written,

$$\frac{1}{p_1}\left(\frac{dp_1}{dt}\right) = -\frac{1}{\mu}\left\{\frac{G}{(1 + g + [(p_1/\rho_o u_1 D)](1 + g - G)}\right\} \qquad (6\text{-}92)$$

where

$$G = 1 - [\rho_o D/(\rho_1 c_1)]^2 \qquad (6\text{-}93)$$

or, in view of the first of Eqs. 6-2

$$G = 1 - [(D - u_1)/c_1]^2 \qquad (6\text{-}94)$$

To determine the sign of the denominator of the term in braces of Eq. 6-92, the equation of the Rayleigh line Eq. 6-14, can be rearranged

$$p_1 - p_o = \rho_o D^2(1 - \rho_o v_1) \qquad (6\text{-}95)$$

and differentiated with respect to v_1 at constant p_o and ρ_o. The resulting expression connects the derivative dD/dp_1 with the slope dp_1/dv_1 of the Hugoniot curve. When it is simplified with the aid of Eq. 6-70 and the definition of g introduced, the expression

$$g = \tfrac{1}{2}\left[1 - \rho_o^2 D^2\left(\frac{dv_1}{dp_1}\right)\right] \qquad (6\text{-}96)$$

is obtained. Since $dp_1/dv_1 < 0$, $g > 1/2$. Therefore, $(1 + g)$ and $(1 + g - G)$—the latter being equal to $g + [\rho_o D/(\rho_1 c_1)]^2$—are positive and the denominator of the term in braces of Eq. 6-92 is positive everywhere on the Hugoniot curve.

In view of the assumption that μ is positive, the sign of dp_1/dt is seen to be opposite to that of G. Therefore, it follows that

$$\frac{dp_1}{dt} < 0 \text{ when } p_1 > p_1^* \text{ and } D < u_1 + c_1$$

$$\frac{dp_1}{dt} = 0 \text{ when } p_1 = p_1^* \text{ and } D = u_1 + c_1$$

$$\frac{dp_1}{dt} > 0 \text{ when } p_1 < p_1^* \text{ and } D > u_1 + c_1$$

where p_1^* is the pressure behind a Chapman-Jouguet detonation wave.

This analysis indicates that both strong and weak detonations are dynamically unstable and tend with time to the Chapman-Jouguet state. It also indicates that the Chapman-Jouguet state is stable since its properties do not change with time. In particular, it is demonstrated that the propagation velocity of the Chapman-Jouguet detonation is constant, a result that is in accord with experimental observations. The analysis must, however, be regarded a plausibility argument since it is subject to the basic

assumption that was made with respect to the nature of the flow behind the detonation wave. We defer to a later chapter further consideration of the Chapman-Jouguet hypothesis and now examine the results that can be obtained with the theory that has been formulated.

6-6 THEORY OF THE DETONATION VELOCITY AND OF THE THERMODYNAMIC STATE OF THE EXPLOSION GAS

When supplemented by an equation of state of the reaction products and the Chapman-Jouguet hypothesis, the conservation conditions across the detonation wave suffice to determine a unique final state, flow velocity, and propagation velocity when the state of the unreacted explosive is specified. In this paragraph, we assemble these relations and effect a partial reduction of the equations. By using thermodynamic relations of general validity, we formulate the general one-dimensional theory of the detonation velocity and detonation properties. We assume, without loss of generality, that the unreacted explosive is at rest with reference to a stationary origin of coordinates.

The conservation conditions across the detonation wave have been expressed by Eqs. 6-2 and 6-3. For the explosive at rest with $u_o = 0$, these relations can be written

$$\rho_o D = \rho_1 (D - u_1) \tag{6-97}$$

$$p_1 - p_o = \rho_o D^2 (1 - \rho_o v_1) \tag{6-98}$$

$$e_1 - e_o = \tfrac{1}{2}(p_1 + p_o)(v_o - v_1) \tag{6-99}$$

The first of these expressions is the equation for the conservation of mass and is identical with the first of Eqs. 6-2. The second, which is the same as Eq. 6-95, can be obtained by rearranging the equation of the Rayleigh line, Eq. 6-14, and is the result of combining the equations for the conservation of mass and momentum. The third is the Hugoniot equation, Eq. 6-3, which is the result of combining the equation for the conservation of energy with the mechanical conservation conditions.

The Chapman-Jouguet hypothesis results in a supplementary condition, Eq. 6-18,

$$D = u_1 + c_1 \tag{6-100}$$

Eliminating the particle velocity u_1 with the aid of Eq. 6-97, we obtain an alternative expression

$$D = \rho_1 c_1 / \rho_o \tag{6-101}$$

It is convenient to eliminate the speed of sound by the introduction of the adiabatic exponent κ defined by

$$\kappa = (\partial \ln p / \partial \ln \rho)_s \tag{6-102}$$

in terms of which the speed of sound is given by

$$c = \sqrt{\kappa p / \rho} \tag{6-103}$$

The adiabatic exponent is a function of the thermodynamic state of the gas. For an ideal gas, it is equal to the ratio of the heat capacity at constant pressure to the heat capacity at constant volume. With the aid of Eq. 6-103, Eq. 6-101 can be transformed to

$$\left.\begin{aligned} D^2 &= \kappa_1 p_1 \rho_1 / \rho_o^2 \\ \kappa_1 &= \kappa(p_1, \rho_1) \end{aligned}\right\} \tag{6-104}$$

Eq. 6-104 can be employed to eliminate the detonation velocity from Eq. 6-98. We then obtain the result

$$1 - \frac{p_o}{p_1} = \kappa_1 \left(\frac{\rho_1}{\rho_o} - 1 \right) \tag{6-105}$$

We have obtained from Eqs. 6-97 to 6-100 a pair of expressions, Eqs. 6-97 and 6-104, from which the detonation velocity and particle velocity of the reaction products can be calculated after the pressure p_1 and specific volume v_1 of the reaction products have been determined, i.e.,

$$\left.\begin{aligned} D &= v_o \sqrt{\kappa_1 p_1 \rho_1} \\ u_1 &= D(1 - \rho_o v_1) \end{aligned}\right\} \tag{6-106}$$

and a pair of expressions, Eqs. 6-99 and 6-105, involving thermodynamic quantities only

$$\left.\begin{aligned} e_1 - e_o &= \tfrac{1}{2}(p_1 + p_o)(v_o - v_1) \\ 1 - p_o/p_1 &= \kappa_1 (\rho_1 v_o - 1) \end{aligned}\right\} \tag{6-107}$$

that suffice to determine p_1 and v_1. We must now consider the solution of the latter pair of equations.

Eqs. 6-107 contain two functions of the state of the reaction products, the specific energy e_1 and the adiabatic exponent κ_1, whose dependence on the state variables p_1 and v_1 is made explicit by the introduction of an equation of state. As a practical matter, it is not convenient to express either of these quantities, either analytically or by means of tables, directly in terms of these two state variables. Consequently, the equation of state introduces an additional state variable—e.g., the entropy or temperature—and Eqs. 6-107 are then to be solved simultaneously with the equation of state for the three state variables. Since the Hugoniot equation expresses a condition on the energy of the reaction products and since the energy is the characteristic thermodynamic function for systems described in terms of entropy and volume, it would be consistent to employ an equation of state having entropy and volume the independent variables. However, again as a practical matter, the thermodynamic data to be employed in the evaluation of the energy difference $e_1 - e_o$ are of such a nature as to require the selection of temperature as an independent state variable and the form of equations of state for nonideal gases makes appropriate the selection of the volume as the second independent state variable. The effect of this choice of variables, which is an unnatural one from a thermodynamic viewpoint, is to confer on the resulting set of equations a degree of algebraic complexity that is not required of the formal presentation of the theory. A method for their solution is presented in Appendix F.

REFERENCES

1. R. Courant and K. O. Friedrichs, *Supersonic Flow and Shock Waves*, Interscience Publishers, Inc., New York, 1948.
2. E. Jouguet, *Mechaniques des Explosifs*, O. Doin e Fils, Paris (1917).
3. J. von Neumann, Office of Scientific Research and Development, Report No. 549 (1942).
4. D. L. Chapman, Phil. Mag. (5) 47, 90 (1899).
5. E. Jouguet, *J. Math.* 347, (1905); *Proc. Int. Cong. Appl. Mech.*, 12-22 (1926).
6. B. Lewis and J. B. Friauf, J. Am. Chem. Soc. 52, 3905 (1930). See also B. Lewis and G. von Elbe, *Combustion, Flames and Explosions of Gases*, 2nd Ed., Academic Press, New York, 1961, pp. 525-527.
7. R. Becker, Z. Physik 8, 321 (1922); Z. Elektrochem. 42, 457 (1936).
8. R. L. Scorah, J. Chem. Phys. 3, 425 (1935).
9. Y. B. Zeldovich, Z. Eksptl i. Teoret. Fiz. 10, 542 (1940), Transl. NACA Tech. Mem. 1261 (1950).
10. S. R. Brinkley, Jr. and J. G. Kirkwood, *Third Symposium on Combustion and Flame and Explosion Phenomena*, Williams and Wilkins Co., Baltimore, 1949, p. 586.

CHAPTER 7 APPLICATION OF THEORY TO CONDENSED EXPLOSIVES

7-1 INTRODUCTION

It has been noted in Chapter 5 that the detonation velocity of solid and liquid explosives is observed to be in the range 4000 to 8000 m per sec, and that for a given explosive in cylinders of large diameter the detonation velocity is very nearly a linear function of the initial bulk density. Since the pressures and temperatures of the reaction products at the detonation wave front lie far outside of the region that can be explored by ordinary experimental methods, the variation of detonation velocity with initial density has constituted the chief experimental fact for determining the pressure, density, and particle velocity. In recent years, this evidence has been supplemented by isolated experimental determinations of the detonation pressure. However, it is necessary to employ the theory to evaluate the state of the detonation products at any point other than that for which a direct experimental determination is available.

Since 1940, a large amount of work has been done in an effort to formulate a generally applicable equation of state to supplement the hydrodynamic equations of the theory of the detonation wave. The work had the objectives of determining the physical and chemical properties of the detonation gas in sufficient detail so as to make possible the evaluation of its thermodynamic state behind the detonation front and during its isentropic expansion from the detonation state. The latter information is necessary for the solution of flow problems when the initial boundary conditions are determined by the detonation wave.

In much of this work, the theory has been employed in an inverted form—using experimental values of the detonation velocity and, when available, of the detonation pressure—to evaluate the parameters of an equation of state of assumed form. The equation of state obtained in this way can be employed to evaluate the unknown properties of the detonation wave in the explosive for which the equation was calibrated. If the parameters of the equation can be related to the basic molecular parameters of the explosive and if the form of the equation is sufficiently general, the theory can be used to predict the properties of other explosives.

Attempts have been made to employ theoretical equations of state, based on molecular models, for *a priori* calculations of the detonation velocity and the properties of the detonation products. The most interesting of these efforts has entailed a very substantial degree of algebraic complexity in the resulting computational procedure. The theoretical approach is of great interest as a program of basic research in the theory of the properties of matter at high temperature and very high density. It may provide valuable qualitative guidance in the formulation of empirical equations in relatively simple analytical form that are in at least approximate agreement with the requirements of basic theory. As a computational procedure to evaluate detonation properties for practical applications, the theoretical approach has been disappointing.

The inverse procedure, involving the calibration of an equation of state of assumed form by experimental values of the detonation velocity, has been pursued with much elaboration of mathematical and numerical detail. The parameters of the equation of state depend upon the composition of the gas. The latter, if not assumed *a priori* on the basis of a conventional reaction scheme, are determined by the thermodynamic equilibrium conditions which depend on the equation of state. Furthermore, it is necessary to conduct the calculation of equilibrium composition and evaluation of the thermodynamic properties of the gas with the temperature as an independent variable, even though this state variable is an unnatural choice from the point of view of the hydrodynamic equations themselves. The introduction of the temperature as a parameter of the problem leads to a degree of algebraic complexity that is absent from the fundamental equations. Because the simplifying assumptions employed by different workers have varied, the literature contains a variety of results on the properties of the detonation products; consequently, a comprehensive review of the field is impossible within the scope of this chapter.

In some applications, estimates of the detonation properties and to first order of their variation with the parameters of the system, e.g., the heat or energy of explosion and the initial density, will suffice. Such calculations do not justify elaborate computational procedures requiring computers and they will usually be based on an *a priori* specification of composition by means of a conventional decomposition scheme. In such calculations, simplicity of procedures is of greater importance than full mathematical rigor, and the equation of state may be of physically unrealistic form provided the properties of basic interest are not seriously affected thereby.

In other applications, it may be desired to secure the most precise evaluation of the detonation properties that is possible. Such calculations will usually, at this time, be conducted on computers. It will commonly be required that the composition of the gas satisfy the thermodynamic equilibrium conditions and that the equation of state have a form that is physically plausible. A computational procedure that is suitable for use on an computer is usually different from one that is suitable for desk calculation, in that iterative methods of solution are extensively employed to reduce the complexity of the program.

In this chapter several equations of state suitable for the two types of application are described. In the case of the forms that are suitable for rapid estimates, the solution of the hydrodynamic equations is developed in some algebraic detail. In the more elaborate case, the solution is extremely laborious when conducted by hand, and we give explicit equations in the form in which they are conveniently utilized in the formulation of a computer program.

7-2 THE ABEL EQUATION OF STATE

The simplest of the various empirical equations that seek to describe the dependence of the pressure of nonideal gases on temperature and volume is that of van der Waal's. In the form, due to Abel, that is appropriate for applications at high temperature, it can be written

$$p(v - \alpha) = nRT \qquad (7\text{-}1)$$

in which α is a constant volume correction or covolume for unit weight of gas. This equation was first employed to solve the Hugoniot and Chapman-Jouguet equations by Taffanel and D'Autriche[1] and it has been extensively used in connection with calculations for condensed explosives by Schmidt[2]. The Abel equation can be obtained as the low density limiting form of the equation of state of a gas at high temperature composed of hard spheres. Therefore, it can be expected to describe the nonideal behavior of gases only if the specific volume is large compared to the covolume constant. This quantity turns out to be of the same order of magnitude as the specific volume of the explosion gases from conventional explosives at customary values of the initial density. Consequently, a theory of the detonation velocity based on this equation of state can be expected to yield accurate results only at initial densities that are much lower than those of practical interest for condensed explosives. In spite of this fundamental limitation, such a theory is of practical value because it yields simple relations giving useful estimates of the detonation properties.

Application of the general relations of Chapter 2 for the nonideal gas correction to the thermodynamic properties of the explosion gas leads to the result that $e(v,T) = e^o(T)$, i.e., that the gas is thermodynamically ideal with a specific energy function independent of the specific volume, a function of temperature only, and equal to the specific energy function of the ideal gas at the same temperature. It follows that $c_v = c_v^o$ and $\gamma = c_p/c_v = \gamma^o$ for a gas described by the Abel equation of state, where the superscript zero refers to the ideal gas and c_p and c_v are the specific heats of the gas at constant pressure and constant volume, repectively. Furthermore,

$$\left.\begin{aligned} h(p,T) &= e + pv = h^o(T) + \alpha p \\ \kappa &= \gamma^o v/(v - \alpha) \end{aligned}\right\} \qquad (7\text{-}2)$$

where h^o is the specific enthalpy function for the ideal gas and κ is the adiabatic exponent, $\kappa = (\partial \ln p/\partial \ln \rho)_s$.

In par. 6-5, it was shown that the detonation pressure p_1 and detonation specific volume are determined by the solution of Eqs. 6-107

$$\left.\begin{aligned} e_1 - e_o &= \frac{1}{2}(p_1 + p_o)(v_o - v_1) \\ 1 - p_o/p_1 &= \kappa_1(\rho_1 v_o - 1) \end{aligned}\right\} \quad (7\text{-}3)$$

When these relations have been supplemented by an equation of state and solved, the detonation velocity D and particle velocity u_1 can be evaluated by Eqs. 6-106

$$\left.\begin{aligned} D &= v_o\sqrt{\kappa_1 p_1 \rho_1} \\ u_1 &= D(1 - \rho_o v_1) \end{aligned}\right\} \quad (7\text{-}4)$$

With a condensed explosive, the pressure p_1 is the order of 10^4 to 10^5 atm. Therefore, p_o can be neglected in comparison to p_1. With this simplification and with the introduction of the enthalpy function and the heat of reaction q, defined by Eq. 6-8, Eqs. 7-3 can be written

$$\begin{aligned} h_1 - h^o(T_o) &= q + \frac{1}{2}p_1(v_o + v_1) \\ \kappa_1(\rho_1 v_o - 1) &= 1 \end{aligned} \quad (7\text{-}5)$$

By use of Eqs. 7-2 and introduction of the average specific heat at constant pressure $\overline{c_p^o}$

$$\overline{c_p^o}\ (T_1 - T_o) = h^o(T_1) - h^o(T_o) \quad (7\text{-}6)$$

Eqs. 7-5 become

$$\left.\begin{aligned} &\overline{c_p^o}\ (T_1 - T_o) \\ &\quad = q + p_1(v_o + v_1 - 2\alpha)/2 \end{aligned}\right\} \quad (7\text{-}7)$$

$$v_1 = (v_o\,\gamma_1^o + \alpha)/(\gamma_1^o + 1) \quad (7\text{-}8)$$

Eq. 7-8 is the desired expression for the specific volume of the explosion gas in the Chapman-Jouguet detonation state. When the pressure is eliminated from Eq. 7-7 by means of the equation of state and the specific volume v_1 by means of Eq. 7-8, we obtain

$$\frac{T_1}{T_o}\left[\frac{\overline{c_p^o}}{nR} - 1 - \frac{1}{2\gamma_1^o}\right] \frac{q}{nRT_o} + \frac{\overline{c_p^o}}{nR} \quad (7\text{-}9)$$

An alternative form, because $\overline{c_p^o} = \overline{c_v^o} + nR$, is

$$\frac{T_1}{T_o}\left[\frac{\overline{c_v^o}}{nR} - \frac{1}{2\gamma_1^o}\right] = \frac{q'}{nRT_o} + \frac{\overline{c_v^o}}{nR} \quad (7\text{-}10)$$

where $q' = q + nRT_o - p_o v_o \approx q + nRT_o$ is the energy of explosion. It will be noticed that the temperature T_1 is a constant independent of the initial density. Because of the form of the Abel equation of state, these expressions for the temperature are the same as those that would be obtained with the ideal gas equation of state. (In fact, Eq. 7-9 can be obtained from Eqs. F-10 by neglecting p_o compared to p_1, as we have done here, and substituting the ideal gas equation of state.)

The specific heats and the heat capacity ratio are slowly varying functions of temperature. Eq. 7-9 or 7-10 is easily solved by iteration. The specific heat and the ratio γ^o are evaluated for an approximate value of the temperature, an improved value of the temperature is obtained by solution of one or the other of the equations, and the process is repeated until successive approximations are in satisfactory agreement. Application of the theory based on the Abel equation is not usually of sufficient accuracy to justify a calculation of the equilibrium composition of the explosion gas. If a special application is such as to justify this elaboration, the composition may be adjusted at each stage of the iteration by a calculation of the equilibrium composition at the approximate values of the temperature and specific volume of the detonation state, using the methods described in Chapter 2. The activity coefficients f_i that are needed for the calculation are easily shown to be $f_i = v/(v - \alpha)$, independent of temperature and composition. It will usually suffice to base the application on a conventional composition as described in Chapter 3.

By substitution of the equation of state and Eq. 7-8 into Eqs. 7-4 and the second of Eqs. 7-2, expressions for the detonation velocity, particle velocity, and adiabatic exponent of the detonation products are obtained.

$$\left.\begin{aligned} D &= \left(\frac{\gamma_1^o + 1}{1 + \alpha\rho_o}\right)\sqrt{nRT_1/\gamma^o} \\ u_1 &= \sqrt{nRT_1/\gamma_1^o} \\ \kappa_1 &= (\gamma_1^o + \alpha\rho_o)/(1 - \alpha\rho_o) \end{aligned}\right\} \quad (7\text{-}11)$$

For an explosion gas described by the Abel equation, the particle velocity u_1 is independent of the initial density ρ_o.

It is a convenient computational device to define hypothetical "ideal" detonation properties calculated for the actual explosion gas composition and initial density but with the ideal gas equation of state. If such quantities are designated with a superscript zero, expressions for their calculation are obtained at once from Eqs. 7-11 by setting $\alpha = 0$. Thus, when the explosion products are described by the Abel equation, $T_1 = T_1^o$ and $u_1 = u_1^o$, we can write

$$\left.\begin{aligned} v_1/v_1^o &= 1 + \alpha\rho_o/\gamma_1^o \\ D/D^o &= (1 - \alpha\rho_o)^{-1} \end{aligned}\right\} \quad (7\text{-}12)$$

where

$$\left.\begin{aligned} v_1^o &= \gamma_1^o/(\gamma_1^o + 1) \\ D^o &= (\gamma_1^o + 1)\sqrt{nRT_1^o/\gamma_1^o} \\ u_1^o &= \sqrt{nRT_1^o/\gamma_1^o} \end{aligned}\right\} \quad (7\text{-}13)$$

and where T_1^o is obtained by the solution of Eq. 7-9 or 7-10.

An approximate solution of Eq. 7-10, sufficiently accurate for estimates of the detonation properties, can be obtained by factoring the term $\overline{c_v^o}/nR$ from the coefficient of T_1/T_o and assuming that the heat capacity is independent of the temperature in evaluating the remainder. If, in addition, we neglect $\overline{c_v^o}T_o$ compared to q, we obtain

$$T_1 = T_1^o = 2q'\gamma_1^o/\left[(\gamma_1^o + 1)\,\overline{c_v^o}\right] \quad (7\text{-}14)$$

Substituting this expression into Eqs. 7-1 and 7-11 and using Eq. 7-8, we obtain

$$\left.\begin{aligned} p_1 &= 2\left(\frac{nR}{\overline{c_v^o}}\right)\frac{q'}{(v_o - \alpha)} \\ D &= \left(\frac{1}{1 - \alpha\rho_o}\right)\sqrt{2q'(\gamma_1^o + 1)nR/\overline{c_v^o}} \\ u_1 &= \sqrt{2q'(\gamma_1^o + 1)nR/\overline{c_v^o}} \end{aligned}\right\} \quad (7\text{-}15)$$

which, together with Eq. 7-8, can be used to furnish estimates of the detonation properties if a value of the covolume α is known. A useful relation is obtained by eliminating q between the first two of these equations

$$p_1 = \rho_o D^2\left(\frac{1 - \alpha\rho_o}{\gamma_1^o + 1}\right) \quad (7\text{-}16)$$

which can be used to estimate the detonation pressure from an experimental value of the detonation velocity if the covolume α is known.

One can estimate the covolume constant by comparison of an observed detonation velocity with a value calculated by the first of Eqs. 7-11. This procedure is not strictly consistent with the assumptions on which that equation are based since it will be found that the covolume, assumed in the derivation to be constant, depends upon the initial density. It does, however provide a simple method of estimating the properties of the explosion gas when a detonation velocity has been experimentally determined that is superior to a total neglect of the effects of gas imperfection. If the detonation velocity has been measured as a function of the initial density, the quantity $g_o = 1 + d\ell nD/d\ell n\rho_o$ can be evaluated from the experimental data. By differentiation of the first of Eqs. 7-11, we obtain the result

$$\alpha = (g_o - 1)/(\rho_o g_o) \quad (7\text{-}17)$$

By substitution into Eqs. 7-8, 7-16, and the third of Eqs. 7-11, we obtain the relations

$$\left.\begin{aligned} \kappa_1 &= g_o(\gamma_1^o + 1) - 1 \\ \frac{v_1}{v_o} &= \frac{\gamma_1^o}{\gamma_1^o + 1}\left[1 + \frac{g_o - 1}{g_o\gamma_1^o}\right] \\ p_1 &= \frac{\rho_o D^2}{\gamma_1^o}\left[\frac{1}{g_o} - \frac{1}{\gamma_1^o + 1}\right] \end{aligned}\right\} \quad (7\text{-}18)$$

that depend only on observed quantities and on the heat capacity ratio for which a sufficiently accurate estimate can be made for an approximate composition and an approximate temperature.

The application of these approximate equations can be illustrated by a calculation for Composition B consisting of 64% RDX, 35%

TNT, and 1% wax, by weight. The detonation velocity for this mixture is accurately known and the adiabatic exponent κ_1 has been evaluated experimentally at a single initial density. These data suffice for the evaluation of experimental values of the detonation pressure, density, and particle velocity at the initial density for which the adiabatic exponent is known. According to Deal[3], the experimental values of the detonation velocity can be represented by

$$D = 2639 + 3127\rho_o$$

where D is in m/sec and ρ_o is in g/cc. At $\rho_o = 1.714$, Deal reports that $\kappa_1 = 2.77$.

We employ the conventional decomposition scheme

$$C_{4.4}H_{5.7}O_6N_{4.9} \rightarrow 4.4CO + 1.25H_2 + 1.6H_2O + 2.45N_2$$

to define the composition of the explosion products, according to which the oxygen is considered to react first to form CO and then to the extent possible with hydrogen to form water. This reaction yields 0.0434 mole of gaseous products per gram of explosive and an energy of explosion $q' = 1.068$ kcal/g at 25°C. The ratio $\gamma^\circ = 1.25$ between 3400° and 5000°K. The results of the calculations are summarized in Table 7-1.

The unexpectedly good agreement between the estimates and the experimental values at $\rho_o = 1.714$ is unquestionably fortuitous, and it cannot be assumed that equally good agreement would extend to lower initial densities, were experimental values to be available. The comparison does imply that very useful estimates can be obtained by simple calculations when experimental values of the detonation velocity are available.

7-3 DETERMINATION OF THE DETONATION STATE FROM VELOCITY DATA

The usual procedure for formulating an equation of state descriptive of the detonation products of condensed explosives has involved the assumption of an analytical form of the equation and the evaluation of its parameters from experimental values of the detonation velocity. It has sometimes been erroneously claimed that the fact that this program can be accomplished implies that the assumed form of the equation of state is valid and that the thermodynamic properties calculated with its aid are accurately evaluated. It turns out that various different forms of the equation lead to approximately the same values of those variables, that are explicit in the hydrodynamic equations but to widely different values of those variables, such as the temperature, that appear as parameters of the problem.

It is instructive to consider the general problem of determining the thermodynamic state of detonation gases using the hydrodynamic theory and an experimental curve $D = D(\rho_o)$. Eqs. 7-3 and the first of Eqs. 7-4 can be rearranged to the form

$$\left.\begin{aligned} p_1 &= \rho_o D^2(1 - \rho_o v_1) \\ e_1 - e_o &= \tfrac{1}{2}D^2(1 - \rho_o v_1)^2 \end{aligned}\right\} \qquad (7\text{-}19)$$

where the Chapman-Jouguet equation is written

$$\kappa_1 = \rho_o v_1/(1 - \rho_o v_1) \qquad (7\text{-}20)$$

In these expressions, we have without loss in generality neglected the initial pressure p_o compared to the detonation pressure p_1. The equation of state is customarily taken to be an expression of the form

TABLE 7-1 ESTIMATES OF THE DETONATION PROPERTIES OF COMPOSITION B

ρ_o, g/cc	g_o	α, cc/g	κ_1		ρ_1, g/cc		p_1, atm		T_1, °K	
			Eq. 7-18	Exp.	Eq. 7-18	Exp.	Eq. 7-18	Exp.	Eq. 7-11	Eq. 7-14
1.0	1.543	0.352	2.47		1.404		94.5		4370	4060
1.25	1.597	0.302	2.61		1.723		146		4370	4060
1.5	1.640	0.260	2.69		2.060		216		4370	4060
1.714	1.670	0.234	2.76	2.77	2.338	2.335	289	290	4370	4060

$$p = p(v, T, \ldots n_i \ldots) \tag{7-21}$$

expressing the pressure as a function of the temperature, specific volume, and the mole numbers of each constituent of the mixture of reaction products. The mole numbers n_i may be fixed *a priori* by an assumed composition or determined as functions of specific volume and temperature by Eq. 7-21 together with the equilibrium conditions. Either case implies the existence of an implicitly defined function

$$p = p(v, T) \tag{7-22}$$

By means of the laws of thermodynamics, the entropy of the detonation products is determined as a function of specific volume and temperature

$$s = s(v, T) \tag{7-23}$$

and Eqs. 7-22 and 7-23 together imply the existence of an implicitly defined function

$$p = p(v, s) \tag{7-24}$$

The usual program for determining an equation of state in the form of Eq. 7-21, subject either to the equilibrium conditions or to an *a priori* specification of the composition, is the formal equivalent of determining function 7-24 for given values of ρ_o, e_o, and $D = D(\rho_o)$ by means of Eqs. 7-19, 7-20 and the laws of thermodynamics. By use of the thermodynamic relations

$$\left(\frac{\partial e}{\partial s}\right)_v = T, \quad \left(\frac{\partial e}{\partial v}\right)_s = -p$$

and the definition

$$\kappa = -(\partial \ln p/\partial \ln v)_s$$

Brinkley[4] has pointed out that the Jacobian

$$J\left(\frac{p, e}{v, s}\right)$$

vanishes at the point (p_1, v_1) satisfying Eqs. 7-19 and 7-20. This means that these equations, the thermodynamic relations, and the observed data can be satisfied together with any arbitrary function $s = s(v)$ or $T = T(v)$. The program of evaluating the thermodynamic state is thus indeterminate in general, and determinacy requires the introduction of some restriction having the effect of specifying the arbitrary function. This is accomplished by assuming a form for the equation of state but the experimental data provide no criterion for the correctness of the assumption.

Jones[5] has remarked that Eq. 7-22 represents a surface in the p,v,T space and that the maximum amount of information that can be derived from a $D(\rho_o)$ relation would fix a line of a certain length on this surface. Thus, when one attempts to analyze detonation velocity data by fixing on one surface by the assumption of an equation of state, the result is largely arbitrary since there are evidently any number of surfaces which contain the same line. Jones concludes that very little information about the form of the equation of state can be obtained from detonation velocity data but that if a form is assumed, then the values of its parameters can in general be determined. It follows that the assumption of a form of equation must be guided in the main by considerations of physical plausibility.

The first of Eqs. 7-19 defines a ruled surface in p_1, v_1, v_o space. The second of these equations determines a curved surface in the same space which, according to the Chapman-Jouguet theory, touches the ruled surface along a line $p_1 = p_1(v_o), v_1 = v_1(v_o)$ that can be called the Chapman-Jouguet locus. In an investigation of the properties of gases that can be deduced from measurements of the detonation velocity, Jones has deduced from this geometrical circumstance a relation that is of great practical value. Eqs. 7-19 are written in implicit form

$$\left.\begin{aligned} F(p_1, v_1, v_o) &= \rho_o D^2(1 - \rho_o v_1) - p_1 = 0 \\ G(p_1, v_1, v_o) &= e_1 - e_o - \tfrac{1}{2}p_1(1 - \rho_o v_1) = 0 \end{aligned}\right\} \tag{7-25}$$

The condition that the surfaces defined by these equations be in contact is that at any point of contact the direction cosines of the normals to the two surfaces be equal. This condition leads to two relations

$$\left.\begin{aligned} (\partial F/\partial v_1)/(\partial F/\partial p_1) &= (\partial G/\partial v_1)/(\partial G/\partial p_1) \\ (\partial F/\partial v_o)/(\partial G/\partial v_o) &= (\partial F/\partial v_1)/(\partial G/\partial v_1) \end{aligned}\right. \tag{7-26}$$

On evaluation of the derivatives, the first relation leads to Eq. 7-20 which is an expression of the Chapman-Jouguet condition. The second relation leads to a new result. Defining a thermodynamic quantity λ by

$$\frac{1}{\lambda} = \frac{1}{p}\left(\frac{\partial e}{\partial v}\right)_p \tag{7-27}$$

and noting the thermodynamic relation

$$\frac{1}{v}\left(\frac{\partial e}{\partial p}\right)_v = \frac{1}{\kappa}\left(1 + \frac{1}{\lambda}\right) \tag{7-28}$$

Jones obtained the relations

$$\left.\begin{aligned} p_1 &= \rho_o D^2/[g_o(2+\lambda)] \\ v_1 &= \frac{1}{\rho_o}\left[1 - \frac{1}{g_o(2+\lambda)}\right] \\ e_1 &= e_o + \frac{D^2}{2}\Big/\left[g_o^2\,(2+\lambda)^2\right] \\ \kappa_1 &= g_o(2+\lambda) - 1 \end{aligned}\right\} \tag{7-29}$$

from the second of Eqs. 7-26, together with Eqs. 7-19 and 7-20. Furthermore, from the second of Eqs. 7-4

$$u_1 = D/[g_o(2+\lambda)] \tag{7-30}$$

In these expressions, $g_v = 1 + d\ln D/d\ln\rho_o$, as defined and employed in the last paragraph.

The utility of these relations resides in the fact that λ contains all of the thermodynamic information that is required when the detonation velocity is known experimentally and g_o can be evaluated. Jones shows that this quantity is essentially positive so that Eqs. 7-29 and 7-30 with $\lambda = 0$ provide upper limits to p_1, e_1, and u_1 and lower limits to v_1 and κ_1. Furthermore, Jones shows that λ is insensitive to the form of the equation of state and that it lies in the range $0 < \lambda << 2$. Rather accurate estimates of λ can be made with approximate equations of state, thus making possible the direct evaluation of those properties of the detonation products that are of principal interest in studies of their subsequent flow. Using available equation of state data for nitrogen, Jones estimated that λ is not likely to be greater than 0.25.

In par. 7-2, reference was made to the experimental determination by Deal of the value of the adiabatic exponent for Composition B at an initial density $\rho_o = 1.714$ g/cc. The measurements made in this investigation permitted the evaluation of the pressure as a function of specific volume along the isentrope passing through the Chapman-Jouguet point. The experimental data were quite well represented, particularly in the neighborhood of the Chapman-Jouguet point, by the simple adiabatic law

$$p_i = p_1\,(v/v_1^*)^{-\kappa^*},\ \kappa^* = 2.77 \tag{7-31}$$

with constant adiabatic exponent, where $p_i = p(v,s_1^*) = p_i(v)$ is the pressure on the isentrope passing through the experimental Chapman-Jouguet point $(p_1^*,\ v_1^*)$. Along an isentrope obeying Eq. 7-31, the specific energy is given by

$$e_i = e_1^* + (p_i v - p_1^* v_1^*)/(\kappa^* - 1) \tag{7-32}$$

where $e_i = e(v,s_1^*)$ and $e_1 = e(p_1^*,\ v_1^*)$. (We have employed an asterisk to designate properties at the experimental Chapman-Jouguet point for $\rho_o = 1.714$ g/cc.)

The equation of state of the detonation products could be determined if, in addition to the known isentrope, the energy were known on a single nonisentropic curve in the same region since the rate of change of energy along an isentrope is defined by the first law of thermodynamics and the nonisentropic curve would provide initial data for the integration. Fickett and Wood[6] have shown that the isentrope and the Chapman-Jouguet locus passing through the experimental point (p_1,v_1) lie close together in the (p,v)-plane. They expand the energy as a Taylor series in the pressure about the point on the isentrope having the same specific volume and assume that the expansion can be terminated after the term of first order. For points near the experimental isentrope, this assumption leads to an equation of state

$$e(p,\ v) = e_i + \beta_i(p - p_i)v \tag{7-33}$$

where β_i is the value on the experimental isentrope of the quantity

$$\beta = \frac{1}{v}\left(\frac{\partial e}{\partial p}\right)_v \tag{7-34}$$

The Chapman-Jouguet locus for varying initial density is completely determined by Eqs. 7-28 to 7-34. Fickett and Wood have obtained the solution by numerical methods. The original paper should be consulted for details. Their results for the coefficients β, κ, and λ are listed for several values of the initial density in Table 7-2. The values of the other detonation properties can be evaluated at once by means of the basic hydrodynamic equations previously given.

The results listed in Table 7-2 depend only on the validity of Eq. 7-33; are independent of any assumptions regarding the form of a temperature explicit equation of state; and did not require evaluation of the composition of the product gas. Eq. 7-33 is correct to terms of first order in the increment $(p - p_i)$ and is probably a very good approximation when employed to determine the Chapman-Jouguet locus since that curve lies close to the experimental isentrope. Although the numerical solution of the equation is tedious, this method is probably the best available for the calculation of p_1, v_1, and κ_1 as functions of ρ_o along the Chapman-Jouguet locus. Its application requires the availability of an experimental Chapman-Jouguet point and, in the absence of an experimental isentrope, the further assumption that the isentrope can be represented by equations in the form of Eqs. 7-31 and 7-32. Additionally, the calculations summarized in Table 7-2 can be employed as a criterion for the physical plausibility of assumed analytical forms of the equation of state.

7-4 MODIFICATIONS OF THE ABEL EQUATION

When the simple Abel equation of state with a constant covolume was employed by Schmidt[2] and others to describe the detonation products of condensed explosives, it was found that the covolume, evaluated to secure agreement with experimental detonation velocities, is a function of the initial density. This theoretical inconsistency should have led the early workers to reappraise the analysis and it has led subsequent workers to remove the inconsistency by adopting less restrictive assumptions. The Abel equation

$$p(v - \alpha) = nRT$$

can be made to describe the state of any substance if α is a suitably prescribed function of two state variables, e.g., $\alpha = \alpha(p,v)$. However, it was shown in the last par. 7-3 that a curve $D(\rho_o)$ does not provide sufficient information to evaluate the function α in this generality, and some restriction must be placed upon it. Restrictions that are sufficient, but less restrictive than the specification $\alpha =$ constant employed in par. 7-2, are $\alpha = \alpha(v)$ or $\alpha = \alpha(p)$. The first of these has been employed by Cook[7] in extensive calculations. The second has been employed by Jones in calculations for the explosive PETN.

Cook employs a modified Abel equation of state in the form

$$p[v - \alpha(v)] = nRT \tag{7-35}$$

According to this equation

$$\left(\frac{\partial e}{\partial v}\right)_T = T\left(\frac{\partial p}{\partial T}\right)_v - p = 0 \tag{7-36}$$

TABLE 7-2 THE DERIVATIVES β, κ, AND λ ALONG THE CHAPMAN-JOUGUET LOCUS FOR COMPOSITION B

ρ_o	β	κ	λ
1.714	1.77	2.77	0.256
1.6	1.79	2.74	0.257
1.4	1.82	2.67	0.260
1.2	1.86	2.59	0.262
1.0	1.91	2.50	0.266

so that a gas described by Eq. 7-35 can be said to be thermodynamically ideal with $e(v,T) = e^o(T)$, $c_v = c_v^o$. Furthermore, the specific enthalpy $h = e + pv = e^o + nRT + p\alpha(v) = h^o + p\alpha(v)$ so that $c_p = c_p^o$ and $\gamma = c_p/c_v = \gamma^o$. At the high density of the detonation products, one would expect the specific energy function to have a substantial contribution from the energy of gas imperfection arising from repulsive terms in the intermolecular potential junction. This expectation is confirmed by molecular theories of the properties of dense gas, such as that of Lennard-Jones and Devonshire, which is at least qualitatively correct. The consequence of Eq. 7-35 that is expressed by Eq. 7-36 does not appear, therefore, to be physically plausible.

The adiabatic exponent κ can be evaluated by Eq. 7-35 and the relation

$$\kappa = -\frac{v}{p}\left(\frac{\partial p}{\partial v}\right)_s = -\gamma\left(\frac{v}{p}\right)\left(\frac{\partial p}{\partial v}\right)_T \qquad (7\text{-}37)$$

We obtain the expression

$$\kappa = \gamma^o\left(\frac{v}{v-\alpha}\right)[1-\alpha'(v)] \qquad (7\text{-}38)$$

where $\alpha'(v)$ is the derivative of α with respect to v. Eqs. 7-3, with the neglect of p_o compared to p_1, become

$$\left.\begin{aligned} v_1 &= (v_o\Gamma + \alpha_1)/(\Gamma+1) \\ \frac{T_1}{T_o}\left[\frac{\overline{c_v^o}}{nR} - \frac{1}{2\Gamma}\right] &= \frac{q'}{nRT_o} + \frac{\overline{c_v^o}}{nR} \end{aligned}\right\} \qquad (7\text{-}39)$$

where

$$\Gamma = \gamma_1^o\,[1 + \alpha_1'(v)] \qquad (7\text{-}40)$$

and where $\overline{c_v^o} = [e^o(T_1) - e^o(T_o)]/(T_1 - T_o)$ is an average specific heat at constant volume and q' is the energy of explosion. It may be noted that Eqs. 7-39 have the same form as the solutions of Taffanel and D'Autriche[1] for the unmodified Abel equation of state, Eqs. 7-8 and 7-10, with the quantity Γ replacing the heat capacity ratio γ^o. Eqs. 7-4 can be written

$$\left.\begin{aligned} D &= \left(\frac{\Gamma+1}{1+\alpha\rho_o}\right)\sqrt{nRT_1/\Gamma} \\ u_1 &= \sqrt{nRT_1/\Gamma} \end{aligned}\right\} \qquad (7\text{-}41)$$

The adiabatic exponent can be evaluated with

$$\kappa_1 = (\Gamma + \alpha\rho_o)/(1 - \alpha\rho_o) \qquad (7\text{-}42)$$

Eqs. 7-41 and 7-42 are analogous to Eqs. 7-11 based on the Abel equation of state.

Cook has applied Eqs. 7-39 through 7-42 to a large number of explosives. His method of calculation was iterative, commencing with the solutions based on the Abel equation. At each state of the iteration, he calculated the equilibrium composition of the detonation products. He has in this way determined the function $\alpha(v)$ from the experiment $D(\rho_o)$ for the explosives considered. He concludes that the function $\alpha(v)$ found in this way is independent of the composition of the detonation gas and may be used for the *a priori* calculation of detonation properties. The function $\alpha(v)$ as determined by Cook is shown in Fig. 7-1. Some of the results obtained with this equation of state are listed in Table 7-3.

If Cook's equation of state is to be employed in a forward calculation of the detonation properties, the calculation must be performed by successive approximations. The Taffanel-D'Autriche[1] solutions expressed by Eqs. 7-8 and 7-10 provide a convenient first approximation. If the calculation is to be elaborated by the assumption that the detonation products are in equilibrium, the compositions can be adjusted at each stage of the iteration by an equilibrium calculation employing the methods detailed in Chapter 2. The activity coefficients f_i, appropriate for an equilibrium calculation at specified temperature and specific volume, are given by

$$\ln f_i = \int_v^\infty \left[\frac{1}{RT}\left(\frac{\partial p}{\partial n_i}\right) - \frac{1}{v}\right] = \int_v^\infty \left[\frac{\alpha(v)}{v - \alpha(v)v}\right] dv \qquad (7\text{-}43)$$

and have been tabulated by Cook. These coefficients are independent of composition and temperature and, as noted in Chapter 2, result in a calculation of the equilibrium composition that is no more difficult than that for an ideal gas.

Jones has employed a modified Abel equation of state in the form

$$p[v - \alpha(p)] = nRT$$

TABLE 7-3 DETONATION PROPERTIES OF SOME PURE EXPLOSIVES[7]

Explosive	ρ_o, g/cm^3	v_1, cm^3/g	n_1, moles/g	T_1, °K	u_1, m/sec	p_1, 10^3 atm
PETN	1.0	0.725	0.0352	5350	1540	85
	1.6	0.478	0.0349	5700	1820	225
RDX	1.0	0.723	0.0405	5250	1660	95
	1.6	0.469	0.0405	5750	2000	255
TNT	1.0	0.740	0.0331	3700	1250	60
	1.6	0.505	0.0245	4170	1340	150
Tetryl	1.0	0.752	0.0370	4200	1340	75
	1.6	0.485	0.0355	4700	1670	200

and applied it to the explosive PETN. According to this equation

$$\left(\frac{\partial h}{\partial p}\right)_T = v - T\left(\frac{\partial v}{\partial T}\right)_p = \alpha(p) \qquad (7\text{-}45)$$

so that a gas described by Eq. 7-44 has the specific enthalpy and energy functions

$$\left.\begin{aligned} h &= h^o(T) + \int_o^p \alpha(p)dp \\ e &= e^o(T) + \int_o^p \alpha(p)dp - p\alpha(p) \end{aligned}\right\} \qquad (7\text{-}46)$$

and $c_p^o = c_p^o$, $c_v = c_v^o$, $\gamma = c_p/c_v = \gamma^o$. Since this form of equation predicts a contribution to the energy from gas imperfection, it appears intuitively to be a more plausible form than that employed by Cook.

This equation of state appears to have been applied only to the explosive PETN. For this material, Jones has employed the detonation velocity data of Friederich[8] to evaluate the function $\alpha(p)$. For an equation of state of the assumed form, the coefficient λ, defined by Eq. 7-27, is

$$\lambda = \gamma^o - 1 \qquad (7\text{-}47)$$

and it may be regarded a constant to a good approximation. Then by means of Eqs. 7-29, the detonation properties can be evaluated directly from the experimental $D(\rho_o)$ curve. Using Eqs. 7-29 and 7-46, Jones shows that $\alpha(p)$ can be evaluated by the numerical solution of

$$p\,\alpha(p) = \Psi + \left(\frac{\lambda}{1+\lambda}\right) p^{\lambda/(1+\lambda)} \int_o^p \left[p^{-\lambda/(1+\lambda)}\,\Psi\right] \frac{dp}{p} \qquad (7\text{-}48)$$

where Ψ is a function of p given parametrically in terms of ρ_o by

$$(1+\lambda)\Psi = \frac{D^2}{2(2+\lambda)}\left(\frac{2g_o - 1}{g_o^2}\right) - \lambda q' \qquad (7\text{-}49)$$

together with the first of Eqs. 7-29, where q' is the energy of explosion. Jones' determination of the function $\alpha(p)$ for PETN is shown in Fig. 7-2. Calculated values of the detonation properties are listed in Table 7-4. The energy of gas imperfection resulting from this form of the equation of state is shown in the last column of the table. The quantity increases strongly with increasing initial density and is responsible for the downward trend of the temperature.

The Jones modification of the Abel equation of state does not appear to have been applied to other explosives, and its application at the present time to an *a priori* calculation would require an assumption that the function $\alpha(p)$ is independent of composition. If such an assumption should turn out to be justified, the equation should provide a useful and relatively simple method for the calculation of detonation products having the desirable feature that the energy of gas imperfection is not neglected. The analytical form of the equation is such as not to yield useful expressions by a partial reduction of the equation, similar to that employed in our description of the Abel equation or of Cook's modification of it. It would be most convenient in this case to conduct the calculation in the general manner described in par. 6-5, using, if desired, the methods of Chapter 2 to evaluate the equilibrium composition.

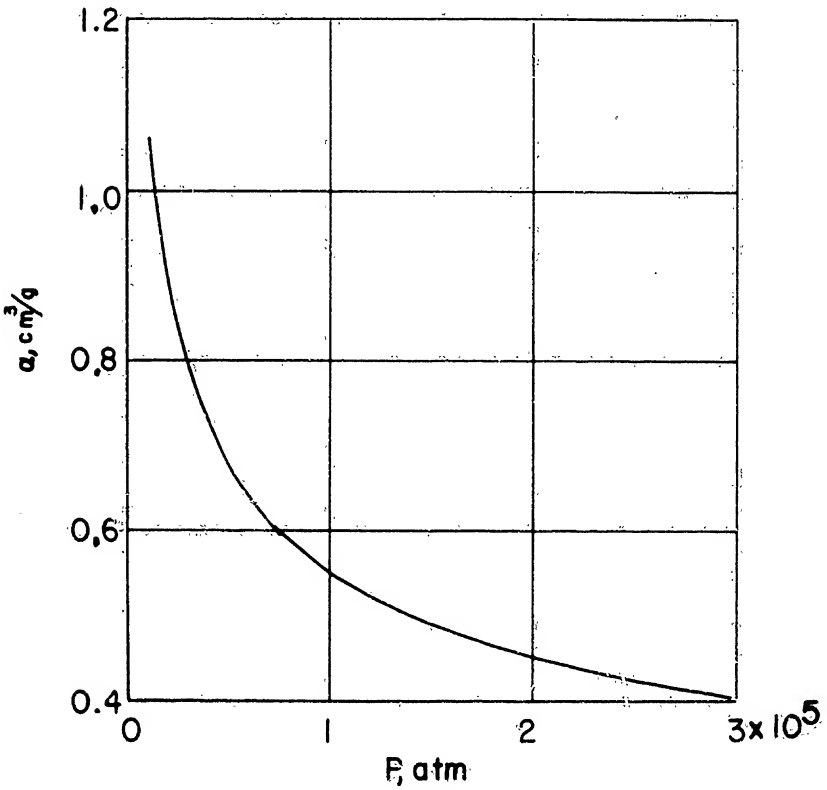

Figure 7-2. Covolume Function for Detonation Products of PETN[5]

TABLE 7-4 DETONATION PROPERTIES OF PETN[5]

ρ_o, g/cm³	D, m/sec	u_1, m/sec	p_1, 10^3 atm	v_1, cm³/g	T_1, °K	E_1, cal/g
0.50	3940	1305	26	1.34	4870	135
0.75	4720	1415	50	0.933	4630	245
1.00	5550	1560	86	0.719	4400	375
1.25	6450	1710	137	0.588	4160	550

The coefficient λ defined by Eq. 7-27 is given by Eq. 7-47 when the modified Abel equation of state employs the assumption $\alpha = \alpha(p)$, and by

$$\lambda = (\gamma^\circ - 1)/[1 - \alpha'(v)] \qquad (7\text{-}50)$$

when the assumption $\alpha = \alpha(v)$ is made. We have employed these expressions together with Eqs. 7-29 and the observed $D(\rho_o)$ to estimate the adiabatic exponent κ on the Chapman-Jouguet locus for Composition B. We employ the same assumptions as were employed in par. 7-2 and take $\gamma^\circ = 1.25$, independent of the initial density. The results are summarized in Table 7-5 where we include for comparison the values obtained by Fickett and Wood, and previously listed in Table 7-2.

The results for α = constant and $\alpha = \alpha(p)$ are identical because both assumptions lead to the same estimate of the coefficient λ, namely $\gamma^\circ - 1$. These results are in rather good agreement with the results of Fickett and Wood. The results based on the assumption $\alpha = \alpha(v)$ are systematically much higher than the other results. If the calculations of Fickett and Wood are used as a standard of comparison, we conclude that the assumption $\alpha = \alpha(v)$ is inferior to the assumption $\alpha = \alpha(p)$. Furthermore, we can conclude that the simple Abel equation when calibrated by observed detonation velocities at each initial density can be used for reliable estimates of the detonation properties in spite of the mathematical inconsistency that attends its use.

7-5 APPLICATION OF THE CHAPMAN-JOUGUET CONDITION TO MIXTURES WITH VARYING COMPOSITION

The application of the Chapman-Jouguet theory to the calculation of the properties of the detonation products has been based on the solution of two equations between thermodynamic properties, Eqs. 7-3, which with the equation of state suffice to specify the thermodynamic state of the product gas. The application of the second of these, which has been employed in the form

$$\kappa_1(\rho_1 v_o - 1) = 1 \qquad (7\text{-}51)$$

TABLE 7-5 THE ADIABATIC EXPONENT FOR COMPOSITION B ALONG THE CHAPMAN-JOUGUET LOCUS

	κ_1			
ρ_o	α = Const.	$\alpha = \alpha(v)$	$\alpha = \alpha(p)$	Table 7-2
1.714	2.76	3.80	2.76	2.77
1.6	2.72	3.66	2.72	2.74
1.4	2.65	3.43	2.65	2.67
1.2	2.57	3.18	2.57	2.59
1.0	2.47	2.92	2.47	2.50

and which is a statement of the Chapman-Jouguet condition, requires further discussion for calculations in which the composition of the product gas is determined by the equilibrium conditions and in which, in consequence, the composition will in general vary in moving from one state point to another.

If we recall that the adiabatic exponent is defined as the derivative

$$\kappa = (\partial \ln p/\partial \ln \rho)_s \qquad (7\text{-}52)$$

it is necessary to specify the way in which the differentiation is to be performed in cases where the composition is a function of state. It has been implicitly assumed in the reduction of the equations presented in the preceding paragraphs of this chapter that the differentiation is performed at constant composition. The quantity so obtained may be called the adiabatic exponent for fixed composition or, more shortly, the "frozen" adiabatic exponent.

For calculations in which the composition is assumed to be fixed, there is no incompleteness in the definition of the quantity κ since the "frozen" quantity is evidently consistent with the *a priori* assumption as to composition.

It has been noted in Chapter 2 that the laws of thermodynamics for mixtures with fixed composition or for mixtures with equilibrium composition assume the same form as for systems of one constituent. The thermodynamic state functions and their derivatives for mixtures are thus completely defined in terms of two state variables either when the composition is fixed *a priori* or the composition is the equilibrium composition. In particular, a differential coefficient such as the adiabatic exponent is a well defined function of the thermodynamic state when it is specified that the equilibrium conditions in differential form are to be satisfied when the differentiation of Eq. 7-52 is performed. The quantity so obtained may be called the adiabatic exponent for equilibrium composition or, more shortly, the "equilibrium" adiabatic exponent.

The sound velocity and the adiabatic exponent are related by the expression,

$$c^2 = \kappa p/\rho \qquad (7\text{-}53)$$

Therefore two sound velocities, a frozen sound velocity or an equilibrium sound velocity, are obtained, depending upon whether the frozen or equilibrium value of the adiabatic exponent is employed in Eq. 7-53. In physical terms, the former quantity is the velocity of propagation of acoustic waves in the limit of very high frequencies; the latter, the velocity for the limit of very low frequencies. Now Eq. 7-52 is an expression of the Chapman-Jouguet condition that the detonation velocity is equal to the local sound velocity with reference to the detonation products. Consequently, the application of the theory is not completely specified until the meaning of sound velocity (and of the quantity κ) is further specified. There is no thermodynamic argument that will define the proper quantity unambiguously.

In Chapter 8, we discuss in some detail the question of completing the statement of the Chapman-Jouguet condition by specifying the nature of the sound velocity. It appears that the equilibrium sound velocity is properly employed in cases that are truly one-dimensional. However, we believe, in at least some instances where the one-dimensional case is employed as a simplified model of an actual two-dimensional explosive charge, it is more appropriate to employ the frozen sound speed in the statement of the Chapman-Jouguet condition. These questions will be more completely considered in Chapter 8. We here wish only to take note of the fact that the numerical results of a calculation of the detonation properties will depend to some extent on the assumption used with respect to the statement of the Chapman-Jouguet condition. As a practical matter, the distinction between the two forms of the Chapman-Jouguet condition is largely academic. Cowan and Fickett[9] report that pressures calculated using an equation of state due to Halford, Kistiakowsky, and Wilson, differed by less than 1% at an initial density of 1.2 g/cm^3 and were almost identical at high initial density, the pressure being higher when calculated from the equilibrium Chapman-Jouguet condition.

Almost all of the calculations that have been reported have employed a Chapman-Jouguet condition based on the frozen sound speed. (Most authors have regarded this an approximation.) If it is desired to base the Chapman-Jouguet condition on the equilibrium

sound speed, two methods of computation are possible. The first, which has been employed by Cowan and Fickett, is to construct the equilibrium Hugoniot curve in the neighborhood of the Chapman-Jouguet point, using only the first of Eqs. 7-3, and to determine by trial or by graphical or numerical interpolation the point on the Hugoniot curve resulting in the minimum detonation velocity. This procedure clearly is equivalent to employing the equilibrium sound velocity in the statement of the Chapman-Jouguet condition. The second, which we prefer because it requires substantially less computation, is to employ the general iterative procedure described in Appendix F which, together with the methods for evaluating equilibrium composition and equilibrium thermodynamic properties described in Appendix E, leads to a direct solution of the problem.

The frozen composition Chapman-Jouguet condition appears generally to be an entirely adequate approximation. It is much more easily employed. Even so, the general iterative procedure of Appendix F remains, in our opinion, the most straightforward computational approach for any equation of state except the simple forms suitable for order of magnitude estimates. In Appendix E, we have described computational procedures in detail for evaluating the thermodynamic properties of equilibrium mixtures. The Chapman–Jouguet point is then determined by an iterative procedure involving thermodynamic quantities only. The computational procedure is thus completely prescribed if the equation of state is presented in analytical form.

7-6 EXPLOSIVES WHOSE PRODUCTS CONTAIN A SOLID PHASE

The products of detonation of an explosive may consist not only of an homogeneous gas mixture but also of a mixture of gas with various condensed constituents. Nongaseous constituents may be present in the products because species found in the reaction condense at the prevailing detonation temperature and density. Explosives such as tetryl or TNT have a marked oxygen deficiency and, as a result, free carbon is formed as a reaction product. Some commercial explosives are compounded with chemically inert diluents present in the original explosive mixture, and these materials form condensed phases in the detonation products.

The first case where some of the reaction products are condensed can be treated in a direct manner. It is natural to assume that such products are in thermal equilibrium with the gaseous reaction products and completely entrained by them. These assumptions applied to explosives containing inert diluents are more arbitrary in nature and will be the more closely applicable the finer the particle size of the diluent and the lower its concentration. For the case of inert diluents, Taylor[11] has compared calculations in which thermal equilibrium is assumed with calculations in which it is assumed that there is no heat transfer to the diluent. Complete entrainment was assumed in each case, and Taylor concludes that the assumption of thermal equilibrium results in the better theoretical model.

The pressure of the gas phase is represented by an equation of state as an expression of the general form

$$p = p(v_g, T) \tag{7-54}$$

where v_g may be defined as the volume of the gas phase for unit total weight of explosion products. Since the volume of gas and of condensed phases is additive

$$v = v_g + v_s \tag{7-55}$$

where v is the specific volume of the mixture as previously defined and v_s is the volume of condensed phases for unit total weight of products. Furthermore,

$$v_s = \sum_{\substack{\text{condensed} \\ \text{phases}}} n_i V_i \tag{7-56}$$

where n_i is the number of moles of the *i-th* condensed species from unit weight of explosive and V_i is the molar volume of the *i-th* condensed species. In the case of an explosive producing solid carbon, such as TNT, this expression is simply

$$v_s = n_c V_c \tag{7-57}$$

The general form of the equation of state for a mixture of gas and condensed species expressed in terms of the specific volume of the mixture, can now be written in the form

$$p = p(v - v_s, T) \tag{7-58}$$

where v_s is, in general, a function of pressure and temperature.

An equation of state of the Abel type can be written in the form

$$\left.\begin{aligned} p(v - \overline{\alpha}) &= nRT \\ \overline{\alpha} &= \alpha + v_s \end{aligned}\right\} \tag{7-59}$$

where n is the number of moles of gas produced by unit weight of explosive. Thus the quantity α becomes an effective covolume, and the equation has the same form for a mixture of gas and condensed phase as for a gas phase alone. In calculations that are calibrated by observed detonation velocities such as have been described previously, α may be considered: (1) an adjustable constant as in the Abel equation, (2) a function $\alpha(v)$ as has been done by Cook, or (3) a function $\alpha(p)$ as would be appropriate in a calculation employing the Jones modification of the Abel equation.

In *a priori* calculations of the detonation properties using an equation of state with known parameters, the quantity v_s must be evaluated. This requires knowledge of the concentration of each condensed species in the detonation products and the molar volume of each species at the temperature and pressure of the detonation gas. The former quantity concentration must be based on an initial estimate that is improved as the overall iteration procedure progresses by successively more accurate determinations obtained from the solution of the equilibrium conditions. The molar volumes of the condensed species can usually be taken as constants of the system unless their concentrations are very large. They can be evaluated, when the necessary compressibility and thermal expansion data exist, at a temperature and pressure in the range of detonation conditions and thereafter held constant. Lacking such data, the molar volume at ambient conditions can be employed as an estimate. The overall precision with which the equation of state of the gas is known does not appear for most applications to warrant an elaborate equation of state for condensed species. Furthermore, as a practical matter, the use of more accurate forms is awkward because such forms are explicit either in the pressure or in the molar volume of the solid and they are not easily combined with the equation of state of the gas which is explicit in the volume of the gas. We cite, however, the work of Cowan and Fickett[9] who have quoted an equation of state for carbon (graphite) with parameters that are derived from experimental measurements of the shock Hugoniot curve in graphite. It is an accurate but extremely cumbersome equation of state for carbon that could be employed in calculations if the high accuracy could be justified by comparable accuracy in the other parameters involved.

7-7 THE VIRIAL EQUATION OF STATE

According to the virial theorem, the equation of state for gases can always be written in the form

$$\frac{pv_g}{nRT} = 1 + \frac{B(T)}{v_g} + \frac{C(T)}{v_g^2} + \frac{D(T)}{v_g^3} + \cdots \tag{7-60}$$

where $B(T)$, $C(T)$, $D(T)$,... are the first, second, third, etc., virial coefficients which are functions of temperature and composition but not of volume. For molecules with an interaction energy that can be expressed as a function of the intermolecular distance, the second virial coefficient can be theoretically evaluated. For nonattracting rigid spherical molecules, the virial coefficients are independent of temperature. For such a gas, the third virial coefficient has been calculated by Boltzmann and Jäger and the fourth virial coefficient by Happel and Majumbar[12]. For the gas of rigid nonattracting spheres, the virial equation to cubic terms in the density has the form

$$\frac{pv_g}{nRT} = 1 + \frac{b}{v_g} + 0.625\left(\frac{b^2}{v_g^2}\right) + 0.2869\left(\frac{b^3}{v_g^3}\right) \tag{7-61}$$

At high temperature, Hirschfelder and Rosevearc[13] proposed the equation

$$\frac{pv_g}{nRT} = 1 + \frac{b}{v_g} + 0.625\left(\frac{b^2}{v_g^2}\right) + 0.2869\left(\frac{b^3}{v_g^3}\right) + 0.1928\left(\frac{b^4}{v_g^4}\right) \tag{7-62}$$

where the second virial coefficient is calculated according to the theory of imperfect gases in the limit of vanishing density and is found at high temperatures to be nearly independent of temperature. Thus, the second virial coefficient can be evaluated theoretically, and its evaluation makes possible a theoretical evaluation of the higher virial coefficients for a hard sphere gas which is taken to be a satisfactory model of a real gas at high temperature. The value of the fifth virial coefficient in the expression given was chosen to make the equation agree at high density with the free volume theory of liquids of Hirschfelder, Stevenson, and Eyring[14].

The calculated high temperature second virial coefficients of some species appearing as explosion products are listed in Table 7-6.

The coefficients in Table 7-6 are for pure gases. Rules for mixtures having a theoretical justification are quite complex in form. In view of the approximation, only the simplest combination rule can be justified and the formula

$$b = \sum_i n_i b_i \tag{7-63}$$

has been employed in applications of Eq. 7-62.

Hirschfelder and his coworkers have employed Eq. 7-62 in extensive calculations of the thermodynamic properties of the products of propellants. Its application to the *a priori* calculation of the properties of the detonation products of condensed explosives is due to Paterson[16]. It is of the form

$$pv_g = nRT\,F\left(\frac{b}{v_g}\right) \tag{7-64}$$

so that if b is a constant

$$\left(\frac{\partial E}{\partial v}\right)_T = T\left(\frac{\partial p}{\partial T}\right)_v - p = 0 \tag{7-65}$$

and $c_v = c_v^o$, $\gamma = c/c_v = \gamma^o$. The equation neglects the energy of gas imperfection and will, for this reason, overestimate the temperature of the detonation products. Paterson justifies this neglect by stating that it is justified at low initial densities and will affect to only a small extent all properties except temperature at higher initial densities.

Eq. 7-62 can be written in the Abel form

$$p\,[v_g - \alpha(v_g)] = nRT \tag{7-66}$$

where

$$\left.\begin{aligned} \alpha(v_g) &= v_g[1 - 1/F(x)] \\ x &= b/v_g \end{aligned}\right\} \tag{7-67}$$

Therefore, the quantity Γ can be calculated by the relation

$$\Gamma = \gamma^o\left[2 - \frac{1}{F} - \frac{x}{F^2}\left(\frac{dF}{dx}\right)\right] \tag{7-68}$$

and the solution for the Chapman-Jouguet point, based on the frozen Chapman-Jouguet condition, is given by Eqs. 7-39. Thus, the modified Boltzmann form of the virial equation of state can be employed to obtain an *a priori*,

TABLE 7-6 HIGH TEMPERATURE SECOND VIRIAL COEFFICIENTS OF GASEOUS DETONATION PRODUCTS[15]

Species i	b_i, cm^3/mole	Species i	b_i, cm^3/mole
CO_2*	37.0	NO	21.2
CO	33.0	N_2	34.0
H_2	14.0	CH_4	37.0
H_2O	7.9	NH_3	15.2
O_2	30.5		

* At densities where the CO_2 molecule is assumed not to rotate. At lower densities, with rotation permitted, the value of b_i for CO_2 is 63.0 cm^3/mole.

theoretical evaluation of the function $\alpha(v)$ that was evaluated empirically by Cook.

The results of some of Paterson's calculations—using the equation of state Eq. 7-62, the frozen Chapman-Jouguet condition, and assuming equilibrium composition of the detonation products—are given in Table 7-7. Paterson has also applied his equation of state to calculations for a large number of commercial blasting explosives.

In these calculations all of the necessary data were determined without reference to detonation experiments. Considering the completely *a priori* nature of the calculations, surprisingly good agreement with experimental detonation velocities was obtained, particularly at the lower values of the initial density.

7-8 HALFORD-KISTIAKOWSKY-WILSON EQUATION OF STATE

An extensive computation of the detonation state was carried out by Brinkley and Wilson[17] employing an empirical form of equation of state that was proposed by Halford, Kistiakowsky, and Wilson[10]. The equation is a modified form of one that was originally employed by Becker to represent an experimental nitrogen isotherm. It was modified by the omission of terms that are significant only at low temperature and in such a way as to provide for a contribution due to gas imperfection to the energy content of the gas. The parameters of the equation were calibrated in part by the use of experimental detonation velocity data and in part from theoretical considerations. Since the original work, this equation has had many modifications as new data became available. The most extensive and most recent revision has been carried out by Cowan and Fickett who were able to supplement experimental velocity data with some experimental pressure measurements.

Cowan and Fickett employ an equation of state in the form

$$\left.\begin{aligned} pv_g &= nRTF(x) \\ F(x) &= 1 + xe^{\beta x} \\ x &= k/[v_g(T+\theta)^{\alpha}] \\ k &= \Sigma_i n_i k_i \end{aligned}\right\} \quad (7\text{-}69)$$

Here, v_g is the volume of gas from unit weight of explosive; n_i is the number of moles of the i-th gaseous constituent from unit weight of explosive; α, β, and θ are empirical constants; and the k_i are empirical constants, characteristic of the individual species, having the nature of covolumes. The constant θ was added to the original form to suppress a spurious minimum that the unmodified form presented in curves of

TABLE 7-7 DETONATION PROPERTIES OF SOME CONDENSED EXPLOSIVES[16]

Explosive	ρ_o, g/cm^3	v_1, cm^3/g	T_1, °K	p_1, 10^3 atm	u_1, m/sec	D, m/sec
Nitroglycerin	1.60	0.505	5640	199	1550	8060
PETN	0.50	1.362	5000	21.3	1175	3670
	1.00	0.760	5150	73.8	1340	5550
	1.50	0.540	5340	188	1550	8150
TNT	0.50	1.354	3873	12.4	894	2770
	1.00	0.769	3873	44.2	1010	4400
	1.50	0.550	3890	124	1196	6970
Tetryl	0.50	1.366	4500	15.6	1000	3140
	1.00	0.770	4600	56.9	1150	5000
	1.50	0.550	4790	160	1375	7850

pressure versus temperature at constant volume. Cowan and Fickett have employed the value θ = 400°K in all of their work.

When Eq. 7-69 is employed as the equation of state, the specific energy e_i of gas imperfection, where $e = e^\circ + e_i$, is given by

$$e_i/(nRT) = \alpha\left(\frac{T}{T+\theta}\right)(F-1) \qquad (7\text{-}70)$$

which is a rapidly increasing function of the gas density at constant temperature.

Eqs. 7-69 and 7-70 can be written in an approximate form

$$e_i = \alpha(pv_g - nRT) \qquad (7\text{-}71)$$

if we neglect θ/T compared to unity. Now, it can be shown from the virial theorem that if attractive forces are neglected in comparison with repulsive forces in the intermolecular potential function and if the latter varies inversely as the *n-th* power of the intermolecular distance, then

$$e_i = (3/n)(pv_g - nRT) \qquad (7\text{-}72)$$

Thus, Eq. 7-71 is of the correct form for the internal energy of a gas that is sufficiently dense so that attractive forces can be neglected in comparison with repulsive forces. Furthermore, the parameter α can be identified with the quantity $3/n$, where n is the exponent of the repulsive term in an intermolecular potential function of the Lennard-Jones type. From theoretical considerations, $n > 6$ so that $\alpha < \frac{1}{2}$. Cowan and Fickett found the best overall fit with experimental data with the value $\alpha = \frac{1}{2}$. The high value of this coefficient reflects the fact that attractive forces are not entirely negligible at any gas density. Also, there is now evidence that an inverse power law for the repulsive term is too "hard" for dense gases.

The discussion of the last paragraph is not, of course, a complete justification of the form of the essentially empirical equation of state, Eq. 7-69. It does, however, indicate that this equation takes account of the energy of gas imperfection in a way that is physically plausible and in this respect, at least, is superior to the other forms of equation of state that have been considered. Unfortunately, its use in routine calculations involves a considerably more elaborate computational program. It is not conveniently employed for desk computations, and it is most suitably employed in calculations employing a computer for which the effort of preparing a computer program can be justified.

We can summarize the values of the equation of state parameters adopted by Cowan and Fickett as follows:

$\alpha = 0.50$
$\beta = 0.09$
$\theta = 400\,°K$

The values of the k_i are given in Table 7-8.

TABLE 7-8 VALUES OF THE CONSTANTS k_i[9]

Species	k_i*	Species	k_i*
H_2	2133	CO	3383
H_2O	3636	CO_2	6407
N_2	6267	NO	4148

Table 7-9 contains values of some detonation properties of several explosives calculated with Cowan and Fickett's form of the Halford-Kistiakowsky-Wilson equation of state. Experimental values and some calculated values by Cook and by Paterson are included for comparison.

Cowan and Fickett conclude that reasonably good agreement between calculated and observed quantities is obtained except for explosives such as TNT with large oxygen deficit. In the case of TNT the calculated values are unsatisfactory even though an elaborate equation of state was used for solid carbon. The cause of this discrepancy is not understood at the present time.

The equation of state employed by Cowan and Fickett leads to detonation temperatures that decrease with increasing initial density. This behavior follows from the fact that the equation of state results in a contribution to the energy due to gas imperfections as a strongly increasing function of density. It will be noted from Table 7-9 that the calculated temperature is

*A more extensive list of the constants fitted to the best available explosives' property data, as contained in reports by C. Mader, LASL, which have not been published.

substantially lower than for equations of state for which the energy of gas imperfection is zero. Cowan and Fickett conclude that the Halford-Kistiakowsky-Wilson equation of state is probably fairly reliable if its use is restricted to explosives which are similar to those that were included in the determination of its parameters, and to pressures and volumes that are not too different from those at the Chapman-Jouguet point. There appears to be no justification for its use in an extended extrapolation.

We conclude this chapter by remarking that the problem of formulating a generally adequate equation of state is not solved. The Halford-Kistiakowsky-Wilson equation appears to be the best available.

TABLE 7-9 COMPARISON OF CALCULATED DETONATION PROPERTIES

Explosive	Source	ρ_o, g/cm³	D, m/sec	$dD/d\rho_o$	T, °K	P, 10^3 atm	κ_1,	λ_1,
RDX	Experimental	1.6	8060	3470		262	2.92	0.32
	Cowan & Fickett	1.6	8037	3250	2788	269	2.79	0.30
	Cook	1.6	8040	~ 3570	5750	255	3.01	~ 0.34
RDX	Experimental	1.8				336	3.05	
	Cowan & Fickett	1.8				344	2..	
TNT	Experimental	1.6	6840	2800		166	3.44	0.68
	Cowan & Fickett	1.6	6894	3120	2715	193	3.88	0.25
	Cook	1.6	7030	~ 3660	4170	150	4.20	0.84
	Paterson	1.6	6790	3310	3900	125	4.81	1.26
TNT	Experimental	1.64				175	3.48	
	Cowan & Fickett	1.64				204	2.91	
RDX/TNT, 78/22	Experimental	1.755				313	2.82	
	Cowan & Fickett	1.755				307	2.90	
Comp. B	Experimental	1.715				288	2.79	
	Cowan & Fickett	1.715				281	2.89	

REFERENCES

1. J. Taffenal and H. D'Autriche, Compt. Rend. 155, 1221 (1912).
2. A. Schmidt, Z. Ges. Schiess-u-Sprengstoffw. 30, 364 (1935); 31, 8 (1936).
3. W. E. Deal, Phys. Fluids 1, 523 (1958).
4. S. R. Brinkley, Jr., *Proc. Conf. Chemistry and Physics of Detonation*, Office of Naval Research, Jan. 1951.
5. H. Jones, *Third Symposium on Combustion and Flame and Explosion Phenomena*, Williams & Wilkins, Baltimore, 1949, p. 590.
6. W. Fickett and W. W. Wood, Phys. Fluids 1, 528 (1958).
7. M. A. Cook, J. Chem. Phys. 15, 513 (1947); see also M. A. Cook, *Science of High Explosives*, Reinhold Publ. Corp., New York, 1958.
8. W. Friederich, Z. Ges. Schiess-u-Sprengstoffw. 28, 2, 51, 80, 113 (1933).
9. R. O. Cowan and W. Fickett, J. Chem. Phys. 24, 932 (1956).
10. G. B. Kistiakowsky and E. B. Wilson, Jr., OSRD Report No. 114, 1941.
11. James Taylor, *Detonation in Condensed Explosives*, Oxford University Press, Oxford, 1952, Chapters 7 and 8.
12. R. Majumbar, Bull. Calcutta Math. Soc. 21, 107 (1929).
13. J. O. Hirschfelder and W. E. Roseveare, J. Phys. Chem. 43, 15 (1939).
14. J. O. Hirschfelder, D. F. Stevenson, and H. Eyring, J. Chem. Phys. 5, 896 (1957).
15. J. O. Hirschfelder, F. G. McClure, and C. F. Curtiss, OSRD Report No. 547, 1942.
16. S. Paterson, Research 1, 221 (1948); see also Reference 11.
17. S. R. Brinkley, Jr. and E. B. Wilson, Jr., OSRD Report No. 905, 1942.
18. R. Becker, Z. fur Physik 4, 393 (1921).

CHAPTER 8 STRUCTURE OF THE PLANE DETONATION WAVE: FINITE REACTION ZONE

8-1 INTRODUCTION

The elementary theory of plane detonation waves, described in Chapter 6, is based on a model in which the reaction zone is idealized as a mathematical plane, thus implying a detonation reaction of infinite rate and a reaction zone of zero thickness. The properties of the detonation wave are then determined by the expressions for the transport of mass, momentum, and energy across the discontinuity; by the Chapman-Jouguet condition which provides a sufficient description of the flow behind the detonation front; and by the equation of state and thermal properties of the detonation products. The properties of the detonation wave are independent of the rate of the detonation reaction according to this idealized model.

This elementary theory correctly describes the main features of the detonation process. In particular, it correctly predicts the detonation velocity and the thermodynamic state of the detonation products of cylindrical explosive charges initiated at one end, provided, the diameter of the charge is not too small. However, extension of the theory to more than one dimension—e.g., to the spherical charge—involves mathematical difficulties that result from the over-idealization of the reaction zone to a mathematical surface. Many details of the detonation process in finite charges—e.g., the effect of charge diameter on the detonation of small cylindrical charges—are determined by the structure of the reaction zone. In this chapter, the consequences of a more realistic model which takes account of finite reaction rates are investigated; however, we limit the treatment to plane waves propagating in one direction.

8-2 CONSERVATION CONDITIONS FOR STEADY REACTION WAVES IN ONE DIMENSION

We assume the existence of a wave of chemical reaction propagating in one direction parallel to the x-axis of a rectangular coordinate system and assume that the properties of the flow are constant on planes perpendicular to the direction of propagation. We fix the origin of the coordinate system in the moving reaction wave and assume that there exists a region of finite extent in the moving coordinate system within which the flow is steady.

The hydrodynamic equations for inviscid flow without heat conduction or diffusion have been given in par. 2-6. For flow in one dimension, they can be written

$$\begin{aligned} \frac{d\rho}{dt} + \rho\left(\frac{\partial w}{\partial x}\right) &= 0 \\ \frac{dw}{dt} + \frac{1}{\rho}\left(\frac{\partial p}{\partial x}\right) &= 0 \\ \frac{de}{dt} - \frac{p}{\rho^2}\left(\frac{d\rho}{dt}\right) &= 0 \end{aligned} \tag{8-1}$$

In these equations, p is the pressure, ρ is the density, e is the specific energy, and w is the particle velocity measured with respect to the moving origin of coordinates. The operator d/dt is the mobile time derivative, denoting the rate of change with respect to time as measured by an observer moving with the fluid, i.e.,

$$\frac{d}{dt} = \frac{\partial}{\partial t} + \frac{\partial}{\partial x} \tag{8-2}$$

For steady one-dimensional flow, partial derivatives with respect to time vanish and Eqs. 8-1 become

$$\begin{aligned} w\left(\frac{d\rho}{dx}\right) + \rho\left(\frac{dw}{dx}\right) &= 0, \\ w\left(\frac{dw}{dx}\right) + \frac{1}{\rho}\left(\frac{dp}{dx}\right) &= 0, \\ \frac{de}{dx} - \frac{p}{\rho^2}\left(\frac{d\rho}{dx}\right) &= 0, \end{aligned} \tag{8-3}$$

where, in the steady state, the properties of the fluid are functions only of the space coordinate x, measured relative to the moving coordinate system. Eqs. 8-3 can be integrated, with the result

$$\left.\begin{aligned} w\rho &= M = \text{constant} \\ p + M^2 v &= P = \text{constant} \\ e + pv + \tfrac{1}{2}w^2 &= \Omega = \text{constant} \end{aligned}\right\} \quad (8\text{-}4)$$

where v is the specific volume. The new constants have the following significance: M is the mass current, P is the dynamic pressure, and Ω is the kinetic enthalpy. The three quantities are constants of the flow in a region where the flow is steady and where the effects of viscosity, heat conduction, and diffusion can be neglected.

Eqs. 8-4 are supplemented by the reaction rate equations of par. 2-6

$$\rho\left(\frac{dn_i}{dt}\right) = R_i \quad (8\text{-}5)$$

and by the stoichiometric conditions given in par. 2-2

$$\sum_i \beta_{ij} n_i = q_j \quad (8\text{-}6)$$

where the stoichiometric constant q_j is the number of moles of the j-th component in unit weight of a hypothetical mixture consisting of components only. Without loss of generality, we can assume that the components are assigned the labels $i = 1, 2, \ldots c$, so that constituents that are not components are assigned the labels $i = c + 1, c + 2, \ldots s$. Eqs. 8-5 and 8-6 can then be written in a more explicit form that takes into account the fact that only the R_i, $i = c + 1, c + 2, \ldots s$, can be independently specified. For the steady state, these expressions are

$$\left.\begin{aligned} \frac{dn_i}{dx} &= \frac{R_i}{\rho w}, & i &= c+1, \ \ldots s \\ \frac{dn_j}{dx} &= -\frac{1}{\rho w}\sum_{i=c+1}^{s} \beta_{ij} R_i, & j &= 1, 2, \ldots c \end{aligned}\right\} \quad (8\text{-}7)$$

The rates R_i are linear combinations of the rate expression for the elementary reactions occurring in the region of reactive flow. These rate expressions depend upon the composition, temperature, and pressure. Therefore

$$R_i = R_i(T, p; n_1 \ldots n_s) \quad (8\text{-}8)$$

and if the mechanism of the reaction is known, the expressions summarized by Eq. 8-8 can, at least in principle, be evaluated. Eqs. 8-4 are also supplemented by an equation of state which we may take to be an expression of the form

$$p = p(v, T; n_1, \ldots n_s) \quad (8\text{-}9)$$

Now, we suppose that fluid is moving from left to right, i.e., $w > 0$. (This convention is opposite to that employed in Chapter 6.) Further, we suppose that the material to the left of the plane $x = 0$ is in the uniform state p_o, ρ_o with $w_o = D$ and $R_i = 0$ for all i. At the plane $x = 0$, we consider two cases. First, assume that the properties of the flow are continuous at this plane. Then the constants of Eqs. 8-4 are given by

$$\left.\begin{aligned} M &= \rho_o D \\ P &= p_o + \rho_o D^2 \\ \Omega &= e_o + p_o v_o + \tfrac{1}{2}D^2 \end{aligned}\right\} \quad (8\text{-}10)$$

where e_o is the specific energy of the nonreacting fluid in the uniform state. Alternatively, assume that the reacting fluid in the region $x > 0$ is connected to the uniform nonreacting fluid in the region $x < 0$ by a shock wave fixed in the plane $x = 0$. If the properties of the shocked fluid at $x = 0$ are designated by a prime, we have

$$\left.\begin{aligned} M &= \rho' w' \\ P &= p' + \rho'(w')^2 \\ \Omega &= e' + p'v' + \tfrac{1}{2}(w')^2 \end{aligned}\right\} \quad (8\text{-}11)$$

Here e' is the specific energy of the material at pressure p' and specific volume v' having the same composition as the material in the uniform state at p_o and v_o. Assuming that the shock can be represented by a discontinuous transition from the unshocked to the shocked state at constant composition, we may employ conservation conditions of par. 2-8 and transform Eqs. 8-11 to expressions that are identical with Eqs. 8-10. Thus Eqs. 8-10 can be employed for the two cases under consideration. Combining them with Eqs. 8-4, we obtain

$$\left.\begin{aligned} \rho w &= \rho_o D \\ p + \rho w^2 &= p_o + \rho_o D^2 \\ e + pv + \tfrac{1}{2}w^2 &= e_o + p_o v_o + \tfrac{1}{2}D^2 \end{aligned}\right\} \quad (8\text{-}12)$$

The left-hand members of Eqs. 8-12 are evaluated at fixed arbitrary values of the x-coordinate, $x>0$. If the first of Eqs. 8-12 is employed to eliminate w from the second, we obtain

$$\rho_o^2 D^2 = -(p - p_o)/(v - v_o) \qquad (8\text{-}13)$$

If the first and second of Eqs. 8-12 are employed to eliminate w and D from the third, we obtain

$$e - e_o = \tfrac{1}{2}(p + p_o)(v_o - v) \qquad (8\text{-}14)$$

If we denote by $u = D - w$ the particle velocity in the region $x>0$ relative to that of the uniform state existing in the region $x<0$, the first of Eqs. 8-12 becomes

$$\rho(D - u) = \rho_o D \qquad (8\text{-}15)$$

If the uniform state is at rest in a laboratory system of coordinates, u is the particle velocity in a laboratory system of coordinates.

Examining Eqs. 8-7 and 8-12, we note that we have $s + 3$ equations connecting the $s + 4$ variables n_i, p, ρ, u, and D when the uniform state is specified. (The equation of state and thermal properties of the explosion products determine the specific energy e as a function of n_i, p, and ρ.) The indeterminacy corresponds, for detonations, to the absence of the Chapman-Jouguet condition from the equations. Insofar as these equations are concerned, we may regard D as a parameter whose value can be specified. Eqs. 8-7 and 8-12 are then in a formal sense determinant, determining each of the dependent variables as functions of x and D. Thus, the solutions of Eqs. 8-7 and 8-12 determine a two parameter sequence of states through the moving reaction wave. It is necessary, in principle, to determine the values of D for which these equations have suitable solutions. For the general case of multiple simultaneous reactions terminating in an equilibrium state, this presents a formidable problem.

A model that is easily visualized and that provides a useful description of the reaction wave is obtained by assuming that the reaction proceeds toward a final invariant composition that can be specified *a priori* independently of final pressure and density. A progress variable ξ can then be introduced by the relation

$$e(\xi) = \xi e_1(p,v) + (1 - \xi)e_o(p,v) \qquad (8\text{-}16)$$

where e_1 is the specific energy of the products and e_o is the specific energy of the reactants, each considered a function of p and v. In this approximation, Eq. 8-14 can be written

$$\xi e_1(p,v) + (1 - \xi)e_o(p,v) - e_o(p_o,v_o) = \tfrac{1}{2}(p + p_o)(v_o - v) \qquad (8\text{-}17)$$

where p and v are to be regarded as functions of the progress variable ξ. When $\xi = 1$, Eq. 8-17 is identical with the Hugoniot equation for instantaneous reaction. Eq. 8-17 describes a family of curves in the (p,v)-plane, each member of which is labeled by a value of ξ with $0 \leqslant \xi \leqslant 1$. For exothermic processes with $e_o(p,v) > e_1(p,v)$ this family consists of nonintersecting curves that are concave upward. Eq. 8-13 is the equation for the Rayleigh line. With p and v regarded as functions of ξ, the reaction in a steady reaction wave is constrained to states on this line. When we employ the subscript unity to identify properties of the flow when $\xi = 1$, Eqs. 8-13 and 8-17 become identical with the analogous expressions of Chapter 6.

8-3 THE STEADY DEFLAGRATION WAVE

The branches of the family of curves given by Eq. 8-17 for which $p(\xi) < p_o$ describe the states in a steady deflagration wave that satisfy the conservation equations. These curves are shown in Fig. 8-1, together with a Rayleigh line $OABC$. This Rayleigh line represents two different processes with the same propagation velocity D. One consists of a discontinuous transition in the unreacted material from the state O to the state C, followed by the reaction zone represented by the segment of the Rayleigh line CB along which ξ changes from 0 to 1, terminating in state B which is a strong deflagration. The other consists of the continuous transition from the state O to the state A, which is a weak deflagration, along the segment of the Rayleigh line OA for which ξ changes from 0 to 1. It has been noted in par. 2-8 that a nonreactive rarefaction shock, as in the transition from O to C, does not exist since it would entail a decrease in entropy and violate

the second law of thermodynamics. It follows that strong deflagrations are impossible for the assumptions made. Therefore, starting at the point O with p_o, v_o, the state point can only reach the upper intersection A without passing through regions for which $\xi > 1$. The only states on the final Hugoniot curve of Fig. 8-1 that are physically admissible are the weak deflagrations lying between (and including) the Chapman-Jouguet deflagration J and the constant pressure deflagration for which $p_1 = p_o$.

In Chapter 6, we noted that a useful description of deflagration waves is not obtained from the hydrodynamic equations in which heat conduction and the diffusion of chemical species are neglected. The propagation velocity of a deflagration wave is determined by these transport processes from the reaction zone upstream into the reactants. In the theory of flame propagation, the differential conservation equations are stated so as to include the effects of viscosity, diffusion, heat conduction, and the rate of chemical reaction. For particular boundary conditions, these equations possess a solution only for a unique value of the wave velocity. In a deflagration wave, the reaction must be initiated by heat conducted upstream from the reaction zone into the medium ahead of the reaction zone.

8-4 THE STEADY DETONATION WAVE

We begin our discussion of the structure of plane detonation waves by commenting on the role of transport processes in the mechanism of the detonation reaction. The solutions of the steady one-dimensional heat conduction-convection equation and of the steady one-dimensional diffusion-convection equation are characterized by

$$e^{-x/x_o}$$

where x is the distance and x_o is a characteristic distance. For thermal conduction, $x_o = \alpha/w$, where α is the thermal diffusivity and w is the particle velocity in the frame of reference within which the motion is steady. For diffusion, $x_o = D/w$, where D is the diffusion constant. The thermal diffusivity and diffusion constant are each of order unity or less, when expressed in units of square centimeters per second. The

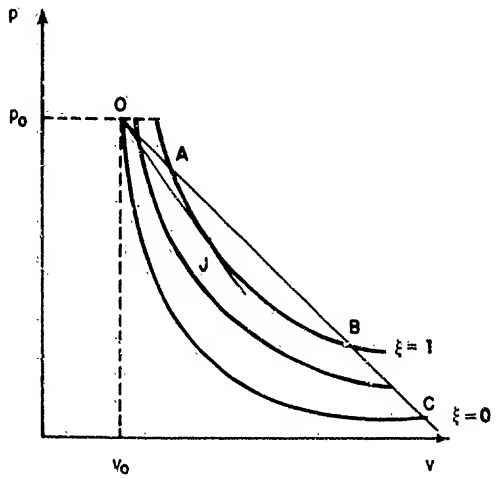

Figure 8-1. Family of Hugoniot Curves for Steady Deflagration Wave

particle velocity associated with a detonation wave is of order 10^5 to 10^6 cm/sec. Therefore, the characteristic length x_o is of order 10^{-5} cm or less.

We need to consider two different possible mechanisms for initiating the chemical reaction. It may be effected by the diffusion of chemical species into the unreacted material or it may consist of an initiation reaction that is *0-th* order in its products. If the initiation is exclusively of the first type, the detonation wave may be conceived of as a shock wave combined with a diffusion wave similar to a diffusion flame. To satisfy the boundary conditions at the reaction front by a temperature or concentration distribution with a characteristic length of 10^{-5} cm or less, it would be necessary to postulate a reaction rate of unreasonably high value, so that the reaction zone width is also of the order of magnitude of the characteristic length. In this connection, it is to be remarked that the particle velocity in diffusion flames is many orders of magnitude less than in detonation waves and the characteristic lengths of the former (diffusion flames) are correspondingly many orders of magnitude greater than those of the latter (detonation waves). It follows that the effects of transport processes can be entirely neglected in the reaction zone of the detonation reaction, except for their occurrence within a shock front where their effects are adequately described by the conservation laws across a discontinuity. The primary contribution to the initiation mechanism must be by an initiation reaction that is *0-th* order in its products.

These considerations lead to a model wherein the initiation reaction has a negligible rate before the front and an appropriately large rate behind it, i.e., to a model wherein the reaction is initiated by the shock front. Such a model was independently postulated by Zeldovich, von Neumann, and Döering [1-3]. The Hugoniot curves prescribed by Eq. 8-17 for the unreacted material immediately behind the shock front ($\xi = 0$), for the completely reacted material ($\xi = 1$), and for an intermediate degree of reaction are sketched in Fig. 8-2. The Rayleigh line *OABC* represents two different processes with the same propagation velocity D. One consists of a continuous transition from the state O to the state A, which is a weak detonation along the segment of the Rayleigh line OA for which ξ changes from 0 to 1. The other consists of a discontinuous transition through a shock front in the unreacted material to the state C on the Hugoniot curve for $\xi = 0$, followed by the reaction zone, represented by the segment of the Rayleigh line CB along which ξ changes from 0 to 1. The state B is evidently a strong detonation and the second process corresponds to that postulated by Zeldovich, von Neumann, and Döering. In Chapter 6, it was remarked that a detonation wave is formally equivalent to a shock wave followed by a deflagration wave. Thus, the detonation states of Fig. 8-2 centered on the initial state O can be regarded as a deflagration wave centered on the state C. It was also remarked that a strong detonation wave is a shock wave followed by a weak deflagration, a weak detonation wave is a shock followed by a strong deflagration, and a Chapman-Jouguet detonation is a shock followed by a Chapman-Jouguet deflagration. In the previous paragraph, it was shown that a strong deflagration does not exist. It follows that, for the assumptions made, a weak detonation does not exist. Therefore, starting from a shock wave in the unreacted material centered on the point O with p_o, v_o, the state point can only reach the upper intersection B. The point J of Fig. 8-2 is the state with lowest pressure on the Hugoniot curve for the unreacted explosive for which the reaction can reach the Hugoniot curve for complete reaction. The Rayleigh line OJ is tangent to the Hugoniot curve for complete reaction; it represents the reaction wave terminating in a Chapman-Jouguet detonation.

Prior to the description of the reaction zone given by Zeldovich, von Neumann, and Döering, it was suggested that the reaction occurs at a constant pressure equal to the Chapman-Jouguet pressure p_J. According to this hypothesis, the process consists of a discontinuous transition through a shock front from the state O to the state J' on the initial Hugoniot curve, followed by a reaction at the constant pressure p_J. It is readily seen that such a process cannot represent a stationary reaction zone since the initial shocked state and final reacted state lie on different Rayleigh lines, OJ' and OJ, respectively.

Weak detonations, under the assumptions made, are impossible. Furthermore, a rarefaction

wave will originate in the explosion products, and will overtake and weaken a strong detonation until it becomes a Chapman-Jouguet detonation. Therefore, the Chapman-Jouguet detonation is the detonation that is stable.

It has been assumed that the family of Hugoniot curves, labeled by a value of the degree of reaction $\xi, 0 \leq \xi \leq 1$, form a family of nonintersecting curves such as has been sketched in Fig. 8-2. This will be the case if, as has been assumed, the reaction proceeds to a fixed invariant mixture of products and if the exothermicity condition, $e_0(p,v) > e_1(p,v)$, is satisfied at all values of the pressure and specific volume. However, von Neumann has pointed out that the family of Hugoniot curves may have a different form if the reaction is not exothermic at all pressures and densities. Such a condition may, in principle, arise if the mechanism of the explosion reaction consists of several different elementary reactions whose relative contribution to the overall decomposition may depend on the strength of the initiating shock wave and one or more of which may be endothermic. In such a case, the Hugoniot curves may intersect and have an envelope, as shown in Fig. 8-3. It would then be possible for the process to consist of a discontinuous transition from the state O to the state B on the Hugoniot curve for $\xi = 0$, followed by a reaction described by the segment of the Rayleigh line BA during which ξ changes continuously from 0 to 1. The point A on the Hugoniot curve for $\xi = 1$ is a weak detonation, and the Rayleigh line OAB is tangent to the envelope to the Hugoniot curves and represents the only process for which ξ takes on all values from 0 to 1. This solution is known as von Neumann's pathological weak detonation. No case of the actual existence of such a detonation is known.

8-5 FLOW BEHIND A CHAPMAN-JOUGUET WAVE

Riemann's equations (see par. 2-7) can be employed to construct the nonsteady flow

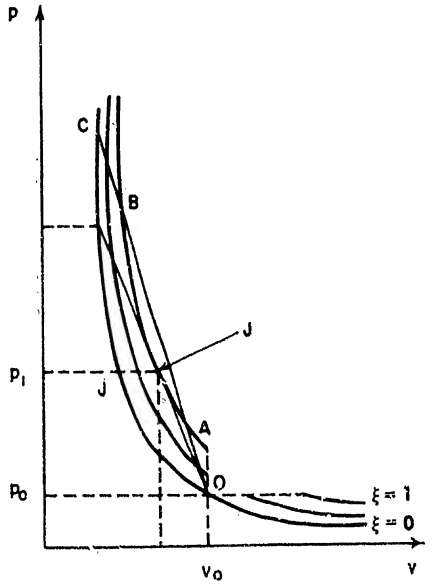

Figure 8-2. Family of Hugoniot Curves for Steady Detonation Wave

behind a Chapman-Jouguet discontinuity. At the discontinuity, located at $x = Dt$, the explosion products are characterized by the quantities u_1, ρ_1, and c_1 which are determined by the Chapman-Jouguet condition, the Hugoniot equations, and the equation of state. One of these quantities may have an arbitrary initial distribution behind the front. The whole flow can then be determined as a simple wave.

For definiteness, we suppose that the steady detonation begins at a piston face located at $x = 0$ at $t = 0$. The Chapman-Jouguet particle velocity u_1 is accommodated to the piston velocity, assumed to be less than u_1, by a centered simple wave, i.e., by an unsteady rarefaction wave. The C_+ characteristics of such a wave are straight lines with the equation

$$x = (u + c)t \tag{8-18}$$

The Chapman-Jouguet point, which is a discontinuity between the steady reaction zone and the nonsteady rarefaction wave, follows a path in the (x,t)-plane which is the C_+ characteristic

$$x = (u_1 + c_1)t = Dt \tag{8-19}$$

In par. 2-7 it was remarked that the Riemann invariant s is constant throughout this simple wave. Because of this circumstance

$$u_1 - \sigma(p_1) = u - \sigma(p)$$

$$\sigma = \int_0^p \frac{dp}{\rho c} \tag{8-20}$$

The function σ can be regarded a known function of the pressure along the isentrope

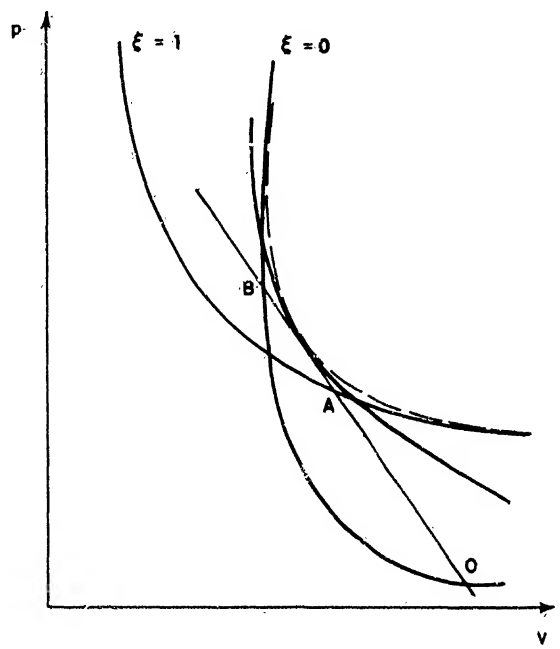

Figure 8-3. The von Neumann Pathological Weak Detonation

passing through the Chapman-Jouguet state. Therefore, Eq. 8-20 provides one relation between the pressure p and the particle velocity u. Along this isentrope, the acoustic velocity c can also be regarded a known function of the pressure. Eq. 8-18 thus provides a second relation, connecting the pressure and particle velocity to the reduced distance variable x/Dt

$$u + c(p) = (u_1 + c_1)(x/Dt) \qquad (8\text{-}21)$$

Eqs. 8-20 and 8-21 determine the particle velocity and pressure in the rarefaction wave as functions of the reduced distance x/Dt. For general equations of state, they can be solved numerically from tables of c and σ versus the pressure. When the pressure distribution through the rarefaction wave is known, the distributions of the other thermodynamic variables through the wave are determined since these variables depend only on the pressure along a prescribed isentrope.

If the explosion products obey a polytropic law, Eqs. 8-20 and 8-21 can be solved explicitly. If the adiabatic exponent is κ, the results can be written in the form

$$\left.\begin{aligned} \frac{u}{u_1} &= 1 + \frac{2}{\kappa+1}\,\frac{D(\zeta-1)}{u_1} \\ \frac{c}{c_1} &= \frac{2}{\kappa+1} + \frac{\kappa-1}{\kappa+1}\,\frac{D\zeta-u_1}{D-u_1} \\ \frac{p}{p_1} &= \left\{\frac{2}{\kappa+1} + \frac{\kappa-1}{\kappa+1}\,\frac{D\zeta-u_1}{D-u_1}\right\}^{2\kappa/\kappa-1} \\ \frac{\rho}{\rho_1} &= \left\{\frac{2}{\kappa+1} + \frac{\kappa-1}{\kappa+1}\,\frac{D\zeta-u_1}{D-u_1}\right\}^{2/\kappa-1} \end{aligned}\right\} \qquad (8\text{-}22)$$

where $\zeta = x/Dt$. It will be noted that the particle velocity and acoustic velocity are linear functions of the reduced distance ζ for this case. The solution for a polytropic gas was obtained by Taylor, and the unsteady flow behind the Chapman-Jouguet detonation is sometimes called the Taylor wave. Eqs. 8-22 assume a particularly simple form when $\kappa = 3$. Then

$$\left.\begin{aligned} \frac{u}{u_1} &= 1 + \tfrac{1}{2}\left[\frac{D(\zeta-1)}{u_1}\right] \\ \frac{c}{c_1} &= \tfrac{1}{2}\left\{\frac{D\zeta-u_1}{D-u_1} + 1\right\} \\ \frac{p}{p_1} &= 1/8\left\{\frac{D\zeta-u_1}{D-u_1} + 1\right\}^3 \\ \frac{\rho}{\rho_1} &= \tfrac{1}{2}\left\{\frac{D\zeta-u_1}{D-u_1} + 1\right\} \end{aligned}\right\} \qquad (8\text{-}23)$$

In this case, the density is also a linear function of the reduced distance ζ. This particular solution is of interest since the explosion products of condensed explosives obey, approximately, a polytropic law with an adiabatic exponent in the neighborhood of 3 [5,6]. It can, therefore, be expected to display qualitatively the features of the flow associated with such explosives.

The transient portion of the flow is terminated by the straight characteristic along which the particle velocity is equal to the piston velocity. The characteristic separates the transient flow from a uniform flow. The uniform flow is found by the solution of Eqs. 8-20 and 8-21 with u set equal to the piston velocity. The case of steady detonation initiated at a rigid fixed wall corresponds to a terminal characteristic along which $u = 0$. In the polytropic case, from the first of Eqs. 8-22, the uniform state at rest extends from the back wall to a point given by

$$\left.\begin{aligned} \zeta &= 1 - \frac{\kappa+1}{2}\left(\frac{u_1}{D}\right) \text{ when } u = 0 \\ &= 1 - 2(u_1/D) \text{ for } \kappa = 3 \end{aligned}\right\} \qquad (8\text{-}24)$$

For condensed explosives, the ratio $u_1/D \approx 1/4$ so that $\zeta \approx 1/2$ when $\kappa = 3$. For this case, the pressure on the back wall can be calculated from the third of Eqs. 8-23. Using $\kappa = 3, \zeta = 1/2$, and $u_1/D = 1/4$, we obtain the order of magnitude result $p/p_1 \approx 8/27$.

From these considerations, we see that the reaction zone is followed by a column of forward-moving explosion products, the length

of which increases linearly with time. For a solid explosive, the length of this column is of the order of one-half the distance traversed by the detonation wave from its point of initiation. If initiation is at a rigid wall, the column of forward-moving products is followed by a column of stationary gas which also increases in length and within which the pressure is constant.

Shear[7] has employed numerical methods to solve Eqs. 8-20 and 8-21 for the explosive pentolite at a loading density of 1.65 g/cm^3. He employed the equation of state of Halford, Kistiakowsky, and Wilson to construct the isentrope through the Chapman-Jouguet state and obtained the function σ by numerical integration. The particle velocity and pressure through the Taylor wave for a detonation originating at a rigid surface as determined by these calculations are shown in Fig. 8-4. It is interesting to note that in Shear's detailed calculations, $u = 0$ and $p/p_1 = 0.295$ at $\zeta = 0.483$. For the polytropic gas with $\kappa = 3$, $D = 4u_1$, we have obtained the estimate, $u = 0$ and $p/p_1 = 0.296$ at $\zeta = 0.5$.

Suppose that the point $x = 0$ represents an interface between explosive and air, i.e., that the plane of initiation is unconfined and that a Chapman-Jouguet detonation is initiated at $t = 0$ on this interface. There will then result a backward flow of explosion products in the negative x-direction. This flow is the same as though the piston of our model is conceived to begin to move at $t = 0$ with a constant velocity sufficient to reduce the pressure on the piston to the ambient air pressure. The velocity of the air-explosion product interface can be determined by solving Eqs. 8-20 and 8-21 with $p = p_o$. For the polytropic case, and neglecting p_o compared to p_1, we obtain from Eqs. 8-22 the result

$$\left.\begin{aligned} \frac{u}{u_1} &= \frac{\kappa + 1}{\kappa - 1} - \frac{D}{u_1}\left(\frac{2}{\kappa - 1}\right) && \text{when } p \approx 0 \\ &= 2 - D/u_1 && \text{for } \kappa = 3 \end{aligned}\right\} \quad (8\text{-}25)$$

Thus, for a condensed explosive with $\kappa = 3$, $D = 4u_1$, we obtain the order of magnitude result that $u/u_1 \approx -2$.

We have seen that when the rear surface of the explosive charge is unconfined, the flow behind the reaction zone consists of a column of forward-moving explosion products, the length of which increases linearly with time, followed by a column of backward-moving products whose length also increases linearly with time. For a solid explosive, the length of the backward-moving products is of the order of twice the length of the forward-moving products and the negative velocity of the air-product interface is of the order of twice the (forward) particle velocity of the Chapman-Jouguet state.

Equations of state of detonation products[5,6,8] have been generated from hydrodynamic properties of the products measured by impedance mismatch methods[9,10]. The early work of Lawton and Skidmore, and Deal showed that shock compressions and adiabatic expansions of the detonation products from the Chapman-Jouguet state in many high explosives are consistent with a polytropic equation of state. The value of the polytropic index above 100 kbar is found to be about 3. Further work by Skidmore and Hart[11] on overdriven detonation waves in Composition B in the 300 kbar regime indicates that the simple polytropic relationship with a constant index appropriate to the Chapman-Jouguet state is adequate for predicting overdriven detonation wave properties, shock compressions, and adiabatic expansions from a given overdriven state. Equations of state of detonation products applicable over a wider pressure range below the Chapman-Jouguet state have been generated for many explosives by Wilkins[12] and coworkers at the Lawrence Radiation Laboratory. The basis of the method is to use the energy-pressure-volume equation of state of the products as a variable in a two-dimensional code for calculating the radial expansion of a copper vessel containing a detonating explosive. Numerical experiments are performed with a computer until calculated expansions agree with those observed experimentally.

8-6 THE DETONATION WAVE WITH EQUILIBRIUM PRODUCT COMPOSITION

In order to provide an easily visualized model of the detonation wave reaction zone, we assumed in par. 8-4 that the detonation reaction proceeds to a fixed composition that is known *a priori*. With this assumption, it was possible to define a "degree of reaction" and to employ this parameter to characterize points within the reaction zone at which the reaction is

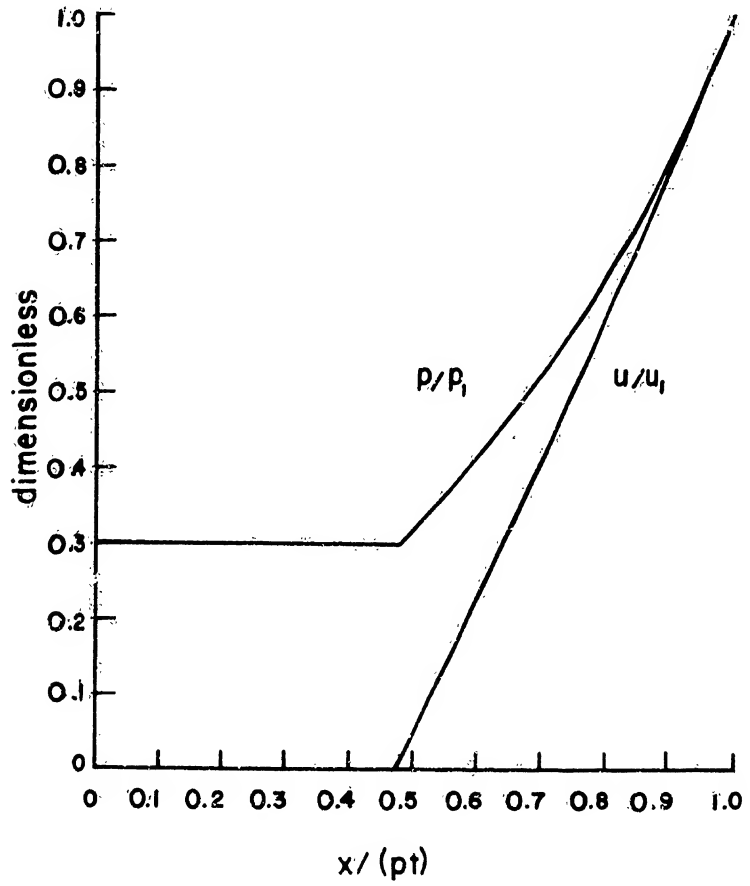

Figure 8-4. Pressure and Particle Velocity Behind an Unsupported Chapman-Jouguet Detonation

incomplete. The degree of reaction was thus described by the progress variable ξ, defined by Eq. 8-16 as the fraction of the energy of explosion released at the point in the reaction zone characterized by a particular value of ξ.

Under these assumptions, Hugoniot curves can be constructed for all points in the reaction zone between the initiating shock wave and the point at which the reaction is complete, each curve being labeled by a value of ξ. Within the context of the model employed, these curves have physical meaning, representing the locus of all states that are compatible with the conservation conditions and for which the amount of energy released is given by Eq. 8-16. Under these assumptions, no ambiguity is encountered in the statement of the Chapman-Jouguet condition since the Hugoniot curve for complete reaction is a curve for constant composition. This curve is tangent to an isentrope along which the composition is constant and whose slope is characterized by the frozen sound speed in which the differentiation is performed at constant composition. The Chapman-Jouguet condition can thus be written in the usual way in terms of the frozen speed of sound.

However, the final Hugoniot curve is supposed to describe the states that are compatible with the conservation conditions when all of the reaction rates R_i of Eqs. 8-7 have vanished, i.e., when the explosion products are in thermodynamic equilibrium. Therefore, the final Hugoniot curve of Fig. 8-2 does not necessarily represent physically accessible states of the explosion products and it may, in fact, not even be a good approximation to the states that can actually be reached from different points on the initial Hugoniot curve.

Suppose that the segment of the Rayleigh line *CB* of Fig. 8-2 represents an actual reaction process, initiated at the state *C* on the initial Hugoniot curve and terminating at the state *B*. In general, the Hugoniot curves labeled with different values of the progress variable ξ and drawn for constant composition represent physically real (i.e., accessible) states only at their points of intersection with this particular Rayleigh line. If a different process—represented by a Rayleigh line from a different point on the initial Hugoniot curve—is considered, the fixed composition Hugoniot curves, drawn for particular values of the progress variable ξ, will not in general coincide with those for the first process. In other words, the sequence of states between the initial Hugoniot curve and the final (equilibrium) Hugoniot curve, each of which represents a locus of physically real states, depends not only on the fraction of energy released but also on the position on the initial Hugoniot curve from which the process starts. Thus, in general, the sequence of states in the reaction zone of a detonation wave depends on a progress variable such as ξ and an additional parameter which may be the detonation velocity *D*.

Although it is evident that a single parameter does not suffice in principle to prescribe a unique family of curves of the von Neumann type (such as those of Fig. 8-2), descriptive of states within the reaction zone that are reached from any point on the initial Hugoniot curve, such a model may provide a useful approximate description. This would be the case if only one reaction process were to be involved, or alternatively if all other reactions were to have much faster reaction rates so that a state of quasi-equilibrium is approximately established at each stage. In practice, a single reaction will hardly ever be sufficient to describe the reaction process, but it may very well happen that one particular step is much slower than the rest. Thus, for example, in granular explosives it can frequently be assumed that grain or surface burning determines the rate of release of energy, and that this process is followed by equilibration among the products at a much faster rate.

It has been customary tacitly to assume that the equilibrium sound speed should be employed in defining the stable velocity of a detonation wave that is not supported by a piston when the reaction terminates in an equilibrium state. Although many numerical calculations have been conducted in which the frozen sound speed was employed for this quantity, it has been assumed, either explicitly or implicitly, that this simplification is an approximation, justified by the fact that the two different statements of the Chapman-Jouguet condition do not lead to very different values of the detonation velocity.

Wood and Kirkwood[13] have shown that if a stable Chapman-Jouguet detonation wave exists, its velocity must be determined by a Chapman-Jouguet condition in which the

equilibrium sound speed is employed. This implies a physical model in which the reaction is initiated in a shock front and terminates at the leading edge of a rarefaction wave at which point the reaction is complete and the explosion products are in thermodynamic equilibrium. Consider the reaction pictured in Fig. 8-5 that is initiated at the point C on the initial Hugoniot curve S and during which the state point moves along the Rayleigh line $CB'B$. Let the point B be an equilibrium state at which the Rayleigh line is tangent to Hugoniot curve F at fixed composition for the composition of the point B. Let the Hugoniot curve E be the curve for equilibrium states that is also centered on the point (p_o, v_o). This curve evidently passes through the point B. It can be shown by the thermodynamic equilibrium conditions that the curve E lies to the left of the curve F for pressures greater than the pressure at the point B. The Rayleigh line CB thus has a point of intersection with the equilibrium at a point, say B', that lies between the points C and B. It follows that the predicated process cannot terminate at the state B' but must terminate at the state B' which also an equilibrium state. Now, the wave of minimum velocity that terminates in a point on the equilibrium Hugoniot curve is the wave whose Rayleigh line is tangent to the equilibrium Hugoniot curve. It has been shown in Chapter 6 that the equilibrium Hugoniot curve is tangent to an equilibrium isentrope at its point of tangency to the Rayleigh line. Thus the slope of the Rayleigh line at this point is characterized by the equilibrium sound speed. Our physical model implies that this is the speed at which the rarefaction wave advances into the explosion products. It is to be noted that this argument does not prove the stability of the postulated flow.

The curves for the rates of the chemical reactions that occur in the reaction zone as functions of time must be asymptotic to the time axis for any reasonable rate laws. Therefore, if the reaction terminates in an equilibrium state, the separation distance between the shock front and rarefaction wave must, in the one-dimensional case, be infinite. This formal result is without substantial practical importance for two reasons. The first is that even in the theoretical one-dimensional case, the reaction of substances of practical interest is substantially complete in a short distance behind the shock front, so that an effective reaction zone thickness exists that is finite but of somewhat indeterminate extent within which all but an infinitesimal amount of the energy of reaction is released. The second is that in detonation waves of explosive charges of finite extent, the position of the rarefaction wave in the flow is unambiguously fixed by other dynamical considerations. Thus, these considerations of the nature of the stability conditions for the one-dimensional detonation wave are mainly of theoretical interest. Although the matter is not satisfactorily settled, it appears from these considerations to be plausible that a detonation wave with a steady reaction zone terminating at a rarefaction wave in an equilibrium state exists only in an asymptotic sense.

On this basis, the results are physically reasonable. The isentropes which appear in a theory based on equilibrium Hugoniot curves must necessarily themselves correspond to equilibrium changes. This is physically acceptable since the infinitesimal rarefactions that enter into the Chapman-Jouguet theory are presumably real rarefactions, involving a change in composition when the system is one in which such changes can occur. Since we are here concerned with the asymptotic properties of a rarefaction wave whose gradient approaches zero with time, it is physically acceptable that the sound speed appearing in the theory be that characteristic for the propagation of sound in the limit of zero frequency.

We have shown that a steady reactive flow exists in which the reaction is initiated in a shock wave and terminated at a rarefaction wave advancing into the equilibrium mixture of explosion products with the equilibrium velocity of sound. (We have not shown that this flow is stable.) We now want to exclude other possibilities. Brinkley and Richardson[14] have supposed that the rarefaction wave is located a finite and fixed distance downstream from the shock wave. They have shown that a steady flow exists between the shock wave and the leading edge of the rarefaction wave, and that the propagation velocity of the rarefaction wave relative to the explosion products is the frozen sound speed. They called such flows subideal

Chapman-Jouguet states. Since the reaction is complete an infinite distance downstream, it follows that the reaction is proceeding in the unsteady rarefaction wave.

Now we wish to show that, if the chemical reaction is still proceeding in the rarefaction wave, a pressure pulse must eventually overtake its front. In a rarefaction wave there are two possibilities: either a signal overtakes the front or a signal does not overtake the front. Let us make the hypothesis that a signal does not overtake the front. Then the rarefaction wave will, in the passing of time, approach a steady state (in most cases this steady state will be a uniform state; however, we do not need to assume this here). Now suppose that upstream ahead of the rarefaction front we have a subideal Chapman-Jouguet state and, consequently, that the rarefaction front is moving with a constant velocity equal to the velocity of the shock front. We have already shown that, in this case, the second law of thermodynamics allows the existence of the steady state only upstream from the rarefaction front. Therefore, the hypothesis must be false since it implies that a steady state is approached on the downstream side of the rarefaction front. Consequently, a signal must overtake the rarefaction front. To complete the argument, we must show that this signal must be a positive pressure pulse. Reasonable assumptions concerning the variation of sound velocity with pressure will imply that a rarefaction wave cannot overtake a rarefaction wave: therefore, the signal must be a positive pressure pulse (which may or may not crest up into a shock).

These arguments are limited to the case in which the reaction is not complete at the rarefaction front. This required use of a subideal Chapman-Jouguet state between the shock and rarefaction fronts, and the corresponding finite separation distance between the fronts. If the

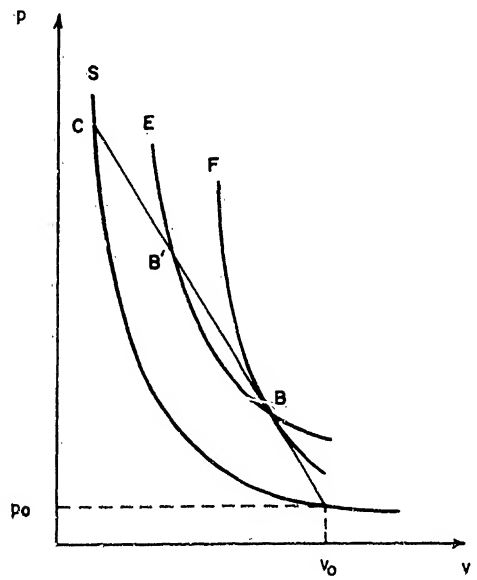

Figure 8-5. Constant Composition and Equilibrium Hugoniot Curves[13]

AMCP 706-180

reaction is complete at the rarefaction front, the ideal Chapman-Jouguet state will exist between the two fronts, and the rarefaction front will be an infinite distance downstream from the shock front. In this case a rarefaction wave can behave in the usual fashion, with no signals overtaking its front, and can approach a uniform steady state without contradiction since there is now no definite limit downstream for the steady state.

These considerations lead us to the conclusion that, in the one-dimensional case, if the reaction is not complete at the rarefaction front, the chemical energy will not be lost forever behind the front. At least a certain fraction of the energy must eventually be delivered upstream in the form of a positive pressure pulse. However, in two- or three-dimensional processes a sidewise expansion in the rarefaction wave is possible with the result that signals may never overtake the front, and the total amount of the chemical energy liberated in the rarefaction may never be delivered upstream.

Brinkley and Richardson erroneously concluded that the propagation velocity, the asymptotic ideal Chapman-Jouguet wave in one-dimension, is defined by the frozen sound speed. We have shown that this cannot be the case and have inferred from arguments of physical plausibility and from the demonstration of Wood and Kirkwood that the asymptotic wave, if it exists, is characterized by the equilibrium sound speed. In an earlier paper, Kirkwood and Wood[15] had reached similarly erroneous conclusions. They had noted that when specialized to one-dimensional flow, the general equations for reactive flow give a system of hydrodynamic equations which is hyperbolic and irreducible, and for which the characteristic sound speed is the frozen sound speed. This property of the equations led them to the same conclusion that had been reached by Brinkley and Richardson. Subsequently, Wood and Kirkwood presented the elementary proof, that has been summarized, that the frozen Chapman-Jouguet state cannot be reached in a one-dimensional steady detonation.

Wood and Salsburg[16] have conducted the most complete theoretical study of the existence and stability of steady state supported one-dimensional detonation waves. It is beyond the scope of our treatment to reproduce their analysis in detail. Their work is, however, the definitive treatment at this time of this subject. They consider the possible steady one-dimensional flows that can occur in a medium in which an arbitrary number of chemical reactions proceed behind an initiating shock wave, and they investigate the stability of solutions to the chemical rate equations in conjunction with such flows. They show that, under suitable conditions on the chemical rate functions, there are stable solutions resulting in equilibrium final states for detonation velocities equal to or greater than those for an equilibrium Chapman-Jouguet condition corresponding to tangency of the Rayleigh line to the equilibrium Hugoniot curve. They suggest that these solutions correspond to piston-supported detonations after the decay of initiation transients, and that the equilibrium Chapman-Jouguet detonation is stable with respect to the removal of the piston after a sufficiently long time. They also show that the frozen Chapman-Jouguet detonation, in which equilibrium is attained at a point where the flow velocity is sonic in terms of the frozen sound speed, is unstable.

8-7 FINE STRUCTURE OF DETONATION IN GASES AND LIQUIDS

Experimental investigations since the late 1950's have shown that self-sustaining gaseous detonations propagate as three-dimensional nonsteady waves rather than as one-dimensional steady-state waves. In view of this discovery, it is necessary to give a brief discussion of recent developments in the study of detonation structure. For more details the reader is referred to the reviews of Wagner[17]; Oppenheim, Manson, and Wagner[18]; Schott[19]; Soloukhin[20]; Shchelkin[21]; van Tiggelen and de Soete[22]; Strehlow[23]; and Edwards[24].

Although Chapman-Jouguet theory predicts gaseous detonation velocities to within a few percent [25], recent experimental studies [19-21, 25-28] have led to the conclusion that the one-dimensional model of the detonation wave is an approximation. Careful examination of gaseous detonation shows that the detonation front has a fine structure composed of a system of unsteady interacting shocks and is not a plane shock. The existence of such fine structure in self-sustaining gaseous detonation shows the detonation to be a three-dimensional nonsteady

phenomenon that exhibits steady gross characteristics. White[26] first associated the fine structure with turbulence in the reaction zone, but it was later identified with Mach interactions[27-30]. In a self-sustaining detonation, points at which the forward propagating curved shocks intersect travel across the detonation front as waves[25]. These transverse waves occur at the detonation front as Mach stems or triple shock intersections of finite amplitude[31-32]. As shown by Oppenheim and Urtiew[23], the motion of the triple points writes the pattern on the smoked surface in studies of detonation structure employing the smoke track technique developed by Denisov and Troshin[33].

The occurrence and structure of transverse waves have been examined extensively by Strehlow and coworkers[24-37]. The experimental evidence suggests that transverse waves are an inherent property of the flow behind a shock that initiates an exothermic reaction. Transverse waves are produced in initiation of detonation in controlled one-dimensional experiments, and are observed repeatedly in self-sustaining, overdriven, and spherical detinations. Examination of cell patterns on smoke track records shows that transverse waves exhibit a well-regulated spacing in many self-sustaining detonations. The regularity depends on the confining geometry and the nature of the chemical system supporting the detonation. In rectangular tubes, the characteristic size of a regular patter is dictated by the initial pressure level and the amount of diluent present in the reactive mixture. At present, transverse wave spacing is thought to be controlled primarily by induction and recombination zone kinetics, but can be influenced by the tube containing the detonation.

A theoretical treatment of the stability of steady one-dimensional detonation waves, based on the assumption of a square wave reaction zone, was started by Shchelkin[38] and continued by many workers. The restrictions imposed by the square wave model have recently been removed by Erpenbeck[39-41] and Strehlow, et al.[42-43] who considered a more realistic reaction zone. The studies of Erpenbeck on the response of an overdriven discontinuity to a transverse harmonic perturbation in the reaction zone indicate that instability depends on the frequency of the disturbance, the activation energy of the assumed first-order exothermic reaction, and the amount the detonation is overdriven. The stability conditions for high frequency transverse waves show systems with sufficiently low activation energy to be stable. The studies of Strehlow and Fernandes[42] and Barthel and Strehlow[43] on the behavior of a high frequency coherent transverse acoustic wave in the reaction zone give two important results. The first of these is that a shock with exothermic reaction, of Mach number greater than 3, is unstable to a transverse acoustic disturbance. The second is the possibility of the wavefront of a sonic disturbance producing multiple shock contacts which asymptotically approach a regular spacing related to the reaction zone thickness.

Theoretical studies show that hydrodynamic instabilities are to be expected in flows where a shock initiates an exothermic reaction, and are consequently consistent with experimental observations.

Although the mechanism of propagation of a self-sustaining gaseous detonation is qualitatively understood, there is no satisfactory model at the present time for calculating quantitative properties of the fine structure. It can be concluded that the gaseous detonation wave with steady gross properties contains an intrinsic unsteadiness on a scale some 1 order of magnitude greater than the one-dimensional reaction zone thickness. The overall motion is sustained by the collisions of Mach interactions which continually provide new centers of reaction as the shocks propagating forward attenuate. The detonation front as a whole propagates at very close to Chapman-Jouguet velocity, even though the velocity of a leading shock in the front varies from a value 10 to 20 percent above to 10 to 20 percent below the Chapman-Jouguet value. Since the Chapman-Jouguet hypothesis is successful in predicting detonation velocity, it must be of some significance even though at the present time it cannot be justified on structural and stability considerations.

Experimental investigations of self-sustaining detonation in liquids have not been as conclusive as those of self-sustaining detonations in gases. Detonations in liquids are more difficult to study experimentally than detonations in gases because they generate pressures in the 100 kbar

regime. The experimental observation of fine structure in the detonation front in nitromethane and its mixtures with acetone led Dremin[44-47] to postulate that detonations in all liquids should exhibit fine structure similar to that in gases. However, the detonation fronts in nitroglycerin, dinitroglycerin, and tetranitromethane were found[48] to be smooth and to exhibit no fine structure.

REFERENCES

1. Y. B. Zeldovich, J. Exp. and Theoret. Physics (USSR) 10, 542 (1940); NACA Tech. Memo. 1261, 1950.
2. J. von Neumann, Office of Scientific Research and Development, Report No. 541, 1942.
3. W. Döering, Ann. Physik 43, 421 (1943).
4. W. Döering and G. I. Burkhardt, Tech. Report No. F-TS-1227-1A (GDAM A9-T-46).
5. H. Lawton and I. C. Skidmore, *Faraday Soc. Discussions*, No. 22, 188 (1956).
6. W. E. Deal, Phys, Fluids 1, 523 (1958).
7. R. E. Shear, BRL Report No. 1159, Aberdeen Proving Ground, Md., 1961.
8. W. Fickett and W. W. Wood, Phys. Fluids 1, 528 (1958).
9. M. H. Rice, R. G. McQueen, and J. M. Walsh, "Compression of Solids by Strong Shock Waves", *Solid State Physics*, Vol. 6, F. Seitz and D. Turnbull, Eds., Academic Press, New York, 1958.
10. L. V. Altshuler, et al., Soviet Phys. JETP 34, 606 (1958).
11. I. C. Skidmore and S. Hart, *Fourth Symposium (International) on Detonation*, ACR-126, Office of Naval Research, Dept. of the Navy, Washington, D. C., p. 47.
12. M. L. Wilkins, et al., *Fourth Symposium (International) on Detonation*, ACR-126, Office of Naval Research, Dept. of the Navy, Washington, D. C., p. 3.
13. W. W. Wood and J. G. Kirkwood, J. Chem. Phys. 25, 1276 (1956); 29, 957 (1958).
14. S. R. Brinkley, Jr. and J. M. Richardson, *Fourth Symposium (International) on Combustion*, Williams and Wilkins Co., Baltimore, 1953, 450-7.
15. J. G. Kirkwood and W. W. Wood, J. Chem. Phys. 22, 1915 (1954).
16. W. W. Wood and Z. W. Salsburg, Phys. Fluids 3, 549 (1960).
17. H. G. Wagner, Agardograph 41, *Fundamental Data Obtained from Shock Tube Experiments*, A. A. Ferri, Ed., Pergamon, New York, 1961, p. 320.
18. A. K. Oppenheim, N. Manson, and H. G. Wagner, AIAA J. 1, 2243 (1963).
19. G. L. Schott, "Structure, Chemistry and Instability of Detonation in Homogeneous Low-Density Fluids—Gases", *Fourth International Symposium on High Explosive Detonation*, White Oak, Maryland, 1964.
20. R. I. Soloukhin, Soviet Physics Uspekhi 6, 523 (1964).
21. K. I. Shchelkin, Soviet Physics Uspekhi 9, 780 (1965).
22. A. van Tiggelen and G. De Soete, Rev. Inst. Franc. Petrole, Ann. Combust. Liquides 21, 239-84, 455-86, 604-78 (1966).
23. R. A. Strehlow, "Gas Phase Detonations: Recent Devlopments", Combust. Flame 12, 81 (1968).
24. D. H. Edwards, *Twelfth Symposium (International) on Combustion*, The Combustion Institute, Pittsburgh, 1969, p. 819.
25. J. Taylor, *Detonation in Condensed Explosives*, Oxford at the Clarendon Press, 1952, pp. 84-5.
26. D. R. White, Phys. Fluids 4, 465 (1961).
27. H. G. Wagner, *Ninth Symposium (International) on Combustion*, Academic Press, New York, 1963, p. 454.
28. K. I. Shchelkin and Y. K. Troshin, Comb. and Flame 7, 143 (1963).
29. Y. N. Denisov and Y. K. Troshin, *Eighth Symposium (International) on Combustion*, Williams and Wilkins Co., Baltimore, 1962, p. 600.
30. R. E. Duff, Phys. Fluids 4, 1427 (1961).
31. V. V. Mitrofanov, V. A. Subbotin, and M. E. Topchian, Zh. prikl. Mekh. i Tekh. Fiz. 3, 45 (1963).
32. A. A. Borisov and S. M. Kogarko, Dokl. Akad. Nank., S.S.S.R. 149, 623 (1963). Translation: Doklady, *Phys. Chem.*, p. 252.
33. Y. H. Denisov and Y. K. Troshin, Dokl. Akad. Nank., S.S.S.R. 125, 110 (1959). Translation: *Phys. Chem.*, Sect. 125, 217 (1960).
34. R. A. Strehlow, AIAA J. 2, 784 (1964).
35. R. A. Strehlow, R. Liaugminas, R. H. Watson, and J. R. Eyman, *Eleventh*

REFERENCES (Continued)

Symposium (International) on Combustion, Mono Book Corp., Baltimore, 1967, p. 177.
36. R. A. Strehlow, R. Maurer, and S. Rajan, AIAA J. 7, 323 (1969).
37. R. A. Strehlow and C. D. Engel, AIAA J. 7, 493 (1969).
38. K. I. Shchelkin, Sov. Phys. JETP 9 (36), 416 (1959).
39. J. J. Erpenbeck, Phys. Fluids 7, 684 (1964).
40. J. J. Erpenbeck, Phys. Fluids 8, 1192 (1965).
41. J. J. Erpenbeck, Phys. Fluids 9, 1293 (1966).
42. R. A. Strehlow, and F. D. Fernandes, Combust. Flame 9, 109 (1965).
43. H. O. Barthel and R. A. Strehlow, Phys. Fluids 9, 1896 (1966).
44. A. N. Dremin and O. K. Rozanov, Dokl. Akad. Nauk. SSSR 139, 137 (1961).
45. A. N. Dremin, O. K. Rozanov, and V. S. Trofimov, *Zh. Prikl. Mekh. Tekh. Fiz.*, No. 1, 130 (1963).
46. A. N. Dremin, O. K. Rozanov, and V. S. Trofimov, Combust. Flame 7, 2 (1963).
47. S. N. Buravova, A. N. Dremin, O. K. Rozanov, and V. S. Trofimov, *Zh. Prikl. Mekh. Tekh. Fiz.* (Gazodynamika Goreniya), No. 4, 101 (1963).
48. A. N. Dremin and S. D. Savrov, *Fiz. Goreniya Vzryva*, No. 1, 36 (1966).

CHAPTER 9 DETONATION WAVES OF CYLINDRICAL AND SPHERICAL SYMMETRY

9-1 INTRODUCTION

The theoretical development of the previous chapters has been limited to detonation waves in one dimension in which the wave front is planar and the flow behind the front is parallel. A rather complete description of this idealized wave is possible, because of the simple geometry. The theory of plane detonation waves is strictly applicable only to a semi-infinite mass of explosive. The treatment becomes a good approximation to charges of finite size if the dimension of the charge perpendicular to the direction of propagation of the wave is large enough so that edge effects become of negligible importance, and if the dimension in the direction of propagation is large compared to the distance in which transients arising from the initiation process exist.

Explosive charges of practical interest are, of course, of finite size. One expects the one-dimensional theory to apply to a cylindrical charge of explosive, initiated at one end and with the wave propagating in the direction of the axis of the cylinder if the cylinder is contained in a perfectly rigid casing and if the interaction of the explosion products with the casing wall has negligible effect on the main flow behind the detonation wave. Such a situation is allowed in the case of an explosive gas mixture contained in a metal tube if the tube diameter is not too small.

The pressures developed in the explosion reaction of a condensed explosive at the reaction front are of the order of 10^5 atm. At such pressures, material cannot be completely contained and it is impossible to conceive of a perfectly rigid envelope. Consequently, the material velocity of the product gases has a radial component and the flow cannot be one-dimensional. One expects, therefore, that the one-dimensional theory will have asymptotic velocity, becoming the more realistic the larger the diameter of the cylindrical charge. Cylindrical charges of finite diameter are expected to differ in their behavior from that of the ideal one-dimensional charge to a degree that depends on the diameter of the charge and on the nature of the confining envelope.

In a cylindrical charge of explosive, the flow of the reaction products must have cylindrical symmetry. The detonation velocity along a finite cylindrical charge is observed, experimentally, to be constant after a short distance in which initiation transients disappear. It is, therefore, appropriate to assume that the flow in the reaction zone of such a charge is stationary (in a coordinate system moving with the wave). The equations of hydrodynamics for steady flow with cylindrical symmetry are approximately as tractable as those for plane unsteady flow. Some progress has been made in the theoretical description of the flow in steady detonation waves in cylindrical charges, but a theory of the effect of finite charge diameter on the detonation velocity in such charges cannot be said to exist.

A further type of nonparallel flow that has received limited theoretical attention is the flow with spherical symmetry resulting from initiation in a large mass of explosive at a point.

These two instances involving nonparallel flow of the reaction products are the only ones that have been amenable to even limited theoretical study. It is thus apparent that the traditional methods of classical physics have not been employed to describe the detonation process in any actual explosive charge of two or three physical dimensions. The material of this chapter is intended to display the limitations of the one-dimensional theory and to assist in the understanding of the reasons why actual detonations may differ in their properties from the predictions of the theory. In the present state of knowledge, the theory cannot provide all of the design data needed for the rational design of an explosive charge for a particular application.

9-2 THE EFFECT OF CHARGE DIAMETER ON THE DETONATION VELOCITY

Soon after detonating explosives began to be studied, it was observed that the detonation velocity of a cylindrical charge of explosive, initiated at one end and with the wave propagating in the direction of the axis of the charge, depends upon the diameter of the charge

and upon the nature of the charge confinement. The velocity increases with increasing charge diameter in charges with the same confining envelope and with increasing strength of confinement at constant finite diameter. At constant confinement and with increasing diameter, the detonation velocity approaches asymptotically a limiting value which, on physical grounds, we consider to be that predicted by the one-dimensional theory. If D is the observed detonation velocity for charge diameter d (i.e., $D = D(d)$) and D_∞ the ideal value given by one-dimensional theory, then

$$D/D_\infty \rightarrow 1 \text{ as } d \rightarrow \infty \qquad (9\text{-}1)$$

This behavior is illustrated in Fig. 9-1, in which the detonation velocity of RDX at a density of 0.9 g/cm^3 is plotted against the reciprocal of the cylinder radius. The experimental data are seen to be well represented by a straight line. (Experimental data on the variation of detonation velocity with charge diameter have been represented in the literature in graphs employing the radius instead of its reciprocal as abscissa. Since the detonation velocity is expected to approach the ideal limit asymptotically as the radius goes to infinity, there can be no justification for this mode of treatment of the data, calling as it does for an extrapolation of infinity.)

It is found experimentally that the slope of curves such as that of Fig. 9-1 depends strongly on the density of the explosive, its chemical nature, and its state of aggregation. The velocity depends on the charge diameter more strongly for explosives at low loading density than for the same explosive at high loading density, for pressed granular explosives than for homogeneous cast explosives, for composite explosives than for pure explosive compounds, and for explosives of low energy release than for

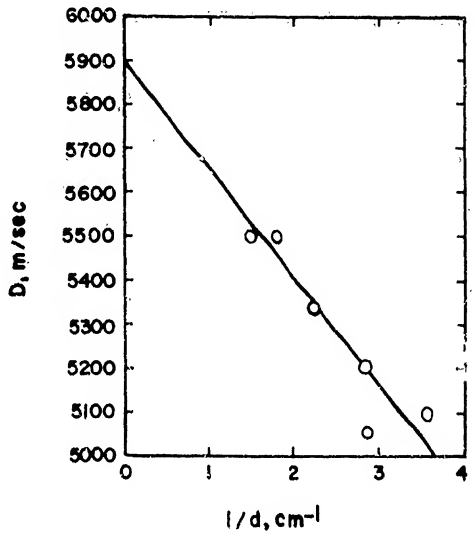

Figure 9-1. Effect of Charge Diameter on the Detonation Velocity of RDX, ρ_o = 0.9 (Ref. 1)

those of high energy release. Thus, a high energy explosive such as PETN has a smaller dependence of velocity on charge diameter than does one such as TNT. Cast TNT has a smaller dependence than does pressed TNT at about the same density. The dependence for a pressed TNT charge of high density is less than that for a pressed charge at low density. At low density, the dependence of the velocity on charge diameter is strongly influenced by the particle size of the explosive, being the greater the greater the particle size. The latter observation suggests that the rate of decomposition of a granular explosive is controlled by the rate of a surface reaction of the individual particles. By contrast, in homogeneous explosives that can be expected to undergo a bulk homogeneous decomposition reaction, only a relatively small dependence of detonation velocity on charge diameter is observed.

Although the general features of the dependence of detonation velocity on charge diameter and the nature of the confinement have been studied experimentally for many years, attempts to explain the effect in terms of the hydrodynamics and thermodynamics of the system were not made until about 1940. Since that time, a qualitative understanding of the effect has been gained but a satisfactory quantitative theory of the phenomenon does not exist.

In the one-dimensional case, the Chapman-Jouguet condition has been shown to define a surface across which energy cannot be transmitted. In the infinite charge of explosive, or alternatively in a finite charge under ideal confinement, the reaction is complete at this surface and this surface lies an infinite distance downstream from the leading edge—the shock wave—of the detonation wave. In the last chapter, it was stated that steady reaction zones can be shown to exist between a surface defined by a frozen sound velocity Chapman-Jouguet condition and the shock wave, where this surface is a finite distance from the shock front in a region where the reaction is incomplete, but that such steady flows are unstable. These theoretically steady but unstable configurations of shock wave and rarefaction front were called subideal Chapman-Jouguet states. If a cylindrical charge of explosive is imperfectly confined, the high pressure explosion products will expand laterally, and this lateral expansion will begin at the intersection between the initiating shock and the boundary of the charge. Thus, both in the reaction zone, which we may assume to be a region of steady flow, and in the expansion wave, which cannot be a region of steady flow, the vector particle velocity of the explosion products will have a nonvanishing radial as well as axial component. The region of steady flow is followed by a two-dimensional rarefaction wave that is determined by boundary conditions prescribed on the interface between explosion products and surrounding medium. As a consequence, the leading edge of the rarefaction wave, propagating into the explosion products with the local velocity of sound, must be fixed in space relative to the position of the shock front. Shock front and head of rarefaction wave are surfaces of revolution about the axis of the cylindrical charge defining a reaction zone having the shape of a meniscus and a volume characterized by two linear dimensions, of which one is the diameter of the explosive charge and the other can be taken to be the distance on the axis of the charges between the shock front and the rarefaction front.

As far as the propagation of the detonation wave is concerned, the reaction is arrested at an intermediate stage corresponding to only a partial release of the energy of explosion. Energy released in the rarefaction wave cannot be transmitted across the sonic surface comprising the head of the rarefaction wave, and it is expended in partial support of the lateral expansion of the gas in the rarefaction wave. Only the energy that is released ahead of the sonic surface is effective in supporting the propagation of the detonation wave. The consequence of the establishment of a two-dimensional analogue of the subideal Chapman-Jouguet state that has previously been considered, with an energy deficit caused by incomplete reaction on the sonic surface, is a decrease in the detonation velocity.

There is a further mechanical consequence of the lateral expansion of the reaction products in finite cylinders of explosive. Work is performed in maintaining the radial component of particle velocity which, as we have already noted, is nonvanishing in the steady reaction zone. As a consequence, not all of the energy released in the region of steady flow is effective in

supporting the axial propagation of the wave, and the detonation velocity is less for diverging flow than for parallel flow with the same energy release.

Divergent flow across a shock front implies a curved shock front and vice versa. Flow crossing an oblique shock is turned toward the shock. Therefore, the shock front is convex toward the intact explosive and concave toward the reaction zone. The assumptions that have been made in formulating the model that has been described are supported by experimental observations of the curvature of the front in cylindrical explosive charges. The observations are made with a streak camera with the axis of the cylinder oriented in the direction of the camera optical axis and with the wave propagating toward the camera. The detonation wave is observed to emerge first from the explosive charge at the axis.

The curvature of the shock front, the divergence of the flow in the reaction zone, and the extent of the region of steady flow are determined by the diameter of the charge and the nature of the confinement. The theoretical calculation of the curvature (or, alternatively, of the flow divergence) would require the solution of a complex hydrodynamical problem involving the formation of shock wave or waves in the exterior medium and requiring the determination of the location of the contact surface between explosion products and exterior medium. In a bare charge, surrounded by air, a cylindrically symmetric shock wave will be propagated outward in the air. If the charge is cased, a shock wave is propagated into the casing. If the casing is thin, the problem is further complicated by the subsequent reflection of this shock wave at the boundary between casing and air, resulting in a reflected wave and a transmitted wave into the air surrounding the cased charge.

The shape of the reaction zone may be characterized by the diameter d of the reaction zone and the axial distance a_o of separation between shock front and the head of the rarefaction wave. If the surrounding medium is defined, and the problem of fully describing its motion could be solved, these two dimensions would fully characterize the region of steady reaction upon which the propagation of the wave depends. The only dimensionless combination of these lengths is the ratio a_o/d, and no other characteristic lengths can occur in the theory. Therefore, from dimensional considerations alone, we can write

$$D/D_\infty = F(a_o/d) \tag{9-2}$$

The function F can always be represented by its MacLaurin expansion. Taking into account the asymptotic behavior summarized by Eq. 9-1, we can write

$$D/D_\infty = 1 + A(a_o/d) + \cdots\cdots \tag{9-3}$$

where A is a constant and where for small values of a_o/d the higher order terms can be neglected. It will be noticed that the data shown in Fig. 9-1 is well represented by an equation linear in $1/d$. It is, in fact, generally true that experimental data for the velocity deficit in finite cylindrical charges can be represented, for small values of the deficit, by Eq. 9-3. The proportionality constant Aa_o is a function of the confinement on the charge for charges of a given density.

9-3 DIVERGING FLOW WITHIN A CYLINDRICALLY SYMMETRIC STEADY REACTION ZONE

When a detonation wave progresses in the direction of the axis of a cylindrical charge of explosive, it is found experimentally that the rate of propagation is constant and that the leading shock wave is convex in the direction of propagation of the wave. These observations imply that a steady reaction zone exists and that the reaction zone has cylindrical symmetry. In order to connect such a flow region with a stationary (in laboratory coordinates) downstream boundary on which the values of the various quantities describing the flow are prescribed, it is necessary to postulate a cylindrically symmetric unsteady expansion wave. Thus, we may consider the flow illustrated schematically by Fig. 9-2, in which the coordinate system is at rest in the wave front, the x-axis being coincident with the axis of the cylindrical charge of explosive with origin in the wave front and with the radial coordinate r measuring the distance from the x-axis. The intact explosive moves from right to left with constant velocity $w_o = D$. To the left of the wave front, the particle velocity vector has an axial component w_x and a radial component w_r.

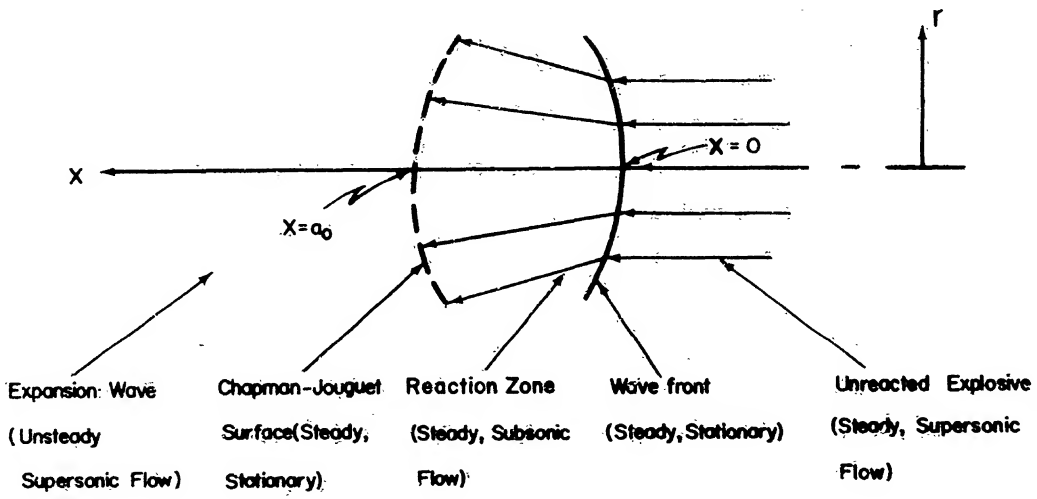

Figure 9-2. Cylindrically Symmetric Flow Through a Detonation Wave

If u and ω are the axial and radial components, respectively, of particle velocity relative to laboratory coordinates,

$$w_x = D - u$$
$$w_r = \omega \tag{9-4}$$

Wood and Kirkwood[2] have considered the flow illustrated by Fig. 9-2, assuming a single chemical reaction in the steady reaction zone. The progress of such a reaction can be described by a progress variable λ which has the value 0 at the wave front where the reaction is initiated and the value 1 when the reaction is complete. The rate equation for such a reaction can be written

$$\frac{d\lambda}{dt} = R \tag{9-5}$$

where the rate function R is a function of the instantaneous state of the system. Since the mobile time derivative is

$$\frac{d}{dt} = \frac{\partial}{\partial t} + (D - u)\frac{\partial}{\partial x} + \omega\frac{\partial}{\partial r} \tag{9-6}$$

Eq. 9-5 becomes

$$(D - u)\frac{\partial\lambda}{\partial x} + \omega\frac{\partial\lambda}{\partial r} = R$$

for the steady flow under consideration.

The differential equations for the conservation of mass, momentum, and energy are given in par. 2-6. For cylindrically symmetric flow, they are the equation of continuity

$$\frac{dp}{d} + \rho\left(\frac{\partial u}{\partial x}\right) + \frac{\rho}{r}\left[\frac{\partial(r\omega)}{\partial r}\right] = 0 \tag{9-7}$$

the equations of motion

$$\left.\begin{aligned}\frac{du}{dt} + \frac{1}{\rho}\left(\frac{\partial p}{\partial x}\right) &= 0\\ \frac{d\omega}{dt} + \frac{1}{\rho}\left(\frac{\partial p}{\partial r}\right) &= 0\end{aligned}\right\} \tag{9-8}$$

and the equation for energy transport

$$\frac{de}{dt} = T\left(\frac{ds}{dt}\right) + \frac{p}{\rho^2}\left(\frac{d\rho}{dt}\right) + R\Delta F \tag{9-9}$$

where ΔF is the change in free energy for the reaction occurring in the reaction zone.

For the postulated steady flow, Wood and Kirkwood[2] transform these hydrodynamic equations into the form

$$\left.\begin{aligned}\left(\frac{D - u}{\rho c^2}\right)\frac{\partial p}{\partial x} - \frac{\partial u}{\partial x} &= \sigma R - \frac{\omega}{\rho c^2}\left(\frac{\partial p}{\partial r}\right) - \frac{1}{r}\left[\frac{\partial(r\omega)}{\partial r}\right]\\ (D - u)\frac{\partial u}{\partial x} + \omega\left(\frac{\partial u}{\partial r}\right) &= \frac{1}{\rho}\left(\frac{\partial p}{\partial x}\right)\\ (D - u)\frac{\partial\omega}{\partial x} + \omega\left(\frac{\partial\omega}{\partial r}\right) &= -\frac{1}{\rho}\left(\frac{\partial p}{\partial r}\right)\\ (D - u)\left[\frac{\partial e}{\partial x} - \frac{p}{\rho^2}\left(\frac{\partial\rho}{\partial x}\right)\right] + \omega\left[\frac{\partial e}{\partial r} - \frac{p}{\rho^2}\left(\frac{\partial\rho}{\partial r}\right)\right] &= 0\end{aligned}\right\} \tag{9-10}$$

where c is here the frozen sound speed

$$c^2 = (\partial p/\partial\rho)_{s,\lambda} \tag{9-11}$$

and σ is the quantity

$$\sigma = -\frac{1}{\rho c^2}\left(\frac{\partial p}{\partial\lambda}\right)_{c,\rho} \tag{9-12}$$

Instead of attempting a complete solution of these equations, Wood and Kirkwood specialize them to the axis of symmetry ($r = 0$) where $w = 0$, $\partial p/\partial r = 0$ and $\partial\rho/\partial r = 0$. When the results are solved for the derivatives of the axial component of particle velocity and pressure with respect to the coordinate x, there are obtained

$$\left.\begin{aligned}\left(\frac{\partial u}{\partial x}\right)^0 &= -\frac{1}{G}\left[\sigma R - 2\left(\frac{\partial\omega}{\partial r}\right)^0\right]\\ \left(\frac{\partial p}{\partial x}\right)^0 &= -\rho\frac{(D - u)}{G}\left[\sigma R - 2\left(\frac{\partial w}{\partial r}\right)^0\right]\\ \frac{\partial e}{\partial x} - \frac{p}{\rho^2}\left(\frac{\partial\rho}{\partial x}\right) &= 0\end{aligned}\right\} \tag{9-13}$$

where

$$G = 1 - (D - u)^2/c^2 \tag{9-14}$$

and where the superscript zero indicates that the derivative so designated is evaluated on the axis, $r = 0$.

Now, the postulated flow has been assumed to consist of a steady reaction zone that is connected to the rear boundary by an unsteady expansion wave. The surface separating these two regimes must be a weak discontinuity. At such a surface, the axial derivatives of pressure and axial component of particle velocity are discontinuous. If these quantities are discontinuous on the surface separating the two regions, and in particular if they are discontinuous at the intersection of this surface with the x-axis at the point labeled $x = a_o$ in Fig. 9-2, the right-hand side of the first two of Eqs. 9-13 are indeterminate at $x = a_o$. Therefore, at $x = a_o$

$$G = 0 \text{ or } D = u + c \tag{9-15}$$

and

$$\frac{\partial \omega}{\partial r} = \sigma R/2 \tag{9-16}$$

Eq. 9-15 is identical in form to the Chapman-Jouguet condition for the plane detonation wave. It is appropriate, therefore, to refer to the surface separating the steady reaction zone and the unsteady expansion wave as the Chapman-Jouguet surface. The relation states that the rarefaction wave advances into the explosion products with the local velocity of sound. However, from Eq. 9-16 we conclude that the Chapman-Jouguet surface is fixed in space relative to the initiating shock wave. The surface intersects the axis of symmetry at the point $x = a_o$ at which, according to Eq. 9-16 the reaction is incomplete; $R > 0$, if $\partial\omega/\partial r > 0$. Therefore, not all of the energy of the explosion reaction is released in the steady reaction zone. Furthermore, the Chapman-Jouguet point defined by Eq. 9-15 is a frozen Chapman-Jouguet point, defined in terms of the frozen sound speed.

The distance a_o is a characteristic length of the cylindrically symmetric diverging flow and may be employed to characterize the thickness of the reaction zone.

Eqs. 9-13 can be integrated to yield integral relations analogous to the Hugoniot equations for plane, one-dimensional flow through a steady reaction zone, obtained in the last chapter. With the aid of the conditions on the axis of symmetry relating the state of the unshocked explosive to the shocked unreacted explosive, Wood and Kirkwood obtained the expressions,

$$\frac{\rho}{\rho_o}\left(1 - \frac{u}{D}\right) = 1 - L(x)$$

$$p = \rho_o D^2 \left(1 - \frac{\rho_0}{\rho}\right) \left\{1 + \frac{2\rho_o/\rho}{1 - \rho_o\rho}\left[2L(x) - \frac{\rho}{\rho_o}\Omega(x)\right]\right\}$$

$$e - e_o = \tfrac{1}{2}p\left(\frac{1}{\rho_o} - \frac{1}{\rho}\right) + D^2\left\{\left(1 - \frac{\rho_o}{\rho}\right)\Omega(x) - 2\frac{\rho_o}{\rho}L(x)\right\} \tag{9-17}$$

where

$$L(x) = \frac{1}{\rho_o D}\int_0^x \rho\left(\frac{\partial \omega}{\partial r}\right)^0 dx$$

$$\Omega(x) = \frac{1}{D}\int_0^x \left(\frac{\partial \omega}{\partial r}\right)^0 dx$$

In deriving Eqs. 9-17, terms quadratic in $(\partial\omega/\partial r)^0$ have been neglected. Eqs. 9-17 are generalized Hugoniot equations for cylindrically symmetric diverging flow through a steady reaction zone. They determine the state of the material in the reaction zone and on the axis in terms of the state of the intact explosive ahead of the wave. For parallel flow, $\partial\omega/\partial r = 0$ and Eqs. 9-17 become identical with the Hugoniot equations that were obtained in the last chapter for parallel flow.

When the conservation conditions, as derived by Wood and Kirkwood, are analyzed, it can be seen that they differ from the analogous expressions for parallel flow in an important aspect. As a mechanical consequence of the divergent flow, the propagation velocity is less than that for parallel flow for the same energy release at the Chapman-Jouguet point. A further decrease in propagation velocity is the result, in principle, of the fact that the reaction is not complete at the Chapman-Jouguet point.

In order to make use of these expressions, it is necessary to obtain a relation for the radial flow

divergence $\partial\omega/\partial x$ on $r = 0$ as a function of x. To do this exactly would require the complete solution of the flow equations subject to boundary conditions prescribed on the interface between explosion gases and exterior medium. Wood and Kirkwood obtain an approximate relation by using the law of conservation of mementum to relate $\partial\omega/\partial r$ to $\partial^2 p/\partial r^2$ and then employing an estimate of the latter quantity. When the second of the equations of motion is differentiated—specialized to the axis $r = 0$—and then integrated with neglect of terms of order $(\partial\omega/\partial r)^2$, they obtain

$$\left(\frac{\partial\omega}{\partial r}\right)^0 = \left(\frac{\partial\omega}{\partial r}\right)^0_{x=0} - \frac{1}{\rho_o D}\int_0^x \left(\frac{\partial^2 p}{\partial r^2}\right)^0 dx \qquad (9\text{-}18)$$

The quantity $(\partial\omega/\partial r)^0$ at $x = 0$ can be expressed in terms of the radius of curvature of the shock front at the axis s by

$$\left(\frac{\partial\omega}{\partial r}\right)^0_{x=0} = \frac{u(0,\,0)}{s} \qquad (9\text{-}19)$$

where $u(0, 0)$ is the particle velocity at $x = 0, r = 0$. The second radial derivative of the pressure is estimated by means of a simplified model of the geometry of the reaction zone, shown schematically by Fig. 9-3. It is assumed that the Chapman-Jouguet surface is a plane perpendicular to the x-axis at $x = a_o$. This surface intersects the curved shock front, as is shown. It is further assumed that the portion of the curved shock front ahead of the Chapman-Jouguet surface can be represented with sufficient precision by a segment of a sphere of radius s. The pressure $p_s(x)$ on the shock front at a point where the axial coordinate is x can be represented approximately be an expansion about the pressure on the axis

$$p_s(x) = p(x,\,0) + r\left(\frac{\partial p}{\partial r}\right)^0 + \frac{r^2}{2}\left(\frac{\partial^2 p}{\partial r^2}\right) + \cdots \qquad (9\text{-}20)$$

The second term on the right-hand side of this equation vanishes because of the cylindrical symmetry. In approximation $r^2 = 2sx$. If the further approximation is made that the shock

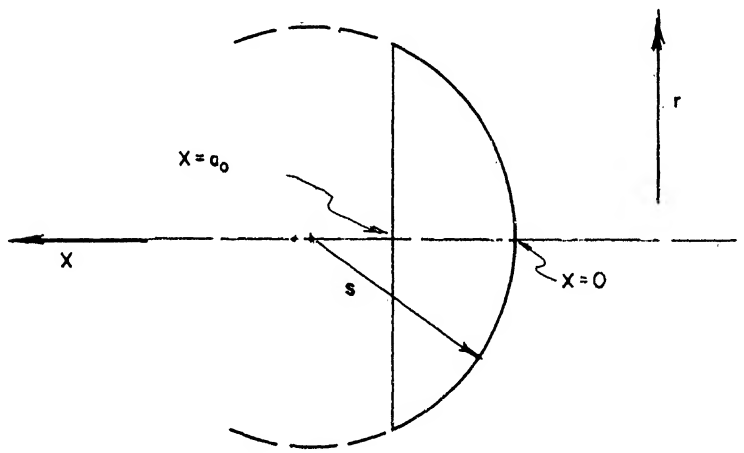

Figure 9-3. Model of the Reaction Zone Employed by Wood and Kirkwood

pressure is constant on the shock surface $p_x = p(0, 0)$, Eq. 9-20 yields the desired relation in approximate form

$$\left(\frac{\partial^2 F}{\partial r^2}\right)^0 = \frac{1}{xs}\left[p(0, 0) - p(x, 0)\right] \quad (9\text{-}21)$$

By use of Eqs. 9-18, 9-19, and 9-21, the expression for $(\partial\omega/\partial r)^0$ becomes

$$\left(\frac{\partial \omega}{\partial r}\right)^0 = \frac{u(0, 0)}{s}\left\{1 - \int_0^x \left[1 - \frac{p(x, 0)}{p(0, 0)}\right]\frac{dx}{x}\right\} \quad (9\text{-}22)$$

where higher order terms have again been neglected.

Additional approximations are made to obtain an approximate explicit solution. Wood and Kirkwood assume that the pressure profile on the axis is square with

$$\left.\begin{aligned} p &= p(0, 0) \quad , \quad x < a_o \\ p &= p_1 \quad , \quad x = a_o \end{aligned}\right\} \quad (9\text{-}23)$$

where p_1 is the pressure on the Chapman-Jouguet surface at the axis. Using a free volume equation of state for the explosion products and the typical values $\rho_o/[\rho(a_o, 0)] = 0.7$ and $\rho_o/[\rho(0,0)] = 0.55$, they finally obtain the relation

$$D/D_\infty = 1. - 3.5 a_o/s \quad (9\text{-}24)$$

This relation, although based on an approximate model of the reaction zone and with the coefficient evaluated for a particular physical explosive, exhibits the nature of the dependence of the detonation velocity in a finite cylindrical charge on the radius of curvature of the shock front.

9-4 THEORIES OF THE CHARGE DIAMETER EFFECT

The analysis by Wood and Kirkwood of the consequences of divergent flow in a steady reaction zone provides a considerable insight into the conditions that obtain in a cylindrical charge of explosive along the axis of which a detonation wave is propagating with constant velocity. However, not even their approximate result, Eq. 9-24 relating the velocity deficit to the radius of curvature of the shock front, is a satisfactory theory of the charge diameter effect since the radius of curvature is difficult to measure experimentally and it cannot at present be calculated in terms of the dimensions of the charge. A complete theory of the charge diameter effect would make possible the calculation of the velocity deficit $U_\infty - U$ from a knowledge of a characteristic time or length characterizing the chemical reaction, the diameter of the charge, and the properties of the confining media. Several authors have attempted this more elaborate program. In each case, the analysis has been based upon a drastically simplified physical model, the mathematical description of which has involved a variety of mathematical and numerical approximations, together with various self-contradictory initial assumptions. These treatments have had as a common aim the evaluations of the function $F(a_o/d)$ of Eq. 9-2.

The resulting theories have always been employed in an inverted sense. Since kinetic data permitting an *a priori* calculation of a characteristic reaction time for condensed explosives is, in the main, nonexistent, the theories have been employed to deduce the characteristics of the reaction zone from the experimentally determined dependence of detonation velocity on charge diameter. When expressed in terms of a "reaction zone length", the various different models yield results differing by a factor of about 2 and thus are in agreement as to order of magnitude. In view of the arbitrary nature of the underlying assumptions and the approximations entering into the subsequent derivations, there exists considerable uncertainty as to the physical significance to be ascribed to the parameters of the various theories. It is the authors' opinion that they have little to recommend them over the simple empirical result expressed by Eq. 9-3. In these circumstances, and because detailed treatments are readily available in the literature, we shall not attempt a detailed exposition of the different theories but shall limit our discussion to a description of the models and a statement of the results.

Two theoretical treatments of the nonideal detonation velocity in a cylindrical charge of explosive of finite radius have a common basic assumption, namely, of the hydrodynamic

equations, only the equation of continuity differs from the form for parallel flow due to the expansion in the reaction zone. Both treatments assume that the reaction is complete a finite distance a_o behind the shock front and that this parameter is, therefore the thickness of the reaction zone.

The physical model employed by Jones is shown schematically in Fig. 9-4(A). Although the shock front is curved when the flow diverges, near the axis it is plane. Jones assumed that it is plane across the cross section of the charge. He approximated the divergence of the flow near the axis by that of a Prandtl-Meyer expansion around a corner a distance from the axis equal to the original radius of the charge. In addition to the assumption of complete reaction, Jones assumed the one-dimensional form of the Chapman-Jouguet condition (Chapter 9) and he employed the Abel equation of state with a covolume appropriate for TNT and an adiabatic exponent of 3. The equations resulting from these assumptions are solved graphically and the results are tabulated. They can be expressed by the relationship

$$(D/D_\infty)^2 = 1 - 0.8\,(2a_o/d)^2 \qquad (9\text{-}25)$$

Eyring, Powell, Duffey, and Parlin[4] adopted a model consisting of curved shock front and a parallel curved surface of complete reaction as shown schematically by Fig. 9-4(B). They assumed that the curved shock front is made up of spherical segments and that the radially divergent flow behind a spherical detonation wave that is described in the next paragraph occurs behind each spherical segment of the curved shock front. The piecewise representation of steady flow in a cylindrical system by spherically divergent flow is self-contradictory since the radius of curvature of a spherical detonation increases with time and, therefore, a spherical detonation is not steady. Eyring and his coworkers obtained relations between the ratio D/D_∞ and the ratio of the radius of curvature to the reaction zone length a_o, assuming that the reaction is complete at the surface a distance a_o behind the shock front. Using these results, they performed calculations of the detonation velocity for a typical solid explosive described by an Abel equation of state for given width of reaction zone and charge radius. In these calculations, the curved front was constructed from connected spherical segments, the spherical radii of which decrease as one moves outward from the axis of the charge. The construction was subject to a requirement that the whole wave have the same constant velocity in the axial direction. For a charge surrounded by air, the wave front was required to reach the surface with an angle of 90 deg between the charge axis and the normal to the final segment. In its detail, the development of this theory is algebraically complex. The results of the calculations were represented by the empirical formula

$$D/D_\infty = 1 - a_o/d \qquad (9\text{-}26)$$

which is identical in form with Eq. 9-3 and in which the proportionality constant is unity.

Cook has based his treatment of the charge diameter effect on a fundamental assumption different from that employed by Jones and by Eyring, and their coworkers. The latter authors have assumed that the reaction is complete on the Chapman-Jouguet surface and have ascribed the velocity deficit in finite cylindrical charges to the mechanical effects of the diverging flow. Cook assumes that the flow is parallel in the reaction zone up to the Chapman-Jouguet surface and ascribes the velocity deficit to the fact that only a portion of the energy of explosion is released in the region of steady flow, the remainder being dissipated in the expansion wave. He visualizes the steady reaction zone as having a conical shape of height a_o as shown schematically in Fig. 9-4(C). This distance is determined by the intersection with the charge axis of the rarefaction wave moving in from the side, calculated from

$$a_o = \alpha\, d' \qquad (9\text{-}27)$$

where α is a constant having a value between 0 and 1 and d' is a corrected diameter

$$d' = d - 0.6 \text{ cm} \qquad (9\text{-}28)$$

Cook assumes that any reaction occurring at $x > a_o$ does not effect the steady zone. According to these assumptions, the velocity deficit is due to the fact that $a_o < a_1$ where a_1 is the distance on the axis at which the reaction would be complete. These assumptions imply that $D = D_\infty$

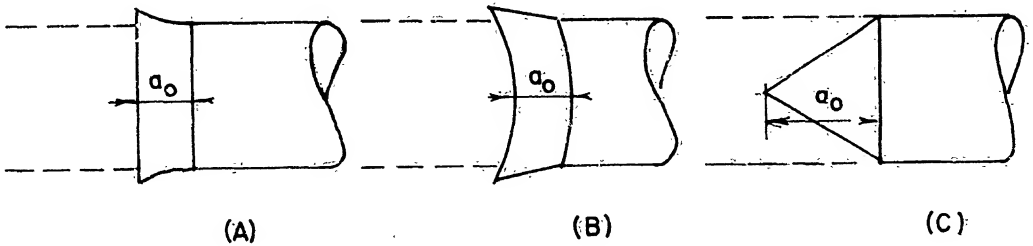

Figure 9-2: Models of the Reaction Zone Employed by (A) Jones, (B) Eyring and Coworkers, and (C) Cook

when $a_o \geq a_1$ and that no diameter effect is then observed. This deduction is not consistent with the experimental observation that D approaches D_∞ asymptotically. Cook made the further assumption that pressure, density, and particle velocity are constant between the shock front and the Chapman-Jouguet plane. With these assumptions, he deduced the relation,

$$\left.\begin{aligned} (D/D_\infty)^2 &= 1 - \left[1 - \frac{4}{3}\,(a_o/a_1)\right]^2, \quad a_o < a_1 \\ D/D_\infty &= 1, \quad a_o \geq a_1 \end{aligned}\right\} \quad (9\text{-}30)$$

The distance a_o is to be calculated from Eq. 9-27. The distance a_1 can in principle be calculated if a reaction mechanism yielding a finite time to complete the reaction is employed, or it may be treated as an adjustable parameter. Such a mechanism is provided if the surface burning of grains of granular explosive is the step controlling the rate of release of explosion energy. In a homogeneous explosive—where the reaction is homogeneous—$a_1 = \infty$, and Eq. 9-30 does not predict a charge diameter effect, which is not in accord with experience.

The assumptions upon which Cook bases his treatment constitute a very substantial oversimplification of the flow within the reaction zone. The results deduced from his model are not in particularly good agreement with experiment. In the next paragraph, we show that the curvature of the wave front can be simply described by a treatment that does not require use of arbitrary assumptions.

9-5 THE RELEASE WAVE MODEL

The release wave model is a description of reaction wave geometry that has been developed by Eichelberger[9] based upon the method of characteristics, for prediction of the impulse imparted to an element of surface area on an explosive charge of arbitrary geometry. Its virtues are simplicity and versatility, but sacrifices of precision are required in order to obtain these advantages.

In principle, the model describes the propagation of isobars in the rarefaction following an idealized detonation wave. The propagation of the detonation front from the initiation source is described by means of Huygen's principle. As the front sweeps the boundary of the explosive charge, it progressively initiates a simple, centered rarefaction. To each isobar, or characteristic surface, in the rarefaction a specific density, pressure, and propagation velocity can be assigned; thus, barring interactions among characteristics initiated from intersecting boundaries or convergence due to complex geometries. Accordingly, Huygen's principle can be used to describe the propagation of each characteristic.

The special simplifications inherent in a polytropic gas law with $\kappa = 3$ are exploited in order to salvage the concept; for this specific condition, rarefactions from different sources penetrate without change. Thus, when rarefactions from several surfaces affect the impulse delivered at a point on the charge—as is generally the case for real, three-dimensional charges—Fermat's principle of least time can be used to determine the earliest time of arrival of a characteristic surface identified with a given pressure. Fortunately for the model, the best measurements of equation of state of explosive products indicate that the polytropic gas law, with a value of $\kappa = 3$ (actually between 2.8 and 2.9) describes the gases through the entire region from the C-J plane to very low pressures.

In applications to date, the reaction zone in the explosive has been neglected, although this is not a necessary feature of the model. A region of constant thickness and pressure distribution, between the detonation front and the rarefaction, could be added without signficant increase in complexity.

The model, then, uses a histogram representation of the pressure behind a one-dimensional pulse, as illustrated in Fig. 9-5. The precision of the results depends upon the number of elements into which the pulse is divided. The values of particle velocity, sound velocity, etc. associated with each finite segment of the pulse are determined by use of one-dimensional theory. The subsequent procedure can follow either of two directions. The pressure distribution behind the detonation front can be developed by constructing the isobars in the detonation products as illustrated in Fig. 9-6. Alternately, the impulse delivered at a selected point on the surface can be estimated by applying Fermat's principle, determining the

time of arrival of each isobar at the selected point, synthesizing the pressure-time history at the selected point, and integrating.

As the ultimate in simplicity, for ease of calculation, a single square pulse has been used to replace the histogram composed of several elements. For rough approximations, a pulse bounded by the detonation wave and by a "release wave" whose propagation velocity is 0.6 times the detonation rate suffices. The amplitude of the square pulse is adjusted to make the total impulse equal to that of the real pulse for a one-dimensional case. In this simplified version, the release wave model very closely resembles the "detonation head" concept described by Cook; there is no claim of physical reality in the square pulse version of the release wave model, however.

Refinements to the model have been developed to permit handling of confined boundaries, using simple, centered rarefactions with an artificial delay time and displacement of the boundary.

9-6 THE SPHERICAL DETONATION WAVE INITIATED AT A POINT

The expanding detonation wave with spherical symmetry is the only instance of a three-dimensional transient wave that has received attention. This case is of practical interest since it represents the immediate result of a localized initiating source embedded in a mass of explosive. G. I. Taylor[7] has analyzed the dynamics of spherical detonation from a point and has demonstrated the theoretical existence of a particular flow, i.e., that the particular flow resulting from his assumptions is compatible with the conservation equations and therefore a possible flow. His analysis does not prove that such a flow is the actual result of the point initiation of a detonating explosive.

Taylor assumed that the reaction is instantaneous, resulting in a wave whose reaction zone is of zero thickness. The model employed is thus the spherical analogue of that used in the elementary theory of plane

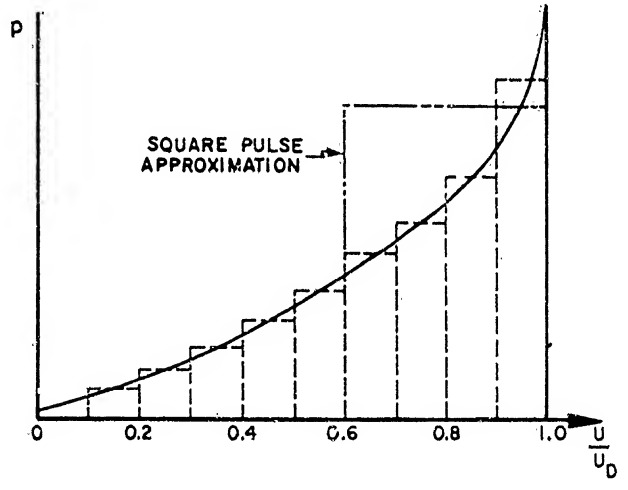

Figure 9-5. Typical Histogram Representation of the Pressure Pulse for Use in "Release Wave" Calculations Together With the Simplified Square Pulse Approximation

detonation waves, given in Chapter 6. He examined the possibility of a flow for which the Chapman-Jouguet condition $D = u_1 + c_1$ is satisfied at a spherical surface expanding with radial velocity D, where D was assumed to be constant. Under these assumptions, all of the properties behind the wave front are easily shown to be functions of the single variable $x = r/t$, where r is the radial coordinate, and the flow is said to be self-similar.

The equations of continuity and motion for spherically symmetric radial flow are given in par. 2-6. They can be written

$$\left.\begin{aligned} \frac{\partial \rho}{\partial t} + u\left(\frac{\partial \rho}{\partial r}\right) + \rho\left(\frac{\partial u}{\partial r}\right) &= -\frac{2\rho u}{r} \\ \frac{\partial u}{\partial t} + u\left(\frac{\partial u}{\partial r}\right) + \frac{1}{\rho}\left(\frac{\partial p}{\partial r}\right) &= 0 \end{aligned}\right\} \quad (9\text{-}31)$$

where u is the radial particle velocity. Since the reaction is assumed to be complete at the wave front, the flow behind the front is isentropic, $\partial s/\partial t + u\partial s/\partial r = 0$, and the pressure can be eliminated from the second of Eqs. 9-31 by the introduction of the sound velocity c. The condition that the density and particle velocity depend only on the variable x can be written

$$\left.\begin{aligned} \frac{\partial u}{\partial t} + x\left(\frac{\partial u}{\partial r}\right) &= 0 \\ \frac{\partial \rho}{\partial t} + x\left(\frac{\partial \rho}{\partial r}\right) &= 0 \end{aligned}\right\} \quad (9\text{-}32)$$

Combining Eqs. 9-31 and 9-32, and introducing the sound velocity, we obtain

$$\left.\begin{aligned} (u - x)\frac{du}{dx} + \frac{c^2}{\rho}\left(\frac{d\rho}{dx}\right) &= 0 \\ (u - x)\frac{d\rho}{dx} + \rho\left(\frac{du}{dx}\right) + \frac{2u\rho}{x} &= 0 \end{aligned}\right\} \quad (9\text{-}33)$$

Following Taylor, we introduce the variables

$$\left.\begin{aligned} \zeta &= u/x \\ \Psi &= u/c \end{aligned}\right\} \quad (9\text{-}34)$$

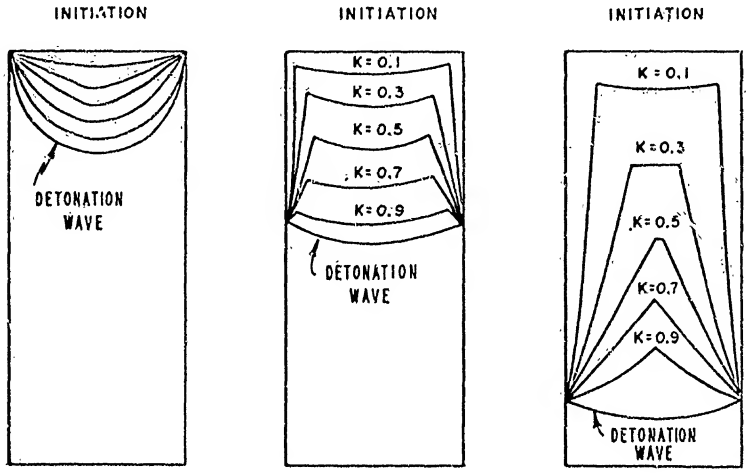

Figure 9-6. Illustration of Progress of Characteristic Surfaces in a Three-dimensional Explosive Charge, as Described in the "Release Wave" Theory

in terms of which Eqs. 9-33 become

$$\left.\begin{aligned} \frac{d\ell n\zeta}{d\ell nx} &= \frac{3\zeta^2 - (1-\zeta)^2\Psi^2}{(1-\zeta^2)\Psi^2 - \zeta^2} \\ \frac{d\ell n\Psi}{d\ell nx} &= \frac{\zeta[2\zeta - (1-\zeta)\Psi^2 f]}{(1-\zeta^2)\Psi^2 - \zeta^2} \end{aligned}\right\} \quad (9\text{-}35)$$

where $f = 2\,(d\ell n\, c/d\ell n\rho)$. To integrate these equations, it is convenient to employ the quantity $\phi = c/D = \zeta x/(\Psi D)$ as independent variable. Employing the relation

$$\frac{d\phi}{\phi} = -\frac{d\Psi}{\Psi} + \frac{d\zeta}{\zeta} + \frac{dx}{x} \quad (9\text{-}36)$$

Eqs. 9-35 are transformed to

$$\left.\begin{aligned} \frac{d\Psi}{d\phi} &= \frac{2\zeta - (1-\zeta)\Psi^2 f}{\phi(1-\zeta)\Psi f} \\ \frac{d\zeta}{d\phi} &= \frac{3\zeta^2 - (1-\zeta)^2\Psi^2}{\phi(1-\zeta)\Psi^2 f} \\ \frac{d\ell nx}{d\phi} &= \frac{(1-\zeta)^2\Psi^2 - \zeta^2}{\phi\,\zeta\,(1-\zeta)\,\Psi^2 f} \end{aligned}\right\} \quad (9\text{-}37)$$

Eqs. 9-37 are integrated numerically inward from the wave front at which point the dependent variables are defined by the Hugoniot equations and the Chapman-Jouguet condition. For the flow behind the wave front, the pressure and density are known functions of the sound velocity along the isentrope terminating in the Chapman-Jouguet state.

Taylor has performed the integration for explosion products treated as an ideal polytropic gas. Shear[8] has performed the integration for the explosion products of the explosive Pentolite at a loading density of 1.65 g/cm^3. His results are given in Figs. 9-7 and 9-8, where they are compared with his calculations for the plane detonation wave that were cited in Chapter 8. The particle velocity becomes zero at $r/(Dt) = 0.43$ and the gas between this point and the center of symmetry is at rest. Approximately 93 percent of the mass of the explosion products is contained by the region at rest.

In Taylor's analysis, the radial gradients of particle velocity, pressure, and density are infinite at the wave front. It is stated that these infinite rates of change probably would not occur if account were taken of the finite reaction time. However, a steady finite reaction zone cannot exist behind a spherically diverging shock front. In connection with the development of his curved front model for the calculation of the charge diameter effect, Eyring deduced for spherical reaction zones of finite width a relation between the radius of curvature of the front and the detonation velocity in which the wave velocity increases with radius and approaches the plane wave velocity in the limit. However, Eyring's analysis is based on the assumption of a stationary reaction zone, which is self-contradictory. It has to be concluded, therefore, that Taylor's description of the flow behind a spherically diverging detonation wave is an approximation and that more detailed theoretical investigations will be required before the degree to which his model is a useful description of the actual flow can be determined. In particular, it must be emphasized that Taylor's analysis does not demonstrate that spherical detonation actually occurs with a constant radial propagation velocity equal to that given by the plane wave Chapman-Jouguet condition.

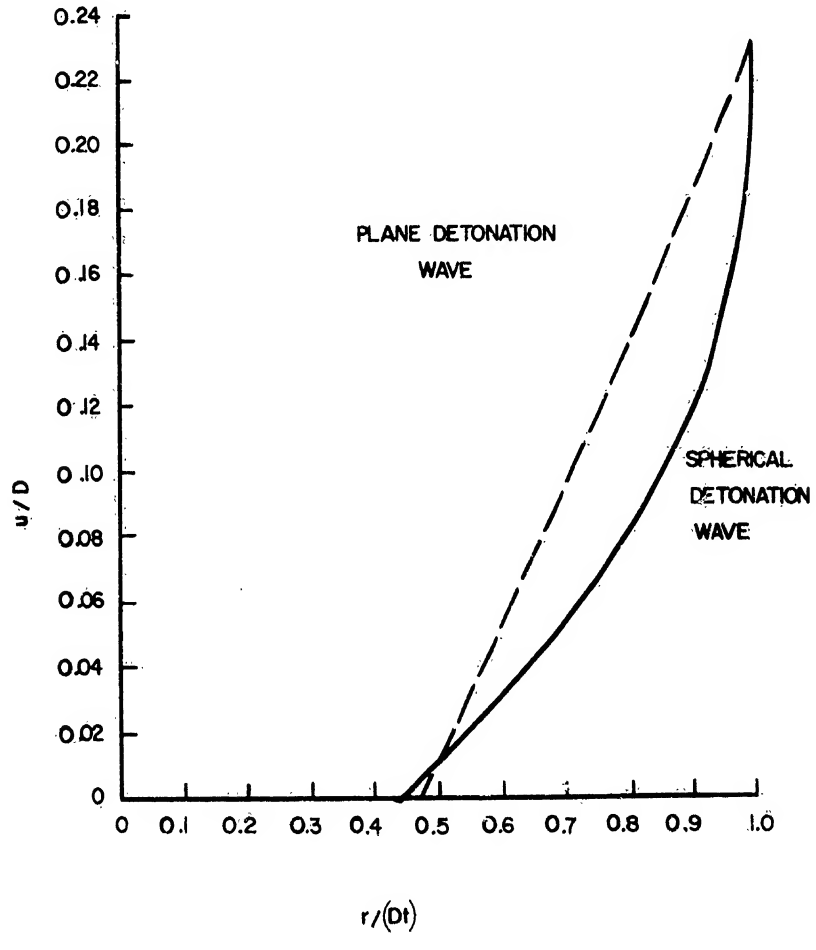

Figure 9-7. Particle Velocity Behind a Spherical Detonation Wave in Pentolite, ρ_o = 1.65

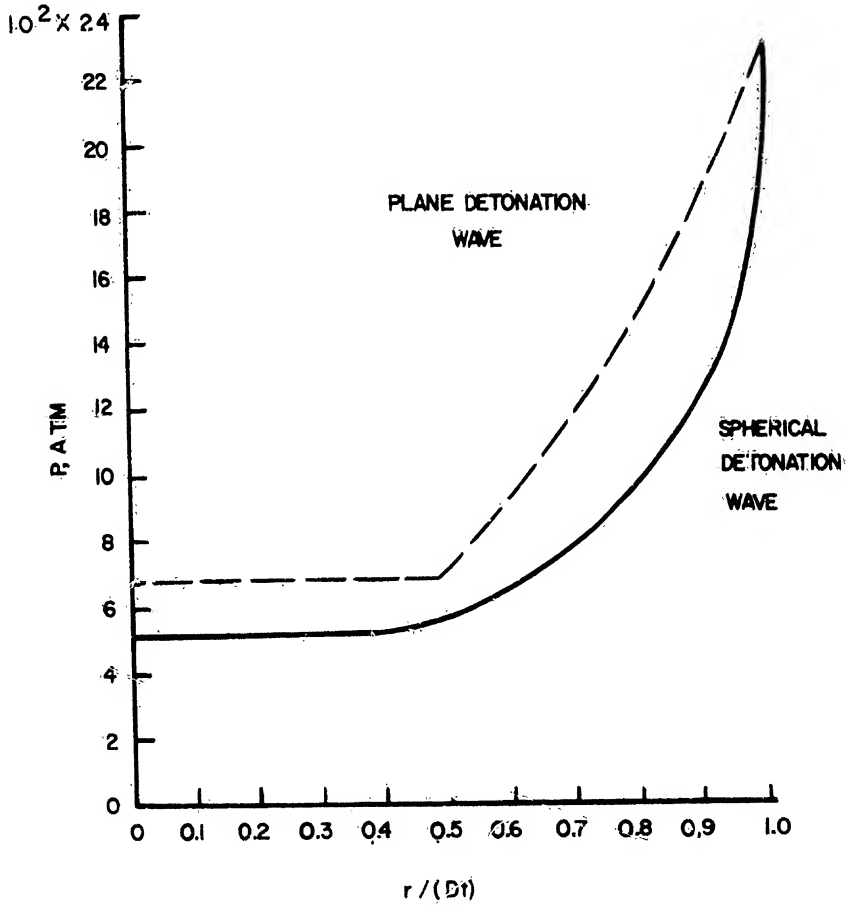

Figure 9-8. Pressure Behind a Spherical Detonation Wave in Pentolite, ρ_o = 1.65

REFERENCES

1. A. Parisot and P. Lafitte, *Compt. rend.*, 18 mc, Congr. Chim. ind., Nancy, 1938, p. 930.
2. W. W. Wood and J. G. Kirkwood, J. Chem. Phys. 22, 1920 (1954).
3. H. Jones, Proc. Roy. Soc. (London), A 189, 415 (1947).
4. H. Eyring, R. E. Powell, G. H. Duffey, and R. B. Parlin, Chem. Rev., 45, 69 (1949).
5. M. A. Cook, *The Science of High Explosives*, Reinhold Publishing Corp., New York, 1958, pp. 125-8.
6. M. A. Cook and F. A. Olsen, A. I Ch. E. Journal 1, 391 (1955).
7. G. I. Taylor, Proc. Roy. Soc. (London) A 200, 235 (1950).
8. R. E. Shear, Ballistic Research Laboratories, Report No. 1159, 1961.
9. R. J. Eichelberger, "Predictions of Shaped Charge Performance from the Release Wave Theory", *Fundamentals of Shaped Charges*, Status Report No. 1, Carnegie Institute of Technology, January 31, 1954. (Originally classified Confidential, declassified January 1966.)

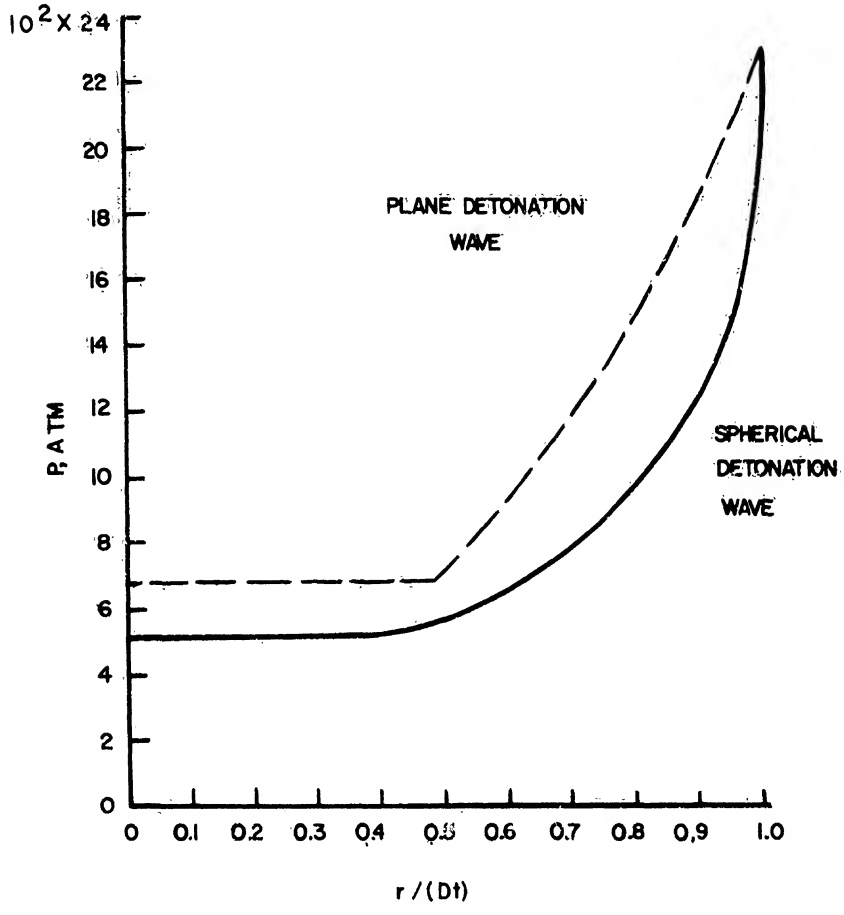

Figure 9-8. Pressure Behind a Spherical Detonation Wave in Pentolite, ρ_o = 1.65

REFERENCES

1. A. Parisot and P. Lafitte, *Compt. rend.*, 18 mc, Congr. Chim. ind., Nancy, 1938, p. 930.
2. W. W. Wood and J. G. Kirkwood, J. Chem. Phys. 22, 1920 (1954).
3. H. Jones, Proc. Roy. Soc. (London), A 189, 415 (1947).
4. H. Eyring, R. E. Powell, G. H. Duffey, and R. B. Parlin, Chem. Rev., 45, 69 (1949).
5. M. A. Cook, *The Science of High Explosives*, Reinhold Publishing Corp., New York, 1958, pp. 125-8.
6. M. A. Cook and F. A. Olsen, A. I Ch. E. Journal 1, 391 (1955).
7. G. I. Taylor, Proc. Roy. Soc. (London) A 200, 235 (1950).
8. R. E. Shear, Ballistic Research Laboratories, Report No. 1159, 1961.
9. R. J. Eichelberger, "Predictions of Shaped Charge Performance from the Release Wave Theory", *Fundamentals of Shaped Charges*, Status Report No. 1, Carnegie Institute of Technology, January 31, 1954. (Originally classified Confidential, declassified January 1966.)

CHAPTER 10 THERMAL EXPLOSION

10-1 INTRODUCTION

Thermal explosion is concerned with the effects of uncontrolled internal heating on explosive systems. Such uncontrolled heating can be initiated by action of external heat sources on the explosive or simply by "spontaneous" decomposition of the explosive itself. Under appropriate (or inappropriate) conditions of temperature, physical dimension, and thermal insulation, all explosive materials can undergo a build-up of chemical reaction leading eventually to fire and/or explosion in the material.

Since thermal explosion concepts have significant application to the safe handling and storage of explosives as well as to the fundamental understanding of the mechanisms of initiation and growth of detonation, it will be desirable to describe the thermal explosion process in some detail. Par. 10-2 is devoted to a description of the important physical processes which give rise to thermal explosions. In par. 10-3, the theoretical treatment of thermal explosions as developed by previous workers such as Semenov[1], Frank-Kamenetskii[2], Chambre'[3], Zinn and Mader[4], Enig[5], and others, is presented. Some specific applications of the theory are discussed in pars. 10-4 and 10-5. The reader will also find reference to the concepts of thermal explosion in Chapters 11 and 12.

10-2 DESCRIPTION OF THE THERMAL EXPLOSION PROCESS

The basis for a thermal explosion is the exponential dependence of chemical reaction rate on temperature, as expressed in the Arrhenius law for the reaction rate proportionality constant k_r

$$k_r = Z \exp[-E/(RT)] \qquad (10\text{-}1)$$

where

Z = pre-exponential factor
E = activation energy for the reaction, cal/mole
R = gas constant, cal/mole-°K
T = absolute temperature, °K*

In a first-order decomposition reaction, which is common in high explosive compounds, the reaction rate constant has the dimensions of $(\text{time})^{-1}$ and its reciprocal is the characteristic life time of the explosive molecules at temperature T.

A typical high explosive compound (see Table 10-1) has a pre-exponential factor equal to about 10^{13} sec^{-1} and an activation energy of the order of 35,000 cal/gram mole. Table 10-2 shows how the characteristic life time changes with temperature for such a material.

The figures in Table 10-2 are illustrative only since the decomposition mechanism may differ in various temperature ranges. In fact, this is common since some of the larger molecular aggregates found among the low-temperature decomposition products of explosives disappear at higher temperatures. In some cases the reaction produces molecules that catalyze further decomposition (autocatalytic reaction). However, the general lifetime behavior exemplified in Table 10-2 is characteristic of virtually all high explosives.

Since the decomposition of an explosive is exothermic and evolves heat, there is a tendency for the decomposing material to become warmer and, thus, for the reaction to become faster and the heat-production rate to increase. Opposing this tendency is the flow and loss of heat to cooler surroundings. The heat production rate depends exponentially on temperature, according to Arrhenius' law, while the rate of heat loss usually increases in a linear fashion with temperature. The difference in the laws governing heat production and heat loss lead to interesting consequences—depending on circumstances, either the opposing effects come into balance and the temperature at some point ceases to rise, and then gradually recedes as the decomposing material becomes used up; or, the opposing tendencies fail to reach a balance. In the latter case the chemical reaction finally dominates, and the result is a catastrophic acceleration of the temperature rise. This is the

*While system temperatures in this chapter may be quoted in degrees centigrade, the reader is cautioned that for calculation purposes the temperature must refer to an absolute temperature unit, i.e., degrees Kelvin.

TABLE 10-1 SPECIFIC RATE CONSTANTS FOR FIRST-ORDER ISOTHERMAL DECOMPOSITION OF EXPLOSIVES

Explosive	Log Z, sec^{-1}	E, kcal/mole	T, °C	*Reference*	
Nitroglycerin	20.5	48	(125-225)	Roginsky	(a)
				Robertson	(b)
TNT	11.4	34.4	275-312	Robertson	(c)
TNT	12.2	43.4	237-277	Cook	(d)
TNT	—	27.8	—	Baum	(f)
Tetryl	15.4	38.4	211-260	Robertson	(e)
Tetryl	12.9	34.9	132-164	Cook	(d)
Tetryl	—	23.1	—	Baum	(f)
Tetryl	22.5	52.0	(solid)	Roginsky	(g)
RDX	18.5	47.5	213-299	Rideal	(h)
RDX	15.5	41.0	(solution)	Robertson	(i)
PETN	15.2	38.6	137-157	Cook	(d)
PETN	19.8	47.0	161-233	Robertson	(b)
HMX	19.7	52.7	271-314	Rideal	(h)
Ammonium Nitrate	12.28	38.3	217-267	Cook	(d)

(a) S. Roginsky, Phys. Zeit Sowjet 1, 640 (1932).
(b) A. J. B. Robertson, J. Soc. Chem. Ind. 61, 221 (1948).
(c) A. J. B. Robertson, Trans. Faraday Soc. 44, 977 (1948).
(d) M. A. Cook and M. T. Abegg, Ind. Eng. Chem. 48, 1090 (1956).
(e) A. J. B. Robertson, Trans. Faraday Soc. 44, 677 (1948).
(f) F. A. Baum, K. P. Stanyakowich, and B. I. Shekhter, "Physics of an Explosion", *Fizmatzig*, Moscow (1959).
(g) S. Roginsky, Z. Phys. Chem. B18, 364 (1932).
(h) E. K. Rideal and A. J. B. Robertson, Proc. Roy. Soc. A195, 135 (1948).
(i) A. J. B. Robertson, Trans. Faraday Soc. 45, 85 (1949).

TABLE 10-2 TYPICAL BEHAVIOR OF A SOLID HIGH EXPLOSIVE COMPOUND FOLLOWING AN ARRHENIUS REACTION LAW

Temperature, °C	*Characteristic Life Time*, k_r^{-1}
20	1 million years
110	1 year
200	1 hour
260	1 minute
325	1 second
375	1 tenth second
435	1 hundredth second
500	1 thousandth second
825	1 millionth second

thermal explosion. The final development is usually sudden and dramatic, and the effect on the observer is heightened by the fact that explosion can be initiated or suppressed by only a slight change in experimental conditions such as temperature, physical dimensions, or thermal insulation.

The way this happens may be illustrated by the following simple experiment. Although the example chosen is hypothetical, such an experiment can safely be carried out in the laboratory if small enough quantities of explosive are used—say, one-tenth gram or less—and if adequate precautions are taken. Fig. 10-1 depicts schematically the conditions of this experiment. A test tube (in practice, preferably made of a high thermal conductivity metal) containing the material is placed in an oil bath that has been previously brought to a selected temperature level T_o and maintained at that point with a thermostat and stirring. A thermocouple in contact with the explosive records its temperature T_1. If the bath temperature is low enough in the first experiment, the temperature of the explosive will be observed to rise to the temperature of the bath, then to continue to a slightly higher point before it levels off. After reaching this maximum, it slowly cools down to the bath temperature again as the explosive decomposes and eventually disappears. When the bath temperature T_o is increased in successive experiments, the maximum level of T_1 will be found to exceed T_o by a wider margin. The decomposition which ensues after the explosive reaches its maximum temperature will also be faster. Then, at some critical bath temperature T_{cr} the material, after seeming to level to a steady condition, will suddenly explode. As the bath temperature is raised still higher, the explosion will occur earlier and the tendency of the temperature to level off near T_o will be less pronounced. Thus, one observes not only a critical temperature effect but also an induction period, or pause, before the explosion. The induction period is an important feature of thermal explosions.

A somewhat oversimplified but informative description of this experiment will point out the basic physical processes occurring in thermal explosions. One assumes, first of all, that the rate $\dot{q}_2$ of heat gain or loss from the explosive can be represented by the product of a constant heat transfer coefficient h, the surface area A of the explosive mass, and the temperature difference; thus

$$\dot{q}_2 = hA(T_o - T_1) \qquad (10\text{-}2)$$

The explosive, of mass m, produces heat at a rate $\dot{q}_1$, given by the product of its reaction rate mk_r (first order reaction) and the heat of decomposition Q, which is the heat produced per unit weight of the decomposing explosive. Thus

$$\dot{q}_1 = mk_r(T_1)Q \qquad (10\text{-}3)$$

where the reaction rate constant $k_r(T_1)$ is expressed as a function of T through Eq. 10-1. The net rate at which heat is accumulated in the material is the sum of $\dot{q}_1$ and $\dot{q}_2$; and the rate of temperature rise will be given by this sum divided by the total heat capacity mc, where c is the specific heat. Thus

$$\frac{dT_1}{dt} = \frac{(\dot{q}_1 + \dot{q}_2)}{mc} \qquad (10\text{-}4)$$

The physical situation represented by Eq. 10-4 may be readily understood in terms of graphs of the functions $\dot{q}_1$ and $\dot{q}_2$, as shown in Fig. 10-2. In the example given, realistic values of the

various parameters of Eq. 10-4 have been chosen. The values are: m = 1.0 g, hA = 0.05 cal/deg, q = 500 cal/g, and c = 0.2 cal/°C-g. For the Arrhenius activation energy E, and the pre-exponential factor Z, the same values have been used as for the example in Table 10-2, namely, 35,000 cal/mole and 10^{13} sec^{-1}.

Fig. 10-2 shows the relationship between the curve for heat production rate, which is an exponential function of temperature, and that for the heat loss rate, which is a straight line of given slope (proportional to the heat transfer coefficient h). The position of the heat loss rate line in reference to the temperature scale depends on the bath temperature T_o. Three different relationships are possible between the straight line and the curve, as shown in Fig. 10-2: (1) the line may cut the curve in two points, (2) the line may touch the curve at a point of tangency, or (3) the line may not intersect the curve at all. In the cases shown, the line for T_o = 200°C is of the first type, that for T_o = 208°C of the second, and that for 210°C of the third.

In physical terms, when the bath is at 200°C, the explosive heats up to the temperature at which the line intersects the curve—i.e., the point A in Fig. 10-2—and since the heat production and heat loss rates are equal at this point, the temperature stabilizes, in this case at about 202°C. When the bath is at 208°C, the temperature stabilizes at a value corresponding to the tangency point B in Fig. 10-2, about 221°C. When the bath temperature is above 208°C, the heat production rate exceeds the heat loss rate, and an explosion occurs. In this example, the temperature of 221°C is the highest point that can be reached by the explosive without exploding.

Fig. 10-3 shows the temperature-time curves corresponding to various bath temperatures, as obtained by numerical integration of Eq. 10-4 based on the data depicted in Fig. 10-2. The curves illustrate the behavior just described,

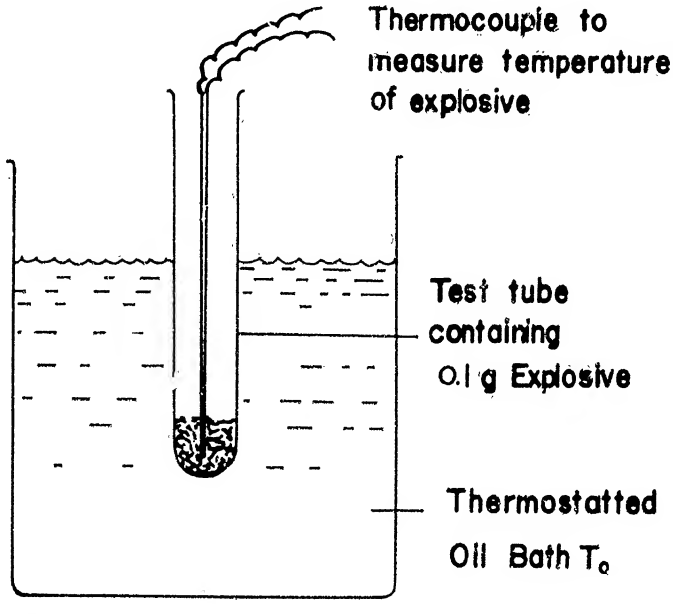

Figure 10-1. An Experiment To Illustrate the Critical Nature of a Thermal Explosion

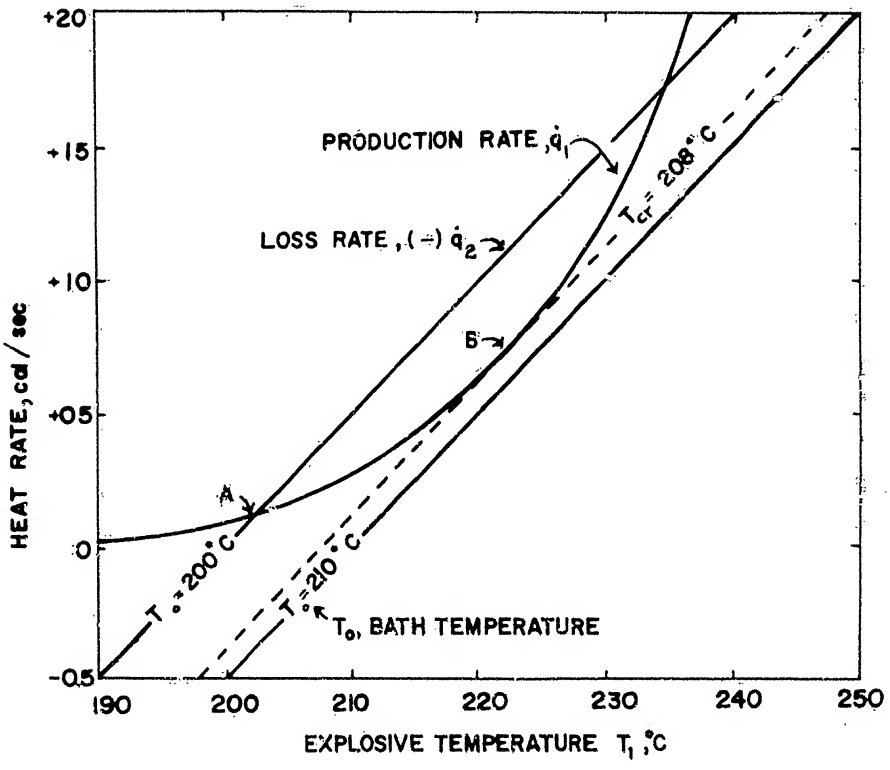

Figure 10-2. Heat Production and Heat Loss Rates in an Experiment of the Type Depicted in Fig. 10-1

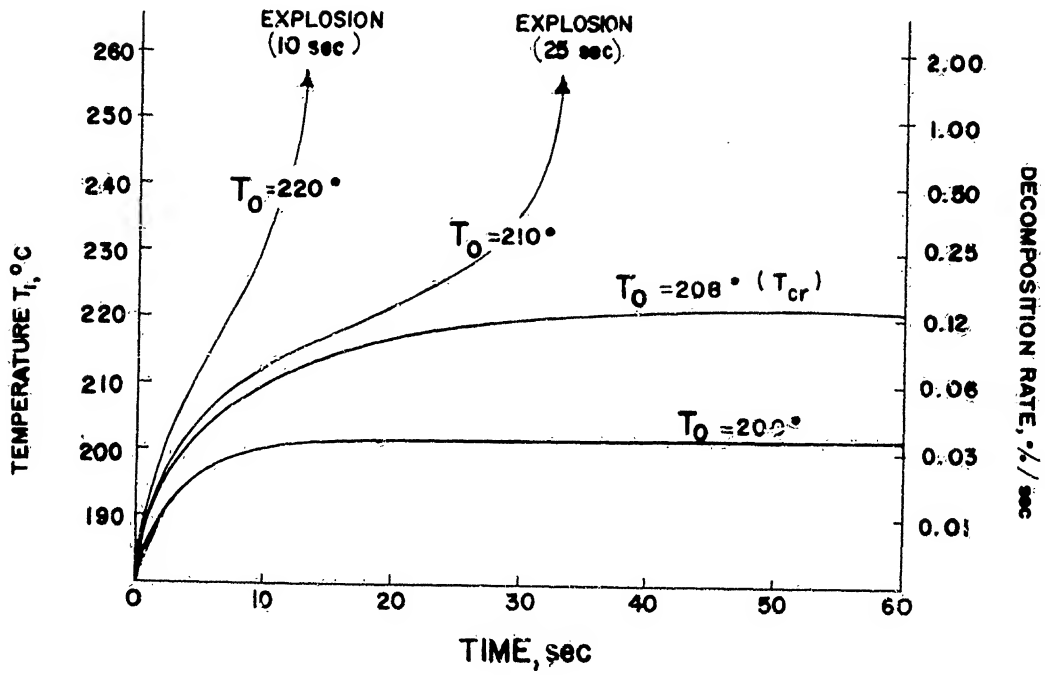

Figure 10-3. Heating Curves (Temperatures vs Time) in an Experiment of the Type Depicted in Fig. 10-1 and Consistent With the Data in Fig. 10-2

namely, explosion when $T_o > 208°C$ and no explosion when $T_o < 208°C$, the temperature 208°C being in this case the critical temperature T_{cr} of the explosive.

Also indicated in Fig. 10-3 is the induction time before explosion. This is equal to 25 sec when T_o = 210°C, and 10 sec when T_o = 220°C. For this purpose, the induction time is defined as the interval between the point when the explosive temperature T_i becomes equal to the bath temperature T_o and the point when the temperature rise becomes extremely steep, the heating curve being almost vertical. The induction time decreases rapidly as the bath temperature is raised above the critical level of 208°C.

Some points illustrated in Fig. 10-3 are worth noting. These observations apply to all materials that have a relatively high heat of decomposition and a high energy of activation for decomposition, conditions which are met by most high explosive compounds. The first point is that the temperature at which the explosive pauses in the induction period before exploding never exceeds by very much the critical explosion temperature T_{cr}.

The second point is that very little of the material reacts during the induction period. Numerical integration under the curves in Fig. 10-3, based on the scale of decomposition rate on the right hand side of the figure, shows that about 4 percent of the material decomposes before explosion when T_o = 210°C, and about 2 percent when T_o = 220°C.

Another important observation concerns the relationship between T_{cr} and the heat loss rate $(-)\dot{q}_2$. It is clear that there is an intimate connection between $\dot{q}_2$ and T_{cr}, because for a perfectly insulated body of explosive, explosion would occur eventually, in principle, even at very low initiation temperatures. That the explosion temperature must increase as the heat transfer coefficient h and surface area A are increased may be seen from the fact that lines representing $(-)\dot{q}_2$ in Fig. 10-2 would then be displaced downward (or toward the right).

Some of the important factors in determining the explosion characteristics of a system are seen from the foregoing discussion to be the following:

(1) Activation energy
(2) Heat of reaction
(3) Thermal conductivity and heat capacity
(4) Effective heated surface area
(5) Mass of explosive.

10-3 MATHEMATICAL TREATMENTS OF THERMAL EXPLOSION

In this paragraph the theory of thermal explosion is given in a somewhat more rigorous form, following the early developments of Frank-Kamenetskii[2] and Chambré[3], and the later numerical and approximate treatments given by Zinn and Mader[4] and Enig[5], for various heated surface boundary conditions.

10-3.1 THE HEAT CONDUCTION EQUATION

In principle the analysis of the behavior of solid explosive materials undergoing nonuniform heating can be accomplished by considering the heat conduction equation which neglects convective heat flow and which includes an energy source term to account for chemical reaction[6], i.e.,

$$\underbrace{\rho c \left(\frac{\partial T}{\partial t}\right)}_{\text{self-heating}} = \underbrace{\lambda \nabla^2 T}_{\substack{\text{heat loss} \\ \text{by} \\ \text{conduction}}} + \underbrace{\rho Q \left(\frac{d\epsilon}{dt}\right)}_{\substack{\text{production of} \\ \text{heat by chemical} \\ \text{reaction}}} \qquad (10\text{-}5)$$

where

T = solid temperature, °K
c = specific heat, cal/g-°K
ρ = density, g/cm^3
λ = thermal conductivity which is assumed temperature independent, cal/cm-°K-sec
Q = heat of reaction, cal/g
ϵ = fraction of explosive reacted, dimensionless

∇^2 = Laplacian operator, which in Cartesian space coordinates x, y, z is

$$\nabla^2 = \frac{\partial^2}{\partial x^2} + \frac{\partial^2}{\partial y^2} + \frac{\partial^2}{\partial z^2} \qquad (10\text{-}6)$$

Since symmetric explosive geometries such that the conduction process depends only on a single space coordinate will be considered here, ∇^2 can be simplified to

$$\nabla^2 = \frac{\partial^2}{\partial x^2} + \frac{\ell}{x}\left(\frac{\partial}{\partial x}\right) \qquad (10\text{-}7)$$

where $\ell = 0$, 1, or 2 for planar, cylindrical, or spherical symmetry and x now refers to the appropriate single space coordinate.

From simple chemical kinetic theory the rate of reaction can be expressed as

$$\frac{d\epsilon}{dt} = (1-\epsilon)^n k_r = (1-\epsilon)^n Z \exp[-E/(RT)] \qquad (10\text{-}8)$$

where n is the reaction order and k_r the reaction rate constant is replaced by its Arrhenius form (see Eq. 10-1).

Thus the heat conduction equation for thermal explosions becomes

$$\rho c\left(\frac{\partial T}{\partial t}\right) = \lambda\left[\frac{\partial^2 T}{\partial x^2} + \frac{\ell}{x}\left(\frac{\partial T}{\partial x}\right)\right] + \rho Q(1-\epsilon)^n Z \exp[-E/(RT)] \qquad (10\text{-}9)$$

It is well known that there are no exact analytical solutions to Eq. 10-9 under any boundary conditions because of the nonlinearity introduced by the exponential chemical reaction term. However, from the description of the thermal explosion process given in the preceding paragraph, two reasonable approximations can be made which give rise to useful solutions. The approximations are:

(1) The temperature T of the explosive just prior to explosion is not too different from the initial explosive temperature T_o, i.e., $(T-T_o)/T_o \ll 1$

(2) The amount of reaction just prior to explosion is slight so that the reaction is essentially zero-order, i.e., $n = 0$.

With these assumptions, Eq. 10-9 simplifies in the following manner: Denoting $T = T_o + \Delta T$, then

$$\frac{E}{RT} = \frac{E}{RT_o}\left(\frac{1}{1+\Delta T/T_o}\right) \approx \frac{E}{RT_o}\left(1-\frac{\Delta T}{T_o}\right) \qquad (10\text{-}10)$$

Defining new space and temperature variables as

$$\theta = \frac{E}{RT_o^2}(T-T_o) \qquad (10\text{-}11)$$

$$\xi = x/a \qquad (10\text{-}12)$$

where a is the significant dimension of the explosive—for example, the one-half thickness of an explosive slab ($\ell = 0$), the radius of a long cylinder ($\ell = 1$) or of a sphere ($\ell = 2$)—the heat conduction equation becomes

$$\frac{\rho c a^2}{\lambda}\left(\frac{\partial\theta}{\partial t}\right) = \frac{\partial^2\theta}{\partial\xi^2} + \frac{\ell}{\xi}\left(\frac{\partial\theta}{\partial\xi}\right) + \delta \exp[\theta] \qquad (10\text{-}13)$$

where

$$\delta = \frac{QEa^2\rho Z}{\lambda RT_o^2}\exp[-E/(RT_o)] \qquad (10\text{-}14)$$

10-3.2 STEADY-STATE CONDITION $\partial T/\partial t = 0$, AND THE CONCEPT OF CRITICAL TEMPERATURE AND SIZE

Frank-Kamenetskii and Chambre' examined the possible steady-state solutions to Eq. 10-14 (i.e., with $\partial\theta/\partial t = 0$) subject to symmetrical heating where the boundary conditions are

$\xi = 0$, $d\theta/d\xi = 0$ (at the center)

$\xi = 1$, $\theta = 0$ (at the surface)

For each of the three geometries ($\ell = 0$, 1, 2), it was found that a maximum value exists for the parameter δ (Eq. 10-14) for which steady-state solutions to Eq. 10-13 are possible. For $\delta \leq \delta_{cr}$, steady-state solutions are possible; but for $\delta > \delta_{cr}$, a stationary temperature distribution is impossible. It is therefore seen that δ_{cr} defines the critical conditions for thermal explosion under uniform surface heating conditions. The values obtained for δ_{cr} and the

corresponding maximum critical stationary temperature distribution $\theta_{max,\,cr}$ are shown in Table 10-3.

The critical explosion temperature T_{cr} is then just that value of the explosive surface temperature T_o which results in $\delta = \delta_{cr}$ in Eq. 10-14, i.e.,

$$T_{cr} = \frac{E/R}{\ell n \left(\frac{QEa^2 \rho Z}{\lambda R T_{cr} \delta_{cr}} \right)} \qquad (10\text{-}15)$$

For given values of Q, E, a, etc. Eq. 10-15 can be readily solved by iteration to yield T_{cr}.

Likewise, from Eq. 10-14 there is a critical size a_{cr} of explosive which can result in $\delta = \delta_{cr}$, i.e.,

$$a_{cr} = \left(\frac{\lambda R \delta_{cr}}{QE\rho Z} \right) T_o \exp\left[E/(2RT_o)\right] \qquad (10\text{-}16)$$

For a given explosive composition it is seen that the critical temperature T_{cr} below which no explosions are obtained is related to the rate at which heat can flow to the explosive surface, which in turn is related to the surface/volume ratio of the explosive geometry. Thus for a given value of a the slab will have the lowest T_{cr}, and the sphere will have the highest T_{cr}.

10-3.3 ADIABATIC HEATING ($\nabla^2 T = 0$) AND THE CONCEPT OF EXPLOSION TIME

The determination of the time to explosion t_e is an important aspect of thermal explosion theory. As described in par. 10-2, the onset of explosion is accompanied by a rapid rise in explosive temperature after a relatively long self-heating or induction period; hence it is convenient to consider the rapid temperature rise as the explosion criterion.

An important case that will now be considered is adiabatic self-heating which is applicable to an infinitely large explosive mass at uniform temperature or to a finite explosive mass that is thermally isolated.

From Eq. 10-15 it is seen that for an infinite explosive size, the critical temperature T_{cr} is zero so that in principle any finite value of initial temperature T_o will lead to a thermal explosion (though the value of t_e may be quite large e.g., see Table 10-2).

The adiabatic heating conditions correspond to the case where the heat conduction term in Eqs. 10-5 and 10-13 is sufficiently small so that it may be neglected (i.e., $\nabla^2 T = 0$). Thus from Eq. 10-13 the variation of temperature with time of an explosive initially at uniform temperature T_o can be expressed as

$$\frac{d\theta}{dt} = \frac{QZE}{cRT_o^2} \exp\left[-E/(RT_o)\right] \exp\left[\theta\right] \qquad (10\text{-}17)$$

It follows that

$$\int_0^{t_e} dt \qquad (10\text{-}18)$$

$$= \frac{cRT_o^2}{QZE} \exp\left[E/(RT_o)\right] \int_{\theta_o}^{\theta_e} \exp\left[-\theta\right] d\theta$$

TABLE 10-3 CRITICAL VALUES FOR THERMAL EXPLOSION PARAMETERS δ AND θ

Explosive Geometry	δ_{cr}	$\theta_{max,\,cr}$
Infinite plane-parallel slab, $\ell = 0$	0.88	1.20
Infinite long cylinder, $\ell = 1$	2.00	1.39
Sphere, $\ell = 2$	3.32	1.61

or

$$t_e = \frac{cRT_o^2}{QZE} \exp[E/(RT_o)] \exp[-\theta] \Big|_{\theta_e}^{\theta_o} \tag{10-19}$$

The integration limits on θ correspond to

$$t = 0; \quad \theta_o = 0$$

$$t = t_e; \quad \theta_e = \frac{E}{RT_o^2}(T_e - T_o)$$

However it may be shown[2,3] that within the approximations used in deriving Eq. 10-13 that $\theta_e \approx 1$. We can, therefore, express the explosion time as

$$t_e \approx \frac{CRT_o^2}{QZE} \exp[E/(RT_o)] \tag{10-20}$$

It will be seen later in this chapter and in subsequent chapters that experimental data on adiabatic explosion times for many explosives generally follow an empirical relationship of the type

$$\ln t_e = A + \frac{B}{T} \tag{10-21}$$

This empirical relationship is consistent with the form of Eq. 10-20.

10-3.4 APPROXIMATE SOLUTIONS FOR t_e WITH NONADIABATIC HEATING

Several investigators[5,7,8] have presented approximate solutions to Eq. 10-9 for the explosion induction time with nonadiabatic surface heating conditions. Enig[5] has approached the problem in a general manner which seems to be applicable to a number of boundary conditions of practical interest. In those particular cases tested, the approximate solutions to t_e yielded values which agreed within ≈20% of the values calculated by more exact numerical methods.

Enig's approach makes use of the fact that in many cases the chemical reaction is small up until the time of explosion, and that the onset of explosion, when the surface temperature of the explosive is much higher than T_{cr}, is accompanied by a maximum temperature very near to the surface. The approach can be described in the following manner for symmetric semi-infinite geometries.

Introducing the dimensionless variables

$$\varphi \equiv \frac{RT}{E}$$

$$z \equiv \left(\frac{\rho QZR}{\lambda E}\right)^{1/2} x$$

$$\tau \equiv \frac{RQZt}{cE}$$

Eq. 10-9 with zero order reaction ($n = 0$) becomes

$$\frac{\partial \varphi}{\partial \tau} = \frac{\partial^2 \varphi}{\partial z^2} = \frac{\ell}{z}\left(\frac{\partial \varphi}{\partial z}\right) + e^{-1/\varphi} \tag{10-22}$$

It will suffice for our purposes to consider only the planar case with $\ell = 0$. The solution to Eq. 10-22 is

$$\int_0^\infty \left(\frac{\partial \varphi}{\partial \tau} - e^{-1/\varphi}\right) dz \tag{10-23}$$

$$= \frac{\partial \varphi}{\partial z} = \frac{\partial \varphi}{\partial z}\Big|_{z=\infty} - \frac{\partial \varphi}{\partial z}\Big|_{z=0}$$

The explosion criterion is expressed as

$$\frac{\partial \varphi}{\partial z}\Big|_{z=0} = 0 \tag{10-24}$$

and since at $z = \infty$, $\varphi(z,\tau) \approx \varphi_o$ the initial temperature for all t, this leads to

$$\int_0^\infty = \left(\frac{\partial \varphi}{\partial \tau} - e^{-1/\varphi}\right) dz = 0 \tag{10-25}$$

The explosion time t_e (or τ_e) is just the root of Eq. 10-25. While exact solutions for $\varphi(z,\tau)$ cannot be found which would allow Eq. 10-25 to be solved, the approximation of negligible chemical reaction over the time period $0 < t \leq t_e$ allows us to replace $\varphi(z,\tau)$ by $\varphi^o(z,\tau)$ in Eq. 10-25, where φ^o represents the solution to the "inert" case of Eq. 10-22 (i.e., the case where $e^{-1/\varphi}$ is set to equal zero).

This leads to

$$-\left.\frac{\partial \varphi^o}{\partial z}\right|_{z=0} = \int_0^\infty e^{-1/\varphi_o}\, dz \qquad (10\text{-}26)$$

A difficulty arises in evaluating the integral of Eq. 10-26 due to the negligible amount of reaction occurring for $\varphi^o = \varphi_o$ at $z = \infty$. This makes the integral infinite. This difficulty is removed by replacing the integrand by $\exp[-1/\varphi^o] - \exp[-1/\varphi_o]$, i.e.,

$$-\left.\frac{\partial \varphi^o}{\partial z}\right|_{z=0} \approx \int_0^\infty \left(e^{-1/\varphi^o} - e^{-1/\varphi_o}\right) dz \qquad (10\text{-}27)$$

Thus an explicit relationship t_e can be found for all cases where analytic solutions can be found for φ^o and where Eq. 10-27 can be integrated in closed form.

Table 10-4 shows derived expressions for t_e for a semi-infinite planar explosive with various boundary conditions. The reader is referred to Enig's original paper[5] for other possible cases.

10-3.5 NUMERICAL METHODS

Numerical methods appear to be the only way of obtaining exact solutions to the heat conduction equation for thermal explosion (Eq. 10-9), and several investigators have carried out such calculations for particular explosive cases[4,9,10]. For the one-dimensional case, the numerical methods are relatively straightforward and can be handled on many modern digital computers. In some instances it has been demonstrated that the numerical results for one particular explosive can be generalized to other explosives by simple graphical techniques.

To solve Eq. 10-9, which is rewritten here as

$$\rho c\left(\frac{\partial T}{\partial t}\right) = \lambda\left(\frac{\partial^2 T}{\partial x^2}\right) + \frac{\ell}{x}\left(\frac{\partial T}{\partial x}\right) + \partial Q\left(\frac{d\epsilon}{dt}\right) \qquad (10\text{-}28)$$

$$\frac{d\epsilon}{dt} = (1-\epsilon)^n\ Z \exp\left[-E/(RT)\right] \qquad (10\text{-}29)$$

by numerical methods in the manner of Zinn and Mader[4], the time scale is considered to be divided into equal increments of τ sec. It is also considered that no chemical reaction occurs during the time τ, but at the end of each time period, the heat produced by chemical reaction can be added to the explosive in the form of an instantaneous temperature correction. The heat produced is taken as that given by $\rho Q d\epsilon/dt$ assuming a constant temperature $T(x,t)$ during the τ time interval. In this manner, Eq. 10-28 is solved with $Q = 0$ over each interval τ but with a different initial temperature distribution $f_j(x)$ for each consecutive time period.

The initial distribution will be given by the expressions

$$f_{j+1}(x) = T(x,j\tau) + \frac{Q}{c}(\Delta\epsilon_j) \qquad (10\text{-}30)$$

$$\Delta\epsilon_j = \tau\left[1 - \epsilon(x,j\tau)\right]^n Z \exp\left\{-E/\left[RT(x,j\tau)\right]\right\} \qquad (10\text{-}31)$$

$$\epsilon(x,j\tau) = \sum_j \Delta\epsilon_j \qquad (10\text{-}32)$$

This numerical procedure is relatively simple but it does require starting solutions to be available for Eq. 10-28 with $Q = 0$. As an example, we can consider the planar case ($\ell = 0$) of a slab ($0 \leq x \leq 2a$), i.e.,

$$\rho c\left(\frac{\partial T}{\partial t}\right) = \lambda\left(\frac{\partial^2 T}{\partial x^2}\right) \qquad (10\text{-}33)$$

with boundary conditions $f_o(x) = T(x,o)$ and $T(2a,t) = T_s$, a constant.

The solution to Eq. 10-33 is given by Carslaw and Jaeger[6] as

$$T(x,t) = T_s + \left\{\frac{1}{a}\sum_{n=1}^{\infty} \exp\left[-\frac{n^2\pi^2\lambda t}{4\rho c a^2}\right]\right\} \times \left\{\sin\left(\frac{n\pi x}{2a}\right)\int_0^{2a}\left[f_o(x) - T_s\right] \sin\left(\frac{n\pi x}{2a}\right) dx\right\} \qquad (10\text{-}34)$$

If $f_o(x)$ is known at a sufficient number of values of x, the integral can be evaluated

TABLE 10-4 APPROXIMATE SOLUTIONS FOR EXPLOSION INDUCTION TIMES FOR A SEMI-INFINITE PLANAR EXPLOSIVE[5]

Surface Condition (at $z = 0$)	*Dimensionless Explosion Time τ_e*
Constant surface temperature, φ_s:	$\tau_e = \frac{1}{\pi}\left(1 - \frac{\varphi_o}{\varphi^*}\right)^2 e^{1/\varphi^*}$
$\varphi_s > \varphi_o$	$\varphi^* = \varphi_s$
Constant Surface Flux:	$\tau_e = \frac{\pi}{4}\left(1 \quad \frac{\varphi_o}{\varphi^*}\right) e^{1/\varphi^*}$
$\varphi_s = \varphi_o + K\tau^{1/2}$	$(\varphi^*)^2 e^{1/\varphi^*} = \left[\kappa(3/2)K\right]^2$
K, a constant	
Heat flux from medium at constant temperature φ_g with a constant coefficient of heat transfer h:	$\tau_e = \frac{\pi}{4}\left[\frac{\varphi_g - \varphi^*}{\varphi_g - \varphi_o}\right]\left[\frac{\varphi^* - \varphi_o}{\varphi^*}\right]^2 e^{1/\varphi^*}$
$-\left.\frac{\partial \varphi^o}{\partial z}\right\|_{z=0} = H\left[\varphi_g - \varphi^o\ (0,\tau)\right]$	$(\varphi^*)^2 e^{-1/\varphi^*} = H^2(\varphi_g - \varphi_o)(\varphi_g - \varphi^*)$
$H \equiv \left[E/(\lambda \rho Q Z R)\right]^{1/2} h$	

numerically and $T(x;t)$ determined. Utilizing Eq. 10-34 for the reactive case involves replacing $f_o(x)$ by $f_f(x)$ and solving for the temperature distribution at each consecutive time period τ. The accuracy of this numerical procedure is limited by how practically small the increments of τ and x can be taken.

Zinn and Mader carried out solutions to Eqs. 10-28 and 10-29 for a number of explosive compositions and geometries assuming zero-order kinetics, and subject to the boundary conditions of uniform initial temperature T_o and constant surface temperature $T_s > T_o$ for $t \geq 0$.

Fig. 10-4 shows the results obtained for the temperature distribution in 1-in. spheres of RDX at various times. Fig. 10-5 depicts the calculated explosion times for one-inch slabs, cylinders, and spheres of RDX for different surface temperatures $T_s > T_{cr}$. In these calculations the values for the physical and kinetic parameters of the explosive are: ρ = 1.8 g/cm^3, c = 0.5 cal/g-°C, $\lambda = 7 \times 10^{-4}$ cal/°C-cm-sec, Q = 500 cal/g, $Z = 10^{18.5}$ sec^{-1}, E = 47500 cal/mole. It also was found that the t_e calculations for one explosive composition could be generalized to all other explosives by ultilizing a t_e vs $1/T_s$ relationship of the form

$$t_e = \frac{\rho c a^2}{\lambda} F(E/T_{cr} - E/T_s) \qquad (10\text{-}35)$$

where F is a function which depends only on the type of geometry (slab, cylinder, or sphere) and the initial temperature T_o. The variation of F in terms of the argument $(E/T_{cr} - E/T_s)$ is shown in Fig. 10-6 for the three geometries all initially at 25°C. T_{cr} can be easily obtained from the Frank-Kamenetskii expression Eq. 10-15. Therefore, Fig. 10-6 makes it possible to readiiy determine the explosion times for any material for which the appropriate physical and kinetic parameters are known.

Several pertinent facts can be gathered from these numerical calculations which indicate that previously discussed approximate solutions must always be used with caution. First, for relatively low values of $T_s > T_{cr}$, the hottest region prior to explosion is at the center of the explosive. This implies that the thermal explosion will initiate at the center. The reverse situation occurs when T_s

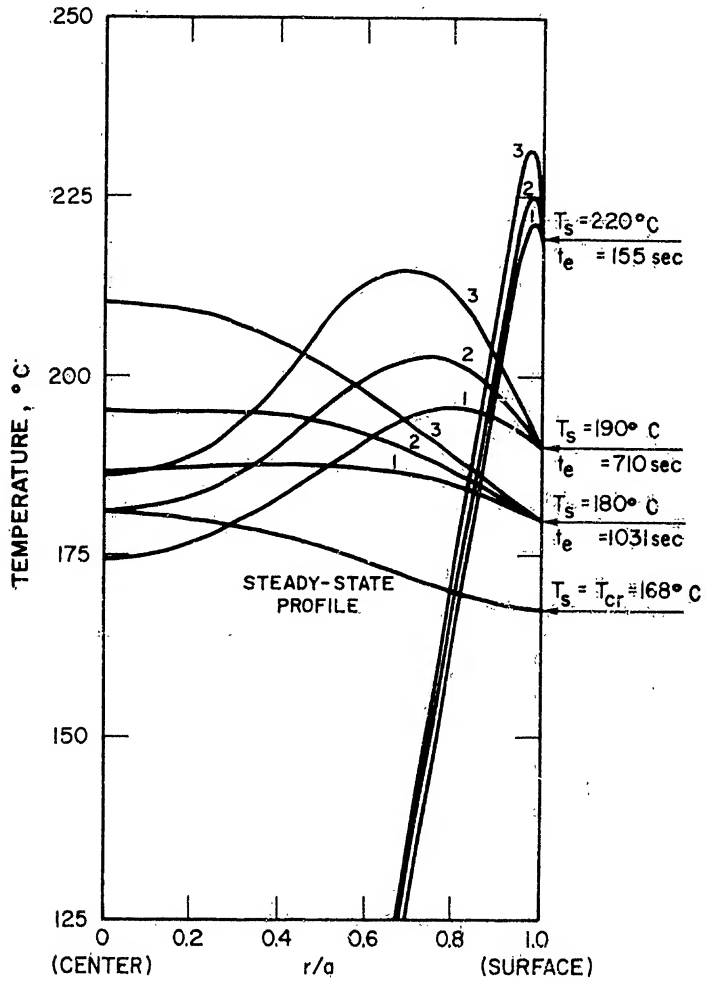

Figure 10-4. Temperature Profiles for Times Near the End of the Induction Period, as Calculated for 1-in. Spheres of RDX Initially at 25°C. [Curve 1: $t = 0.90\ t_e$; Curve 2: $t = 0.95\ t_e$; Curve 3: $t = 0.98\ t_e$. Also shown is the steady-state profile at the critical temperature T_{cr} (Ref. 4).]

is much higher than T_{cr}. Here the temperature near the surface is hottest prior to explosion while the center temperature remains relatively unchanged. Thus approximations based upon a semi-infinite geometry are only applicable for $T_s >> T_{cr}$. Second, it is seen from Fig. 10-5 that the temperature dependence of t_e does not follow an Arrhenius curve (such as Eq. 10-21, which is often used to curve fit experimental data) over all values of T_s. Therefore, one must be cautious in identifying the slope of such empirical curves with an activation energy for chemical reaction (i.e., E or E/R). The experimental studies of Gross and Amster[11], which are discussed in Chapter 12, are a good example of the considerations that must be taken in deriving kinetic parameters from measured explosion times.

Another point that should be considered in connection with the Zinn and Mader calculations, as well as with most of the available approximate solutions, is the effect of assuming a zero-order chemical reaction. This assumption applies that the source of chemical energy cannot be used up prior to explosion regardless of the heat loss rate or the time to explosion. For small explosive masses this may not be valid since the total heat content of the explosive may be relatively small compared to the effective heat capacity of the medium immediately surrounding the explosive. This point will be discussed further in the next paragraph.

10-4 THERMAL EXPLOSION OF HOT SPOTS

A concept of great importance for the initiation of detonation in high explosives is that of "hot spots". This topic is discussed in greater detail in Chapter 11. However at this point, it is

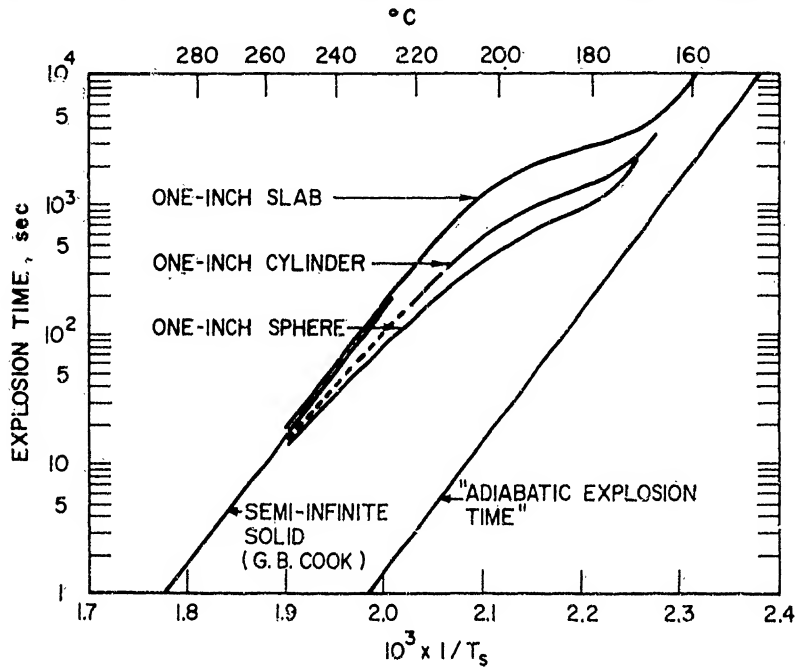

Figure 10-5. Explosion Times vs $1/T_s$ for RDX in Various Geometries, Initially at 25°C (Ref. 4)

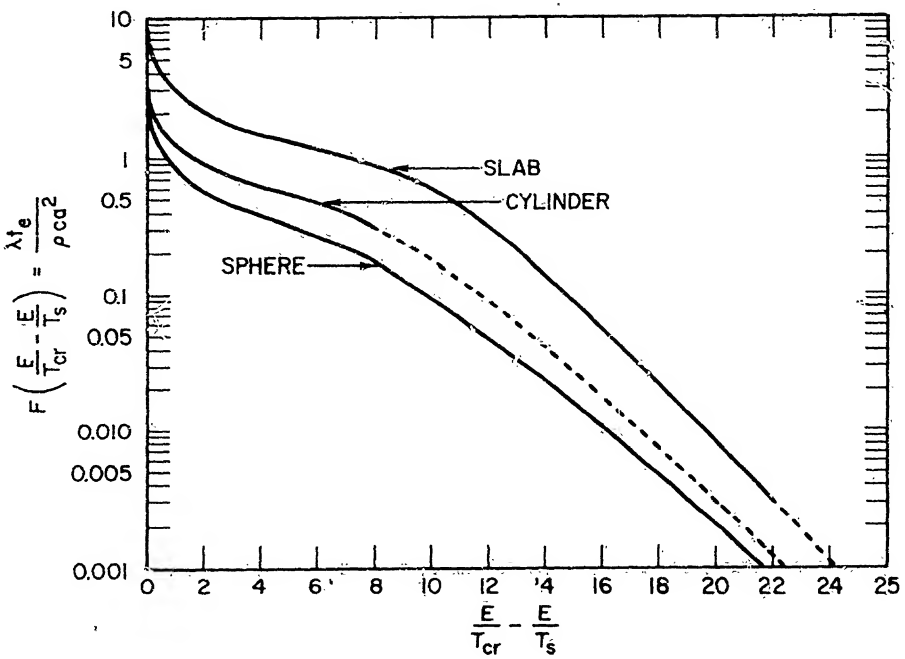

Figure 10-6. Graphs of $\lambda t_e/(\rho c a^2)$ vs $E/T_{cr} - E/T_s$ for Spheres, Cylinders, and Slabs, All Initially at 25°C (Ref. 4)

cooling of the sphere in subsequent periods of time would be represented by the temperature distribution curves in Fig. 10-7. These are derived from the classical treatment of the differential equation for heat conduction and may be found in Carslaw and Jaeger[6]. Time is depicted in terms of a dimensionless parameter $\alpha t/a^2$, where a is the radius of the sphere and α the thermal diffusivity $[\alpha = \lambda/(\rho c)]$ where λ is thermal conductivity, ρ the density, and c the specific heat).

The sudden creation of a hot spot by mechanical action in an explosive material causes the reaction to occur in the affected region at a measurably higher rate than that in the body of the explosive, where it may be virtually zero[12]. However, during most of the induction period before explosion the amount of heat produced by chemical reaction is very small and the cooling behavior is little affected by the fact that reaction is taking place. To state this more exactly: the temperature rise at any point in the hot spot caused by chemical reaction in the induction period is small compared to the initial difference in temperature between the hot spot and the body of the explosive; therefore, the temperature gradient that develops at this point, and consequently the flow of heat during this time, is affected very little by the fact that the material is reactive and not inert. The temperature profiles in Fig. 10-7 are, therefore, a close approximation to those that would obtain in an explosive hot spot during the period prior to explosion.

where t_{ind} is the induction time. Equating t_{ind} to the adiabatic explosion time given by Eq. 10-20, allows one to obtain the criterion in terms of the properties of the explosive, i.e.,

$$\frac{T_o^2}{X} \exp\,[E/(RT_o)] < \frac{0.04QEa^2}{\alpha^2 cR} \quad (10\text{-}37)$$

This relationship, Eq. 10-37, can be used to calculate typical quantities for hot spots of various sizes. Such figures are given in Table 10-5, based on the explosive properties quoted in par. 10-3.4 for RDX. It is significant that the induction period is in the order of microseconds for a hot spot in the order of microns in diameter. This is consistent with the fact that the total time for initiation and reaction in detonating high explosives is usually in the order of microseconds. The critical temperature 550°-600°K also falls in a physically plausible range. The fourth column in the table gives the total chemical energy per unit area available for heating the explosive medium just external to the hot spot. It is seen that the values of q/s are also strongly dependent on the size of the hot spot. This points to the possibility that while hot spots may explode, they may have insufficient energy content to ignite the surrounding cooler medium. For the case of RDX there is evidence from adiabatic gas compression studies (3 msec duration) that the minimum ignition energy is ≈0.3 cal/cm² (Ref. 13), which is somewhat consistent with a hot spot size of the order of microns.

It should be noted that this treatment of the thermal explosion of hot spots assumes adiabatic

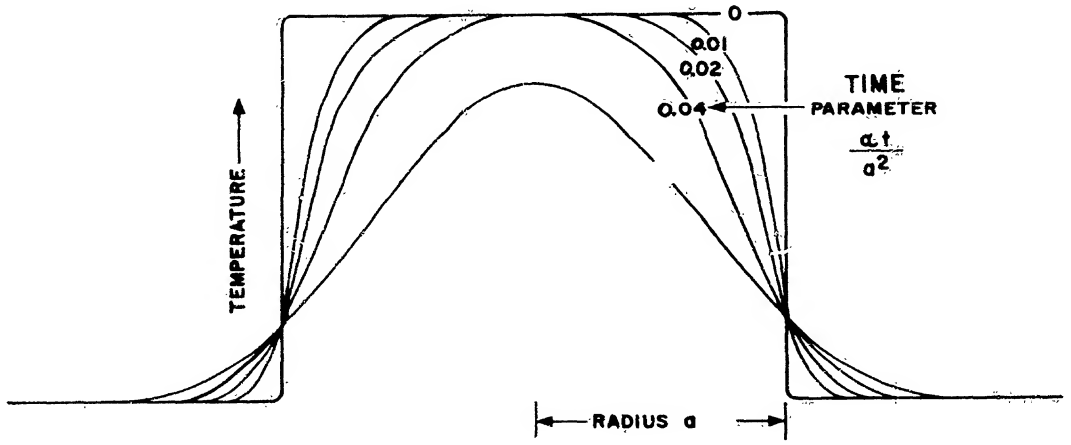

Figure 10-7. Temperature Distribution During Cooling of a Spherical Element of Inert Material That Has Been Raised Initially to a Uniform Temperature Greater Than That of the Surroundings

explosion times and zero-order reaction. Neither of these assumptions may be valid for the small explosive mass that makes up the hot spot.

Friedman, for example, carried out numerical solutions for the critical quantities of a nonadiabatic hot spot which was assumed to be a thin slab[14]. A good analytical approximation to the numerical value of the critical one-half slab thickness d_{cr} was found to be

$$d_{cr}^2 = \left[\frac{\lambda(T_o - T_1)}{\rho Z Q}\right] \exp\left[\frac{E}{RT_o}\right] \quad (10\text{-}38)$$

For conditions of T_o = 550°K and an ambient environment temperature T_1 = 300°K, the value of d_{cr} for RDX is 220 microns, which is one order of magnitude greater than the value a_{cr} in Table 10-5 for the same T_o. Part of this difference in calculated critical hot-spot size is undoubtedly due to the fact that the two calculations refer to different geometries (slab and sphere). However it is reasonable to suggest that a significant part of the difference is actually due to nonadiabatic vs adiabatic heating conditions.

Friedman also investigated by numerical calculations the extent of reaction in the hot spot prior to explosion. Although he states that typically a maximum reaction of 1-8% is indicated, it can be readily calculated from his results that an explosive having the properties E = 20 kcal/mole, c = 0.25 cal/g-°C, Q = 250 cal/g, T_o = 800°K, T_1 = 300°K, will undergo 80% reaction by first order reaction kinetics. The possible effects of nonzero-order chemical reaction in thermal explosion theory warrants considerable more attention, particularly when application is to be made to small quantities of explosive.

10-5 THERMAL EXPLOSION AND SAFETY IN HANDLING HIGH EXPLOSIVES

High explosives are prime examples of materials that can undergo thermal explosion, and it is not suprising that this is an important aspect of their behavior. The mechanism is most apparent in phenomena related to initiation and transition to detonation, subjects which are treated in the following and subsequent chapters. The potential for self-heating is also a matter for serious consideration in connection with safety in handling and storing explosives.

Several disasters with great loss of life and property have resulted from the failure to appreciate the possibilities of self-heating in explosive materials and the suddenness with which a thermal explosion develops when it occurs[15]. Although numerous severe explosions following fires in dynamite factories and ammunition dumps had warned people of the hazard of fighting fire in which high explosives

TABLE 10-5 VARIOUS CALCULATED QUANTITIES FOR HOT SPOTS IN RDX

Hot-spot Temperature T_o, °K	*Hot-spot Radius* a_{cr}, *microns*	*Explosion Times* t_{ind}, *microsec*	*Total Energy Available* q/S, cal/cm²*
450	710	260000	21
500	56	1600	1.7
550	6.9	25	0.21
600	1.3	0.83	0.04
700	0.08	0.0036	0.002
800	0.01	0.000066	0.0003

* $q/S = (1/3)\,\rho Q a$, the total chemical energy available in the hot spot per unit of surface area.

were involved by the customary method , it was not generally appreciated that relatively insensitive materials such as ammonium nitrate and nitromethane have basically the same tendency toward thermal explosion. The catastrophe at Texas City in 1947, in which several million pounds of ammonium nitrate fertilizer exploded following a fire, drew sharp attention to the critical size phenomenon in this material. This had been overlooked in this case because countless fires in smaller quantities of the material had occurred and had not resulted in explosion.

One of the lessons to be learned from these tragic events is that explosives should always be stored in ways that will provide for the maximum possible dissipation of heat and never in large consolidated piles if it can be avoided. It is of interest in this connection to calculate the critical diameter at various surface temperatures for spherical mass of RDX, Eq. 10-16, and the adiabatic explosion time for various initial uniform temperatures, Eq. 10-20. The physical and kinetic parameters considered in these calculations are the same ones used in previous calculations in this chapter. The calculated values are given in Table 10-6.

The values of explosion time in Table 10-6 refer to the condition in which a mass of the explosive is at a uniform temperature initially; therefore, these figures do not apply specifically to the situation in a fire. The actual relationship among surface temperature, geometry, size, and time to explosion can be obtained by the numerical methods described in par. 10-3.5.

In assessing the potential explosion hazards of an explosive mass at elevated surface temperature, useful information can be gained from the temperature distribution just prior to the thermal explosion (theoretically represented by a rapid increase in temperature or rate of reaction at some point in the mass). If rapid reaction starts at or near the surface, the reaction will be unconfined and will probably lead to a less violent surface deflagration. However if rapid reaction starts in the interior of the explosive mass, the reaction will be confined and have a greater probability of building up to a detonation.

Referring to Fig. 10-4, we see that the temperature distribution varies significantly with the ratio T_s/T_{cr}. As this ratio increases above unity, the position of the maximum temperature (which defines the position of runaway reaction) moves closer to the surface. In the example shown (1-in. RDX spheres) when $T_s/T_{cr} = 1.05$, the explosion starts at a distance of $r/a \approx 0.7$, while for $T_s/T_{cr} \approx 1.12$ it starts at $r/a \approx 0.95$.

In the particular case where an explosive mass is burning, it can be suggested that T_s/T_{cr} will not be too much greater than unity. If the mass is sufficiently large and the burning time

TABLE 10-6 CRITICAL DIAMETER AND ADIABATIC EXPLOSION TIME FOR RDX

Temperature, °C	*Critical Diameter**		*Adiabatic Explosion Time***	
50	540	meters	9200	years
75	148	meters	6.8	years
100	41	meters	27	weeks
125	5.8	meters	3.8	days
150	1	meter	3	hours
200	5.6	cm	30	seconds

* Surface of explosive sphere at constant temperature.

** Sphere of explosive at uniform initial temperature.

sufficiently long, it is reasonable to expect that the surface burning will lead to a violent explosion. However if the mass is sufficiently small, the surface burning can consume the entire explosive prior to the build-up of a violent explosion. Thus, in disposing of high explosives it is common to set the material afire but only when it is dispersed in small chunks on the ground, and never when it is in large consolidated masses.

The application of these principles to operations involving the heating of high explosive materials, such as melting in preparation for casting and drying in ovens, will be obvious. The importance of good temperature control in these operations cannot be overstressed; and an overriding control should always be provided in addition to a thermostat to prevent overheating.

REFERENCES

1. N. N. Semenov, *Some Problems in Chemical Kinetics and Reactivity*, Vol. 2 (English translation by M. Boudart), Princeton University Press, Princeton, N. J., 1959.
2. D. A. Frank-Kamenetskii, *Diffusion and Heat Exchange in Chemical Kinetics* (English translation by N. Thon), Princeton University Press, Princeton, N. J., 1955.
3. P. L. Chambre', J. Chem. Phys. 20,1795 (1952).
4. J. Zinn and C. L. Mader, J. Appl. Phys.31, 323 (1960).
5. J. W. Enig, Proc. Roy. Soc. A05A, 205 (1968).
6. H. S. Carslaw and J. C. Jaeger, *Conduction of Heat in Solids*, Oxford University Press, 1959.
7. M. H. Fried[illegible]omb. and Flame 11, 239 (1967).
8. Y. B. Zeldovich [illegible]oviet Phys. Dokl. 8, 461 (1963).
9. G. B. Cook, Proc. Roy. Soc. A246, 154 (1958).
10. E. W. Price, H. H. Bradley, Jr., G. L. Doherity, and M. M. Ibiricu, AIAA Journal 4,1153 (1966).
11. D. Gross and A. B. Amster, *Eighth Symposium (International) on Combustion*, Williams & Wilkins Co., Baltimore, Md., 1962, p. 728.
12. F. P. Bowden and A. D. Yoffe, *Initiation and Growth of Explosion in Liquids and Solids*, Cambridge University Press, 1952.
13. F. P. Bowden and A. D. Yoffe, *Fast Reactions in Solids*, Academic Press, New York, 1958, p. 63.
14. M. H. Friedman, *Ninth Symposium (International) on Combustion*, Academic Press, New York, 1963, p. 294.
15. C. S. Robinson, *Explosives, Their Anatomy and Destructiveness*, McGraw-Hill, New York, 1944.

CHAPTER 11 INITIATION OF DETONATION BY SHOCK WAVES

11-1 UNDERDRIVEN AND OVERDRIVEN DETONATION

Steady-state detonation is a self-supporting shock wave in which chemical energy constantly restores the deficit of mechanical energy that would otherwise be created because of dissipation at the shock front (into heat) and external losses. An inert or neutral shock wave without such a source of energy loses strength and ultimately disappears. The Chapman-Jouguet (C-J) detonation represents a dynamic "stable" condition. If there is a slight disturbance, such as a small gap in the explosive charge or a narrow region with greater explosive energy, the shock wave (or detonation front) will weaken or grow stronger temporarily, but will tend to return to the original stable condition when the perturbation is removed. Thus, when the shock at the detonation front is slightly weaker than the C-J wave, the energy supplied by chemical reaction causes the front to accelerate; and when the shock at the detonation front is stronger than the C-J wave, the chemical energy supplied is insufficient to maintain it and the front slows down. This behavior does not depend on whether the rate of chemical energy conversion is sufficient or insufficient *per se*, but rather whether the conditions in the flow is such that the released energy is transmitted to the front, i.e., whether the flow near the end of the reaction zone is supersonic, sonic, or subsonic (see Chapter 8).

In the situation represented in Fig. 11-1, where detonation is transmitted from a "donor" explosive to an "acceptor" explosive, there are three possibilities: the shock wave transmitted to the acceptor may be stronger than, of the same strength as, or weaker than the stable C-J wave in the acceptor. The first and last cases may be referred to as overdriven and underdriven detonations, respectively. The degree of overdrive and underdrive may be of any given magnitude, and it is of interest to determine the consequences of large departures from the C-J condition on the ultimate fate of the transmitted shock.

In the case of an overdriven wave, it is found that the strength always decays until the C-J condition is reached; but, for an underdriven wave in a given experimental arrangement, there is some limiting shock strength below which the wave decays and does not gain the increased strength needed to reach the C-J condition. The question of interest in this chapter may be stated: "What conditions are required for development of stable detonation from an underdriven shock wave?". The answer, obviously, bears on the question of safety in handling high explosives and materials, such as rocket propellants, that are potential high explosives. It also relates importantly to the problem of designing reliable initiating mechanisms in the practical use of explosives.

11-2 THE GAP TEST

Experimentally, a simple way to determine the sensitivity of an explosive to initiation by shock waves is represented in the gap test. This test comprises a method of producing underdriven waves of variable strength by inserting varying thicknesses of inert material between a donor and an acceptor charge (Fig. 11-2). Commonly, the inert material consists of a number of uniform "cards" which may be paper or plastic, for example. (An air-filled gap is not desirable because the hot explosive product gases from the donor would impinge directly on the acceptor.)

As in other tests of critical "go, no-go" behavior in explosives, the gap test experiments must be interpreted statistically. An efficient way to perform the test is the so-called "up-and-down" method, whereby, in a sequence of experiments, the number of cards is increased or decreased by one in each successive trial (or by some other standard incremental number) depending on whether the previous trial results in detonation or failure, respectively (see Chapter 12). The result of such a series of experiments is usually reported as the number of cards in the gap that produces, on the average, a 50 percent chance of detonation.

The gap test has been developed at the U. S. Naval Ordnance Laboratory into a useful means for comparing the sensitivity of solid rocket propellants[1]. The standard test assembly is

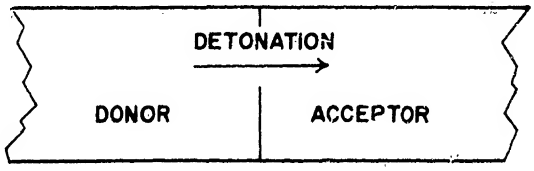

Figure 11-1. Transmission of Detonation From a Donor to an Acceptor Charge

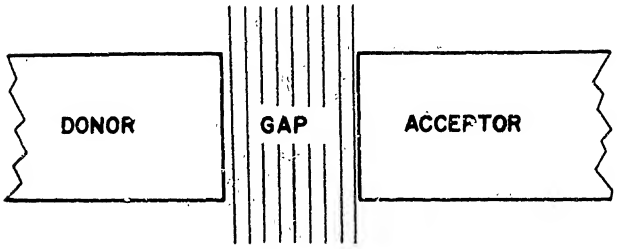

Figure 11-2. The Gap Test

illustrated in Fig. 11-3 and is described as follows: "a 5.08-cm length of pressed tetryl (ρ_o = 1.51 g/cc) to supply the shock; Lucite, or the equivalent cellulose acetate, as the shock attenuator; a moderately confined acceptor charge of 3.65-cm diameter by 13.97-cm length; and a mild steel witness (test) plate 0.952-cm thick. The criterion of 'detonation' used is the punching of a hole in the witness plate. The measure of charge sensitivity is the length of attenuator (gap length) at which there is 50 percent probability of detonation according to the above criterion.".

Gap test results become more significant when they are equated not simply to the number of cards or thickness of the gap but to the strength of the shock wave at the critical "go, no-go level". The Naval Ordnance Laboratory has "calibrated" the NOL test to make it possible to interpret the results in this manner. The method is described in the paragraph which follows.

11-3 SHOCK-PRESSURE MEASUREMENTS IN THE GAP TEST

By means of simultaneous shock wave velocity and free surface velocity measurements, such as those described in Chapter 5, the "Hugoniot adiabat" for Lucite has been determined. (The method of erecting the Hugoniot curve from the experimental data is explained in Chapter 8.) With this basic information the shock wave strength at the end of the gap can be determined from either shock wave velocity or free surface velocity measurements, with various thicknesses of Lucite in the gap, under actual conditions of the test, i.e., with the donor charge shown in Fig. 11-3. This kind of determination was carried out at NOL, with the results shown in Fig. 11-4, i.e., axial shock pressure at the end of the Lucite gap in kbar (1 kbar = 987 atm) vs thickness of gap.

The shock pressure at the end of the Lucite

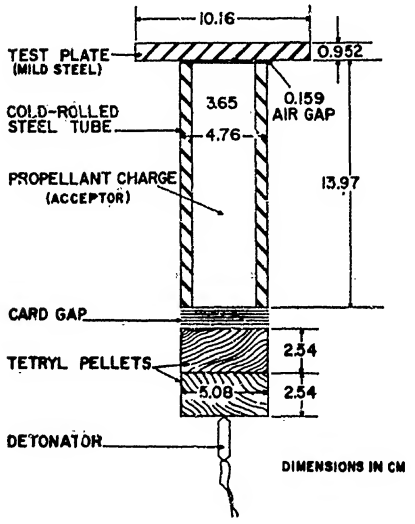

Figure 11-3. Charge Assembly and Dimensions for NOL Gap Test

gap, however, is not in general equal to the shock wave pressure transmitted to the acceptor explosive because there is usually an acoustic impedance mismatch between Lucite and the test explosive. The transmitted shock wave pressure can be readily determined from the Hugoniot adiabat of the acceptor. Experimental shock Hugoniots (or Hugoniot adiabats) have been determined for many of the military explosives (see Ref. 2). However, the impedance mismatch with Luicte does not differ very much for many of the common high explosives in the cast or pressed condition; therefore, the transmitted shock pressure in the explosive is approximately proportional to the incident pressure in the Lucite, Fig. 11-5 shows this relationship, the data points being the critical 50 percent explosion points for nine explosives for which sufficient equation of state data were available to calculate the initial pressure in the transmitted shock. It may be observed that for these materials no error would be made in ranking the explosives for shock wave sensitivity if one were to use incident pressures in the Lucite rather than transmitted pressures in the explosive. This statement would not necessarily apply, however, if explosives differing widely in density were being compared, e.g., a loose crystalline powder and a cast material.

Table 11-1 lists some of the results obtained on solid rocket propellants at the Naval Ordnance Laboratory. The term "loading pressure" in the table refers to the pressure of the incident wave at the end of the Lucite gap. A notable feature of the measurements is the effect of voids in composite propellants. (These propellants are based on ammonium perchlorate as oxidizer with an organic, rubber-like binder.) Composite propellants in their service condition and containing no high explosives such as HMX are generally nondetonable in this test, even when the tetryl donar charge is in direct contact with the propellant (zero gap). However, a negative result of the gap test cannot be taken to imply that a propellant is nondetonable under all conditions of initiation charge diameter and confinement. When the propellant is shredded and recompressed, leaving some air-filled voids, it becomes very sensitive to initiation. Voids, therefore, appear to influence sensitivity very markedly in this case.

11-4 EFFECTS OF SHOCK WAVES IN CONDENSED EXPLOSIVES

In a homogeneous material, lacking voids or discontinuities of any kind, a shock wave raises the pressure, density, and temperature uniformly in the plane immediately behind the front. Condensed media are, of course, very much less compressible than gases; therefore, the increases in density and temperature that accompany a given rise in pressure are much smaller than in gases. However, the pressures developed in the detonation of condensed materials are in the order of 10,000 times the detonation pressures of gaseous mixtures at an initial pressure of one atmosphere—e.g., 200,000 atm pressure for condensed explosives compared to 20 atm for gaseous explosives. Under such tremendous forces, even seemingly incompressible materials are highly densified and heated by the compression. It is perhaps not surprising to find, therefore, that the detonation front in a condensed explosive detonation heats the medium to a temperature in the neighborhood of 1,000°C or higher, a temperature quite high enough to start

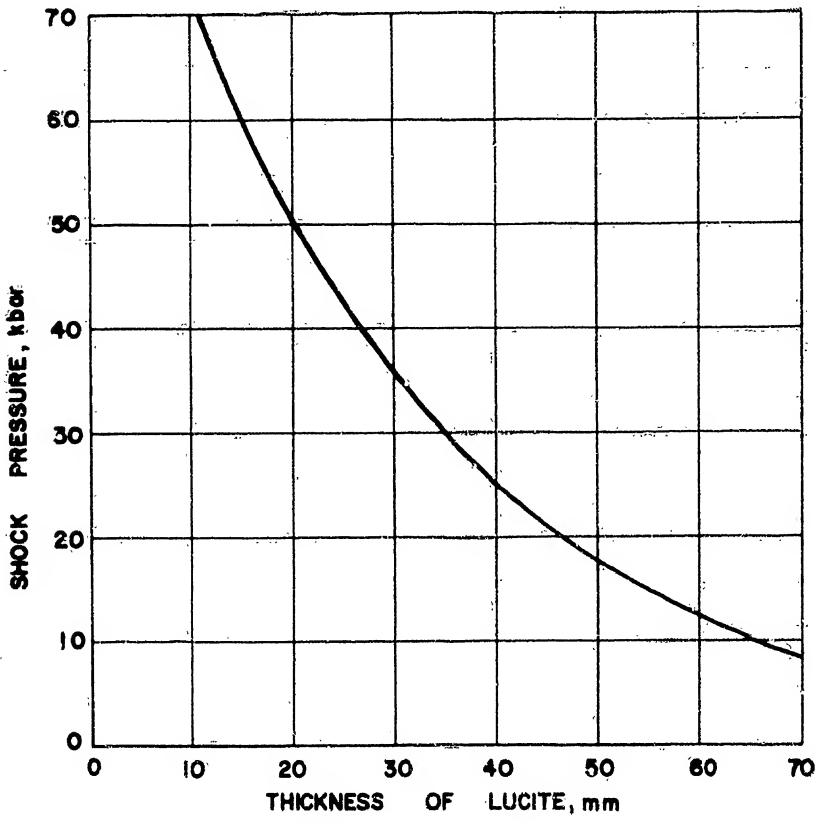

Figure 11-4. Shock Wave Pressure at the End of the Lucite Gap in the NOL Gap Test

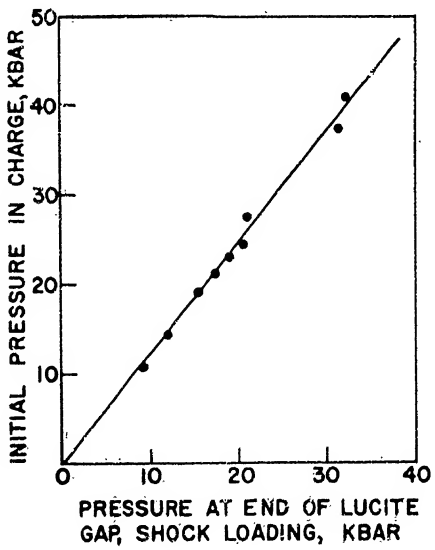

Figure 11-5. Comparison of Shock Loading at 50 Percent Point With Initial Pressure in Charges

decomposition at a rapid rate. The Zeldovich-von Neumann-Döering model of detonation is, therefore, equally as plausible when applied to condensed explosives as it is in the case of gaseous explosives.

There is, in fact, in the case of condensed materials a phenomenon that markedly increases their susceptibility to initiation by shock waves. This is the so-called "hot spot". An important class of hot spots is hydrodynamic in origin and results exclusively from the action of strong shock waves at discontinuities. The formation of the hydrodynamic hot spot and its subsequent behavior are, therefore, of primary importance in a discussion of shock initiation of explosives.

11-5 SHOCK INITIATION IN HOMOGENEOUS AND NONHOMOGENEOUS EXPLOSIVES

Although much valuable work has been done at several laboratories on initiation of detonation by underdriven shock waves, perhaps the most decisive experimentation of this kind has been carried out at the George Washington University Laboratory and the Los Alamos Scientific Laboratory. This work, largely summarized in Refs. 3-6, established that there is an essential difference between explosives that are completely homogeneous and free from discontinuities of any kind, and those which contain a multitude and a variety of such discontinuities. The presence of discontinuities is, of course, by far the most common practical condition, and it is only with extreme care that the number and size of discontinuities can be reduced to a point where the clearly defined behavior of a truly homogeneous material is evident.

The basic requirements for well-controlled experiments on shock wave initiation are:

(1) High degree of planarity in the incident shock wave. This is achieved by a plane-wave generator (Chapter 5).

(2) Sufficient run length of the plane detonation wave in a booster charge so that the decay of pressure behind the shock front (due to

TABLE 11-1 SHOCK SENSITIVITY OF SOLID ROCKET PROPELLANTS IN THE NOL GAP TEST

Propellant	*Physical State*	*Loading Pressure at the 50 percent Point, kbar*
various composites	service condition; nonporous	no-go
double base	service condition; nonporous	80-47
composite with 17-18 percent high explosive	service condition; nonporous	69-58
composite	shredded and pressed; 16-22 percent connected pores	11-7

the Taylor expansion described in Chapter 8) is small for a time period of some microseconds.

(3) Large enough diameter in the donor shock wave production system so that lateral expansion effects (described in Chapter 9) do not seriously affect the planarity of the shock wave or decrease the period of sustained high pressure behind the front.

(4) Variable attenuation of the donor shock wave. This is produced by inserting between the donor and acceptor charge a gap filled with an inert material of various composition and thickness.

A number of different experimental arrangements were used to elucidate various aspects of the phenomena. These cannot be described in detail here. Typical arrangements —taken from Refs. 5,6—are shown in Fig. 11-6(A) and 11-6(B), and illustrate how the various requirements previously enumerated were met in these experiments.

The major aspects of initiation phenomena in homogeneous and nonhomogeneous explosives as derived from a long series of experiments with liquid and solid explosives can be stated as follows:

(1) *In Nonhomogeneous Explosives.* If the entering shock wave is above a critical strength, it begins to accelerate at the point of entry, gaining strength relatively slowly at first, but ever more rapidly until steady-state C-J velocity is reached. The development of detonation in this case may be described as a smooth transition from a shock wave at first only weakly supported by chemical reaction to a fully supported steady detonation. The final stages of acceleration to detonation, in which the greater part of the increase in shock strength occurs, comprise only a small fraction of the total time between the initial entrance of the wave and the final achievement of full detonation. Material lying in the region between the point of entry of the shock wave and the region between the point where detonation first starts remains essentially unreacted, and retonation (a detonation wave moving back toward the point of shock entry) is often observed.

(2) *In Homogeneous Explosives.* The entering shock behaves as would a chemically unsupported shock in an inert material, decaying slightly and losing speed as it travels forward because of normal dissipation. After an induction period which bears a strong inverse relationship to the strength of the entering shock, detonation starts, not at the shock front but at the entering face of the acceptor. This detonation wave is characteristic of the explosive medium in the precompressed (and heated) condition created by the initial shock, and it travels at a hypervelocity (higher than the C-J velocity at normal density) characteristic of these conditions plus the velocity of forward motion imparted to the medium by the initial

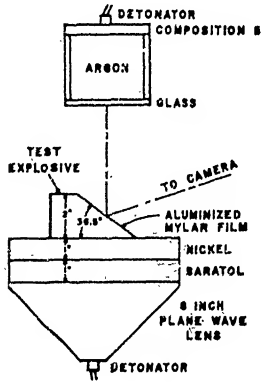

Figure 11-6(A). Arrangement to Measure Shock and Detonation Travel in a Nonhomogeneous Solid Explosive Using the Wedge Technique[6]

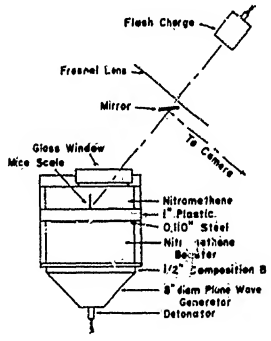

Figure 11-6(B). Arrangement to Measure Shock and Detonation Travel in a Homogeneous Liquid Explosive (Nitromethane)[6]

shock. This hypervelocity detonation, traveling at a higher speed than the initial shock wave overtakes it, and the combined wave moves from that point as an overdriven detonation the medium ahead. Eventually, the detonation wave decays to the characteristic, steady-state velocity of the explosive.

The distance-time relationships in these two contrasting situations are depicted in Fig. 11-7. Traces of essentially this nature were obtained by smear-camera techniques.

The induction time in the initiation of homogeneous explosives is sensitive to many factors. Indeed, the effects of various experimental variables are so important that only by taking extreme care is it possible to sort them out. Fig. 11-8, taken from Ref. 5, is a smear record taken from a camera viewing from the top (through a slit) the shock wave which is progressing upward toward the camera from the bottom of a vessel containing nitromethane. The light in this photograph is self-light from detonation; therefore, the original unreactive shock, starting at a point in time marked *F* in Fig. 11-8, is not visible. For this experiment the Plexiglas attenuator plate which formed the bottom of the nitromethane vessel (e.g., Fig. 11-6(B) was scored over half of the surface with triangular grooves, 0.020 in deep, spaced 0.025 in. apart. The other half of the surface was polished smooth. In Fig. 11-8, the scored half of the plate corresponds to the upper half of the photograph, and the smooth half to the lower. The photograph shows at the time marks *A* and *C* the sudden appearance of a faint light. This is light from the detonation when it originates in the precompressed medium at the Plexiglas surface. The time marks *B* and *D*, indicating the appearance of a much brighter front, indicate the points when the detonation in the precompressed medium overtakes the shock front producing an overdriven detonation in the undisturbed fluid. The induction time—represented by the distance between *F* and *A*, and *F* and *C* in the two regions—is seen to be about 2μsec on the smooth portion of the Plexiglas plate and less than one microsecond on the roughened portion. The explanation, presumably, is that the grooves in the Plexiglas produce distortions and interaction on the shock front which result in regions of somewhat higher temperature than that in the undisturbed shock,

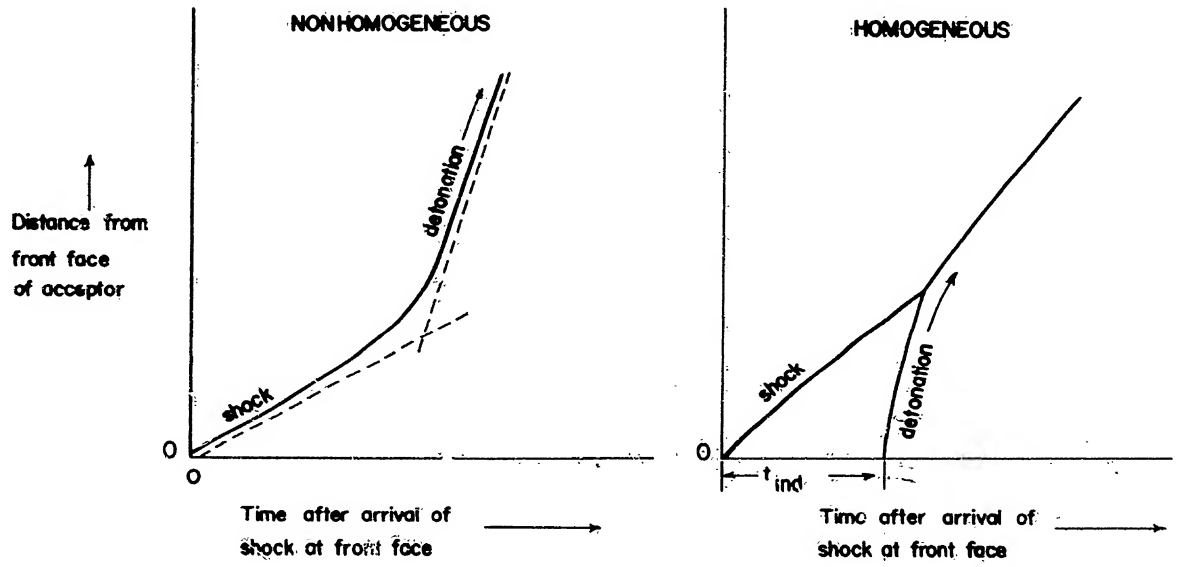

Figure 11-7. Distance vs Time Behavior in Shock Wave Initiation of Nonhomogeneous and Homogeneous Explosives

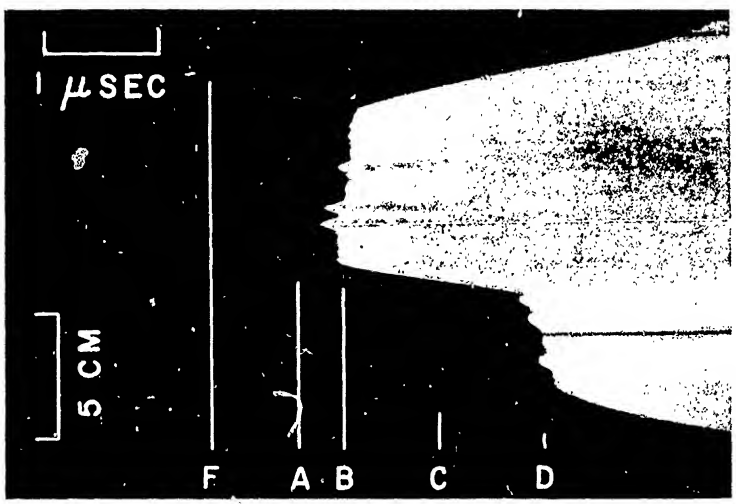

F: Shock enters nitromethane.

A: Detonation is initiated in compressed nitromethane at interface between nitromethane and grooved attenuator plate.

B: Detonation over grooved plate overtakes shock.

C: Detonation is initated at interface of nitromethane and smooth attenuator plate.

D: Detonation over smooth plate overtakes shock.

Induction time, t_{ind}: Over grooved plate *F* - *A*
Over smooth plate *F* - *C*

Figure 11-8. Smear Camera Record of Effect of Rough Shock Wave on Induction Time

with the result that thermal explosion occurs sooner on the roughened plate than it does on the smooth plate.

The induction time in a thermal explosion is very sensitive to temperature (Chapter 10). Therefore, the time for shock initiation of nitromethane would be expected to depend critically on shock pressure. That this is so can be readily seen from Fig. 11-9 which is taken from a recent analysis[7] of data reported by three different laboratories[3,5,8]. From Fig. 11-9 it also appears that increasing the initial temperature of the nitromethane causes a decrease in induction time.

The effect of hot-spot sites in nitromethane was also very nicely deomonstrated in the work described in Ref. 5. This was done by carefully locating air bubbles of various size at the Plexiglas-nitromethane interface. Other types of potential hot-spot sites have also been studied, including, for example, tiny rods of metal and glass that would produce a disturbance in the initiating shock front. A hot spot was usually visible as a flash of light at the moment of its creation by the shock wave; then, after a variable delay in time, a detonation was observed to spread out in a spherical front from the hot spot. (The hot spot produced no visible light during the induction period.) The effect is illustrated in Fig. 11-10, taken from Ref. 5. This photograph, taken in the same way as Fig. 11-8, shows the flash of light created by the interaction of the shock wave with a bubble at the time mark *F*. After a variable delay, explosions occur at *C* and *D* for the 1.0-mm and 0.75-mm bubbles, respectively; but no explosion occurred for the 0.5-mm bubble, presumably because the hot-spot temperature was too low or the size too small for an explosion to develop. The delayed homogeneous detonation occurs at the Plexiglas-nitromethane interface at the time mark *A* in Fig. 11-10, and the catch-up and formation of the overdriven detonation occurs at *B*. The dependence of the explosion induction period on the size of the hot spot site is clearly shown by this experiment. Also evident is a critical-size phenomenon in relation to hot spots since the smallest of the three bubbles did not produce a detonation.

The variable induction period, the critical "go, no-go" behavior of hot spots, and the important influence of temperature in these experiments point clearly to the explosion mechanism discussed Chapter 10. This inference has been investigated by C. L. Mader at the Los Alamos Laboratory[10] and Enig and Petrone at the U.S. Naval Ordnance Laboratory[11] in a series of "computer experiments," the results of which are discussed in the paragraph which follows.

11-6 THERMAL EXPLOSION THEORY APPLIED TO SHOCK INITIATION

11-6.1 HOMOGENEOUS EXPLOSIVES

The experimental phenomena described in par. 11-5 strongly suggest a thermal explosion mechanism in the shock wave initiation of homogeneous explosives. Detonation starts, not at the shock front but behind it, at the point where the wave entered the explosive and, therefore, where the high temperature produced by the shock has existed for the longest time. And, as it should in a thermal explosion, the induction period depends very sensitively on the temperature produced at this point. Proof that the phenomenon is indeed a thermal explosion would be provided if one could predict independently the magnitude of the induction period from the strength of the shock wave and the properties of the explosive.

The data needed for this calculation are the shock-Hugoniot properties of the explosive, a *PVT* equation of state and, the kinetic and thermal data for the chemical deposition (see Eq. 10-20). Unfortunately, reliable experimental *PVT* data are unavailable for shocked explosives. However, Mader[10] and Enig and Petrone[11], utilizing the same shock Hugoniot and kinetic data but different assumed *PVT* equations of state, were able to calculate induction times for nitromethane, liquid TNT, and single crystal PETN in reasonable agreement with experiment (see Table 11-2). While these calculations show that a thermal explosion mechanism is consistent with the observed shock initiation process in homogeneous explosives, they do not prove it.

How detonation develops from an underdriven shock wave in nitromethane is shown in the calculated pressure vs distance curves in Fig. 11-11. These curves are taken from Ref. 10. They were plotted by automatic equipment which took its input directly from the computer.

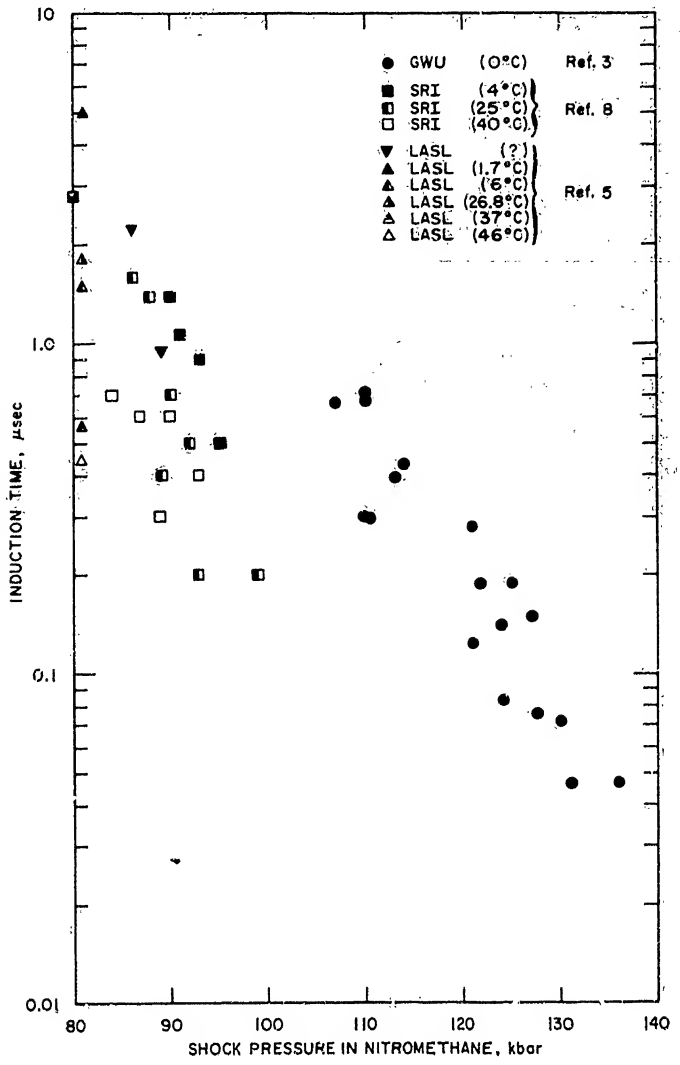

Figure 11-9. Shock Initiation Induction Times in Nitromethane at Different Shock Pressures and at Different Initial Temperatures

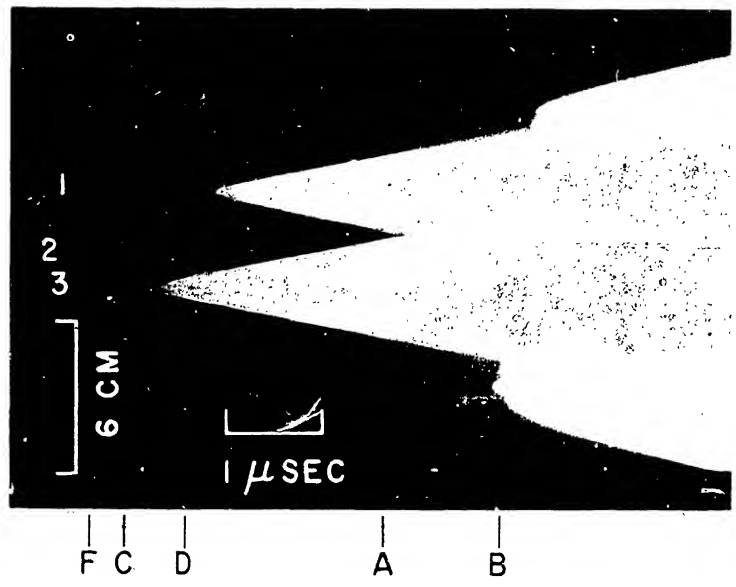

Argon bubbles: 1. 0.75-mm diameter
2. 9.50-mm diameter
3. 1.0 -mm diameter

F: Shock enters nitromethane. (Flash of bubbles number 1 and 3 may be seen.)

C: Local detonation starts at 1.0-mm bubble.

D: Local detonation starts at 0.75-mm bubble.

A: Detonation starts in precompressed nitromethane at interface with attenuator plate.

B: Detonation overtakes shock front.

Figure 11-10. Smear Camera Record Showing Effect of Bubbles in Initiation of Nitromethane

TABLE 11-2 CALCULATED SHOCK INITIATION INDUCTION TIMES IN HOMOGENEOUS EXPLOSIVES

Shock Pressure, kbar	*Shock Temperature, °K*		*Induction Times, μsec*		*Observed*
	Enig & Petrone	*Mader*	*Enig & Petrone*	*Mader*	
Nitromethane (T_o = 300° K)					
86	1103	1180	2.31	1.34	~1.0
170	1560	2100	—	—	—
201	1662	2472	—	—	—
Liquid TNT (T_o = 358° K)					
125	1154	1132	0.50	0.68	0.7
265	1992	2409	—	—	—
Single Crystal PETN (T_o = 298° K)	—	not shown	—	0.337	0.3

11-6.2 BEHAVIOR OF HOT SPOTS

The power of modern computer techniques is even more forcefully demonstrated in the treatment of hot spots reported by Mader in Ref. 10. Here the behavior is much too complex for analytical description. Even to anticipate what will happen, qualitatively, is difficult.

Mader treats the problem of describing all events set in motion by creation of a spherical hot spot, starting with various initial boundary conditions. In general, the following processes may be important:

(1) Production of heat by chemical reaction
(2) Dispersion of energy by wave motion
(3) Dispersion of energy by heat conduction.

The competition between (1) and (3) is treated in par. 10-4, where the following condition, Eq. 10-36, first derived by Zinn[12], is shown to apply:

$$t_{Ind} < 0.04\, a^2/\alpha \qquad (11\text{-}1)$$

The characteristic heat flow time on the right-hand side of the expression is seen to depend on the square of the radius a. For the "hydrodynamic" hot spots in nitromethane considered by Mader the size is so large (a = 0.03 to 0.3 cm) that this heat flow time is of the order of some thousands of microseconds. On the other hand, fluid dynamical energy dispersion (wave motion) occurs in a time of the order of a/c, where c is the speed of sound. Since c is of the order of 10^5 - 10^6 cm/sec, the time period characteristic of this mode of energy transfer is in the range of 0.01 - 0.1 μsec. Heat conduction can, therefore, be disregarded in this case and only the first two of the processes listed need be considered. However, this still poses a task that is impossible without the aid of a modern high speed computer.

The computer was programmed to integrate the partial differential equations of fluid dynamics (Chapter 2) in which the energy transport equation includes a term for chemical reaction. In principle, the problem is one of spherical shock wave propagation as treated in Chapter 13, with the added complication of variable energy sources at every point in the medium. Special methods, such as the von Neumann-Richtmyer artificial viscosity technique (Chapter 14), are needed to handle the shock wave problem alone.

Figs. 11-12, 11-13, and 11-14 are taken from Mader's paper[10], and the discussion which follows is quoted directly from that source. The model discussed here is termed the "temperature" hot spot—i.e., one in which the temperature is higher than in the surrounding (shocked) medium, but in which the density is the same as that of the surroundings. The pressure is, therefore, higher in the hot spot than

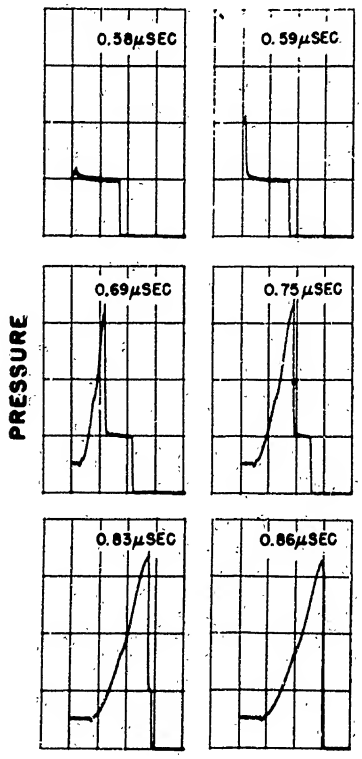

Figure 11-11. Pressure-distance Profiles at Various Times for the Shock Initiation of Nitromethane by a 92-kbar Shock (The ordinate is pressure in scale divisions of 100 kbar and the abscissa is Eulerian distance in scale divisions of 0.1 cm.)

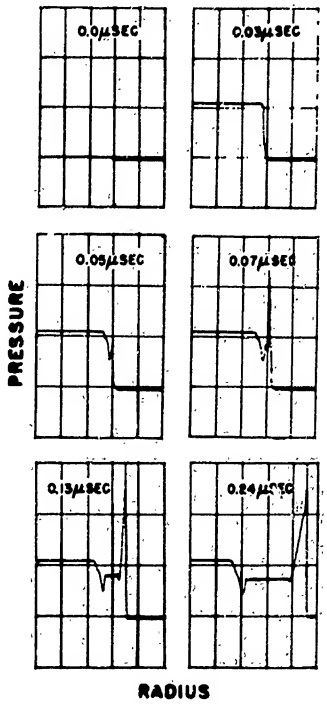

Figure 11-12. Pressure-radius Profiles at Various Times for the Development of a Detonation in Shocked Nitromethane (94.7 kbar, 1230°K) from a Spherical Temperature Hot Spot (1404°K) of 0.292-cm Radius (The ordinate is pressure in scale divisions of 100 kbar and the abscissa is Eulerian radius in scale divisions of 0.1 cm.)

in the bulk medium but the pressure difference is of somewhat minor importance in this case. Mader also treats the "pressure" hot spot, where density as well as temperature is higher than in the surroundings. This case will not be described here. The quotation from Ref. 10 follows:

"Fig. 11-12 shows the pressure-radius profiles for a 0.292-cm radius, temperature hot spot (1404°K) in nitromethane which has been shocked to 94.7 kbar. Initially, at the boundary between the hot spot and the shocked nitromethane, a small shock is sent into the outer nitromethane and a rarefaction is sent back into the hot spot. At about 0.03 μsec, part of the hot spot explodes and initiates the remainder of the hot spot, which has been

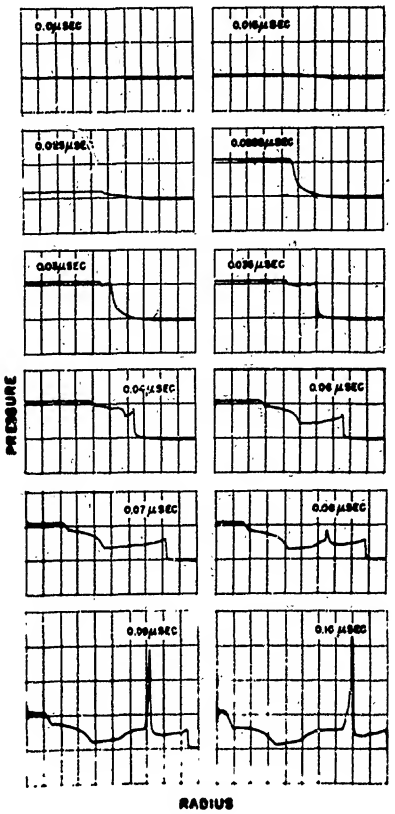

Figure 11-13. Pressure-radius Profiles at Various Times for the Development of a Detonation in Shocked Nitromethane (94.7 kbar, 1230°K) from a Spherical Temperature Hot Spot (1404°K) of 0.06-cm Radius (The ordinate is pressure in scale divisions of 100 kbar and the abscissa is Eulerian radius in scale divisions of 0.01 cm.)

cooled by the rarefaction. A strong shock goes into the undetonated nitromethane and a rarefaction goes back into the explosion products. The strongly shocked nitromethane at the hot spot boundary explodes at about 0.06 μsec and initiates a detonation which propagates through the rest of the nitromethane. The detonation propagates at a velocity of 0.856 cm/μsec, which is the computed equilibrium detonation velocity of the shocked nitromethane. The experimental hypervelocities in shocked nitromethane are approximately 0.8 cm/μsec[3,5].

"Fig. 11-13 shows in considerable detail the mechanism of initiation of detonation from a 0.06-cm radius, temperature hot spot (1404°K). Initially, at the hot spot boundary, a small shock is sent into the shocked nitromethane and a rarefaction is sent back into the hot spot. The pressure of the hot spot increases as a result of a chemical reaction. At 0.288 μsec, the inner 0.045 cm of the original hot spot explodes. At 0.035 μsec, the entire hot spot has exploded. A shock is sent into the undetonated explosive and a rarefaction is sent into the explosion products. The undetonated explosive at the hot spot boundary does not explode until 0.08 μsec, or after an initial induction period of 0.045 μsec. At 0.1 μsec, the detonation is propagating at full velocity and pressure.

"Fig. 11-14 shows the pressure-radius profiles for a 0.0292-cm radius, temperature hot spot (1404°K) in shocked nitromethane. The initial behavior is essentially the same as for larger hot spots. However, the pressure and temperature of the undetonated explosive at the hot spot interface decay more rapidly because of the greater divergence of the flow, and initiation of detonation fails to occur.

"Numerous other calculations were also performed varying the hot spot temperature and the temperature of the exterior nitromethane. The results can be summarized as follows. Temperature hot spots in shocked (≈ 90 kbar) nitromethane of 0.06-cm radius and larger will explode before the rarefaction reaches the center of the hot spot. Cooler hot spots may explode even after the rarefaction arrives at the center of the hot spot, since the rarefaction is weak. For example, it was observed that a

1300°K, 0.06-cm-radius hot spot exploded and initiated propagating detonation, even though the rarefaction had arrived at the center of the hot spot before the hot spot exploded.

"Temperature hot spots in shocked (≈ 90 kbar) nitromethane of 0.03-cm radius and smaller will not initiate propagating detonation. The spherical divergence of the shock is too strong. For example, it was observed that a 1400°K, and even a 1600°K, 0.03-cm-radius-temperature hot spot failed to initiate propagating detonation.

"As the pressure and temperature of the shocked exterior nitromethane decrease, the critical size of the hot spot increases. For example, a 0.27-cm-radius, 1400°K temperature hot spot in unshocked nitromethane will not initiate propagating detonation, while the same hot spot in nitromethane shocked to 90 kbar will initiate propagating detonation. Similarly, as the pressure and temperature of the shocked nitromethane increase, the critical size of the hot spot decreases. For example, a 0.03-cm-radius, 1400°K-temperature hot spot in

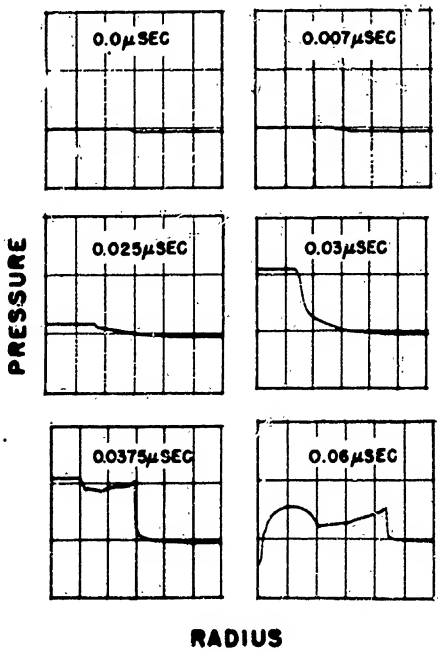

Figure 11-14. Pressure-radius Profiles at Various Times for the Failure of a 0.0292-cm-radius Temperature Hot Spot (1404°K) to Initiate Propagating Detonation in Shocked Nitromethane (94.7 kbar, 1230°K) (The ordinate is pressure in scale divisions of 100 kbar and the abscissa is Eulerian radius in scale divisions of 0.01 cm. The nitromethane at the boundary of the hot spot is cooling at 0.06 μsec, having a temperature of 1393°K. At 0.08 μsec the temperature has decreased to 1370°K at the boundary.)

1300°K shocked nitromethane will initiate propagating detonation, while the same hot spot in 1200°K shocked nitromethane will not initiate propagating detonation."

In summary, one may make the following generalizations concerning the behavior of hydrodynamic hot spots:

(1) The question whether or not a hot spot starts a self-propagating spherical detonation depends on its size, temperature, and pressure and on the temperature of the surrounding shocked medium.

(2) The first stage in the development of detonation from a hot spot is the explosion of material at the center of the hot spot. Such an explosion, however, does not necessarily lead to detonation.

(3) The critical phenomenon that prevents development of detonation from an exploding hot spot is usually the spherical divergence of the shock wave propagating into the surrounding explosive. In some cases, however, it is the spherical convergence of the rarefaction moving toward the center of the hot spot that chokes off the explosion.

(4) In any case, the development of a hydrodynamic hot spot is influenced mainly by chemical reaction and wave motion, and not appreciably by heat conduction.

(5) Results of the detailed investigation of hot spot behavior in nitromethane correlate well with experimental observations with respect to the critical size of hot spots and the shock wave conditions required to create hot spots that lead to local detonation.

11-7 HOT SPOT CREATION BY SHOCK WAVES

The contrasting behavior of homogeneous and nonhomogeneous explosives in the initiation of detonation by shock waves described in par. 11-5 can be readily understood if it is assumed that a shock wave in nonhomogeneous explosives creates hot spots as it passes through the material. Some of these hot spots explode and create shock waves that produce reaction, or, possibly, local detonation in the surrounding precompressed explosive. Since the initiating shock is underdriven with respect to a C-J detonation, energy liberated behind it can be transmitted to the front; hence, the shock wave gains added strength by the liberation of energy in the hot spots it has created in its wake. As the shock wave builds up, it produces hot spots of higher temperature which are, therefore, more apt to explode and produce local self-sustained shock waves or detonations. In the final full-scale detonation, initiation of reaction by the precursor shock may still depend on hot spot formation rather than initiation by uniform compression of the medium.

The concept of hot spots in connection with explosives originated from the study of initiation by friction and impact[13,15]. In experiments where hot spots are developed in inert material associated with the explosive—such as grit particles in the case of friction experiments and occluded gas pockets in the case of impact experiments—heat flows from the hot spots to the adjacent explosive and starts decomposition there. A delay of the order of 100 μsec is often involved between the impact that creates the hot spots and the explosion. Such a period of time is characteristic for diffusion of heat over a distance of the order of 10 microns.

A delay as high as 100 μsec, obviously, is impossible in most cases of shock initiation since in this period of time the shock wave would travel something like half a meter. From such considerations one concludes that hot spots, to be effective in shock wave initiation, must be created within the explosive medium itself and not in gas pockets or inert particles. In the case of initiation at the site of small air bubbles in nitromethane, as photographed in Fig. 11-10, the initial flash of light when the shock wave strikes the bubble is caused, no doubt, by the sudden compression of the gas in the bubble. But, the local detonation, which is initiated about one microsecond later, must arise from a hot spot created simultaneously in the nitromethane itself near the bubble, because this period of time is insufficient for heat transfer.

The paper by Evans, Harlow and Meixner[14] provides some insight into how hot spots can be produced in the medium surrounding a small discontinuity such as a gas bubble by interaction with a shock wave. The cases treated in detail by these authors involve only gases: specifically, the case of a bubble of neon in a helium continuum, and a bubble of helium in a neon continuum. The results are instructive, but obviously not

necessarily transferable to condensed explosives. Figure 11-15, taken from Ref. 14, shows how a bubble is deformed and the shock front distorted by interaction with the shock wave. Fig. 11-16 from the same paper shows the temperature distribution after the shock wave has passed through the bubble for the case of a neon bubble in a helium continuum. High temperature areas comparable in size to the bubble are formed in the adjacent medium due to the interaction.

Ref. 14 also describes the results of calculations for a shock wave interacting with a vacuum bubble in nitromethane. The bubble in this case collapses completely when struck by the shock, and a high temperature hot spot is formed in the adjacent liquid. Computational difficulties prevented this phenomenon from being more fully explored.

The formation of hot spots in nonhomogeneous explosives may be understood in terms of several different mechanisms (see References 13, 15-19, also Chapters 10 and 12). In a loose crystalline explosive, for example, hot spots within the crystals undoubtedly arise because of shock wave distortion caused by the sharp discontinuities in the medium. Also, physical impact of crystals at points of contact when they are propelled into motion by the shock wave may be an important hot spot mechanism in this case. In a pressed or cast polycrystalline explosive, the anisotropy of the crystals may give rise to shock wave interactions of important magnitude. And, even in a highly densified explosive, voids of microscopic size which produce shock wave interferences are not entirely absent.

Generally, an increase in void space causes an increase in sensitivity for any condensed explosive. The difference between a voidless material and a loose crystalline powder, for example, covers one or two orders of magnitude in the shock wave strength required for initiation. Thus, a homogeneous single crystal of PETN requires a shock pressure of about 100 kbar for initiation[20], whereas pressed granular

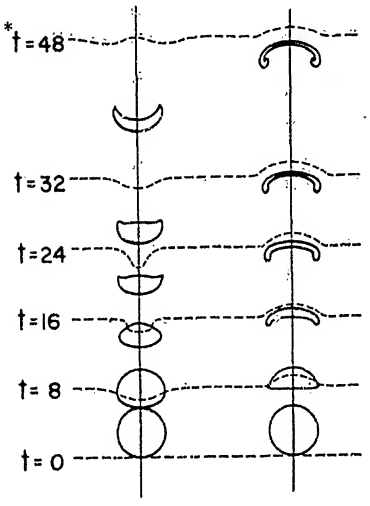

* Time scale is arbitrary; the relative values of the numbers are important.

Figure 11-15. Successive Configurations of Shock and Bubble (Left-hand sequence is for neon bubble in helium; right-hand sequence is for helium bubble in neon.)

PETN with 40 percent voids (density = 1.0 g/cm^3) requires only 2.5 kbar[21].

In the compressed granular explosive approaching crystal density, or in a plastic-bonded explosive, for example, hot-spot sites may be few in number and relatively "inactive". Such materials might be expected to show "homogeneous behavior" when initiated by a strong shock. In fact, it is quite possible to have hot-spot initiation and homogeneous initiation proceeding simultaneously, as the photograph in Fig. 11-10 shows.

11-8 SENSITIVITY TO SHOCK INITIATION

In most applications the main explosive charge is initiated by a detonator cap or primer, possibly in conjunction with a booster charge. Such an initiating system often produces an underdriven shock wave; therefore, many of the principles discussed in this chapter have a bearing on problems connected with the design and performance of these systems. Also, in the use of explosives for blasting, it frequently happens that an inert object may fall between two sticks of dynamite in a borehole, or that an air gap may result from not tamping the sticks in the borehole firmly enough. It is, therefore, important that explosives used for this purpose be sufficiently sensitive to shock wave initiation so that detonation will not fail to propagate under these circumstances.

In principle, one may distinguish between the shock wave sensitivity of explosives and sensitivity to other stimuli such as impact and friction. Indeed this distinction has been drawn in the division of subject matter in this handbook, the present chapter dealing with initiation by shock waves, and the next chapter dealing with initiation from thermal sources. Nevertheless, these two subjects have important factors in common.

The term "shock wave sensitivity" has been used rather loosely up to now, and it is important to clarify its meaning. One can, of course, define it arbitrarily in terms of some standard test, e.g., the gap test. The results of such a test may be treated in a more or less sophisticated way, by defining the sensitivity either in terms of the actual shock strength produced in the explosive at the critical, "go, no-go" threshold, or, more simply, in terms of the critical thickness of the gap material. But, either way, the point remains that any such definition is arbitrary in some degree because there is at least one other factor that may be important besides the peak pressure in the shock wave. This factor is *time*, i.e., the duration of the shock pulse or its characteristic decay time.

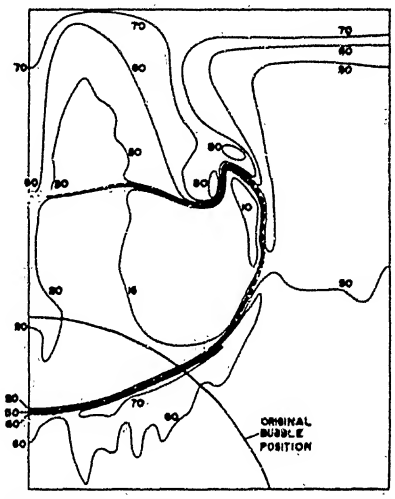

Figure 11-16. Isotherm Plots for the Shock in Helium Hitting a Neon Bubble (The numbers are 100 times the specific internal energy; behind the initial shock, the value is 50. Dashed lines show the bubble configuration. Cylindrical axis is to the left. Late-time heating at the top is caused by collision with wall. t = 30.)

The time factor in the initiation of solid explosives is of interest, because it could be important in determining shock sensitivity. In a shock sensitivity experiment, such as the gap test, the time period over which the initiating shock can be sustained in the acceptor charge without chemical reaction is limited either by (1) the diameter of the donor charge, (2) the length of the donor charge (i.e., the pulse width of the incoming shock), or (3) the diameter of the acceptor charge. This arises because

rarefactions (release waves) will always propagate towards the shock front from the charge boundaries (Chapter 9). The release waves are associated with a drop in pressure and temperature, and hence will effectively quench chemical reaction. Therefore, if detonation is to be initiated in an acceptor charge, significant chemical reaction (e.g., thermal explosion) must occur prior to the arrival of the release waves.

This criterion for shock initiation of detonation can be stated as

$$\tau(d^*) \geq t_e(P_I) \qquad (11\text{-}2)$$

where $\tau(d^*)$ is the time period available for chemical reaction when the limiting charge dimension is d^*, and $t_e(P_I)$ is the thermal explosion time for an initiating shock pressure P_I. The equality sign in Eq. 11-2 will then define the critical shock pressure (i.e., $P_I = P_{cr}$) for a "go or no-go" result in a gap test experiment. Since τ can be expected to decrease with decreasing d^*, and t_e to decrease with increasing P_I (see Eqs. 10-20 and 10-21), it can, therefore, be inferred that P_{cr} must increase with decreasing d^*.

This effect on P_{cr} has been borne out in a series of gap test experiments carried out by Aerojet-General Corporation with solid composite propellants[22]. Fig. 11-17 shows the experimental variation in P_{cr} with acceptor charge diameter for three different propellants*. In these gap tests the acceptor was a right cylinder with a diameter greater than the critical diameter d_c (i.e., the minimum charge diameter in which a steady-state detonation will propagate). The donor charge in each case was a conical TNT booster that is three base diameters in height with the base diameter equal to the diameter of the acceptor. The region below each of the curves defines the "no-go" region for the propellant, and above the curve, the "go" region†.

It is clear from the figure that there are values of the acceptor diameter, particularly near to d_c, where a decrease in charge dimension causes an increase in P_{cr}. It can be construed from these results that the acceptor diameter is acting as a limiting dimension d^* and that its effect becomes less important at larger charge diameters.

Table 11-3 shows the effect of variations in diameter of the donor charge on the shock pressure required for initiation of one of the propellants from Fig. 11-17 (i.e., propellant A with 9.2% RDX; d_c = 2.7 in.). Here the cylindrical acceptor charge diameter was kept constant at 6 in. and the donor charges were cylindrical TNT boosters whose diameters were varied. While the values for P_{cr} are not well defined by these data, it is clear that shocks of higher strength were required for a "go" result when the donor charge diameter was made smaller. This would again indicate that there is a limiting charge dimension d^*, namely the donor diameter, at least for those cases where the diameter is less than that of the acceptor. It is interesting to note from Table 11-3, that a "go" result can be obtained even when the donor size is less than the critical diameter of the acceptor, however the value of P_{cr} apparently is greatly increased in this case.

Fig. 11-18 depicts the results of a shock sensitivity experiment with Propellant A, d_c = 2.7 in., using the flyer-plate technique. In this test explosively driven flyer plates (5 sq. in., 1/32 to 1/2 in.) are impacted against the acceptor charge (4 in. diameter). In this manner planar shock waves with varying peak pressure, (proportional to plate velocity) and pulse width (proportional to plate thickness) are introduced into the acceptor. As in the gap-test, a "go or no-go" result is determined. It is quite evident from Fig. 11-18 that P_{cr} varies quite drastically when the pulse width is less than 1-2 μsec, but approaches a constant value at larger pulse widths. Since the pulse width in microseconds is governed by the release wave which moves directly behind and toward the shock front, the data of Fig. 11-18 can be interpreted as indicating the existence of a limiting dimension d^* which would be equivalent to the length of a donor charge. In this particular case, the d^* corresponding to a 2 μsec pulse width would be $\approx$7 mm.

One can conclude from these results that the critical shock strength for initiation may be controlled by factors which are not intrinsic to

* Compositions containing ammonium perchlorate, aluminum, RDX, and PBAN binder (polybutadiene-acrylonitrile copolymer).

† A "go" result was interpreted when detonation was initiated and sustained over the entire length of the acceptor (2-4 charge diameters).

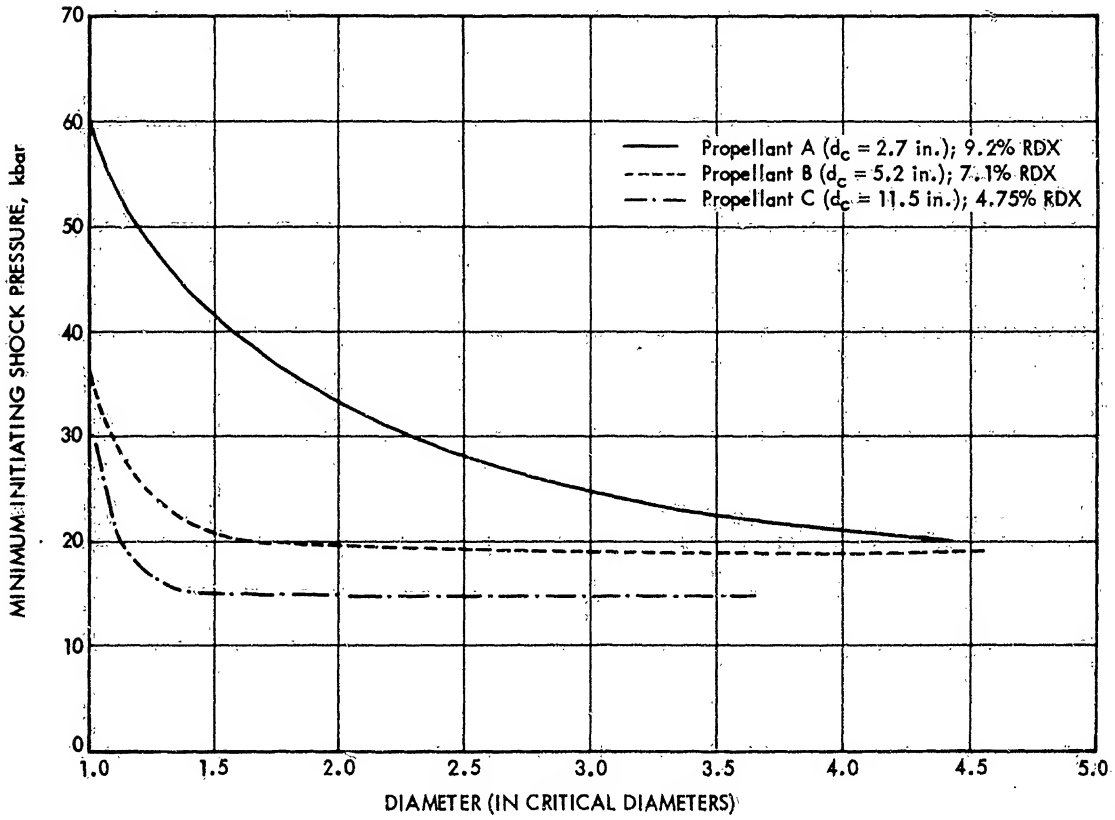

Figure 11-17. Normalized Initiation Criteria

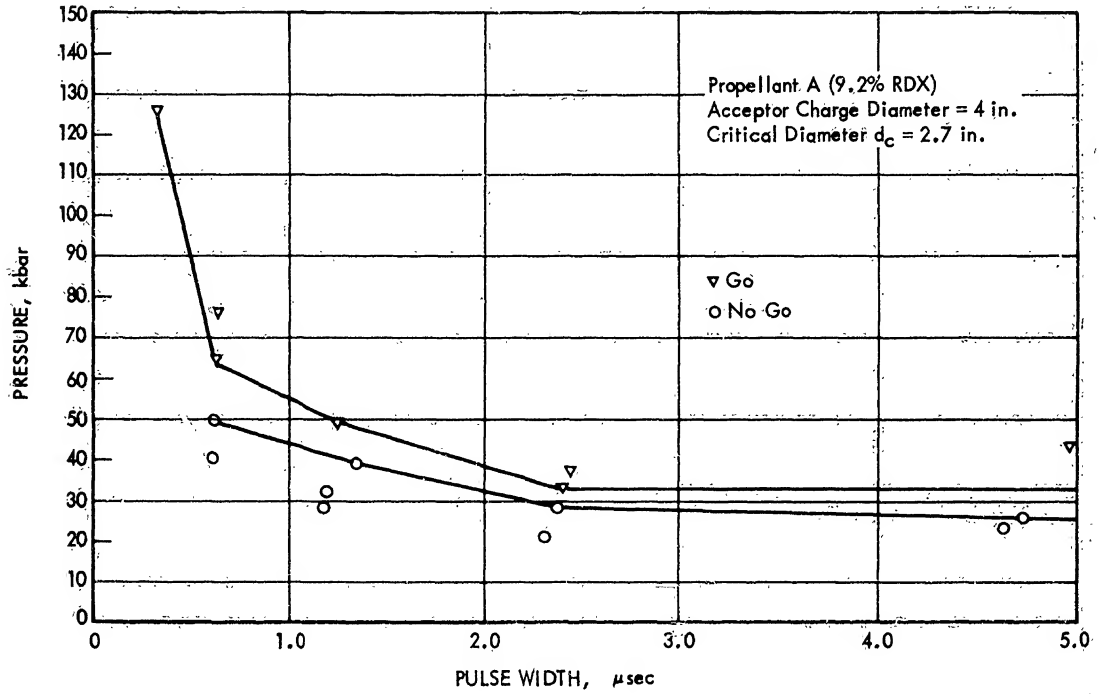

Figure 11-18. Effect of Pulse Width on Minimum Initiating Shock Pressure

AMCP 706-180

TABLE 11-3 EFFECT OF DONOR CHARGE DIAMETER ON SHOCK SENSITIVITY

Acceptor Charge: 6-in. right cylinder (critical diameter = 2.7 in.)

Donor Charge Diameter, in.	*Initial Shock Pressure, kbar*	*Gap Test Result*
1.00	250*	No-Go
1.50	250	No-Go
1.75	150	No-Go
1.75	250	Go
2.00	125	No-Go
2.00	150	Go
2.00	250	Go
3.00	50	No-Go
6.00	≈30	Go

* Maximum shock pressure attainable (i.e., zero-gap).

the explosive composition, in which case one must be cautious in comparing the experimental results from different test arrangements, and even with the same test arrangements. However, it is also evident that it is possible to minimize the effects of charge geometry on P_{cr} by utilizing charge diameters both for the acceptor and donor which are larger than the critical diameter of the test material.

11-9 THEORY OF SHOCK WAVE INITIATION IN SOLID EXPLOSIVES

The contrasting behavior of homogeneous and nonhomogeneous explosives when subjected to underdriven shock waves was described in par. 11-5. Solid explosives, except for single crystals, are nonhomogeneous; and, typically, unless the wave decays without producing detonation, it begins to accelerate immediately, and smoothly develops to a steady-state detonation. Acceleration of the front indicates that reaction is occurring close behind the shock. Electrical resistivity measurements derived by Campbell, Davis, Ransay, and Travis[6] tend to confirm this. Their experiments seem to show that the region immediately behind the underdriven shock front is electrically conductive, and that the conductivity in this region increases continually as the wave progresses until steady state detonation is reached. This indicates that weak chemical reaction occurs behind the entering shock front and becomes stronger as the shock wave builds up. This finding is somewhat at variance, however, with conclusions reported by Gipson and Macek[23], who interpreted their experimental results to mean that the reaction at first lags at a distance behind the shock. They explain the acceleration of the front as resulting from the action of compression waves emanating from the reaction zone. In their picture, the reaction catches up to the shock wave only when full detonation is established. The conditions were not the same in the two sets of experiments: Campbell, et al., employed plane, essentially nondecaying (step-like) shocks, whereas Gipson and Macek used a typical gap-test geometry where neither of these conditions were fully met. Also, the conclusions of Gipson and Macek are based on an observed difference in location of a pressure front as detected by pressure collapsing probes and a "flame front" as detected by a common type of ionization probe. The pressure detectors were located on the central axis of the cylindrical charge, and the ionization detectors at the interface of the explosive and the steel tube used to confine the charge. Possibly, the interpretation of the experimental results could be reconciled in the two cases if the electrical

response characteristics of the different ionization probes were carefully analyzed, and if the curvature of the front in the Gipson and Macek experiments were taken into account. The theory of hot spots as described in the previous paragraphs suggests that initiation takes place within 0.1 μsec or less after passage of the shock. It is to be expected that ionization will increase with time as the initiation process spreads, and as the reaction becomes general throughout the mass of the explosive. Therefore, the somewhat disparate conclusions of these two investigations may not be really at variance with this theoretical picture.

Although experimental work has not as yet yielded a clear picture of the nature of the reaction that supports a shock wave in the early stages of the initiation process in solid explosives, it is quite certain that energy release occurs not far behind the initiating front. This is in distinct contrast to the behavior of homogeneous liquid explosives where detonation develops at the back face where the shock first enters the explosives. Obviously the model of a simple first-order, Arrhenius-type reaction—which describes the latter phenomenon so well—does not represent the entire behavior of solid explosives. Indeed, there is little doubt that the actual mechanism involves initiation by hot spots followed by some sort of surface-erosive deflagration, or grain burning. The formulation of a mathematical model along these lines, however, presents some rather formidable problems not encountered in the homogeneous case.

The general approach to this question has been discussed by Adams[24], who shows that a pressure-dependent burning law as displayed by solid propellants, i.e.,

$$r = kSp^n \qquad (11\text{-}3)$$

where r is the linear surface erosion rate; S, the surface area; p, the pressure; and k and n constants, will meet many of the model requirements provided the reaction is supposed to start on all the grain surfaces when the shock advances over them. Warner[25] has formulated the equations of motion for a computer program with this type of heat release term. As a technical matter, it is necessary to set an arbitrary pressure level below which decomposition does not occur to prevent the explosive from decomposing even before the shock passes through it. Essentially this device performs the function of hot spots in the actual case. Another practical problem is to find an equation of state that satisfactorily describes the two-phase system representing the surface burning explosive grains and the product gases. In spite of obvious imperfections, a simple model with a pressure-dependent burning law does show the desired behavior: steady build-up of the shock front to detonation without overshoot. Some of the results reported in Ref. 25 are depicted in Fig. 11-19 and 11-20. These figures illustrate the calculations for an initiating shock of finite duration applied by means of piston motion at the left boundary of the explosive ($x = 0$), the motion of the piston being adjusted to support the flow at all times as reaction builds up. Full development of the von Neumann "spike" (Chapter 8) to the steady-state condition occurs in this case in about one microsecond.

Boyer and coworkers[26] have attempted to simulate the behavior of hot spots combined with grain burning by a "two-zone" model. The explosive grains are considered to be enveloped in a thin initiating layer which comprises a fraction F_1 of the total explosive. This initiating layer behaves as a homogeneous explosive, following a first order Arrhenius law. The activation energy is adjusted to give a suitably short ignition delay time. By means of this device the grain burning mechanism is brought into action in the second, inner zone. Behavior of this model is similar to that of Warner's model, showing a steady build-up to full detonation at the shock front. Interesting studies can be made in this case by varying the fraction F_1, which might be thought of as the "hot-spot" fraction. Boyer and Grandey[26] have also considered the effect of varying grain size on the behavior of the two-zone model. Larger grains lead to a longer reaction zone and a slower build-up to detonation, as expected (cf. Chapter 9).

Boyer, on the basis of the two-zone model, has investigated some interesting ideas pertaining to the effect of void spaces, or porosity in the charge. The following remarks are quoted from a discussion in the *Ninth Combustion Symposium*, p. 551 (Academic Press, 1963): "An interesting

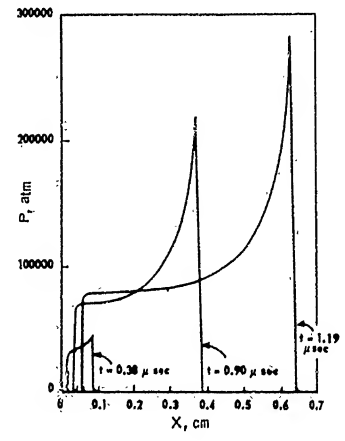

Figure 11-19. Build-up of Shock Wave in Solid Explosive to Detonation for a Surface-erosion (grain burning) Law of Heat Release[25] (The shock enters the explosive at X = 0 with a pressure of 10,000 atm.)

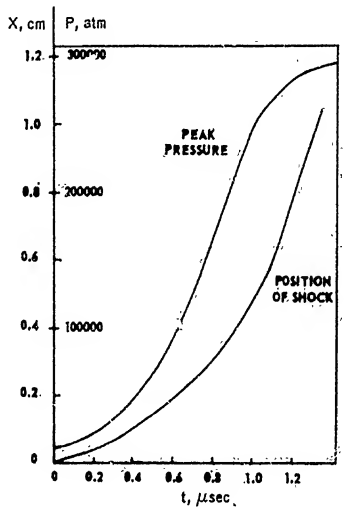

Figure 11-20. Peak Pressure and Position of the Wave as a Function of Time for the Case in Fig. 11-19

type of ignition occurs when there are pores or voids in the charge. It is found that if, upon passage of a shock over porous material, the pores are compressed to zero volume, then the energy deposition in excess of that deposited by a shock of similar intensity in a nonporous material is approximately proportional to the initial pore volume. This excess energy represents work done in compressing the pore. It is associated with motion and viscous dissipation, and presumably is deposited in the vicinity of the pore. If the volume of material so affected is approximately equal to the pore volume, then the temperature rise will be twice in bulk material. A hot spot approximately equal to the pore volume is, therefore, created (cf. Ref. 10, 14, and 22); this logically becomes the volume of the ignition region, and it is concluded that in the initiation of porous explosives by such a mechanism, the parameter F_1 can be taken to be equal to the fractional porosity of the charge. It is to be noted that the foregoing arguments do not depend significantly upon the type, or even the presence of occluded gas.

"This relation between porosity and the ignition process provides a resonable interpretation of many widely observed characteristics of detonation waves.. It is first necessary to realize that representation of the ignition reaction by an Arrhenius function means that the ignition reaction zone is very narrow. Its energy contribution to support of the wave is, therefore, not seriously degraded by lateral expansions, even at small charge diameters. This will be equally true of Taylor expansions (Chapter 8) behind the wave after a very short propagation distance. It follows that if a large fraction of the charge material is consumed in the ignition process, as would be the case, according to the previous argument, with loosely packed, porous charges (i.e., large F_1) one would expect a very short wave run up to steady state and a small critical diameter.

With a high density, nonporous charge, the converse would be expected. Such behavior is in general accord with experiment."

Boyer also makes these remarks concerning the effect of grain radius R_g. "The parameter R_g has a similar effect on the surface regressive process. A small R_g provides a thin reaction zone width and, consequently, a short run-up distance and small critical diameter, whereas the converse is true with large R_g. We have observed that computed waves in charges defined to have an R_g combined with a small F_1 (i.e., initiating fraction) will run for large distances at a velocity of about 4 mm/μsec before accelerating to a steady value. Since these waves were computed with one-dimensional geometry, the effect of lateral losses could not be ascertained (cf. Chapter 9), but it is believed that had such losses been present, these low velocity waves could have been indefinitely stabilized. Experimentally, it is reported that the condition of large grain size, high density, and small charge diameter is just that which results in stable low order detonation" (cf. Refs. 27 and 28).

The term "low-order" detonation is a loosely defined concept referring to reaction waves which travel at velocities much less than that predictable by C-J theory. These processes, which can be considered as intermediate between deflagrations and detonations, undoubtedly involve a critical balance between energy production by heterogeneous reaction processes and energy loss due to lateral expansion (Chapter 9). Hence the observed reaction wave depends critically on charge diameter, porosity, explosive composition, confinement, etc. A comprehensive review of this general subject can be found in Ref. 28 which is a U.S. Army Research Office STAF report.

A special case of "low-order" detonation is the so-called "low-velocity detonation wave" (LVD) which can occur in certain liquids and solids and in charge geometries which can also sustain a "normal" C-J type detonation. This special case is discussed in some detail in par. 11-10.

11-10 LOW-VELOCITY DETONATION (LVD)

The discussions of shock wave initiation have referred so far primarily to the establishment of a "normal" detonation wave whose velocity is commensurate with that predictable from hydrothermodynamic theory. For many years, however, it has been known that certain solid and liquid explosives (e.g., granular TNT and nitroglycerin) can detonate in two different velocity regimes (see Ref. 28). There is the stable "normal" mode or high-velocity detonation (HVD) which we have referred to previously, and an apparently stable low-velocity detonation (LVD) that propagates near the sonic velocity of the unreacted material. The LVD mode occurs only under special conditions of charge diameter, confinement, and initiation. This can be seen in Fig. 11-21 which presents the detonation velocities found in a typical blasting gelatin[29].

The HVD mode is seen to propagate essentially at the Chapman-Jouguet velocity of 7500 m/sec, while the LVD mode propagates at 1500-2500 m/sec, which is near sonic in the unreacted blasting gelatin. In this case, either HVD or LVD could be obtained at the same charge diameter simply by changing the initiation source from a high strength Briska detonator to a lower strength fulminate-chlorate detonator. Similar HVD-LVD phenomena have been reported for granular TNT[30].

The different shock strengths required to initiate HVD and LVD is one of the striking differentiating characteristics of the two modes of detonation. For example, HVD in homogeneous liquid explosives requires shock initiation pressures of 50-100 kbar, whereas an LVD in these same liquids might be initiated with shock pressures one to two orders of magnitude less. A good example of this difference can be seen in the gap-test sensitivity data (see Table 11-4) reported by the U. S. Bureau of Mines for a 50/50 nitroglycerin-ethylene glycol dinitrate explosive mixture (NG-EGDN) and a nitric acid-fuel solution (Cavea B110)[31].

The extreme shock sensitivity of materials to LVD has considerable significance in the safe handling of liquids which can undergo this mode of detonation. Accidental explosions have occurred in nitroglycerin and liquid monopropellant manufacturing facilities as the result of relatively mild initiation stimuli. This suggests that LVD may have been the responsible factor in the initiation of the explosion.

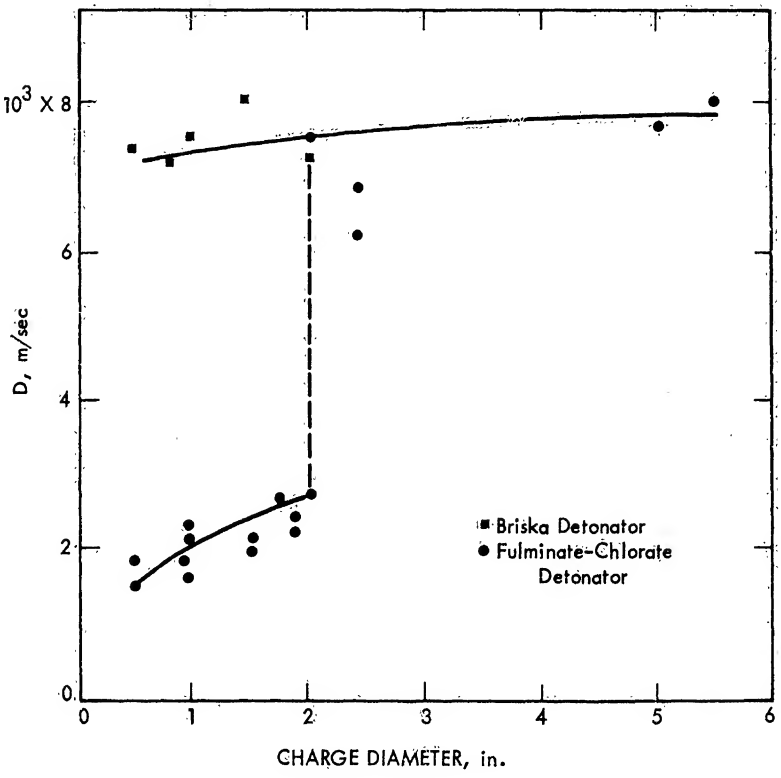

Figure 11-21. Propagation Failure in Blasting Gelatin[29]

TABLE 11-4 EXPERIMENTAL CARD-GAP TEST RESULTS

Confinement Material	Sonic Velocity,* m/sec	P_t/P_i**	Gap Values† (in. of Lucite)			
			NG-EGDN		Cavea B	
			HVD-LVD	LVD-NI	HVD-LVD	LVD-NI
Lucite	1840	1.00	2.2	> 12	1.2††	—
Lead	1190	1.73	1.8	> 12	1.5	—
Aluminum	5000	1.73	1.2	> 12	0.1	3.0
Copper	3810	1.87	1.0	> 12	< 0.1	4.0
Steel	5200	1.90	0.4	> 12	< 0.1	6.0

* Sonic velocity in thin rods of confinement material.

** Ratio of transmitted to incident pressures from Lucite gap.

† Gap values for HVD-LVD refer to threshold between HVD and LVD.
Gap values for LVD-NI refer to threshold between LVD and no initiation (NI).

†† Only HVD observed.

At the present time there is no adequate theory for LVD initiation and propagation, however, experimental studies at the U. S. Bureau of Mines[31-33] and Stanford Research Institute[34-36] have characterized some of the properties of LVD in liquid explosives. These studies suggest that the phenomenon involves complex shock interactions between the liquid and the container walls, and the formation of vapor bubbles by cavitation.

Table 11-5 shows some of the results found by the U. S. Bureau of Mines for the stability of an LVD wave in NG-EGDN under various conditions of confinement[33]. It is evident that wave stability is enhanced by increased container wall thickness and increased wall sound speed. These results along with high speed photographic evidence of cavitation in the liquid led Watson, et al.[33] to suggest the following four step model for LVD initiation and propagation.

In the first step, shocks (precursor waves) moving up through the container walls cause bow waves in the liquid explosive which compress the fluid. In step 2, the compressed liquid is expanded by the rarefaction waves which are associated with a radially outward motion of the container walls. In step 3, the liquid cavitates resulting in the formation of large numbers of gas bubbles. In the final step, the gas bubbles ignite to release the energy required to support the precursor shock wave in the container wall.

The mechanism by which these steps are coupled to yield a steady state reaction wave has yet to be worked out. However, the model is somewhat similar to the grain burning mechanism often postulated for granular solid explosives (e.g., see discussions in previous paragraph). In the solids case the surfaces necessary to support bulk grain burning are associated with the individual grains of explosive. In the liquids case, the necessary surfaces are formed *in situ* by cavitation behind the precursor waves.

Amster and coworkers[34] at Stanford Research Institute suggested a somewhat different model for LVD propagation. In this model the bow waves in the liquid coalesce to form a high pressure "Mach disc" which travels with the speed of the precursor wave. The pressure just behind the "Mach disc" could be quite high (≈ 85 kbar) which would be marginally sufficient to initiate the same type of reactions that support HVD in the liquid. This model would explain the observations that (1) a propagating

TABLE 11-5 RESULTS OF LOW-VELOCITY DETONATION STABILITY STUDIES WITH NG-EGDN

(c_o = 1.48 mm/μsec, ρ = 1.55 g/cm^3)

Wall Thickness, in.	*Result*	*Detonation Velocity, mm/μsec*
	Lead Tubes: c_o = 1.21 mm/μsec	
1/16	Unstable	----
1/8	Unstable	----
1/4	Unstable	----
	Plexiglas Tubes: c_o = 1.84 mm/μsec	
1/16	Unstable	----
1/8	Stable	2.14
1/4	Stable	1.84
1/16	Steel Tubes: c_o = 5.20 mm/μsec	
1/16	Stable	1.96
1/8	Stable	1.88
1/4	Stable	2.11
	Aluminum Tubes: c_o = 5.00 mm/μsec	
1/16	Unstable	----
1/4	Stable	2.04

LVD wave often changes in a jump fashion to an HVD wave, (2) an LVD wave is more stable in cylindrical containers (wall shocks in noncylindrical containers will not give rise to a "Mach disc"), and (3) LVD wave stability is sensitive to wall composition and wall thickness.

However, in subsequent studies Woolfolk and Amster[35] observed an apparent LVD propagation with 1,2 difluoraminopropane (1,2-DP) in cylindrical lead and square aluminum containers (see Table 11-6). This is inconsistent with the "Mach disc" model because with lead having a sound speed (c_o = 1.2 mm/μsec) just slightly above that of 1,2-DP (c_o = 0.96 mm/μsec) a high pressure "Mach disc" would not be expected to form in the liquid. Also, a well defined "Mach disc" is not expected to be formed when the liquid is contained in a noncylindrical geometry.

Indirect evidence in support of a cavitation type model comes from an extensive experimental study by Stanford Research Institute (SRI) of the sensitivity of an isomeric series of difluoramino propanes (1,2-DP; 2,2-DP; 1,3-DP)[36]. These liquid explosives consistently exhibit an LVD of ≈ 1 mm/μsec in charges of less than ≈ 9 mm diameter and an HVD of ≈ 6 mm/μsec at larger charge diameters. In some cases the LVD wave can be initiated by extremely weak shocks as can be seen from the

TABLE 11-6 LVD GAP TEST FOR 1,2-DP: EFFECT OF CONFINEMENT GEOMETRY AND SONIC VELOCITY

Tube Material	Sonic Velocity, mm/μsec	Geometry	Dimensions ID, cm	Dimensions Wall, cm	50% Gap, cm of Plexiglas
Aluminum	5.2	Cylinder	1.27	0.23	> 214
Aluminum	5.2	Square	1.27	0.318	> 61 – <91.5
Brass	3.7	Cylinder	1.27	0.23	> 95 – <122
Steel	5.1	Cylinder	1.27	0.63	> 91 – <126
Lead	1.2	Cylinder	1.27	0.63	> 95.0†

† No further test was made above this gap because the average propagation velocity had become subsonic.

positive gap test result for 1,2-DP with a 214 cm gap (see Table 11-6).

It was found by the SRI group that the order of increasing shock initiation sensitivity for the difluoraminopropanes is just that order which would be expected on the basis of increasing gas-phase reaction rates (see Table 11-7). In addition, the drop weight and spark sensitivities for the compounds follow the same order. On the other hand the order of HVD shock sensitivity as deduced from measured shock initiation induction times (see par. 11-5) is exactly opposite to that for LVD. These results suggest the following: (1) the controlling chemical reactions in LVD are gas-phase decompositons (i.e., in gas bubbles formed by cavitation of the liquid), and (2) the controlling chemical reaction step in LVD is not the same as that in HVD, at least for the two compounds shown in Table 11-7. The first suggestion is consistent with a cavitation type model for LVD, while the second suggestion is inconsistent with the "Mach disc" model.

The various observations of LVD in liquids indicate that a quantitative understanding of the phenomena cannot be obtained by application of the Chapman-Jouguet theory. Consideration must be given to the multiple shock wave interactions that occur and to heterogeneous bulk burning in the liquid.

TABLE 11-7 CORRELATION OF SENSITIVITY TESTS WITH REACTION RATES

Gas-Phase Reaction Rate	Sensitivity Test: LVD Gap	Sensitivity Test: Drop Weight	Sensitivity Test: Spark	Reaction Time HVD Gap
2,2-DP ↑ ‡	2,2-DP ↑	2,2-DP ↑	2,2-DP ↑	2,2-DP ↓ **
1,2-DP	1,2-DP	1,2-DP	1,2-DP	1,2-DP
1,3-DP	---	1,3-DP	---	---

‡ ↑ = increasing sensitivity or reactivity.

** ↓ = increasing reactivity.

REFERENCES

1. Donna Price, and I. Jaffe, Am. Rocket Soc. Journ. 31, 595 (1961).
2. *Fourth Symposium (International) on Detonation*, Sponsored by the U. S. Naval Ordnance Laboratory and the Office of Naval Research, Office of Naval Research Report ACR-126 (1965).
3. R. F. Chaiken, *Eighth Symposium (International) on Combustion*, Williams and Wilkins Co., Baltimore, Md., 1962, p. 759.
4. R. F. Chaiken, J. Chem. Phys. 33, 760 (1960).
5. A. W. Campbell, W. C. Davis, and J. R. Travis, Phys. of Fluids, 4, 498 (1961).
6. A. W. Campbell, W. C. Davis, J. B. Ramsay, and J. R. Travis, Phys. of Fluids, 4, 511 (1961).
7. R. F. Chaiken, Unpublished work at Stanford Research Institute, Menlo Park, Calif., 1969.
8. J. Berke, L. B. Seely, D. Tegg, and R. Shaw, Unpublished work at Stanford Research Institute, Menlo Park, Calif., 1969.
9. J. R. Travis, Reference 2, p. 386.
10. C. L. Mader, Phys. of Fluids 6, 375 (1963).
11. J. W. Enig and F. J. Petrone, Phys. of Fluids 9, 398 (1966).
12. J. Zinn, J. Chem. Phys. 36, 1949 (1962).
13. F. P. Bowden and A. D. Yoffe, *Initiation and Growth of Explosion in Liquids and Solids*, Cambridge University Press, 1952.
14. M. W Evans, F. H. Harlow, and B. D. Meixner, Phys. of Fluids 5, 651 (1962).
15. F. P. Bowden and A. D. Yoffe, *Fast Reactions in Solids*, Academic Press, New York, 1958.
16. M. A. Cook, *The Science of High Explosives*, Reinhold Publishing Co., New York, 1958.
17. *Proceedings of the International Conference on Sensitivity and Hazards of Explosives*, London, October 1963, sponsored by the Explosives Research and Development Establishment, Ministry of Aviation, Watham Abbey, Essex, England.
18. *Ninth Symposium (International) on Combustion*, Academic Press, New York, 1963.
19. C. E. Melton, D. F. Strenzwilk, and P. D. Yedinak, *Microscopic Theory of Detonation in Solids*, BRL TN 1715, Aberdeen Proving Ground, Md., April 1969.
20. T. E. Holland, A. W. Campbell and M. E. Malin, J. Appl. Phys. 28,1217 (1957).
21. G.E. Seay and L. B. Seely, Jr., "Initiation of a Low-Density PETN Pressing by a Plane Shock Wave", *Third Symposium on Detonation*, p. 562, Vol. 2, 1960, published by Office of Naval Research.
22. *Large Solid Propellant Boosters Explosive Hazards Study Program (Project SOPHY)*, Technical Documentary Report Nos. AFRPL-TR-65-11, Nov. 1965 and AFRPL-TR-67-211, August 1967.
23. R. W. Gipson, and A. Macek, "Flame Fronts and Compressions Waves During Transition from Deflagration to Detonation in Solids", *Eigth Symposium on Combustion*, Williams and Wilkins, Baltimore, Md., 1962, p. 847.
24. G. K. Adams, Reference 18, p. 545.
25. F. J. Warner, Reference 18, p. 536
26. M. H. Boyer and R. Grandey, "Theoretical Treatment of the Detonation Behavior of Solid Propellants", *Symposium of Amer. Rocket Soc. on Detonation and Two Phase Flow*, April 26-28, 1961. Published by Academic Press, 1962, S.S. Penner and F.A. Williams, Eds., 75. See also disscussions by M. H. Boyer, Reference 18, pp. 543 and 551, and additional paper in Reference 17.
27. A. Macek, "Sensitivity of Explosives", Chem. Rev. 62, 41 (1962).
28. J. A. Brown and M. Collins, *Explosion Phenomena Intermediate Between Deflagration and Detonations*, Esso Research and Engineering Co. Report on Contract No. DA-49-092-ARO-140, Oct. 1967, AD-662 778.
29. J. Taylor, *Detonation in Condensed Explosives*, Oxford University Press, 1952.

REFERENCE (Cont'd)

30. E. Jones and L. C. Cumming, *Second Detonation Symposium*, sponsored by the Office of Naval Research, 1955, p. 483.
31. R. W. Van Dolah, R. W. Watson, F. C. Gibson, C. M. Mason and J. Ribovich, Reference 17.
32. F. C. Gibson, C. R. Summers, C. M. Mason and R. W. Van Dolah, *Third Symposium on Detonation*, ONR Symposium Report ACR-52, Vol. 2, 1960, p 436.
33. R. W. Watson, C. R. Summers, F. C. Gibson, and R. W. Van Dolah, Reference 2, p. 117.
34. A. B. Amster, D. M. McEachern, Jr., and Z. Pressman, Reference 2, p. 126.
35. R. W. Woolfolk, and A. B. Amster, *Twelfth Symposium (International) on Detonation*, The Combustion Institute, Pittsburgh, Pa., 1969, p. 731.
36. Stanford Research Institute, *Sensitivity Fundamentals*, Reports on Contract NONR-3760(00); Annual Report No. 66-2, March 1966.

CHAPTER 12 INITIATION AND GROWTH OF DETONATION FROM IMPACT, FRICTION, AND THERMAL SOURCES

12-1 SENSITIVITY TO IMPACT AND FRICTION

Safety is, of course, a constant concern in handling explosives; from the beginning of their development, methods were sought to test the "sensitivity" of explosives to various types of stimuli. Explosives that are more sensitive to impact and friction are not necessarily more powerful; therefore, it should be quite possible in principle to produce explosives that are just as effective or more effective than those now in use and which, at the same time, are safer to handle and use. This has been the reason for much of the work on this subject. At the same time attempts have been made to interpret the sensitivity behavior in terms of properties that are better characterized and better understood.

The difficulty of the sensitivity problem stems, indeed, just from the fact that it is so poorly understood and, therefore, so poorly defined. Even at the present time there are no standards in this field; tests results from one laboratory may not entirely concur with those from another. In the United States there are perhaps three nonofficial "standard" impact test machines—one at the Bureau of Mines, Bruceton, Pennsylvania; one at Picatinny Arsenal; and one at the Naval Ordnance Laboratory (NOL). Because there are no guiding principles in this area, the design and dimensions of each of these devices was quite arbitrarily arrived at. However, to obtain meaningful and consistent results, great pains must be taken to control conditions in the test whatever they are arbitrarily established to be. The painstaking nature of this work is illustrated by the following description of the apparatus and methods presently in use at the Bureau of Mines, a typical piece of apparatus.

The Bureau of Mines impact apparatus shown in Fig. 12-1 is essentially a device in which a sample of explosive is subjected to an impact of a free-falling drop-hammer of 5-kg weight. It consists of a framework of steel T-beams which rise vertically from a massive steel base resting on a concrete pier. The drop-hammer and the yoke move between the steel beams which are 12.5 ft in height. The yoke is provided with an electromagnet so that it can be magnetized. It is raised or lowered by means of a windlass located at the base of the machine. When the yoke is magnetized, it attracts and holds the drop-hammer which may be raised to any desired height up to 330 cm. When the yoke is demagnetized, it releases the steel hammer. A recording device attached to the windlass measures the height from which the hammer is released. The anvil assembly is mounted on the base of the machine and consists of a hardened steel anvil and a plunger, 1.25 in. in diameter and 6 in. in length, machined to give a sliding fit through a steel guide ring. The drop-hammer, when released, strikes the plunger which transmits the forces developed on impact to a small striking pin that fits into a steel cup containing the test sample.

The striking pins—0.5-in. diameter by 0.75-in. length—are of type 440-C stainless steel, hardened to 55-60 on the Rockwell scale, and ground and polished to give a snug, freely sliding fit in the sample cup. The sample cups are approximately 0.5-in. in diameter and 0.25-in. in depth, and are of type 302 stainless steel with a wall thickness of 0.007-in.

The test sample of approximately 35 mg is placed in the stainless steel sample cup, and the striking pin is gently pressed down upon the sample. This assembly is then centered on the anvil by a shallow socket at the lower end of the plunger. The hammer is raised to a given height and then allowed to drop on the plunger. If no explosion or reaction occurs, the hammer is raised to successively greater heights and the test repeated with a fresh charge until a reaction occurs or until the maximum range of the equipment is reached. If a reaction does occur, fresh samples are tested at successively lower initial heights of fall until a point of no reaction is reached. Once the initial height is determined, a sample will be tested at a given increment below the level at which the previous sample was tested if that sample reacted, and a given increment above the level at which the previous one was tested if it did not react. By using this "up-and-down" method and analyzing the data

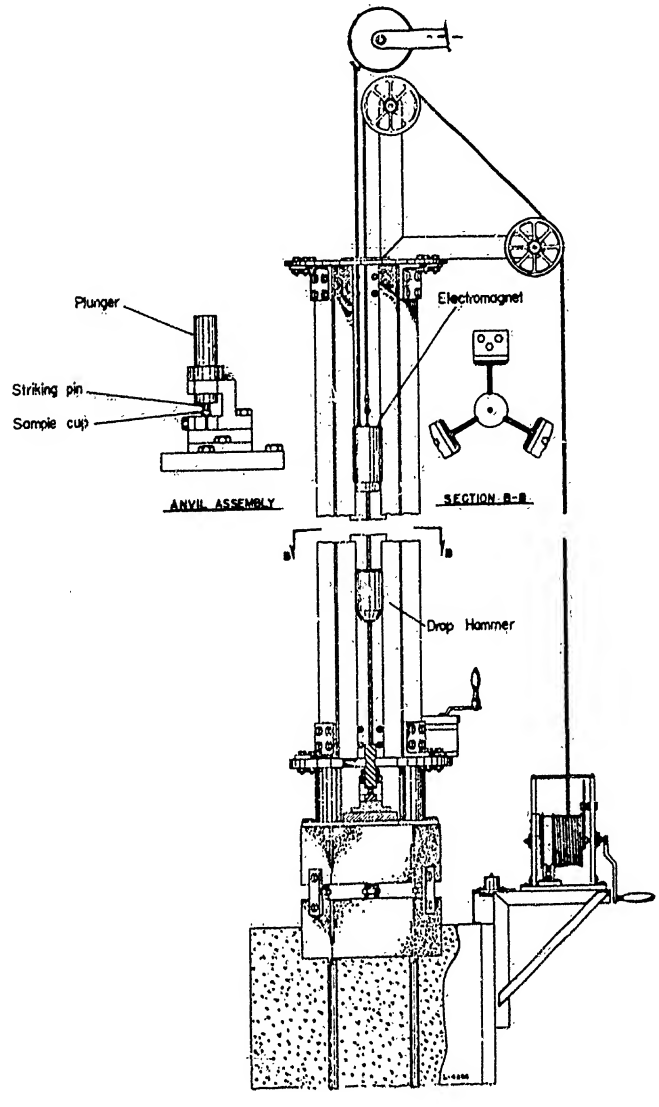

Figure 12-1. Impact Apparatus Showing Anvil-striking Pin Assembly

statistically, a height for 50-percent ignition probability is attained.

The determination of an "explosion or reaction" is based on visual and aural observation. Any indication of decomposition—explosion, burning, flash, smoke, or charring—is considered a "go".

One difference between the Bureau of Mines test and that at NOL is the use at NOL of a piece of sandpaper placed under the sample on the test anvil. This possibly has the effect of more nearly standardizing the mechanism by which the mechanical energy of the falling weight is converted to heat in the explosive sample.

Other differences are present in the tooling, drop weight, size and criteria for judging a "go". All differences combine to give different 50-percent drop height values for the same explosives; however, in general, when properly determined on adequate equipment, the results have a differential validity in that they correctly order explosives with respect to impact sensitivity.

Friction testing of explosive has not been as common as impact testing. However, interesting

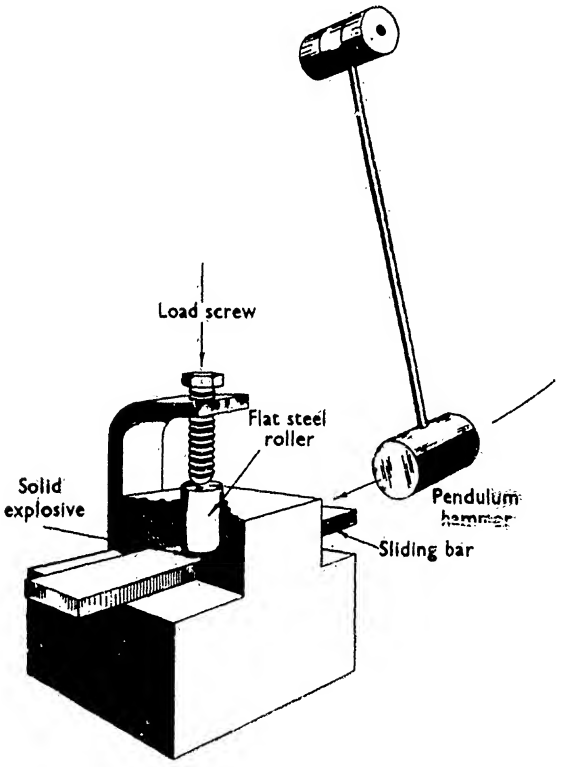

Figure 12-2. Illustration of Apparatus Used for Determining the Friction Sensitivity of Solid Explosives

results have been obtained by Bowden[1] and coworkers using friction apparatus such as that illustrated in Fig. 12-2. Some of the results are described in par. 12-3. The device in Fig. 12-2 is designed so that a thin layer of solid explosive is subjected to rapid shear while held under a known load.

12-2 DESIGN AND ANALYSIS OF SENSITIVITY EXPERIMENTS

Explosive sensitivity tests are among the few examples of what might be described as one-shot, "go or no-go" experiments. Certain types of biological tests, e.g., lethal dosage, also fall into this category. In experiments of this nature, only a single trial can be performed on each specimen because it is so altered by the test, regardless of outcome, that it cannot be subjected to further testing. Thus, it is not possible to determine the critical level of the independent variable—e.g., the drop height of the impact test—in this case for each specimen and, therefore, an element of indeterminacy is inherent in each trial result. One consequence of this situation is that more tests are necessary to determine the sample mean and standard deviation with given precision than in experiments where a definite critical threshold value can be assigned as a result of each trial. Another consequence is that a certain method of testing, the so-called "up and down" method, is considerably more efficient than other methods in deriving this information.

The up-and-down method was developed by the Explosives Research Laboratory, Bruceton, Pa., and the statistical analysis appropriate to it was developed by the Statistical Research Group at Princeton University during World War II. A full treatment of the subject may be found in Ref. 2; the essentials are given in the following discussion which refers specifically to the drop-weight impact sensitivity test.

In performing a test on a given sample of explosive, one first of all fixes certain points on the height scale at which trials will be made. Individual trials are then made by setting the drop hammer at one of these points, never at intermediate positions. The fixed points, which we designate by the general symbol h_i to indicate the *i-th* point on the scale, are separated by equal intervals d on a *normalized* scale. The normalized scale is defined as that scale function of height on which the *actual* critical drop heights—if these could be determined—of an infinite number of specimens of the explosive would be normally distributed (in the statistical sense). Experience indicates that the normalized scale in the impact test is the logarithm of the drop height; therefore, the intervals should be equal increments of log height. If equal linear intervals on the height scale are used, it would lead, in principle, to errors in the application of the statistics. (A test for normality of scale is described in Ref. 2.) Ideally, the interval d should be chosen, equal to the standard deviation σ. Obviously, since σ is not known in advance, the magnitude of d had to be selected on the basis of experience. A choice of interval either larger or smaller than σ simply makes the test less efficient but does not invalidate the results.

The "up-and-down" test is carried out in a sequential manner, the choice of test level for the drop hammer in each trial being dictated by the result of the trial just preceding it. The drop hammer is raised by one interval d to the next higher point h_{i+1} if the preceding trial at h_i was "no-go" and is lowered by one interval d to the next lower point h_{i-1} if the preceding trial was "go". This procedure results in a nearly equal number of "go's" and "no-go's", and guarantees that a great majority of trials is grouped around the mean. An example of an actual test involving 100 trials is shown in Fig. 12-3. In this type of testing, 100 or more trials are considered necessary if reasonably good estimates are to be made of the mean height.

The formula for calculation of the mean height (or mean log height if the log scale is used) follows. The computation is based either on the "no-go's" (zeros) or the "go's" (x's), depending upon which is *least* in number; if the number of each is the same, either may be used. When the numbering of the fixed points starts with zero at the lowest level at which tests were made, the mean level m is given by

$$m = c + d\left[\frac{1}{N(o)}\Sigma i n_i(o) + \tfrac{1}{2}\right] \qquad (12\text{-}1a)$$

where c refers to the normalized scale value at the zero level—e.g., the value of h_o in Fig. 12-3;—$N(o)$ refers to the total number of zeros, or "no-go's"; i is the number of the level; and

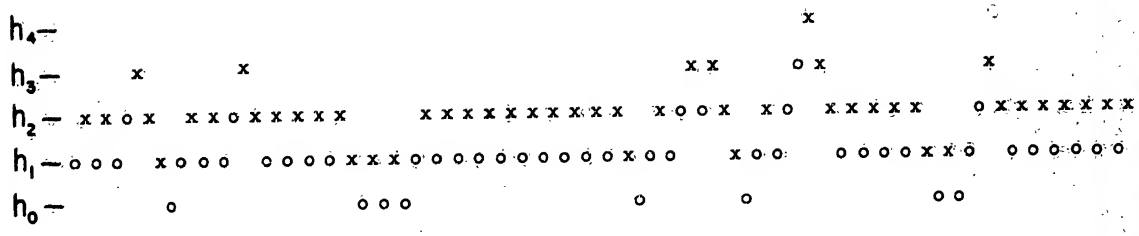

Figure 12-3. Example of a Sensitivity Test Result Comprising 100 Trials Following the Up-and-down Method (x indicates "go", and o indicates "no-go")

$n_i(o)$ the number of zeros at that level, the sum being taken over all levels above the zero level. A similar formula applies if one counts the "go's" or x's, as follows:

$$m = c + d\left[\frac{1}{N(x)}\Sigma i n_i(x) - \tfrac{1}{2}\right] \qquad (12\text{-}1b)$$

where $N(x)$ refers to the total number of x's, and the other symbols are defined consistently with those previously given. Eqs. 12-1a and 12-1b are, of course, identical with usual formulas for calculating the mean, except for the correction ± 1/2, which takes account of the fact that the independent variable is not continuous, but "quantized".

Calculation of the standard deviation σ is not so direct. One first calculates a number M defined by

$$M = \frac{\Sigma i^2 n_i}{N} - \left[\frac{\Sigma i n_i}{N}\right]^2 \qquad (12\text{-}2)$$

where N and n_i refer to either the zeros or the x's, the choice being of the one for which N is the smaller if N is not the same for both. If $M > 0.40$, a number s is calculated from it by the approximate formula

$$s = 1.60\,(M + 0.04) \qquad (12\text{-}3)$$

If $M < 0.40$, the curves in Fig. 12-4 are used to find s. The actual curve to be used depends on how close the mean value m is to the nearest test point h. Interpolation can be made between the curves in Fig. 12-4 when the difference $m - h$ does not correspond to a value for which a curve is given. When s has been evaluated, the estimated standard deviation σ is calculated by the formula

$$\sigma = sd \qquad (12\text{-}4)$$

These formulas, of course, give *estimated* values for m and σ based on tests on a finite sized sample. The standard error of the estimates depends, as in ordinary statistics, on $1/\sqrt{n}$ where n is the total number of trials. It also depends on the relative size of d and σ, and on where m happens to fall within an interval on the height scale. For the formulas used to compute standard errors of various estimates, the reader is referred to the original publications[2]. However, it should be noted that Martin and Sanders[3] compared the analysis of the Bruceton method to that of large sample theory employing the results on as many as 150,000 trials obtained in a simulated computer experiment. They concluded that for a sample size of 100, the Bruceton type of test will give a good estimate of the mean m, but a relatively poor estimate of the standard deviation σ. With a sample size of 25, the spread in m becomes excessive.

12-3 THEORY OF IMPACT SENSITIVITY

It is now widely accepted that initiation in all the common sensitivity tests depends on thermal explosion. Usually, the temperature rise produced by the test stimulus is not uniform throughout the mass of explosive; instead, heat is concentrated in one or more small-volume elements, i.e., hot spots, created by the stimulus. Explosion occurs in these areas and spreads into the mass by the action of hot gases or of compression waves, or of both. A complete theory of the phenomena in any given type experiment would have to treat the following aspects: (1) process by which heat is produced in a hot spot as a result of the initial stimulus, (2) distribution of size and temperature level among the hot spots as a function of intensity of the initial stimulus, (3) temporal behavior of a hot spot after it is formed as a function of size and initial temperature, and (4) spread of reaction to the bulk explosive following explosion of the hot spots.

Because of the obvious complexity of the problem, a complete theory such as this has never been formulated, but considerable attention has been given to the problem (see Chapters 10 and 11). The types of processes by which hot spots are produced as a result of impact and friction have been the subject of much artful research by Bowden, Yoffe, and coworkers[1]. This work has demonstrated that there are a number of mechanisms by which part of the mechanical energy may appear as heat concentrated in a number of small volume elements or hot spots in the explosive mass. These findings are as yet only semi-quantitative, and in no instance is it possible to calculate with certainty the size or temperature of a hot spot that is produced, for example, by some given impact. Neither is anything yet known about the

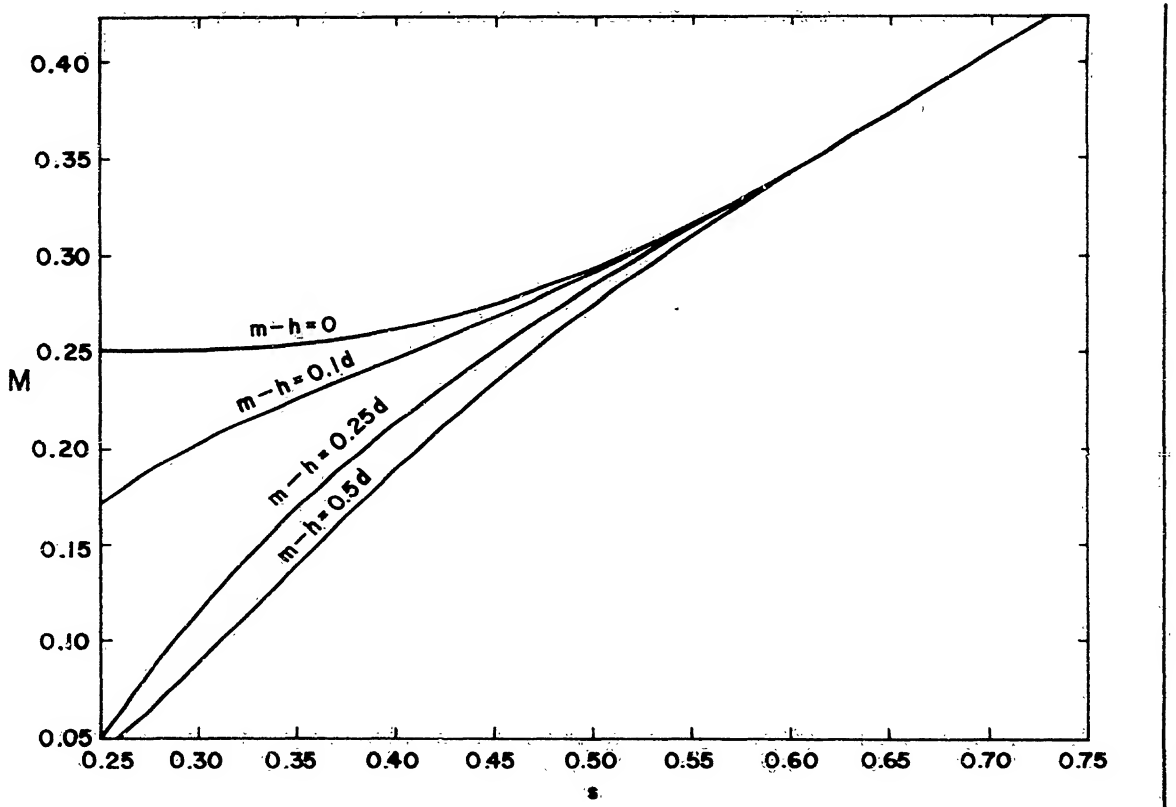

Figure 12-4. Curves for Calculating s from m When m < 0.40 in the Statistical Reduction of Impact Sensitivity Data

distribution of temperature and size among the hot spots produced, or how these distributions affect the behavior of the explosive. The theory of thermal explosion was applied to hot spot behavior by Rideal and Robertson[4] and their work has been extended by several others, including Gross and Amster[5], Boddington[6] and Friedman[7]. The final growth of the explosion following decomposition of the hot spot has not been specifically treated. What has evolved to the present time, then, is a partially complete and still largely qualitative model. Comparison between theory and experiment consist in correlation rather than quantitative calculation.

Bowden[1] has listed the possible effects of impact or shock as follows:

(1) Adiabatic heating of compressed gas spaces
(2) Frictional hot spot on the confining surface or on a grit particle
(3) Intercrystalline friction of the explosive itself
(4) Viscous heating of the explosive flowing under high rates of shear
(5) Heating of a sharp point when it is deformed plastically
(6) Mutual reinforcement by interference of shock waves.

The adiabatic heating of compressed gas bubbles proves to be an important source of hot spots in liquid explosives like nitroglycerin. The importance of this effect is illustrated by the following experimental finding. With nitroglycerin, when a bubble as small as 5×10^{-3} cm in radius is present, an explosion efficiency of 100 percent may be obtained with a 40-g weight falling 10 cm; but, when no gas bubble is present something like 5 kg falling through one meter may be needed to initiate explosion. Nitroglycerin can be initiated when a 40-g striker falls a distance of only 0.5 cm with the apparatus depicted in Fig. 12-5. (Fig. 12-5 is taken from Ref. 1.) Trapped air pockets may also be the source of hot spots in the impact testing of granular solid explosives but this is not so readily demonstrated.

A fact overlooked in early speculations on the effect of trapped bubbles on impact is that the heat made available by the compression of the air in a small bubble does not flow rapidly enough into the surrounding liquid explosive to heat it to a temperature necessary for explosion. Evidence has been adduced by Johannson and coworkers[8] to show that impact on a liquid containing a gas bubble causes a fine spray or foam inside the bubble. The tiny particles explode when heated by the hot compressed gas in the bubble, and the heat in these explosion products is then communicated to the bulk. Because of this mechanism, therefore, a compressed bubble is actually a much more potent source of heat than a simple calculation based on the gas alone would indicate. Similar effects, caused by fracturing and splintering of crystals, may occur in the impact test on solids.

In the frictional mechanism of hot spot formation; melting point, thermal conductivity, and viscous flow play an important role. Melting point is significant because a low-melting material subjected to a given impact stimulus may take up so much heat by melting (latent heat) that it is prevented from reaching the explosion temperature. A convincing series of experiments on this point has been performed by Bowden and coworkers[1] who added various kinds of grit to an explosive and subjected it to a given stimulus, either friction or impact. Typical results are given in Table 12-1 which lists the hardness as well as the melting point of the various grit materials used. While there is apparently no correlation between test results and the hardness of the grit particles, there is a very significant relationship of the behavior to the melting point. Clearly, there is a sharp threshold effect when the melting point of the grit particles lies in the region of 400°C or higher.

It is interesting to note that for some primary explosives, like lead azide, lead styphnate, and mercury fulminate—and secondary explosives, like PETN and TNT—that the secondary explosives melt at a temperature below the point at which they normally explode, whereas the primary explosives explode below the temperature at which they melt. This may help to explain the marked difference in sensitivity between the two types of explosive. However, melting point alone cannot explain the differences in sensitivity of pure secondary explsives; for example, PETN (m.p. = 142°C; 50 percent impact height ≈ 25 cm) and RDX (m.p. = 204°C; 50 percent impact height ≈ 25 cm). Chaiken and Cheselske[9] suggested that in these cases the rate of heating by friction (and impact) may be controlled by surface rate processes involving viscous melt flow. Quantitative

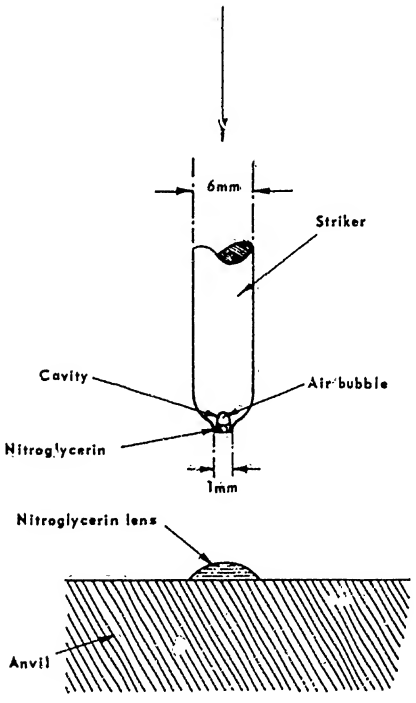

Figure 12-5. Cavity Striker, Showing Small Air Bubble Inside Cavity

measurements of the rates of viscous melt flow for PETN, RDX, tetryl, and TNT under surface heating conditions showed that at a given energy input the observed melt temperatures follow the same order as the sensitivity, i.e., PETN > RDX > tetryl > TNT. These studies indicate the possible importance of endothermic rate processes in determining the sensitivity of explosives to external stimuli.

A simplified derivation of the relationship between hot-spot size and temperature at the critical conditions for explosion was given in par. 10-4, which is

$$\frac{T_{cr}^2}{Z}\exp\left[E/T_{cr}\right] = \frac{0.04\ QEa_{cr}^2}{\alpha^2 cR} \qquad (12\text{-}5)$$

where a_{cr} is the critical radius of a hot spot that has a temperature T_{cr} (or vice versa). The attempts at correlating thermal explosion theory with impact sensitivity data have usually started with the assumption that hot spots of the same size (i.e., same value a_{cr}) are produced in various explosives by the impact machine, and proceeded to calculate from an equation like Eq. 12-5 the critical temperature T_{cr}. This involves the use of kinetic decomposition data (see Table 10-1). The temperatures so calculated are then correlated with the critical heights in the drop-weight test.

Of the several papers that have treated this kind of correlation, the one by Gross and Amster[5] is of special interest because of the uniquely appropriate way in which decomposition data for the explosives were obtained. Most decomposition kinetics studies

TABLE 12-1 INITIATION OF EXPLOSION OF PETN IN THE PRESENCE OF GRIT

Grit	*Hardness, Moh scale*	*Melting Pt., °C*	*Friction Explosion Efficiency, %*	*Impact Explosion Efficiency, %*
Nil (pure PETN)	2	141	0	2
$AgNO_3$	2-3	210	0	3
KNO_3	2-3	334	0	0
$K_2Cr_2O_7$	2-3	398	0	0
AgBr	2-3	434	50	6
AgI	2-3	550	100	-
Glass	7	800	100	100
Galena	2-3	1114	100	60

on explosives have used the evolution of gas (build-up of pressure) to follow the course of reaction. Chemical analysis of the gas and identification of the decomposition products permit one to calculate the heat of reaction, and thus to infer the rate of heat release from the measured reaction rate. Measurements over a range of temperature give the activation energy (cf. Fig. 4-2); with this and the absolute rate determination, the frequency factor Z is calculated (Eq. 4-5). There are several reasons why information derived in this somewhat roundabout manner may lead to erroneous results when applied to self-heating calculations. In the method employed by Gross and Amster[5], however, heat release rates are inferred directly from experiments involving self-heating under adiabatic conditions. The method is outlined in the paragraphs which follow.

If no heat escapes from a body of explosive that is decomposing according to a first order law, the temperature rises according to the differential equation

$$\frac{dT}{dt} = \frac{qZ}{c} \exp\left[-E/(RT)\right] \qquad (12\text{-}6)$$

where c and q are the specific heat and heat of decomposition per gram, respectively. The equation strictly applies only to instantaneous conditions at the start of the reaction but—provided the decomposition does not proceed very far during an experiment, i.e., approximately zero-order reaction—the equation can be applied to the behavior of a body of explosive that is decomposing over a period of time under adiabatic conditions. Therefore, if the T vs t curve is measured at several points in such an experiment, one should find that $\ln (dT/dt)$ plotted against $1/T$ is a straight line.

The experiments of Gross and Amster were carried out in a special furnace designed to supply heat automatically to a vessel enclosing an explosive sample, the heat being supplied at such a rate as to maintain the vessel at all times virtually at the same temperature as the self-heating sample, thus preventing any exchange of heat with the surroundings. The sample was initially in the form of a solid right cylinder 2 in. × 2 in., and was contained in a stainless steel cup. The sample was heated slowly under manual control to a temperature at which self-heating became noticeable; then the device was switched to automatic control which maintained the adiabatic condition. In some cases, e.g., with TNT, the explosive was in the liquid state during the self-heating stage of the experiment; in others, e.g., RDX, the melting point was not reached. Thus, in the extrapolation of some of Gross and Amster's data to higher temperature, a change from solid to liquid is involved which has an unknown effect on the reaction kinetics. Two figures showing the adiabatic self-heating data for several explosive materials are reproduced in Fig. 12-6(A) and 12-6(B). The data points in Fig. 12-6 generally fall on a straight line as predicted by Eq. 12-6. From the slope of the line the activation energy E was calculated. The specific heat was measured in independent experiments; thus the quantity qZ was obtained from the data. The values computed for these derived quantities are given in Table 12-2. (The value of qZ for Propellant C, given in Ref. 3 appears to be in error; this has been corrected in Table 12-2.) Gross and Amster have also included some conventional kinetic measurements in the table for comparison.

For Explosive Q two values of E are given in Table 12-2 along with corresponding values of qZ, the higher value of E being the one used by Gross and Amster. The data points for Explosive Q in Fig. 12-6(A) show an abrupt change of slope in the dT/dt vs $1/T$ curve near the high temperature end. However, the authors used the points at low temperatures as a basis for evaluating E. Since the value of E is to be used in extrapolating the behavior to higher temperatures than those at which experimental data were obtained, it seems more appropriate to choose the points at high temperatures as the basis. The values given in parentheses in Table 12-2 are, therefore, based on a line of lower slope, as drawn through the high temperature points for the Explosive Q in Fig. 12-6(A).

With the adiabatic furnace data of Gross and Amster as a basis, the critical explosion temperatures for hot spots in the various explosives have been calculated from Eq. 12-5. These are given in Table 12-3, based on three values for the hot-spot radius—10^{-3}, 10^{-2}, and 10^{-1} cm. Similar calculations based on the conventional kinetic data of Table 12-2 are also given. The two different types of data give generally consistent results. (An average value,

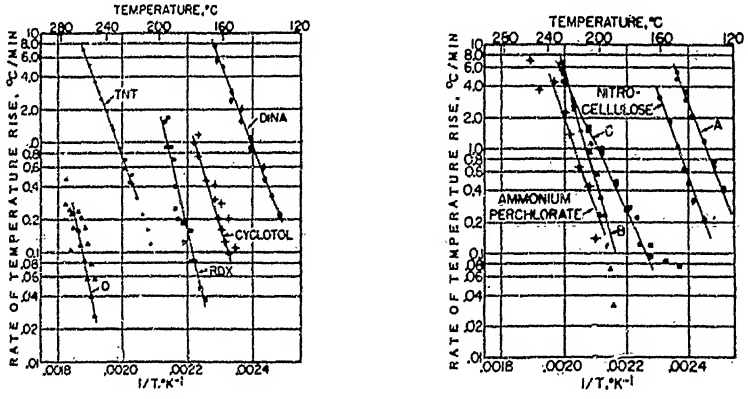

(A) (B)

Figure 12-6. Explosive Decomposition Data From the Adiabatic Furnace[3]

10^{-2} cm^2/sec, was used for the thermal diffusivity α for all the calculations in Table 12-3.)

In order to select from Table 12-2 a set of temperatures for correlation with sensitivity test data, a choice has to be made of some "standard" hot-spot size on which to base the comparison. Although this choice is in a degree arbitrary, there is reason to believe that a radius of about 10^{-3} cm (10μ) is fairly representative for hot spots produced in impact experiments. One line of evidence comes from data such as those in Table 12-1 which show that the critical hot-spot temperatures for relatively sensitive explosives like PETN and RDX lie in the region of 400°C (670°K). To judge from the temperatures listed in Table 12-3, this would indicate that the hot-spot radius is in the neighborhood of 10^{-3} cm, or perhaps somewhat less.

Another argument for this choice of hot spot size may be based on the induction time measurements of Rideal and Robertson[4]. In their experiments the interval was measured between the instant of impact of the drop weight and the time when the explosion was recorded by a microphone placed as close as possible to the edge of the sample. In various ways the authors demonstrated that this time interval was mainly due to an induction or lag period, and not to the time required for explosion to propagate through the explosive. (Indeed, in some of their experiments the explosion probably started on the edge of the sample near the microphone but in no case—although there is the usual random scatter in the data—did they ever find a delay time less than about 150μsec.) The average time interval increased as the energy of the impact (height of fall) was reduced toward the critical level required for ignition. The induction period measured by Rideal and Robertson for PETN, RDX, and tetryl was found to lie in the range from 200 to 500μsec when the drop height was near the critical value. According to the theory of thermal explosions, the critical induction period is of the order of 0.1 a^2/α (cf. Eq. 10-36). Thus with $a = 10^{-3}$ cm and with $\alpha = 10^{-3}$ cm^2/sec the induction period should be of the order of 100 μsec; but if a were 10^{-2} cm, for example, it would be of the order of 10,000 μsec. This points to 10μ as the correct magnitude (see Table 10-4).

An empirical correlation of hot-spot explosion temperature in °C and with the logarithm of the 50 percent drop height (cm) is shown in Fig.

TABLE 12-2 KINETIC PROPERTIES OF EXPLOSIVE MATERIALS FROM ADIABATIC SELF-HEATING EXPERIMENTS

	Adiabatic Furnace Data			*Conventional Kinetic Data*		
*Explosive**	*Temp. Range and State, °C†*	*Activation Energy E, kcal/mol*	*qZ, cal/sec-g*	*Temp. Range and State, °C†*	*Activation Energy E, kcal/mol*	*qZ, cal/sec-g*
TNT	220-260; L	37	5×10^{13}	275-310; L	34	1×10^{14}
				238-277; L	43	5×10^{14}
RDX	170-200; S	57	2×10^{24}	213-299; L	48	3×10^{21}
Comp.B	155-180; L	44	6×10^{18}			
DINA	130-175; L	36	2×10^{16}	166-189; L	50	5×10^{23}
Q	250-270; S	66	4×10^{23}			
		(39)	(7×10^{12})			
AP	205-270; S	41	1×10^{16}	215-240; S	28	
				240-270; S	19	
Prop. A	100-170; S	39	4×10^{18}			
Prop. B	190-242; S	49	9×10^{19}			
Prop. C	165-235; S	29	1×10^{13}			

* Comp. B (or Cyclotol) is RDX/TNT, 60/40.
DINA is diethylnitramine dinitrate.
Explosive Q is a high-melting CHNO explosive.
Propellant A is a double-base (nitrocellulose-nitroglycerin-type) propellant.
Propellant B is a composite propellant containing ammonium perchlorate (AP), aluminum, and polyvinyl chloride.
Propellant C is a composite containing AP, aluminum, and polyurethane.

† L = Liquid
S = Solid

TABLE 12-3 HOT-SPOT EXPLOSION TEMPERATURES CALCULATED ON BASIS OF DATA IN TABLE 12-2

	Critical Explosion Temperature, °K					
	Adiabatic Furnace Data			*Conventional Kinetic Data*		
Explosive	$a = 10^{-3}$ cm	$a = 10^{-2}$ cm	$a = 10^{-1}$ cm	$a = 10^{-3}$ cm	$a = 10^{-2}$ cm	$a = 10^{-1}$ cm
TNT	900	710	580	780	640	540
				930	770	650
RDX	610	550	510	600	530	490
Comp. B	660	580	510			
DINA	650	560	480	550	500	460
Q	740	670	610			
	(1050)	(830)	(690)			
AP	770	660	570			
Prop. A	590	520	460			
Prop. B	670	600	530			
Prop. C	750	600	500			

12-7. The explosion temperatures (converted to °C) are taken from the first column of Table 12-3 (for $a = 10^{-3}$ cm), and the sensitivity data from the paper of Gross and Amster. (The explosion temperature used for Explosive Q in locating the point in Fig. 12-7 is that given in parentheses in Table 12-3, i.e., the figure predicted on the lower value of E in Table 12-2.) It is evident from the data points that the hot-spot temperature increases with increasing impact *insensitivity* or decreasing *sensitivity*. The overall correlation (represented by the heavy line in Fig. 12-7) is apparently improved when the data are grouped into the two "families" of points joined by the dashed lines in Fig. 12-7. One of these families consists of TNT, RDX, and the mixture of these, Comp. B; the other, of ammonium perchlorate (AP) and the two composite propellants based on it (B and C). While these results are consistent with a thermal explosion theory of initiation, it should be pointed out that other factors—e.g., endothermic surface rate processes—may be involved in determining impact sensitivity.

12-4 TRANSITION OF DEFLAGRATION TO DETONATION

In deflagration or simple burning, as exemplified in ordinary flames and solid propellants, fresh material is caused to react as a result of heat transfer from the flame zone and diffusion of matter back and forth between intact and burning regions. In detonation, on the other hand, reaction is initiated in successive layers by the advance of a shock wave, and transfer processes play little if any part. Compared on the basis of either mass reaction rate or propagation velocity, detonation is 10^3-10^4 times as fast as deflagration. The change from the deflagration regime to the detonation regime, when it occurs, is almost always extremely sudden and unpredictable (or nonreproducible). For this reason the phenomenon has been difficult to study experimentally, and little understanding of it has been obtained until quite recently.

Detonation almost invariably starts at some distance ahead of the burning front. The

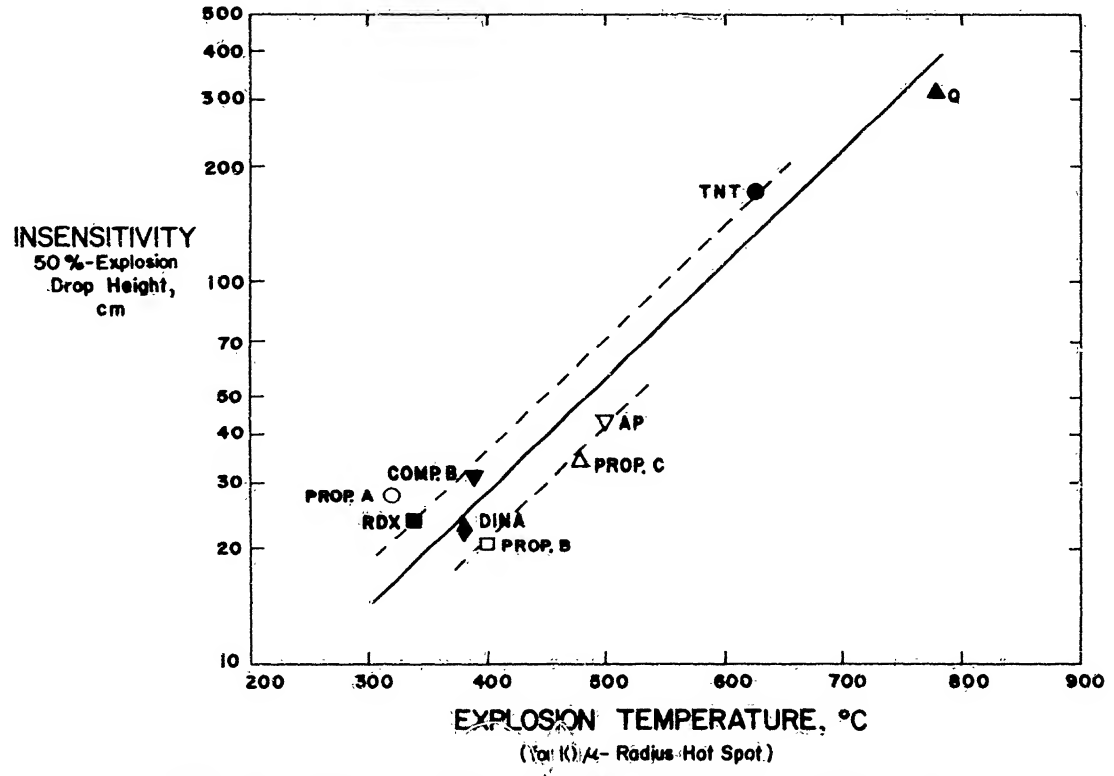

Figure 12-7. Correlation Plot of 50 Percent Explosion Drop Height in the Sensitivity Test vs Critical Explosion Temperature for Hot Spot of Radius 10μ. (Calculations based on adiabatic furnace measurements of Gross and Amster[5].)

detonation wave moves forward from the point of initiation, and a "retonation" wave is sometimes observed to travel back into the undecomposed material between that point and the flame front. The explanation of this behavior seems quite straightforward: (1) a compression wave builds up, emanating from the deflagration zone, (2) the rise in pressure accelerates the decomposition and the pressure, therefore, increases exponentially, and (3) the compression front changes into a shock; when this reaches critical strength, it initiates reaction at hot spots and quickly develops to detonation.

Initiation of detonation after a strong shock front forms follows the mechanisms described in Chapter 11. The new phenomenon here is the development of a compression wave from a deflagration zone. The treatment of this subject is drawn mainly from the papers of Macek and his coworkers[10-13].

According to this mechanism, the transition will not occur unless the explosive is confined because a shock pressure of the order of several kilobars is required to initiate detonation. This fact is well known in practice. For example, a common method of disposing of high explosives without producing detonation is simply to burn them in the open. On the other hand, heavy-cased explosive projectiles and bombs often detonate when involved in fire. The strength and weight of confinement needed to cause deflagration to change to detonation depends on several properties of the explosive: state of aggregation, bulk density, burning rate (in deflagration), and shock sensitivity. It also depends on the size of the charge. A large mass of finely powdered, granular explosive requires little if any confinement because of the large burning surface available and the ease with which deflagration can spread from grain to grain. If such a mass of explosive is ignited in the middle, it may detonate with only the self-confinement provided by the inertia of the outer layers. A cast or plastic-bonded explosive, on the other hand, is much less prone to detonate when ignited and may require very heavy confinement. Both the strength and inertia of the walls confining an explosive charge are important because the pressure development is slow in the early stages; when the walls burst and relieve the internal pressure, the transition to detonation may be stopped. On the other hand, since the final pressures produced during the transition are much higher than any vessel can withstand without bursting, rupture will usually occur before detonation starts; at this stage, the inertia of the walls is the factor that limits the rate of the expansion. The quantity of explosive is also important, both because of the effect of the mass in self-confinement and because of the time and distance available for compression waves to build up. Some materials, such as primary explosives, have such a high intrinsic burning rate and high sensitivity to shock initiation that the transition occurs even with small quantities and very little confinement. The effect of these various factors may be inferred from the discussion which follows of experimental studies on this problem.

The deflagration to detonation transition experiments of Macek and coworkers[10] at the Naval Ordnance Laboratory were performed with cast explosives, namely: DINA, Pentolite (PETN/TNT), and TNT. The first two explosives detonated readily in these experiments but, under the same conditions, TNT did not. This illustrates the combined effect of burning rate and sensitivity since TNT is notably more sluggish than the other two. (See, for example, the positions of TNT and DINA on the sensitivity curve in Fig. 12-7.) The explosives were confined in a heavy-walled steel tube, as shown in Fig. 12-8. They were ignited by an electrically-heated nichrome wire, retained by a threaded plug at one end of the cylinder. The pressure produced in the deflagrating zone was measured by a strain gage on the outside of the steel tube, as shown in Fig. 12-8. Several ionization probes (Chapter 5) were used to detect the detonation wave and locate the approximate point at which detonation was established. The description of results in the paragraphs which follow refers to experiments with DINA. Quite similar results were obtained with Pentolite.

Although the pressure build-up in the deflagration zone was not identical from one experiment to the next—presumably, because of random variations in minute details of the ignition process—the general form was always approximately exponential

$$p = p_o \exp [kt] \qquad (12\text{-}7)$$

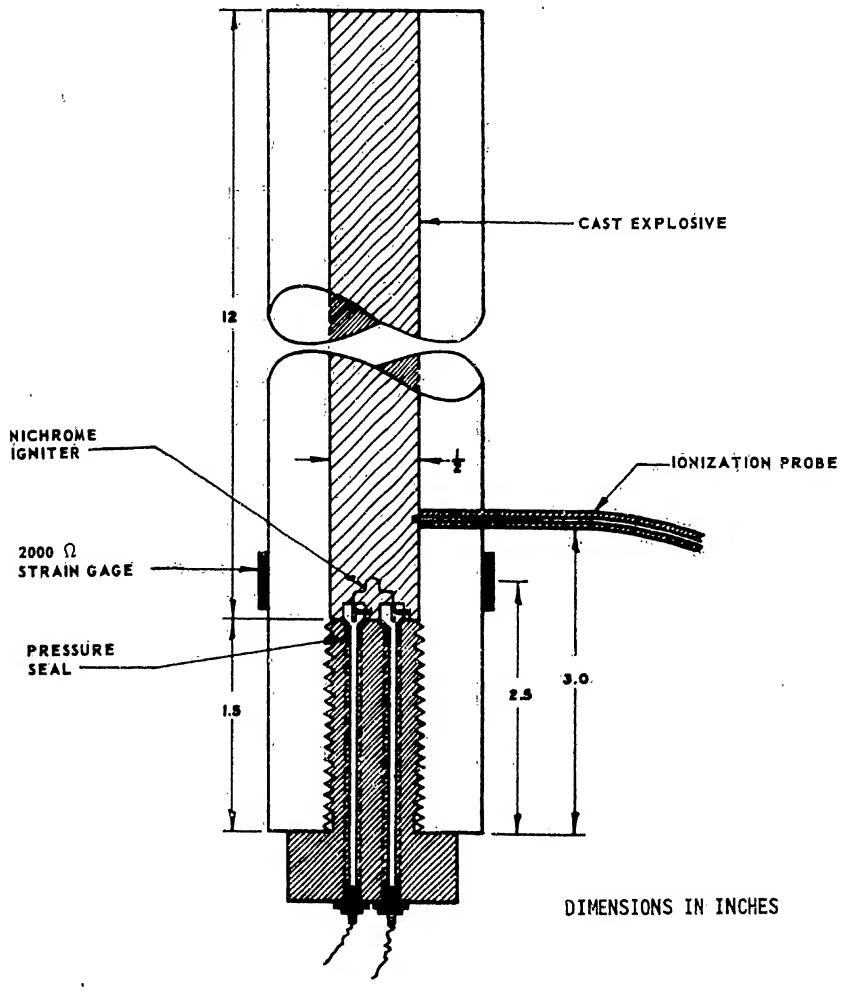

Figure 12-8. Charge Arrangement Used by Macek[10] to Study Deflagration to Detonation Transition (Three other ionization probes were located at regular intervals in addition to the one shown.)

the time constant k having a value in the range 0.10-0.12 μsec^{-1}. The point of origin of the detonation wave was variable but usually was located a distance of 10-15 cm from the igniter. Pressures of several kilobars magnitude were recorded by the strain gage; higher pressures were undoubtedly reached after the strain wire broke. The bursting strength of the tube was in the neighborhood of 5-10 kbar but inertial confinement allowed the pressure in the deflagration zone to reach higher values. This can be appreciated from the calculations which follow of the expansion that would occur in the tube if only inertial forces were involved, i.e., under the assumption of zero strength. As a basis for the calculations we take from Ref. 10 a typical pressure-time relation recorded by the strain gage, $p = 0.08 \exp [0.1\ t]$ where p is measured in kbars and t in μsec. The strain gage registered pressures in some cases as high as 10 kbar. Under the assumption that this relationship continues to apply as the pressure rises beyond this point, the following figures show the pressure and percent expansion of the tube at various times:

Time, μsec:	30	40	50	60	70
Pressure, kbar:	1.6	4.5	12	33	90
Expansion, %:	4	10	29	86	266

On the basis of these calculations, one may guess that the pressure will actually rise to a maximum in the neighborhood of, perhaps, 30-40 kbar. Such a shock wave pressure should easily produce detonation in cast explosives like DINA and Pentolite. Although direct measurements are not available. Jacobs, Liddiard and Drimmer[14] report a pressure of 20 kbar as the threshold shock strength needed to initiate Composition B-3, a less sensitive explosive than DINA. These calculations, therefore, show that the proposed explanation of the transition is quite reasonable. More convincing evidence is obtained by the analysis which follows of the build-up of the compression wave, based on a calculation of characteristics (Chapter 2). This analysis is also due to Macek[10].

In the analysis, the pressure produced at the deflagration surface is considered to act as a piston which creates motion at that surface and produces a compression wave traveling ahead into the explosive. The generating pressure at the deflagration surface is assumed to be given, for a certain period of time at least, by an extrapolation of the pressure-time function indicated by the strain gage (Eq. 12-7). The diagram of positive (C_+) characteristics is shown in Fig. 12-9 and, based on this, the compression wave development is represented in Fig. 12-10. For the purpose of this figure, it is assumed that the pressure-time function is unaffected by expansion of the tube until the pressure reaches about 30 kbar. Beyond that, it is assumed that the pressure levels off and eventually begins to fall. The lower part of the pressure curve, on the assumption that the deflagration pressure is known, is indicated by solid lines; the upper part, based only on conjecture, by broken lines. The position of the deflagration boundary—i.e. the "piston"—is indicated by the vertical line terminating the pressure curve on the left. (This line is not meant to indicate that the pressure drops to zero at this point.) The shaded areas in Fig. 12-10, therefore, represent at various times the pressure in that portion of the intact explosive affected by the compression wave.

Fig. 12-10 shows the expected steepening of the compression wave front, the high pressure portion of which develops into a shock at a distance of about 12-14 cm from the igniter and at a time about 90-100 μsec after ignition, (see Fig. 12-9). This result comports quite well with the experimental findings. Other calculations reported by Macek, based on pressure-time curves from several different experiments, give similar results.

The basis for these characteristics calculations, as outlined by Macek, follows. The equation of state of the solid explosive under adiabatic restraint is assumed to have the form

$$p = a[(\rho/\rho_o)^3 - 1] \qquad (12\text{-}8)$$

where a is a constant with dimensions of pressure. This is a modification of the Tait equation. The constant a is evaluated from the value of the sound velocity c_o in the explosive, the sound velocity c being given in general by

$$\begin{aligned} c &= \sqrt{(dp/d\rho)_s} \\ &= \left(\sqrt{3a/\rho_o^3}\right)\rho \\ &= c_o(\rho/\rho_o) \end{aligned} \qquad (12\text{-}9)$$

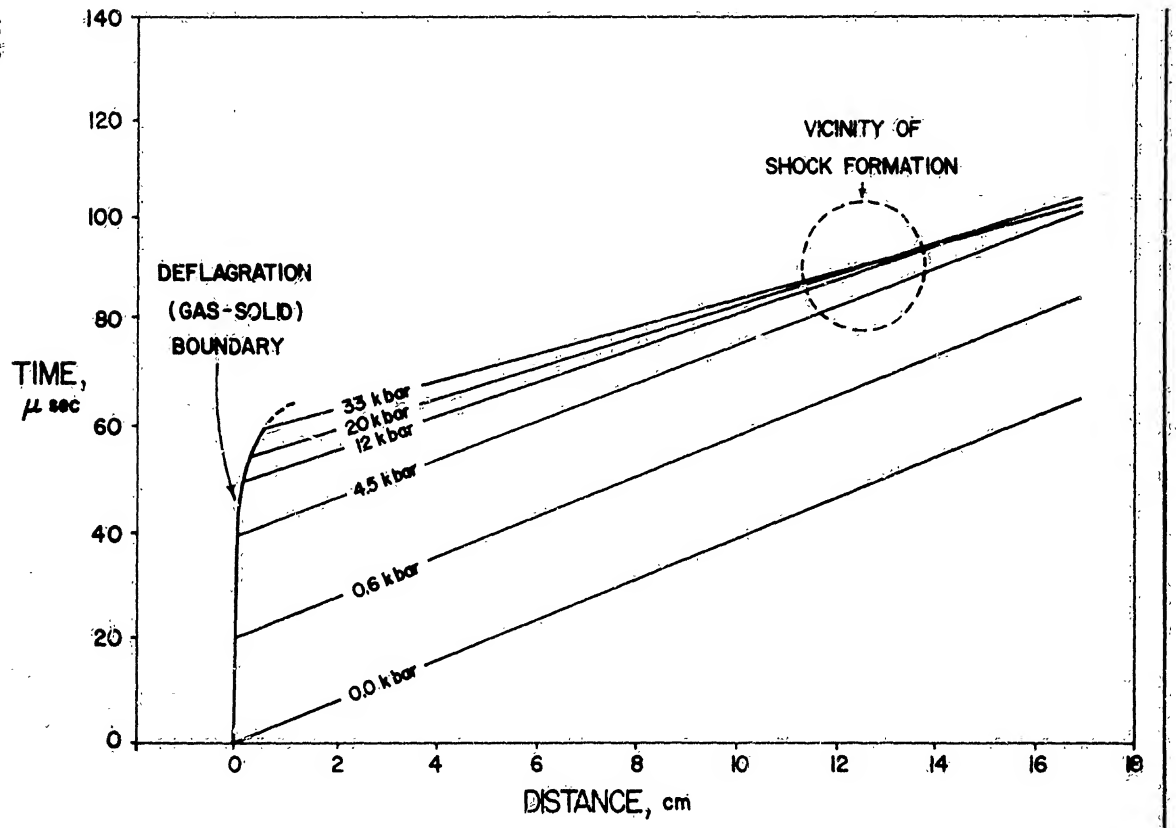

Figure 12-9. Characteristics Diagram (C_+) for the Development of a Compression Wave From Deflagration in a Rigidly Confined High Explosive[10]

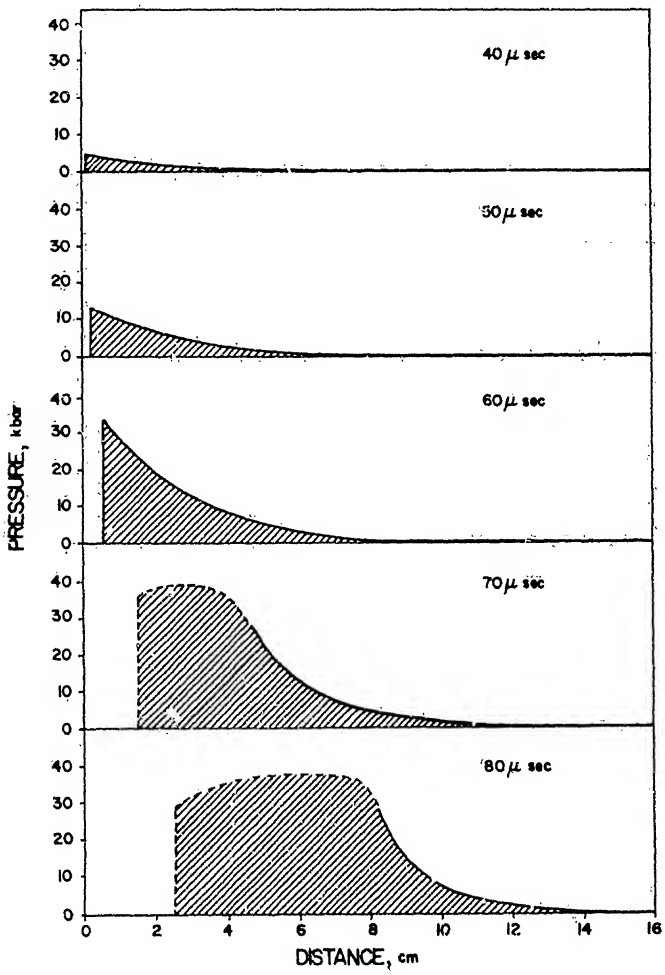

Figure 12-10. Development of Compression Wave From Deflagration as Transposed From the Characteristics Diagram in Fig. 12-9 (The left boundary of the shaded area represents the position of the deflagration surface.)

The Riemann quantity σ, defined by

$$\sigma = \int^{\rho} (c/\rho)d\rho \qquad (12\text{-}10)$$

is thus readily shown to be given by

$$\sigma = c - c_o \qquad (12\text{-}11)$$

if the lower limit of integration in Eq. 12-10 is taken to be ρ_o. Since the C_- characteristics originate on the $x = 0$ axis—where the particle velocity u equals zero and where $\sigma = 0$ also, and since on any C_- characteristic $u - \sigma$ is constant—it follows that $u = \sigma$ everywhere, i.e.,

$$u = c - c_o$$

$$= c_o[(\rho/\rho_o) - 1] \qquad (12\text{-}12)$$

The calculation of the characteristics diagram proceeds as follows. Eq. 12-7, in which the constants p_o and k have been experimentally evaluated, gives the relationship of pressure to time at the deflagration boundary. Combination of Eq. 12-7 and Eq. 12-8 then gives the p,t-relationship at the boundary. Evaluation of the integral $\int_o^t u dt$, using Eq. 12-12, then describes the motion of this boundary. Each point on the boundary terminates a C_+ characteristic on which the state properties p,ρ and c, and the velocity u are constant. The terminal values of these quantities at the boundary can be evaluated through Eqs. 12-7, 12-8, 12-9, and 12-12, and since the slope of the C_+ characteristic is given by $u + c$, which is constant, the C_+ lines can be plotted and the properties determined everywhere to the right of the boundary in the x,t-domain. The analysis can be extended along any characteristic C_+ line only to the point where it crosses another C_+ line, which is interpreted to be the point at which the flow becomes discontinuous, i.e., the point at which a shock develops. The pressure-distance curves in Fig. 12-10 are readily obtained by transposing from Fig. 12-9, where the characteristics are labeled according to the pressure.

Macek[10] also shows that the observed exponential rise in pressure agrees quite well with the behavior of a model based on "cigarette-type" burning at the deflagration boundary (with constant burning area), perfectly rigid cylindrical walls, and a pressure exponent unity in the erosive burning law (cf. Eq. 11-3). This demonstration completes the rationalization of the observed behavior in these experiments.

REFERENCES

1. F. P. Bowden and A. D. Yoffe, *Initiation and Growth of Explosion in Liquids and Solids*, Cambridge University Press, Cambridge, England, 1952.
2. Statistical Research Group, Princeton University, *Statistical Analysis for a New Procedure in Sensitivity Experiments*, report to Applied Mathematics Panel, NDRC, AMP Rep. No. 101.1R, SRG-P No. 40, (1944); also see W. J. Dixon and J. Mood, Amer. Statistical Assn. 43, 109 (1948); W. J. Dixon and F J. Massey, Jr., *Introduction to Statistical Analysis*, McGraw-Hill, New York, 2nd Ed., 1957, pp. 318-327.
3. J. W. Martin and J. Saunders, *Proceedings of the International Conference of Sensitivity and Hazards of Explosives*, Session 6, London, October 1963.
4. E. K. Rideal and A. J. B. Robertson, Proc. Roy. Soc. A 195, 135 (1948).
5. D. Gross and A. B. Amster, *Eighth Symposium (International) on Combustion*, Williams and Wilkins, Baltimore, Md., 1962, p. 728.
6. T. Boddington, *Ninth Symposium (International) on Combustion*, Academic Press, New York, 1963, p. 287.
7. M. H. Friedman, *Ninth Symposium (International) on Combustion*, Academic Press, New York, 1963, p 294.
8. C. H. Johansson, Proc. Roy. Soc. A 246, 160 (1958).
9. R. F. Chaiken and F. J. Cheselske, J. Chem. Phys. 43, 3228 (1965).
10. A. Macek, J. Chem. Phys. 31,162 (1959).
11. R. W. Gipson, and A. Macek, *Eighth Symposium (International) on Combustion*, Williams and Wilkins Co., Baltimore, Md. 1962, p. 847.
12. C. T. Zovko and A. Macek, "A Computational Treatment of the Transition from Deflagration to Detonation in Solids", *Third Symposium on Detonation*, Princeton University, Sept. 1960, published by Office of Naval Research, Rep. No. ACR-52, Vol. 2, p. 606.
13. A. Macek, Chem. Rev. 62,41 (1962).
14. S. J. Jacobs, T. P. Liddiard, Jr., and B. E. Drimmer, *Ninth Symposium (International) on Combustion*, Academic Press, New York, 1963, p. 517.

CHAPTER 13 SHOCK WAVES FROM EXPLOSIVE CHARGES

13-1 INTRODUCTION

Spherically-symmetric blast waves resulting from explosions in air, water, and solid media are considered in this chapter. Explosions in air and water are dealt with in detail; references to blast waves in solid media are given.

Compared to the duration of its after-effects in air the decomposition of an explosive charge by a detonation is very rapidly completed. If the detonation process is considered to occupy one unit of time, for example, the shock wave in air is capable of inflicting serious damage to structures at points some 200 charge radii distant from the center and at times in the order of 3500 of these time units later. For some purposes, therefore, the detonation process can be considered instantaneous. In cases involving dense media, however, the detonation time may be of the order of the damage times in the media.

Passage of the detonation wave leaves the explosive product gases at an extremely high pressure and in a state of motion. However, neither the pressure nor the particle velocity is uniform throughout the volume of the explosive gases. The simplest geometry results if the charge is spherical and initiated at the center so that the detonation wave reaches the boundaries of the charge everywhere at the same instant. In this case, the velocity of outward motion of the explosion products is the highest at the boundary and decreases toward the center, at which point material must remain motionless. Pressure and density are also at a maximum at the boundary, and at a minimum at the center. For any geometry of a finite, three-dimensional charge other than the centrally initiated sphere, interaction with the external medium begins before detonation is everywhere complete within the charge, giving rise to a much more complex flow of the explosion products.

As the explosion products begin to expand, the pressure at the interface separating them from the exterior medium falls rapidly. An intense pressure wave is propagated outward in the exterior medium and an outward flow of the medium results. In Chapter 2, it was mentioned that a compression wave of finite amplitude always propagates as a shock wave at a velocity that is greater than the velocity of sound in the undisturbed medium and which depends upon the amplitude of the wave. The shock is characterized by a very rapid increase in pressure that may—as a very good approximation—be considered instantaneous, so that the leading edge of the shock wave can be regarded a mathematical discontinuity. The shock wave in air generated by an explosive charge is often called the blast wave. The initial shock front pressure of the shock wave generated in air at atmospheric pressure by conventional explosives is of the order of 10^3 atm. In water the initial shock front pressure is of the order of 10^4 atm, and in metals is of the order of 10^5 atm. The shock front pressure is often called the peak pressure.

As the shock wave propagates away from the generating explosive charge, its peak pressure decreases. The shock wave decay can be attributed to two causes. If the shock wave is not planar, the decay is due to geometrical divergence. Also, because of the finite entropy increment across the shock front, the decay is due to progressive dissipation of energy in the shocked air in accord with the requirement of the second law of thermodynamics. The decay of shock waves because of the dissipation of energy leads to a decay more rapid than would be expected from geometrical considerations alone.

For the purpose of discussion, we may consider a cylindrical charge of explosive in air, initiated at one end. The development of the shock wave in the surrounding medium is shown qualitatively in Fig. 13-1, for three times after the instant of initiation. As the detonation wave progresses down the charge, the laterally expanding products generate a shock wave that has cylindrical symmetry For definiteness, suppose that the origin of cylindrical coordinates is fixed at the point of initiation with the detonation wave moving in the positive direction of the axial coordinate. Then the profile of the shock wave at any instant and the flow behind the shock front depend only on the axial and radial coordinates relative to this fixed origin and are determined by the hydrodynamic

equations for cylindrically symmetric flow. At points in space with positive axial coordinates greater than about one or two charge radii and less than the length of the charge, the shock wave is, to a good approximation, the same as would be generated by an infinitely long explosive charge. At smaller positive values of the axial coordinate and all negative values, the flow is more complicated because of end effects connected with the finite length of the charge. When the detonation wave reaches the end of the charge, a shock wave is generated off the end which is connected discontinuously with the shock wave that has been propagating laterally. Although the shock wave profile and the flow behind the shock front retain cylindrical symmetry, the flow becomes very complicated after the detonation wave has progressed through the charge and it has not been analyzed in detail.

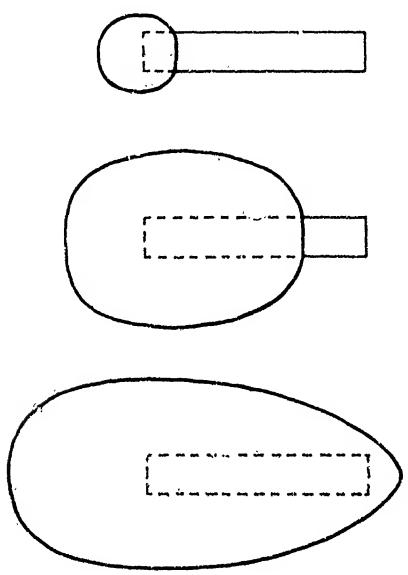

Figure 13-1. Development of Shock Wave About Cylindrical Explosive Charge Initiated at One End

As the shock wave continues to propagate, the effects of charge geometry and of the initiating detonation wave become progressively less important in comparison with the effects of radial divergence. The shock wave profile becomes progressively more spherical. At distances that are several times the largest linear dimension of the charge, the shock wave can be considered spherical to a good degree of approximation. The approximation is the better the more nearly the ratio of charge length to charge diameter is unity. At such distances, a model that is amenable to theoretical analysis is obtained by consideration of a spherical charge of explosive of the same weight as the charge of interest, in which the detonation wave is initiated at the center. The shock wave profile from such a charge is spherical and the flow behind the shock front depends only on the time and the radial coordinate of a spherical coordinate system.

Further simplifications may be justified for the sake of theoretical simplicity. One further step in this direction is to consider the globe of explosion gases formed by detonation of a spherical charge to be uniform in pressure and density, and at a state of rest. This is the result of hypothetical, homogeneous, instantaneous constant-volume explosion.

Asymptotically, at distances that are large compared to the radius of the equivalent sphere of explosive, an even simpler model is obtained by considering a point source in which the energy of explosion of the charge of interest is instantaneously released.

In this chapter, we shall restrict the discussion to shock waves in one-dimension with radial symmetry, i.e., those from a spherically symmetric explosion. This is not only the case that has been studied in greatest detail but also the case that provides a simple model that is approximately descriptive of actual explosive charges. We shall further limit the discussion to the shock wave in an infinite isotropic medium, regarding as outside of the scope of this handbook such topics as shock wave reflection at rigid or free surfaces and shock wave interactions with structures of various types. A nonsuperficial treatment of these topics cannot be undertaken in a chapter of reasonable length. Each treatment requires a knowledge of the parameters of the incident wave and it is with these parameters that this chapter is concerned.

13-2 EXPANSION OF THE EXPLOSION PRODUCTS

Given a spherical globe of gas at an extremely high pressure, there follows immediately as it begins to expand the establishment of a shock front running outward into the medium and a rarefaction moving in toward the center of the sphere. There is a boundary requirement that the particle velocity normal to the surface and pressure be continuous across the contact surface between the explosion product gases and the external medium. The flow is somewhat similar to that occurring in a shock tube. However, the spherical divergence of the flow introduces complications for a theoretical treatment that are not encountered in the plane case. The pressure at the shock front, instead of being constant as in the shock tube, falls rapidly as the front moves out. This changes the terminal condition for the rarefaction. The characteristics of the solution of the partial differential equations are not straight lines; neither are the integrals of the motion along these characteristic lines simple functions as in the plane case. For a considerable period of time after the expansion begins, therefore, the temporal changes in pressure, density, and particle velocity occurring at any point depend on the configuration of the entire flow field from the center out to the shock front. A complex numerical integration is required to obtain an accurate description of the motion.

To make certain order-of-magnitude assessments, one may simplify the actual process and consider that the explosive gas globe expands uniformly, the boundary coming to rest at a radius r_m when the pressure within the globe has dropped to the ambient pressure of the medium p_o. Acutally, the distance moved by the boundary and the velocity of its motion depend on the original size of the gas globe, the conditions and properties of the gases inside it, and on the properties of the external medium. Motion within the globe is not uniform; when the boundary first comes to rest, there are still pressure, density, and motion gradients within the sphere. However, if the expansion is considered to be quasi-static and isentropic, and the explosive products are treated as a polytropic gas, the final volume V_m will be related to the initial volume V_e by the relation

$$V_m = V_e(p_e/p_o)^{1/\bar{\kappa}} \tag{13-1}$$

where $\bar{\kappa}$ is the average or effective value of the adiabatic exponent κ during the expansion process. (In fact, the gas globe does not remain isentropic because of the inward-facing shock as described in the discussion which follows.) If the total expansion energy available in the gas globe, which for a polytropic gas would be equal to $p_e V_e/(\kappa - 1)$, is equated to the energy of the explosion E_o, one obtains from Eq. 13-1 an approximate expression for the maximum expansion radius r_m of the gas globe in terms of a characteristic length $(E_o/p_o)^{1/3}$ as follows:

$$\frac{r_m^3}{(E_o/p_o)^{1/3}} = \frac{3(\bar{\kappa} - 1)}{4\pi}\left(\frac{p_o}{p_e}\right)^{(\bar{\kappa}-1)/\bar{\kappa}} \tag{13-2}$$

The expression on the right side of Eq. 13-2 is not very sensitive to the value assumed for $\bar{\kappa}$; and, if p_o and p_e are given values of 1 atm and 10^5 atm, respectively, and $\bar{\kappa}$ a value of 1.4 (its value for an ideal gas), r_m in terms of the unit $(E_o/p_o)^{1/3}$ assumes a value of about 0.15.

The velocity of the contact surface in the expansion of the gas globe depends on the properties of the explosion gases and the properties of the medium. For an explosion in air where the resistance to expansion is relatively small, the initial motion will approach the velocity u_{esc} for escape into a vacuum, given approximately by the equation

$$u_{esc} \approx \left(\frac{2}{\kappa_e - 1}\right) c_e \tag{13-3}$$

where c_e is the initial acoustic velocity in the gas globe and κ_e the adiabatic exponent at the constant volume explosion state. For explosives, c_e is equal approximately to 0.8 times the detonation velocity D, and the effective value of

κ_e is about three*. By equating the average value of the boundary velocity during the expansion to one-half the initial velocity, one obtains, to an order of magnitude, the time t_m required for the gas globe to deliver substantially all of its energy to the pressure wave

$$t_m \approx \frac{r_m}{0.4D} \approx \frac{0.4\ (E_e/p_o)^{1/3}}{D} \qquad (13\text{-}4)$$

Putting this time in terms of units $(E_e/p_o)^{1/3}/c_o$, where c_o is the acoustic velocity in the medium, one obtains

$$\tau_m = \frac{t_m\, c_o}{(E_e/p_o)^{1/3}} \approx \frac{0.4\ c_o}{D} \qquad (13\text{-}5)$$

Substituting the value of c_o for air and a typical value for D of a high explosive, one obtains for τ_m the approximate value 0.025. On the other hand, in terms of the same dimensionless units, the total time of interest for the air blast wave at sea level—i.e., the time in which it is able to inflict serious damage on structures—is of order unity.

The main interest in the air blast wave at sea level is, therefore, in the period after the explosive has passed on essentially all the available energy to the blast wave. The hydrodynamic laws governing the wave propagation are such that the influence of details in the process by which the wave was formed tends to diminish with the passage of time. This explains why the point-energy release model gives a fairly good description of the air blast from explosions at sea level.

It is of interest to examine the effect of altitude (lower ambient pressures) in the light of this analysis. To do this it is first necessary to consider briefly the potential of an explosion to inflict damage on a target at a distance. For some targets, such as window glass, the energy involved in the destruction is small. For these, it is the level of overpressure in the blast wave that mainly determines whether or not destruction of the target occurs. However, for most structures substantial amounts of energy are required to cause the displacements and deformations that constitute damage. For such typical targets the total energy flux per unit area of the blast wave provides in first order approximation a criterion for the damaging effectiveness. On this basis one can conclude that, for a given target and a given explosive source with energy E_e, there must be some absolute limiting distance r_t where the quantity $E_e/(4\pi r_t^2)$ is just sufficient to inflict critical damage**. This absolute distance limit is independent of the nature of the medium intervening between the explosion and the target.

It is apparent from Eq. 13-2 that when the ambient pressure p_o is reduced, the maximum radius reached by the expanding gas cloud increases. In the limit of perfect vacuum, of course, the expansion continues indefinitely. Consideration of the blast effects of explosives at various altitudes, therefore, shows that although the details of the expansion process play a relatively minor role at sea level, they become increasingly important at lower ambient pressures and, in vacuum, constitute the entire phenomenon.

For an explosive fired under water, the expansion of the gas globe assumes a key role in the development of the shock wave. Nothing analogous to the point-energy release model seems to be possible for this case. Because of the relative incompressibility of water, the sound velocity is much higher and the flow velocities smaller for water than for air. The motion of the gas-water interface is very slow relative to the outward movement of the shock wave. For many applications the strength of the

* The appropriate value of κ_e to be used in Eq. 13-3 is different in principle from the value of K that is appropriate to Eq. 13-2. By use of Eq. 13-3, we wish to estimate the initial flow velocity which is a characteristic of the initial state of the gas; whereas by Eq. 13-2 we want to calculate the final expansion volume which depends in large degree on the properties of the gas at low pressure. The work of Deal[1] and that of Fickett and Wood[2] shows that in isentropic expansion from the detonation state, where the pressure is in the order of 10^5 atm, down to a pressure of about 10^3 atm the explosive products behave nearly as a polytropic gas with a K-value of 3.0. At much lower pressures—below, e.g., 100 atm—the gases assume more normal properties and the effective K becomes something less than 1.4. It is when the gases are at a relatively low pressure level, of course, that they undergo the greater part of the increase in volume.

** The energy criterion of damage effectiveness is necessary but obviously not sufficient. Therefore, r_t is an upper limit to the radius of damage effect. The actual radius may be considerably smaller and will depend on what pressure or impulse levels may be required to perform the destructive effects.

underwater shock wave decays below a level of interest before the gas bubble reaches its maximum extension. The theoretical treatment of underwater explosions depends, therefore, critically on the behavior of the gas globe as well as on the propagation of the shock wave in water.

The interaction of detonation products with solid materials will be discussed in more detail in subsequent paragraphs.

13-3 ENERGY TRANSPORT BY SHOCK WAVE PROPAGATION

The foregoing considerations show that the problem of air blast from high explosives fired at sea level and up to certain altitudes can be considered largely as the problem of shock wave propagation. The input energy from the explosion determines the scale of the phenomenon. The shock wave provides a mechanism for the outward transmission and dissipation of this energy (in the sense of the second law of thermodynamics). The shock wave plays a similar role for explosives fired under water or underground. Other mechanisms are heat conduction and radiation. These various means for the diffusion of energy do not interact to an appreciable extent for the chemical high explosives. For nuclear explosives, however, the three mechanisms do interact importantly for a short period in the beginning, after which shock wave transmission becomes dominant.

It is of interest to consider what information thermodynamics can yield about the transfer of energy via the shock wave. Designating the rate at which mechanical work is performed per unit area at the shock front when it has reached a radius R as $\dot{w}(R)$, we note that*

$$\dot{w}(R) = p_1 u_1 \tag{13-6}$$

where p_1 and u_1 are the pressure and particle velocity, respectively, immediately behind the front. This work serves to raise the internal energy of, and impart kinetic energy to, the adjacent layer in the medium which is being enveloped by the shock front, i.e.,

$$\dot{w}(R) = \rho_o\, U(R)\, [(e_1 - e_o) + u_1^2/2] \tag{13-7}$$

where $U(R)$ is the velocity of the shock wave at R, and e_1 and e_o the specific energy immediately behind and in front of the shock, respectively. (We assume the medium is initially at rest, i.e., $u_o = 0$.)

Part of the energy change represented by $(e_1 - e_o)$ is irreversible in the sense that, after shock wave compression, subsequent expansion of the medium back to ambient pressure p_o does not yield an amount of work equivalent to $(e_1 - e_o)$, but a quantity which is less by an amount which we will designate $\Delta e[s_1(r_o)]$. This notation signifies Δe to be the "irreversible" increment of energy connected with the entropy rise in the shock and $s_1(r_o)$ denotes that this particular entropy state is associated with the element of the medium (originally) at the Lagrangian coordinate r_o. Quantitatively, $\Delta e[s_1(r_o)]$ is given by

$$\Delta e[s_1(r_o)] = e(p_o, s_1) - e(p_o, s_o) \tag{13-8}$$

The significance of this "retained" energy is illustrated graphically in Fig. 13-2.

If no other shock waves or irreversible processes occur behind the initial shock front, $\Delta e[s_1(r_o)]$ represents the ultimate legacy of the explosion to this element of the medium. Thus, the total energy released by the explosive in going from the initial state to the final state of the explosion products at p_o can be equated to the total of such residual energy in the medium plus the net work done by expansion of the explosion products and the shock-heated medium

$$E_e(p_o) - E_p(p_o) = \int_{a_o}^{\infty} 4\pi r_o^2\, \rho_o\, \Delta e[s_1(r_o)]\, dr_o + p_o[V_p(p_o) - V_e(p_o)] + p_o \int_{a_o}^{\infty} 4\pi r_o^2\, \rho_o \left\{ v[p_o, s_1(r_o)] - v_o \right\} dr_o \tag{13-9}$$

where $E_e(p_o)$ and $E_p(p_o)$ are the total energy of the intact explosive and the explosive products

* The notation "subscript one" denotes values at or immediately behind the shock front.

at pressure p_o, respectively; $V_e(p_o)$ and $V_p(p_o)$ are the corresponding total volumes; $v[p_o, s_1(r_o)]$ is the specific volume of the medium in the state represented by (p_o, s_1); v_o is the specific volume of the medium initially; and a_o is the initial radius of the explosive charge. By rearrangement of terms, Eq. 13-9 can be written

$$H_e(p_o) - H_p(p_o) = \int_{a_o}^{\infty} 4\pi r_o^2 \rho_o \Delta h[s_1(r_o)]\, dr_o \quad (13\text{-}10)$$

where $H_e(p_o)$ and $H_p(p_o)$ are the total enthalpy of the intact explosive and the explosive products at p_o, respectively, and the quantity $\Delta h[s_1(r_o)]$ is defined, like $\Delta e[s_1(r_o)]$; thus,

$$\Delta h[s_1(r_o)] = h[p_o, s_1] - h[p_o, s_o]$$

Eq. 13-10 expresses the thermodynamic requirement that for the total system, explosive and medium, enthalpy is conserved in the explosion process.

Eq. 13-10 is based on division of the total system into two parts separated by the boundary between the explosive and the medium. The surface of such division is arbitrary. Therefore, one may equally well define a spherical boundary in Lagrangian coordinates that includes not only the explosive but also a portion of the medium out to radius R in one part, and the rest of the medium from R to infinity in the other. Then, one can write on the basis of arguments identical to those which led to Eq. 13-10

$$H_o(R) - H_\infty(R) = \int_{R}^{\infty} 4\pi r_o^2 \rho_o \Delta h[s_1(r_o)]\, dr_o \quad (13\text{-}11)$$

where $H_o(R)$ and $H_\infty(R)$ represent the total enthalpy in the explosive plus the medium out to Lagrangian coordinate $r_o = R$ initially and at infinite time, respectively. The change in enthalpy can be equated to the change in energy plus the change in pV and, since the pressure is equal to p_o in both the initial and final states, we can write

$$H_o(R) - H_\infty(R) = E_o(R) - E_\infty(R) - p_o \Delta V \quad (13\text{-}12)$$

where $E_o(R)$ and $E_\infty(R)$ are the total energy in the initial and final states, respectively, and ΔV is the total change of volume. The latter quantity can be computed from the movement of the boundary at $r_o = R$; thus

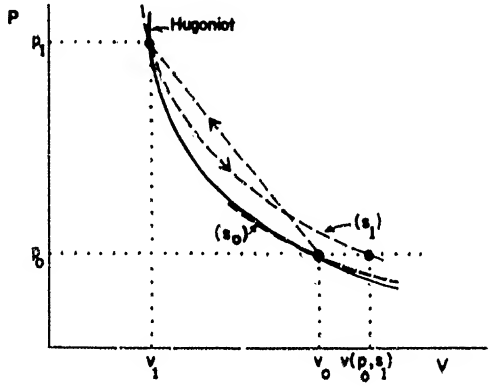

Figure 13-2. Schematic Illustration of the Energy Retention Resulting From the Entropy Increase at the Shock Front [The area under the curve between the initial and final states represents the energy change in both the shock compression (upward arrow) and isentropic expansion back to p_o (downward arrow).]

$$\Delta V = (r_o = R) \int_{t(R)}^{\infty} 4\pi r^2 u\,dt \qquad (13\text{-}13)$$

where the notation in front of the integral sign is meant to signify that the integral is along the particle path $r_o = R$, u is the particle velocity, and $t(R)$ is the time at which the shock wave reaches R and at which u, therefore, takes on a value different from zero. From the first law of thermodynamics, the change in energy may be equated to the work done on the medium external to R; thus

$$E_o(R) - E_\infty(R) = (r_o = R) \int_{t(R)}^{\infty} 4\pi r^2 p u\,dt \qquad (13\text{-}14)$$

Combining Eqs. 13-11, 13-12, 13-13, and 13-14 we may

$$E(R) \quad {}_{o} = R) \int_{t(R)}^{\infty} 4\pi r^2 \ (p - p_o)\ u\,dt \qquad (13\text{-}15)$$

$$= \int_{R}^{\infty} 4\pi r_o^2\ \rho_o \Delta h[s_1(r_o)]\,dr_o$$

where we have defined $E(R)$ to represent the integral for total work involving the overpressure $p - p_o$ along the particle path $r_o = R$. It will be noted that $E(R) = H_o(R) - H_\infty(R)$, and, in particular, $E(a_o) = H_e(p_o) - H_p(p_o)$.

By differentiating Eq. 13-15, we derive the differential equation for the total transport of enthalpy associated with transmission of a spherical shock wave; thus

$$\frac{dE(R)}{dR} = 4\pi R^2\ \rho_o \Delta h[s_1(R)] \qquad (13\text{-}16)$$

It should be noted that Eq. 13-16 contains no information not implicit in the Hugoniot relations since they take full account of the conservation of energy. When the Hugoniot relations are combined with an equation of state, all the basic information it is possible to derive from thermodynamics in this connection is implicitly contained. However, the concept of total enthalpy transport expressed in Eq. 13-16, which was first derived by Kirkwood and Brinkley[3], provides an insight not immediately given by the Hugoniot relations alone.

13-4 BLAST WAVES IN AIR FROM EXPLOSIVE CHARGES

Before considering the quantitative analysis of the shock wave in air generated by an explosive charge, it is desirable to describe the qualitative features of the wave. We limit the discussion to the spherical wave with a center of symmetry, propagating radially outward from the center of the explosion in a space free of obstacles.

As the blast wave in air travels away from the source, the peak pressure steadily decreases and the pressure behind the front falls off in a regular manner. After the shock front has propagated a certain distance, the pressure behind the shock front falls below the original ambient pressure of the atmosphere, creating a suction phase of negative overpressures. The pressure as a function of distance from the center of explosion is shown schematically in Fig. 13-3 for several successive times, increasing as the wave propagates from left to right. It may be noted that the suction phase of the blast wave is a consequence of the geometrical divergence of the wave. Waves propagating without divergence do not exhibit a suction phase.

It will be recalled from Chapter 2 that the Hugoniot equations, expressing the conservation laws across the shock discontinuity, prescribe all of the shock front variables in terms of any one of them. Thus, if the peak pressure is chosen as the independent variable, the shock front particle velocity is a monotonic function of the peak pressure so that it decreases during propagation of the wave in a manner determined by the instantaneous value of the peak pressure through the Hugoniot equation. The particle velocity decreases behind the shock front in a manner that is determined by the pressure distribution through the hydrodynamic equations. The particle velocity is shown as a function of distance from the center of explosion schematically in Fig. 13-4 for several successive times as the wave propagates from left to right. The particle velocity changes direction in consequence of the suction phase of the blast wave.

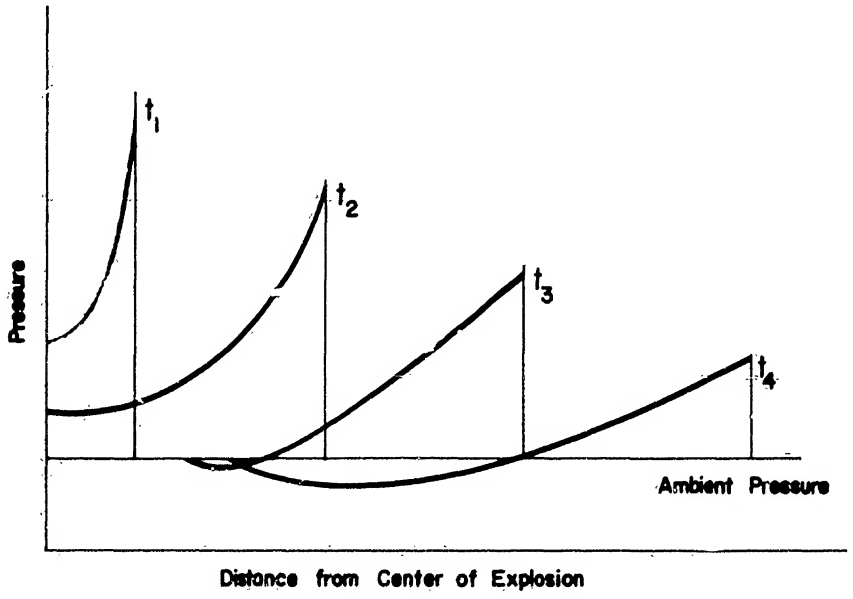

Figure 13-3. Pressure-distance Curves for Blast Waves in Air at Successive Times

Qualitatively similar curves are obtained if the pressure or particle velocity is plotted as functions of time at a fixed distance from the center of the explosion. Such curves are called the Eulerian pressure-time of particle velocity-time curve because the position is taken as fixed in a laboratory system of coordinates. Pressure-time curves at two distances, R_1 and $R_2 > R_1$, are shown schematically in Fig. 13-5. At R_1, the blast wave does not exhibit a suction phase. At the greater distance R_2, the suction phase exhibited in the pressure-distance curves is reproduced by the pressure-time curve.

At distances close enough to the explosion so that the blast wave is of the form as shown to the left in Fig 13-5, it may be represented by the empirical equation*

$$p(t) = p_i \; e^{-t/\theta} \tag{13-17}$$

where p is the pressure in excess of the ambient pressure p_o, i.e., the excess pressure or the overpressure; p_i is the peak value of the excess pressure at the shock front, i.e., $p_i = p_1 - p_o$; t is the time measured from the instant of arrival of the shock wave; and θ is called Eulerian time constant of the pressure-time curve. It is the time required for the overpressure to fall to a value $1/e$ of its peak value. It can be calculated by the relation

$$-\frac{1}{\theta} = \frac{1}{p_i}\left(\frac{\partial p}{\partial t}\right)_{R,\,t=0} \tag{13-18}$$

where the partial derivative is formed at constant radial coordinate R and evaluated at the time of arrival of the shock front at R. Asymptotically, at large distances and low overpressures, it has been shown by Kirkwood

* The notation "subscript prime" is used only with pressure and refers to shock front pressure above atmospheric pressure.

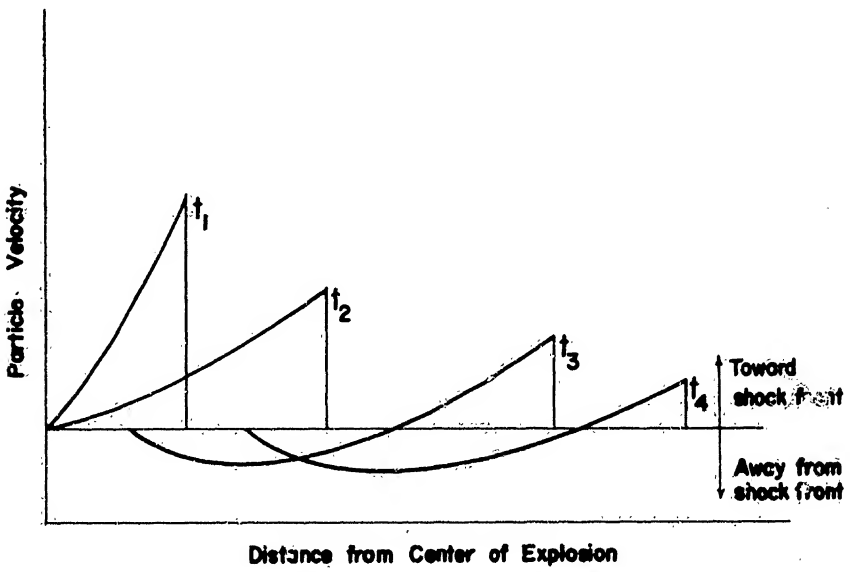

Figure 13-4. Particle Velocity-distance Curves for Blast Waves in Air at Successive Times

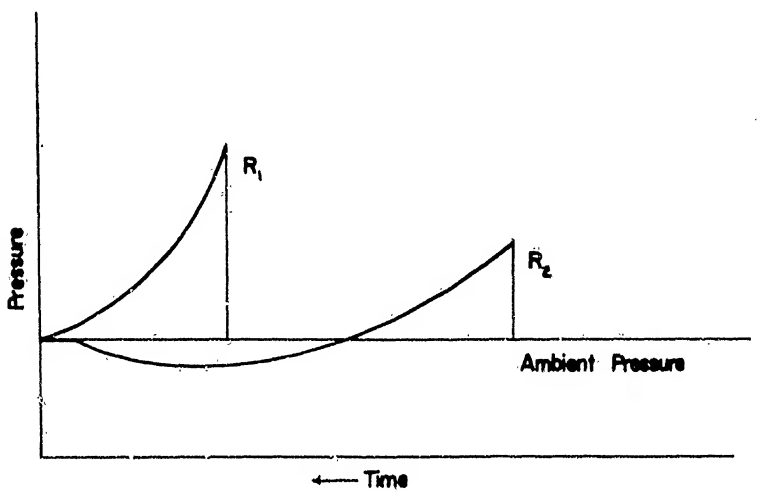

Figure 13-5. Pressure-time Curves for Blast Waves in Air

and Bethe[8] that the positive portion of the pressure-time curve is the straight line

$$p(t) = p_1(1 - t/\theta),\ t > \theta \qquad (13\text{-}19)$$

For the asymptotic pressure-time curve, θ is the duration of the positive portion of the wave. It satisfies the definition of Eq. 13-18. At intermediate distances and peak pressures, the pressure-time curve cannot be represented by a simple, one-parameter, empirical equation.

The properties of the shock front, expressed as functions of the peak pressure, can be calculated by the use of the Hugoniot equations supplemented by an equation of state for the air. Fig. 13-6 has been constructed on the assumption that air is polytropic with $\gamma = 1.4$. This assumption is adequate for shock waves whose peak pressure is relatively low. At higher amplitudes, the high temperature of the shock wave causes extensive dissociation and the polytropic assumption is no longer valid. Hugoniot curves for air in which dissociation is taken into account have been constructed Hilsenrath and Beckett[9].

The dynamic pressure π is defined as the quantity

$$\pi = \rho u^2/2 \qquad (13\text{-}20)$$

This property of the shock wave determines the aerodynamic drag forces to which a structure is exposed. The dynamic pressure is characterized by a peak value at the shock front, determined through the Hugoniot equations by the peak pressure, and a decaying dynamic pressure-time curve. The peak dynamic pressure is shown as a function of shock front pressure in Fig. 13-6. A peak approximation, similar in form to Eq. 13-17, is appropriate to describe the variation of dynamic pressure with time at points near the explosion. Asymptotically, at large distances and low overpressures, Kirkwood and Bethe[8] have shown that the portion of the dynamic pressure corresponding to the positive part of the wave is represented by the quadratic expression

$$\pi(t) = \pi_1(1 - t/\theta)^2,\ t > \theta \qquad (13\text{-}21)$$

This expression involves the same constant θ as Eq. 13-19 because the durations of positive pressure and forward facing particle velocity are asymptotically equal.

The impluse delivered to unit area by the positive portion of the shock wave is the area under the positive portion of the pressure-time curve. For the pressure-time curve of Eq. 13-1

$$I_p = p_1\,\theta \qquad (13\text{-}22)$$

which is valid close to the explosion. Asymptotically, when Eq. 13-19 applies, then

$$I_p = \tfrac{1}{2}p_1\,\theta \qquad (13\text{-}23)$$

If the peak approximation for the dynamic pressure is written in terms of a time constant θ'

$$-\frac{1}{\theta'} = \frac{1}{\pi_1}\left(\frac{\partial \pi}{\partial t}\right)_{R,t=0} \qquad (13\text{-}24)$$

analogously to Eq. 13-18, the dynamic impulse per unit area is given by an expression similar to Eq. 13-22

$$I_u = \pi_1\,\theta' \qquad (13\text{-}25)$$

which is valid close to the explosion. Asymptotically, when Eq. 13-21 applies, the dynamic impulse for the positive phase of the wave is given by

$$I_u = 2/3\pi_1\,\theta \qquad (13\text{-}26)$$

These simple expressions for the impulses require a knowledge only of two parameters of the shock wave, each of which are evaluated at the shock front. At intermediate distances and shock wave amplitudes, the evaluation of pressure impulse or dynamic impulse requires either additional information on the structure of the wave or an interpolation procedure between the expressions resulting from the peak approximation and those resulting from the asymptotic equations.

13-5 RESULTS OF NUMERICAL INTEGRATION OF THE HYDRODYNAMIC EQUATIONS FOR BLAST WAVES IN AIR

A complete theoretical development of the consequences of a simple model such as the spherical shock wave from a centrally initiated spherical charge is attended by considerable

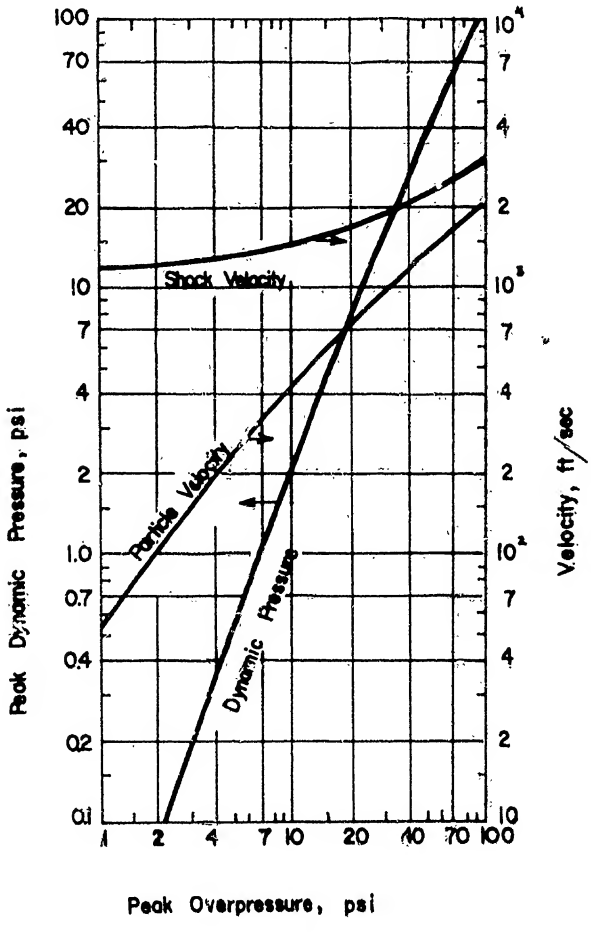

Figure 13-6. Hugoniot Properties of the Shock Wave for Ideal Polytropic Air

difficulty. In principle, the theoretical analysis is to be based on the partial differential equations of hydrodynamics. They are to be solved subject to the Hugoniot equaitons which express the conservation laws across the discontinuous shock front and which implicitly prescribe the path of the shock front in space as a function of time. The solutions depend upon initial and boundary conditions that are prescribed on the interface separating explosion products and air. The latter themselves pose a difficult problem since the position of the surface and the conditions on it depend on the flow of the detonation products at all times subsequent to the passage of the detonation wave. Now, when the detonation wave reaches the surface of the explosive and generates the initial shock wave in the surrounding medium, a wave is reflected back into the explosion products. In the spherical case, this wave is again reflected at the center and on reaching the interface between explosion products and air modifies both the position of the interface and the properties on it. As the motion develops, a complex set of waves is generated, both in the explosion products and in the air, and these have to be followed in detail in order to construct an exact solution, even for the spherical model.

The point source model of a spherical shock wave is much easier to exploit since the complicated conditions on the interface between explosion products and air are replaced by a single condition specifying the total energy released by the explosion. There is theoretical and experimental evidence that this model reproduces the main features of the explosively generated shock wave, especially at large distances from the explosion, and it provides a useful basis upon which to continue our description of the properties of blast waves in air. A more exact treatment taking into account the motion of the explosion products can be considered as adding a kind of "fine structure" to the picture obtained from the simpler considerations. The point of view appears to be valid in the present instance for two reasons, namely: (1) at distances where measurements of shock wave parameters are normally made experimentally, and where their magnitudes are important for practical problems such as specification of critical damage radii, the so-called fine structure is not resolved by the instrumentation employed, and (2) at distances nearer to the explosion where the so-called fine structure is more important, the assumption of spherical symmetry is an increasingly poor approximation to charge configurations usually employed.

Brode[6-7] has obtained the numerical solutions of the differential equations of hydrodynamics for the point source model of the spherical blast wave in air. The computational method employed is due to von Neumann and Richtmyer[10] in which an artificial viscosity is introduced into the equations as a mechanism for avoiding shock front discontinuities. The artificial viscosity is defined in such a way as to replace the shock front with steep but finite gradients in the properties of the flow, across which the Hugoniot equations are satisfied. Simultaneously, as defined, it has negligible effect on the flow in all other regions. The integrating process then consists of the step-wise solution of difference equations which approximate the differential equations of motion of the gas.

For the point source model, one can define a characteristic length λ and time τ

$$\lambda = (E/p_o)^{1/3}, \tau = \lambda/c_o \qquad (13\text{-}27)$$

where E is the total energy transmitted by the explosion to the shock wave, and p_o and c_o are the pressure and sound velocity, respectively, in the undisturbed air. Then, it is easy to show that the solutions of the hydrodynamic equations are similar, i.e., that scaling is preserved, if distances are expressed in units of length λ and times in units of the characteristic time τ. Thus, the point source solutions are independent of the nature of the explosive, so long as the energy released to the shock wave is properly employed in evaluating the scaling parameters λ and τ.

The solid line of Fig. 13-7, which is taken from Brode's paper, shows the variation of peak pressure with distance for a point explosion in an ideal gas in which it is assumed that the heat capacity ratio γ is constant and equal to 1.4. The effect of the assumption of ideality is shown by comparison with the dashed curve of the same figure, which results from calculations in which the thermodynamic properties of real air were employed and in which account was taken of the dissociation of air at the high

temperatures associated with strong shocks. The curves are qualitatively similar but show the importance of the equation of state in the actual shock amplitude at a given distance. This figure also shows for comparison experimental values for TNT.

These calculations afford a complete description of the flow associated with the shock wave. Brode presents the results in his paper by means of graphs and by empirical equations fitted to the various curves. The results are too voluminous for inclusion in this chapter and for them reference is made to the original reports. For later reference, however, we reproduce in Fig. 13-8 the instantaneous pressure-distance curves calculated for isotropic air with the point source model. The curves for real air are of similar form.

In the point source approximation, the explosion is described by a single parameter, i.e., the energy transmitted to the shock wave. The results of the calculation are thus independent of size, density, or chemical nature of the explosive, and, when scaled by a characteristic length and characteristic time determined by the energy of explosion, the results are applicable to any explosive. The effect of the parameters of the explosive that are neglected by the point source approximation is revealed by consideration of a numerical integration, carried out by Brode, in which the integration is continued from the spherical detonation wave of Taylor of the case of TNT at initial density of 1.5 g/cm^3. It was carried out using the artificial viscosity technique of von Neumann and Richtmyer. This calculation is substantially more involved than that of the point source model, and it does not appear to have been repeated for other explosive charges. Unfortunately, obsolete equation of state data for the explosion products and an incorrect energy of explosion were employed, so that the numerical results are likely to be somewhat in error. However, this calculation provides the most complete and detailed description of the air shock wave that is in existence. It has special value in providing a test of the validity of simplified models.

When a spherical shock wave is generated by a sphere of gas of finite volume at high pressure, the establishment of continuity of pressure and radial particle velocity across the contact surface between explosion products and air results in a rarefaction wave moving toward the center in the explosion products. (If the explosion products are generated by a spherical detonation wave of the type described by Taylor, the rarefaction wave moves into and modifies the structure of Taylor wave.) In general, as Brode points out, when a spherical shock wave of finite volume is backed up to an inward moving rarefaction wave, the negative pressure gradient of the rarefaction joins the positive gradient of the shock through a compression which grows as a shock as the rarefaction develops. No such condition exists for a plane wave in a shock tube. Thus, in the numerical calculations, a shock wave is seen to follow the rarefaction wave into the explosion gases. It starts with zero strength and grows as it moves inward through these gases. The gases themselves are expanding radially at a velocity that is initially high, so that this shock is swept outward in space until the expansion of the explosion products is nearly complete. Then it implodes on the origin and is reflected outward to the contact surface. At the time of reaching this surface, the explosion gases are denser and cooler than the air outside. Therefore, on passing through the surface the wave establishes a second shock wave in the air and a new inward rarefaction wave which, like the initial rarefaction wave, is followed by a shock wave moving inward. This shock implodes on the origin, reflects, and propagates outward in the wake of the earlier shocks. The succession of shocks continues in this manner until the residual energy of the explosion products is dissipated.

A rather complicated series of shock waves and rarefactions thus develops which affect the motion of the contact surface. Instead of moving monotonically from the initial radius of the explosive to the radius at which the products are at rest, a series of damped oscillations are observed. Fig. 13-9, which is taken from Brode's paper, shows the trajectories of the shock waves and of the contact surface.

By neglecting shock waves in the explosion products, the specific energy of explosion q' has been defined as

$$q' = e_o - e(\rho_o, s_1) \qquad (13\text{-}23)$$

where e_o is the specific energy content of the intact explosive, and the specific energy content

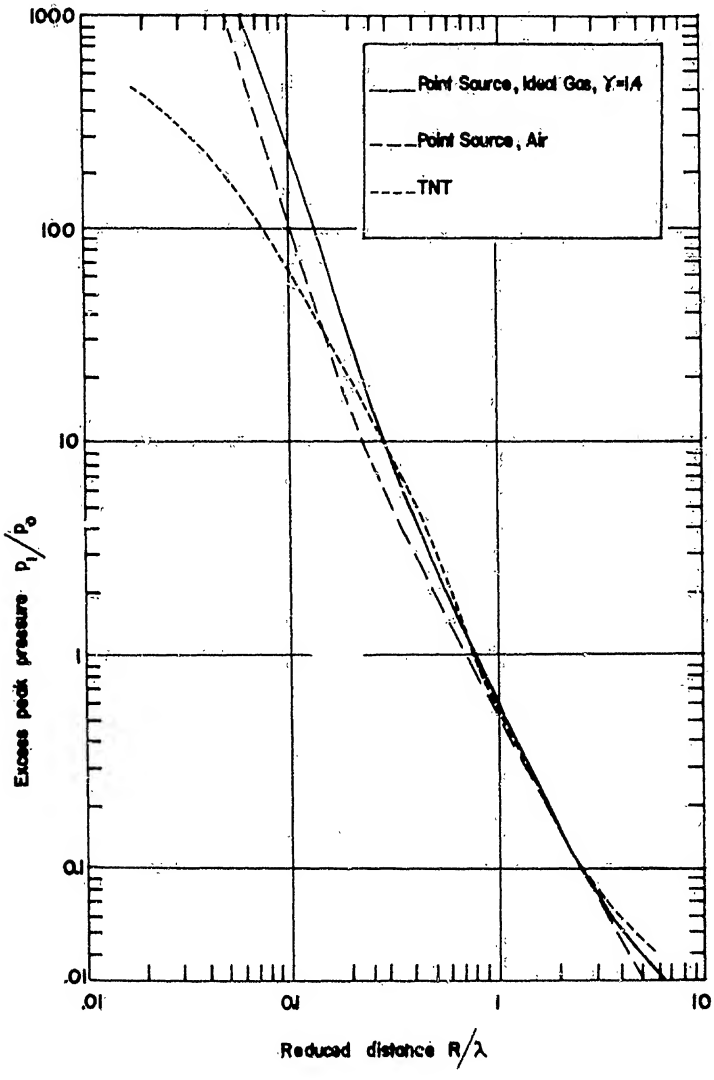

Figure 13-7. Peak Pressure-distance Curves for Shock Waves in Air Calculated With the Point Source Model (Brode)

e of the explosion products is evaluated at ambient pressure p_o and the entropy s_1 of the Chapman-Jouguet detonation state. However, the final entropy is greater than s_1 by the increments across all of the shocks in the explosion products, so that Eq. 13-28 is an overestimate of the energy transmitted to the air. It may be retained as a reasonable approximation since the energy dissipated across the shock waves is a small fraction of the total energy released by the explosion. The dissipation assumption employed in par. 13-3 is that all of the energy of the explosion is dissipated in the air as a result of the entropy increment across the initial shock. This assumption, also, is not strictly correct because of the entropy increments associated with each of the later shocks. These increments are small compared to that across the primary shock and consequently the description of energy propagation that takes account only of the primary shock wave is a good approximation.

These subsidiary shocks, as is shown by Fig. 13-10, follow the main shock at such a time and distance as to be behind the minimum of the negative phase. The pressure-distance curves of this figure are to be compared with those of Fig. 13-8, which results from the point source model. They show how the structure of the wave is affected by the finite size of the explosive charge. Since the subsidiary shocks are located in the negative phase of the primary shock wave, they cannot overtake and merge with the primary shock. It will be noted that the shape of the positive portion of the pressure-time curve as calculated from the point source model is qualitatively quite similar to that from the finite charge.

The variation of peak pressure with distance as calculated for the finite charge of TNT is

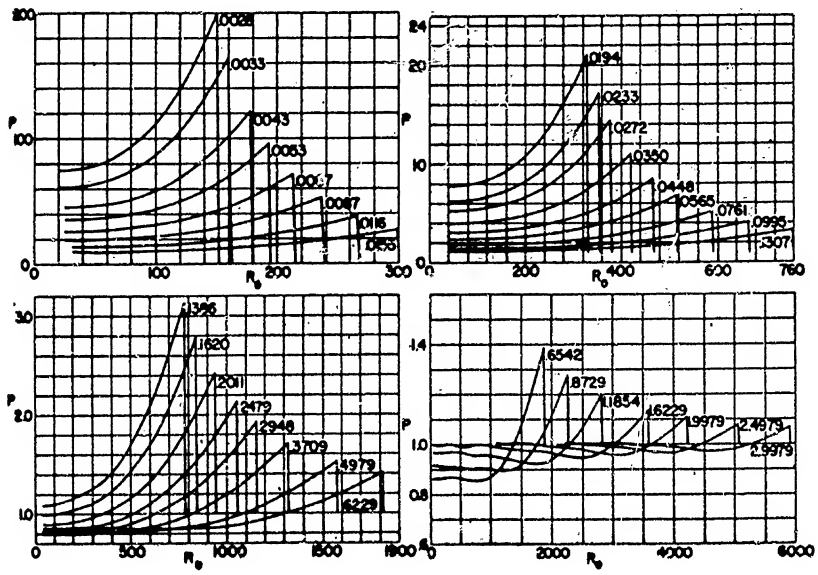

Figure 13-8. Pressure in Atmospheres as a Function of the Lagrange or Mass Position for the Point Source Solution at Times Indicated (The position is in arbitrary units of λ/1627.2 and the time is in units of τ.) (Brode)

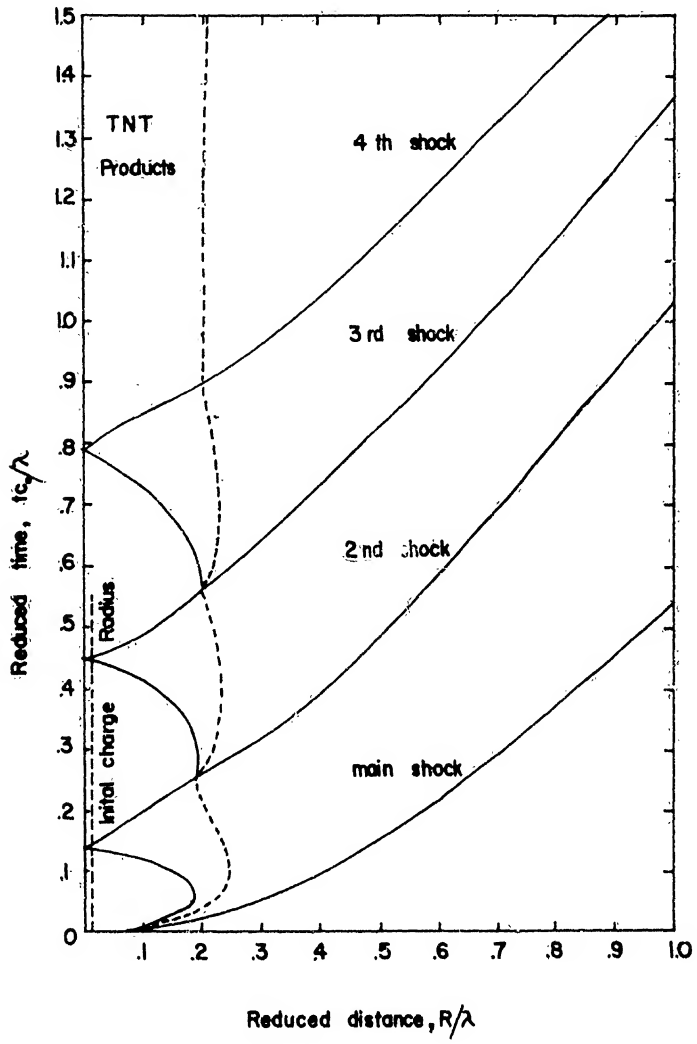

Figure 13-9. Space-time Diagram for Shocks and Contact Surface for TNT Blast in Air (Brode)

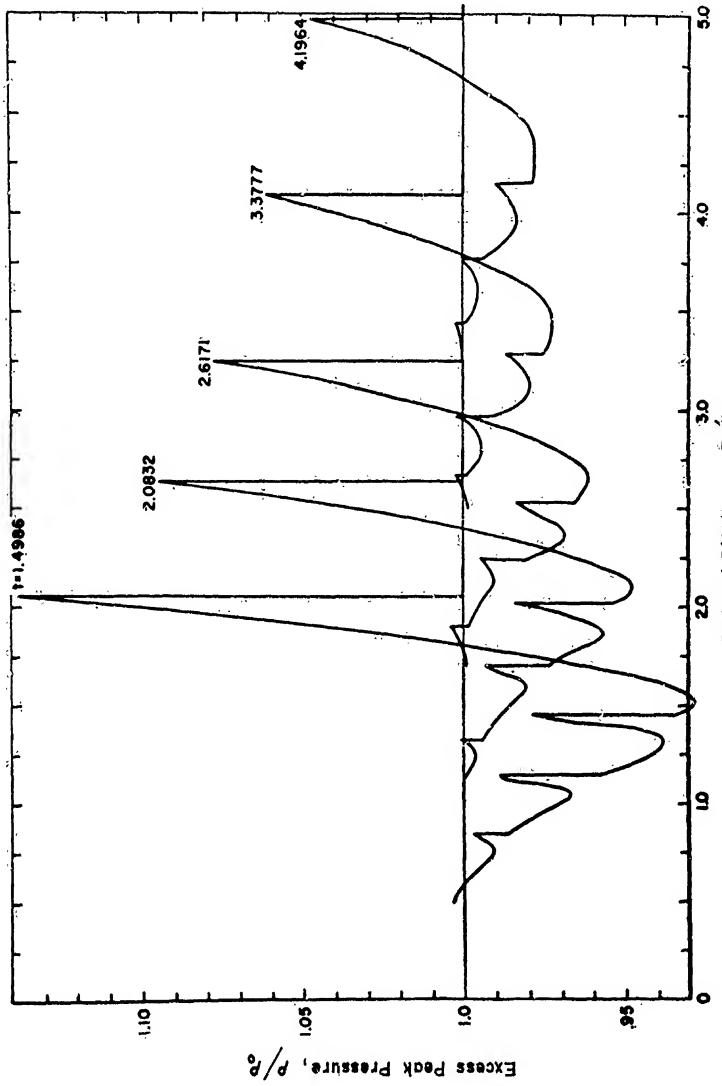

Figure 13-10. Pressure-distance Curves at Successive Times for TNT Blast Waves in Air (Brode)

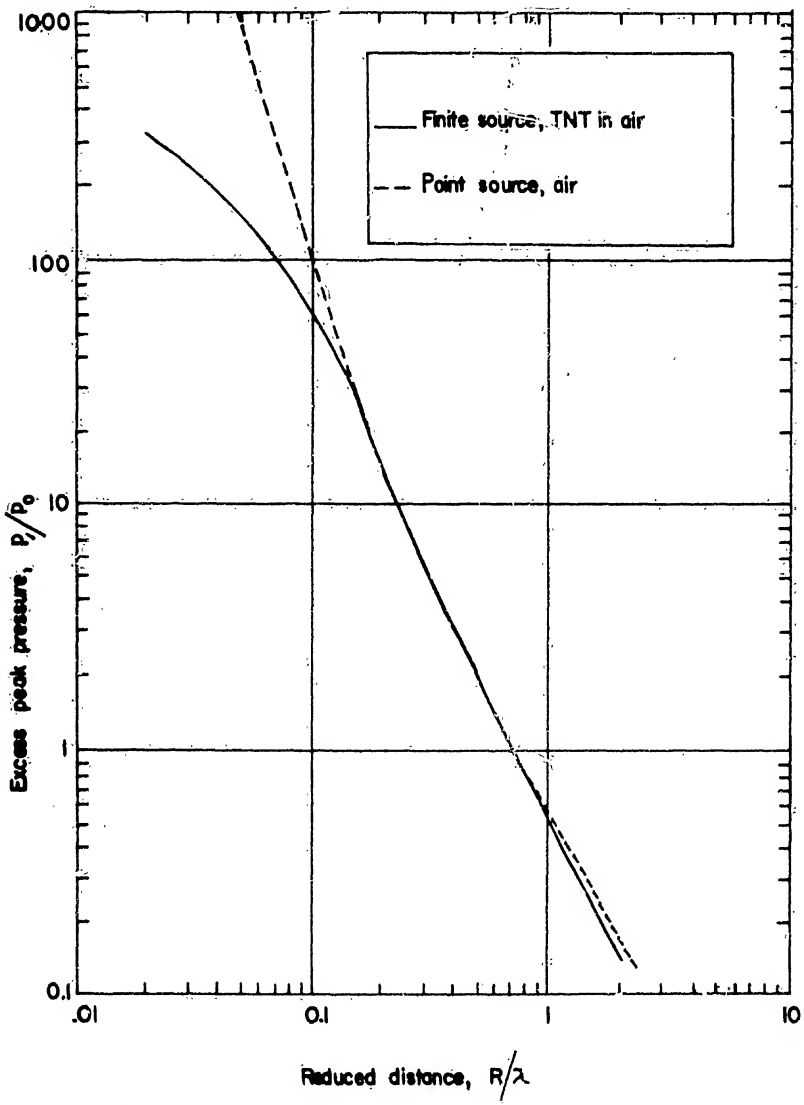

Figure 13-11. Peak Pressure-distance Curve for TNT Blast Waves in Air (Brode)

compared with results for the point source model in Fig. 13-11. At no distance are the results the same, although the slopes at large distances are similar. Close to the charge, the point source curve is, as expected, much higher than that for the finite TNT charge. Because of excessive dissipation of shock wave energy in this region, the point source curve falls below that for the finite charge releasing the same energy. It seems fair to conclude that the point source model provides at best only a qualitatively correct description of the shock wave. At distances of primary practical interest, it overestimates the most important of the shock wave parameters, the peak pressure.

Although the numerical integration of the basic equations—using the von Neumann-Richtmyer or an equivalent technique—provides the most detailed and probably the most accurate description of the shock wave, calculations of this kind are time-consuming and expensive in computational cost. They would seem to serve best as standards against which simpler approximate treatments can be compared. Any simplified theory of shock wave propagation will result in a loss in the detail with which the phenomenon is described. The simplified theory is justified if it is able to provide estimates of acceptable accuracy of those properties of the shock wave that are of practical importance, as for example, in the design of protective structures.

13-6 UNDERWATER AND UNDERGROUND EXPLOSIONS

The rapid expansion of the gas bubble formed by an underwater explosion results in a shock wave being propagated outward through the water in all directions. The shock wave is similar in form to the shock wave in air, and it obeys the same laws of hydrodynamics. It differs in detail, the differences arising solely from the differences in the equations of state of the two media. Just as in air, there is a sharp rise in overpressure at the shock front. The peak values for an underwater explosion are much higher than at the same distance from the same explosive charge in air. The peak overpressure in water does not decay with distance as rapidly as it does in air. Furthermore, the shock wave velocity which is always greater than and asymptotically equal to the velocity of sound, is greater in water than in air, except near the charge surface.

In spite of these differences, an underwater shock wave is qualitatively similar to one in air, as is seen from the summary of its characteristics which follows. The velocity of propagation near the charge is several times the limiting acoustic velocity, this limiting value being approached quite rapidly as the wave advances outward and the pressure falls. In water, the acoustic velocity is about 5,000 ft/sec. The peak pressure in the spherical wave decays more rapidly with distance than inversely as the first power of the distance, as would be predicted for a disturbance obeying acoustic laws. The rate of decay approaches this acoustic behavior in the limit of large distances. The nonacoustic decay is to be attributed, as in the case of shock waves in air, to the dissipation of energy in the water through which the shock wave has passed. However, because of the properties of the equation of state of water, the entropy increment across the shock front is very much less in water than for shock waves of the same amplitude in air. Indeed, a successful theoretical treatment of underwater shock waves has been based on the approximation that entropy changes across the shock front can be neglected with the result that the Hugoniot curve for water is approximated by the isentrope through the initial state. Thus, the nonacoustic decay of shock wave amplitude is less important in the theoretical description of underwater shock waves than in the case of shock waves in air. Finally, as in the case of air, the profile of the wave broadens gradually as the wave propagates outward. The increase in duration is most marked in the early stages of the shock wave propagation near the explosive charge. Pressure-distance curves for an underwater explosion of a 300-lb TNT charge are sketched in Fig. 13-12 for three different instants of time. In Fig. 13-13, there is shown a pressure-time curve for the same charge at a single distance. These examples are taken from a comprehensive treatment of underwater explosions by Cole[12].

The initial portion of the pressure-time curve, to pressures of the order of 30 percent of the peak value, is well described by the peak approximation, Eq. 13-17. In the later portions of the wave, however, the pressure falls off

much more slowly than is predicted by an exponential law.

Because of the long duration of the positive portion of the pressure-time curve, the definition of a limit of integration in order to obtain the impulse delivered by the primary shock wave is somewhat arbitrary. For example, duration of positive excess pressure for a 300-lb charge of TNT is about 160 times the time constant 30 ft from the charge. An integration to this limit poses difficult problems both in experimental arrangements and in analysis of data. The impulse is actually employed as a measure of short-lived transient pressure. For these reasons, it has become customary to evaluate the impulse from underwater shock waves under only the earlier high pressure region to an arbitrarily assigned upper limit on time which is long enough to include the characteristic features of the pressure-time curve when the pressures are a significant fraction of the initial peak value. One way of specifying the time limit of integration is as a constant multiple of the experimentally observed time constant. Cole suggests that the integration under the pressure-time curve be carried to a time that is five times the experimental time constant.

In several theoretical treatments of underwater shock waves, e.g., that of par. 13-8, it is assumed that the pressure-time curve can be represented by the peak approximation. This assumption imposes a constraint to which the solutions are forced to comply. It is found that theoretical time constants so calculated are greater than experimental values but that the impulse, calculated by means of Eq. 13-22, is in quite good agreement with values obtained from experimental pressure-time curves to the arbitrary time limit described above.

In a spherically diverging shock wave, the exterior medium is left with an outward velocity following the passage of the shock wave. In underwater explosions, this flow has been called the afterflow. In air, the outward flow continues past the time at which the pressure has fallen to the ambient pressure, and the flow is not brought to rest until after the pressure has fallen below the ambient value. Thus, in air, the

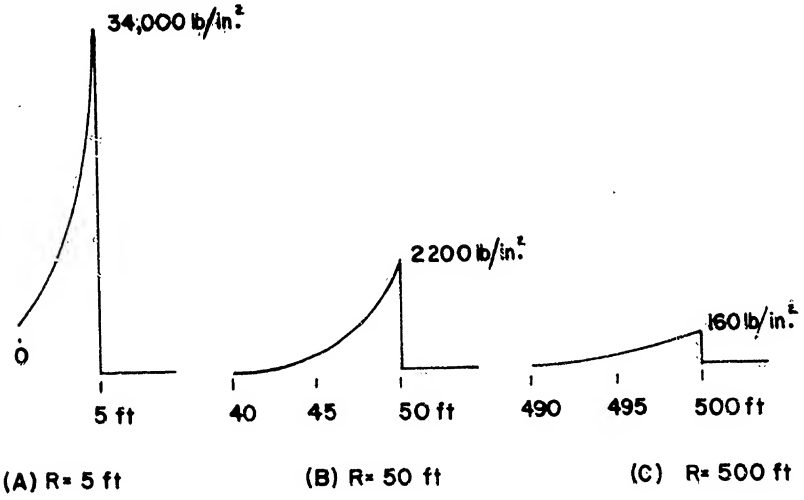

Figure 13-12. Pressure-distance Curves for the Underwater Shock Wave Produced by a 300-lb TNT Charge

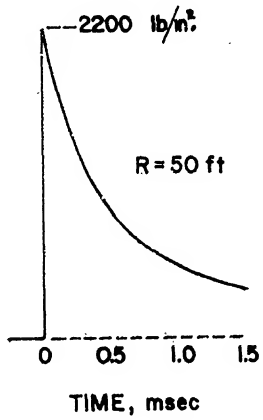

Figure 13-13. Pressure-time Curve for the Underwater Shock Wave Produced by a 300-lb TNT Charge

divergence of the flow results in a negative phase of the shock wave. We note that the explosion gases are more dense than the exterior air.

During the first part of the expansion of the gas bubble in an underwater explosion and the emission of the major part of the shock wave, the pressure and density of the explosion gases are substantially reduced. The density becomes much less than that of the exterior water but the pressure remains for a time substantially higher than the equilibrium hydrostatic pressure. The water in the vicinity of the contact surface has a high outward velocity and the diameter of the bubble increases rapidly. Because of the inertia of the water determined by its relatively high density, the afterflow continues for a relatively long time. During this period, the gas pressure falls below the equilibrium hydrostatic pressure while the water pressure approaches the equilibrium static pressure from above. Ultimately, the pressure differential brings the outward flow to a stop, and the bubble begins to contract at an increasing rate. This motion continues until it is abruptly reversed by the compression of the explosion products. Thus, the conditions for an oscillating system are provided by the inertia of the water and the compressibility of the gas. The bubble does in fact undergo repeated cycles of expansion and contraction. The process is illustrated by Fig. 13-14. It is seen that the bubble spends most of its time in an expanded state.

A pressure wave is propagated into the water by each expansion cycle of the bubble oscillations. The primary shock wave and the first bubble pulse for the underwater explosion of a TNT charge are shown in Fig. 13-15. The amplitude of the bubble pulse is seen to be much lower than that of the primary shock wave. However, the wave is of long duration and the impulse delivered by it is comparable to that delivered by the shock wave. The bubble pulses can thus contribute significantly to the damage from an underwater explosion. The time constant of the primary shock wave (the time required for the pressure to fall to a value of p_s/e) is of the order of 0.5 msec. In order of magnitude, the time of arrival of the bubble pulse is 1,000 times the time constant of the shock wave. The secondary pressure waves described here have their origin in the dynamical properties of water. They are not to be identified with the secondary shock waves in air that were described in the last paragraph.

A comprehensive discussion of the oscillations of the gas bubble and of the secondary bubble pulses emitted during the bubble motion is given by Cole. It is shown that the theoretical description of the phenomenon can be based on the incompressive approximation of the equations of hydrodynamics, however, the force of gravity cannot be neglected in the description of the bubble motion. One result of this theoretical treatment is of particular interest. It is shown that the period of the oscillation is proportional to the one-third power of the energy transmitted to the water during the bubble oscillations and inversely proportional to the five-sixths power of the hydrostatic pressure

$$T = KE_b^{1/3}/p_o^{5/6} \qquad (13\text{-}29)$$

where T is the period, E_b is the bubble energy, and K is a proportionality constant. This result, which as been derived by a number of writers, is usually known as the Willis formula. This result makes possible the determination of the bubble energy from measurements of the variation of the period with charge depth and charge size. It is found that approximately 50 percent of the

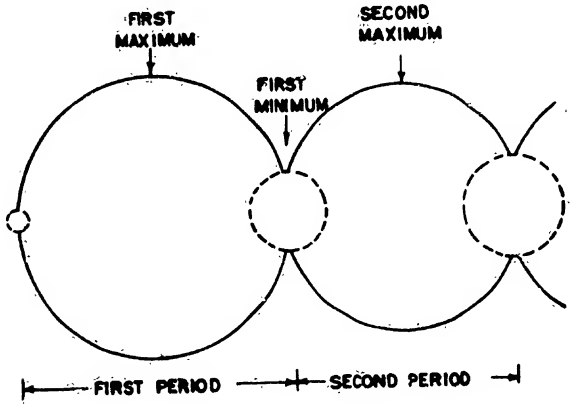

Figure 13-14. Bubble Oscillations From an Underwater Explosion[13]

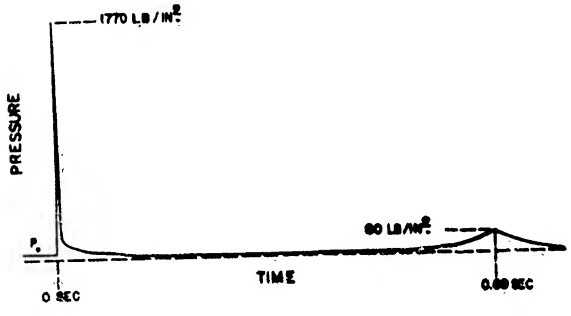

Figure 13-15. Pressure-time Curve for Underwater Pressure Waves 50 ft From a 300-lb TNT Charge

energy of explosion is transmitted during the primary shock wave*, the remainder being dissipated during the oscillations of the gas bubble. The most precise data are available for the underwater explosion of TNT, for which the energy of explosion has been evaluated as 1060 cal/g. From the observed period of oscillation of the gas bubble, a bubble energy of 480 cal/g is calculated. The difference, 580 cal/g, is the energy of the initial shock wave.

In water, as in air, all of the properties at the shock front are determined as functions of the peak pressure by the Hugoniot equations and an equation of state. The Tait equation of state is an expression of simple form that gives a good representation of pvT data. Along an isentrope, it can be written

$$p = B[(\rho/\rho_o)^{\kappa} - 1] \qquad (13\text{-}30)$$

The exponent κ is taken to be 7.15 for sea water. The quantity B is a slowly varying function of entropy. For sea water at 20°C, it has been assigned the value 3.047 kbars. It will be noted that Eq. 13-30 has a form similar to that for a polytropic gas. Richardson, Arons, and Halverson[11] have employed Eq. 13-30 to evaluate the properties of sea water along the Hugoniot curve. The shock wave velocity and the particle and sound velocities at the shock front are shown as functions of peak pressure by Fig. 13-16.

As in the case of shock waves in air, a straightforward mathematical approach to the theoretical description of the shock wave from underwater explosions can be based on the numerical integration of the equations of hydrodynamics. A calculation of this nature has been performed by Penney and Dasgupta[12] for TNT. The integration was continued from the spherical detonation wave described by Taylor. The peak pressure-distance curve obtained by this procedure is shown in Fig. 13-17 which also shows some experimental values. At distances for which experimental data are available, the rate of decay of the theoretical curve is closely similar to that for the experimental curve. The low values obtained by calculation are to be attributed to the low energy release that was assumed in the calculation of the initial conditions. It seems reasonable to assume that a revision and extension of these calculations, employing the more accurate value of the energy of explosion that is now available, would give results in good agreement with experiment.

The principal commercial application of explosives has been to blasting with the explosive detonated underground. An underground explosion is very difficult to describe quantitatively, and the present state of knowledge in this area is very limited. In practical cases, the terrain is rarely even approximately uniform over any considerable distance from the charge. Even where uniform, the exterior medium cannot be described by any simple equation of state. Finally, the explosion in a medium of infinite extent, to which we have elected to limit the treatment of this chapter, does not correspond to the geometry of any blasting application of practical interest. On the other hand, more recent problems involving underground storage of ammunition, and simulation of underground nuclear bursts, have led to experimental and theoretical work on underground detonations in "infinite" media[20-25].

In an underground explosion, the pressure wave transmitted to the exterior medium is, of course, affected by the mechanical properties of the medium. If the medium is an elastic solid, such as rock, there is a region of plastic deformation and permanent displacement in the region close to the charge where the pressure is greater than the elastic limit of the material. At greater distances, both transverse and longitudinal elastic waves are generated by the explosion which travel, in general, at different velocities and which are modified on reflection at free surfaces, such as the ground level or a pit face, and on passing from material at one density to material at another. In general, it can be stated that most of the energy of explosion is dissipated close to the explosion in the region of permanent displacement, and that the amount of energy transmitted by elastic or seismic waves is at most a few percent of the energy of explosion. If the solid is elastic, it most commonly fractures under tension as the result of the tension wave produced on reflection of a compression wave at a free surface.

* Not all of the energy transmitted by the primary shock wave appears in the shock wave at moderate distances from the charge. A portion of the energy is dissipated as heat in the fluid through which the shock wave has progressed (see par. 4-8).

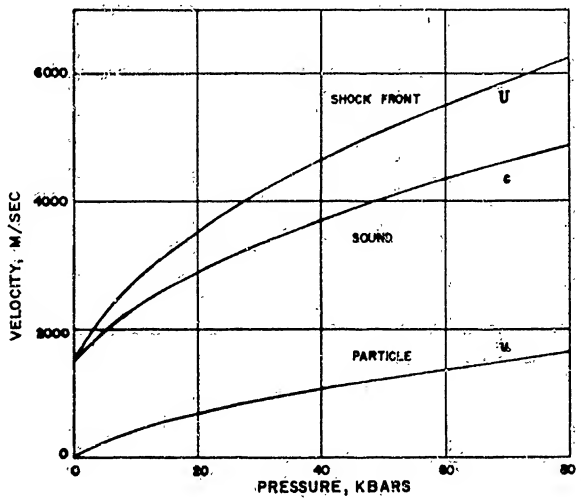

Figure 13-16. Hugoniot Properties for Shock Waves in Sea Water[11]

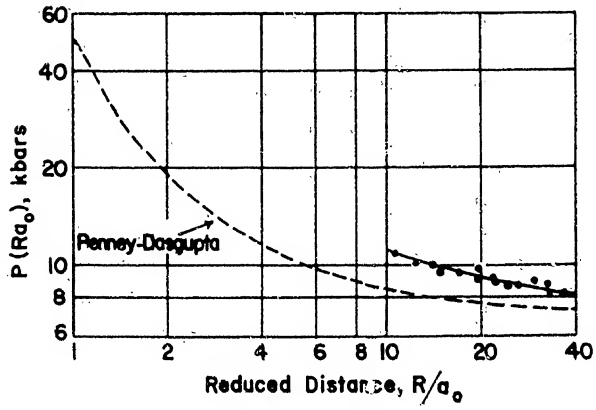

Figure 13-17. Peak Pressure-distance Curve for the Underwater Explosion of TNT as Calculated by Penney and Dasgupta[12]

A considerable amount of empirical information has been compiled on the behavior of explosives in varying terrains. The selection of an explosive and its arrangements for a particular blasting job are, as a practical matter, entirely dictated by experience. It seems fair to state that blasting is at the present time an art almost completely without a quantitative scientific basis.

13-7 THE INITIAL SHOCK WAVE PRESSURES

At the contact surface between explosion products and exterior medium, the pressure and normal component of the particle velocity are equal on each side of the surface at all times. In particular, for a spherical explosive charge of initial radius a_o, these conditions can be expressed by

$$p_1(a_o) = p_*(a_o),\ u_1(a_o) = u_*(a_o) \qquad (13\text{-}31)$$

where $p_1(a_o)$ is the initial excess peak pressure in the exterior medium, $p_*(a_o)$ is the pressure in excess of the initial pressure p_o of the explosion products on the surface $R = a_o$, $u_1(a_o)$ is the initial radial shock front particle velocity, and $u_*(a_o)$ is the radial particle velocity of the explosion products on the contact surface. When these conditions are established, a shock wave advances into the exterior medium and a rarefaction wave recedes into the explosion products. The rarefaction wave is initially characterized by the fact that the Riemann $\bar{r}$ function (see Chapter 2) is an invariant on a particle path, i.e., on the surface $R = a_o$. This condition can be stated in the form

$$\left.\begin{aligned} \bar{r} &= u + \sigma = \text{constant} \\ \sigma &= \int^{p+p_o} \frac{dp}{\rho c} \end{aligned}\right\} \qquad (13\text{-}32)$$

The constant in Eq. 13-32 is fixed when the difinition of the σ-function is completed by specification of a lower limit of integration. The integral defining the σ-function is along a path of constant entropy (which because of the entropy transport equation is also a particle path).

The solution for the propagation of shock waves should, of course, be based on a continuation of the solution for the spherical detonation wave, described in Chapter 9. If we here designate by p_d the pressure of the detonation wave front and by u_d the corresponding value of the particle velocity, Eqs. 13-32 can be written

$$u_*(a_o) + \sigma(p_*) = u_d \qquad (13\text{-}33)$$

where

$$\sigma(p) = \int_{p_d}^{p+p_o} \frac{dp}{\rho c} \qquad (13\text{-}34)$$

Using Eqs. 13-31, the Riemann condition can be written in the form

$$u_1(a_o) + \sigma(p_1) = u_d \qquad (13\text{-}35)$$

The σ-function is to be evaluated using an equation of state for the explosion products. It is necessary to calculate the detonation state; to construct the isentrope through this state; to evaluate the integrand of Eq. 13-34 along the isentrope; and, finally, to evaluate the σ-function by quadrature. Methods for the construction of the isentrope are described in Chapter 2.

The shock front in the exterior medium must satisfy the Hugoniot conservation equations (see Chapter 2). These can be written

$$\left.\begin{aligned} p_1 &= \rho_o u_1 U \\ u_1 &= U(1 - \rho_o v_1) \\ h_1 - h_o &= p_1(v_o + v_1)/2 \end{aligned}\right\} \qquad (13\text{-}36)$$

in terms of the excess peak pressure p_1, where U is the velocity of propagation of the shock wave. These equations are supplemented by an equation of state for the exterior medium. They make it possible to express each of the shock front properties as functions of any one of them (usually in tabular form) for given values of the properties of the undisturbed medium. In particular, it is possible to express the shock front particle velocity as a function of the peak excess pressure

$$u_1 = u_1(p_1) \qquad (13\text{-}37)$$

Thus, Eqs. 13-35 and 13-36 imply a relation

$$u_1(p_r) + \sigma(p_r) = u_d \qquad (13\text{-}38)$$

which can be solved for the initial excess shock front pressure p_r by numerical or graphical methods.

Kirkwood and Bethe[8] have constructed a theory of the propagation of shock waves in water in which it is shown that the function

$$G = r\left(w + u^2/2\right)$$
$$w = \int_{p_o}^{p+p_o} dp/\rho \qquad (13\text{-}39)$$

propagates according to a relation that can be written

$$G(r,t) = G_a(\tau) \qquad (13\text{-}40)$$

where G_a is the value of the function G on the contact surface at a time τ. If $G(r,t)$ is known everywhere in the (r,t)-plane, all of the properties of the shock wave can be deduced in a straightforward manner. Eq. 13-40 states that the function $G(r,t)$ is equal to the value of the same function on the contact surface at a time τ which is a function $\tau(r,t)$. Kirkwood and Bethe give a prescription for evaluating $G_a(\tau)$ and $\tau(r,t)$, and they have thus formulated a theory of propagation of the shock wave. We do not wish to describe this theory in further detail but only to comment on an implication of Eq. 13-40. Kirkwood and Bethe show that the time τ is an increasing function of time for any constant value of r. This means that the properties of the shock wave, including those at the shock front, are determined by properties on the contact surface at times that increase as the shock front propagates. We may, therefore, picture modification of the wave during its propagation as the result of a process in which the wave front is continually destroyed by dissipation in response to the finite entropy increment across the shock front and in which the properties of the wave as it propagates are determined by properties on the contact surface at successively later times. The process is illustrated schematically by the pressure-time profiles at two distances of Fig. 13-18, in which the dashed curve of the curve at the greater distance is intended to represent the portion of the earlier wave that has been destroyed by dissipation. The Kirkwood-Bethe theory is based on an assumption that the flow behind the shock front can be considered to be isentropic, as assumption that is valid in water but not in air. The picture that it affords of the dissipation mechanism, is however, qualitatively true for shock waves in air, where the dissipation of energy is more rapid than in water.

It can be concluded on the basis of the insight afforded by the analysis of Kirkwood and Bethe that simpler models of the initial state of the explosion products can be employed to calculate the initial shock wave pressure, provided the energy of the explosion is correctly specified. The shock wave parameters are seen to be relatively insensitive to the initial shock wave pressure. It is, therefore, frequently assumed that the explosion can be adequately approximated by assuming that it takes place instantaneously at constant volume. One then defines the σ-function by

$$\sigma(p) = \int_{p_e}^{p+p_o} \frac{dp}{\rho c} \qquad (13\text{-}41)$$

where p_e is the pressure of the constant volume explosion state. The constant of Eq. 13-32 is then zero and the expression corresponding to Eq. 13-38 is

$$u_1(p_r) + \sigma(p_r) = 0 \qquad (13\text{-}42)$$

which can be solved for the initial excess shock front pressure by numerical or graphical methods.

13-8 AN APPROXIMATE THEORY OF SHOCK WAVE PROPAGATION

In the analysis of damage to structures by blast waves in air or underwater explosion waves, and in the establishment of an order of merit among explosives with respect to damage power, the pressure-time curves and peak pressure-distance curves of the shock waves produced by the explosives are of primary importance. While experimental techniques have been sufficiently developed so as to lead to the accumulation of a large body of reliable data,

there exists a need for more flexible and convenient theoretical methods of analysis of the problem.

The theoretical analysis of explosion waves in air, water, or in other media characterized by a well-defined equation of state, involves the integration of the hydrodynamic equations subject to initial conditions determined by the explosive source and subject to the Hugoniot conditions at the shock front. It has been seen, for the case of blast waves in air, that the point source model is insufficiently exact for a quantitative description of the shock wave and that a more realistic model of the explosion must be employed. A straightforward attack on the mathematical problem can be based on the numerical integration of the hydrodynamic equations. The complexity of this approach has thus far limited the procedure to a few special applications. The need for a more rapid and flexible theoretical method, based on well-defined approximations as necessary, is therefore clear. In the case of underwater explosions such a method, which has been extensively applied, has been developed by Kirkwood and Bethe[8]. Brief reference was made to their theory in par. 13-7. It is described in detail, with the results of calculations, by Cole[13].

Underwater explosion waves are simpler to treat than blast waves in air since the relatively small entropy increment produced at the shock front permits the use of the approximation of adiabatic flow. This approximation cannot be employed for blast waves in air. Kirkwood and Brinkley[3] have described a theory of propagation of one-dimensional waves—i.e., plane, cylindrical, or spherical—that takes proper account of the finite entropy increment in the fluid resulting from the passage of the shock wave. It also permits the use of the exact Hugoniot equation of the fluid and is in this respect superior to treatments for air based or the use of ideal gas isentropes with constant heat capacity, an approximation that fails badly near the explosion. The treatment is based upon a

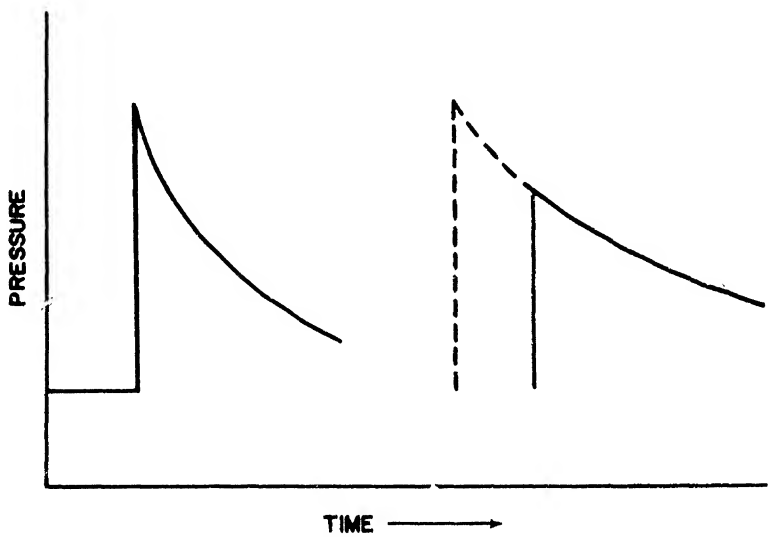

Figure 13-18. Pressure-time Curves of Shock Wave in Water, Showing Dissipation at the Front as Described by Kirkwood and Bethe

similarity restraint imposed upon the energy-time curve of the wave. The theory results in the formulation of a pair of ordinary differential equations which can easily be integrated by numerical procedures. A similar approach has been employed by Kirkwood and Brinkley[3] for the shock wave generated in an infinitely. long cylindrical charge with a detonation wave progressing at constant velocity in the axial direction. In this paragraph the theory will be described for the spherical wave.

The equations of hydrodynamics for radial flow in the absence of viscosity or heat conduction can be written in the usual Eulerian form

$$\left.\begin{aligned} \frac{1}{\rho c^2}\left(\frac{dp}{dt}\right) + \frac{\partial u}{\partial r} &= -\frac{2u}{r} \\ \frac{du}{dt} + \frac{1}{\rho}\left(\frac{\partial p}{\partial r}\right) &= 0 \end{aligned}\right\} \qquad (13\text{-}43)$$

where p is the excess pressure, u is the particle velocity, ρ is the density, and r is the radial space coordinate whose origin is at the center of the explosion. The sound velocity c is defined by $c^2 = (\partial p/\partial \rho)_s$. These equations are supplemented by the entropy transport equation which we do not employ explicitly. The conservation of mass for radial flow requires that

$$\frac{4}{3}\pi r_o^3 \rho_o = 4\pi \int_{r(o,t)}^{r(r_o,t)} \rho(r',t)\left(r'\right)^2 dr' \qquad (13\text{-}44)$$

where $r(r_o,t)$ is the Eulerian space coordinate of the material particle whose Eulerian coordinate was r_o at $t = 0$, and where ρ_o is the constant density of the fluid at $t = 0$. Differentiating Eq. 13-44 with respect to r_o at constant t, we obtain the Lagrangian equation of continuity for spherical symmetry

$$\left(\frac{\partial r}{\partial r_o}\right)_t = \frac{\rho_o}{\rho}\left(\frac{r_o}{r}\right)^2 \qquad (13\text{-}45)$$

Also, by definition

$$u = \left(\frac{\partial r}{\partial t}\right)_{r_o} \qquad (13\text{-}46)$$

In terms of the Lagrangian space coordinate r_o, Eqs. 13-43 can be written

$$\left.\begin{aligned} \frac{1}{\rho c^2}\left(\frac{\partial p}{\partial t}\right) + \frac{\rho}{\rho_o}\left(\frac{r^2}{r_o^2}\right)\frac{\partial u}{\partial r_o} &= \frac{2u}{r} \\ \frac{\partial u}{\partial t} + \left(\frac{r^2}{\rho_o r_o^2}\right)\frac{\partial p}{\partial r_o} &= 0 \end{aligned}\right\} \qquad (13\text{-}47)$$

where we now understand the independent variables to be r_o and t. Eqs. 13-47 are of hybrid form in that the Eulerian form of the equation of continuity is retained. They are supplemented by the entropy transport equation and by the equation of state of the fluid, and they are to be solved subject to initial and boundary conditions specified on a curve in the (r_o,t)-plane and to the Hugoniot conditions, Eqs. 13-36

$$\begin{aligned} p_1 &= \rho_o u_1 U \\ u_1 &= U(1 - \rho_o v_1) \\ h_1 - h_o &= (p_1/2)(v_o + v_1) \end{aligned} \qquad (13\text{-}48)$$

(p is the pressure in excess of the pressure p_o of the undisturbed fluid) which are to be satisfied at the shock front. Eqs. 13-48 are compatible with Eqs. 13-47 and specified boundary conditions only if the shock front follows an implicitly prescribed curve $R(t)$ in the (r_o,t)-plane.

We denote a derivative in which the shock front is stationary by

$$\frac{d}{dR} = \left(\frac{\partial}{\partial r}\right)_1 + \frac{1}{U}\left(\frac{\partial}{\partial t}\right)_1 \qquad (13\text{-}49)$$

where the subscript unity means that the quantity so designated is to be evaluated at the shock front. If this operator . applied to the first of Eqs. 13-48, one obtains the relation

$$\left.\begin{aligned} \left(\frac{\partial u}{\partial t}\right)_1 + U\left(\frac{\partial u}{\partial r}\right)_1 &= \frac{g}{\rho_o}\left[\frac{1}{U}\left(\frac{\partial p}{\partial t}\right)_1 + \left(\frac{\partial p}{\partial r}\right)_1\right] \\ g = \rho_o U\frac{du_1}{dp_1} &= 1 - \frac{p_1}{U}\frac{dU}{dp_1} \end{aligned}\right\} \qquad (13\text{-}50)$$

where the partial derivatives are to be evaluated at the shock front and where the function g is to be calculated from the Hugoniot relations.

When specialized to the shock front $r = r_o = R$, Eqs. 13-47 become

$$\left.\begin{aligned} \frac{\rho_1}{\rho_o}\left(\frac{\partial u}{\partial r}\right)_1 + \frac{1}{\rho_1 c_1^2}\left(\frac{\partial p}{\partial t}\right)_1 &= -\frac{2u_1}{R} \\ \left(\frac{\partial u}{\partial t}\right)_1 + \frac{1}{\rho_o}\left(\frac{\partial p}{\partial r}\right)_1 &= 0 \end{aligned}\right\} \quad (13\text{-}51)$$

Eqs. 13-50 and 13-51 provide three relations between the four partial derivatives $-p/\partial t$, $\partial p/\partial r$, $\partial u/\partial t$, and $\partial u/\partial r$—all evaluated at the shock front, with coefficients that can be expressed as functions of excess peak pressure alone for given ambient conditions, by means of the Hugoniot equations and the equation of state of the fluid. If they could be supplemented by a fourth independent relation, it would be possible to solve algebraically for each of the partial derivatives as a function of p and R and, with the aid of Eq. 13-19, to formulate an ordinary differential equation

$$\frac{dp_1}{dR} = \left(\frac{\partial p}{\partial r}\right)_1 + \frac{1}{U}\left(\frac{\partial p}{\partial t}\right)_1 = F(p,R) \quad (13\text{-}52)$$

for the peak pressure p_1 of the shock wave as a function of the distance R and also to obtain the initial slope of the Euler pressure-time curve of the wave.

It is, of course, futile to seek such a fourth relation that does not itself involve an integral of Eqs. 13-47. It is possible, however, to formulate a relation of the desired type that requires only a knowledge of the form of the energy-time curve of the shock induced flow and that is insensitive to changes in form attending the propagation of the wave. By imposing a similarity restraint on the energy-time curve, an approximate theory of propagation is obtained.

The physical basis for the supplementary relation derives from the fact that the nonacoustic decay of waves of finite amplitude is closely associated with the finite entropy increment experienced by the fluid in passing through the shock front and the resulting dissipation of energy. As the shock wave propagates through the fluid, it leaves in its path a residual internal energy increment determined by the entropy increment produced in it by the passage of the shock wave. In consequence, the energy propagated ahead by the shock wave decreases as the distance it has traveled from the source increases.

In par. 13-3, it was shown that the shock wave energy $E(R)$, defined by Eq. 13-15

$$E(R) = 4\pi \int_{r_o(R)}^{\infty} r^2 pu\,dt \quad (13\text{-}53)$$

(in this paragraph p denotes the excess pressure) is related to the Hugoniot properties at the shock front by the ordinary differential equation

$$\frac{dD}{dR} = -4\pi R^2 \rho_o \Delta h(p_1) \quad (13\text{-}54)$$

where $\Delta h(p_1)$ is the specific enthalpy dissipated at a shock front whose peak pressure is p_1. The integral of the energy-time curve is expressible through Eq. 13-54 in terms of the peak pressure-distance curve of the shock wave for distances beyond R by Eq. 13-54. The dissipation assumption does not violate conservation of momentum since, through spreading of the wave, the total momentum can remain finite while the particle velocity everywhere and the total kinetic energy tend to zero. The dissipation assumption breaks down if the first shock wave can be overtaken by secondary shocks built up in its wake. This will not occur if the pressure-time curve is initially monotonically-decreasing with asymptotic value p_o. If the excess pressure has a negative phase, second shocks may develop in the negative portion of the wave but they cannot overtake the initial positive shock. In this case, the theory will apply to the positive portion of the wave if the line integral of Eq. 13-53 is extended to the time at which the excess pressure vanishes, instead of to infinity.

The energy-time curve can now be expressed in reduced form as follows:

$$\left.\begin{aligned} E(R) &= 4\pi R^2 p_1 u_1 \mu\epsilon \\ \frac{1}{\mu} &= -\left[\frac{\partial}{\partial t}\ln r^2 p\,u\right]_{t=t_o(R)} \\ &= -\frac{1}{p_1}\left(\frac{\partial p}{\partial t}\right)_1 - \frac{1}{u_1}\left(\frac{\partial u}{\partial t}\right)_1 - \frac{2u_1}{R} \\ \epsilon &= \int_o^{\infty} f(R,\tau)\,d\tau \\ \tau &= [t - t_o(R)]/\mu \\ f(R,\tau) &= r^2 p\,u/\left(R^2 p_1 u_1\right) \end{aligned}\right\} \quad (13\text{-}55)$$

The function $f(R,\tau)$ is the energy-time integrand, normalized by its peak value at the shock front, expressed as a function of R and a reduced time which normalizes its initial slope to -1, if μ does not vanish, i.e.,

$$f(R, 0) = 1$$

$$(\partial f/\partial \tau)_{\tau=0} = -1$$

We assume f to be a monotonically-decreasing function of τ. Elimination of μ between the first two of Eqs. 13-55 yields the desired supplementary relation between the partial derivatives at the shock front. It, of course, involves integrals of Eqs. 13-47 for a knowledge of the reduced energy-time function. However, if $f(a_o,\tau)$—a_o is initial charge radius—is initially a monotonically-decreasing function of τ, $f(R,\tau)$ will remain so and will, at large R, become asymptotically a quadratic function of τ corresponding to the linear form of the pressure-time curve shown by Kirkwood and Bethe[8] to be asymptotically stable. This means that ϵ is a slowly varying function of R for which a sufficiently accurate estimate can be made without explicit integration of the equations of hydrodynamics.

The initial pressure-time curve and energy-time curves of an explosion wave are rapidly decreasing. An expansion of the logarithm of the function in a linear Taylor series in the time, the peak approximation, is appropriate for an initial estimate of ϵ. This corresponds to an exponential $f(\tau)$, independent of R

$$f = e^{-\tau}, \ \epsilon = 1$$

For the asymptotic energy-time curve of quadratic form corresponding to a linear positive portion of the pressure-time curve

$$f = (1 - \tau/2)^2, \ \tau \leq 2$$

$$f = 0, \tau > 2, \ \epsilon = 2/3$$

As an empirical interpolation formula between these two limiting values, Kirkwood and Brinkley[3] have employed the relation

$$\epsilon(p) = 1 - \frac{1}{3} \exp[-p/p_o] \qquad (13\text{-}56)$$

When the four relations expressed by Eqs. 13-50, 13-51, and 13-55 between the four partial derivatives $\partial p/\partial t$, $\partial p/\partial r$, $\partial u/\partial t$, and $\partial u/\partial r$, all at the shock front, are combined with Eq. 13-52; we obtain an ordinary differential equation

$$\frac{dp_1}{dr} + \frac{p_1}{R} m(p_1) = -4\pi \frac{\epsilon R^2}{D} p_1^2 \, n(p_1) \qquad (13\text{-}57)$$

where

$$m(p_1) = \frac{2G(1 - \rho_o/\rho_1) + 4\rho_o/\rho_1}{2(1 + g) - G}$$

$$n(p_1) = \frac{G(1 - \rho_o/\rho_1)}{2(1 + g) - G}$$

$$G = 1 - (\rho_o U/\rho_1 c_1)^2$$

which is to be solved simultaneously with Eq. 13-54. The constants of integration are the initial value of the peak pressure, the evaluation of which is discussed in par. 13-7, and the energy $E(a_o)$ delivered to the shock wave. For a shock wave in air, this quantity may be taken equal to the energy of explosion since substantially all of the explosion energy is dissipated by the shock wave. For an underwater shock wave, it can be assumed for *a priori* calculations that 50 percent of the energy of explosion is transferred to the initial shock wave, the remainder being transmitted as secondary pulses by the oscillation of the bubble. These equations can also be employed to extrapolate an experimental peak pressure-distance curve to distances nearer to or farther from the explosion than those covered by the experiments. In this application, the constants of integration are chosen from experimental values of p_1 and of dp_1/dR at some value of R.

The Eulerian time constant θ of the pressure-time curve is

$$-\frac{1}{\theta} = \left[\left(\frac{\partial \ell n \, p}{\partial t}\right)_r\right]_{t=t_o} = \frac{1}{p_1}\left(\frac{\partial p}{\partial t}\right)_1 - \frac{u_1}{p_1}\left(\frac{\rho_1}{\rho_o}\right)\left(\frac{\partial p}{\partial r}\right)_1 \qquad (13\text{-}58)$$

Using Eqs. 13-50, 13-51, and 13-55, we obtain

$$\frac{1}{\theta} = \frac{2u_1}{R} a(p_1) + 4\pi \frac{\epsilon R^2 \, p_1 u_1}{D} b(p_1) \qquad (13\text{-}59)$$

where

$$a(p_i) = b(p_i) + \frac{2(\rho_o/\rho_1) - 1}{(1 - \rho_o/\rho_1)[2(1 + g) - G]}$$

$$b(p_i) = \frac{(\rho_1/\rho_o)(1 + g) - (\rho_1/\rho_o - 1)G}{2(1 + g) - G}$$

For the peak approximation, the positive impulse I is given by Eq. 13-22

$$I = p_i\theta \qquad (13\text{-}60)$$

For the asymptotic linear pressure-time curve, the positive impulse I is given by Eq. 13-23

$$I = \frac{1}{2} p_i \theta \qquad (13\text{-}61)$$

Kirkwood and Brinkley[3] have interpolated between these limiting values by means of the empirical formula

$$I = \left\{1 - \frac{1}{2} \exp\left[-\, p_i/p_o\right]\right\} p_i\theta \qquad (13\text{-}62)$$

an expression that has no theoretical justification and of which the form was chosen to give agreement with experimental values of the positive impulse.

It is convenient for shock waves in air to express the excess peak pressure in units of p_o and the distance in units of the initial charge radius a_o. Therefore, we define

$$\left.\begin{aligned} \underline{p} &= p_i/p_o \\ \underline{R} &= R/a_o \end{aligned}\right\} \qquad (13\text{-}63)$$

We also define a reduced energy variable $\underline{D}$ by

$$\underline{D} = \frac{3}{\pi}\left(\frac{\gamma_o^3}{\gamma_o + 1}\right)\left(\frac{D}{c_o^2 a_o^3 \rho_o}\right) \qquad (13\text{-}64)$$

where c_o and γ_o are the sound velocity and heat capacity ratio, respectively, of the undisturbed air. With these definitions, Eqs. 13-54 and 13-57 can be written

$$\left.\begin{aligned} \frac{d\underline{p}}{d\underline{R}} + \frac{\underline{p}}{\underline{R}}\, m(\underline{p}) &= -\frac{\epsilon \underline{R}^2 \underline{p}^4}{\underline{D}}\, F(\underline{p}) \\ \frac{d\underline{D}}{d\underline{R}} &= -\,\underline{p}^3 \underline{R}^2 f(\underline{p}) \end{aligned}\right\} \qquad (13\text{-}65)$$

where

$$F(\underline{p}) = \frac{12\gamma_o}{\gamma_o + 1}\left[\frac{1}{\underline{p}}\left(\frac{c_o}{U}\right)^2\right]\left[\frac{G}{2(1 + g) - G}\right]$$

$$f(\underline{p}) = \frac{12\,\gamma_o^3}{\gamma_o + 1}\left[\frac{\Delta h(\underline{p})}{c_o^2\, \underline{p}^3}\right]$$

and where we have already defined

$$m(\underline{p}) = \frac{2G(1 - \rho_o/\rho_1) + 4\rho_o/\rho_1}{2(1 + g) - G}$$

with

$$\ell = 1 - \frac{d\ell n\, U}{d\ell n\, p_i}$$

$$G = 1 - \left(\frac{\rho_o\, U}{\rho_1\, c_1}\right)^2$$

The normalization of these functions has been so arranged that

$$\left.\begin{aligned} &\text{Lim } (\underline{p} \to 0)\ m(\underline{p}) = 1 \\ &\text{Lim } (\underline{p} \to 0)\ F(\underline{p}) = 3/2 \\ &\text{Lim } (\underline{p} \to 0)\ f(\underline{p}) = 1 \end{aligned}\right\} \qquad (13\text{-}66)$$

For shock waves in water, it is convenient to retain the definition of the reduced distance $\underline{R}$ but to define

$$\underline{p} = p_i/B$$

$$\underline{D} = \frac{3\kappa^3}{\pi(\kappa + 1)}\left(\frac{D}{c_o^2\, a_o^3\, \rho_o}\right) \qquad (13\text{-}67)$$

where B and κ are parameters of the Tait equation of state

$$p = \left[B\,(\rho/\rho_o)^\kappa - 1\right]$$

With these definitions, Eqs. 13-54 and 13-57 reduce to Eqs. 13-65 with the quantity γ_o replaced by the quantity κ. In this form, the normalization leading to Eqs. 13-66 is preserved.

The propagation equations can be stated in another reduced form that is particularly useful for the discussion of scaling. We have defined a

characteristic length λ by Eq. 13-27, which we write in the form

$$\lambda = (Wq'/p_o)^{1/3} \tag{13-68}$$

where W is the weight of the explosive charge and q' is the energy released by unit weight of explosive. We also define a new reduced energy variable K by

$$K = \left(\frac{a_o}{\lambda}\right)^3 \underline{D} = \frac{3\gamma_o^2}{\pi(\gamma_o + 1)} \left(\frac{D}{Wq'}\right) \tag{13-69}$$

In terms of a reduced distance $Z = R/\lambda$, the propagation equations can be written

$$\left.\begin{aligned} \frac{d\underline{p}}{dZ} + \frac{\underline{p}}{Z} m(\underline{p}) &= -\frac{\epsilon Z^2 \underline{p}^4}{K} F(\underline{p}) \\ \frac{dK}{dZ} &= -Z^2 \underline{p}^3 f(\underline{p}) \end{aligned}\right\} \tag{13-70}$$

For the shock wave in air, where all of the energy of explosion may be assumed to be dissipated in the shock wave, the initial value of K can be calculated with $D/(Wq') = 1$. For an underwater shock wave, an approximate initial value can be obtained $D/(Wq') = 1/2$ (and with γ_o replaced by k).

For numerical integration, it is convenient to let

$$\left.\begin{aligned} x &= \ln \underline{R} \\ P &= \underline{R}\,\underline{p} \\ Q &= \underline{D}/(\underline{R}\,\underline{p}) \end{aligned}\right\} \tag{13-71}$$

or

$$\left.\begin{aligned} x &= \ln Z \\ P &= Z\underline{p} \\ Q &= K/(Z\underline{p}) \end{aligned}\right\} \tag{13-72}$$

Then both Eqs. 13-65 and Eqs. 13-70 can be written

$$\frac{d\ln P}{dx} = 1 - m(\underline{p}) - \frac{P^2}{Q}\epsilon F(\underline{p}) \tag{13-73}$$

$$\frac{d\ln Q}{dx} = m(\underline{p}) - 1 + \frac{P^2}{Q}\left[\epsilon F(\underline{p}) - f(\underline{p})\right].$$

In view of Eqs. 13-66, and recalling that $\epsilon \to 2/3$ as $p \to 0$, the asymptotic form of Eqs. 13-73 is

$$\left.\begin{aligned} \frac{dP}{dx} &= -\frac{P^3}{Q} \\ \frac{dQ}{dx} &= 0 \end{aligned}\right\} \tag{13-74}$$

Their solution can be written

$$P = P_i[\ln(R/R_i)]^{-1/2}$$

$$Q = 2P_i^2$$

where R_i and P_i are constants. These results are in accord with those obtained by Kirkwood and Bethe[8] for the asymptotic nonacoustical decay of spherical waves of finite amplitude.

In terms of the reduced distance $\underline{R}$ and the reduced energy variable $\underline{D}$, the first of Eqs. 13-59 can be written

$$\frac{1}{\theta}\left(\frac{\tau_o}{c_o}\right) = \frac{2}{\underline{R}} A(\underline{p}) + \left(\frac{\epsilon \underline{R}^2 \underline{p}}{\underline{D}}\right) B(\underline{p}) \tag{13-75}$$

where

$$\left.\begin{aligned} A(\underline{p}) &= (u_1/c_o)\, a(\underline{p}) \\ B(\underline{p}) &= \left(\frac{12\gamma_o^2}{\gamma_o + 1}\right)(u_1/c_o)\, b(\underline{p}) \end{aligned}\right.$$

In terms of the reduced distance Z and the reduced energy variable K, the same equation has the form

$$\frac{\tau}{\theta} = \frac{2}{Z} A(\underline{p}) + \left(\frac{\epsilon Z^2 \underline{p}}{K}\right) B(\underline{p}) \tag{13-76}$$

where τ is the characteristic time that has been defined by Eq. 13-27. These expressions are applicable to shock waves in water if the heat capacity ratio γ_o is replaced by the exponent κ.

Kirkwood and Brinkley[3], in a calculation cited by Cole[13], have employed the propagation theory described in this paragraph to extrapolate the experimental peak pressure-distance curve, shown in Fig. 13-17, for the underwater explosion of TNT, to distances closer to the charge. The results of the calculation are shown in Fig. 13-19. The calculated peak pressures are, as is to be expected, in good agreement with the experimental values, although it is significant

that the theory is able to reproduce the experimentally observed rate of decay of peak pressure over the whole experimental range. The extrapolated value of the shock wave energy at the surface of the explosive is 561 cal/g, which is in excellent agreement with the experimental value of 580 cal/g and which constitutes a significant test of the reliability of the theory for underwater shock waves.

Kirkwood and Brinkley[3] and Makino[15] have employed the theory to carry out a complete *a priori* calculation of the shock wave parameters for the blast waves produced by TNT and Pentolite. Their calculations employed a Hugoniot curve for air that has been made obsolete by more accurate thermodynamic data and, in consequence, their results are somewhat inaccurate. The calculations have been repeated by Shear and Wright[16], using an accurate Hugoniot curve for air. Unfortunately, these authors evaluated only the peak pressure-distance curve and do not report values of the impulse. In Figs. 13-20 and 13-21, we reproduce the peak pressure-distance curves for TNT and Pentolite that were calculated by Shear and Wright[16]. For illustrative purposes, we reproduce the impulse-distance curve of Makino[15] for Penolite, Fig. 13-22, even though the experimental data shown in that figure are not the latest values and the theoretical curve is not based on the same Hugoniot curve as that employed by Shear and Wright. These curves have not been adjusted in any way by the experimental data and the good agreement between experiment and the theory indicates that the approximate propagation theory provides a description of the shock wave that is of acceptable accuracy.

13-9 SHOCK WAVE SCALING

Three different types of scaling procedures are involved in the application of theoretical or experimental determinations of shock wave parameters to the prediction of the actual effects of explosives. These involve scaling as to the size of the explosive charge, as to the ambient conditions of the undisturbed medium, and as to the nature of the explosive. Rules for the first are easily derived from the fundamental hydrodynamic equations. Rules for the second and third cannot be deduced apart from a description of the explosion. If it can be assumed that the approximate propagation theory is of adequate accuracy, the discussion is simplified since the propagation theory defines the information that is required about the explosion. In this paragraph, we assume it to

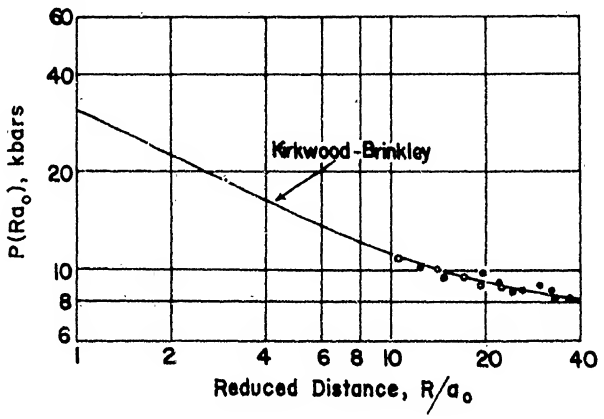

Figure 13-19. Peak Pressure-distance Curve for the Underwater Explosion of TNT as Calculated by Kirkwood and Brinkley

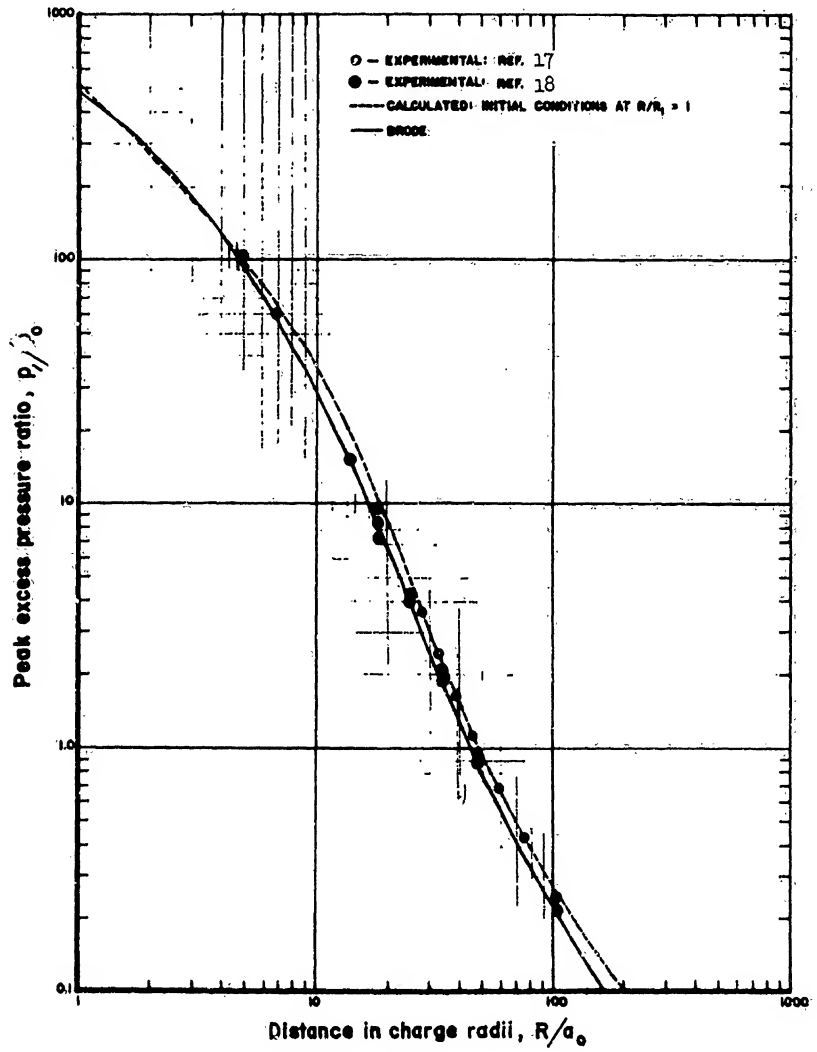

Figure 13-20. Peak Excess Pressure Ratio vs Distance in Charge Radii for TNT at a Loading Density of 1.5 g/cm³ (Experimental values of Ref. 17 are for small charges in free air. Experimental values of Ref. 18 are from the surface explosion of a 20-ton charge uncorrected for surface reflection.) (Shear and Wright)

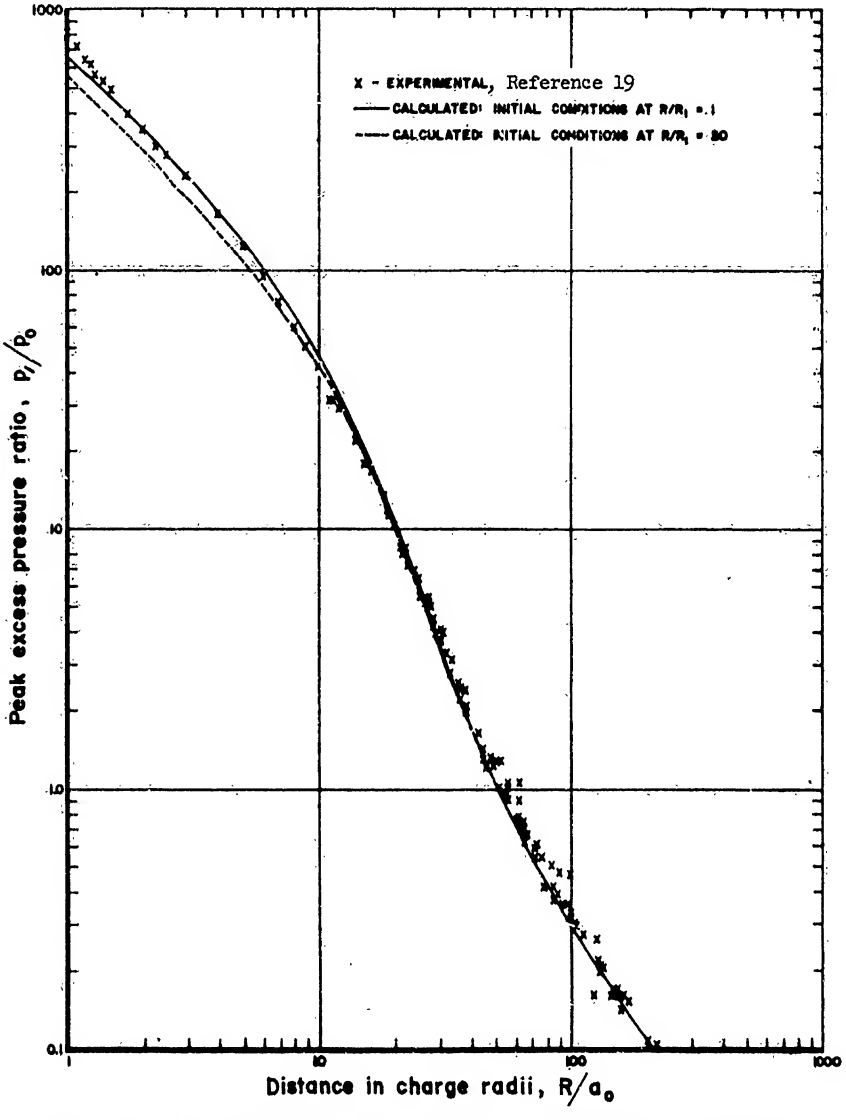

Figure 13-21. Peak Excess Pressure Ratio vs Distance in Charge Radii for Pentolite at a Loading Density of 1.65 g/cm³ (Shear and Wright)

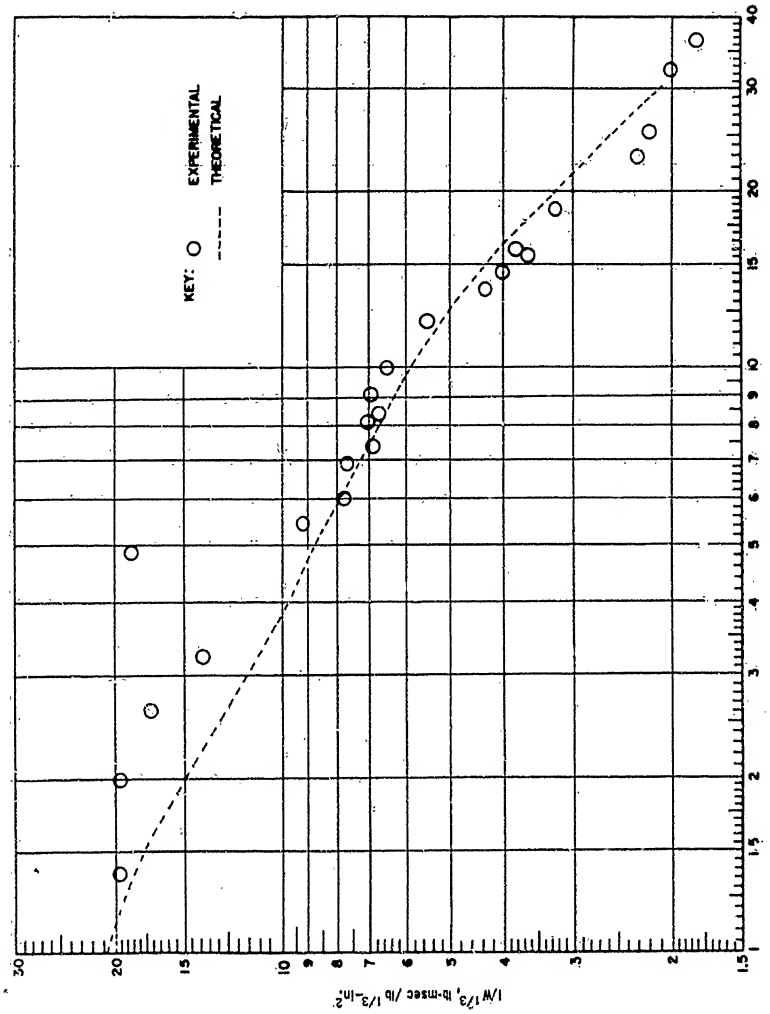

Figure 13-22. Positive Impulse-distance Curve for Pentolite (Making)

have been established that the point source model of the explosion is insufficiently accurate for shock waves generated by chemical explosives and that the approximate propagation theory described in the preceding paragraph provides a description of the shock wave that is sufficiently accurate for practical purposes.

The solution of Eqs. 13-65 and 13-75 can be represented by the expressions

$$\left.\begin{aligned} p_1 &= p_o f_1[\underline{R}\,;\underline{p}\,(a_o),\underline{D}\,(a_o);p_o,T_o] \\ D &= a_o^3 f_2[\underline{R}\,;\underline{p}\,(a_o),\underline{D}\,(a_o);p_o,T_o] \\ \theta &= a_o f_3[\underline{R}\,;\underline{p}\,(a_o),\underline{D}\,(a_o);p_o,T_o] \end{aligned}\right\} \quad (13\text{-}77)$$

and it follows that the impulse is of the form,

$$I = a_o p_o f_4[\underline{R}\,;\underline{p}\,(a_o),\underline{D}\,(a_o);p_o,T_o] \quad (13\text{-}78)$$

where f_1, f_2, etc., are functions whose form is determined by the actual solution of the equations, and where we indicate the dependence of the shock wave parameters on (1) the reduced distance $\underline{R} = R/a_o$; (2) the constants of integration, the initial reduced excess peak pressure $\underline{p}\,(a_o)$, and reduced shock wave energy $\underline{D}\,(a_o)$; and (3) the ambient conditions of the medium which we describe by the ambient pressure p_o and temperature T_o. Alternatively, the solutions of Eqs. 13-70 and 13-76 can be symbolized by

$$\left.\begin{aligned} p_1 &= p_o\, g_1[Z\,;\underline{p}(a_o);p_o,T_o] \\ D &= Wq'\, g_2[Z\,;\underline{p}(a_o);p_o,T_o] \\ \theta &= (Wq'/p_o)^{1/3}\, c_o^{-1}\; g_3 \\ &\quad [Z\,;\underline{p}(a_o);p_o,T_o] \end{aligned}\right\} \quad (13\text{-}79)$$

and it follows that the impulse is of the form

$$I = (Wq')^{1/3}\, p_o^{2/3}\, c_o^{-1}\, g_4[Z\,;\underline{p}(a_o);p_o,T_o] \quad (13\text{-}80)$$

where g_1, g_2, etc., are also functions whose form is determined by the actual solution of the equation, but where we need to indicate their dependence only on the integration constant $\underline{p}(a_o)$, since the initial value of the reduced energy variable K can be taken to be a constant.

For shock waves from explosive charges of different size but of the same explosive in the same medium at the same ambient conditions, these solutions can be symbolized by the simplified expressions

$$\left.\begin{aligned} p_1 &= F_1(R/a_o) = G(R/W^{1/3}) \\ D &= a_o^3 F_2(R/a_o) = WG(R/W^{1/3}) \\ \theta &= a_o F_3(R/a_o) = W^{1/3}\, G(R/W^{1/3}) \\ I &= a_o F_4(R/a_o) = W^{1/3}\, G(R/W^{1/3}) \end{aligned}\right\} \quad (13\text{-}81)$$

Eqs. 13-81 are a statement of the usual rules for geometrical scaling. They state that the quantities p_1, D/a_o^3, θ/a_o, and I/a_o are similar when presented as functions of the reduced distance R/a_o, or alternatively that the quantities p_1, D/W, $\theta/W^{1/3}$, and $I/W^{1/3}$ are similar when presented as functions of the distance variable $R/W^{1/3}$.

The functions on the Hugoniot curve in the integrands of Eqs. 13-70 and those defined in connection with Eq. 13-76 are functions not only of the reduced excess peak pressure $\underline{p}$, but also, in general, of the ambient state of the medium which we have designated by p_o and T_o. If the medium is a polytropic gas or if it can be described by an equation of the form of the Tait equation, as is the case for water, it is easy to show that the functions on the Hugoniot curve of Eqs. 13-70 and 13-76 are universal functions of the reduced excess peak pressure $\underline{p}$ and do not depend explicitly on the ambient state of the medium. In this event, Eqs. 13-79 and 13-80 can be simplified to

$$\left.\begin{aligned} p_1 &= p_o\, g_1[Z\,;\underline{p}\,(a_o)] \\ D &= Wq'\, g_2[Z\,;\underline{p}\,(a_o)] \\ \theta &= (Wq'/p_o)^{1/3}\, c_o^{-1}\; g_3[Z\,;\underline{p}\,(a_o)] \\ I &= (Wq')^{1/3}\, p_o^{2/3}\, c_o^{-1}\, g_4[Z\,;\underline{p}\,(a_o)] \end{aligned}\right\} \quad (13\text{-}82)$$

Since the Tait equation provides a satisfactory equation of state for water, the scaling implied by Eqs. 13-82 can evidently be employed for shock waves in water. It has been shown by actual calculation that the propagation equations for shock waves in air can, as a good approximation, employ a polytropic equation of state to evaluate the functions appearing in Eqs. 13-79 and 13-80, provi[illegible] the evaluation of the constant of integration $\underline{p}(a_o)$ is based on the

actual Hugoniot curve for air. This result, which can properly be termed a "numerical accident", means that the scaling implied by Eqs. 13-82 is a good approximation for shock waves in air.

It is a widely adopted practice to represent the shock wave parameters for some particular explosive by defining an "equivalent weight" of a reference explosive, usually TNT. It is then assumed that the shock wave parameters of the explosion of interest are those for the explosion of the equivalent weight of the reference explosive, in the same medium at the same ambient conditions. If peak pressures are shown for the explosion of interest, the equivalent weight may be evaluated by matching such pressures with those for a fixed weight of the reference explosive. The equivalent weight is properly defined by energy considerations based on Eqs. 13-82.

The description of the shock wave from an explosion by the statement that it can be represented by the shock wave from an equivalent weight of a reference explosion assumes that Eqs. 13-82 can be approximated by

$$\left.\begin{aligned} p_1 &= p_o g_1(Z) \\ D &= W q' g_2(Z) \\ \theta &= (W q'/p_o)^{1/3} c_o^{-1} g_3(Z) \\ I &= (W q')^{1/3} p_o^{2/3} c_o^{-1} g_4(Z) \end{aligned}\right\} \quad (13\text{-}83)$$

This approximation is valid if the value $p(a_o)$ is the same for both explosions or if the shock wave parameters are insensitive to this constant of integration. Because of the phenomenon of dissipation at the front, discussed in par. 13-7, it turns out that the parameters of the shock wave in air for shock waves of equal energy are quite insensitive to the value of the initial shock wave pressure. Eqs. 13-82 are thus a reasonably good approximation to Eqs. 14-82 provided the initial shock wave pressure of the explosions being compared are of the same order of magnitude. For such cases, the description of the effect of the explosion by that of an equivalent weight of a reference explosive is then a valid procedure. The procedure becomes invalid for widely different values of the initial shock wave pressure. For shock waves in water, the shock wave parameters are much more sensitive than in air to the initial shock wave pressure because of the relatively smaller dissipation of energy at the shock front. The range of utility of the concept of a weight equivalent of another explosive is correspondingly more limited.

Sachs[14] has based a procedure for scaling shock waves in air to different ambient conditions on the assumption that the blast wave parameters depend dominantly on the energy of explosion. This scaling procedure is also implied by Eqs. 13-83. However, the initial shock wave pressure $p(a_o)$ is not, even approximately, independent of the ambient conditions, and Eqs. 13-83 are not, strictly, a good approximation to Eqs. 13-82 for scaling explosions with the same explosive as to changes in the ambient conditions of the medium.

In spite of this conclusion, Sachs scaling is experimentally verified as a procedure having asymptotic validity. This asymptotic validity is the result of the insensitivity of the shock wave parameters to the initial shock wave pressure. At points close to the explosion, deviations must be anticipated from the predictions of the Sachs scaling procedure.

13-10 EXPLOSIVELY-PRODUCED SHOCK WAVES IN SOLIDS

There is an extensive literature covering the response of solids to explosive loading. Reviews have been given by Duvall[26] and by McQueen[27]. In most of the work the explosive has simply been used as a tool to provide loading of the solid at high stresses and high strain rates. The development of explosive plane wave generators has made it possible to produce plane detonation waves in solid explosives, and these plane detonation waves have been used to produce shock waves in solid samples under conditions of uniaxial strain. When the explosive is in direct contact with the solid, shock wave pressures of the order of 10^5 atm and strain rates of the order of 10^6 sec^{-1} are typically produced in a solid. The simple uniaxial strain conditions make it relatively easy to calculate the developing shock waves and flow fields, using the standard computational techniques discussed earlier and in Chapter 14, e.g., the artificial viscosity method of von Neumann and Richtmyer[10].

The detailed response of a solid to explosive loading is, of course, a function of the material

properties. In general, the constitutive equation for the material must be known, and this depends in turn on the microscopic properties of the material. For example, in a metal the stress history due to explosive loading with a given explosive will depend on such things as the stress dependence of the mobile dislocation density and mobility[28].

Thus, explosively-produced shock waves are currently serving as productive tools for investigating both macroscopic and microscopic behavior of solids undergoing rapid loading.

REFERENCES

1. W. E. Deal, Phys. of Fluids 1, 523 (1958).
2. W. Fickett and W. W. Wood, Phys. of Fluids 1, 528 (1958).
3. J. G. Kirkwood and S. R. Brinkley, Jr., OSRD Report No. 4814, 1945.
4. S. R. Brinkley, Jr. and J. G. Kirkwood, Phys. Rev. 71, 606 (1947).
5. H. L. Brode, J. Appl. Phys. 26, 766 (1955).
6. H. L. Brode, Rand Corporation Research Memorandum RM-1824, 1956.
7. H. L. Brode, Phys. of Fluids 2, 217 (1959).
8. J. G. Kirkwood and H. Bethe, OSRD Report No. 588, 1942.
9. J. Hilsenrath and C. W. Beckett, National Bureau of Standards Report No. 3991, 1955.
10. J. von Neumann and R. D. Richtmyer, J. Appl. Phys. 21, 232 (1950).
11. J. M. Richardson, A. B. Arons, and R. R. Halverson, J. Chem. Phys. 15, 785 (1947).
12. W. G. Penney and H. K. Dasgupta, British Report RC-333, 1942.
13. R. H. Cole, *Underwater Explosions*, Princeton University Press, Princeton, N.J., 1948.
14. R. G. Sachs, BRL Report No. 486, Aberdeen Proving Ground, Md., 1944.
15. R. Makino, BRL Report No. 750, Aberdeen Proving Ground, Md., 1951.
16. R. E. Shear and E. Q. Wright, BRL Memorandum Report No. 1423, Aberdeen Proving Ground, Md., 1962.
17. E. M. Fisher and J. F. Pittman, NAVORD Report 2890, U. S. Naval Ordnance Laboratory, 1953.
18. Suffield Experimental Station, Ralston, Alberta, Canada, *Canadian Observations on 20-ton TNT Explosion*, 1961, cited by Reference 16.
19. H. Goodman, BRL Report No. 1092, Aberdeen Proving Ground, Md., 1960.
20. A. J. Chabai and R. C. Bass, *Measurements on a Spherical Shock Wave in a Granite Medium*, Sandia Corporation, SC-4741 (RR).
21. H. L. Brode and B. R. Parkin, "Calculation of the Blast and Close-In Elastic Response of the Cavity Explosion in the Cowboy Program", Journal of Geophysical Research 68, No. 9, 2761-2789 (1963).
22. R. H. Bishop, "Spherical Shock Waves from Underground Explosions", *Section 4, Close-In Phenomena of Buried Explosions*, Sandia Corporation SC-4907 (RR).
23. P. C. Loken, *Calculation and Observation of the Ground Shock from Underground Detonations in Rock*, Int. Rpt., X-112, Norwegian Defense Research Establishment, Kjeller, Norway, May 1966.
24. "Prevention of and Protection against Accidental Explosion of Munitions, Fuels, and Other Hazardous Mixtures", Annals of the New York Academy of Sciences 152, Art. 1, 1-913 (1968).
25. J. T. Cherry, "Computer Calculations of Explosion-Produced Craters", Int. J. Rock Mech. Min. Sci. 4, 1-22 (1967).
26. G. E. Duvall, "Some Properties and Applications of Shock Waves", *Response of Metals to High Velocity Deformation*, P. G. Sherman and V. F. Zackay, Eds., Interscience Publishers, New York, 1961.
27. R. G. McQueen, "Laboratory Techniques for Very High Pressures and the Behavior of Metals under Dynamic Loading", *Metallurgy at High Pressures and High Temperatures*, K. A. Gschneidner, Jr., M. T. Hepworth, and N. A. D. Parlee, Eds., Gordon and Breach Science Publishers, New York, 1964.
28. J. N. Johnson, and L. M. Barker, "Dislocation Dynamics and Steady Plastic Wave Profiles in 6061-T6 Aluminum", J. Appl. Phys. 40, 11, 4321 (1969).

CHAPTER 14 COMPUTER PROGRAMS FOR EXPLOSIVE CALCULATIONS

14-1 INTRODUCTION

A great many large-scale computer programs have been developed for handling explosive calculations. This chapter presents a discussion of the types of problems solved and some of the techniques used to solve them. The relative advantages of the techniques are described and several general-purpose computer programs, or codes, are referenced.

Stress wave computations analyze the detonation of an explosive, expansion of the products, and propagation of resulting stress or shock waves into adjacent materials. Three elements are required for these calculations: (1) hydrodynamic* calculations—a procedure for following the progress of a shock or stress wave; (2) equation of state of the reacted, unreacted, and inert materials; and (3) a mathematical model of the reaction process—a procedure for following the transformation of the explosive from unreacted material to explosive products. These three elements will be described separately in the chapter, although they may be interwoven in computer programs. Computer programs are available which handle all three aspects of wave propagation; others deal only with the construction of an equation of state for the explosion products.

14-2 METHODS OF HYDRODYNAMIC CALCULATIONS

14-2.1 INTRODUCTION

A number of well-developed procedures are available for solving problems of wave propagation. Each is a technique for integrating the governing set of differential equations. These equations are the flow equations, representing conservation of mass, momentum, and energy, plus the associated equations of state and the reaction mechanisms.

The two most popular techniques are the methods of characteristics and of artificial viscosity. Several subcategories are available under both of these methods. The procedures are outlined in the discussion which follows and their appropriateness for certain types of problems is discussed. The description is not given in sufficient detail for guiding a computation, but is only intended to indicate the nature of the computation, point out inherent weaknesses of the methods, and anticipate some of the difficulties in each approach; the references contain details of the procedures.

14-2.2 METHOD OF CHARACTERISTICS

In the method of characteristics the governing differential equations are integrated along certain preferred lines, called characteristic lines, in the distance-time (x,t)-plane for one-dimensional flow. The characteristics are surfaces for problems depending on two space dimensions and the time, and hypersurfaces for three space dimensions. The characteristics derive their importance from the fact that the governing set of equations may be converted into an equivalent set, each member of which contains only derivatives in one of the characteristic directions. Hence, problems in wave propagation can be solved by integrating this second set of equations along the characteristic lines. The lines correspond to the motion of wave fronts or particles in the (x,t)-plane and therefore have physical as well as mathematical significance. Shock waves do not, in general, travel along characteristics; therefore, a separate treatment is usually required for shocks. A complete solution is produced by combining the characteristic and shock calculations.

We collect here—from Eqs. 2-113, 2-104, 2-103, and 2-108—the mass and momentum equations for one-dimensional plane flow,

* "Hydrodynamic" refers here to computations providing for the conservation of mass, momentum, and energy in the flows. Originally, these computations dealt with pressure, not stress, and so were hydrodynamic. More recently material strength has been added to many calculations, but the name has not changed.

expressed in Eulerian* variables, together with the equations that depend only on material properties but not on geometry:

$$\frac{\partial \rho}{\partial t} + u\left(\frac{\partial \rho}{\partial x}\right) + \rho\left(\frac{\partial u}{\partial x}\right) = 0 \qquad \text{(mass)} \qquad (14\text{-}1)$$

$$\frac{\partial u}{\partial t} + u\left(\frac{\partial u}{\partial x}\right) + \frac{1}{\rho}\left(\frac{\partial p}{\partial x}\right) = 0\,. \qquad \text{(momentum)} \qquad (14\text{-}2)$$

$$\frac{de}{dt} - T\left(\frac{dS}{dt}\right) - \frac{p}{\rho^2}\left(\frac{d\rho}{dt}\right) - \frac{1}{\rho}\sum_i \mu_i R_i = 0 \qquad \text{(energy)} \qquad (14\text{-}3)$$

$$\frac{dn_i}{dt} = \frac{R_i}{\rho} \qquad \text{(reaction)} \qquad (14\text{-}4)$$

$$\frac{dS}{dt} = \frac{\delta S}{dt} \text{ for shock}$$

$$= -\frac{1}{\rho T}\sum_i \mu_i R_i = 0 \text{ for reaction} \qquad \text{(entropy)} \qquad (14\text{-}5)$$

$$= 0 \text{ for isentropic flow}$$

$$p = p(\rho, e, n_1 \ldots n_i \ldots) \qquad \text{(eq. of state)} \qquad (14\text{-}6)$$

where x is the Eulerian space coordinate, u is the particle velocity, R_i is the reaction rate, μ_i is the chemical potential, n_i is the mole number, and S is entropy. The total derivatives refer to differentiation along a particle path.

As noted in par. 2-7 the three characteristic directions are

$$\frac{dx}{dt} = u + c; \quad \frac{dx}{dt} = -c \quad \frac{dx}{dt} = u \qquad (14\text{-}7)$$

where c is the isentropic sound speed. The differential equations along the first two characteristic directions are obtained from Eqs. 14-1 and 14-2 (see Courant and Friedrichs[1], p. 82)**

$$\left.\begin{aligned} dp + \rho c\, du &= + \sum_j \left(\frac{\partial p}{\partial \lambda_j}\right)_{e,\rho} d\lambda_j \\ dp - \rho c\, du &= + \sum_j \left(\frac{\partial p}{\partial \lambda_j}\right)_{e,\rho} d\lambda_j \end{aligned}\right\} \qquad (14\text{-}8)$$

Here p, the pressure, is related to ρ and c by

$$c^2 = \left(\frac{\partial p}{\partial \rho}\right)_{s, n_1 \ldots \bar{n}_i \ldots} \qquad (14\text{-}9)$$

The λ_j is a reaction coordinate, varying from 0 to 1 as the *j-th* reaction goes to completion Eqs. 14-3 through 14-6, together with the path relations, Eqs. 14-7, comprise a complete set for the solution of reactive flow problems in the absence of shocks. The shock fronts are treated using the Hugoniot jump conditions, Eqs. 2-133 and 2-134†, together with the equation of state. Two numerical procedures for integrating the equations and solving for the flow are presented: the Massau and the Hartree methods. The discussion here pertains only to points within the flow, not along the initial characteristic or on boundaries. (The reader is referred to Courant and Friedrichs[1], Chou, Karpp and Huang[2], Hartree[3], and Meyer[4] for more complete treatment.)

The Massau computational procedure (see Meyer[4]) is explained with reference to Fig. 14-1, a set of time-distance diagrams for the flow. Lines with positive slope in Fig. 14-1(A) are characteristics for which $dx/dt = u + c$; the others are for $u - c$. The solution is obtained at the intersection points of these two characteristics. Because the slopes depend on the flow variables, the grid is constructed (in the numerical order of the points) concurrently with the computation. Fig. 14-1(B) shows a typical intersection at point D of all three characteristics. An iteration scheme is adopted to define the location (x,t) and thermodynamic state (p, u, e, c) at point D. First, u and c are estimated at D; X_D and t_D are computed and the thermodynamic properties at B are found by interpolation between those at A and C. Then the characteristic equations (Eqs. 14-8), energy equation (Eq. 14-3), and reaction rate equation (14-4) are integrated, taking into account the equation of state (Eq. 14-6), to obtain improved values of the six quantities at point D. This integration is repeated until the differences

* Eulerian variables form a fixed grid in space; the flow moves past them. By contrast, a Lagrangian coordinate system moves with the particles of the flow.

**The reaction terms on the right hand side are obtained from works such as that of Stanyukovich[52].

† If the reaction is presumed to occur at the shock front, the energy equation becomes

$$e_1 = e_o + \tfrac{1}{2}(p_1 + p_o)(v_o - v_1) + Q.$$

between the quantities on two successive cycles are less than a desired limit.

One disadvantage of the Massau technique is the lengthy iteration in space and time to locate the intersection point D. The Hartree[3] technique simplifies this problem by choosing all the grid points on constant time lines as shown in Fig. 14-2. The known points are A, B, and C. The point D is on the particle path from B. Points A' and C' are found by extending the estimated characteristic lines back to the time associated with A, B, and C. After locating points D, A' and C' approximately, the iteration proceeds as in the Massau technique. The Hartree method has two distinct advantages over Massau's:

(1) Computations occur at constant times, thereby imposing a natural order on the computations.

(2) Information is obtained along particle paths. These data are directly comparable to records from embedded gages which move with the material.

Comparison computations suggest that the

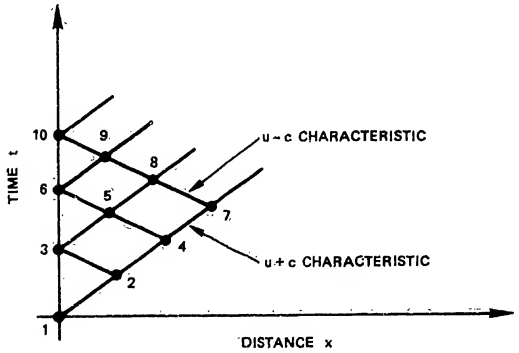

(A) GRID FOR A RIGHT-MOVING WAVE

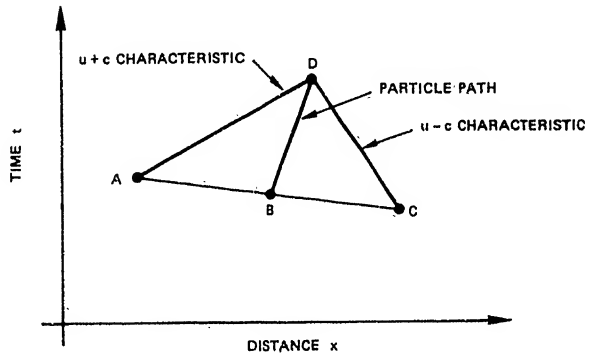

(B) GRID FOR MASSAU COMPUTATION SCHEME

Figure 14-1. Typical Characteristic Grids in the Distance- time Plane

errors from the two techniques are similar (see Chou, Karpp, and Huang[2]).

If shocks occur, their trajections in the (x,t)-plane must be constructed during the computation. Thermodynamic state variables on either side of the shock line are computed from the Hugoniot jump conditions. Normally, the starting point of each shock trajectory must be anticipated by the programmer; special provision must be made for each possible occurrence and disappearance of a shock front. If the computation begins with a strong shock, as in an impact, the shock is easily followed. If a shock develops or disappears, as in a transistion from deflagration to detonation, then the computations are much more difficult and the shock location is established by trial.

For computational purposes, a shock is assumed to be initiated at a point where two successive characteristic lines of the same sign intersect. To avoid the computational difficulties associated with the presence of shocks, approximate procedures are sometimes used to eliminate these intersections. In the NIP code of Lambourn and Hartley[5] the lower pressure characteristic is simply discarded. Another approach is to average the sound velocities of the intersecting characteristics to produce a pseudo-characteristic; this is the weak-shock analysis of Friedrichs[6], Whitham[7], and Blackstock[8].

Because of the inherent complexities introduced by the presence of shocks, a quite different technique for using the method of characteristics has been developed. In this approach, exemplified by the Stress Wave Analyzing Program (SWAP) computer program (see Barker[9,10]), all waves are represented by a series of shock waves. Hence, the Hugoniot jump conditions are used throughout the (x,t)-plane, replacing the differential equations for continuous flow, Eqs. 14-1 to 14-8. The grid used is similar to that for the Massau technique. The isentropic sound speed c is replaced by shock speed U for defining the directions of characteristics. SWAP is rare among characteristics codes, because it is designed to treat a wide variety of one-dimensional problems (radiation deposition, plate impact, and detonation). Shock trajectories are located by the program; they do not need to be pre-positioned by the programmer. The current program (SWAP-9) does not handle rate-dependent phenomena; hence reaction mechanisms are excluded, although a C-J detonation is permitted.

For simplicity, this discussion has been limited to planar one-dimensional flow. However, characteristics have been used for cylindrical and spherical one-dimensional problems (see Chou, Karpp and Huang[2]), in two-dimensional planar problems (Barthel and Strehlow[11]), in

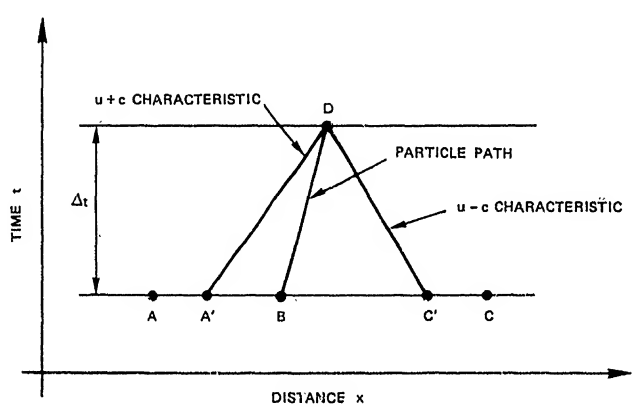

Figure 14-2. Characteristic Grid for Hartree Computation Scheme

two-dimensional axially symmetric calculations (Richardson[12]), and in three-dimensional flows (Chushkin[13]).

14-2.3 METHOD OF ARTIFICIAL VISCOSITY

One approach to calculating wave propagation is to simply put the governing differential equations in finite difference form, and integrate numerically. Computations of this type generally lead to fictitious pressure oscillations near discontinuities such as shocks. The amplitude of these oscillations may increase indefinitely with time, thus effectively terminating the computation. To reduce these oscillations and produce a stable scheme which could account for shocks, von Neumann and Richtmyer[14] suggested adding an artificial viscosity. The viscous stresses are significant only at shock fronts, and they act to smooth the shock fronts over several cells of the finite difference grid and reduce oscillations at the wave fronts. The artificial viscous stress is intrepreted physically as the difference between mechanical or external stress (which follows the Rayleigh line*) and thermodynamic stress (which lies on the equation-of-state surface) as shown in Fig. 14-3.

Many types of artificial viscosity have been introduced† but in one-dimensional problems only the linear[15] and quadratic[14] forms are in general use.

The linear and quadratic artificial stresses are given by

$$\left.\begin{aligned} q_L &= -\rho C_L c \left(\frac{\partial u}{\partial x}\right)\Delta X \\ q_Q &= +\rho C_Q^2 \left(\frac{\partial u}{\partial x}\right)^2 \Delta X^2 \end{aligned}\right\} \frac{\partial u}{\partial x} < 0 \qquad (14\text{-}10)$$

$$q_L = q_Q = 0 \qquad \frac{\partial u}{\partial x} \geqslant 0 \qquad (14\text{-}11)$$

where ρ and c are density and sound velocity, respectively; u is particle velocity; and ΔX is the grid spacing. The dimensionless coefficients, C_L and C_Q, which govern the amount of viscous dissipation, normally have values around 0.1 and 2.0, respectively. The quadratic term provides dissipation only very near the shock front but is not very effective in eliminating small and low-frequency oscillations. Since the linear form does damp out oscillations but increases rise time excessively, it is usually advantageous to use a combination of both forms. Examples of the use of each form in impact calculations are shown in Figs. 14-4(A) and (B); note that the wave front remains steep with quadratic viscosity, while the oscillations die out quickly with the linear form.

Finite difference computations have been based on Eulerian, Lagrangian, and hybrid formulations of the flow equations, and have treated one-, two-, and three-dimensional problems. For simplicity, the discussion of details of the computational procedure is restricted to one-dimensional, planar Lagrangian coordinates. For this geometry the material may be considered discretized into a large number of cells in the directions of motion and with unit cross-sectional area. The computations then treat motion through this grid or array of cells. For the most stable and accurate results, the numerical integrations are not based on the differential equations, but on integral forms of the conservation relations. These conservation relations are, in finite difference form:

$$X_1 = X_o + \overline{U}\Delta t \qquad \text{(velocity)} \qquad (14\text{-}12)$$

$$D_1 = \frac{Z}{\Delta X} \qquad \text{(mass)} \qquad (14\text{-}13)$$

$$U_1 = U_o = \frac{1}{\overline{D}}\left[\frac{\Delta(S+Q)}{\Delta X}\right]\Delta t \qquad \text{(momentum)} \qquad (14\text{-}14)$$

$$E_1 = E_o + (\overline{S}+\overline{Q})(1/D_o - 1/D_1) + \frac{1}{\overline{D}}\sum_i \mu_i R_i \qquad \text{(energy)} \qquad (14\text{-}15)$$

where Z is the constant mass per unit area of a cell; X and U are position and velocity of the cell boundaries, respectively; ΔX is the current distance between adjacent cell boundaries; D and E are density and internal energy, respectively; and S and Q are thermodynamic and artificial viscous stresses, respectively. The subscripts o and 1 refer to time t_o and $(t_o + \Delta t)$,

* The Rayleigh line is a straight line in the (P,V)- or (P,u)-planes connecting the initial state to a final shocked state on the Hugoniot curve. It is the locus of P,V or P,u states consistent with a single shock velocity.

† Forms of von Neumann and Richtmyer[14] Landshoff[15], Langley[16], and Lax and Wendroff[17] are discussed by Frank and Lazarus[18] and by A.F. Emery[19]. Richtmyer and Morton[20] describe the effective viscosity form of Godunov[21] and some of the above. Additional, more complex forms are used for two- and three-dimensional problems[22].

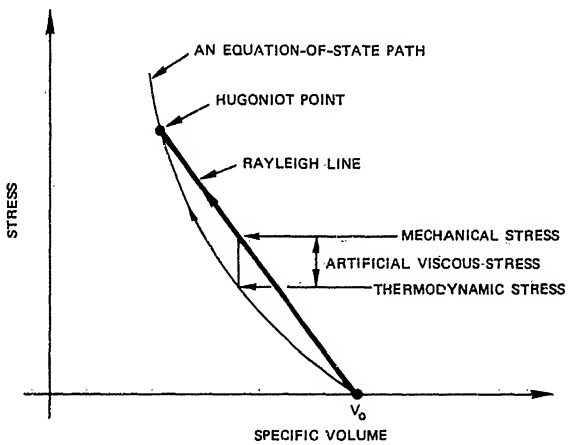

Figure 14-3. Paths Traversed by Thermodynamic and Mechanical Stress Through a Shock Front; Definition of Artificial Viscous Stress

respectively. The quantities used for $\overline{U}$, $\overline{D}$, $\overline{S}$, and $\overline{Q}$, ΔS, ΔQ, and Δt are chosen to provide an accurate representation of the conservation laws; the differences between methods lie in these choices.

The progress of computation is illustrated in the distance-time plane in Fig. 14-5 which shows coordinate points (labeled C and O) and other points (labeled H and A). The flow and thermodynamic variables are computed at some or all of these points. Calculations proceed from left to right, one coordinate (set of A, C, H points) at a time, updating X, U, D, etc., to the new time, $t_o + \Delta t$. When the right boundary is reached, computations begin again at the left for the next time increment. The simplest computation scheme is the leapfrog method of von Neumann and Richtmyer[14] in which density, energy, and stresses are computed at H points, particle velocity at coordinate C points, and X at A points. With this layout, the computed velocity equals U (the average velocity between times associated with X_o and X_1) in Eq. 14-12, the two derivatives in Eq. 14-14 [$\partial U/\partial t$ and $\partial(S + Q)/\partial X$] are centered at the same point, and the density calculation of Eq. 14-13 is exact. The stress quantities in Eq. 14-15 are averages at two H points for successive times, hence the stress at $(t_o + \Delta t)$ must be known to integrate Eq. 14-15. For equations of state in which density is linearly related to energy, Eq. 14-15 can be solved simultaneously with the equation of state. For more complex equations of state, E and D are found by iteration (see Brodie[23] for an example).

Another integration procedure is typified by the two-step Lax-Wendroff method of Richtmyer and Morton[20]. In that, all flow and thermodynamic quantities are computed for both C and H points. The H points are treated as subsidiary, so the difference equations (Eqs. 14-12 to 14-15) for those points are not required to be centered. The energy equation (Eq. 14-15) is directly integrable because $(S + Q)$-term is taken as the average of the stresses one-half time step earlier, and these are known at the time of integration. Hence, for complex equations of state, this two-step method has an advantage over the leapfrog method. Because there are twice as many hydrodynamic computations in the two-step as in the leapfrog method, the computing time is longer for simple equations of state.

Besides the leapfrog and two-step Lax-Wendroff integration schemes, there are several others which have been used successfully.

Among these are schemes due to Lax[24] (a method which uses second derivatives and only C points in Fig. 14-5), Lax and Wendroff[17,20] (one-step with second derivatives), Godunov[21], and Seaman[25] (a double-leapfrog scheme combining features from the two-step Lax-Wendroff and leapfrog methods). The double-leapfrog method allows direct integration of the energy equation, yet remains stable in the presence of boundaries and high density gradients, unlike the two-step Lax-Wendroff method. Wilkins[22] developed a two-dimensional version of the leapfrog scheme; this version is the basis of the general-purpose codes HEMP and PIPE[26]. Other practical two-dimensional schemes are those of Trulio[27], Lax[24], Rusanov[28], and Herrmann[29].

In setting up the integration schemes for a computer program, the following general rules should be followed to avoid stability problems:

(1) Centered, first order differences should be used to represent first order derivatives.

(2) The time increment must be less than $\Delta X/C$ for all cells (the Courant-Friedrichs-Lewy conditions[20]). It should be much smaller (e.g., $0.02\ \Delta X/C$) for the first few cycles, and should be allowed to increase only gradually (e.g., 20 percent) at any step.

(3) The artificial viscosity must be

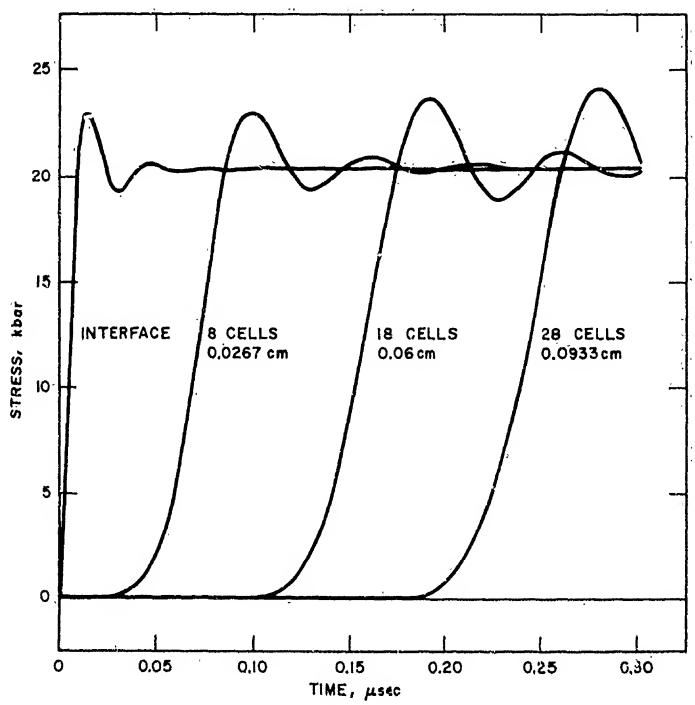

Figure 14-4(A). Stress Histories Generated in Tungsten by an Impact With C-7 Epoxy: Quadratic Artificial Viscosity Only, With a Coefficient of 4.0

sufficient to force the mechanical stress to follow the Rayleigh line, but not so large that the stress-volume path is markedly concave downward.

(4) The computation scheme in a two-step method should exhibit sufficient feedback in the computation of velocity and stress to maintain stability; i.e., the equations must be so arranged that an overestimate in velocity on one cycle will lead immediately to a stress gradient which will correct the velocity on the next cycle. The double-leapfrog scheme[25] features this feedback, and therefore is usable with high density gradients, seriously mismatched materials, and equations of state with regions of imaginary sound speed.

For each problem, a grid or cell size must be selected which is appropriate to the materials and to the detail required in the results.

Normal values of artificial viscosity will smear shock fronts over three or four cells; the cell size should be chosen with this in mind. At interfaces between materials the cell thickness, ΔX_1 and ΔX_2 should be chosen for equal crossing times, i.e.,

$$\frac{\Delta X_1}{c_1} \approx \frac{\Delta X_2}{c_2} \qquad (14\text{-}16)$$

where c is the relevant wave or shock velocity.

The artificial viscosity method is well suited to the construction of general purpose programs. Shock formation and disappearance, and shock

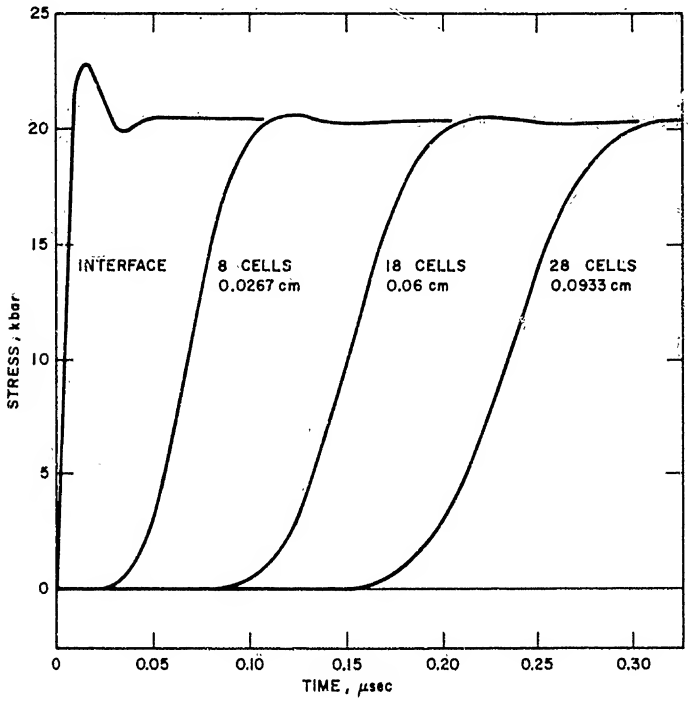

Figure 14-4(B). Stress Histories Generated in Tungsten by an Impact With C-7 Epoxy: Linear Artificial Viscosity Only, With a Coefficient of 0.5

fronts are provided for naturally in the computations, without requiring that the program or programmer know in advance the locations of these phenomena. After a stable scheme for handling the hydrodynamic integrations is produced, arbitrarily complex equations of state, strain-rate-dependence, combustion reactions, radiation deposition, heat conduction, fracturing, and other capabilities may be readily added. For this reason, many artificial viscosity computer programs can handle wave propagation initiated in three ways: by impact, radiation deposition, and detonation. The method is also readily extended to two- and three-dimensions.

The principal difficulties with the artificial viscosity method are the erosion of wave fronts, and the computer times required. The wave front erosion is serious if details of the wave front, such as time-dependent precursor decay, are of interest (see Fig. 14-6 for a comparison of precursor decay from a viscosity calculation with that obtained from an analytical calculation). For attenuating waves, the viscosity augments the rate of dissipation. Computing times are usually much longer than for characteristics codes for comparable problems. For multi-dimensional problems, the computing costs can be very high. To minimize costs, the grid is usually very coarse on these problems; then the results are also coarse.

Many computations are not suited to the Lagrangian formulation. Lagrangian is most appropriate if the motions and distortions of the material are sufficiently limited for the cells to retain their basic shape (e.g., a square cell stretched to a long rod no longer represents the material very well). During some computations the distortion is eliminated periodically by "rezoning", i.e., redefining the Lagrangian cells. When there are large distortions, however, such as in a fluid flow problem, Eulerian (nonmoving) variables are probably appropriate. The Eulerian approach is often faster than Lagrangian, but is less accurate for solids, and requires extensive programming to handle material interfaces and elastic-plastic behavior. The OIL code[30] is one example of an Eulerian program.

In an effort to combine the advantages of Eulerian and Lagrangian variables, many programs have been written with a mixture of the two types of variables. Frank and Lazarus[1,8] treated a two-dimensional problem in which the variables were Eulerian in one direction, Lagrangian in the other; this technique is appropriate for many laminar flow problems in

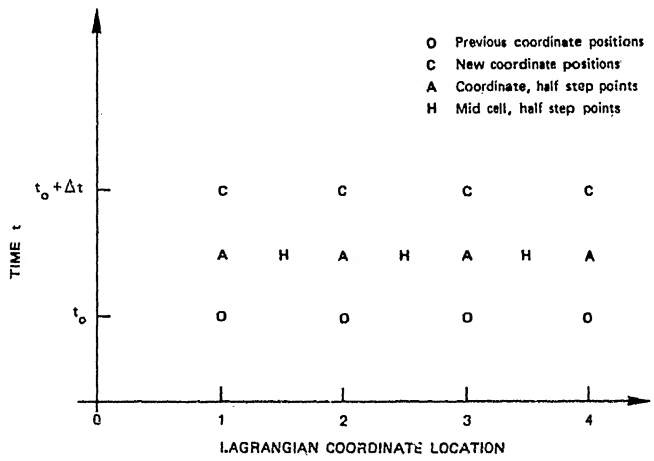

Figure 14-5. Grid for Depicting Coordinates and Time Increments

which the motion is primarily in one direction. The STRIP code was developed by Trulio[31] to handle two-dimensional spherical problems with the radial variables being Lagrangian, but variables in the θ direction being Eulerian. Noh[32] wrote the CEL code for fluid flow past solid objects; for that problem it was convenient to use Lagrangian variables for the solid, and Eulerian for the fluid. In the AFTON codes Trulio[33] attempted to follow the flow with Lagrangian or other moving variables and to rezone frequently to reduce grid distortion; the rezoning tended to erode wave fronts excessively. More recently he has developed a moving coordinate system[34] which emphasizes (with a fine mesh) the wave fronts. The moving coordinates were designed specifically for the problem of radiation deposition in a thin surface layer; at early times, very fine cells are needed in that surface layer, later the small cells are needed elsewhere and the surface layer can be represented by large cells. For the two-dimensional radiation problem it has been appropriate to use an Eulerian or PIC (discussed later) computation during the early, violent motion, and a Lagrangian grid later. Evidently, a grid system appropriate to the problem at hand can usually be found and used successfully.

The preceding artificial viscosity formulations are all of the explicit type, except for iterations associated with the equation of state. This approach, in which the variables at each time are determined by extrapolative formulas from the previous time, is by far the most common. By contrast, in implicit methods[22] the variables at each time are a function of all other variables at the new time as well as those at previous times. The flow equations are solved by "closed" numerical integration schemes. Implicit methods may be designed so as not to require short time steps like those needed for explicit methods. Therefore, if details of the wave fronts or other information requiring short time steps are not of interest, an implicit scheme may be advantageous. The solution at each time increment is produced by iteration, the first set of values being obtained from equations of "open" type, and the later values from "closed" type equations. A code based on an implicit method was derived from an integration of the flow equations along approximately characteristic lines by Muller[35] for the

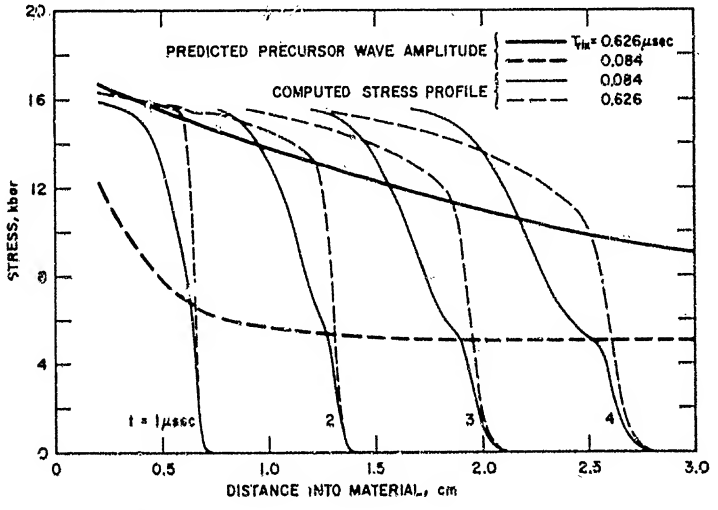

Figure 14-6. Stress Profiles Following Impact in a Material Represented by Simple Anelastic Model

computation of nonlinear acoustic flow without shocks.

14-2.4 PARTICLE-IN-CELL METHOD

The particle-in-cell (PIC) method[35,37] is a mixture of Lagrangian and Eulerian techniques, and generally requires a computer with both a large memory and high speed. It is especially useful for problems in which there are large distortions. The fluid may be visualized as discretized into small Lagrangian particles with mass, velocity, and energy, but no shape. During the computation, these cells are passed through a fixed Eulerian grid. During each time step, two types of calculations occur: a computation of pressure and energy in the Eulerian cell based on the number of particles in the cell, then a determination of the motion of each Lagrangian particle from the pressure gradients on the particle. The stability of the computations arises, according to Harlow[36], from an artificial viscosity introduced unintentionally in the averaging process. Some of the disadvantages of the method are its high computing cost[36], the jumps in pressure associated with quantized changes in density, and difficulty in handling elastic-plastic properties. Harlow presented figures from two-dimensional PIC computations of a crater formed by the explosion of a spherical charge on the surface of the ground; this exemplifies well the large distortions treated in PIC problems.

14-3 EQUATION-OF-STATE COMPUTATIONS

An equation of state is a relationship between thermodynamic variables which describe equilibrium states of a material. The relationship can be visualized as a multidimensional surface whose coordinates are the thermodynamic variables. In an equilibrium process, the material state moves across the surface; in a shock or reaction process, the end points are on the surface but intermediate points may be off the surface. An example of Hugoniot curves on equation-of-state surfaces is shown in Fig. 14-7. In the shock front the material state follows the Rayleigh line from O to A. In the subsequent reaction, the state follows the Rayleigh line from A to the C-J point.

In this paragraph, computer codes are discussed which develop the equation-of-state relationships for reaction products, given the equations of state of each constituent; i.e., these codes could be used to develop the upper curve in Fig. 14-7. The computations generally follow the analyses in Chapter 2 and Appendices A, B, and D. Examples of these codes are the STRETCH, BKW[38], RUBY[39], and TIGER[40]. The TIGER code was constructed with the aid of experience gained from the earlier two; its characteristics are described in the paragraphs which follow.

The TIGER computer code calculates the composition and thermodynamic variables associated with equilibrium states of reaction products. The user supplies the chemical formula (or formulas, for a mixture) of the condensed explosive and specifies the state points of interest. State points which are obtainable are the C-J point, the constant volume explosion point, a series of Hugoniot points, a series of points on an isentrope, or any arbitrary point for which two thermodynamic variables are specified. The program uses the analysis of Chapter 2 to satisfy the stoichiometric and chemical equilibrium conditions, and the equations of state of each constituent—combined with the Hugoniot, isentropic, and C-J conditions—to find the state. The printed output for each state point includes the constituents, the thermodynamic variables, and derivatives—such as the specific heat, the thermal expansion coefficient, and the adiabatic exponent. For each point the constituents may be represented by either a perfect gas law or a Becker-Kistiakowsky-Wilson equation of state. The resulting states are equilibrium states and, therefore, do not represent a reaction process. To be able to estimate properties of nonequilibrium states, points may be computed with the constituents either frozen to those of a prior equilibrium state, or free to assume a new equilibrium configuration. The transient state may be presumed to lie between these two states.

Within the TIGER program there is a basic thermodynamics routine (THERMO) which solves for equilibrium composition given two equation-of-state variables. Within THERMO the basic variables are the n_i (mole numbers for all gas phase constituents), η_k (parameters related to chemical potentials—one per element present), temperature T, and a pressure-related variable P_1. Because of the highly nonlinear relations

among these variables, a two-level iteration procedure was devised. To start the procedure the n_j are estimated; the n_j may be taken as equal for all constituents. This estimate serves as a basis for determining the η_k, T, and P_1 values from the stoichiometric conditions (which require conservation of each element in a reaction, see Eqs. 2-5 and 2-10) and the equation of state. With fixed η_k, T, and P_1; the n_j are determined from the chemical equilibrium conditions (Eq. 2-30) in the inner iteration loop by the Newton-Raphson method. With new values for the n_j; the η_k, T, and P_1 are determined in the outer iteration loop. The inner and outer loops are repeated in order until values computed in successive cycles meet the convergence criteria.

Hugoniot points, the C-J points, isentropes, etc., are calculated by repeated calls to THERMO. For example, to compute the C-J point, the constant volume explosion state is first computed by providing THERMO with two state variables, the energy of formation and initial specific volume. The first approximation to the C-J point is obtained by providing THERMO with T_o and V_1 where T_o is the temperature at the constant volume explosion point and

$$V_1 = V_o \left(\frac{\kappa_o}{\kappa_o + 1}\right)$$

V_o and κ_o are specific volume and adiabatic exponent, respectively, of the constant volume explosion point. The equation for V_1 is derived from the C-J condition. By use of this initial approximation, the iteration procedure finds improved values of pressure and specific volume which are used in the next call to THERMO.

In wave propagation programs the principal thermodynamic variables are pressure, internal energy, and specific volume (or density). In the artificial viscosity codes, the equation-of-state subroutines are provided with energy and density and expected to yield values of pressure.

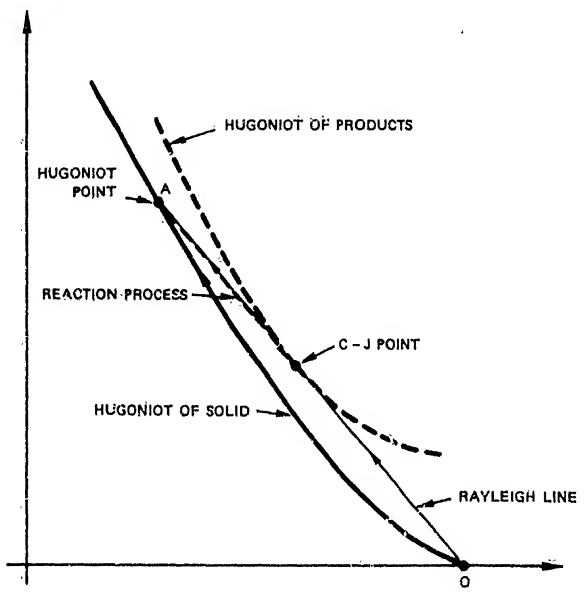

Figure 14-7. Hugoniots and Paths for Steady-state Shock and Reaction in a Homogeneous Explosive

Therefore, for use in wave propagation calculations, the most convenient equation of state is one in which pressure is an explicit function of energy and density. An example of the transformation which may be required to put an equation of state in tractable form is given by Zernow, et al.[41]. Initially, they used the equation of state to compute pressure for a grid of points in (E,ρ)-space, and then interpolated in this grid for the wave propagation calculation.

14-4 REACTION MECHANISMS FOR COMPUTATIONS

The reaction mechanism is the process by which the unreacted material burns or detonates to become the reaction product. If the reaction process is not of interest, then a very simple computational scheme can be used. However, for a study directed toward determining the induction time, initiation and fadeout of detonation, and other phenomena governed by the reaction zone; the reaction process is modeled more carefully. For a homogeneous explosive the Arrhenius equation for the reacted fraction f is used[41, 42, 43]

$$\frac{\partial f}{\partial t} = A(1-f)^{\lambda} \exp\left[-E^*/(RT)\right] \qquad (14\text{-}17)$$

where A is the frequency factor, E^* is the activation energy, R is the gas constant, and λ is the order of the reaction (either $\lambda = 0$ or 1 is used). While the material is reacting, part of the material is obeying the product equation of state and part the explosive equation of state. The products are in pressure equilibrium but not necessarily in thermal equilibrium. Possible computational treatments of this two-phase problem are given by Petrone[42] and by Zernow, et al[41].

For an inhomogeneous (condensed) explosive Warner[44] and Boyer[45] have suggested methods for describing the hot-spot initiation, burning of adjacent material, and detonation. Warner let $\lambda = 2/3$, corresponding to a process depending on surface area rather than volume, and made T the temperature of the reacted gas. Boyer[45] considered the condensed explosive to consist of two phases, one of which would detonate by an Arrhenius law (the hot-spot part), and the other would burn by a law like Warner's with $\lambda = 2/3$. Both Warner's and Boyer's methods were able to model an underdriven detonation, with subsequent build up of reaction and production of a steady C-J wave front.

Where details of the reaction process are unimportant, simple reaction mechanisms have been employed, for example, an instantaneous conversion to the C-J state of the explosive at the front of the detonation wave. This mechanism, available in TOODY[29] and in NIP[46] may be adequate when the explosive propels a flyer plate, and only the terminal velocity of the plate is of interest. For a little more fidelity to the reaction process, Wilkins[22] has suggested two computational mechanisms:

(1) The detonation is required to travel at the known detonation velocity D, and the time of arrival of the wave at each cell is calculated in advance. When the detonation time is reached at a cell, the heat of reaction is added to the internal energy of the cell over several time increments. As with the simpler mechanism previously described, the detonation wave is forced to reach the C-J velocity and achieve the C-J pressure.

(2) An alternate possibility is to set the burn fraction f to

$$f = \frac{1 - V/V_o}{1 - V_{CJ}/V_o} \qquad (14\text{-}18)$$

where V, V_{CJ}, V_o are the current, C-J, and initial specific volume, respectively. With this mechanism, the detonation wave is allowed to establish itself.

Wilkins has found that the second mechanism does not establish a steady state very rapidly. To eliminate this problem and also to allow for an overdriven wave, he recommends computing f as the maximum from the two mechanisms.

14-5 SUMMARY OF CALCULATIONS OF WAVE PROPAGATION WITH REACTIVE MECHANISMS

The preceding paragraphs have contained descriptions of the three basic elements of wave propagation in reactive flow: hydrodynamics, equations of state, and reactive mechanisms. Here, some of the ways in which these elements have been combined are mentioned, and the nature of the resulting solutions are discussed.

One example of a method of characteristics calculation with reactive flow is that of Barthel

and Strehlow[11] to study the effect of transverse waves on one-dimensional flow. Another is the study of Osborn[47] on the thermal decomposition, induction, and burning of propellants.

Unsteady aspects of detonation waves have been considered by Warner with artificial viscosity computations. The initiation, induction, and gradual build up to the steady state, instability, and fadeout were treated from a continuum mechanics viewpoint. The details of hot-spot and bubble collapse mechanisms for initiation have been studied by Mader[48,49,50] who treated the hot spot in detail.

Without treating the reaction process in detail, Wilkins[51] has performed multiple detonation computations to determine the equation of state of reactant products. The equation of state was altered and the calculations were repeated until there was satisfactory agreement between computed and measured motion of the explosive casing. The preceding references only hint at the variety of problems which have been tackled with wave propagation codes.

Before constructing a code for wave propagation calculations, it is well to decide on the nature of the results desired, whether the code must be general-purpose, etc. Some of these code characteristics have been discussed previously; three more will be mentioned here.

First, the code should be easy for the user to understand and even modify. Normally, this requirement lengthens the program and extends running time somewhat, but it saves programmer time and encourages people to use the code. If possible, the code should be modular, i.e., with separate routines for hydrodynamics, equations of state, reaction mechanisms, input and output; this simplifies code modification.

Second, an estimate of the number of computations required in a given project depends strongly on the role that the computations are to play. If the observed detonation velocity or fracture lines are pre-planned for the computation, the computed results serve mainly to correlate the experimental data. Then there may be one or two computations per experiment. On the other hand, if the computed detonation velocity is the result of hydrodynamic and reaction rate calculations, then it is properly termed a theoretical prediction. With such a code, a variation of parameters is usually helpful, this will require a large number of computations.

The third item is accuracy. With all computations there will be some errors and, in wave propagation, these tend to grow with time. One aspect of accuracy has been discussed, namely, the comparison of computed results with an exact analytical prediction. Normally, this type of error is of less interest (and smaller) than those associated with uncertainties in the parameters of the reaction process and the equations of state. In most of the foregoing computations these parameters are not known closely so that the computed results are primarily of a semi-quantitative nature, although the results may be relied upon to indicate the relative importance of input parameters. In spite of this drawback, the computations are useful for extending our understanding of the detonation process.

REFERENCES

1. R. Courant and K. O. Friedrichs, *Supersonic Flow and Shock Waves*, Interscience Publishers, Inc., New York, 1948.
2. Pei Chi Chou, Robert R. Karpp, and Shih Lien Huang, "Numerical Calculation of Blast Waves by the Method of Characteristics", Amer. Inst. of Aero. & Astro Journal, 5, No. 4, 618 (1967).
3. D. R. Hartree, *Numerical Analysis*, 2nd Edition, Oxford University Press, London, 1958.
4. R. E. Meyer, "The Method of Characteristics", *Modern Developments in Fluid Dynamics, High Speed Flow*, L. Howarth, Ed., Clarendon Press, Oxford, 1953.
5. B. O. Lambourn and J. E. Hartley, "The Calculation of the Hydrodynamic Behavior of Plane One-Dimensional Explosive/Metal Systems", *Fourth Symposium (International) on Detonation*, p. 538, Naval Ordnance Lab., October 1965.
6. K. O. Friedrichs, "Formation and Decay of Shock Waves", Commun. Pure and Appl. Math. 1, 211 (1948).
7. G. B. Whitham, "The Flow Pattern of a Supersonic Projectile", Commun. Pure and Appl. Math. 5, 301 (1952).
8. David T. Blackstock, "Connection between the Fay and Fubine Solutions for Plane Sound Waves of Finite Amplitude", Jour. of Acoustical Society of America 39, No. 6, 1019 (1966).
9. L. M. Barker, *SWAP-A Computer Program for Shock Wave Analysis*, SC-4796 (RR), Sandia Corp., Albuquerque, New Mexico, Oct. 1963.
10. L. M. Barker, *SWAP-9: An Improved Stress Wave Analyzing Program*, SC-RR-69-233, Sandia Laboratories, August 1969.
11. Harold O. Barthel and Roger A. Strehlow, "Wave Propagation in One-Dimensional Reactive Flows", The Physics of Fluids 9, No. 10, 1896 (1966).
12. D. J. Richardson, "The Solution of Two-Dimensional Hydrodynamic Equations by the Method of Characteristics", *Methods in Computational Physics*, B. Alder, S. Fernbach, and M. Rotenberg, Eds., Vol. 3 *Fundamental Methods in Hydrodynamics*, Academic Press, New York, 1964.
13. P. I. Chushkin, "Numerical Method of Characteristics for Three-dimensional Supersonic Flows", *Progress in Aeronautical Sciences*, D. Kuchemann, Ed., Pergamon Press, Oxford, Vol. 9, 1968, p.41.
14. J. von Neumann and R. D. Richtmyer, "A Method for the Numerical Calculation of Hydrodynamic Shocks", J. Appl. Phys. 21, 232 (1950).
15. R. Landshoff, *A Numerical Method for Treating Fluid Flow in the Presence of Shocks*, LASL LA-1930, Los Alamos Scientific Laboratory, New Mexico, 1955.
16. H. J. Longley, *Methods of Differencing in Eulerian Hydrodynamics*, LAMS-2379, Los Alamos Scientific Laboratory, 1960.
17. P. D. Lax, and B. Wendroff, "Systems of Conservation Laws", *Communications on Pure and Applied Mathematics*, 13, 217.
18. R. M. Frank and R. B. Lazarus, "Mixed Eulerian-Lagrangian Method", *Methods in Computational Physics—Advances in Research and Application*, Vol. III, Academic Press, New York, 1964, pp. 47-67.
19. A. F. Emery, *An Evaluation of Several Differencing Methods for Inviscid Fluid-Flow Problems*, Sandia Corporation Monograph SCL-DC-66-78, Albuquerque, New Mexico, March 1967.
20. R. D. Richtmyer and K. W. Morton, *Difference Methods for Initial-Value Problems*, 2d Ed., Interscience Publishers, New York, 1967.
21. S. K. Godunov, "Finite Difference Method for Numerical Computation of Discontinuous Solutions of the Equations of Fluid Dynamics", Mat. Sbornik 47 (89), No. 3, 271-306 (1959).
22. Mark L. Wilkins, "Calculation of Elastic Plastic Flows", *Methods in Computational Physics*, Vol. 3, Berni Alder, Ed., Academic Press, New York, 1964.
23. R. N. Brodie and J. E. Hormuth, *The PUFF 66 and P PUFF 66 Computer Programs*, Research and Technology Division, Air

REFERENCES (Cont'd)

Force Weapons Laboratory, Kirtland Air Force Base, New Mexico, May 1966.

24. P. D. Lax, "Weak Solutions of Nonlinear Hyperbolic Equations and Their Numerical Computations", Communication on Pure and Applied Mathematics 7, 159 (1954).
25. L. Seaman, *SRI PUFF 3 Computer Code for Stress Wave Propagation*, Stanford Research Institute for Air Force Weapons Laboratory under Contract F29601-70-C-0001, January 1970.
26. C. S. Godfrey, D. J. Andrews and E. T. Trigg, *Prediction Calculations for Free Field Ground Motion*, Tech. Doc. Report No. WL-TDR-64-27, Physics International for Air Force Weapons Laboratory, May 1964.
27. J. G. Trulio, *Theory and Structure of the AFTON Codes*, Tech. Rept. No. AFWL-TR-66-19, Nortronics for Air Force Weapons Laboratory, June 1966.
28. V. Rusanov, *Calculation of Interaction of Non-Steady Shock Waves with Obstacles*, National Research Council of Canada, Translation No. 1027, 1962.
29. B. J. Thorne and W. Herrman, *TOODY, A Computer Program for Calculating Problems of Motion in Two Dimensions*, Sandia Laboratories Report No. SC-RR-66-602, Albuquerque, New Mexico, July 1967. See also S. E. Benzley, L. D. Bertholf, and G. E. Clark, *TOODY 11-A*, Sandia Laboratories Report No. SC-DR-69-516, November 1969.
30. W. E. Johnson, *OIL, A Continuous Two-Dimensional Eulerian Hydrodynamic Code*, General Atomic Division of General Dynamics Corporation for Advanced Research Projects Agency under Contract DA-04-495-AMC-116(X), Jan. 1965.
31. John G. Trulio, "The STRIP Code and the Jetting of Gas Between Plates", *Methods in Computational Physics*, Vol. 3,Berni Alder, Ed., Academic Press, New York, 1964, p. 69.
32. W. F. Noh, "CEL: A Time-Dependent, Two-Space-Dimensional, Coupled Eulerian Lagrange Code", *Methods in Computational Physics*, Vol. 3, Berni Alder, Ed., Academic Press, New York, 1964, p. 117.
33. John G. Trulio, *Theory and Structure of the AFTON Codes*, Tech. Rept. No. AFWL-TR-66-19, Nortronics, A Division of Northrop Corporation, for Air Force Weapons Laboratory, June 1966.
34. John G. Trulio, William E. Carr, and John B. Muller, *PUFF Rezone Development*, Tech. Rept. No. AFWL-TR-69-50, Applied Theory, Inc., for Air Force Weapons Laboratory, October 1969.
35. George M. Muller, *Numerical Calculation of the Near Field for Spherically Symmetric Nonlinear Acoustic Flows in an Unbounded Ideal Gas*, Stanford Research Institute for Air Force Systems Command, Wright-Patterson Air Force Base, Ohio, under Contract F33615-67-C-1751, February 1970.
36. Francis H. Harlow, "The Particle-in-Cell Computing Method for Fluid Dynamics", *Methods in Computational Physics*, Vol. 3, Berni Alder, Ed., Academic Press, New York, 1964, p. 319.
37. R. Bjork, N. Brooks, and R. Papetti, *A Numerical Technique for Solution of Multidimension Hydrodynamic Problems*, Memorandum RM-2628-PR of Rand Corporation for U. S. Air Force under Contract AF 49(638)-700, Dec. 1963.
38. C. L. Mader, *Detonation Properties of Condensed Explosives Using the Becker-Kistiakowsky-Wilson Equation of State*, Los Alamos Scientific Lab Rept. LA-2900, 1963.
39. H. B. Levine and R. E. Sharples, *Operator's Manual for RUBY*, LRL Rept., UCRL-6815, 1962.
40. W. E. Wiebenson, Jr., W. H. Zwisler, L. B. Seely, and S. R. Brinkley, Jr., *TIGER Computer Program Documentation* (4 volumes), Stanford Research Institute for Ballistic Research Laboratories under Contract DA-04-200-AMC-3226(X), November 1968.
41. L. Zernow, E. A. Tkachenko, Nancy B. Brooks, R. L. Laradale, and G. E. Lewis, "Application of Two-Dimensional Computations to the Study of Sub-Critical Initiation and Fadeout in a Homogeneous

REFERENCES (Cont'd)

Explosive", *Eleventh Symposium (International) on Combustion*, 1957, p. 645.

42. Francis J. Petrone, "Validity of the Classical Detonation Wave Structure for Condensed Explosives", Phys. of Fluids 11, 1473 (1968).
43. Charles L. Mader, "One- and Two-Dimensional Flow Calculations of the Reaction Zones of Ideal Gas, Nitromethane, and Liquid TNT Detonations", *Twelfth Symposium (International) on Combustion*, The Combustion Institute, 1969, p. 701.
44. F. J. Warner, "The Initiation of Detonation in Solid Explosives", *Ninth Symposium (International) on Combustion*, The Combustion Institute, 1963.
45. M. H. Boyer, "Calculation of the Characteristics of Detonation Waves in Real Materials", J. Appl. Phys. 40, 654 (1969).
46. B. D. Lambourn and J. E. Hartley, "The Calculation of the Hydro-dynamic Behavior of Plane One-Dimensional Explosive/Metal Systems", *Fourth Symposium (International) on Detonation*, Naval Ordnance Lab., Oct. 1965, p. 538.
47. J. R. Osborn and G. M. Lehmann, "On the Interaction of a Finite Amplitude Pressure Pulse with a Combustion Region", *Eleventh Symposium (International) on Combustion*, 1967, p.739.
48. Charles L Mader, "Shock and Hot Spot Initiation of Homogeneous Explosives", Phys. of Fluids 6, No. 3, 375 (1963).
49. Charles L. Mader, "Initiation of Detonation by the Interaction of Shocks with Density Discontinuities", Phys. of Fluids 6, No. 10 (1965).
50. Charles L. Mader, "Theoretical Studies of Shock and Hot Spot Initiation of Homogeneous Explosives", *Proceedings of the International Conference on Sensitivity and Hazards of Explosives*, Chairman G. K. Adams, Explosives Res. and Dev. Establishment, Oct. 1963.
51. Mark L. Wilkins, Squier Bailey, and Bertram Halperin, "Equation of State for Detonation Products of PBX 9404 and LX04-01", *Tenth Symposium (International) on Combustion*, The Combustion Institute, 1965, p. 769.
52. K. P. Stanyukovich, *Unsteady Motion of Continuous Media*, Translated by Maurice Holt and J. George Adashko, Pergamon Press, London, 1960.

REFERENCES (Cont'd)

Explosive", *Eleventh Symposium (International) on Combustion*, 1957, p. 645.

42. Francis J. Petrone, "Validity of the Classical Detonation Wave Structure for Condensed Explosives", Phys. of Fluids 11, 1473 (1968).
43. Charles L. Mader, "One- and Two-Dimensional Flow Calculations of the Reaction Zones of Ideal Gas, Nitromethane, and Liquid TNT Detonations", *Tweifth Symposium (International) on Combustion*, The Combustion Institute, 1969, p. 701.
44. F. J. Warner, "The Initiation of Detonation in Solid Explosives", *Ninth Symposium (International) on Combustion*, The Combustion Institute, 1963.
45. M. H. Boyer, "Calculation of the Characteristics of Detonation Waves in Real Materials", J. Appl. Phys. 40, 654 (1969).
46. B. D. Lambourn and J. E. Hartley, "The Calculation of the Hydro-dynamic Behavior of Plane One-Dimensional Explosive/Metal Systems", *Fourth Symposium (International) on Detonation*, Naval Ordnance Lab., Oct. 1965, p. 538.
47. J. R. Osborn and G. M. Lehmann, "On the Interaction of a Finite Amplitude Pressure Pulse with a Combustion Region", *Eleventh Symposium (International) on Combustion*, 1967, p.739.
48. Charles L Mader, "Shock and Hot Spot Initiation of Homogeneous Explosives", Phys. of Fluids 6, No. 3, 375 (1963).
49. Charles L. Mader, "Initiation of Detonation by the Interaction of Shocks with Density Discontinuities", Phys. of Fluids 6, No. 10 (1965).
50. Charles L. Mader, "Theoretical Studies of Shock and Hot Spot Initiation of Homogeneous Explosives", *Proceedings of the International Conference on Sensitivity and Hazards of Explosives*, Chairman G. K. Adams, Explosives Res. and Dev. Establishment, Oct. 1963.
51. Mark L. Wilkins, Squier Bailey, and Bertram Halperin, "Equation of State for Detonation Products of PBX 9404 and LX04-01", *Tenth Symposium (International) on Combustion*, The Combustion Institute, 1965, p. 769.
52. K. P. Stanyukovich, *Unsteady Motion of Continuous Media*, Translated by Maurice Holt and J. George Adashko, Pergamon Press, London, 1960.

APPENDIX A EVALUATION OF THE THERMODYNAMIC PROPERTIES

A-1 INTRODUCTION

The thermodynamic relations of general validity, summarized in par. 2-4, provide the basis for the evaluation of the thermodynamic properties of a system. Since it is a characteristic of these relations that they are in differential form, it is necessary to integrate them in order to obtain expressions that can be employed for numerical work. Furthermore, since they are characteristically relations between partial derivatives, the integral expressions are most conveniently stated in terms of line integrals. Physically a line integral is a way of expressing the change in some property during a process between two different states. In the present application, one state is taken to be that of the system of interest and the other that of a reference system whose properties are known. If the reference state is properly defined, the line integrals needed to evaluate the thermodynamic properties of real systems can be made to involve only properties of the system that are determined by the equations of state of its constituent phases.

In successive paragraphs of this Appendix, expressions are deduced for the thermodynamic properties of pure condensed phases and of a gas mixture. Relations are then given for the properties of a general heterogeneous system. It is assumed that the composition of each phase is given. A procedure for the determination of the composition at equilibrium (which is the only composition uniquely determined by thermodynamic considerations alone) is given in Appendix B.

A-2 THERMODYNAMIC PROPERTIES OF PURE CONDENSED PHASES

In the interest of simplicity of notation, we dispense in this paragraph with the component index that has been employed in Chapter 2 to identify the chemical species of which the phase is composed, and with the prime-notation that has been employed to distinguish a condensed phase from a gaseous phase as in Eq. 2-11.

We assume that the molar volume of a pure condensed phase is a known function of pressure and temperature, $V = V(p,T)$. Writing the second of Eqs. 2-65 and integrating, we obtain an expression for the molar enthalpy H of the phase

$$H = H^* + \int_1^p \left[V - T\left(\frac{\partial V}{\partial T}\right)_p\right] dp \qquad \text{(A-1)}$$

where H^* is the molar enthalpy in a reference state at one atmosphere. The quantity H^* is a function of temperature only, $H^* = H^*(T)$, and the integral is along a path of constant temperature. The quantity H^* is undefined to the extent of an additive constant, the specification of which can be arbitrary. The specification of this constant is equivalent to the selection of a standard state or datum base in terms of which the enthalpy is to be measured. The standard state is defined by a reference temperature, reference pressure, and reference state (liquid or solid) of each element. We select absolute zero and one atmosphere as the reference temperature and pressure. The reference state is the phase which is stable at room temperature and atmospheric pressure. The quantity H^* may then be defined formally by

$$H^* = H_T^* - H_o^* + \Delta_f H_o^*$$

where $(H_T^* - H_o^*)$ is the enthalpy function in the reference state at temperature T measured relative to the same state at a temperature of absolute zero and $\Delta_f H_o^*$ is the molar heat of formation of the materials from the elements at absolute zero and at a pressure of one atmosphere. The quantities $(H_T^* - H_o^*)$ and $\Delta_f H_o^*$ are listed in standard tables of thermodynamic properties[1]. The standard state here defined is consistent with that employed for gas mixtures. The molar energy is obtained from the definition of the enthalpy

$$E = H^* - pV + \int_1^p \left[V - T\left(\frac{\partial V}{\partial T}\right)_p\right] dp \qquad \text{(A-2)}$$

The heat capacities can be obtained by differentiation of Eq. A-1 and the use of Eq. 2-69

$$\left.\begin{aligned} c_p &= c_p^* - \int_1^p T\left(\frac{\partial^2 V}{\partial T^2}\right)_p dp \\ c_v &= c_p^* + T\left(\frac{\partial V}{\partial T}\right)_p^2 \left(\frac{\partial p}{\partial V}\right)_T \\ &\quad - \int_1^p T\left(\frac{\partial^2 V}{\partial T^2}\right)_p dp \end{aligned}\right\} \quad \text{(A-3)}$$

where $c_p^* = dH^*/dT = c_p^*(T)$ is the molar heat capacity at constant pressure in the reference state of unit pressure. It can be obtained from standard tables of thermodynamic properties.

The chemical potential (equal for a pure phase to the molar Gibbs energy) is expressed by a relation obtained by integrating the first of Eqs. 2-67

$$\mu = \mu^* + \int_1^p V dp \quad \text{(A-4)}$$

where μ^* is the chemical potential in the reference state of unit pressure. This quantity is a function of temperature only, $\mu^* = \mu^*(T)$, that is tabulated in standard tables of thermodynamic properties. The entropy can be obtained from the relation

$$S = (H - \mu)/T \quad \text{(A-5)}$$

which results from the definition of the Gibbs free energy.

As a first approximation, the molar volume may be assumed to be a constant, independent of p and T. With this assumption

$$\left.\begin{aligned} H &= H^* + V(p - 1) \\ E &= E^* \\ c_p^* &= c_p = c_v = c_v^* \\ \mu &= \mu^* + (p - 1)V \end{aligned}\right\} \quad \text{(A-6)}$$

where E^* and c_v^* denote the molar energy and molar heat capacity at constant volume, respectively, in the reference state at 1 atm. At low pressures, it is possible to simplify these expressions still further by neglecting the product pV compared to E^* and μ^* so that $H \approx E^*$, $\mu \approx \mu^*$. This approximation is valid for systems in which a condensed phase is in equilibrium with a gas phase if $npV/RT << 1$, where n is the number of moles of condensed phase per mole of gas phase. For the explosion products of a condensed explosive for which—as we shall see, the density of the gas phase is of the order of the densities of normal solids—this approximation is not valid even if it is possible to assume that the condensed phase molar volumes are constant.

A second approximation may be obtained by assuming that the coefficient K_p of isothermal compressibility

$$K_p = -\frac{1}{V}\left(\frac{\partial V}{\partial p}\right)_T$$

and the coefficient K_T of isobaric thermal expansion

$$K_T = \frac{1}{V}\left(\frac{\partial V}{\partial T}\right)_p$$

are constants independent of temperature and pressure. With these assumptions the pressure-volume-temperature equation of state is

$$V = V_o \exp[K_T T] \exp[K_p (1 - p)]$$

where V_o is the molar volume at a temperature of absolute zero and a pressure of one atmosphere. Then Eq. A-1 becomes

$$H = H^* + (1 - TK_T)\frac{V^*}{K_p}\left\{1 - \exp\left[K_p(1-p)\right]\right\} \quad \text{(A-7)}$$

where $V^* = V_o \exp[K_T T]$, and the expression for E follows directly by adding pV to the right hand side. Differentiating Eq. A-7 with respect to temperature at constant pressure and combining the result with Eq. 2-69 gives the following expressions for the heat capacities,

$$\left.\begin{aligned} c_p &= c_p^* - \frac{TK_T^2 V^*}{K_p}\left\{1 - \exp\left[K_p(1 - p)\right]\right\} \\ c_v &= c_v^* \end{aligned}\right\} \quad \text{(A-8)}$$

For the chemical potential, we obtain the expression

$$\mu = \mu^* + \frac{V^*}{K_p}\left\{1 - \exp[K_p(1 - p)]\right\} \quad \text{(A-9)}$$

A-3 THERMODYNAMIC PROPERTIES OF A GAS MIXTURE

In this paragraph, we present expressions by means of which the thermodynamic properties of a phase consisting of a gas mixture can be evaluated in terms of certain thermal properties of its constituents and an equation of state of the mixture. A comprehensive account of these matters is given in a review by Beattie[2].

Our procedure is to define a reference state of the mixture and to calculate the change in the various thermodynamic properties of the mixture during a process that transforms the mixture in the reference state into the mixture in the actual state of interest. If the thermodynamic properties of the mixture in the reference state are known in terms of the properties of the pure constituents, the properties of the mixture in the actual state are then known. It is not necessary that the reference state have physical existence; it is only necessary that it be possible to determine its properties and to perform an accurate calculation of its change in the process resulting in the actual state of interest. The reference state may, therefore, be an hypothetical state and its definition may be arbitrary.

As reference state, we select the hypothetical perfect gas mixture of the same composition at the pressure and temperature of the actual system or, alternatively, at the volume and temperature of the actual system. The data for the mixture are taken to be the thermal properties of the pure constituents when they are in an hypothetical ideal gas state at a pressure of one atmosphere. For a constituent i in this state, we let E_i^o be the molar energy and S_i^o be the molar entropy. By definition, E_i^o and S_i^o are functions of temperature only

$$E_i^o = E_i^o(T), S_i^o = S_i^o(T)$$

From a knowledge of the energy states and structure of the molecules of gaseous substances, the methods of statistical mechanics have been employed to calculate the quantities $E_T^o - E_o^o$ and S_T^o for pure substances regarded as ideal gases at atmospheric pressure. E_T^o and S_T^o are the molar energy and entropy, respectively, at absolute temperature T; E_o^o is the molar energy at $T = 0°K$; and the statistically calculated quantity $S_T^o = 0$ when $T = 0$.

We may now complete the specification of the E_i^o and S_i^o by defining

$$\left.\begin{aligned} S_i^o &= (S_T^o)_i \\ E_i^o &= (E_T^o - E_o^o)_i + (\Delta_f H_o^o)_i \end{aligned}\right\} \quad \text{(A-10)}$$

where $(\Delta_f H_o^o)_i$ is the heat change of the hypothetical reaction at atmospheric pressure and zero absolute temperature (equal at absolute zero to the energy absorbed) that produces one mole of substance i from the elements, the elements being assumed to be in the state of aggregation that is stable at room temperature and atmospheric pressure. More briefly, $(\Delta_f H_o^o)_i$ is called the heat of formation at zero temperature. Thus, the energy E_i^o is measured relative to a datum base or standard state consisting of the elements at absolute zero. The entropy S_i^o is measured relative to the same standard state because the entropy of the elements in their standard states is zero. It may be noted that the specification of a standard state independent of the composition of the mixture is essential if changes in the composition are to be considered. The quantities $E_T^o - E_o^o$, $\Delta_f H_o^o$, and S_T^o are listed in standard tabulations of thermodynamic data.

The ideal gas pure components satisfy the equation of state

$$pV_i^o = RT \quad \text{(A-11)}$$

where R is the molar gas constant and V_i^o is the ideal molar volume of substance i. The ideal molar enthalpy of substance i at one atmosphere pressure is

$$H_i^o = E_i^o + pV_i^o = E_i^o + RT = H_i^o(T) \quad \text{(A-12)}$$

and the ideal molar Gibbs free energy (chemical potential) of substance i at a pressure of one atmosphere is

$$\mu_i^o = H_i^o - TS_i^o = E_i^o + RT - TS_i^o = \mu_i^o(T) \quad \text{(A-13)}$$

The ideal heat capacities of substance i at a pressure of one atmosphere are the functions

$$\left.\begin{aligned} c^o_{v_i} &= dE^o_i/dT = c^o_{v_i}(T) \\ c^o_{p_i} &= dH^o_i/dT = c^o_{p_i}(T) \end{aligned}\right\} \quad \text{(A-14)}$$

Evidently, $c^o_{p_i} - c^o_{v_i} = R$. From Eqs. 2-66. we have

$$d(\mu^o_i/T)/dT = -H^o_i/T^2 \quad \text{(A-15)}$$

From Eqs. 2-64 and 2-65, written for one mole of a substance i, we find that for a substance obeying Eq. A-11

$$(\partial H_i/\partial p)_T = 0;\ (\partial S_i/\partial p)_T = -R/p$$

Integrating these expressions between $p = 1$ and $p = p$ at constant temperature, we obtain the relations

$$\left.\begin{aligned} H_i(p, T; \text{ ideal}) &= H^o_i \\ S_i(p, T; \text{ ideal}) &= S^o_i - R\,\ell n\, p \end{aligned}\right\} \quad \text{(A-16)}$$

and from the definition of the chemical potential, we obtain the additional relation

$$\mu_i(p, T; \text{ ideal}) = \mu^o_i + RT\,\ell n\, p \quad \text{(A-17)}$$

We now define the hypothetical perfect gas mixture as one for which

$$\left.\begin{aligned} \mu^*_i(p, T) &= \mu^o_i + RT\,\ell n\, p + RT\,\ell n\, x_i \\ x_i &= n_i/n, \quad n = \textstyle\sum_i n_i \end{aligned}\right\} \quad \text{(A-18)}$$

for every constituent i of the mixture, where we employ an asterisk to designate a property in the reference state. All of the properties of the mixture in the reference state are deducible from Eq. A-18. In particular, since the chemical potential is the partial molar Gibbs free energy, the Gibbs free energy g^* of the perfect gas mixture described by the mole numbers $n_1, \ldots n_s$ is given by

$$g^* = \textstyle\sum_i n_i\mu^o_i + nRT\,\ell n\, p + RT\sum_i n_i\,\ell n\, x_i \quad \text{(A-19)}$$

Since, from Eqs. 2-31, $(\partial g^*/\partial p)_{T,n} = \tau^*$, the equation of state of the perfect gas mixture can be obtained by differentiation of Eq. A-19

$$p\tau^* = nRT \quad \text{(A-20)}$$

Eq. A-20 is in accord with Dalton's law of partial pressures. Dalton's law of itself does not, however, form a sufficient basis for the definition of the reference state since Eq. A-18 cannot be deduced from it without an additional assumption that introduces the concept of equilibrium between the mixture in the reference state and the pure constituents (as through appropriately defined semi-permeable membranes).

With the aid of Eq. A-20, the Helmholtz free energy f^* of the perfect gas mixture can be obtained from Eq. A-19.

$$\left.\begin{aligned} f^* &= g^* - p\tau^* = g^* - nRT \\ &= \textstyle\sum_i n_i(\mu^o_i - RT) + nRT\,\ell n\,(RT/\tau) \\ &\quad + RT\textstyle\sum_i n_i\,\ell n\, n_i \end{aligned}\right\} \quad \text{(A-21)}$$

Expressions for the other thermodynamic properties of the mixture in the reference state are easily deduced.

The equation of state of the actual mixture is an expression in one of the forms

$$p = p(\tau, T;\ n_1, \cdots n_s)$$

$$\tau = \tau(p, T;\ n_1, \cdots n_s)$$

We assume the equation of state, expressed in either way, has the property that $p\tau/(nRT) \to 1$ as $p \to 0$ or $\tau \to \infty$, and further that $p\tau/(nRT)$ differs from unity by terms of at least first order in p or $1/\tau$ at finite pressures. Thus the actual mixture becomes identical with the reference mixture in the limit as $p \to 0$ or $\tau \to \infty$.

If the equation of state is explicit in temperature and volume, we evaluate the Helmholtz free energy of the actual mixture from that of the perfect gas mixture in a reference state at the same temperature and volume by means of

$$f(\tau, T) = f^*(\tau, T) - [f^*(\tau, T) - f^*(\infty, T)] + [f(\tau, T) - f(\infty, T)]$$

where we use the fact that $f^*(\infty, T) = f(\infty, T)$. From Eqs. 2-31, $(\partial f/\partial v)_{T,n} = -p$. Therefore

$$f^*(\tau, T) - f^*(\infty, T) = -\int_\infty^\tau \left(\frac{nRT}{\tau}\right) d\tau$$

$$f(\tau, T) - f(\infty, T) = -\int_\infty^\tau p\, d\tau$$

where the integration is along a path of constant temperature and composition, and thus

$$\left.\begin{aligned} f(\tau,T) - f^*(\tau,T) &= \int_{\infty}^{\tau}\left(\frac{nRT}{\tau} - p\right)d\tau \\ f^*(\tau,T) &= \sum_i n_i(\mu_i^o - RT) \\ &\quad + RT\sum_i n_i \ln (n_iRT/\tau) \end{aligned}\right\} \quad \text{(A-22)}$$

All of the thermodynamic properties can be derived from Eq. A-22 by means of the general relations of thermodynamics. Using Eq. 2-25, we obtain

$$\left.\begin{aligned} \mu_i(\tau,T) - \mu_i^*(\tau,T) &= \int_{\infty}^{\tau}\left(\frac{RT}{\tau} - p_i\right)d\tau \\ \mu_i^*(\tau,T) &= \mu_i^o + RT \ln (n_iRT/\tau) \end{aligned}\right\} \quad \text{(A-23)}$$

where p_i has been defined as $p_i = (\partial p/\partial n_i)_{\tau,T}$. From Eq. 2-31, we have $s = -(\partial f/\partial T)_{v,n}$ and therefore

$$\left.\begin{aligned} s(\tau,T) - s^*(\tau,T) &= \int_{\infty}^{\tau}\left[\left(\frac{\partial p}{\partial T}\right)_{\tau,n} - \frac{nR}{\tau}\right]d\tau \\ s^*(\tau,T) &= \sum_i n_i S_i^o + R\sum_i n_i \ln [\tau/(n_iRT)] \end{aligned}\right\} \quad \text{(A-24)}$$

Using Eq. 2-34, we obtain the expression for the energy

$$\left.\begin{aligned} e(\tau,T) - e^*(\tau,T) &= \int_{\infty}^{\tau}\left[T\left(\frac{\partial p}{\partial T}\right)_{\tau,n} - p\right]d\tau \\ e^*(\tau,T) &= \sum_i n_i E_i^o \end{aligned}\right\} \quad \text{(A-25)}$$

and by differentiation with respect to temperature, an expression for the frozen heat capacity at constant volume

$$\left.\begin{aligned} c_{v,n}(\tau,T) - c_{v,n}^*(\tau,T) &= \int_{\infty}^{\tau} T\left(\frac{\partial^2 p}{\partial T^2}\right)_{v,n} d\tau \\ c_{v,n}^* &= \sum_i n_i c_{v_i}^o \end{aligned}\right\} \quad \text{(A-26)}$$

In Eq. 2-61, there is defined the derivative $E_i = (\partial e/\partial n_i)_{\tau,T}$. From Eq. A-25 we obtain the expression

$$E_i - E_i^o = \int_{\infty}^{\tau}\left[T\left(\frac{\partial p_i}{\partial T}\right)_{\tau} - p_i\right]d\tau \quad \text{(A-27)}$$

Eqs. A-22 to A-27 are the desired expressions for the thermodynamic properties when the equation of state is explicit in the temperature and volume. We note that the argument of the logarithm in Eqs. A-22 to A-24 is expressed in units of atmospheres.

If the equation of state of the mixture is explicit in temperature and pressure, we evaluate the Gibbs free energy of the actual mixture g from that of the perfect gas mixture g^* in a reference state at the same temperature and pressure by means of

$$g(p,T) = g^*(p,T) - [g^*(p,T) - g^*(0,T)] + [g(p,T) - g(0,T)]$$

where we use the fact that $g^*(0,T) = g(0,T)$. From Eqs. 2-31, $(\partial g/\partial p)_{T,n} = v$. Therefore

$$g^*(p,T) - g^*(0,T) = \int_0^p \left(\frac{nRT}{p}\right)dp$$

$$g(p,T) - g(0,T) = \int_0^p v\,dp$$

where the integration is along a path of constant temperature and composition, and thus

$$\left.\begin{aligned} g(p,T) - g^*(p,T) &= \int_0^p \left(v - \frac{nRT}{p}\right)dp \\ g^*(p,T) &= \sum_i n_i \mu_i^o + nRT \ln p \\ &\quad + RT\sum_i n_i \ln x_i \end{aligned}\right\} \quad \text{(A-28)}$$

All of the thermodynamic properties can be derived from Eq. A-28 by means of the general equations of thermodynamics. Using Eq. 2-25, we obtain

$$\left.\begin{aligned} \mu_i(p,T) - \mu_i^*(p,T) &= \int_0^p \left(\overline{V}_i - \frac{RT}{p}\right)dp \\ \mu_i^*(p,T) &= \mu_i^o + RT \ln p + RT \ln x_i \end{aligned}\right\} \quad \text{(A-29)}$$

From Eqs. 2-31, we have $s = -(\partial g/\partial T)_{p,n}$ and therefore

$$\left.\begin{aligned} s(p,T) - s^*(p,T) &= \int_0^p \left[\frac{nR}{p} - \left(\frac{\partial \tau}{\partial T}\right)_{p,n}\right] dp \\ s^*(p,T) &= \sum_i n_i S_i^\circ - nR \ln p - R\sum_i n_i \ln x_i \end{aligned}\right\} \quad \text{(A-30)}$$

Using Eq. 2-34, we obtain the expression for the enthalpy

$$\left.\begin{aligned} h(p,T) - h^*(p,T) &= \int_0^p \left[\tau - T\left(\frac{\partial \tau}{\partial T}\right)_{p,n}\right] dp \\ h^*(p,T) &= \sum_i n_i H_i^\circ \end{aligned}\right\} \quad \text{(A-31)}$$

and by differentiation with respect to temperature an expression for the frozen heat capacity at constant pressure

$$\left.\begin{aligned} c_{p,n}(p,T) - c^*_{p,n}(p,T) &= -\int_0^p T\left(\frac{\partial^2 \tau}{\partial T^2}\right)_{p,n} dp \\ c^*_{p,n}(p,T) &= \sum_i n_i c^\circ_{p_i} \end{aligned}\right\} \quad \text{(A-32)}$$

By differentiating Eq. A-31, we obtain an expression for the partial molal enthalpy of the *i-th* constituent,

$$\bar{H}_i - H_i^\circ = \int_0^p \left[\bar{V}_i - T\left(\frac{\partial \bar{V}_i}{\partial T}\right)_{p,n}\right] dp \quad \text{(A-33)}$$

Eqs. A-28 to A-33 are the desired expressions for the thermodynamic properties when the equation of state is explicit in pressure and temperature. We note that the argument of the logarithm in Eqs. A-28 to A-30 is expressed in units of atmospheres.

Activity coefficients f_i are sometimes defined by one of the relations

$$\left.\begin{aligned} \ln f_i &= \int_0^p \left(\bar{V}_i - \frac{RT}{p}\right) dp \\ \ln f_i &= \int_\infty^\tau \left(\frac{RT}{\tau} - p_i\right) d\tau \end{aligned}\right\} \quad \text{(A-34)}$$

the first expression being used if the equation of state is explicit in pressure and temperature, and the second if the equation of state is explicit in volume and temperature. These quantities are used as abbreviations for the definite integrals that express the effect of gas imperfection on the chemical potential.

A-4 THERMODYNAMIC PROPERTIES OF HETEROGENEOUS SYSTEMS

For the general heterogeneous system of unit weight which consists of a gas phase whose composition is described by the mole numbers n_i ($i = 1, 2, \ldots s$) together with one or more condensed phases whose sizes are described by the mole numbers n'_j, the extensive properties are the sums of the contributions of each phase. Therefore, the specific energy is given by

$$\left.\begin{aligned} e = \sum_i n_i E_i^\circ + \int_\infty^\tau \left[T\left(\frac{\partial p}{\partial T}\right)_{\tau,n} - p\right] d\tau \\ + \sum_j n'_j (H'_j - pV'_j) \end{aligned}\right\} \quad \text{(A-35)}$$

the specific enthalpy by

$$\left.\begin{aligned} h = \sum_i n_i H_i^\circ + \int_0^p \left[\tau - T\left(\frac{\partial \tau}{\partial T}\right)_{p,n}\right] dp \\ + \sum_j n'_j H'_j \end{aligned}\right\} \quad \text{(A-36)}$$

and the specific entropy by either of

$$\left.\begin{aligned} s = \sum_i n_i \left\{S_i^\circ + R \ln [(\tau/(n_i RT))]\right\} \\ + \int_\infty^\tau \left[\left(\frac{\partial p}{\partial T}\right)_{\tau,n} - \frac{nR}{\tau}\right] d\tau + \sum_j n'_j S'_j \end{aligned}\right\} \quad \text{(A-37)}$$

$$\left.\begin{aligned} s = \sum_i n_i [S_i^\circ - R \ln (pn_i/n)] \\ + \int_0^p \left[\frac{nR}{p} - \left(\frac{\partial \tau}{\partial T}\right)_{p,n}\right] dp + \sum_j n'_j S'_j \end{aligned}\right\} \quad \text{(A-38)}$$

where the properties of the condensed phases are expressed as functions of pressure and temperature in par. A-2.

The specific enthalpy is an implicitly prescribed function of the pressure, temperature, and the mole numbers n_i and n_j'. It has the partial derivatives

$$\left.\begin{aligned}
\frac{\partial h}{\partial T} &= \sum_i n_i c_{p_i}^{\circ} - \int_{\circ}^{p} T\left(\frac{\partial^2 \tau}{\partial T^2}\right) dp + \sum_j n_j' c_{p_j}' = c_{p,n} \\
\frac{\partial h}{\partial p} &= \tau - T\frac{\partial \tau}{\partial T} + \sum_j n_j'\left[V_j' - T\left(\frac{\partial V_j'}{\partial T}\right)\right] = v - T\left(\frac{\partial v}{\partial T}\right) \\
\frac{\partial h}{\partial n_i} &= H_i^{\circ} + \int_{\circ}^{p}\left[\overline{V}_i - T\left(\frac{\partial \overline{V}_i}{\partial T}\right)\right] dp = \overline{H}_i \\
\frac{\partial h}{\partial n_j'} &= H_j'
\end{aligned}\right\} \quad \text{(A-39)}$$

The specific entropy may be regarded an implicitly defined function of the same variables with the partial derivatives

$$\left.\begin{aligned}
\frac{\partial s}{\partial T} &= c_{p,n}/T \\
\frac{\partial s}{\partial p} &= -\frac{\partial v}{\partial T} \\
\frac{\partial s}{\partial n_i} &= (\overline{H}_i - \mu_i)/T \\
\frac{\partial s}{\partial n_j'} &= (H_j' - \mu_j')/T
\end{aligned}\right\} \quad \text{(A-40)}$$

The specific energy can be regarded an implicitly prescribed function of the gas phase volume τ, temperature, and the mole numbers n_i and n_j'. If we recall that $V_j' = V_j'(p,T)$, the partial derivatives of the specific energy are

$$\left.\begin{aligned}
\frac{\partial e}{\partial T} &= \sum_i n_i c_{v_i} + \int_{\infty}^{\tau} T\left(\frac{\partial^2 p}{\partial T^2}\right) d\tau + \sum_j n_j'\left[c_{v_j}' - p\left(\frac{\partial V_j'}{\partial T}\right)\right] \\
&\quad - \frac{\partial p}{\partial T}\sum_j n_j'\left[T\left(\frac{\partial V_j'}{\partial T}\right) + p\left(\frac{\partial V_j'}{\partial p}\right)\right] = c_{\tau,n} \\
\frac{\partial e}{\partial \tau} &= T\left(\frac{\partial p}{\partial T}\right) - p - \frac{\partial p}{\partial \tau}\sum_j n_j'\left[T\left(\frac{\partial V_j'}{\partial T}\right) + p\left(\frac{\partial V_j'}{\partial p}\right)\right] \\
\frac{\partial e}{\partial n_i} &= E_i^{\circ} + \int_{\infty}^{\tau}\left[T\left(\frac{\partial p_i}{\partial T}\right) - p_i\right] d\tau = E_i \\
\frac{\partial e}{\partial n_j'} &= H_j' - pV_j'
\end{aligned}\right\} \quad \text{(A-41)}$$

The specific entropy can also be regarded an implicitly prescribed function of the gas phase volume τ, temperature, and the mole numbers n_i and n_j', with the partial derivatives

$$\left.\begin{aligned}
\frac{\partial s}{\partial T} &= \frac{1}{T}\left[c_{\tau,n} + \sum_j n_j' p\left(\frac{\partial V_j'}{\partial T}\right) + \frac{\partial p}{\partial T}\sum_j n_j' p\left(\frac{\partial V_j'}{\partial p}\right) - nR\right] \\
\frac{\partial s}{\partial \tau} &= \frac{\partial p}{\partial T} - \frac{\partial p}{\partial \tau}\sum_j n_j'\left(\frac{\partial V_j'}{\partial T}\right) \\
\frac{\partial s}{\partial n_i} &= (E_i - \mu_i)/T \\
\frac{\partial s}{\partial n_j'} &= (H_j' - \mu_j')/T
\end{aligned}\right\} \quad \text{(A-42)}$$

In Eqs. A-30 to A-42, all of the variables except the variable in terms of which the differentiation is performed are to be held constant during the differentiation.

REFERENCES

1. D. R. Stull, et al., *JANAF Thermochemical Tables*, Dow Chemical Company, Contract No. AF 04(611)-7554, Sponsored by Project Principia of the Advanced Research Projects Agency, August 1965, with addenda published in August 1966 and 1967.
2. J. A. Beattie, "The Computation of the Thermodynamic Properties of Real Gases and Mixtures of Real Gases", Chem. Rev. 44, 141 (1949).

APPENDIX 3 GENERAL PROCEDURE FOR THE CALCULATION OF EQUILIBRIUM COMPOSITION

B-1 INTRODUCTION

This Appendix describes a procedure for the calculation of the equilibrium composition of a heterogeneous system consisting of a gas phase, whose composition is described by the mole numbers n_i ($i = 1, 2, \ldots, s$), in equilibrium with one or more condensed phases, each of which we have assumed to consist of a pure component and whose sizes are determined by the mole numbers n_j'. The relations for a system consisting only of a homogeneous gas phase can be obtained by setting all of the n_j' equal to zero.

The procedure is designed for calculations to be carried out on large computers. For this reason, it takes advantage of the possibilities offered for a general program by the general nature of the notation that has been employed to describe the chemistry of the system. An objective in formulating the procedure is to make the computer program as simple as possible. Simplicity of program is achieved at the expense of the number of individual arithmetic operations that need to be carried out.

If the equilibrium composition is to be evaluated in calculations performed by hand (as with a desk calculator), it is desirable to reduce the number of arithmetic operations as much as possible by a partial reduction of the problem in which the chemical nature of the system is explicitly considered. A procedure of this type for systems consisting of compounds of carbon, hydrogen, oxygen, and nitrogen is presented in Appendix C.

B-2 LINEARIZATION OF THE EQUILIBRIUM CONDITIONS

The equilibrium conditions, Eqs. 2-30, can be written for the heterogeneous system under consideration in the form,

$$\mu_i = RT \sum_{k=1}^{c} \beta_{ik} \lambda_k \quad (i = 1, \ldots, s) \qquad \text{(B-1)}$$

and

$$\mu_j' = RT\lambda_j \quad \text{if} \quad n_j' \neq 0 \quad (j = 1, \ldots, c) \qquad \text{(B-2)}$$

where μ_i and μ_j' are the chemical potentials of the *i-th* gaseous constituent and the *j-th* condensed component in the heterogeneous mixture.

The stoichiometric conditions for the same system are

$$\sum_i \beta_{ij} n_i + n_j' = q_j \quad (j = 1, \ldots, c) \qquad \text{(B-3)}$$

where for generality we have assumed that every component may exist as a condensed phase. In practice n_j' will be zero for most j and if $n_j' = 0$ for all j, the system consists of a gas phase only.

The number of Eqs. B-1 to B-3 is equal to the sum of the number of components, the number of gaseous constituents, and the number of condensed phases. This number is equal to the number of unknowns n_i, n_j', and λ_k. We will consider the temperature and either the gas phase volume τ or the pressure p to be additional unknown variables, and we will supplement Eqs. B-1 and B-2 by two independent specifications of the state of the system.

The number of equations to be solved can be reduced by the number of components by algebraic elimination of the parameters λ_k from Eqs. B-1 to B-3. If this is done, it turns out that the number of arithmetical operations in calculating the coefficients of the remaining unknowns and in the subsequent solution of the equations is just the same as the number of arithmetical operations required to solve the larger set of equations. (The two alternatives are, in fact, formally identical.) If the λ_k are eliminated algebraically, a more elaborate program is required. Therefore, there is no benefit from such a procedure if the memory capacity of the computer is adequate to accommodate the problem with the larger number of variables.

The dominant parts of Eq. B-1 are linear in the logarithms of the mole numbers n_i, while Eq. B-3 are linear in the mole numbers. Two computational procedures are possible, each resulting in an approximate set of equations linear in all of the variables. One is to expand the logarithms of the mole numbers (and the contributions from the equation of state) in

terms of the mole numbers, retaining only linear terms. The other is to expand the mole numbers (and the contributions from the equation of state) in terms of the logarithms of the mole numbers, retaining only linear terms. The second procedure employs the exponential expansion to represent the mole numbers n_i in terms of their logarithms. The first procedure leads to a computation method proposed for ideal gases by White, Johnson, and Dantzig[3] (although their method of derivation is less direct). The second procedure leads to computation methods proposed by Brinkley[1] and by Huff, Gordon, and Morrel[2]. The second procedure clearly leads to the better linearization of the problem since the exponential expansion is much more rapidly convergent than the expansion of the logarithm.

The linearized equations, in either form, constitute the basis for the solution of Eqs. B-1 to B-3 by successive approximations. The coefficients of the linearized equations are evaluated with each approximation to the equilibrium composition. An improved approximation is then obtained by solution of the set of linear equations. The process, consisting of evaluation of the coefficients of the linearized equations and their solution is continued until successive approximations to the composition are identical to some desired degree of precision. The procedure, in whatever form the equations are linearized, is an example of the well-known Newton-Raphson method for the solution of nonlinear algebraic equations.

Efficient and well standardized computer programs exist for the solution of simultaneous linear equations, and the methods employed do not need to be discussed here. This Appendix will therefore, be limited to the presentation of the necessary equations.

We elect to express the mole numbers n_i as linear functions of their logarithms, in the form

$$\left.\begin{aligned} n_i &= n_i^0 + n_i^0\Delta_i + \cdots \\ \Delta_i &= \ln n_i - \ln n_i^0 \end{aligned}\right\} \quad \text{(B-4)}$$

Eq. B-4 is just the Taylor expansion of n_i, regarded a function of $\ln n_i$ about a value n_i^0 to terms of first order in Δ_i. With this approximation, Eq. B-3 becomes

$$\sum_i \beta_{ij} n_i^0 \Delta_i + n_j' = q_j - \sum_i \beta_{ij} n_i^0 \qquad \text{(B-5)}$$

($j = 1, 2, \ldots c$). Eqs. B-5 are the linearized form of the stoichiometric conditions in which the variables are regarded to be the increments Δ_i and the mole numbers n_j' which describe the sizes of condensed phases.

B-3 RELATIONS FOR AN EQUATION OF STATE EXPLICIT IN PRESSURE AND TEMPERATURE

Now we suppose that the equation of state of the gas phase is explicit in pressure, temperature, and the mole numbers n_i. The linear Taylor expansion of the chemical potential $\mu_{i'}$ of gaseous constituent i' can be written

$$\left.\begin{aligned} \frac{\mu_{i'}}{RT} = \left(\frac{\mu_{i'}}{RT}\right)^0 &+ \sum_i \gamma_{i'i}^0 \Delta_i \\ &+ \left(\frac{p\overline{V}_{i'}}{RT}\right)^0 \Delta_p - \left(\frac{\overline{H}_i}{RT}\right)^0 \Delta_T + \cdots \end{aligned}\right\} \quad \text{(B-6)}$$

where

$$\Delta_p = \ln (p/p^0)$$

$$\Delta_T = \ln (T/T^0)$$

and where the superscript zero means that the quantities so designated are to be evaluated at the point $(p^0, T^0; n_1^0, \ldots n_s^0)$. In writing Eq. B-6, Eqs. 2-66 are employed, together with the following relation that can be derived from Eqs. A-29:

$$\gamma_{i'i} = \left(\frac{\partial(\mu_{i'}/RT)}{\partial \ln n_i}\right)_{p,T} = \delta_{i'i} - \frac{n_i}{n} + \frac{n_i}{RT}\int_0^p \frac{\partial \overline{V}_{i'}}{\partial n_i}\, dp \qquad \text{(B-7)}$$

where $\delta_{i'i}$ is the Kronecker delta ($\delta_{i'i} = 1$ when $i = i'$, and $\delta_{i'i} = 0$ when $i \neq i'$.) With the approximation expressed by Eq. B-6, the linearized form of Eqs. B-1 is

$$-\sum_i \gamma_{i'i}^0 \Delta_i + \sum_j \beta_{i'j}\lambda_j - \left(\frac{p\overline{V}_{i'}}{RT}\right)^0 \Delta_p + \left(\frac{\overline{H}_{i'}}{RT}\right)^0 \Delta_T = \left(\frac{\mu_{i'}}{RT}\right)^0 \qquad \text{(B-8)}$$

($i' = 1, 2, \ldots s$). The linear Taylor expansion of the chemical potential $\mu_{j'}'$ of Eqs. 2-67 is of the form

$$\frac{\mu_{j'}'}{RT} = \left(\frac{\mu_{j'}'}{RT}\right)^0 + \left(\frac{pV_{j'}'}{RT}\right)^0 \Delta_p - \left(\frac{H_{j'}'}{RT}\right)^0 \Delta_T + \cdots \qquad \text{(B-9)}$$

With this approximation, the linearized form of Eq. B-2 is

$$\delta_{j'j}\lambda_j - \left(\frac{pV_{j'}}{RT}\right)^{\circ}\Delta_p + \left(\frac{H_{j'}}{RT}\right)\Delta_T = \left(\frac{\mu'_{j'}}{RT}\right)^{\circ} \quad \text{(B-10)}$$

($j' = 1, 2, \ldots c$). Eqs. B-5, B-8, and B-10 are $(s + 2c)$ linear relations between the $(s + 2c + 2)$ quantities, $\lambda_1, \ldots \lambda_c; n'_1, \ldots n'_c; \Delta_1, \ldots \Delta_s; \Delta_p, \Delta_T$. They will be supplemented by two additional relations prescribing the state of the system.

If a condensed form of a particular component—e.g., j'—is excluded *a priori* on physical grounds, then n'_j is set equal to zero and the corresponding member of Eq. B-10 is eliminated.

If the solution of the equations leads to the result that $n'_j \leq 0$, then n'_j is set equal to zero and the corresponding member of Eq. B-10 is eliminated from consideration. As a formal computation device, this can be done by defining

$$\left.\begin{aligned} &\delta_{j'j} = 1 \text{ if } j = j' \text{ and } n'_j > 0 \\ &\delta_{j'j} = 0 \text{ otherwise} \end{aligned}\right\} \quad \text{(B-11)}$$

It is now necessary to express the two independent specifications of the state of the system in a manner compatible with the linearized equilibrium and stoichiometric conditions. If the pressure is specified, $p = p^{\circ}$ and

$$\Delta_p = 0 \quad \text{(B-12)}$$

Similarly, if the temperature is specified, $T = T^{\circ}$ and

$$\Delta_T = 0 \quad \text{(B-13)}$$

Suppose that it is desired to evaluate the composition and thermodynamic properties at a specified value of the enthalpy. With the aid of Eqs. A-39, the linear Taylor expansion of the enthalpy can be written in the form

$$\left.\begin{aligned} h = h^{\circ} &+ \Sigma_i n_i^{\circ}(\overline{H}_i)^{\circ}\Delta_i + \sum_{j'}(H'_{j'})^{\circ}\left[n'_{j'} - (n'_{j'})^{\circ}\right] \\ &+ \left(pV - Tp\left(\frac{\partial v}{\partial T}\right)\right)^{\circ}\Delta_p + (Tc_{p,n})^{\circ}\Delta_T + \cdots \end{aligned}\right\} \quad \text{(B-14)}$$

Rearranging, the condition imposed by specified enthalpy can be written

$$\left.\begin{aligned} &\Sigma_i n_i^{\circ}\left(\frac{\overline{H}_i}{RT}\right)^{\circ}\Delta_i + \sum_{j'}\left(\frac{H'_{j'}}{RT}\right)^{\circ}n'_{j'} \\ &\quad + \left[\frac{pv}{RT} - \frac{p}{R}\left(\frac{\partial v}{\partial T}\right)\right]^{\circ}\Delta_p + \left(\frac{c_{p,n}}{R}\right)^{\circ}\Delta_T \\ &\quad = \frac{h - h^{\circ}}{RT^{\circ}} + \sum_{j'}(n'_{j'})^{\circ}\left(\frac{H'_{j'}}{RT}\right)^{\circ} \end{aligned}\right\} \quad \text{(B-15)}$$

where h is the specified value of the specific enthalpy. The mixture volume and its fixed composition temperature derivative are to be calculated from Eq. 2-41. Proceeding similarly, the condition imposed by specified entropy can be written with the aid of Eqs. A-40 in the form

$$\left.\begin{aligned} &\Sigma_i n_i^{\circ}\left(\frac{\overline{H}_i}{RT} - \frac{\mu_i}{RT}\right)^{\circ}\Delta_i + \sum_{j'}\left(\frac{H'_{j'}}{RT} - \frac{\mu'_{j'}}{RT}\right)^{\circ}n'_{j'} \\ &\quad - \left[\frac{p}{R}\left(\frac{\partial v}{\partial T}\right)\right]^{\circ}\Delta_p + \left(\frac{c_{p,n}}{R}\right)^{\circ}\Delta_T \\ &\quad = \frac{s - s^{\circ}}{R} + \sum_{j'}(n'_{j'})^{\circ}\left(\frac{H'_{j'}}{RT} - \frac{\mu'_{j'}}{RT}\right) \end{aligned}\right\} \quad \text{(B-16)}$$

where s is the specified value of the specific entropy.

If the volume is specified but the equation of state is explicit in the pressure and temperature, the condition imposed by specified volume can be obtained in a similar manner. It is expressed by

$$\left.\begin{aligned} &\Sigma_i n_i^{\circ}\left(\frac{p\overline{V}_i}{RT}\right)^{\circ}\Delta_i + \sum_{j'}\left(\frac{pV'_{j'}}{RT}\right)^{\circ}n'_{j'} + \left[\frac{p^2}{RT}\left(\frac{\partial v}{\partial p}\right)\right]^{\circ}\Delta_p \\ &\quad + \left[\frac{p}{R}\left(\frac{\partial v}{\partial T}\right)\right]^{\circ}\Delta_T \\ &\quad = \frac{p^{\circ}(v - v^{\circ})}{RT^{\circ}} + \sum_{j'}(n'_{j'})^{\circ}\left(\frac{pV'_{j'}}{RT}\right)^{\circ} \end{aligned}\right\} \quad \text{(B17)}$$

where v is the specified specific volume of the system. The fixed composition derivatives of the mixture specific volume are to be evaluated with the aid of Eq. 2-41. If the energy is specified but the equation of state is explicit in the temperature and pressure, the condition imposed by specified energy can be obtained by making use of the relation $e = h - pv$. There is obtained

$$\left.\begin{aligned}\sum_i n_i'\left(\frac{H_i}{RT}-\frac{pV_i}{RT}\right)^{\circ}\Delta_i+\sum_i\left(\frac{H_i'}{RT}-\frac{pV_i'}{RT}\right)^{\circ}n_i'-\left[\frac{p}{RT}\left(\frac{\partial v}{\partial T}\right)+\frac{p^2}{RT}\left(\frac{\partial v}{\partial p}\right)\right]^{\circ}\Delta_\tau\\ +\left[\frac{c_{p_0}}{R}-\frac{p}{R}\left(\frac{\partial v}{\partial T}\right)\right]^{\circ}\Delta_T+\frac{e-e^{\circ}}{RT^{\circ}}+\sum_i n_i'\left(\frac{H_i'}{RT}-\frac{pV_i'}{RT}\right)^{\circ}\end{aligned}\right\} \quad \text{(B-18)}$$

Eqs. B-5, B-8, and B-10 may be employed together with any two of Eqs. B-12, B-13, and B-14 to B-18 to determine by an iterative calculation the equilibrium composition and thermodynamic properties for two independently specified state properties. Pairs that are independent are: *(p,T), (p,h), (p,s), (p,v), (p,e), (h,s), (h,v), (h,e), (s,v), (s,e), (v,T),* and *(v,e).* The coefficients of the set of linear equations selected for the particular problem can all be evaluated at an approximate determination of the composition and state of the system in terms of tabulated thermal properties of the constituents of the system and explicit equations of state for each phase by means of expressions given in Appendix A.

B-4 RELATIONS FOR AN EQUATION OF STATE EXPLICIT IN VOLUME AND TEMPERATURE

Now we suppose that the equation of state of the gas is explicit in gas phase volume, temperature, and the mole numbers n_i. We employ the same procedure as that of the previous discussion. The linearized for of Eq. B-1 becomes

$$\left.\begin{aligned}-\sum_i\gamma_{i'i}^{\circ}\Delta_i+\sum_j\beta_{i'j}\lambda_j+\left(\frac{p_{i'}\tau}{RT}\right)^{\circ}\Delta_\tau\\ +\left(\frac{E_{i'}}{RT}\right)^{\circ}\Delta_T=\left(\frac{\mu_{i'}}{RT}\right)^{\circ}\end{aligned}\right\} \quad \text{(B-19)}$$

where

$$\Delta_\tau=\ln(\tau/\tau^{\circ})$$

$$\Delta_T=\ln(T/T^{\circ})$$

and where, when the chemical potential is considered a function of volume and temperature, Eq. A-23 can be used to define the coefficient $\lambda_{i'i}$ as

$$\left.\begin{aligned}\gamma_{i'i}&=\left(\frac{\partial\ln(\mu_{i'}/RT)}{\partial\ln n_i}\right)_{\tau,T}\\ &=\delta_{i'i}-\frac{n_i}{RT}\int_{\infty}^{\tau}\frac{\partial p_{i'}}{\partial n_i}\,d\tau\end{aligned}\right\} \quad \text{(B-20)}$$

The linearized form of Eq. B-2 is

$$\left.\begin{aligned}\delta_{j'j}\lambda_j-\left(\frac{pV_{j'}'}{RT}\right)^{\circ}\left[\frac{\tau}{p}\left(\frac{\partial p}{\partial\tau}\right)\right]^{\circ}\Delta_\tau\\ +\left[\frac{H_{j'}'}{RT}-\frac{V_{j'}'}{R}\left(\frac{\partial p}{\partial T}\right)\right]^{\circ}\Delta_T\\ -\sum_i\left(\frac{n_ip_iV_{j'}'}{RT}\right)^{\circ}\Delta_i=\left(\frac{\mu_{j'}'}{RT}\right)^{\circ}\end{aligned}\right\} \quad \text{(B-21)}$$

The comments made in connection with Eq. B-10 apply to Eq. B-21. Eqs. B-5, B-19, and B-21 are the linearized form of the stoichiometric and equilibrium conditions for use when the equation of state of the gas phase is explicit in temperature and gas phase volume.

It is now necessary to express the two independent specifications of the state of the system in a manner compatible with these linearized conditions. If the temperature is specified, Eq. B-13 applies. The analogue of Eq. B-12, namely that $\Delta_\tau = 0$ for specified τ is of no interest except in a system consisting of a gas phase only. If the volume of the mixture v is specified, one may employ the condition

$$\left.\begin{aligned}\sum_j\left(\frac{pV_j'}{RT}\right)^{\circ}n_j'+\left[\frac{p\tau}{RT}\left(\frac{\partial v}{\partial\tau}\right)\right]^{\circ}\Delta_\tau+\left[\frac{p}{R}\left(\frac{\partial v}{\partial T}\right)\right]^{\circ}\Delta_T\\ +\frac{p^{\circ}}{RT^{\circ}}\sum_i\sum_j\left[n_in_{j'}\left(\frac{\partial v_j}{\partial n_i}\right)_{p_i}\right]^{\circ}\Delta_i\\ =\frac{p^{\circ}(v-v^{\circ})}{RT^{\circ}}+\sum_j(n_j')^{\circ}\left(\frac{pV_j'}{RT}\right)^{\circ}\end{aligned}\right\} \quad \text{(B-22)}$$

where v is the specified specific volume of the mixture. For a homogeneous system, Eq. B-22 yields the relation $\Delta_\tau = 0$ when $v = \tau = v^{\circ}$. Suppose that it is desired to evaluate the composition and thermodynamic properties at a specified value of the energy or entropy. If we

use the linear Taylor expansions of these functions, the conditions imposed by specified energy or entropy can be written

$$\left.\begin{aligned}\sum_i n_i^\circ \left[\frac{1}{RT}\left(\frac{\partial e}{\partial n_i}\right)\right]^\circ \Delta_i + \sum_j \left[\frac{1}{RT}\left(\frac{\partial e}{\partial n_j'}\right)\right]^\circ n_j' \\ + \left[\frac{\tau}{RT}\left(\frac{\partial e}{\partial \tau}\right)\right]^\circ \Delta_\tau + \left[\frac{1}{R}\left(\frac{\partial e}{\partial T}\right)\right]^\circ \Delta_T \\ = \frac{e - e^\circ}{RT^\circ} + \sum_j \left[\frac{1}{RT}\left(\frac{\partial e}{\partial n_j'}\right)\right]^\circ (n_j')^\circ\end{aligned}\right\} \quad \text{(B-23)}$$

$$\left.\begin{aligned}\sum_i n_i^\circ \left[\frac{1}{R}\left(\frac{\partial s}{\partial n_i}\right)\right]^\circ \Delta_i + \sum_j \left[\frac{1}{R}\left(\frac{\partial s}{\partial n_j'}\right)\right]^\circ n_j' + \left[\frac{\tau}{R}\left(\frac{\partial s}{\partial \tau}\right)\right]^\circ \Delta_\tau \\ + \left[\frac{T}{R}\left(\frac{\partial s}{\partial T}\right)\right]^\circ \Delta_T = \frac{s - s^\circ}{R} + \sum_j \left[\frac{1}{R}\left(\frac{\partial s}{\partial n_j'}\right)\right]^\circ (n_j')^\circ\end{aligned}\right\} \quad \text{(B-24)}$$

respectively. The derivatives of the energy are given explicitly by Eqs. A-41 and the derivatives of the entropy are given explicitly by Eqs. A-42.

If the pressure is specified but the equation of state of the gas phase is explicit in the gas volume and temperature, the condition imposed by specified pressure can be written

$$\left.\begin{aligned}\sum_i n_i \left(\frac{p_i T}{RT}\right)^\circ \Delta_i + \left[\frac{\tau^2}{RT}\left(\frac{\partial p}{\partial \tau}\right)\right]^\circ \Delta_\tau \\ + \left[\frac{\tau}{R}\left(\frac{\partial p}{\partial T}\right)\right]^\circ \Delta_T \\ = \frac{(p - p^\circ)\tau^\circ}{RT^\circ}\end{aligned}\right\} \quad \text{(B-25)}$$

If the enthalpy is specified but the equation of state of the gas phase is explicit in temperature and gas volume, the condition imposed by specified enthalpy can be obtained from the relation $h = e + pv$, in the form

$$\left.\begin{aligned}\sum_i n_i^\circ \left[\frac{1}{RT}\left(\frac{\partial e}{\partial n_i}\right) + \frac{pv}{RT} + \frac{p}{RT}\left(\frac{\partial v}{\partial n_i}\right)\right]^\circ \Delta_i + \sum_j \left(\frac{H_j'}{RT}\right) n_j \\ + \left[\frac{\tau}{RT}\left(\frac{\partial e}{\partial \tau}\right) + \frac{pv}{RT}\left(\frac{\partial v}{\partial \tau}\right) + \frac{vT}{RT}\left(\frac{\partial p}{\partial \tau}\right)\right]^\circ \Delta_\tau \\ + \left[\frac{1}{R}\left(\frac{\partial e}{\partial T}\right) + \frac{p}{R}\left(\frac{\partial v}{\partial T}\right) + \frac{v}{R}\left(\frac{\partial p}{\partial T}\right)\right]^\circ \Delta_T = \frac{h - h^\circ}{RT^\circ} + \sum_j (n_j')^\circ \left(\frac{H_j'}{RT}\right)^\circ\end{aligned}\right\} \quad \text{(B-26)}$$

Eqs. B-22 to B-26 reduce to expressions that are algebraically much simpler for the case of a system consisting only of a gas phase. A considerable amount of simplification is achieved if the molar volumes of the condensed phases can be considered constant.

Eqs. B-5, B-19, and B-21 can be employed together with any two of Eqs. B-13, and B-22 to B-26 to determine by an iterative calculation the equilibrium composition and thermodynamic properties for two independently specified state properties. Pairs that are independent are: *(v,T)*, *(v,e)*, *(v,s)*, *(v,p)*, *(v,h)*, *(e,s)*, *(e,p)*, *(e,h)*, *(s,p)*, *(s,h)*, *(p,T)*, and *(p,e)*. The coefficients of the set of linear equations selected for the particular problem can all be evaluated at an approximate determination of the composition and state of the system in terms of tabulated thermal properties of the constituents of the system and explicit equations of state for each phase by means of expressions given in Appendix A.

For the ideal gas equation of state and for some forms of equations of state of imperfect gas mixtures, the coefficients $\gamma_{i'i}$ are diagonal ($\gamma_{i'i} = 0$ when $i' \neq i$). If this is true for an equation of state explicit in the temperature and pressure, the gas mixture obeys the Lewis and Randall rule for imperfect gas mixture. If it is true for an equation of state explicit in the temperature and volume, the gas mixture obeys the Gibbs-Dalton rule for imperfect gas mixture. It is then possible algebraically to eliminate the linearized equilibrium conditions from the equations to be solved in the method of successive approximations and so to reduce the dimensions of the simultaneous linear equations by the number s. There is no benefit derived from this procedure unless the computer memory capacity is limited, since the reduction in the number of arithmetic operations resulting from the reduced number of equations is exactly offset by the increase in the number of arithmetic operations required to calculate the coefficients of the resulting equations.

B-5 THE INITIAL APPROXIMATION

In order to complete the description of a computation procedure employing the method of successive approximations, it is necessary to specify a way of obtaining the initial approximation. The hypothetical system

consisting of components only provides a convenient initial approximation to the composition. Our procedure requires that the n_i must not vanish (although they may be negligibly small). This requirement is met if, in the absence of a better approximation, the initial approximation is taken to be

$$n_i^o = \epsilon \text{ if } i \neq i(j)$$

where $i(j)$ is the constituent label of the j-th component and ϵ is an arbitrarily chosen constant smaller than the precision with which the equilibrium composition is to be calculated, and

$$n_i^o = q_j \text{ if } i = i(j)$$

and a condensed phase of the j-th component is excluded *a priori*, or

$$n_j^o = \epsilon \text{ if } i = i(j)$$

and a condensed phase of the j-th component may exist, in which case

$$(n_i')^o = q_j$$

If the temperature and pressure or volume of the system is not prescribed, initial estimates of these quantities can be entirely arbitrary (but preferably of the correct order of magnitude) or, when available, the results of some simplified approximate calculation.

The state for which enthalpy and pressure are specified is called the constant pressure combustion state. That for which the energy and volume are specified is called the constant volume explosion state. The latter is frequently employed to describe the reaction products of a condensed explosive.

B-6 CALCULATION OF THE EQUILIBRIUM PARTIAL DERIVATIVES

The equilibrium derivatives $(\partial v/\partial T)_p$, $(\partial v/\partial p)_T$, and c_p can be evaluated by means of Eqs. 2-48 and 2-62 if the partial derivatives of the mole numbers n_i and n_j' with respect to temperature and pressure in equilibrium mixtures are determined. Expressions for these quantities can be obtained by differentiating, with respect to temperature and with respect to pressure, Eqs. B-1 to B-3. We obtain for the change in equilibrium composition with respect to temperature at constant pressure the simultaneous linear equations

$$\left.\begin{aligned} &\sum_i \beta_{ij} n_i \left(\frac{\partial \ln n_i}{\partial T}\right) + \frac{\partial n_j'}{\partial T} = 0 \\ &-\sum_i \gamma_{ii'} \left(\frac{\partial \ln n_i}{\partial T}\right) + \sum_j \beta_{ij} \left(\frac{\partial \lambda_j}{\partial T}\right) = -\frac{\overline{H}_{i'}}{RT^2} \\ &\delta_{j'j} \left(\frac{\partial \lambda_j}{\partial T}\right) = -\frac{H_{j'}'}{RT^2} \end{aligned}\right\} \quad \text{(B-27)}$$

For the change in equilibrium composition with respect to pressure at constant temperature, we obtain the simultaneous linear equations

$$\left.\begin{aligned} &\sum_i \beta_{ij} n_i \left(\frac{\partial \ln n_i}{\partial p}\right) + \frac{\partial n_j'}{\partial p} = 0 \\ &-\sum_i \gamma_{ii'} \left(\frac{\partial \ln n_i}{\partial p}\right) + \sum_j \beta_{ij} \left(\frac{\partial \lambda_j}{\partial p}\right) = \frac{\overline{V}_{i'}}{RT} \\ &\delta_{j'j} \left(\frac{\partial \lambda_j}{\partial p}\right) = \frac{V_{j'}'}{RT} \end{aligned}\right\} \quad \text{(B-28)}$$

In Eqs. B-27 and B-28, the coefficients $\gamma_{ii'}$ are defined by Eq. B-7. The coefficients of the variables of Eqs. B-27 and B-28 are the same and their matrix is the same as the matrix of the coefficients of Eqs. B-5, B-8, and B-10. Since the triangular or inverse form of the latter is obtained in the course of the calculation of the equilibrium composition, the solution of Eqs. B-27 and B-28 can be economically performed.

The equilibrium derivatives $(\partial p/\partial T)_v$, $(\partial p/\partial v)_T$, and c_v can be evaluated by the procedure described in par. 2-4 if the partial derivatives of the mole numbers n_i and n_j' with respect to temperature and gas phase volume in equilibrium mixtures are determined. Expressions for these quantities can be obtained by differentiating, with respect to temperature and with respect to gas phase volume, Eqs. B-1 to B-3. For the derivatives with respect to temperature at constant τ, we obtain

$$\left.\begin{aligned}
&\Sigma_i \beta_{ij} n_i \left(\frac{\partial \ln n_i}{\partial T}\right) + \frac{\partial n'_j}{\partial T} = 0 \\
&-\Sigma_i \gamma_{i'i} \left(\frac{\partial \ln n_i}{\partial T}\right) + \Sigma_j \beta_{i'j} \left(\frac{\partial \lambda_j}{\partial T}\right) = -\frac{E_{i'}}{RT^2} \\
&\delta_{j'j} \left(\frac{\partial \lambda_j}{\partial T}\right) = -\frac{E'_{j'}}{RT^2} + \frac{V'_{j'}}{RT}\left(\frac{\partial p}{\partial T}\right)
\end{aligned}\right\} \quad \text{(B-29)}$$

For the derivatives with respect to τ at constant temperature, we obtain

$$\left.\begin{aligned}
&\Sigma_i \beta_{ij} n_i \left(\frac{\partial \ln n_i}{\partial \tau}\right) + \frac{\partial n'_j}{\partial \tau} = 0 \\
&-\Sigma_i \gamma_{i'i} \left(\frac{\partial \ln n_i}{\partial \tau}\right) + \Sigma_j \beta_{i'j} \left(\frac{\partial \lambda_j}{\partial \tau}\right) = -\frac{p_{i'}}{RT} \\
&\delta_{j'j} \left(\frac{\partial \lambda_j}{\partial \tau}\right) = +\frac{V'_{j'}}{RT}\left(\frac{\partial p}{\partial \tau}\right)
\end{aligned}\right\} \quad \text{(B-30)}$$

In Eqs. B-29 and B-30, the coefficients $\gamma_{i'i}$ are defined by Eq. B-20. The coefficients of the variables of Eqs. B-29 and B-30 are the same and their matrix is the same as the matrix of the coefficients of Eqs. B-5, B-19, and B-21. The triangular or inverse form of the latter is obtained in the course of the calculation of the equilibrium composition, and thus the solutions of Eqs. B-29 and B-30 can be economically obtained.

REFERENCES

1. a. S.R. Brinkley Jr., J. Chem. Phys. 15, 107 (1947).
   b. *High Speed Aerodynamics and Jet Propulsion*, Princeton Univ. Press, Princeton, 1956, Vol. II, pp. 64-97.
   c. *Proc. Conf. on Kinetics, Equilibrium and Performance of High Temperature Systems*, Butterworth's, London, 1960, pp. 74-81.
2. V. N. Huff, S. Gordon, and V. E. Morrell, National Advisory Committee for Aeronautics Report 1037, 1951.
3. W. B. White, S. M. Johnson and G. B. Dantzig, J. Chem. Phys. 28, 751 (1958).

APPENDIX C METHOD FOR THE DESK CALCULATION OF EQUILIBRIUM COMPOSITION OF SYSTEMS CONTAINING COMPOUNDS OF CARBON, HYDROGEN, OXYGEN, AND NITROGEN

C-1 INTRODUCTION

In this Appendix, we outline a simple iterative procedure for the calculation of the equilibrium composition of systems containing compounds of carbon, hydrogen, oxygen, and nitrogen. The procedure is designed for hand computations. It is now well adapted to calculations on computers since convergence is not guaranteed for all possible combinations. This is not an important characteristic for hand calculations since the computist can exercise judgment to force convergence by adjusting the approximate solution employed as the basis for each iterative step.

We assume that the calculation is to be performed with independent variables, temperature and pressure, when an equation of state is explicit in temperature and pressure; or with independent variables, temperature and gas volume, when the equation of state is explicit in these variables. If the state of the system is specified in another way, it is best—in using these methods—to perform the calculation at several appropriate values of the independent variables and to interpolate in the resulting table of the thermodynamic properties with respect to the property or properties that are specified.

The procedure described in this Appendix does not lead to an exact calculation of the equilibrium derivatives, such as the heat capacity. If these quantities are required, they must be evaluated either by the exact methods described in Appendix B, using the composition calculated by the method of this Appendix C, or by numerical differentiation in a table of the appropriate property prepared by performing the calculations at several values of the independent variables.

The chemical species considered in this Appendix, together with the label assigned to each species, are listed

Species	C(s)	CO	CO_2	H_2	H_2O	N_2
i or j	1	2	3	4	5	6
Species	O_2	O	OH	H	NO	N
i or j	7	8	9	10	11	12

Elemental carbon, if present, is assumed to be solid.

We define a quantity φ_i for each constituent by the following scheme:

$$\varphi_1 = \mu_1'/(RT) \qquad \text{(C-1)}$$

where μ_1' is the chemical potential of solid carbon, to be evaluated by Eq. A-4, and

$$\varphi_i = \mu_i/(RT) - \ell n\, n_i,\ i = 2, 3, \ldots 12 \qquad \text{(C-2)}$$

where μ_i is the chemical potential of the i-th gaseous constituent, φ_i is the same quantity less the leading concentration term, and n_i is the number of moles of the i-th constituent in a unit weight of mixture. The quantity μ_i is to be evaluated with the aid of Eq. A-29 if the equation of state is explicit in temperature and pressure, or with the aid of Eq. A-23 if the equation of state is explicit in temperature and gas phase volume. We define equilibrium constant k_i for the i-th species by the relation

$$\log_{10} k_i = 0.43429(\Sigma_j \beta_{ij}\varphi_j - \varphi_i) \qquad \text{(C-3)}$$

Tables of the coefficients β_{ij} are given in tables which follow.

The method is based on the fact that, with one exception receiving special treatment, the k_i as calculated by Eq. C-3 for the particular values of the β_{ij} employed here are all much less than unity at the pressures of interest in the description of the explosion products of condensed explosives.

Generally, solid carbon is not produced in systems containing more oxygen than required for complete oxidation of the carbon and hydrogen. Usually, it is necessary to determine the equilibrium composition on the assumption that solid carbon is present. If this calculation results in a negative amount of carbon, the calculation is then repeated with the knowledge that solid carbon is absent.

We denote by q_C, q_H, q_O, q_N the number of gram atoms of carbon, hydrogen, oxygen, and nitrogen, respectively, that are present in one gram of mixture. We affix a superscript zero to

the symbol n_i to denote that the symbol so designated is an approximation to the composition of the system, and to the symbol k_i to denote that the equilibrium constant so designated is to be calculated with the approximation $n_2^0, \ldots n_{12}^0$ to the composition of the system.

C-2 SYSTEMS WITH SOLID CARBON

The equilibrium constants k_i are calculated with the aid of the following table of the β_{ij} for each value of i for which entries are given:

β_{ij}		C	CO	H_2	N_2
	j =	1	2	4	6
	i				
CO_2	3	-1	2	0	0
H_2O	5	-1	1	1	0
O_2	7	-2	2	0	0
O	7	-1	1	0	0
OH	9	-1	1	1/2	0
H	10	0	0	1/2	0
NO	11	-1	1	0	
N	12	0	0	0	

Steps in the calculation are:

(1) n_2, n_4, and n_6 are calculated from the conservation relationships for oxygen, hydrogen, and nitrogen atoms:

$$\left.\begin{aligned} n_2 &= q_O - 2n_3^0 - n_5^0 - 2n_7^0 - n_8^0 - n_9^0 - n_{11}^0 \\ n_4 &= \tfrac{1}{2}q_H - n_5^0 - \tfrac{1}{2}n_9^0 - \tfrac{1}{2}n_{10}^0 \\ n_6 &= \tfrac{1}{2}q_N - \tfrac{1}{2}n_{11}^0 - \tfrac{1}{2}n_{12}^0 \end{aligned}\right\} \text{(C-4)}$$

Initially, all of the n_j^0 in these relationships can be taken to be zero.

(2) The remaining mole numbers are calculated with the equilibrium conditions:

$$\left.\begin{aligned} n_3 &= k_3^0 n_2^2 \\ n_5 &= k_5^0 n_2 n_4 \\ n_7 &= k_7^0 n_2^2 \\ n_8 &= k_8^0 n_2 \\ n_9 &= k_9^0 n_2 \sqrt{n_4} \\ n_{10} &= k_{10}^0 \sqrt{n_4} \\ n_{11} &= k_{11}^0 n_2 \sqrt{n_6} \\ n_{12} &= k_{12}^0 \sqrt{n_6} \end{aligned}\right\} \text{(C-5)}$$

(3) Steps (1) and (2) are repeated in sequence until successive iterations give the same values of n_2, n_4, and n_6. The amount of solid carbon is then calculated from

$$n_1 = q_c - n_2 - n_3 \qquad \text{(C-6)}$$

The calculations for $n_1 < 0$ are given in the next paragraphs.

C-3 RICH SYSTEM WITHOUT SOLID CARBON, $q_O < 2q_C + q_H/2$

The equilibrium constants k_i are calculated with the aid of the following table of the β_{ij} for each value of i for which entries are given:

β_{ij}		CO	H_2	H_2O	N_2
	j =	2	4	5	6
	i				
CO_2	3	1	-1	1	0
O_2	7	0	-2	2	0
O	8	0	-1	1	0
OH	9	0	-1/2	1	0
H	10	0	1/2	0	0
NO	11	0	-1	1	1/2
N	12	0	0	0	1/2

Steps in the calculations are:

(1) The Quantities A, B, C are evaluated from the definitions

$$\left.\begin{aligned} A &= q_C \\ B &= \tfrac{1}{2}q_H - q_O + q_C + 2n_7^0 + n_8^0 \\ &\quad + \tfrac{1}{2}n_9^0 - \tfrac{1}{2}n_{10}^0 + n_{11}^0 \\ C &= q_O - q_C - 2n_7^0 - n_8^0 - n_9^0 - n_{11}^0 \end{aligned}\right\} \quad \text{(C-7)}$$

Initially, all of the n_i^0 in these relationships can be taken to be zero.

(2) n_3 is the positive root of the quadratic

$$(1-k_3^0)n_3^2 + (Ak_3^0 + B + Ck_3^0)n_3 - ACk_3^0 = 0 \quad \text{(C-8)}$$

(3) n_2, n_4, n_5, and n_6 are evaluated from the relations

$$\left.\begin{aligned} n_2 &= A - n_3 \\ n_4 &= B + n_3 \\ n_5 &= C - n_3 \\ n_6 &= \tfrac{1}{2}q_N - \tfrac{1}{2}n_{11}^0 - \tfrac{1}{2}n_{12}^0 \end{aligned}\right\} \quad \text{(C-9)}$$

Initially, the values of n_{11}^0 and n_{12}^0 can be taken to be zero.

(4) The remaining mole numbers are calculated with the relations

$$\left.\begin{aligned} n_7 &= k_7^0 n_5^2/n_4^2 \\ n_8 &= k_8^0 n_5/n_4 \\ n_9 &= k_9^0 n_5\sqrt{n_4} \\ n_{10} &= k_{10}^0\sqrt{n_4} \\ n_{11} &= k_{11}^0 n_5\sqrt{n_6}/n_4 \\ n_{12} &= k_{12}^0\sqrt{n_6} \end{aligned}\right\} \quad \text{(C-10)}$$

(5) Steps (1) through (5) are repeated in sequence until successive iterations give the same values of n_2, n_4, n_5, and n_6.

C-4 LEAN SYSTEMS WITHOUT SOLID CARBON, $q_O \geq 2q_C + q_H/2$

The equilibrium constants k_i are calculated with the aid of the following table of the β_{ij} for each value of i for which entries are given:

β_{ij}			CO_2	H_2O	N_2	O_2
		j =	3	5	6	77
	i					
CO	2		1	0	0	-1/2
H_2	4		0	1	0	-1/2
O	8		0	0	0	1/2
OH	9		0	1/2	0	1/4
H	10		0	1/2	0	-1/4
NO	11		0	0	1/2	1/2
N	12		0	0	1/2	0

Steps in the calculations are:

(1) n_3, n_5, n_6, and n_7 are calculated from the relations

$$\left.\begin{aligned} n_3 &= q_C - n_2^0 \\ n_5 &= \tfrac{1}{2}q_H - n_4^0 - \tfrac{1}{2}n_9^0 - \tfrac{1}{2}n_{10}^0 \\ n_6 &= \tfrac{1}{2}q_N - \tfrac{1}{2}n_{11}^0 - \tfrac{1}{2}n_{12}^0 \\ n_7 &= \tfrac{1}{2}q_O - \tfrac{1}{4}q_H - q_C \\ &\quad + \tfrac{1}{2}n_2^0 + \tfrac{1}{2}n_4^0 - \tfrac{1}{2}n_8^0 - \tfrac{1}{4}n_9^0 \\ &\quad + \tfrac{1}{4}n_{10}^0 - \tfrac{1}{2}n_{11}^0 \end{aligned}\right\} \quad \text{(C-11)}$$

Initially, the values of the n_i^0 may be taken to be zero. If $q_O = \frac{1}{2}q_H - 2q_C$, it is necessary initially to take n_7 to be some arbitrary small number, e.g., 10^{-6}, so that it will not vanish.

(2) The remaining mole numbers are calculated with the relations

$$
\left.
\begin{aligned}
n_2 &= k_2^0 n_3 / \sqrt{n_7} & n_{10} &= k_{10}^0 \sqrt{n_5 / \sqrt{n_7}} \\
n_4 &= k_4^0 n_5 / \sqrt{n_7} & n_{11} &= k_{11}^0 \sqrt{n_6 \sqrt{n_7}} \\
n_8 &= k_8^0 \sqrt{n_7} & n_{12} &= k_{12}^0 \sqrt{n_6} \\
n_9 &= k_9^0 \sqrt{n_5 \sqrt{n_7}}
\end{aligned}
\right\} \quad \text{(C-12)}
$$

(3) Steps (1) and (2) are repeated in sequence until successive iterations give the same values of n_3, n_5, n_6, and n_7.

APPENDIX D IMPERFECT GAS CONTRIBUTIONS TO THE THERMODYNAMIC PROPERTIES FOR SEVERAL EQUATIONS OF STATE

D-1 INTRODUCTION

In this Appendix, we list for easy reference expressions for the imperfect gas part of the thermodynamic properties of a gaseous phase, employing several of the equations of state that have been used to describe the gaseous products of condensed explosives. These expressions are obtained by the use of the relations deduced in Appendix A.

D-2 THE ABEL EQUATION OF STATE

The Abel modification of the van der Weal's equation of state has been employed to describe the gaseous products of condensed explosives. The equation is written

$$p\tau = nRT + \alpha p \tag{D-1}$$

where α is a constant covolume. (For references, see par. 7-9.) The partial derivatives of the equation of state are

$$\left.\begin{aligned} \frac{\partial \tau}{\partial T} &= \frac{nR}{p} \\ \frac{\partial \tau}{\partial p} &= -\frac{nRT}{p^2} \\ \frac{\partial \tau}{\partial n_i} &= \frac{RT}{p} \end{aligned}\right\} \tag{D-2}$$

With this equation of state, the nonideal parts of the thermodynamic parts of the gas mixture are given by

$$\left.\begin{aligned} h(T,p) - h^*(T) &= \alpha p \\ e(T,p) - e^*(T) &= 0 \\ s(T,p) - s^*(T,p) &= 0 \\ c_{p,n}(T,p) - c^*_{p,n}(T) &= 0 \\ \mu_i(T,p) - \mu^*_i(T,p) &= 0 \end{aligned}\right\} \tag{D-3}$$

The derivative $\gamma_{i/i}$ employed in the calculation of the equilibrium composition is

$$\gamma_{i/i} = \delta_{i/i} - n_i/n \tag{D-4}$$

where δ is the Kronecker delta. Although this equation of state has been used to calculate detonation parameters, it does not satisfy the identiy for volume, Eq. 2-45.

D-3 THE ABEL EQUATION OF STATE AS MODIFIED BY JONES

Jones had modified the Abel equation of state for calculations of the properties of gaseous explosion products of condensed explosives by assuming that

$$\alpha = \alpha(p) \tag{D-5}$$

(For references, see Chapter 7.) With Eq. D-5, the partial derivatives of Eq. D-1 are

$$\left.\begin{aligned} \frac{\partial \tau}{\partial T} &= \frac{nR}{p} \\ \frac{\partial \tau}{\partial p} &= -\frac{nRT}{p^2} + \alpha'(p) \\ \frac{\partial \tau}{\partial n_i} &= \frac{RT}{p} \end{aligned}\right\} \tag{D-6}$$

The nonideal parts of the thermodynamic properties of the gas mixture are given by

$$\left.\begin{aligned} h(T,p) - h^*(T) &= \int_0^p \alpha(p)dp \\ e(T,p) - e^*(T) &= \int_0^p \alpha(p)dp - \alpha p \\ s(T,p) - s^*(T,p) &= 0 \\ c_{p,n}(T,p) - c^*_{p,n}(T) &= 0 \\ \mu_i(T,p) - \mu^*_i(T,p) &= 0 \end{aligned}\right\} \tag{D-7}$$

The coefficient $\gamma_{l'l}$ employed in the calculation of the equilibrium composition is given by

$$\gamma_{l'l} = \delta_{l'l} \tag{D-8}$$

This form of the Abel equation does not satisfy the thermodynamic identity for volume, Eq. 2-45.

D-4 THE ABEL EQUATION OF STATE AS MODIFIED BY COOK

Cook has modified the Abel equation of state for calculations of the properties of gaseous explosion products of condensed explosives by assuming that

$$\alpha = \alpha(\tau) \tag{D-9}$$

(For references see Chapter 7.) With Eq. D-9, the partial derivatives of Eq. D-1 are

$$\left.\begin{aligned} \frac{\partial p}{\partial T} &= \frac{nR}{\tau - \alpha} \\ \frac{\partial p}{\partial \tau} &= -\frac{nRT}{(\tau - \alpha)^2}\left[1 + \alpha'(\tau)\right] \\ \frac{\partial p}{\partial n_l} &= \frac{RT}{\tau - \alpha} \end{aligned}\right\} \tag{D-10}$$

The nonideal parts of the thermodynamic properties of the gas mixture are given by

$$\left.\begin{aligned} e(\tau,T) - e^*(T) &= 0 \\ s(\tau,T) - s^*(\tau,T) &= nR\int_{\infty}^{\tau}\frac{\alpha}{\tau(\tau - \alpha)}\,d\tau \\ c_{v,n}(\tau,T) - c^*_{v,n}(T) &= 0 \\ \mu_l(\tau,T) - \mu_l^*(\tau,T) &= -RT\int_{\infty}^{\tau}\frac{\alpha}{\tau(\tau - \alpha)}\,d\tau \end{aligned}\right\} \tag{D-11}$$

The coefficient $\gamma_{l'l}$ employed in the calculation of the equilibrium composition is given by

$$\gamma_{l'l} = \delta_{l'l} \tag{D-12}$$

This form of the Abel equation does not satisfy the thermodynamic identity for volume, Eq. 2-45.

D-5 THE VIRIAL EQUATION OF STATE OF HIRSCHFELDER AND ROSEVEARE

An equation of state in viral form proposed by Hirschfelder and Roseveare has been applied to the calculation of the properties of the gaseous explosion products of condensed explosives by Patterson. Patterson employs the expression

$$\left.\begin{aligned} \frac{p\tau}{nRT} = 1 + \frac{b}{\tau} + A\left(\frac{b}{\tau}\right)^2 + B\left(\frac{b}{\tau}\right)^3 \\ + C\left(\frac{b}{\tau}\right)^4 \end{aligned}\right\} \tag{D-13}$$

where A, B, and C are numerical constants. $A = 0.625$, $B = 0.287$, $C = 0.193$, and

$$b = \sum_l n_l b_l \tag{D-14}$$

where b_l is the high temperature second virial coefficient of the k-th gaseous constituent, regarded as independent of temperature. (For references, see Chapter 7.) The partial derivatives of the equation of state are

$$\left.\begin{aligned} \frac{\partial p}{\partial T} &= \frac{nR}{\tau}\left\{1 + \frac{b}{\tau} + A\left(\frac{b}{\tau}\right)^2 + B\left(\frac{b}{\tau}\right)^3 + C\left(\frac{b}{\tau}\right)^4\right\} \\ \frac{\partial p}{\partial \tau} &= -\frac{nRT}{\tau^2}\left\{1 + 2\left(\frac{b}{\tau}\right) + 3A\left(\frac{b}{\tau}\right)^2 + 4B\left(\frac{b}{\tau}\right)^3 + 5C\left(\frac{b}{\tau}\right)^4\right\} \\ \frac{\partial p}{\partial n_l} &= \frac{RT}{\tau}\left\{1 + \left(1 + \frac{nb_l}{b}\right)\frac{b}{\tau} + \left(1 + \frac{2nb_l}{b}\right)A\left(\frac{b}{\tau}\right)^2 \right. \\ &\quad \left. + \left(1 + \frac{3nb_l}{b}\right)B\left(\frac{b}{\tau}\right)^3 + \left(1 + \frac{4nb_l}{b}\right)C\left(\frac{b}{\tau}\right)^4\right\} \end{aligned}\right\} \tag{D-15}$$

The nonideal parts of the thermodynamic properties are given by

$$\left.\begin{aligned} e(\tau,T) - e^*(T) &= 0 \\ s(\tau,T) - s^*(\tau,T) &= -nR\left\{\frac{b}{\tau} + \frac{A}{2}\left(\frac{b}{\tau}\right)^2 + \frac{B}{3}\left(\frac{b}{\tau}\right)^3 + \frac{C}{4}\left(\frac{b}{\tau}\right)^4\right\} \\ c_{v,n}(\tau,T) - c^*_{v,n}(T) &= 0 \\ \mu_l(\tau,T) - \mu_l^*(\tau,T) &= RT\left\{\left(1 + \frac{nb_l}{b}\right)\frac{b}{\tau} + \left(\tfrac{1}{2} + \frac{nb_l}{b}\right)A\left(\frac{b}{\tau}\right)^2 \right. \\ &\quad \left. + \left(\tfrac{1}{3} + \frac{nb_l}{b}\right)B\left(\frac{b}{\tau}\right)^3 + \left(\tfrac{1}{4} + \frac{nb_l}{b}\right)C\left(\frac{b}{\tau}\right)^4\right\} \end{aligned}\right\} \tag{D-16}$$

AMCP 706-180

The coefficient $\gamma_{l'l}$ employed in the calculation of the equilibrium composition is given by

$$\gamma_{l'l} = \frac{\sum_{m=1}^{4} A_m \left(\frac{b}{\tau}\right)^m}{1 + \sum_{m=1}^{4} mA_m \left(\frac{b}{\tau}\right)^m} \left(\frac{n_l b_l}{b} - \frac{n_l}{n}\right) \left[n(m-1)\frac{b_{l'}}{b} + m\sum_{m=1}^{4} A_m \left(\frac{b}{\tau}\right)^m\right] \quad \text{(D-17)}$$

where

$$A_1 = 1$$

$$A_2 = A$$

$$A_3 = B$$

$$A_4 = C$$

D-6 THE HALFORD-KISTIAKOWSKY-WILSON EQUATION OF STATE

Halford, Kistiakowsky, and Wilson have proposed an empirical equation of state for the description of the gaseous products of condensed explosives. As subsequently modified by Cowan and Fickett, it has the form

$$\left.\begin{aligned} p\tau &= nRT\,(1 + xe^{\beta x}) \\ x &= k/[\tau(T+\theta)^{\alpha}] \\ k &= \sum_l n_l k_l \end{aligned}\right\} \quad \text{(D-18)}$$

Here, α, β, and θ are constants to which Cowan and Fickett assign the values $\alpha = 0.5$, $\beta = 0.09$, $\theta = 400°\text{K}$. The k_l are "covolume" constants characteristic of the individual species. (For references, see Chapter 7.) The partial derivatives of the equation of state are

$$\left.\begin{aligned} \frac{\partial p}{\partial T} &= \frac{nR}{\tau}\left\{1 + xe^{\beta x} - \left(\frac{\alpha T}{T+\theta}\right)(1+\beta x)xe^{\beta x}\right\} \\ \frac{\partial p}{\partial \tau} &= -\frac{nRT}{\tau^2}\left\{1 + xe^{\beta x} + (1+\beta x)xe^{\beta x}\right\} \\ \frac{\partial p}{\partial n_l} &= \frac{RT}{\tau}\left\{1 + xe^{\beta x} + \frac{nk_l}{k}(1+\beta x)xe^{\beta x}\right\} \end{aligned}\right\} \quad \text{(D-19)}$$

With this equation of state, the nonideal parts of the thermodynamic properties of the gas mixture are given by

$$\left.\begin{aligned} e(T,\tau) - e^*(T) &= nRT\left(\frac{\alpha T}{T+\theta}\right)xe^{\beta x} \\ s(T,\tau) - s^*(T,\tau) &= nR\left\{\left(\frac{\alpha T}{T+\theta}\right)xe^{\beta x} - (e^{\beta x} - 1)/\beta\right\} \\ c_v(T,\tau) - c_v^*(T) &= nR\left(\frac{\alpha T}{T+\theta}\right)xe^{\beta x}\left\{2 - \frac{T}{T+\theta}(1 + \alpha + \alpha\beta x)\right\} \\ u_l(T,\tau) - u_l^*(T,\tau) &= RT\left\{k_l x e^{\beta x}/k + (e^{\beta x} - 1)/\beta\right\} \end{aligned}\right\} \quad \text{(D-20)}$$

In the calculation of the equilibrium composition, we employ the derivative

$$\gamma_{l'l} = \delta_{l'l} - \frac{n_l}{n} + \frac{e^{\beta x}}{k}\left(\frac{n_l k_l}{k} - \frac{n_l}{n}\right)\left[\frac{kx(1 + e^{\beta x}) + nk_{l'}x^2(\beta - e^{\beta x})}{1 + 2xe^{\beta x} - \beta^2 x^2 e^{\beta x}}\right] \quad \text{(D-21)}$$

APPENDIX E CALCULATION OF THE DETONATION VELOCITY OF THE THERMODYNAMIC STATE OF THE EXPLOSION GAS

As shown in Chapter 6 (Eqs. 6-106 and 6-107), the detonation velocity D and the thermodynamic state at the detonation front satisfy the equations

$$\left.\begin{aligned} D &= v_0\sqrt{\kappa_1 p_1 \rho_1} \\ e_1 - e_0 &= \tfrac{1}{2}(p_1 + p_0)(v_0 - v_1) \\ 1 - p_0/p_1 &= \kappa_1(\rho_1 v_0 - 1) \end{aligned}\right\} \quad \text{(E-1)}$$

where the subscripts o and 1 denote initial conditions and conditions at the detonation front, respectively; κ is the adiabatic exponent; and e, specific energy function.

Let us suppose that the equation of state is an expression of the form

$$p = p(v,T) \quad \text{(E-2)}$$

and that with this expression together with tables of the thermal properties of the individual reaction products, the specific energy, and adiabatic exponent are represented as functions of the same independent variables

$$\left.\begin{aligned} e &= e(v,T) \\ \kappa &= \kappa(v,T) \end{aligned}\right\} \quad \text{(E-3)}$$

Thus, in the solution of Eqs. E-1, we are required to satisfy the functions represented by Eqs. E-2 and E-3, in which the temperature appears as a parameter.

If the composition of the reaction products is known, if the analytical form of the equation of state is a simple one, and if the thermal properties of the reaction products can be represented with sufficient accuracy by simple empirical equations; then an algebraic solution of Eqs. E-1, E-2, and E-3 can in principle be obtained. As an example of the theory, we derive in Appendix F the solution for the case when Eq. E-2 is the equation of state for an ideal gas. In general, however, the thermal properties of the reaction products are not analytic functions of the temperature, and the composition of the mixture of reaction products is to be determined on the assumption that the products are in thermodynamic equilibrium at the temperature and specific volume behind the detonation front. The solution of the equilibrium conditions, necessary for calculating the detonation parameters with Eqs. E-2 and E-3, is itself a problem of considerable complexity. This problem has been discussed in Appendixes B and C where methods for its solutions are discussed in detail. It is apparent that the solution of Eqs. E-1, satisfying the functions represented by Eqs. E-2 and E-3 and subject to the equilibrium conditions for the composition of the mixture, must be obtained by an iterative method. With the understanding that the procedures described in Appendix A can be employed to evaluate the functions of Eqs. E-2 and E-3 for specified values of specific volume and temperature, these functions can be regarded as known and we can proceed to formulate an iterative method for the solution of Eqs. E-1.

Suppose that an approximate solution, e.g., (v_1', T_1'), to Eqs. E-1 has been found and that

$$\begin{aligned} p_1' &= p(v_1', T_1') \\ e_1' &= e(v_1', T_1') \\ \kappa_1' &= \kappa(v_1', T_1') \end{aligned}$$

have been evaluated. It is convenient to define the abbreviations

$$\left.\begin{aligned} x &= p_1/p_1' \\ y &= v_1/v_1' \end{aligned}\right\} \quad \text{(E-4)}$$

which are the corrections to be applied to the approximate values p_1' and v_1' to obtain an improved approximation. We also define the quantities

$$\left.\begin{aligned} a &= p_0/p_1' \\ b &= v_0/v_1' \\ c &= 2(e_1' - e_0)/(p_1' v_1') \end{aligned}\right\} \quad \text{(E-5)}$$

which can be evaluated at (v_1', T_1'). Now, as an approximation, we assume that the detonation

products are polytropic between (v_1', T_1') and the correct solution to Eqs. E-1, (v_1, T_1), with adiabatic exponent $\kappa_1 = \kappa_1'$. With this assumption

$$e_1 - e_1' = \frac{1}{\kappa_1' - 1}(p_1 v_1 - p_1' v_1') \qquad \text{(E-6)}$$

By use of Eqs. E-4, E-5, and E-6 the bottom two equations in E-1 can be written as

$$\left.\begin{aligned} x &= \frac{(\kappa_1' - 1)(c - ab + ay) - 2}{(\kappa_1' - 1)\, b - (\kappa_1' + 1)y} \\ y &= \frac{\kappa_1'}{\kappa_1' + 1}\, b + \left(\frac{a}{\kappa_1' + 1}\right)\frac{y}{x} \end{aligned}\right\} \qquad \text{(E-7)}$$

and solved for x and y.

For a condensed explosive, the ratio p_1/p_o is the order of 10^5. Since the ratio p_1/p_1' is of order unity, $a \approx 0$ to a very good approximation for condensed explosives, and the solution of Eqs. E-7 can be written

$$\left.\begin{aligned} x &= -(\kappa_1' - 1)(c/b) + 2/b \\ y &= \kappa_1' b/(\kappa_1' + 1) \end{aligned}\right\} \qquad \text{(E-8)}$$

For a gaseous explosive, p_1/p_o is of order 10 and it is not permissible to neglect p_o in comparison to p_1' in the solution of Eqs. E-7. The separation of variables in Eqs. E-7 results in a pair of simultaneous quadratic equations. Instead of solving them in this form, it is convenient to use successive approximations—employing the second of Eqs. E-8 to begin the iteration—and then employing Eqs. E-7 in sequence to determine successive approximations to x and y, a process that converges very rapidly.

Having determined x and y, and these improved estimates of p_1 and v_1; we can obtain an improved estimate of the temperature T_1 from the equation of state. For a condensed explosive, requiring the use of a nonideal equation of state explicit in temperature and volume, the evaluation of the temperature must usually be carried out by successive approximations because of the practical impossibility of inverting the equation of state to obtain an expression giving temperature as function of volume and pressure. For a gaseous explosive, for which the ideal gas equation of state is sufficiently accurate, we can write

$$T_1 = T_1' xy \qquad \text{(E-9)}$$

and this expression can be used to start the successive approximations to determine T.

We have developed a procedure to obtain an improved estimate (v_1, T_1) to the solution of Eqs. E-1, satisfying the functional relations of Eqs. E-2 and E-3, when an approximation solution (v_1', T_1') is known. We have thus, without assumption regarding the form of the equation of state, formulated an iterative procedure for the solution of these equations. At each stage of the iteration the equilibrium composition and thermodynamic properties are evaluated, using standard computational procedures, for the thermodynamic state specified by the approximate solution. When $x = y = 1\, p_1 = p_1'\, v_1 = v_1'\, T_1 = T_1'$, and the detonation can be calculated with the top equation in E-1. The comparison of x and y with unity affords a test, at each stage of the iteration, of whether or not the iteration has converged. The usefulness of this computational procedure results from the facts that the adiabatic exponent is an insensitive function of state and that the polytropic assumption, Eq. E-6, is employed between states whose separation tends to zero as the iteration proceeds. In application, this procedure has been found to converge very rapidly.

In order to complete the formulation of the computational procedure, it is necessary to specify a way to obtain a first approximation to the desired solution. For this purpose, it is convenient to employ the polytropic gas relation between the Chapman-Jouguet pressure and the constant volume explosion pressure p_e.

$$e(p_e, v_o) = e_o \qquad \text{(E-10)}$$

can be used to calculate the thermodynamic properties of the constant volume explosion state by the methods described in Appendix B.

On the assumption that the detonation products are polytropic between the states (p_1, v_1) and $)p_e, v_o)$, we can write

$$\left.\begin{aligned} e(p_1,v_1) - e(p_e,v_o) &= \frac{1}{\kappa_e - 1}(p_1 v_1 - p_e v_o) \\ \kappa_e &= \kappa(p_e,v_o) \end{aligned}\right\} \quad \text{(E-11)}$$

With Eqs. E-10 and E-11, the Hugoniot equation can be written

$$\left.\begin{aligned} \frac{p_1}{p_e}\left(\frac{\kappa_e + 1}{\kappa_e - 1} - \frac{v_o}{v_1}\right) &= \frac{p_o}{p_e}\left(\frac{v_o}{v_1} - 1\right) \\ &\quad + \frac{2}{\kappa_e - 1}\left(\frac{v_o}{v_1}\right) \end{aligned}\right\} \quad \text{(E-12)}$$

Eliminating the ratio of the specific volume by means of the third of Eqs. E-1, we obtain the quadratic equation

$$\left.\begin{aligned} \left(\frac{p_1}{p_e}\right)^2 - 2\left(\frac{p_1}{p_e}\right) + \left[(1-\mu^2)\frac{p_o}{p_e}\right. \\ \left. + \mu^2\left(\frac{p_o}{p_e}\right)^2\right] = 0 \end{aligned}\right\} \quad \text{(E-13)}$$

where $\mu^2 = (k_e - 1)/k_e + 1)$. Since $p_1 > p_e$, the desired root is

$$\left.\begin{aligned} \frac{p_1}{p_e} &= 1 \\ &+ \left[1 - (1-\mu^2)\frac{p_o}{p_e} - \mu^2\left(\frac{p_o}{p_e}\right)^2\right]^{1/2} \end{aligned}\right\} \quad \text{(E-14)}$$

The expansion

$$\frac{p_1}{p_e} = 2 - \left(\frac{1-\mu^2}{2}\right)\frac{p_o}{p_e} - \tfrac{1}{2}\left(\frac{1+\mu^2}{2}\right)^2\left(\frac{p_o}{p_e}\right)^2 \cdots \quad \text{(E-15)}$$

is correct to terms of order $(p_o/p_e)^2$. For a condensed explosive, p_o can be neglected in comparison to p_e, and Eq. E-14 reduces to

$$p_1/p_e = 2 \quad \text{(E-16)}$$

Even for a gaseous explosive, the approximation given by Eq. E-16 differs from the result of Eq. E-14 or Eq. E-15 by at most a few percent.

From this analysis, we conclude that an appropriate first approximation to the pressure p_1 can be obtained from the constant volume explosion pressure p_e through Eq. E-16. The corresponding first approximations to the specific volume v_1 and temperature T_1 can then be obtained from the second of Eqs. E-1 and the equation of state, respectively. With the specification of the initial approximation and the formulation of an iterative procedure, the computational procedure for the solution of Eqs. E-1 is completely formulated.

APPENDIX F CALCULATION OF THE DETONATION VELOCITY FOR IDEAL GASES

As shown in Chapter 6 the detonation pressure p_1 and the detonation specific volume v_1 are determined by solving the equations

$$\left.\begin{aligned} e_1 - e_2 &= \tfrac{1}{2}(p_1 + p_o)(v_o - v_1) \\ 1 - p_o/p_1 &= \kappa_1(\rho_1 v_o - 1) \end{aligned}\right\} \quad \text{(F-1)}$$

and the solution requires the introduction of an equation of state. When it has been obtained, the detonation velocity D and the particle velocity u_1 can be evaluated using the equations

$$\left.\begin{aligned} D &= v_o\sqrt{p_1\rho_1} \\ u_1 &= D(1 - \rho_o v_1) \end{aligned}\right\} \quad \text{(F-2)}$$

As an example of the application of the theory, we derive in this Appendix the solution of Eqs. F-1 for the case where the explosion products are described with sufficient accuracy by the ideal gas equation of state

$$pv = nRT \quad \text{(F-3)}$$

where n is the number of moles of gas produced by unit weight of explosive. We also assume that the composition of the explosion gas is frozen and is known. In order to calculate the detonation velocity and detonation properties of a gaseous detonation, to which case the ideal gas equation of state is accurately applicable, the results of this Appendix can be employed iteratively with the procedure for the calculation of the equilibrium composition that has been described in Chapter 2. The results also provide a basis for approximate relations that are of practical interest for the estimation of the explosion properties of condensed explosives.

It is convenient to transform Eq. F-1 by the introduction of the specific enthalpy $h = e + pv$ and of the specific heat of explosion, defined by Eq. 6-8. When this is done, we obtain

$$h_1 - h(p_o, T_o) = q + \tfrac{1}{2}(p_1 - p_o)(v_1 + v_o) \quad \text{(F-4)}$$

where $h(p_o, T_o)$ is the specific enthalpy of the explosion products at pressure p_o and temperature T_o. For an ideal gas, the enthalpy is independent of the pressure and a function of the temperature only. Therefore, the left-hand side of Eq. F-4 can be written

$$\left.\begin{aligned} h_1 - h(p_o, T_o) &= h^\circ(T_1) - h^\circ(T_o) \\ &= \overline{c_p^\circ}(T_1 - T_o) \end{aligned}\right\} \quad \text{(F-5)}$$

where $h^\circ(T) = h(T, p = 1 \text{ atm})$ is the ideal gas specific enthalpy of the explosion products and $\overline{c_p^\circ}$ is the average specific heat of the explosion products between temperatures T_o and T_1. When this expression is substituted into Eq. F-4 and the temperature T_1 eliminated by means of Eq. F-3, we obtain

$$\overline{c_p^\circ}\left(\frac{p_1 v_1}{nR} - T_o\right) = q + \tfrac{1}{2}(p_1 - p_o)(v_1 + v_o) \quad \text{(F-6)}$$

When the abbreviations $x = v_1/v_o$, $y = p_1/p_o$, $a = 2\,\overline{c_p^\circ}/nR$, $b = 2\,(q + \overline{c_p^\circ}\,T_o)/(p_o v_o)$ are introduced, Eq. F-6 becomes

$$(a - 1)xy + x - y = b - 1 \quad \text{(F-7)}$$

In the special case that the average specific heat $\overline{c_p^\circ}$ is a constant, Eq. F-7 describes a rectangular hyperbola.

For an ideal gas, the adiabatic exponent κ is equal to the ratio of the heat capacity at constant pressure to that at constant volume,

$$\kappa = c_p^\circ/c_v^\circ = \gamma^\circ \quad \text{(F-8)}$$

By using the abbreviations x and y, the second of Eqs. F-1 can be transformed to the expression

$$(\gamma_1^\circ + 1)xy - x - \gamma_1^\circ y = 0 \quad \text{(F-9)}$$

Eqs. F-7 and F-9 are to be solved simultaneously for x and y.

Upon separation of the variables, a pair of quadratic equations is obtained

$$\left.\begin{aligned}&(\gamma_1^{\circ} + a)x^2 - (\gamma_1^{\circ} + 1)bx + \gamma_1^{\circ}(b-1) = 0\\&[\gamma_1^{\circ}(a-1) - \gamma_1^{\circ} - 1]y^2\\&\quad - (\gamma_1^{\circ} + 1)(b-2)y + b - 1 = 0\end{aligned}\right\} \quad \text{(F-10)}$$

These equations can be solved with the aid of the usual formula for the roots of a quadratic equation. Each has two real roots. The Chapman-Jouguet detonation, which is here the solution of interest, corresponds to the pair for which $x < 1, y > 1$. (The pair for which $x > 1, y < 1$ corresponds to a Chapman-Jouguet deflagration.) After x and y have been obtained, v_1 and p_1 can be evaluated and the temperature T_1 of the Chapman-Jouguet state can be evaulated with the aid of the equation of state, Eq. F-3.

Both the average specific heat and the heat capacity ratio are functions of temperature, although the temperature dependence is not very strong. If an attempt is made to include the temperature dependence explicitly by expanding these quantities as a power series of the temperature, the expressions replacing Eqs. F-10 become of order higher than the second and their solution becomes awkward. It seems better, therefore, if precise results are desired, to conduct the calculations iteratively. The average specific heat and ratio γ° are evaluated at an approximate temperature. The solution of Eqs. F-10 and F-3 will then yield an improved value of the temperature, upon which a second solution can be based. If it is desired to elaborate the calculation to the extent of requiring that the explosion products be in thermodynamic equilibrium, the composition of the products can be adjusted at each stage of the iteration by calculating the equilibrium composition at the approximate temperature and pressure of the particular iteration. Whether the equilibrium calculation is performed or not, the successive approximations will be found to converge rapidly.

As a useful approximation to obtain estimates of the detonation properties, one can assume that the explosion gas is polytropic with a constant heat capacity. Then

$$\left.\begin{aligned}a &= 2\gamma^{\circ}/(\gamma^{\circ} - 1)\\b &= \frac{2}{p_o v_o}[q + \gamma^{\circ} nRT_o/(\gamma^{\circ} - 1)]\end{aligned}\right\} \quad \text{(F-11)}$$

In this approximation, Eqs. F-10 can be written

$$\left.\begin{aligned}&x^2 - \left(\frac{\gamma^{\circ} - 1}{\gamma^{\circ}}\right)bx\\&\quad + \left(\frac{\gamma^{\circ} - 1}{\gamma^{\circ} + 1}\right)(b - 1) = 0\\&y^2 - (\gamma^{\circ} - 1)(b - 2)y\\&\quad + \left(\frac{\gamma^{\circ} - 1}{\gamma^{\circ} + 1}\right)(b - 1) = 0\end{aligned}\right\} \quad \text{(F-12)}$$

In the polytropic approximation, γ° is a known constant, independent of the temperature. Therefore, Eqs. F-12 can be solved at once and an iterative calculation is not required.

Relations that are convenient for order of magnitude estimates of the detonation properties can be obtained from a further approximation to Eqs. F-12. On the detonation branch of the Hugoniot curve, x is of order unity, and y and b are large compared to unity. As a first approximation, the roots of Eqs. F-12 corresponding to the Chapman-Jouguet detonation can be written

$$\left.\begin{aligned}x &= \gamma^{\circ}/(\gamma^{\circ} + 1)\\y &= (\gamma^{\circ} - 1)b\end{aligned}\right\} \quad \text{(F-13)}$$

Futhermore, q is much greater than $\bar{c_p^{\circ}}\, T_o$. Therefore, Eqs. F-13 result in the approximate relations,

$$\left.\begin{aligned}v_1 &= v_o\gamma^{\circ}/(\gamma^{\circ} + 1)\\p_1 &= 2q(\gamma^{\circ} - 1)/v_o\end{aligned}\right\} \quad \text{(F-14)}$$

The corresponding approximation to the detonation temperature is obtained by substitution in the equation of state

$$T_1 = \left(\frac{2q}{nR}\right)\frac{\gamma^{\circ}(\gamma^{\circ} - 1)}{\gamma^{\circ} + 1} \quad \text{(F-15)}$$

and the corresponding approximations to the detonation velocity and particle velocity are obtained by substitution in Eqs. 6-56

$$\left.\begin{aligned} D &= \sqrt{2q(\gamma^\circ + 1)(\gamma^\circ - 1)} \\ u_1 &= \sqrt{2q(\gamma^\circ - 1)/(\gamma^\circ + 1)} \end{aligned}\right\} \quad \text{(F-16)}$$

In order to estimate the accuracy of the approximate relations, Eqs. F-14, we may use the formula for the roots of a quadratic to write the exact solutions of Eqs. F-12. If this is done and the resulting radical expanded in powers of $1/b$, the result to terms of order $1/b$ can be written

$$\left.\begin{aligned} x &= \frac{\gamma^\circ}{\gamma^\circ + 1}\left\{1 - \left[1 + \tfrac{1}{4}\frac{(\gamma^\circ)^2}{(\gamma^\circ)^2 - 1}\right]\frac{1}{b} + \cdots\right\} \\ y &= (\gamma^\circ - 1)b\left\{1 - \left[2 + \frac{1}{(\gamma^\circ)^2 - 1}\right]\frac{1}{b}\right\} \end{aligned}\right\} \quad \text{(F-17)}$$

Thus, the approximations expressed by Eqs. F-14 differ from the exact solutions of Eqs. F-12 by terms in the quantity $1/b$ of first and higher orders.

INDEX

A

Abel 7-2
  equation of state 9-10, D-1
Accidents 11-26
Accuracy 14-14
Activation energy 4-1, 4-3, Table 4-1, 10-1
Activity coefficient 7-3, A-6
Adams 11-24
Adiabat, Hugoniot 11-2
  exponent 2-14, 2-16, 7-2, 7-9, Table 7-5, 14-11, E-1
  heating 10-9
Aerodynamic drag 13-10
AFTON 14-10
Air-blast 3-5
Amatol Table 1-2
Ammonium
  nitrate Table 1-1
    dynamite Table 1-2
  perchlorate Table 1-1
  picrate Table 1-1
  salts 4-16
Amster 11-28
AN See: Ammonium nitrate
Andreev 4-5
AP See: Ammonium perchlorate
Argon
  flash 5-3
  gap method 5-15
Arrhenius equation 10-2, 12-10, Fig. 12-6, Table 12-2, 14-13
Avrami and Erofeev 4-2

B

Ballast, thermal 1-3
  function of in explosives, commercial 1-3
Ballistic Mortar test 3-7, Table 3-11, 5-25
Baratol, composition of Table 1-2
Barium nitrate, in baratol Table 1-3
Barker 14-4
Barthel and Strehlow 8-15, 14-4, 14-13, 14-14
Beattie A-3
Becker 6-21, 7-13
Becker-Kistiakowsky-Wilson See: BKW code
Berthelot
  and Vieille 1-1
  detonation, theory of 1-1
Bikini gage 5-19
Bircumshaw 4-16
Bis (2,2-dinitro-2-fluoroethyl) formal See: FEFO
Bis (N, N'-trinitromethyl), urea See: BTNEU
BKW code 14-11
Black powder, constituents of 1-1
Blackstock 14-4
Blast
  pressure 5-19, 13-1
  propagation theory 1-3
  wave 13-1, 13-7, 13-10
Blasting
  caps 1-9, 1-4
  gelatin Table 1-2, 11-26
Boddington 12-8
Boltzmann and Jäger 7-16
Bowden 12-4, 12-6, 12-8
  and Yoffe 12-6
Boyer 11-24, 14-13
  and Grandey 11-24
Bridgman 5-10
Brinkley B-2
  and Kirkwood 6-21, 13-7, 13-30, 13-31, 13-32
  and Richardson 8-12
  and Wilson 7-18
  stoichiometric conditions 2-8
Brisance 5-24, 5-25
Brode 13-12, 13-13
Brodie 14-6
BTNEU Table 1-1
Bubble pulse 5-19
Burning law 11-24, 12-20

C

Camera
  framing 5-3
  image dissection 5-3
  rotating-mirror or -drum 5-1, 5-2, Fig. 5-1
  "streak camera 1-2, 5-1
  See: Photography, high-speed
Campbell, Davis, Ramsay, and Travis 11-23
Carslaw and Jager 10-11, 10-16
CEL 14-10
Chaiken and Cheselske 12-8
Chambre', 10-1, 10-7
Chapman and Jouguet 1-1, 6-1
  See: C-J
Characteristics, method of 2-21, 14-1

Charge
cylindrical 8-1, 13-1
diameter, effect on detonation velocity 9-1, 9-9
spherical 8-1, 13-1
Chemical kinetics 1-2
Chemical potential 2-7, 14-11, A-2, A-4, A-5, B-2, B-4, C-1, D-1, D-2, D-3
definition of 2-7
Chemical reaction 1-1
detonation wave 1-1, 1-2, 14-2, 14-4
Chou, Karpp, and Huang 14-2, 14-4
Chushkin 14-5
C-J
detonation F-2
hypothesis 6-19
parameters Table 3-5, 3-6
points 14-11
state
detonation velocity F-3
energy 7-7
particle velocity F-3
pressure 5-9, 7-4, 7-7, E-2, F-2
solution for 6-24
subideal 8-12, 9-3
temperature 7-3, 7-4, F-2
volume F-2
theory 1-1
Code
BKW 14-11
Eulerian-Lagrangian 14-9, 14-10
modular 14-14
Codes, computer See: Computer codes (or programs)
Coefficient
activity 7-3, A-6
thermal expansion A-2
Cole 13-19, 13-21, 13-27, 13-32
Components, definition of 2-2
Composition, theoretical description 2-1
Composition B Table 1-2, 5-23
Compressibility, isothermal A-2
Computer codes (or programs)
AFTON 14-10
CEL 14-10
explosion phenomena, use in 1-2
HEMP 14-7
hydrodynamic, time dependent 1-3, 14-1
NIP 14-4, 14-13
OIL 14-9
PIC 14-10
PIPE 14-7
RUBY 14-11
STRETCH 14-11
STRIP 14-10
SWAP 14-4
THERMO 14-11
thermodynamic, equilibrium 1-3
TIGER 14-11
TOODY 14-13
See: Chapter 14
Conductivity, as measurable parameter 5-1, 5-4, 5-22
Conservation
equations 2-18, 2-19, 5-7, 8-1
shock front 2-28, 2-29
Constants
Gurney Table 3-8
Rydberg 4-9
stoichiometric 2-2
Constant volume explosion point 14-11
Constituent, definition of 2-1
Conventional decomposition equation See: Decomposition, equation
Cook 5-5, 7-8, 7-9, 9-10
Courant
and Friedrichs 2-29, 6-15, 14-2
-Friedrichs-Lewy conditions 14-7
Courtney-Pratt, J. S. 5-4
Covolume 7-2, D-1, D-2, D-3
Cowan and Fickett 7-14, 7-16, 7-18, D-3
Cyclotetramethylene tetranitramine See: HMX
Cyclotol, composition of Table 1-2
Cyclotrimethylene trinitramine See: RDX
Cylindrical charge 13-1

D

Dalton's law A-4
DATNB Table 1-1
D'Autriche method 5-5
Deal 5-18, 7-5, 8-9, 13-4
Deb 4-9
Decomposition
covalent explosives 4-3
data from adiabatic furnace Fig. 12-6
equation 2-1, 2-3
heat of 4-1
ionic solids 4-6
mechanisms 4-3
of azides 4-6
of nitrates 4-14
products 2-3
of TNT 2-4

Decomposition (cont.)
rate of 4-1
reaction 4-5, 4-6, 4-16, 4-18, 10-1
spontaneous 10-1
thermal 4-1, Table 4-2
Deflagration 6-3
propagation of 1-3, 1-6, 1-8
strong 8-3
transition to detonation 12-15
wave 8-3
Denisov and Troshin 8-15
Densitometry, flash X-ray 5-7
Dependence, domain of 2-23
Detonation
energy 1-2, 1-3
fadeout of 14-13
hypervelocity 11-17
in liquid 8-16
initiation of 14-13
low-order 11-26
low-velocity 11-26, 11-28
stability 11-26, Table 11-5
overdriven 11-1
parameters, measurement of 5-4
pressure 5-5, 5-9
properties Table 7-3, Table 7-4, Table 7-5, Table 7-7
solids and liquids 7-1
theoretical/experimental comparison Table 7-9
products
composition of 3-2, 3-3, Table 3-4, 7-13
equation of state 3-3
stability of 6-21, 8-6
strong 6-4, 8-10
temperature 5-21
theories of 1-1
underdriven 11-1, 11-10, 11-17, Fig. 11-11
velocity 5-1, 5-8, F-1
charge effect on 9-2, 9-9
equation for 3-6, 6-14, 7-3, 7-4
low, initiation process 11-26,
waves
cylindrical 9-1
definition of 1-8
elementary theory of 6-1
front of 1-1
planar 1-2
plane 8-1
spherical 9-13
steady 8-4
weak 6-4
Dewey 5-19
Diaminotrinitrobenzene See: DATNB
Diaphragm gage 5-19
Diethylnitramine dinitrate See: DINA
DINA Table 1-1, 12-15
Döering 5-18, 8-5
and Burkhardt 5-18
Drag, aerodynamic 13-10
Dremin 8-16
Duff and Houston 5-9, 5-10
Duvall 13-38
Dynamic pressure 13-10
Dynamite 1-1, Table 5-2
ammonium nitrate type Table 1-2
commerical 1-3
composition of Table 1-2
nitroglycerin-based 1-1
Nobel 1-1
See: Explosive, secondary

E

EDGN Table 1-1
EDNA Table 1-1, Table 5-2
Edwards 8-14
Effect
See: Faraday effect
See: Kerr effect
See: Magneto-optic effect
Eichelberger 9-12
Electrical systems, ionization probes 5-4
Emery 14-5
Energy
activation 10-1, Table 10-1
as property of explosive 1-3, 3-1
as thermodynamic property 2-10
free 3-2
internal A-1, A-3, A-5, A-6, D-1, D-2, D-3, E-1
of detonation 1-2, 1-3
of explosion 13-23
of explosive 3-1
specific internal, of C-J state 7-7
Enig 10-1, 10-7, 10-10
and Petrone 11-10
Enthalpy 2-7, 2-9, 13-6, A-1, A-3, A-6 B-3, F-1
as thermodynamic property 2-10
definition of 2-7
Entropy A-2, A-3, A-5, A-6, D-1, D-2, D-3,
function of
mole number 2-9

Entropy (cont.)
temperature 2-9
volume 2-9
in reversible process 2-8
in thermodynamics, second law 2-5
Equation
See: Arrhenius equation
See: Conservation equations
See: Decomposition equation
See: Eulerian equations of motion
See: Hyperbolic equations
See: Rankine-Hugoniot equation
See: Stoichiometric equations
Equation of state 3-3, 3-6, 5-1, 5-22, 8-2, A-2, A-3, A-4, B-2, B-3, B-5, C-1, D-1, D-2, D-3, F-1
Abel's 7-2, 9-10, D-1
as requirement for stress wave calculations 14-1
Becker-Kistiakowsky-Wilson 14-11
caloric 2-10
Cook's 7-8
definition of 2-10, 14-11
Fickett and Wood 7-7, Table 7-2
for solid or liquid explosives 7-1
general derivation 7-5
Halford, Kistiakowsky, and Wilson 8-9, D-3
Jones' 7-9
modified Abel 7-8, 7-16
by Jones 7-9, D-1
by Cook 7-8, D-2
of condensed species 7-16
of products 8-9
Tait 12-17, 13-30, 13-37
van der Waal D-1
virial 7-16, D-2
table of coefficients, Table 7-6
Equilibrium
composition 14-11, B-1, B-6, C-1, D-1
conditions B-4, C-2
general conditions for 2-8
mechanical, chemical, and thermal 2-8, 2-9
Equivalent weight, Table 3-9, Table 3-10, 5-25, 13-38, 3-5
Erpenbeck 8-15
Ethylenedinitramine See: EDNA
Ethylene glycol dinitrate See: EGDN
Eulerian
equations of motion 2-16, 2-18, 2-20
variables 14-1, 14-9
Eulerian-Lagrangian code 14-9, 14-10
Eyring 9-15
and Powell, Duffey, and Parlin 9-10
Experimental technique 5-1
Exploding wire 5-3
Explosion
description of 1-2
energy of 14-27
point, constant volume 14-11
pressure, constant 6-3
products 1-4, 2-1
in thermodynamic equilibrium 2-3
thermal 1-3, 1-8, 10-1
critical temperature for 10-9, Table 10-3, Table 10-4
dependence on sensitivity tests 12-6
of cylinders Fig. 10-5
of slabs Fig. 10-5
of spheres 10-12, Fig. 10-4, Fig. 10-5, Table 10-6
shock initiation of 11-10
stability 10-3
time 10-9, 10-12, Fig. 10-4, Fig. 10-5, Fig. 10-6, 10-19, Table 10-6
underground 12-19, 13-23
underwater 13-4, 13-19
volume, constant 6-3, E-3
work of 3-6, Table 3-11
Explosive
acceptor 11-1, 11-20
commercial 1-3
condensed 14-13
covalent 4-4
damage from 13-4, 13-26
definition of 1-2, 1-4, 3-1
donor 11-1, 11-20
homogeneous 11-5, 11-10, 11-17, 11-23
Hugoniot adiabat 11-2
inhomogeneous 14-13
lens 5-9
nonhomogeneous 11-17, 11-23
performance 1-2
evaluation of 1-3
primary 1-4, 12-8, 12-15
processes of 1-2
products 5-1
secondary 1-4, 12-8
size, critical 10-9
Explosive D See: Ammonium picrate

F

Faraday
effect 5-4
foil 5-16
FEFO Table 1-1, Table 3-1

Fermat's principle 9-12
Fickett Table 3-5
  and Wood 7-7, 7-13, 13-4
Figure of merit 5-25
Formula vector 2-2
  of components 2-3
  of constituents 2-2, 2-3
Flash, argon 5-3
Flash X-ray, densitometry 5-7
Fragments, velocities of 3-4
Frank and Lazarus 14-5, 14-9
Frank-Kamenetskii 10-1, 10-7
Free energy function, Table 3-3
Friedman 12-8, 3-2
Friederich 7-10
Friederich 14-4
'Frozen" composition, of mixture 2-1
Fuel, types Table 3-1

G

Gage
  Bikini 5-19
  diaphragm 5-19
  in-material 5-10, 5-13
  manganin 1-2, 5-10, 5-13
  piezoelectric 5-10
  piezoresistive 5-10, 5-13
  polarization 5-14
  quartz 5-10
  sulfur 5-15
Galwey and Jacobs 4-18
Gap test 11-1, 11-20, 11-26, Table 11-3, Table 11-4
  argon 5-15
  pressure measurement in 11-2
Gas
  imperfect, properties of D-1
  polytropic 13-23, 13-37, E-2
Geometry, spherical 13-1, 13-2, 13-12
Gibbs-Dalton rule B-5
Gibbs free energy 2-7, A-2, A-3, A-5
  in standard state 2-9
  specific 2-9
Gibson 5-21, 5-22
Gipson and Macek 11-23
Godunov 14-5, 14-7
Goranson 5-8
Gray 4-4
  and Williams 4-4
Gross and Amster 12-8, 12-9, 12-10
Gross composition, specification of 2-2
Gurney
  constants, Table 3-8
  comparison of with Q, Table 3-8
  formula, definition 3-5

H

Haleite See: EDNA
Halford, Kistiakowsky, and Wilson 7-18, 8-9, D-3
  equation of state 8-9, D-3
Happel and Majumdar 7-16
Harlow 14-11
Hartree method 14-2, 14-3
Hat 5-23
He
  capacity A-1, A-3, A-5, A-6
  conduction 10-7, 10-8, 13-5
  of formation A-3
  radiation of 13-5
  release 3-1, Table 3-6, Table 3-7, 6-2
    computation 3-5
    equation for Hess' law 3-1
    in detonation 3-1
    sample values Table 3-2
  specific 2-10, 2-12, 7-3, 14-11, D-1, D-2, D-3, F-1
  transport, cause of detonation 1-3
Helmholtz free energy 2-17, A-4
  in standard state 2-9
HEMP 14-7
Herrmann 14-7
Hess' law 3-1
Heterogeneous explosives See: Explosive, nonhomogeneous
Heterogeneous system B-1
Hilsenrath and Beckett 13-10
Hirschfelder
  and Roseveare 7-16, D-2
  Stevenson, and Eyring 7-17
HMX Table 1-1, Table 1-2
Homogeneous explosives See: Explosive, homogeneous
Hot spots 10-22, Table 10-5, 11-5, 11-10, 11-13, 11-17, 14-13, 14-14, 11-24, 12-6, 12-9, 12-11
  critical 12-11
  pressure 11-14
  temperature 11-14, 11-15, 11-16, Table 12-3
  See: Explosion, thermal
Huff, Gordon, and Morrell B-2

Hugoniot 2-29, 13-7
adiabat 11-2
and Rankine 1-1
curve 2-29, 5-10, 6-3, Fig. 6-2
definition for an explosion 8-11
equations, cylindrically symmetric flow 9-7
jump conditions 14-2
of explosive 11-2
points 14-11
relations 8-6
shock front 1-1
Huygen's principle 9-12
Hydrodynamics
cause of detonation 1-3
conservation equations 1-1
definition 14-1
equations 2-18, 2-20, 8-1, 14-2
Eulerian equation of 13-28
explosion phenomena of 1-1, 1-6, 2-1
for point source model 13-12
of reacting continua 2-16
theoretical development 2-1
Hyperbolic equations 2-27

I

Illumination 5-3
Image-converter tube 5-4
Image dissection 5-3
Impact
sensitivity 1-8
tests 12-1
Implicit methods 14-10
Impulse, positive, as parameter of shock wave 5-19
Induction time 10-6, 10-12, 10-16, Table 10-5, 11-7, 11-30, Fig. 11-8, Table 11-2, 12-11, 14-13
Inerts as ballast 1-3
Inhomogeneous explosives See: Explosive, inhomogeneous
Initiating mechanisms 11-1
Initiation 11-1, 14-13
air bubbles effect 11-10, 11-17,
by friction 11-17, 12-1, 12-14, 12-8
by impact 11-17, 12-1, 12-6
cavitation model 11-28, 11-29
confinement effect 12-15
diameter, critical 11-20, Table 11-3
duration of shock pulse effect 11-19
grain size effect 11-24
in gas bubble 12-8
inhomogeneities effect 11-5
Mach disc model 11-28
porosity effect 11-3, 11-18
process of low-velocity detonation 11-26, 11-28
thermal 12-1, 12-6
time, critical 11-20
Initiator, types of
mechanical shock 1-4
thermal source 1-4
In-material gage 5-10, 5-13
Interferometer, laser 5-16
Inviscid motion 2-17
Ionic solids 4-6
Ionization probes 5-4
Irreversibility 13-5
Irreversible process 2-7, 2-18, 2-19, 2-28
Isentrope, properties of 2-16

J

Jacobs, Liddiard, and Drimmer 12-17
Jameson 5-23
Johannson 12-6
Jones 5-8, 5-18, 5-21, 7-6, 9-10
Jouquet rule 6-6, 6-7, 6-11, 6-14

K

Kerr effect 5-3
Kinetics, chemical 1-2
Kirkwood
and Bethe 13-8, 13-10, 13-26, 13-27, 13-30, 13-32
and Brinkley 13-7, 13-27, 13-28
and Wood 8-11, 8-14

L

Lagrangian 14-5, 14-9
equations of motion 2-16, 2-20
Lambourn and Hartley 14-4
Landau and Lifshitz 3-5
Landshoff 14-5
Langley 14-5
Laser interferometer 5-16
Law
See: Arrhenius equation
See: Burning law
See: Conservation equations
See: Dalton's law
See: Hess' law

Law (cont.)
See: Perfect gas law
See: Planck's distribution law
See: Wien displacement law
Lawton and Skidmore 8-9
Lax 14-7
and Wendroff 14-5, 14-7
Lax-Wendroff 14-6
Lead azide Table 1-1
Lead block test 5-25
Lead styphnate Table 1-1
Leapfrog 14-6
double 14-7
Le Chatelier See: Mallard, detonation, theory of
Lens, plane wave 5-9
Lewis
and Friauf 6-20
and Randall rule B-5
Lucite wedge 5-15

M

Macek 12-15, 12-17, 12-20
Mader Table 3-5, 11-10, 14-14
Magneto-optic effect 5-4
Makino 13-33
Makovsky
and Gruenwald 4-6
and Lenji 4-5
Mallard, detonation, theory of 1-1
Manganin gage 1-2, 5-10, 5-13
Massau 14-2, 14-3
Martin and Saunders 12-6
McQueen 13-38
Measurement of detonation parameters 5-1
Mercury fulminate Table 1-1
Method
See: Argon gap method
See: Characterisitics, method of
See: D'Autriche method
See: Hartree method
See: Implicit method
See: Method of characteristics
See: Newton-Raphson method
See: Up-and-down method
Method of characteristics 14-1
Meyer 14-2
Microballoons 5-15
Mixture
composition of 2-1
constant composition of 2-10
constituents of 2-4
heterogeneous 2-10
Mitchell 4-9
Modular codes 14-14
Mole number 14-11
Muller 14-10

N

Newton-Raphson method B-2
Nicholson 4-6
NIP 14-4, 14-13
Nitrobenzene 5-3
Nitroglycerin 1-1, Table 1-1, Table 1-2, Table 5-2, 5-22, 11-26, 12-8
Nitromethane Table 1-1, Table 5-2, 5-23, Table 11-2, 11-7, 11-10, 11-13, 11-14, 11-15, 11-16, 11-17
NG See: Nitroglycerin
NM See: Nitromethane
Nobel 1-1
Noh 14-10
Nonequilibrium states 14-11
Nuclear tests 5-10

O

OIL 14-9
Oppenheim
and Urtiew 8-14
Manson, and Wagner 8-14
Ornellas 3-2
Osborn 14-14
Oxidizer
in explosives 1-3
types Table 3-1
Oxygen balance Table 3-6

P

Particle-in-cell 14-10, 14-11
Particle velocity 5-7, 5-15, F-1
equation for 6-24, 7-3, 7-4, 7-7
Paterson 7-17
PBX 9404, composition of Table 1-2
Penney and Dasgupta 13-23
Pentaerythritol tetranitrate See: PETN
Pentolite 13-33
composition of Table 1-2
Perfect gas law 14-11
PETN Tables 1-1, 1-2, 5-2; 5-22
as homogeneous explosive 11-10, Table 11-2
charge diameter 9-3
Petrone 14-13

Phase
  condensed, in mixture 2-1, 2-3, 2-10
  gas in mixture 2-1, 2-3
  rule 2-3
PHERMEX 5-18
Photography
  argon flash 5-3
  Deal 5-18
  Dewey 5-19
  Döering and Burkhardt 5-18
  exploding wire 5-3
  framing 5-3
  high-speed 5-1
  illumination 5-3
  image dissection 5-3
  PHERMEX 5-18
  Schall 5-18
  spark discharge 5-3
  See: Camera
Photo-optical systems 5-4
PIC See: Particle-in-cell
Picric acid Table 1-1
Piezoelectric gage 5-10
Piezoresistive gage 5-10, 5-13
Pin technique 5-15
PIPE 14-7
Planck's distribution law 5-21
Plane wave lens 5-9
Plate-dent test 5-25
Point source model 13-12, 13-27
Polarization 5-14
Polytropic gas 13-23, 13-37
Power of an explosive 5-24
Pressure
  as property
    of explosive 1-3, 1-4
    of homogeneous phase 2-4, 2-5
    thermodynamic 2-10
  blast 5-19
  C-J, equation for 3-6
  dynamic 13-10
  in reversible process 2-8
  of detonation 5-5, 5-9
  of reaction 1-2
  transducer 5-10
Price 3-5
Principle
  See: Fermat's principle
  See: Huygen's principle
Probes, ionization 5-4
Process
  equations for 2-9
  infinitesimal 2-5, 2-7, 2-8
  irreversible 2-5, 2-7
  natural 2-5
  of isolated system 2-8, 2-8
  reversible 2-5, 2-7
  thermodynamic 2-5
  unnatural 2-5
Propagation
  blast See: Blast, propagation theory
  velocity, definition of 1-6
Propellant 1-3, 11-3, 11-20, 11-26
Prout and Tompkins 4-2

Q

Quartz gage 5-10

R

Radiation
  damage 4-18
  of heat 13-5
Rankine 2-29
  shock front, discontinuous 1-1
Rankine-Hugoniot equation 2-29, 6-1
Rarefaction 13-3
  wave 2-24
Rayleigh
  line 6-3, 14-5, 14-8
  shock waves 1-1
RDX Table 1-1, Table 1-2, Table 5-2, 5-22
Reaction
  decomposition 1-2, 2-2, 4-5
  heat of 6-2
  initiation 8-5
  order of 10-8
  process 14-1, 14-13
    progress variable for 8-3
  products Table 3-1
  rate 2-17, 2-18, 10-1, Table 10-1, 10-3
    equation 8-2, 10-8
  water-gas 3-2
  waves
    boundary
      rigid 8-9
      free 8-9
    general 8-6
    polytropic gas 8-8
    stability 8-12, 8-14, 8-15
  zone 8-1, 11-23
    cylindrical charge 9-3, 9-4, 9-9
    diverging flow 9-4

Reaction Zone (Cont.)
fine structure 8-14
length 9-9
Mach interactions 8-15
mechanisms 11-24
turbulence 8-15
Release wave model 9-12
Retonation 12-15
Reversible process 2-7, 2-18, 2-19, 2-28
Rezoning 14-9
Richardson, Arons, and Halverson 13-23
Richtmyer and Morton 14-5, 14-6
Rideal and Robertson 12-8, 12-11
Riemann
function 13-25
invariants 2-22
shock waves 1-1
RUBY 14-11
Rule
See: Gibbs-Dalton rule
See: Jouquet's rule
See: Lewis and Randall rule
See: Phase, rule
Rusanov 14-7
Rydberg constant 4-9

S

Sachs 13-38
Safety in handling 4-1, 10-1, 10-18, 11-1, 11-26, 12-1
Schall 5-18
Schmidt 7-2, 7-8
Schott 8-14
Scorah 6-21
Seaman 14-7
Secco 4-16
Seismic waves 13-23
Self-heating 4-1
Semenov 10-1
Sensitivity 11-26, Table 11-7, 12-1, 12-4, 12-6, 12-8
of explosive 1-8
relation to melting temperature 12-9
Shchelkin 8-14, 8-15
Shear 8-9, 9-15
and Wright 13-33
Shock
front 13-3
velocity 5-7
wave 2-25
chemical reaction 1-1
detonation 1-1
from explosive charge 13-1
in solids 13-38
line 14-4
nonreactive 1-1
propagaton of 1-3, 13-5, 13-26
properties of 1-1
scaling of 13-33, 13-37
stability 1-29
weak 14-4
Shuster 1-1
detonation wave 1-1
Simple waves 2-23
Skidmore and Hart 8-9
Smith and Calvert 4-6
Smoke trails 5-21
Soloukhin 8-14
Sombrero 1-1
Sonic 2-19
subsonic 2-19
supersonic 2-19
Sound velocity 2-14
equilibrium 7-14
frozen 7-14, 8-12
Spacelike 2-22
Spark
as external initiating stimuli 1-3
discharge 5-3
types of 1-3
Specific heat See: Heat, specific
Spherical geometry 13-1, 13-2, 13-12
Standard state 2-9
Steady-state
detonation
charge diameter effect on 1-3
theory of 1-1
of wave 1-6
Stimuli, initiating
See: Heat
See: Impact
See: Shock
See: Spark
Stoichiometric
conditions B-1, B-2, B-4
mathematical expressions of 2-3, 2-8
constants 2-2
equations 8-2
Strehlow 8-14, 8-15
and Fernandes 8-15
STRETCH 14-11
STRIP 2-19
Subsonic 2-19

Sulfur gage 5-15
Supersonic 2-19
SWAP 14-4
Systems
  See: Electrical systems
  See: Heterogeneous system

T

Taffanel and D'Autriche 7-2, 7-9
Tait equation of state 13-23, 13-31, 13-37
Target 13-4
Taylor 7-15, 13-13, 13-23
  wave 5-10, 8-8, 13-13
Taylor, G. I. 9-13
Technique
  See: Experimental technique
  See: Pin technique
Temperature
  as property
    of homogeneous phase 2-4
    thermodynamic 1-10, A-1, A-3
  in equation of state relation 2-10
  in reversible process 2-8
Test
  See: Ballistic Mortar test
  See: Gap test
  See: Impact tests
  See: Lead block test
  See: Nuclear tests
  See: Place-dent test
Tetranitromethane See: TNM
Tetryl Table 1-1, Table 5-2
Thermal expansion coefficient 14-11, A-2
THERMO 14-11
Thermochemical data on explosives Table 3-1
Thermodynamic(s)
  cause of detonation 1-3
  first law of 2-5, 2-7, 2-7
  process, definition 2-5
  properties 2-10, A-5, A-6, D-1
    gas mixture A-1, A-3
    heterogeneous systems A-6
    pure condensed phase A-1
  second law of 2-5, 2-7
  state E-1
  theory of 1-2, 2-4
Theory
  See: Berthelot, detonation, theory of
  See: Blast, propagation theory
  See: C-J theory
  See: Detonation, theories of
  See: Mallard, detonation, theory of
  See: Thermodynamics, theory of
  See: TNT, propagation theory
TIGER 14-11
Timelike 2-22
TNETB Table 1-1
TNM Table 1-1
TNT Table 1-1, Table 1-2
  as equivalent weight 13-38
  as homogeneous explosive 11-10, Table 11-2
  burning rate and sensitivity 12-15
  charge diameter 9-3
  conductivity profile in detonation zone 5-23
  decomposition equation of 2-1
  energy of explosion of 13-23
  "equivalent" 1-3
  finite charge of 13-15
  granular 11-26
  pressure-distance curves for 13-19
  pressure ratio vs charge radii Fig. 13-20
  pressure-time curve for 13-19
  propagation theory 13-32
TOODY 14-13
Transducer, pressure 5-10
Transfer
  electron 4-18
  proton 4-18
Trinitrophenyl methylnitramine See: Tetryl
Trinitrotoluene See: TNT
Trulio 14-7, 14-10

U

Underwater performance 3-5
Up-and-down method 12-1, 12-4
  statistical analysis of 12-4

V

van der Waal D-1
van Tiggelen and de Soete 8-14
Velocity
  deflagation 1-8
  particle 5-7, 5-15, F-1
    equation for 6-24, 7-3, 7-4, 7-7
  shock 5-7
  See: Detonation, velocity
  See: Sound velocity
Vieille See: Berthelot

Viscosity, artificial 13-12, 13-13, 14-1, 14-5
  linear 14-5
  other forms 14-5
  quadratic 14-5
Volume
  as property of homogeneous phase 2-4
  in reversible process 2-8
  molar A-1
  specific 2-9
  of C-J state 8-3, 7-7, 7-9
Von Neumann 8-5, 8-6
  and Richtmyer 13-12, 13-13, 14-5, 14-6
  spike 5-9

W

Wagner 8-14
Warner 11-24, 14-13, 14-14
Wave 1-1
  blast 13-1, 13-7, 13-10
  deflagration 8-3
  detonation 1-1, 1-8
  propagation 14-1
    multidimensional 14-4, 14-5
  rarefaction 2-24
  reaction 1-1
  retonation 12-15
  seismic 13-23
  shock 7-25, 13-38
  simple 2-23
  stability 2-29
  steady-state of 1-6
  three-dimensional 8-14
  See: Taylor, wave
Welding 1-2
White 8-15
  Johnson, and Dantzig B-2
Whitham 14-4
Wien displacement law 5-21
Wilkins 3-9, 14-7, 14-13
Willis formula 13-21
Wood
  and Kirkwood 8-12, 8-14, 9-6, 9-9
  and Salsburg 8-14
Woolfolk and Amster 11-29

X

X-ray, flash 1-2
  densitometry 5-7
  photography 5-18

Z

Zeldovich 6-21, 8-5
Zernow 14-13
Zinn and Mader 10-1, 10-7, 10-12
Zubarev Table 3-5